TESTING CERT # 2937.01

Midwest States Regional Pooled Fund Research Program
Fiscal Years 2008-2009 (Years 18 and 19)
Research Project Numbers SPR-3(017) and TPF-5(193)
NDOR Sponsoring Agency Codes RPFP-08-09 and RPFP-09-06

DEVELOPMENT OF A LOW-COST, ENERGY-ABSORBING BRIDGE RAIL

Submitted by

Jeffrey C. Thiele, M.S.C.E, E.I.T.
Former Graduate Research Assistant

Dean L. Sicking, Ph.D., P.E.
Professor and MwRSF Director

Ronald K. Faller, Ph.D., P.E.
Research Assistant Professor

Robert W. Bielenberg, M.S.M.E., E.I.T.
Research Associate Engineer

Karla A. Lechtenberg, M.S.M.E., E.I.T.
Research Associate Engineer

John D. Reid, Ph.D.
Professor

Scott K. Rosenbaugh, M.S.C.E., E.I.T.
Research Associate Engineer

MIDWEST ROADSIDE SAFETY FACILITY
University of Nebraska-Lincoln
130 Whittier Building
2200 Vine Street
Lincoln, Nebraska 68583-0853
(402) 472-0965

Submitted to

MIDWEST STATES REGIONAL POOLED FUND PROGRAM
Nebraska Department of Roads
1500 Nebraska Highway 2
Lincoln, Nebraska 68502

MwRSF Research Report No. TRP-03-226-10

August 11, 2010

TECHNICAL REPORT DOCUMENTATION PAGE

1. Report No. TRP-03-226-10	2.	3. Recipient's Accession No.
4. Title and Subtitle Development of a Low-Cost, Energy-Absorbing Bridge Rail		5. Report Date August 11, 2010 6.
7. Author(s) Thiele, J.C., Sicking, D.L., Faller, R.K., Bielenberg, R.W., Lechtenberg, K.A., Reid, J.D., and Rosenbaugh, S.K.		8. Performing Organization Report No. TRP-03-226-10
9. Performing Organization Name and Address Midwest Roadside Safety Facility (MwRSF) University of Nebraska-Lincoln 130 Whittier Building 2200 Vine Street Lincoln, Nebraska 68583-0853		10. Project/Task/Work Unit No. 11. Contract © or Grant (G) No. SPR-3(017) and TPF-5(193)
12. Sponsoring Organization Name and Address Midwest States Regional Pooled Fund Program Nebraska Department of Roads 1500 Nebraska Highway 2 Lincoln, Nebraska 68502		13. Type of Report and Period Covered Final Report: 2008– 2010 14. Sponsoring Agency Code RPFP-08-09 and RPFP-09-06
15. Supplementary Notes Prepared in cooperation with U.S. Department of Transportation, Federal Highway Administration.		

16. Abstract (Limit: 200 words)

A new, low-cost bridge rail was designed to be compatible with the Midwest Guardrail System (MGS) such that an approach transition would not be required between the two barriers. It was desired that the system minimize bridge deck and rail costs.

Several concepts for an energy-absorbing bridge post were developed and tested. These concepts included strong-post systems designed with plastic hinges and weak-post systems designed to bend near the attachment to the bridge deck. The final post concept incorporated S3x5.7 (S76x8.5) steel sections which were designed to bend at their bases. Each post was housed in a socket placed at the vertical edge of the deck and anchored to the deck with one through-deck bolt. A W-beam section was used as the rail element and was attached to the posts with a bolt that was designed to break during an impact event.

Two full-scale crash tests were performed according to the Test Level 3 impact conditions provided in the *Manual for Assessing Safety Hardware* (MASH), in which the system successfully met all safety performance criteria. The dynamic deflection of the new bridge rail and BARRIER VII modeling demonstrated that the new bridge rail would not require a transition when used with the MGS.

17. Document Analysis/Descriptors Highway Safety, Crash Test, Roadside Appurtenances, Compliance Test, MASH, Longitudinal Barrier, Bridge Rail, Approach Transition, MGS		18. Availability Statement No restrictions. Document available from: National Technical Information Services, Springfield, Virginia 22161	
19. Security Class (this report) Unclassified	20. Security Class (this page) Unclassified	21. No. of Pages 421	22. Price

DISCLAIMER STATEMENT

This report was funded in part through funding from the Federal Highway Administration, U.S. Department of Transportation. The contents of this report reflect the views and opinions of the authors who are responsible for the facts and the accuracy of the data presented herein. The contents do not necessarily reflect the official views or policies of the state highway departments participating in the Midwest Sates Regional Pooled Fund Program nor the Federal Highway Administration, U.S. Department of Transportation. This report does not constitute a standard, specification, regulation, product endorsement, or an endorsement of manufacturers.

UNCERTAINTY OF MEASUREMENT STATEMENT

The Midwest Roadside Safety Facility (MwRSF) has determined the uncertainty of measurements for several parameters involved in standard full-scale crash testing and non-standard testing of roadside safety features. Information regarding the uncertainty of measurements for critical parameters is available upon request by the sponsor and the Federal Highway Administration. Test nos. MGSBRB-1 through 7 and MGSBRS-1 through 3 were non-certified component tests conducted for research and development purposes only.

INDEPENDENT APPROVING AUTHORITY

The Independent Approving Authority (IAA) for this project was Mr. Mario Mongiardini.

ACKNOWLEDGEMENTS

The authors wish to acknowledge several sources that made a contribution to this project: (1) the Midwest States Regional Pooled Fund Program funded by the Illinois Department of Transportation, Iowa Department of Transportation, Kansas Department of Transportation, Minnesota Department of Transportation, Missouri Department of Transportation, Nebraska Department of Roads, Ohio Department of Transportation, South Dakota Department of Transportation, Wisconsin Department of Transportation, and Wyoming Department of Transportation for sponsoring this project; and (2) MwRSF personnel for constructing the barriers and conducting the crash tests.

Acknowledgement is also given to the following individuals who made a contribution to the completion of this research project.

Midwest Roadside Safety Facility

J.R. Rohde, Ph.D., P.E., Associate Professor
J.C. Holloway, M.S.C.E., E.I.T., Test Site Manager
C.L. Meyer, B.S.M.E., E.I.T., Research Associate Engineer
A.T. Russell, B.S.B.A., Shop Manager
K.L. Krenk, B.S.M.A, Maintenance Mechanic
Tom McMaster, Laboratory Mechanic
Undergraduate and Graduate Research Assistants

Illinois Department of Transportation

David Piper, P.E., Highway Policy Engineer

Iowa Department of Transportation

David Little, P.E., Assistant District Engineer
Deanna Maifield, P.E., Methods Engineer
Chris Poole, P.E., Litigation/Roadside Safety Engineer

Kansas Department of Transportation

Ron Seitz, P.E., Bureau Chief
Rod Lacy, P.E., Metro Engineer
Scott King, P.E., Road Design Leader

Minnesota Department of Transportation

Michael Elle, P.E., Design Standard Engineer

Missouri Department of Transportation

Joseph G. Jones, P.E., Engineering Policy Administrator

Nebraska Department of Roads

Amy Starr, P.E., Research Engineer
Phil TenHulzen, P.E., Design Standards Engineer
Jodi Gibson, Research Coordinator

Ohio Department of Transportation

Dean Focke, P.E., Road Safety Engineer (Retired)
Michael Bline, P.E., Standards and Geometrics Engineer

South Dakota Department of Transportation

David Huft, Research Engineer
Bernie Clocksin, Lead Project Engineer

Wisconsin Department of Transportation

John Bridwell, P.E., Standards Development Engineer
Erik Emerson, P.E., Standards Development Engineer

Wyoming Department of Transportation

William Wilson, P.E., Standards Engineer

Federal Highway Administration

John Perry, P.E., Nebraska Division Office
Danny Briggs, Nebraska Division Office

TABLE OF CONTENTS

LIST OF FIGURES

LIST OF TABLES

1 INTRODUCTION

1.1 Background

The Midwest Guardrail System (MGS) is a semi-rigid, W-beam guardrail that has been accepted by the Federal Highway Administration (FHWA) as a Test Level 3 (TL-3) barrier under National Cooperative Highway Research Program (NCHRP) Report 350 [1-2]. The system has been tested in several specialized applications, including a long-span application in which three guardrail posts were removed, creating an open span of 25 ft (7.62 m) [3]. This configuration provides a clear span for small culverts or other obstructions, eliminating the need for a special culvert guardrail and a transition between the two systems. However, the guardrail posts near the culvert must be installed with their back faces flush with the front face of the culvert headwall, which may require lateral extension of the culvert and/or contraction of the roadway shoulder, and separate bridge rail systems are still required for culverts and bridges with lengths greater than 25 ft (7.62 m).

In general, existing bridge rail systems are both costly and much stiffer than approach guardrails. This difference in stiffness between guardrail and bridge rail requires installation of approach guardrail transitions, which are also costly and further increase the cost of constructing a bridge rail system. A bridge rail with a lateral stiffness comparable to that of an approach guardrail system embedded in soil and with similar rail geometry could eliminate the need for the costly transition sections. Additionally, a more flexible bridge rail system that uses less material than existing bridge rails could substantially reduce the cost of construction. Such a barrier would also reduce dead loads on the bridge, thereby reducing the effective cost of the bridge rail even further. This system would be ideal for low-volume highway applications, in which the expected frequency of vehicle impacts is low and the need for controlling costs and bridge rail dead loads is high. Even though the cost of repairing this type of barrier would likely be higher than conventional bridge rails, the low initial cost and low crash frequencies on low-volume roadways could provide significant reductions in life-cycle costs.

In recognition of the potential benefits of a low-cost bridge rail that could eliminate the need for transitions and/or reduce the required width of culverts, the Midwest States Regional Pooled Fund Program funded a research project to develop such a system that was compatible with the MGS.

1.2 Research Objectives

The purpose of this research study was to develop a W-beam bridge rail that would satisfy the TL-3 criteria described in the *Manual for Assessing Safety Hardware* (MASH) [4] and eliminate the need for an approach guardrail transition when used with the MGS. The new bridge rail, designated the MGS Bridge Rail, was to have the following features:

- attach to the edge of a bridge deck or culvert head wall with spans greater than 25 ft (7.62 m);
- provide a lateral stiffness and strength comparable to that of the MGS with posts embedded in soil;
- allow controlled post rotation when lateral loads become high; and
- provide a yielding post or post-to-deck connection that does not damage the bridge deck during most impacts.

1.3 Research Approach

The research project began with a literature review of previously crash-tested W-beam and other light-post bridge rails and their components, as well as W-beam guardrail systems and components deemed relevant to the design of the bridge rail. Concepts for the new design were developed through a brainstorming process and, eventually, were evaluated both analytically and through static and dynamic testing.

Computer simulations were then undertaken to further evaluate the most promising design concepts when incorporated into a complete barrier system. These analyses were then used as a tool for finalizing the new barrier design. A prototype system was then constructed and subjected to full-scale crash tests under MASH criteria to verify the safety performance of the new barrier. Finally, conclusions and recommendations were made that pertain to the safety performance of the MGS Bridge Rail system.

2 LITERATURE REVIEW

The first phase of the research project consisted of an extensive literature search of previous studies deemed relevant to the development of a bridge rail compatible with the MGS. Prior research concerning W-beam bridge and culvert railing systems, other steel bridge railing systems, weak-post guardrail systems, and connections between guardrail and system posts were reviewed and summarized in this section.

2.1 Bridge Rail Design

Design of roadside appurtenances, such as bridge rails, has evolved over time as improved guidelines and practices have been developed. Prior to the 1980s, bridge rail design was performed in accordance with the standards in various editions of the American Association of State Highway and Transportation Officials (AASHTO) *Standard Specifications for Highway Bridges* [5]. This document stipulated that bridge rails were to meet certain allowable stress design (ASD) requirements, which were based on an assumed elastic behavior. Alternatively, bridge rails could be crash tested for designs that did not meet the ASD requirements.

As the importance of full-scale crash testing barriers became more apparent, guidelines and performance criteria were put forth by various organizations. Several of these were used for developing and testing bridge rails, including Transportation Research Circular (TRC) 191 [6], NCHRP Report 230 [7], the AASHTO *Guide Specifications for Bridge Rails* [8], NCHRP Report 350 [2], and MASH.

Beginning in 1986, the FHWA required that all bridge rails for use on federal aid projects meet full-scale crash testing criteria. Currently, NCHRP Report 350 criteria are required, pending approval of MASH to supersede this document. The FHWA released a memorandum in 1997 which provided NCHRP Report 350 equivalency ratings to barriers tested under prior crash testing standards [9]. Additionally, an FHWA memorandum released in 2000 [10] specified that barriers may be approved without testing should they be similar to previously-tested systems and would perform similarly based on analysis as described in the AASHTO *LRFD Bridge Design Specifications* [11].

2.2 Testing of Steel Bridge and Culvert Rails

Various W-beam and other steel bridge and culvert railing systems currently accepted by the FHWA have been subjected to full-scale crash tests. These systems include nearly-rigid, semi-rigid, and flexible designs. Testing has been performed according to requirements set forth in various crash testing standards as discussed previously. Studies deemed relevant to this research effort included flexible bridge railing designs, side-mounted bridge railing designs, and top-mounted bridge railing designs in which the railing intruded a short distance onto the bridge deck.

2.2.1 W-Beam Bridge Rails and Culvert Guardrails

A number of W-beam bridge rails and culvert guardrails have been developed for both TL-2 and TL-3 performance criteria. These systems tend to be more flexible than most bridge railing systems and typically utilize steel post-to-deck attachment hardware. These systems are very close to the system to be designed in this study and are summarized below.

2.2.1.1 California Type 15 Bridge Barrier Rail

In 1959, the California Division of Highways Bridge Department developed the California Type 15 Bridge Barrier Rail [12]. This bridge railing was designed as an economical railing for use on bridges on secondary roads. The barrier incorporated a single steel 12-gauge (2.66-mm thick) W-beam rail mounted on steel W6x15.5 (W152x23) posts bolted to the outside edge of the concrete bridge deck at 6 ft - 3 in. (1.91 m) spacing. During testing, a 4,000-lb (1,814-kg) passenger vehicle impacted the rail at 55 mph (88.5 km/h) and at an angle of 30 degrees, which produced severe wheel entrapment on posts and excessive rail deflections.

Although the behavior was deemed inadequate for freeway use, this design was considered suitable for low-speed secondary roads. However, as heavier, vehicles began using secondary roads with higher speeds, failures of the bridge rail began to occur [12]. In response to these failures, in 1967, the single W-beam was replaced with two 3½-in. (89-mm) square, structural steel tubular rails. This new tubular section proved capable of redirecting a 4,500-lb (2,041-kg) sedan travelling at a nominal speed of 60 mph (96.6 km/h) and at an angle of 15 degrees, but created a much more rigid rail section. Maximum permanent set of the rail was 0.21 ft (0.06 m), which indicated that the barrier would require approach guardrail transitions for both stiffness and geometry considerations when used with standard guardrail.

2.2.1.2 Texas Type T6 and T8 Bridge Rails

A tubular W-beam bridge rail was developed and tested in a 1978 study [13]. This bridge rail, the Texas Type T6, consisted of standard W6x8.5 (W152x12.6) guardrail posts spaced at 6 ft - 3 in. (1.91 m) and attached to a base plate with welds that were designed to break during impact. The front flange of the post was fully welded while only a portion of the rear flange was welded to the plate. The tubular W-beam rail was fabricated by welding two standard 12-gauge (2.66-mm thick) W-beams back-to-back, which allowed the rail to act as its own blockout. A pipe-sleeve and ⅝-in. (15.9-mm) diameter button-head bolt connection was used between the rail and support posts. Stiffness and strength of the rail were considered comparable to the standard Texas Guard Fence, its guardrail counterpart [13]. Thus the rail did not require an approach transition. To connect to the approach guardrail, the tubular beam was extended 12 ft - 6 in. (3.81 m) past each end of the bridge and attached to two guardrail posts.

Note that the Type T6 bridge rail did not meet the elastic analysis and allowable stress design requirements of the AASHTO *Standard Specifications for Highway Bridges, 12th Edition* [5]. However, this barrier was successfully crash tested to meet the Transportation Research

Circular (TRC) 191 criteria [6]. The T6 smoothly redirected a 4,500-lb (2,041-kg) vehicle that impacted the barrier at 61.6 mph (99.1 km/h) and at an angle of 27.5 degrees and a 2,280-lb (1,034-kg) vehicle that impacted the rail at 58 mph (93.3 km/h) and at an angle of 14 degrees. The breakaway weld mechanism worked as desired, cleanly releasing several system posts during impact from the larger vehicle. Maximum dynamic deflection of the bridge rail in these tests was 33.1 in. (840 mm). Thus, the T6 bridge rail was deemed suitable for use on culverts and low bridges according to provisions in the AASHTO specification, and later according to the multiple-service-level 2 (MSL-2) requirements in NCHRP Report 230.

With the adoption of NCHRP Report 350 by the FHWA, it was mandated that all barriers used on new construction projects on the National Highway System (NHS) must be tested according to the revised criteria. In an FHWA memorandum, the Texas T6 was classified as a TL-2 system based on successful performance in the NCHRP 230 MSL-2 tests [9]. However, the Texas Department of Transportation (DOT) believed that the barrier could meet TL-3 performance criteria, which required that the system be subjected to testing at 62 mph (100 km/h).

In a 1998 full-scale crash test, the T6 bridge rail was impacted by a 4,409-lb (2,000-kg) pickup truck traveling 62.1 mph (99.9 km/h) and at an angle of 26.6 degrees [14]. Although the bridge rail contained and redirected the vehicle, the breakaway welds did not release, and significant wheel snag occurred on system posts. The posts that detached pulled some of the anchor bolts out of the deck, thereby damaging it. The vehicle rolled onto its left side, which caused the test to be classified as a failure according to NCHRP Report 350 criteria. Maximum dynamic deflection of the bridge rail during this test was 32.3 in. (820 mm), which closely matched the results of the TRC 191 testing.

In a later study, the post-to-base plate connection welds were redesigned based on static and dynamic test results to ensure weld failure and thereby prevent wheel snag [15]. The new weld detail specified a weld on only one side of the front flange instead of both in order to significantly lower the capacity of the connection.

Test designation no. 3-11 of NCHRP Report 350 was then repeated in which a 4,409-lb (2,000-kg) pickup truck impacted the barrier at a speed of 63.1 mph (101.6 km/h) and at an angle of 25.4 degrees. The vehicle was successfully contained and redirected, but again rolled onto its side upon exiting the system. Peak dynamic deflection was 28 in. (710 mm).

The repeated rollovers of the 2000P vehicle indicated that the T6 barrier was either too short, too stiff, or both. Note that the 27¾-in. (706-mm) tall, T6 railing was significantly stiffer than standard guardrail. Maximum dynamic deflections of the rail were in the range of 2.33 to 2.69 ft (0.71 m to 0.82 m), which was significantly less than the 3.28 to 3.71 ft (1.0 to 1.13 m) deflections observed during tests of steel post, metric height guardrail [16-17]. Further, note that crash tests of strong-post, W-beam guardrail at the 27-in. (686-mm) top mounting height also produced vehicle rollover when subjected to test designation no. 3-11 of NCHRP Report 350 [18].

After the second failed test, the post-to-deck connection was again redesigned to alter its failure mechanism [19]. The redesigned connection consisted of fully welding the front flange to the plate with non-breakaway welds to improve the weak-axis capacity of the post. Two ½-in. (13-mm) slots were cut in the front flange of the post to facilitate rupture under strong-axis loads. A plate was also welded to the back of the rear flange to induce tensile loads in the post-plate connection upon post rotation, thus facilitating failure. With these changes, another full-scale crash test was performed according to NCHRP Report 350 criteria, during which the connection behaved as desired, but the pickup rolled once again.

A finite element model of the Texas T6 bridge rail system was developed in a 2004 study to determine the performance trends causing failure and evaluate potential design changes [20]. Pendulum testing of the post-to-deck connection was used to support model development. This model was then calibrated to the most recent failed full-scale test, from which it was determined that a 27¾-in. (706-mm) top rail mounting height was inadequate for preventing rollover of a pickup truck due to rail height reduction upon post rotation. Thus, a modified T6 rail system was designed that used a 12-gauge (2.66-mm thick) tubular thrie-beam rail element in place of the tubular W-beam. Top-of-rail height for the system was raised to 31 in. (787 mm) due to the increased depth of the rail. Simulation results indicated that the tubular thrie-beam system should redirect the pickup truck while maintaining its stability.

Texas Transportation Institute (TTI) revisited its finite element model of the Texas Type T6 bridge rail in a 2008 study [21]. Updated LS-DYNA software and vehicle models were used to calibrate a new model to the third failed full-scale test, which again demonstrated insufficient rail height. It was decided again to use a 12-gauge (2.66-mm thick) tubular thrie-beam element in place of the tubular W-beam rail to mitigate the chance for the small car test vehicle to underride the rail. The resulting system was renamed the Type T8 bridge rail.

A series of pendulum tests was performed on the post-to-deck connection in which the size of the slots cut into the posts was varied. A design was sought that would mitigate bridge deck damage during an impact, or be usable on decks as thin as 6½ in. (165 mm) thick. An increased slot length of ⅞ in. (22 mm) was selected and implemented into the finite element model. The T8 bridge rail, with both the smaller and larger slot sizes, demonstrated satisfactory performance in simulations of NCHRP Report 350 test designation no. 3-11.

A full-scale crash test was then performed on the T8 bridge rail using NCHRP Report 350 criteria [22]. Posts with ⅞-in. (22-mm) slots were mounted on a 6½-in. (165-mm) thick bridge deck. A 4,570-lb (2,073-kg) pickup truck impacted the bridge rail at a speed of 62.1 mph (99.9 km/h) and at an angle of 25.4 degrees, during which the bridge deck failed prior to the breakaway mechanism of the posts. The posts did not fully release, causing the rail to be pulled downward and significant wheel snag. Both these behaviors contributed to vehicle instability, and the truck rolled over. Maximum dynamic deflection was 2.44 ft (0.74 m). Post-test analysis showed that the load was applied to the posts at a lower height than anticipated. Thus, the force required to cause failure in the front flange of the posts was too large for the bridge deck to withstand, and the deck failed.

A second full-scale crash test was performed on the T8 bridge rail mounted on a 6½-in. (165-mm) thick bridge deck [23]. Length of the slots in the tension flanges of the system posts was increased to 1 in. (25 mm). A plastic blockout was added that offset the rail 1 in. (25 mm) from the post to maintain the height of load application. In this test, a 4,522-lb (2,051-kg) pickup truck impacted the barrier at 62.1 mph (99.9 km/h) and at an angle of 23.8 degrees. The bridge deck once again failed, and the breakaway connection did not release as intended. The truck wheel again snagged on these posts and the rail was pulled down by the posts, both of which caused the vehicle to roll upon exiting the system. Maximum dynamic deflection was 1.91 ft (0.58 m).

Following the failed test, the researchers concluded that a deeper offset block and longer slots in the front flanges of the posts may be required for successful system performance. Additionally, they recommended modifying the rail section to include tubular steel elements. These modifications could ensure load application on the posts is at sufficient height to maintain a large moment arm, such that the post flanges would rupture as desired and release the posts from the deck. However, no further testing has been performed.

The failure mechanisms utilized in the T6 and T8 bridge rail posts have proven unreliable. Due to variation in the baseplate welds, system posts, bridge deck strength, and/or height of load application on the post, the breakaway mechanisms have not released consistently during full-scale crash testing. This behavior has resulted in reduction of rail height and wheel snag on posts, both of which cause vehicle instability, and unacceptable bridge deck damage. While deeper blockouts could help maintain a higher moment arm of the applied force and rail height, the reliability of the rupturing mechanism has yet to be proven. Further increase in slot length will also decrease the already diminished capacity of the posts.

2.2.1.3 Texas Low-Fill Culvert Guardrail

A 1987 study investigated the use of a continuous W-beam guardrail across an entire bridge-length culvert [24]. This option was considered to be safer and more economical than using a rigid bridge rail and would eliminate the need for a transition section between the approach guardrail and the culvert rail.

W-beam guardrail with reduced post spacing and shallow embedment over the culvert was crash tested and proved unsatisfactory. It was determined that the posts needed to be attached directly to the culvert deck to develop the required bending strength and lateral load capacity. Thus, a standard 12-gauge (2.66-mm thick) W-beam rail was mounted on W6x9 (W152x13.4) posts and blockouts spaced at 6 ft - 3 in. (1.91 m). Posts were welded to steel base plates that were bolted to the culvert slab and embedded 18 in. (457 mm) into cohesion-less soil.

In full-scale testing according to NCHRP Report 230 criteria, a 4,450-lb (2,019-kg) vehicle impacted the guardrail at 61.8 mph (99.4 km/h) and 25.3 degrees. The car was smoothly redirected and the maximum rail deflection was 32.4 in. (823 mm). Stiffness was considered similar to that of its approach rail, so no transition section was used. Performance met MSL-2 criteria as defined in NCHRP Report 230 which has been deemed equivalent to TL-2 of NCHRP Report 350.

2.2.1.4 Nested W-Beam Guardrail for Low-Fill Culverts

In a 1992 study, the Texas Low-Fill Culvert Guardrail was modified to decrease deflection of the system [25]. The Texas design required that the face of the W-beam be installed 3 ft (0.91 m) from the head wall of the culvert, which increased the size and cost of the culvert system. The new design utilized nested, 12-gauge (2.66-mm thick) W-beam rail mounted on W6x9 (W152x13.4) posts and blockouts spaced at 3 ft - 1½ in. (095 m). Posts were welded to steel base plates that were bolted to the culvert deck and embedded 9 in. (229 mm) into soil. Splices were located at posts. The distance between the face of the W-beam and the head wall of the culvert was 1 ft - 4½ in. (0.42 m). Half-post spacing and nested guardrail were extended for two post spaces on both sides of the culvert system, after which standard guardrail continued.

In crash testing, a 4,500-lb (2,041-kg) vehicle impacted the guardrail system at 61.0 mph (98.2 km/h) and at an angle of 28.2 degrees. The vehicle was smoothly redirected, and the system met all of the required NCRHP Report 230 safety performance criteria. Lateral permanent set of the barrier was 18⅝ in. (473 mm), which was significantly less than the 2.20 ft (0.67 m) observed in testing of the Texas Low-Fill Guardrail design, and the culvert was not damaged. Thus, the system satisfied the performance requirements for MSL-2 in NCHRP Report 230, which was deemed equivalent to a TL-2 rating under NCHRP Report 350.

This system proved to be significantly stiffer than the approach guardrail. For example, dynamic deflection of the MGS under NCHRP 350 impact conditions was 43.1 in. (1,094 mm) [1]. Thus, this system may need an approach transition due to its high stiffness.

2.2.1.5 Tennessee Type TBR-3 Bridge Rail

The Tennessee Type TBR-3 Bridge Rail was analyzed in a 1994 study on Tennessee bridge rails [26]. This bridge rail utilized standard, 12-gauge (2.66-mm thick) W-beam rail mounted on W6x16 (W152x23.8) steel posts spaced at 6 ft - 3 in. (1.91 m) and bolted to either the bridge deck or a 6-in. (152-mm) high concrete curb. An Allowable Stress Design (ASD) analysis indicated that the rail could resist a one-span load of 13.6 kips (60.5 kN) at a height of 21 in. (533 mm) when installed on a curb. Installation without the curb reduced the post capacity from 21.8 kips (97 kN) to 15.6 kips (69.4 kN). However, the one-span capacity of the rail remained 13.6 kips (60.5 kN), which was ruled sufficient to redirect 4,500-lb (2,041-kg) vehicles impacting at 30 mph (48.3 km/h) and 25 degrees. Based on analysis and crash tests of similar bridge rails, the Tennessee Type TBR-3 was accepted as a Test Level 1 (TL-1) barrier according to NCHRP Report 350.

2.2.1.6 Top-Mounted W-Beam Bridge Rail for Low-Volume Roads

A flexible, top-mounted W-beam bridge rail was developed in a 1996 study for use on longitudinal glulam timber bridge decks located on low-volume, low-speed roads [27]. The bridge rail utilized 12-gauge (2.66-mm thick) W-beam rail supported by W6x9 (W152x13.4) steel posts and blockouts spaced 6 ft - 3 in. (1.91 m) on center. Splices were located at posts, and W-beam backup plates were used at non-splice locations. Top rail mounting height was 27¾ in. (706 mm). The posts were bolted to a steel plate which was attached to the bridge deck surface. No transition section was used between the approach guardrail and bridge rail.

In crash testing, a 4,412-lb (2,001-kg) pickup truck impacted the bridge rail at a speed of 31.8 mph (51.2 km/h) and at an angle of 25.2 degrees, resulting in a maximum dynamic deflection of 13.5 in. (343 mm). The pickup was smoothly redirected and the test was deemed acceptable according to the TL-1 criteria in NCHRP Report 350.

2.2.1.7 Flexible Bridge Railing for Low-Volume Roads

A flexible, W-beam bridge railing with a breakaway wood post system for use on longitudinal timber bridge decks on low-volume, low-speeds roads was developed in a 1997 study [28]. The low-cost bridge rail utilized 12-gauge (2.66-mm thick) W-beam rail supported by 4-in. x 6-in. (102-mm x 152-mm) nominal wood posts spaced 6 ft - 3 in. (1.91 m) on center. The posts were connected to the deck through two 5-in. x 5-in. x ⅜-in. (127-mm x 127-mm x 9.5-mm) steel angles that were each anchored to the exterior edge of the bridge deck with a ¾-in. (19-mm) diameter, 12-in. (305-mm) long lag screw. Two ⅝-in. (15.9-mm) diameter bolts passed through the angles and the post. When loaded, these bolts caused a vertical split to develop in the post that allowed it to break free of the deck. As the railing was designed to be flexible, no transition section was used between the approach guardrail and bridge rail.

Two full-scale crash tests were performed using NCHRP Report 350 TL-1 criteria. The first test resulted in the vehicle vaulting over the bridge rail, after which the top mounting height of the W-beam rail was increased from 24 in. (610 m) to 27¾ in. (706 mm). In the second full-scale test, a 4,504-lb (2,043-kg) pickup truck impacted the bridge rail at 30.6 mph (49.2 km/h) and 24.9 degrees, resulting in a maximum dynamic deflection of 51.9 in. (1,318 mm). The truck was redirected but came to rest with the right wheels of the vehicle hanging off the bridge deck, and the bridge rail satisfied all criteria for TL-1 of NCHRP Report 350.

2.2.1.8 TL-3 Guardrail with Half-Post Spacing for Low-Fill Culverts

A 2002 study developed a W-beam guardrail for rigid attachment to box culverts that would meet the TL-3 criteria of NHCRP Report 350 [29]. The system utilized standard 12-gauge (2.66-mm thick) W-beam rail with a top mounting height of 27¾ in. (706 mm) mounted on steel W6x9 (W152x13.4) posts and 6-in. x 8-in. x 14-in. (152-mm x 203-mm x 356-mm) wood blockouts. Posts were spaced at 3 ft - 1½ in. (0.95 m) and attached with a base plate and bolts to a simulated box culvert with a 7-in. (178-mm) thick concrete slab. A soil fill of 9 in. (229 mm) was used on the culvert. Post spacing in the approach guardrail was reduced from 6 ft - 3 in. (1.91 m) to 3 ft - 1½ in. (0.95 m) for six post spaces on either side of the culvert.

Crash tests were performed on two different designs that featured different clear distances between the back of the guardrail posts and the culvert head wall. These clear distances were 18 in. (457 mm) for the first test and 1 in. (25 mm) for the second test. The intended failure mechanism was for the post and plate to yield without any bolt or weld failure. In the first test, the barrier successfully redirected a 4,394-lb (1,993-kg) pickup truck impacting at a speed of 64.2 mph (103.3 km/h) and at an angle of 25.3 degrees. In the second test, a 4,396-lb (1,994-kg) pickup truck impacted the barrier at a speed of 62.0 mph (99.7 km/h) and at an angle of 24.8 degrees. The truck was redirected but rolled over upon exiting the system. Maximum dynamic deflection in the tests was 18.6 in. (473 mm). Based on the test results, it was recommended that the backside face of the steel posts be positioned at least 10 in. (254 mm) away from the front face of the culvert headwall. This system was considered an NCHRP Report 350 TL-3 barrier, provided this offset criterion was met.

It is noted that the approach transition was not explicitly addressed in the research. No TL-3 testing for 27¾-in. (706-mm) high guardrail with half-post spacing has been performed to compare stiffness of the approach guardrail to the culvert rail. Simulation data for standard guardrail with half-post spacing impacted by a 4,400-lb (2,000-kg) sedan travelling at 60 mph (97 km/hr) and at an angle of 25 degrees to the rail predicted a maximum dynamic deflection of 21.3 in. (541 mm) [30], which suggests that the systems were indeed compatible. However, without full-scale crash testing for verification, this cannot be stated conclusively.

2.2.1.9 TL-3 Guardrail with Standard-Post Spacing for Low-Fill Culverts

In a 2008 study, a W-beam guardrail with standard, 6 ft - 3 in. (1.91 m) post spacing was developed for use on low-fill culverts [31]. The 12-gauge (2.66-mm thick) W-beam was mounted on W6x9 (W152x13.4) posts and 6-in. x 8-in. x 14-in. (152-mm x 203-mm x 356-mm) wood blockouts with a top mounting height of 27 in. (686 mm) Guardrail splices were located at posts. A new connection was developed between the post and the box culvert through use of dynamic pendulum testing. This connection consisted of four ⅞-in. (22-mm) diameter threaded rods embedded in a proprietary epoxy. Posts were welded to steel base plates that were attached to these threaded rods.

A full-scale crash test was performed on the system in which the back face of the guardrail posts were positioned 18 in. (457 mm) from the front face of the culvert headwall and embedded in 9 in. (229 mm) of soil. A 9-in. (229-mm) thick deck was used for the culvert. During testing, a 4,614-lb (2,093-kg) pickup truck impacted the barrier at 62.9 mph (101 km/h) and at an angle of 23.9 degrees. The vehicle was smoothly redirected, even though the W-beam guardrail ruptured as the vehicle exited the system. The culvert was not damaged, and the post-to-deck connection performed in a satisfactory manner. Thus, the system was deemed to satisfy the criteria of TL-3 in NCHRP Report 350, according to the researchers.

While testing was done within acceptable tolerances for impact severity as defined in NCHRP Report 350, it should be noted that actual impact severity in the test was somewhat lower than nominal impact severity for test designation no. 3-11. As the W-beam rail element ruptured, the system had little to no reserve capacity for redirection. Therefore, even a slightly more severe accident, which could also fall within acceptable tolerances for impact severity, might result in a system failure. Thus, further investigation of this system may be warranted. Note that this system did not receive FHWA acceptance [32].

2.2.2 W-Beam with Tube-Section Backup Bridge Rails

Several bridge rails and culvert guardrails use W-beam rail sections with tubular backups. These systems tend to be quite stiff and require transitions, but several have post-to-deck attachment hardware that minimizes intrusion of the system onto the bridge deck.

2.2.2.1 Texas T101 Bridge Rail

A 1984 study investigated the performance of the Texas T101 bridge rail [33]. The T101 bridge railing incorporated 12-gauge (2.66-mm thick) W-beam rail and two 4-in. x 3-in. x $^{3}/_{16}$-in. (102-mm x 76-mm x 4.8-mm) structural steel tubes mounted on W6x20 (W152x29.8) posts that were welded to base plates and bolted to the top of the bridge deck. The steel posts were spaced at 8 ft - 4 in. (2.54 m), and the top mounting height of the W-beam was 27 in. (686 mm). The T101 system required an approach transition when used with standard strong-post guardrail.

Seven full-scale crash tests were performed on the T101 bridge rail utilizing passenger vehicles and buses. In three crash tests with passenger vehicles, clean and smooth redirections occurred and the system met all safety criteria of TRC 191, with the exception that lateral decelerations were higher than permitted. However, greater decelerations were later permitted by NCHRP Report 350, therefore these decelerations were acceptable. In four full-scale crash tests utilizing buses, the vehicles were contained and redirected. However, in tests with a 32,000-lb (14,528-kg) intercity bus and a 7,000-lb (3,178-kg) school bus, the buses rolled onto their sides after impact with the bridge rail. The particular vehicle characteristics and interaction with the rail may have also contributed to the successful system performance with the other buses. Based on the performance in these tests, the Texas T101 Bridge Rail has been classified as TL-3 under NCRHP Report 350.

Observations of extensive bridge deck damage in impacts with the Texas T101 prompted a 1985 study in which design variations were investigated [34]. Standard concrete bridge decks were unable to withstand the required loads without significant cracking. Several design revisions were recommended, including strengthening the concrete bridge deck and changing the washers and base plate to induce tensile failure in the bolts.

2.2.2.2 Ohio Box Beam Rail

The Ohio Box Beam Rail utilized standard 12-gauge (2.66-mm thick) W-beam rail with an 8-in. x 4-in. x $^{3}/_{16}$-in. (203-mm x 102-mm x 4.8-mm) tubular backup beam. Top mounting height of the W-beam was 27 in. (686 mm), and posts were W6x25 (W152x37.2) sections spaced at 6 ft - 3 in. (1.91 m) centers. Additional 6-in. (152-mm) long box beams were used above and below the backup rail at each post as blockouts. Posts were mounted with anchor bolts that extended through the exterior edge of the bridge deck and passed through the front flanges of the posts. As the system was near-rigid, it required an approach guardrail transition.

The Ohio Box Beam Rail was crash tested under NCHRP Report 230 criteria for MSL-2 in a 1987 study [35]. During testing, a 1,980-lb (898-kg) vehicle impacted the rail at 60.6 mph (97.5 km/h) and at an angle of 19.6 degrees, and a 4,790-lb (2,172-kg) vehicle impacted the rail at 60 mph (97 km/h) and at an angle of 25 degrees. In both tests, the vehicles were smoothly redirected, while the bridge rail and deck received only minor damage. The Ohio Box Beam Bridge Rail met all performance criteria for MSL-2, which is considered equivalent to TL-2 of NCRHP Report 350.

2.2.2.3 Ohio Type 5 Culvert Guardrail

The Ohio Department of Transportation (ODOT) Type 5 W-Beam Guardrail with a Tubular Backup originated from the Ohio Box Beam Bridge Rail, and is also known as ODOT GR-2.2 [36]. The standard system consisted of 12-gauge (2.66-mm thick) W-beam rail backed up with 8-in. x 4-in. x $^{3}/_{16}$-in. (203-mm x 101-mm x 4.8-mm) structural tubing and supported by W6x25 (W152x37.2) steel posts spaced at 6 ft - 3 in. (1.91 m). Two additional 8-in. x 4-in. x $^{3}/_{16}$-

in. (203-mm x 101-mm x 4.8-mm) structural tubes were used as blockouts above and below the backup rail at each post. The W-beam rail had a top mounting height of 27¾ in. (706 mm). The system had a range of stiffness values depending on the post mounting conditions to the culvert, but always required a transition to connect to standard guardrail, which is the ODOT GR-3.4 system.

LS-DYNA finite element analyses of NCHRP Report 350 test designation nos. 3-10 and 3-11 were performed on the standard system with the posts embedded in both concrete and soil. Based on these results, the standard ODOT GR-2.2 guardrail was classified as a TL-3 system across its range of stiffness. Additional analyses were performed to determine potential improvements to the rail, which included using two tubular backup rails, a lower rub-rail, and/or nested W-beams. All were found to reduce the propensity for wheel snag on system posts.

Evaluation of the ODOT GR-3.4 transition revealed that it was much less stiff than the GR-2.2 guardrail. Thus, a modified transition was developed which used nested W-beam rails. With this modification, the guardrail and transition were accepted as a TL-3 system. However, no full-scale crash tests were performed.

2.2.2.4 Michigan Side-Mounted W-Beam Rail

The Michigan Side-Mounted W-Beam system was quite similar to the Ohio Box Beam Rail. The Michigan system used W6x25 (W152x37.2) posts spaced at 6 ft - 3 in. (1.905 m) that supported a 8-in. x 4-in. x $^{3}/_{16}$-in. (203-mm x 102-mm x 4.8-mm) box beam and standard, 12-gauge (2.66-mm thick) W-beam. Posts were attached directly to the bridge deck edge using anchor bolts. Alternatively, posts could be welded to spacer sections that were then bolted to the deck, which reduced rail encroachment onto the deck surface. Four 1¼-in. (31.8-mm) diameter anchor bolts were used, with the upper anchors positioned 8 in. (203 mm) above the lower anchors. Additional box beam blockouts were used above and below the box beam rail at each post. The system was quite stiff and required an approach guardrail transition. No research, crash testing reports, or FHWA approval letters were found for this system during the literature review.

2.2.3 Thrie-Beam Bridge Rails

Many bridge rails utilizing thrie-beam rail elements have been developed and successfully tested. While these systems tend to be relatively stiff, several have post-to-deck attachment hardware that minimizes intrusion of the system onto the bridge deck.

2.2.3.1 NCHRP SL-1 Barrier

NCHRP Report 239 details the design and testing of a thrie-beam barrier rated Service Level 1 (SL-1) [37]. The 12-gauge (2.66-mm thick) thrie-beam guardrail had a top mounting height of 32 in. (813 mm). Posts were either 6-in. x 6-in. (152-mm x 152-mm) wood sections or steel TS6x3x¼ (TS152x76x6.4) sections spaced at 8 ft - 4 in. (2.54 m), both of which were designed to break away during impact. Wood posts were housed in sockets anchored to the side of the deck that developed the ultimate capacity of the posts, while steel posts were attached to the deck edge with a breakaway connection. This connection utilized two bolts anchored in the side of the concrete deck that passed through a steel base plate which extended above the deck. A bolt was passed through this plate, the post, and a bearing plate on the back side of the post that was designed to fail during impact. Wood posts were attached to the thrie-beam rail with $^{5}/_{16}$-in. (7.9-mm) diameter bolts and washers, while hooked beam hangers were used to attach the thrie-beam to steel posts. A bolt was passed through the straight end of the hanger to attach it to the thrie-beam, while the hooked end rested on top of the tube-section post. Following unsatisfactory performance of this connection, the wood-post connection was applied to the steel-post system.

In testing, the steel-post SL-1 barrier was impacted by a 4,500-lb (2,041-kg) vehicle at 61.7 mph (99.3 km/h) and at an angle of 16.6 degrees, twice with a 2,250-lb (1,021-kg) vehicle at 58.6 mph (94.3 km/h) and 60.0 mph (96.6 km/h), both at angles of 16.0 degrees, and once with a 20,000-lb (9,072-kg) vehicle at 44.7 mph (71.9 km/h) and at an angle of 7.7 degrees. In all tests, the vehicles were smoothly redirected. Maximum barrier deflection of 30 in. (762 mm) occurred during the 4,500-lb (2,041-kg) vehicle impact. The wood-post system was also tested five times, but displayed varying results due to lack of uniformity in the wood posts. However, both systems were deemed acceptable as SL-1 barriers, which are considered equivalent to TL-2 barriers under NCHRP Report 350.

2.2.3.2 Nebraska Tubular Thrie-Beam

The Nebraska Tubular Thrie-Beam Bridge Rail utilized a tubular thrie-beam rail formed by placing two separate 10-gauge (3.42-mm thick) thrie-beam elements back-to-back. Center mounting height of the rail was 23 in. (584 mm). The rail was supported by W6x25 (W152x37.2) posts which were welded to a base-plate and bolted to the deck with five cast-in-place bolts.

Two crash tests were performed on the barrier in a 1987 study [35]. The barrier successfully redirected a 1,970-lb (893-kg) vehicle which impacted at 61.4 mph (98.8 km/h) and at an angle of 20 degrees and a 4,700-lb (2,132-kg) vehicle which impacted at 58.4 mph (94.0 km/h) and at an angle of 24.3 degrees. The barrier met the MSL-2 criteria of NCHRP Report 230 and was later classified as a TL-3 system under NCHRP Report 350.

2.2.3.3 California Thrie-Beam Bridge Rail

The California Thrie-Beam Bridge Rail consisted of 10-gauge (3.42-mm thick) thrie-beam rail mounted on W6x15.5 (W152x23) posts and blockouts with a top mounting height of 32 in. (813 mm). Posts were spaced at 6 ft - 3 in. (1.91 m) and side-mounted to the bridge deck with two 1¼-in. (31.8-mm) diameter upper anchors and two ¾-in. (19.1-mm) diameter lower anchors that passed through the front flange of each post. The upper anchors were positioned 5 in. (127 mm) above the lower anchors. Minimum deck thickness for this system was 12 in. (305 mm), and an approach guardrail transition was required.

Crash testing was performed on the California Thrie-Beam Bridge Rail in a 1993 study [38]. The barrier successfully redirected a 5,400-lb (2,449-kg) pickup truck impacting at 44.9 mph (72.3 km/h) and at an angle of 21 degrees, and a 1,770-lb (803-kg) car impacting at 48.7 mph (78.4 km/h) and at an angle of 18.3 degrees. Successful crash testing was also performed on the approach guardrail transition. Thus, the system performance satisfied Performance Level 1 (PL-1) criteria as defined by AASHTO *Guide Specifications for Bridge Rails*, which was deemed equivalent to a TL-2 rating under NCHRP Report 350.

2.2.3.4 Oregon Side-Mounted Thrie-Beam Bridge Rail

The Oregon Side-Mounted Thrie-Beam Bridge Rail utilized 10-gauge (3.42-mm thick) thrie-beam rail mounted on W6x15 (W152x22.3) posts with a top mounting height of 27 in. (690 mm). Posts were anchored to the edge of bridge decks with two ¾-in. (19.1-mm) diameter upper bolts and two lower concrete inserts. Minimum deck thickness for the rail was 15 in. (381 mm), and the system required an approach guardrail transition.

Two full-scale crash tests were performed on the Oregon Side-Mounted Thrie-Beam Bridge Rail in a 1997 study [39]. The system successfully redirected a 1,970-lb (894-kg) car impacting at 52.2 mph (84.0 km/h) and at an angle of 19.7 degrees and a 5,737-lb (2,605-kg) pickup truck impacting at 46.1 mph (74.2 km/h) and at an angle of 20.9 degrees. Performance was deemed acceptable for PL-1, which was considered equivalent to a TL-2 rating under NCHRP Report 350.

2.2.3.5 TBC-8000 Bridge Rail

The thrie-beam and channel, or TBC-8000 bridge rail, was designed for use on longitudinal glulam timber bridge decks [40]. The system consisted of W6x15 (W152x22.3) posts and blockouts spaced at 6 ft - 3 in. (1.905 m) that supported 10-gauge (3.42-mm thick) thrie-beam rail and a C8x11.5 (C200x17) channel section. Top mounting height of the channel section was 33¼ in. (845 mm). Posts were side-mounted to exterior base plates on the edge of the deck using four 1-in. (25.4-mm) diameter bolts. These plates were anchored with two 1-in. (25.4-mm) diameter threaded rods that extended 4 ft (1.22 m) into the deck and through an anchor plate. An approach guardrail transition was used with the system.

The TBC-8000 was successfully crash tested to Performance Level 2 (PL-2) with an 18,000-lb (8,165-kg) single-unit truck travelling 47.4 mph (76.3 km/h) and at an angle of 16.1 degrees to the bridge rail. In the test, the vehicle was smoothly redirected, and maximum permanent set of the rail was 8³⁄₁₆ in. (208 mm). This barrier was considered a TL-4 system under NCHRP Report 350.

2.2.3.6 TL-4 Thrie-Beam Bridge Rail for Glulam Timber Decks

A TL-4 steel bridge rail for use on transverse glulam timber decks was developed in a 2002 study [41]. Posts were side-mounted, W6x15 (W152x22.3) sections spaced at 8 ft (2.44 m) and bolted to upper and lower anchor plates. These anchor plates were attached to the top and bottom of the bridge deck with twelve ⅞-in. (22.2-mm) diameter through-deck bolts. Additional W6x15 (W152x22.3) sections were used to block the 10-gauge (3.42-mm thick) thrie-beam rail away from the posts. A steel 8-in. x 3-in. x ³⁄₁₆-in. (203-mm x 76-mm x 4.8-mm) tube section was used as a second rail section that was mounted above the thrie-beam. An approach guardrail transition was used with the system.

The system was crash tested according to NCHRP Report 350 criteria with a 4,396-lb (1,994-kg) pickup travelling at 58.2 mph (93.7 km/h) and at an angle of 25.5 degrees to the rail and with a 17,785-lb (8,067-kg) single-unit truck travelling at 47.5 mph (76.4 km/h) and at an angle of 14.6 degrees. Both vehicles were successfully redirected with maximum permanent sets of 4⅝ in. (117 mm) and 5⅜ in. (137 mm), respectively. Thus, the system met the TL-4 criteria presented in NCHRP Report 350.

2.2.3.7 TL-2 Thrie-Beam Bridge Rail for Glulam Timber Decks

A TL-2 steel bridge rail for use on transverse glulam timber decks was developed in a 2003 study [42]. This system was similar to the previously developed TL-4 system, but used W6x12 (W152x17.9) posts and blockouts, a C8x11.5 (C200x17) channel as the second beam element, and eight ⅞-in. (22.2-mm) diameter through-deck bolts in the post-to-deck attachment. This system also used an approach guardrail transition.

In NCHRP Report 350 crash testing, a 4,334-lb (1,966-kg) pickup truck impacted the rail at a speed of 41.4 mph (66.6 km/h) and at an angle of 25.6 degrees. The vehicle was smoothly redirected, and maximum dynamic deflection of the rail was 3 in. (78 mm). Thus, the system met the TL-2 criteria presented in NCHRP Report 350.

2.2.4 Tube-Section Bridge Rails

Several bridge rails utilizing tube-section rail elements have been developed and successfully tested. These systems tend to be relatively stiff, but several have post-to-deck attachment hardware that minimizes intrusion of the system onto the bridge deck.

2.2.4.1 California Type 18 Bridge Rail

The California Type 18 Bridge Rail utilized W8x31 (W203x46.1) posts spaced at 8 ft (2.44 m) which supported a TS4x4x¼ (TS102x102x6.4) upper rail and blockout and a TS3x12x¼ (TS76x305x6.4) lower rail that was mounted on a pipe section blockout designed to crush and absorb energy during an impact. An additional, smaller rail could be mounted above the top rail if desired. Posts were anchored to the side of the deck with two 1¼-in. (31.8-mm) diameter upper bolts and two 1-in. (25.4-mm) diameter lower bolts. Upper bolts were positioned 4½ in. (114 mm) above the lower bolts, and loops of rebar formed a cage around the bolts. Minimum bridge deck thickness for the bridge rail was 12 in. (305 mm), and the system required an approach guardrail transition.

Crash testing was performed on the California Type 18 Bridge Rail in a 1983 study [43]. The system successfully redirected a 1,850-lb (839-kg) car impacting at 59.7 mph (96.1 km/h) and 12 degrees and a 4,530-lb (2,055-kg) car impacting at 60.7 mph (97.7 km/h) and 23 degrees. Thus, the barrier met the safety criteria of MSL-2 defined in NCHRP Report 230 and was deemed equivalent to a TL-2 system under NCHRP Report 350.

2.2.4.2 California Type 115, 116, and 117 Bridge Rails

Three similar side-mounted, tubular bridge rails have been developed by the California DOT. The Type 115 Rail utilized W8x31 (W203x46.1) posts spaced at a minimum of 6 ft (1.83 m) and a maximum of 8 ft (2.44 m) which supported two TS4x4x¼ (TS102x102x6.4) rails. Posts were anchored to the side of the deck with two 1¼-in. (31.8-mm) diameter upper bolts and two 1-in. (25.4-mm) diameter lower bolts. The upper bolts were located 10 in. (254 mm) above the lower bolts, and the minimum deck thickness was 18 in. (457 mm). Alternatively, the upper bolts could be placed as close as 4½ in. (114 mm) to the lower bolts if additional loops of rebar were placed around the bolts, which reduced the required deck thickness to 12 in. (305 mm). The Type 116 and 117 Bridge Rails were similar to the Type 115 Rail, but the Type 116 used one additional, smaller upper rail element and the Type 117 used two additional, smaller, upper rail elements. All three systems required approach guardrail transitions.

The Type 115 Bridge Rail was crash tested in a 1993 study [38]. A 1,800-lb (816-kg) car impacting at 59.0 mph (95.0 km/h) and 19 degrees and a 5,470-lb (2,481-kg) pickup impacting at 64.2 mph (103.3 km/h) and 21 degrees were successfully redirected. However, wheel snag occurred in the test with the car, and as such the system did not satisfy criteria for PL-2. However, the system met PL-1, and was considered equivalent to TL-2 under NCHRP Report 350. The Type 116 and 117 Bridge Rails are also considered TL-2 barriers [44].

2.2.4.3 Illinois Side-Mounted Bridge Rail

The Illinois Side-Mounted Bridge Rail utilized a TS8x4x$^5/_{16}$ (TS203x102x7.9) upper rail and TS6x4x¼ (TS152x102x6.4) lower rail. Both rails were mounted on W6x25 (W152x37.2) posts spaced at 6 ft - 3 in. (1.91 m) that were side-mounted to the edge of the bridge deck using two 1-in. (25.4-mm) diameter upper bolts and two ⅝-in. (15.9-mm) diameter lower bolts. The upper bolts were placed 10 in. (254 mm) above the lower bolts, and deck thickness was 17 in. (432 mm), not including the bituminous wearing surface. Additional tube sections were placed between the post and deck as spacer sections. Due to the stiffness of the system, an approach guardrail transition would be required.

The Illinois Side-Mounted Bridge Rail was full-scale crash tested three times in a 1997 study [39]. The barrier redirected a 1,961-lb (890-kg) car impacting at 58.7 mph (94.4 mph) and 20 degrees, a 5,797-lb (2,632-kg) pickup truck impacting at 63.6 mph (102.3 km/h) and 19.2 degrees, and an 18,000-lb (8,172-kg) single-unit truck impacting at 50.8 mph (81.8 km/h) and 15.1 degrees. Thus, the barrier met all performance criteria for PL-2 as defined by AASHTO and was considered equivalent to a TL-4 rating under NCHRP Report 350.

2.3 Prior Weak-Post W-Beam Guardrail System Testing

Weak-post, W-beam barriers have been investigated in prior research, including full-scale crash tests and finite element modeling. This section summarizes the research and testing of these systems that are relevant to the current project, including post-to-rail connections and rail splices.

2.3.1 TL-2 Weak-Post W-Beam Guardrail System (SGR02a)

The weak-post W-beam guardrail system, also known as the G2 guardrail or SGR02a, has been used in several states, including Pennsylvania, New York, Connecticut, Virginia, and North Carolina. The standard system utilizes S3x5.7 (S76x8.5) posts spaced at 12 ft - 6 in. (3.81

m), standard 12-gauge (2.66-mm thick) W-beam guardrail with a top mounting height of 30 in. (762 mm), and splices located at posts. A $\frac{5}{16}$-in. (7.9-mm) diameter hex bolt and nut and a 1¾-in. x 1¾-in. x ⅛-in. (44-mm x 44-mm x 3.2-mm) square washer attach the guardrail to each post. A $\frac{9}{16}$-in. (14.3-mm) diameter shelf bolt located beneath the rail provides additional support against environmental loads. The design intent of the post-to-rail connection was for the bolt to fracture upon deflection of the post, ensuring that the rail is not pulled down upon post rotation. A median barrier variant of the system, the SGM02, was created by placing W-beam guardrails on both sides of the posts.

Although the weak-post W-beam guardrail performed adequately under NCHRP Report 230 criteria, the system has not performed well with higher center-of-gravity vehicles. This problem was first observed after the system caused a van to roll during crash testing [45]. The system was first tested under NCHRP Report 350 TL-3-11 conditions in a 1995 FHWA study, in which a 4,409-lb (2,000-kg) truck impacted the guardrail at a speed of 62.0 mph (99.8 km/h) and at an angle of 24.4 degrees [18]. During the test, the W-beam rail dropped, allowing three of the vehicle's tires to override the guardrail and straddle it for the length of the system. The authors concluded that the vehicle most likely would have completely vaulted over the rail if the guardrail system had been longer.

The most likely cause of the test failure was that the post-to-rail connection was inadequate. The connection must be strong enough to hold the rail in place until the guardrail posts begin to pull it down and then must break to avoid pulling the rail down. The report appears to indicate that, for this test, the rail dropped due to premature failure of the post-to-rail bolt connection.

The G2 system was then tested under TL-2 conditions [18]. A 4,409-lb (2,000-kg) truck impacted the barrier at a speed of 44.1 mph (71.0 km/h) and at an angle of 26.1 degrees. In the test, the guardrail system successfully redirected the vehicle while sustaining a maximum dynamic deflection of 4 ft - 6 in. (1.4 m). Thus, the system was accepted as an NCHRP Report 350 TL-2 barrier.

2.3.2 TL-3 Weak-Post W-Beam Guardrail System (SGR02b)

Full-scale pickup truck crash tests were performed on the Pennsylvania Type 2 Class A weak-post W-beam guardrail in a 1999 study [46]. Although the barrier passed the first two tests, the speed was too low to meet TL-3 requirements. A third test was performed in which the pickup truck impacted the guardrail at a speed of 64 mph (103 km/h) and at an angle of 26.3 degrees. In this test, the rail ruptured at a splice location and the pickup truck penetrated the barrier.

In 2000, a study was undertaken to investigate the causes of unsatisfactory performance of the weak-post W-beam guardrail [47-48]. Under static testing, the post-to-rail connection for the existing system was found to fail inconsistently. Failure mechanisms in these tests consisted of bending and pullout of the square washer and stripping the threads off of the bolt. The bolt did not fracture as desired in any of the tests. Both failure mechanisms occurred at force levels greater than desired and required what the authors considered to be excessive displacement, which might allow the rail to be pulled downward by the post. Static testing of the $^{5}/_{16}$-in. (7.9-mm) diameter, ASTM A307 Grade A bolts revealed a wide range of failure stresses, as some fractured at stresses less than the minimum specified ultimate stress while others sustained significantly higher stresses before fracture.

Maximum loading of the guardrail normally occurs as it is bent around a post. The weakest point in the guardrail is at the splice, where approximately 15 percent of the cross-section is missing. Thus, the normal guardrail design places the weakest point of the guardrail at the point of maximum loading.

A revised post-to-rail connection system was designed which used an additional square washer and nut and a smaller, ¼-in. (6.4-mm) diameter bolt to isolate bolt fracture as the failure mechanism. Guardrail splices were moved to the midspan locations between the posts. This revised system was subjected to a test in which a 4,409-lb (2,000-kg) pickup impacted the guardrail at a speed of 62.3 mph (100.2 km/h) and at angle of 25.9 degrees [49]. During the test, a small tear initiated in the guardrail as it was pressed against the edge of a post flange. This tear produced a rupture of the entire guardrail element, which allowed the truck to penetrate the barrier. Small nicks were found in the guardrail at each post in the impact region, indicating that the failure was likely to be a common occurrence.

Additionally, as the rail element dropped in front of the vehicle in the first TL-3 test, a stronger or more ductile connection may have been required. Isolation of bolt fracture as the failure mechanism resulted in a more consistent failure mechanism, but it decreased the ductility of the connection, as the bolts cannot yield appreciably before failure whereas the washers can. Stress waves that pass through a W-beam rail upon impact of a vehicle can be managed better by a ductile connection which can yield without failing, preventing premature release of the rail from downstream posts.

A finite element model was developed for the guardrail system to examine the guardrail-post interaction. This model confirmed that as the posts rotated and twisted, the flanges of the posts caused stress concentrations at the base of the rail which developed the nicks observed during testing. The post-to-rail connection was further revised with the addition of a 12-guage (2.66-mm thick) W-beam section backup plate at each post to prevent these nicks. Shelf bolts were eliminated on all but the end posts. The updated system was crash tested with a 4,409-lb (2,000-kg) pickup truck traveling at a speed of 62.3 mph (100.3 km/h) and at an angle of 25.3 degrees to the guardrail [50]. In this test, the guardrail system initially contained and redirected the pickup truck, but the guardrail dropped in front of the impact region and the vehicle was allowed to override the barrier.

The rail mounting height was then increased to 32¼ in. (820 mm), and the post-to-rail connection bolt diameter was increased to $^{5}\!/_{16}$ in. (7.9 mm). Shelf bolts were again added to support the W-beam rail. The redesigned system was tested with a 4,409-lb (2,000-kg) pickup truck travelling at a speed of 63.6 mph (102.4 km/h) and at an angle of 26.5 degrees [51]. The truck was successfully redirected by the guardrail and met all required performance criteria for an NCHRP Report 350 TL-3 barrier.

Following the successful performance of the system in test designation no. 3-11, the same revised system was subjected to test designation no. 3-10 conditions to ensure the system still performed adequately in a small-vehicle impact [52]. The system successfully redirected a 1,806-lb (820-kg) car which impacted the rail at a speed of 62.4 mph and at an angle of 21.1 degrees. Thus, the modified weak-post W-beam guardrail met all performance criteria for an NCHRP Report 350 TL-3 barrier.

2.3.3 New York DOT W-Beam on Light Post Median Barrier

The New York DOT W-Beam on Light Post Median Barrier consisted of standard 12-gauge (2.66-mm thick) W-beams mounted on both sides of S3x5.7 (S76x8.5) posts. Guardrail splices were located at the posts, which were spaced at 12 ft - 6 in. (3.81 m), and the top mounting height of the W-beam guardrail was 32⅞ in. (835 mm). A $^{5}\!/_{16}$-in. (7.9-mm) diameter hex bolt and nut and a 1¾-in. x 1¾-in. x ⅛-in. (44-mm x 44-mm x 3.2-mm) square washer attached the guardrails on both sides of each system post, and $^{9}\!/_{16}$-in. (14.3-mm) diameter shelf bolts located beneath the rail provided additional support against environmental loads. This barrier was crash tested with a 4,409-lb (2,000-kg) pickup truck travelling at a speed of 63.1 mph

(101.5 km/h) and at an angle of 24.8 degrees [53]. In this test, the guardrail system successfully redirected the truck and met all performance criteria for an NCHRP Report 450 TL-3 barrier.

2.4 Other Post-to-Rail Connections

The connections between guardrail and system posts have been investigated under several research projects. Studies relevant to the current project are discussed in the following sections.

2.4.1 Strong-Post (G4) Guardrail Post-to-Rail Connection

The behavior of the post-to-rail connection of the G4 strong-post guardrail system was investigated in a 2002 study [54]. A total of 8 quasi-static tests were performed in which a standard ⅝-in. (15.9-mm) diameter button-head bolt was pulled through the ¾-in. (19.1-mm) wide slot in standard 12-gauge (2.66-mm thick) W-beam guardrail sections. Two tests were performed for each of four different load cases. For Cases 1 and 2, bolts were pulled through a single layer of W-beam, whereas for Cases 3 and 4, bolts were pulled through two layers of W-beam. For Cases 1 and 3, bolts were positioned at the center of the slot in the W-beam(s), while in Cases 2 and 4, bolts were positioned at the edge of the slot. In all 8 tests, the connection failed when the guardrail deformed and allowed the bolt head to slip through.

The tests demonstrated that the forces necessary to pull the bolt through the W-beam sections varied dramatically. These tests showed that the number of layers of guardrail at the pullout location has a greater effect on failure loads than bolt location within the slot. The average force recorded for Case 4 was more than three times that of Case 1. These results suggested that this connection does not create consistent failure loads, particularly for systems which have both splice and non-splice rail sections at posts.

2.4.2 T-31 Guardrail Countersunk Bolt Connection

A 2006 paper presented the design of a proprietary strong-post W-beam guardrail system that utilized a countersunk bolt to attach the guardrail to system posts [55]. This bolt had a tapered head that ensured more uniform pullout forces, regardless of bolt position within the slot. Rail splices were placed at midspan locations to further reduce the post bolt pullout force. The connection was incorporated into a proprietary guardrail system that featured modified line posts and no blockouts, known as the T-31 Guardrail System.

2.4.3 GMS Guardrail Mini Spacer Releasable Fastener

A 2007 paper examined the behavior of guardrail post-to-rail connections for use in design of a proprietary guardrail system [56]. After analyzing the mechanics of rail release for existing post-to-rail connections in strong-post systems, the author asserted that relying on the motion of the system for guardrail release was disadvantageous. Motion of guardrail systems that use blockouts can be highly variable based on actual installation conditions, resulting in highly variable release loads and potentially preventing rail release. A connection was designed which consisted of a $\frac{5}{16}$-in. (7.9-mm) diameter hex bolt and nut, a dome washer, a dome nut, and two circular release washers. This connection was designed to be strong under shear loads to prevent premature release of the rail, and weak in tension to prevent posts from pulling the rail down. Guardrail splices for the proprietary GMS Guardrail System were located at the posts.

2.4.4 Nu-Guard 31 Connection

Another proprietary guardrail system was developed in which the guardrail was released from system posts through fracture of the posts themselves [57]. In the system, W-beam guardrail was connected to U-channel line posts through vertical slots near the tops of the posts with a bolt, nut, and an oversized washer positioned between the guardrail and the post. Upon post rotation, the bolt slid upward and fractured the edge of the slot. Guardrail splices for the proprietary Nu-Guard Guardrail System were located at the posts.

3 BARRIER DESIGN

3.1 Design Goals

Two important components of the MGS Bridge Rail were the post-to-deck and post-to-rail connections. To eliminate the need for an approach guardrail transition, the post design was required to develop rail stiffness, strength, and deflection characteristics comparable to those of guardrail posts embedded in soil. Further, a post system was needed that would transmit loads into the bridge deck without causing damage during most impacts. It was also desirable to minimize barrier encroachment onto the deck surface in order to reduce bridge construction costs. Finally, the post design and mounting system needed to be simple, economical, and usable on both newly constructed bridges as well as for retrofitting existing structures.

The primary design goals for the bridge rail post were to develop sufficient stiffness and strength to match the lateral deflection of the MGS guardrail and absorb sufficient energy to limit tensile loading in the rail element. These objectives can be accomplished in one of two ways. A plastic hinge can be designed into a strong post that allows the post to bend at a prescribed load. Alternatively, a post can be selected that absorbs energy by bending at its base. The plastic hinge concept can be designed to absorb more energy, but it is also more costly to implement. Both of these design approaches were pursued as described in the following sections.

3.1.1 Plastic Hinge Concepts

Five plastic hinge concepts were identified as possible solutions to the bridge rail post problem. As described in the following sections, three of the plastic hinge concepts relied on a bolt tearing through a steel plate, a fourth relied upon rupture of a tube, and the last utilized crushing of an energy-absorbing foam.

3.1.1.1 Top-Mounted, Lateral Steel Plate Tear-out

One bolt tear-out concept was the top-mounted, lateral steel plate tear-out design. This concept utilized a steel plate that was connected to the top of the deck with a bolt that passed completely through the bridge deck. Upon impact, the post would bear against and rotate about the bottom of the deck and cause the through-deck bolt to tear through the top plate. Tear-out force would be tuned by adjusting the thickness of the tear-out plate. Sketches of this concept in deformed and undeformed states are shown in Figure 1.

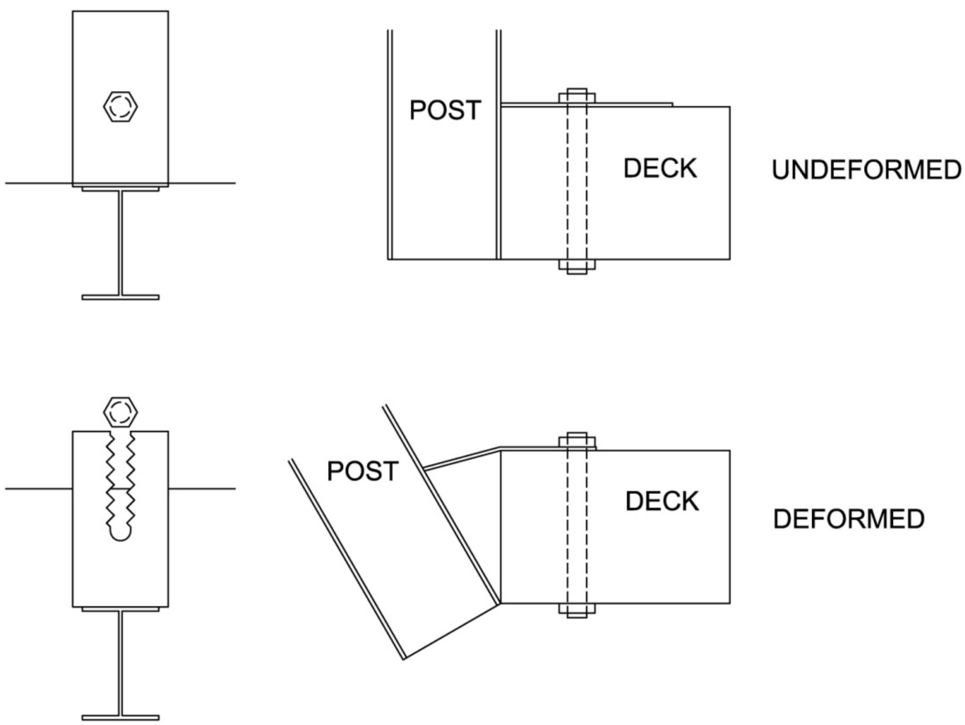

Figure 1. Lateral Plate Tear-out Concept

Several different variations were developed for connecting the post to the bridge deck, but one final design was selected which displayed the greatest likelihood of behaving as desired. This design utilized one through-deck bolt and a tear-out plate that was butted against the post and attached with fillet welds on both sides to ensure adequate weld strength to initiate and sustain tearing. A lower angle section was bolted to the post and attached to the deck with the through-deck bolt. Slots were cut into the angle to attach the post, which allowed for variation in bridge deck thickness. Gusset plates were welded to the angle to prevent it from bending during post rotation.

To limit the pre-impact friction between the tear-out plate and the deck, the tear-out plate was designed with metal strips welded to its lower side on either side of the bolt hole, which created a small span with the plate. Spacing between the strips and the plate thickness were tuned such that the plate was unable to support excessive preload from the bolt without collapsing. Directions for installation specified that the bolt should be tightened down without collapsing the plate, thereby limiting the maximum amount of preload on the plate. Finally, a small offset was left between the edge of the post and the bridge deck to allow for tolerance in placing the through-deck bolt. A sketch of the final design of the lateral plate tear-out concept is shown in Figure 2.

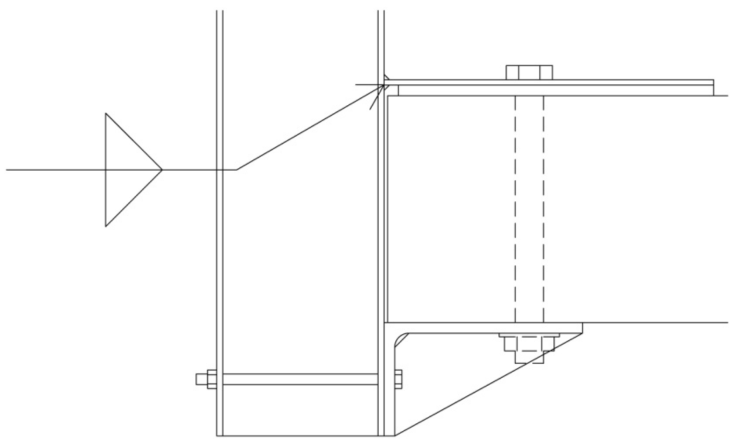

Figure 2. Final Lateral Plate Tear-out Concept

An advantage of this concept was that tearing of the plate was expected to generate constant resistance to post rotation. When loaded, the through-deck bolt would bend and apply out-of-plane stress to the plate, which would help initiate tearing. Placement of the post on the side of the deck also minimized rail intrusion onto the deck.

The greatest weakness of the concept was its ability to limit friction between the plate and the deck due to bolt preload. While a rudimentary mechanism was designed into the system for this purpose, its effectiveness was unknown. Another weakness was that the tear-out plate would have to be butt-welded to system posts, creating an awkward section for states to stock and ship. Finally, extension of the tear-out plate several inches past the rail on the deck surface could allow for it to be damaged by snow plow operations.

3.1.1.2 Flange Splice with Bolt Tear-out

Another strong-post bolt tear-out concept was based on previous research performed by Safety By Design [58]. This concept utilized a wide-flange beam that was mounted to the side of the bridge deck. The tension flange and web of the beam were cut such that only the compression flange was a continuous member. Splice plates and bolts were then used to reconnect the tension flange of the post. Upon impact, the post would rotate about its compression flange at the location of the cut, causing the splice bolts to tear through either the tension flange or the splice plate.

Two variations of the flange splice with bolt tear-out concept were developed. The first concept utilized two thin splice plates placed on the interior side of the tension flange on either side of the web. During impact, the bolts rotate with the post and tear through the splice plates. The second concept used a thick splice plate located between the bridge deck and the post. During impact, the bolts remain stationary relative to the post, tearing through the tension flange of the post as it rotates. One proposed modification was to install the tear-out bolts at angles to apply out-of-plane deformations in the tear-out material, thereby facilitating fracture. Sketches of the rotating bolts concept in deformed and undeformed states are shown in Figure 3, and a sketch of the stationary bolts concept is shown in Figure 4.

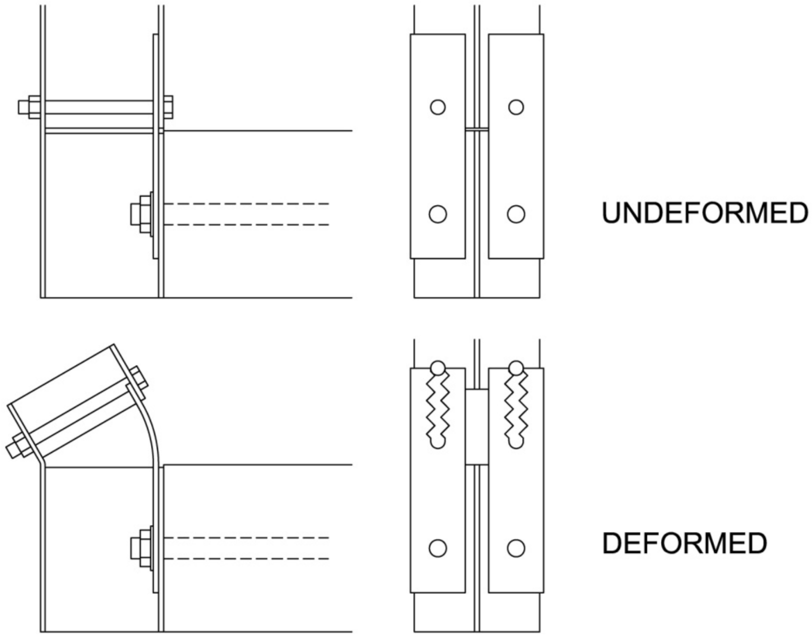

Figure 3. Flange Splice with Rotating Bolts Tear-out Concept

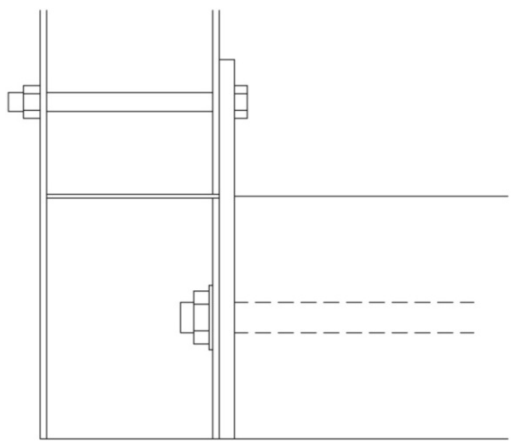

Figure 4. Flange Splice with Stationary Bolts Tear-out Concept

Upon further investigation of the tension flange splices, it was determined that both splice options were unsatisfactory. The stationary bolts design was expected to develop resistance forces that were significantly larger than desired due to the thickness of post flanges, while the rotating bolts design required wide splice plate sections to prevent the bolts from rupturing the plates in tension. This in turn required a wider and heavier post section, such as a W6x15 (W152x22.3), to accommodate the wider plates.

A revised concept that used a stationary bolt was developed based on these concerns. A hollow structural section (HSS) member was used in place of a wide-flange beam as the bridge rail post. The tube was cut through its front face and both of its side faces while its rear face was left intact. A splice plate was placed between the post and the deck, and one or two tear-out bolts were passed through the splice plate and post. Upon impact, the bolts would tear through the post face. A sketch of the tube-splice connection is shown in Figure 5.

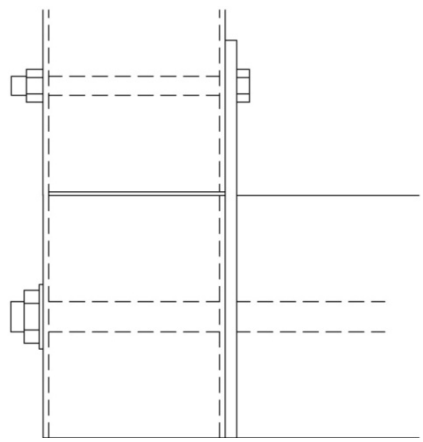

Figure 5. Tube Splice, Stationary Bolts with HSS Post

Strengths of this concept were that it minimized intrusion onto the bridge deck and the hardware required should be easy to fabricate.

However, one weakness of this side-mounted connection was its anchoring system. To avoid contacting reinforcing bar in a standard slab-on-girder bridge deck, approximately 4 in. (102 mm) was required between the top of the deck and the anchor. This severely restricted the moment arm of the anchors, which resulted in much higher anchor bolt loads. There was concern that these high loads may not be attainable in retrofit applications.

3.1.1.3 Side-Mounted Post with Bolt Tear-out

Another concept was developed which used side-mounted anchor brackets and bolt tear-out to absorb energy. Two variations of this concept were considered. For both, a bolt was passed through the post and would tear through the post itself upon rotation. An alternative was considered in which the bolt tore through the mounting bracket, but due to fabrication costs of the brackets, it was decided to design the brackets such that they were reusable and the tear was produced in the posts. Tear-out force for these concepts could be tuned through selection of different post thicknesses and the location of the tear-out bolt.

The first variation of this concept utilized a wide-flange post placed between two gusseted angle sections which were side-mounted to the deck. These angles were welded to a base plate to aid in installation. A bolt was passed through the wide-flange beam near its compression flange that extended through both angles. Upon impact, the post would rotate and cause the bolt to tear through the web of the post. A second, smaller bolt was positioned near the base of the post to prevent the post from rotating toward the deck under environmental loads. Sketches of this design are shown in Figure 6.

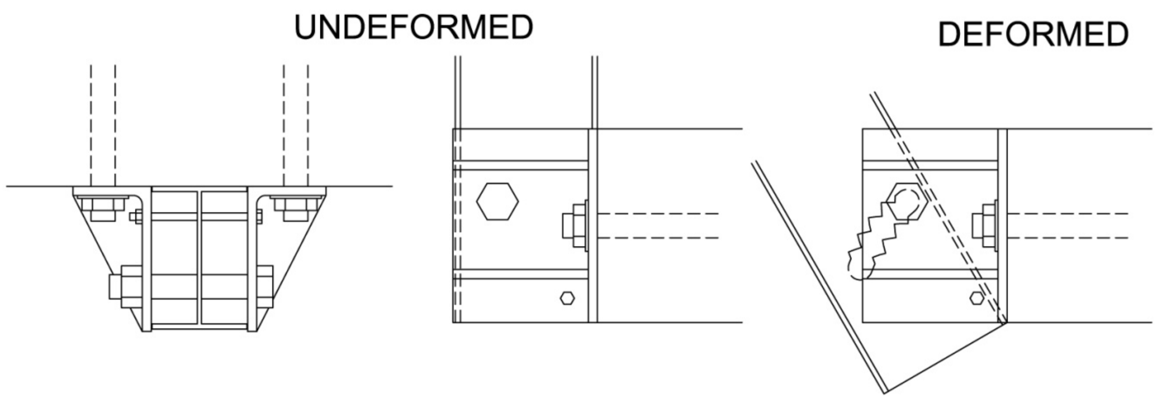

Figure 6. Side-Mounted Post with Bolt Tear-out Concept with W-Beam Post

The second variation of the post tear-out concept used a tubular post that was also side-mounted between two gusseted angles. A bolt was passed through the post and both angles. This bolt would tear through both side faces of the post upon rotation. Again, a second, smaller bolt was added near the base of the post to prevent the post from rotating toward the deck. Sketches of this concept are shown in Figure 7.

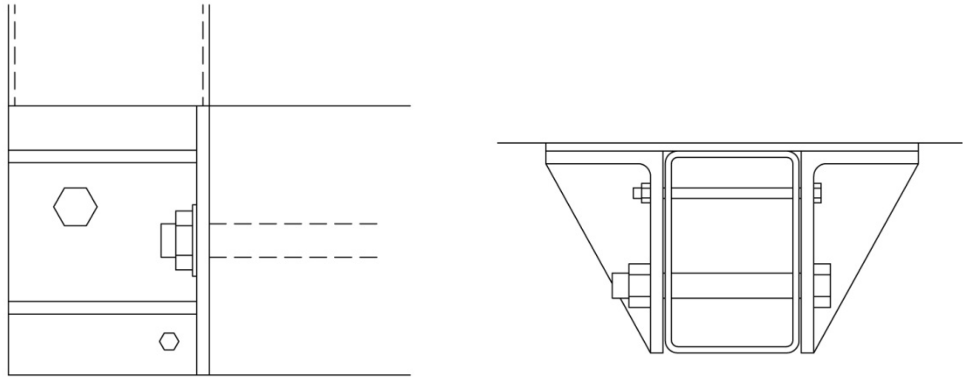

Figure 7. Side-Mounted Post with Bolt Tear-out Concept with Tubular Post

An advantage of this concept was that the side-mounted anchor brackets, which were reinforced with gussets, prevented preload in the tear-out bolt from applying friction to the post. Thus, posts were expected to develop more consistent resistance forces.

A weakness of this concept was that the mounting brackets, which required significant strength in order to be reusable, would be expensive. The variation incorporating a wide-flange post also required the tear-out bolt to sustain load at its center-span, which would result in significant bending stresses. Thus, it was believed that the tubular post represented a better option as it would load the bolt near its supports and reduce bending in the bolt.

3.1.1.4 Foam Crush

Another energy absorbing mechanism considered for use in the design of the post-to-deck connection was crushing of an energy-absorbing foam as the post rotated. Foam was considered ideal as it can generate a relatively constant resistance across most of its crush distance. One concept was developed which consisted of a bent-plate steel socket that was side-mounted to the bridge deck and housed a mass of crushable foam material and the post. Both a triangular-shaped socket, in which crush of the foam was approximately uniform across the face of the post, and a rectangular-shaped socket were considered. For both, a bolt was passed through the lower edge of the post to prevent it from slipping out of the socket. Sketches of the triangular socket and rectangular socket are shown in Figure 8.

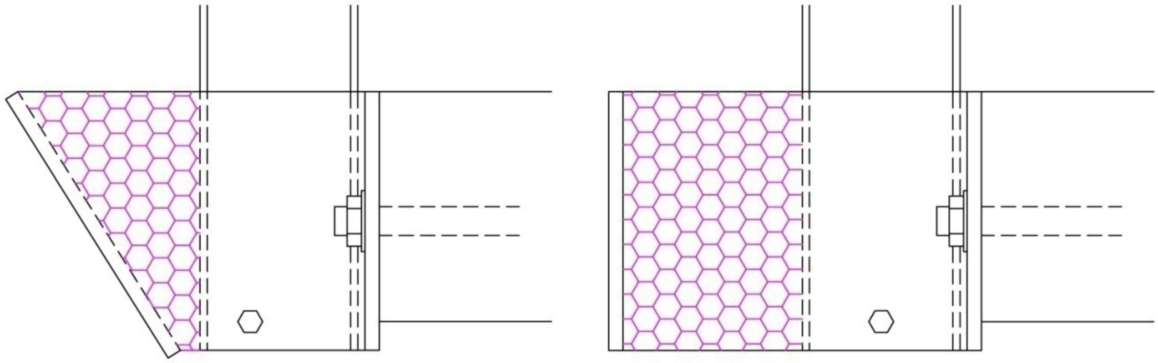

Figure 8. Foam Crush Concepts – Triangular (left) and Rectangular (right)

Strength of this concept was that it was expected to display consistent post force-deflection behavior. It was believed that due to its simple mechanism, it could easily be tuned to work as desired, provided the anchorage system was adequate.

Weakness included that the concept required large and expensive sockets. Aging effects on the foam were also potentially problematic. An additional concern with the triangle-shaped socket was that post rotation would cause the foam to be pushed out of the socket.

3.1.1.5 Socket Rupture

Another concept was developed which absorbed energy through the rupture of a steel socket which housed the post. One embodiment of this concept consisted of a side-mounted, bent plate socket. A bolt was passed through both sides of the socket to support the post. Upon impact, the post was pressed against the socket, stretching it and eventually causing Mode III, or out-of-plane shear failures along both edges of the post flange. As the post rotated, these tears would move downward on the socket until, at a sufficiently low height, the post would be released from the socket. Notches could be cut into the top of the socket to facilitate fracture initiation. Sketches of this concept are shown in Figure 9.

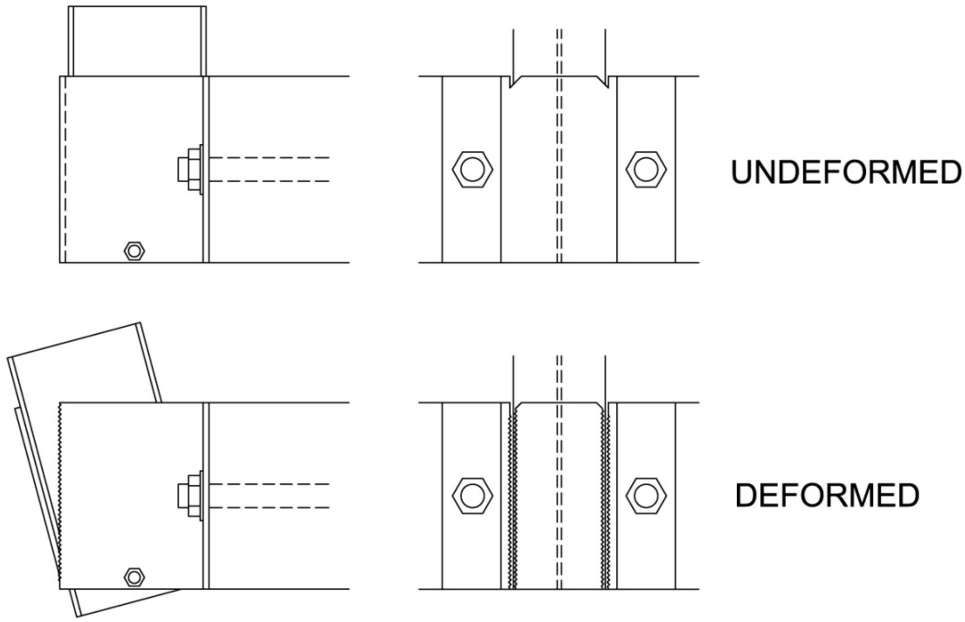

Figure 9. Socket Rupture Concept

A variation to the socket rupture concept was to place notches on the sides of the socket, rather than the back face. This would change the failure mode of the socket to Mode I fracture, in which the plate was fractured in tension. However, it was believed that this failure method would generate higher forces and be less consistent than Mode III, or out-of-plane shear fracture. Thus, this concept was not further pursued.

Another proposed variation to the socket rupture concept was to place a post blockout between the bridge deck and the post. Essentially, this would place the post at the exterior of the socket. Notches would again be placed at the upper end of the blockout that would initiate either Mode I or Mode III fracture, and the blockout would be attached to the post with either bolts or welds and bolted to the edge of the bridge deck. To prevent the blockout from crushing during post rotation, internal reinforcement would be required at its lower end. The advantage of this concept was that it would allow a rail blockout to be used between the W-beam and bridge rail posts without encroaching onto the deck surface. A sketch of the post blockout is shown in Figure 10.

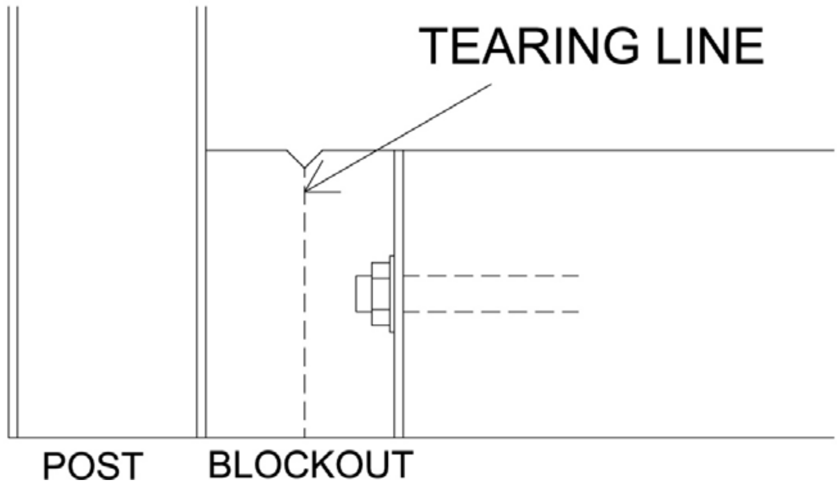

Figure 10. Socket Rupture with Blockout Concept

The greatest weakness of the socket rupture concept was that it would not generate a constant resistance force at the top of the post. Upon post rotation, the fracture would begin at the top of the socket and then move downward. While the force required to propagate the fracture would remain constant, the decreasing moment arm due to the downward movement of the fracture location would cause resistance force at the top of the post to decrease. Energy absorbed by the post-to-deck connection would therefore decrease at a second-order rate, and developing sufficient total energy absorption would be difficult. Calculations showed that increasing the tear-out force early in the event would result in overly large top-of-post forces at the beginning of an impact with minimal gains in energy absorption due to the ratio of the tear-out moment arm length to height of impact. Increases in the depth of the socket were considered to alter this ratio, but over the range of depths which were practical for construction, all gains in the amount of energy absorbed were accompanied by unacceptably large increases in force at the top of the post.

3.1.1.6 Selection of Designs for Component Testing

The top-mounted lateral steel plate tear-out and side-mounted post bolt tear-out concepts were selected as the primary strong-post designs for component testing. These were selected as they were believed to provide the most reliable failure mechanisms. Specifically, the side-mounted post tear-out concept eliminated the problem of bolt preload friction resisting post rotation. While this issue was not fully resolved for the lateral plate tear-out concept, it was believed that the design might mitigate its effects. The foam crush concept was also expected to work as desired, but due to potential problems with the foam aging, this concept was abandoned.

The flange splice concept was not selected due to concerns that the post would not rotate as desired, and therefore the bolts would not tear through the posts. In design, it was assumed that the post would rotate about its rear flange, producing ideal motion of the front flange for tearing. However, the validity of this assumption was questioned, and this design was not selected for further analysis. As discussed previously, the socket rupture concept would not provide the desired results even under the assumed ideal behavior, thus it was not selected for testing.

3.1.2 Post Yield Design Concepts

The second design approach was to develop a post system that relied on post yield to absorb energy. Several different post types were considered, but S3x5.7 (S76x8.5) posts were selected based on their demonstrated performance and use in previously-developed systems, including cable barriers and weak-post W-beam guardrails. Prior research has shown that these posts generate roughly one-half the resistive force and energy absorption as standard W6x9 (W152x13.4) guardrail posts rotating in soil. Thus, S-posts with half-post spacing should generate similar stiffness, strength, and deflection characteristics as the approach guardrail.

For this design approach, a post-to-deck connection was sought that could attach the post in essentially a fixed configuration and be replaced or repaired quickly following impact. The attachment should not be damaged during impacts and it should not cause damage to the bridge deck.

3.1.2.1 Top-Mounted Post Welded to Base Plate

One concept incorporated a base plate that was welded to the post and bolted to the top of the bridge deck. A second plate would be placed on the lower side of the bridge deck. During impact, the welds would develop the full capacity of the post, allowing it to yield. The post and base plate would require replacement after each significant impact. Sketches of this concept are shown in Figure 11.

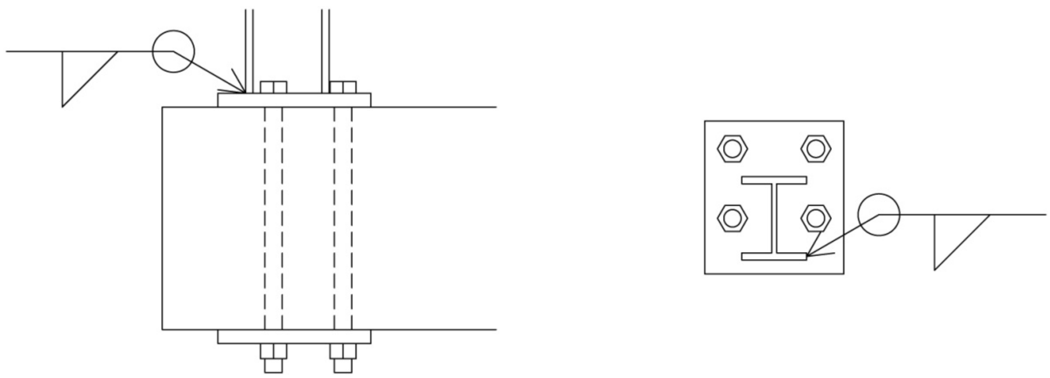

Figure 11. Top-Mounted Post Welded to Base Plate Concept

The major strength of this design was its simplicity. However, it also had several weaknesses. First, similar connections have historically damaged bridge decks [14-15, 19-23, 34]. As this concept was top-mounted, it also encroached significantly more onto the bridge deck than side-mounted designs. Further, the posts would have to be welded to base plates, which would create an awkward piece for states to store and ship, and post replacement could not be accomplished from the top of the bridge.

3.1.2.2 Top-Mounted Socket Welded to Base Plate

To eliminate the need to re-weld and replace a post and base plate assembly following each impact event, a concept was developed that consisted of a socket welded to a base plate which was bolted to the bridge deck. In this design, the post would rest in the socket and a shim would be inserted to snug the connection and prevent post release. Only the post would require replacement following an impact. Sketches of the top-mounted socket are shown in Figure 12.

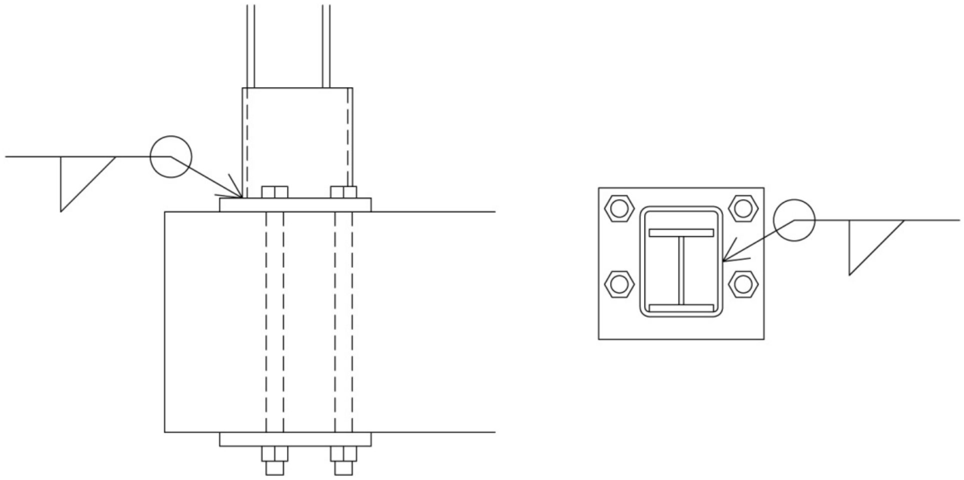

Figure 12. Top-Mounted Socket Welded to Base Plate Concept

Although this concept eliminated the problem of replacing non-standard parts following impacts, it had several weaknesses. One problem was that the socket, which would extend several inches above the bridge deck, could cause wheel snag. As the socket would also move the location of post bending higher, it would effectively make the barrier stiffer. Finally, the design still encroached significantly onto the bridge deck.

3.1.2.3 Cast-in-Place Socket

Another concept utilized a socket for the bridge rail post that would be cast-in-place in the bridge deck. The socket would be selected from either standard HSS or mechanical tubing sections, and a shim would be inserted to secure the post and prevent it from releasing. Only the post would require repair following impact. Deck capacity to resist applied loads would need to be provided through either internal reinforcement or other means. Sketches of this concept are shown in Figure 13.

A weakness of this design was that the bridge rail encroached significantly onto the bridge deck. Retrofit applications of this concept may require the posts to be located even further inward onto the bridge deck for the deck to safely withstand post forces. Thus, the system may encroach onto the deck even further in retrofit applications.

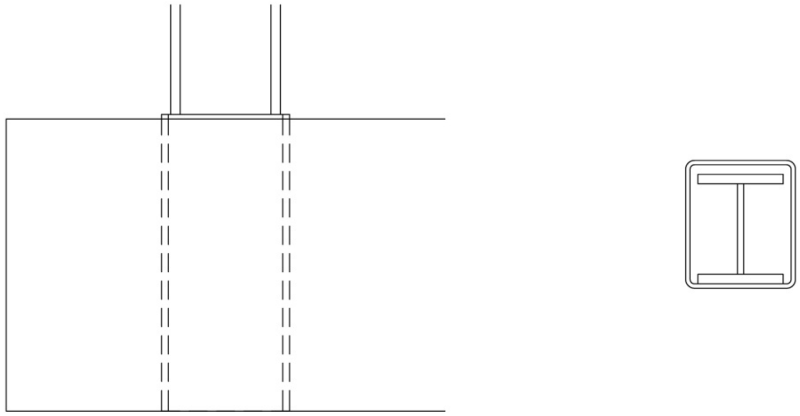

Figure 13. Cast-in-Place Socket Concept

3.1.2.4 Side-Mounted Post Welded to Base Plate

Another concept utilized a post welded to a base plate that was side-mounted to the edge of the bridge deck. Cast-in-place anchors or threaded rods embedded in epoxy would be used to anchor the base plate to the deck. Sketches of this concept are shown in Figure 14.

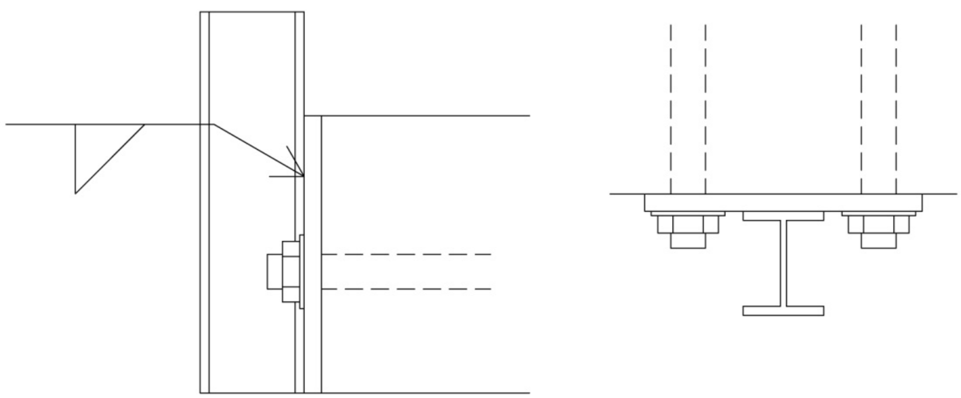

Figure 14. Side-Mounted Post Welded to Base Plate Concept

This concept did not encroach onto the bridge deck and its estimated cost was low. However, the small moment arm of the side-mounted anchors would result in large loads on the anchors themselves, thereby increasing the risk of failure. Additionally, the part would have to be galvanized after the post was welded to the plate, and the size of the total structure would not be ideal for shipping and storage. Finally, the post would potentially bend at the height of the bolts, which would reduce wheel snag, but also would reduce the stiffness of the barrier.

3.1.2.5 Side-Mounted Post in Socket Welded to Base Plate

Another side-mounted connection concept consisted of a tube section welded to a base plate which would be anchored to the side of the deck. The tube would be selected from standard HSS shapes, and the anchors would either be cast-in-place bolts or threaded rods embedded in epoxy. Alternatively, the socket could be formed from one continuous bent plate. Sketches of the connection are shown in Figure 15.

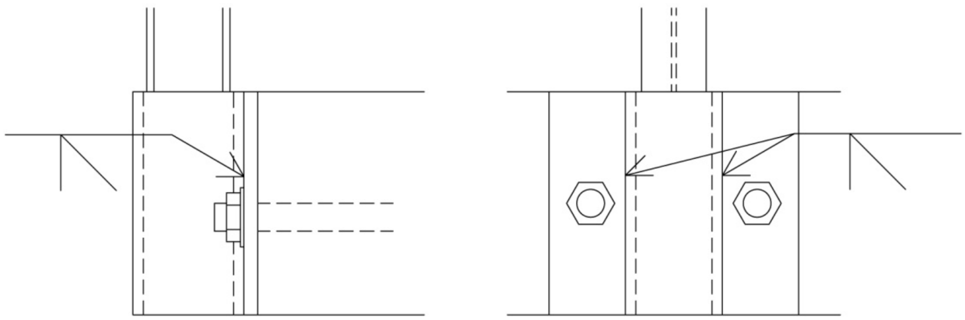

Figure 15. Side-Mounted Post in Socket Welded to Base Plate Concept

Strengths of this concept were that it did not encroach onto the bridge deck and that it eliminated the awkward section problem of the side-mounted post welded to base plate concept. However, weaknesses of this concept were that it still placed large loads on the anchors due to their small moment arms and that the socket might be damaged during impact.

3.1.2.6 Side-Mounted, Top-Anchored Post

Several variations of a concept featuring posts placed on the side of the deck with through-deck anchorage systems were considered. The upper anchorage utilized a steel strap that was either welded or bolted to the post. If bolted, a plate washer would be positioned on the backside of the post to help distribute the load. The lower anchorage was either a smaller anchor embedded in the side of the deck or a lower angle plate attached to the through-deck bolt. Sketches of these variations are shown in Figures 16 and 17.

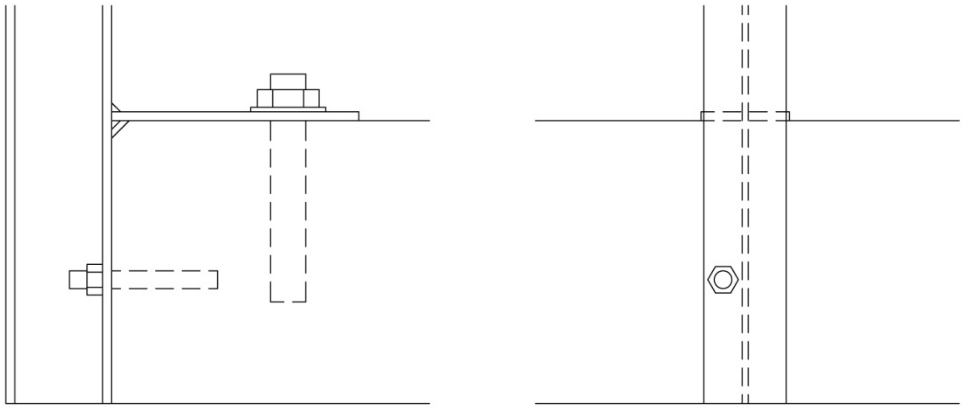

Figure 16. Top-Anchored, Side Mounted Post Welded to Strap

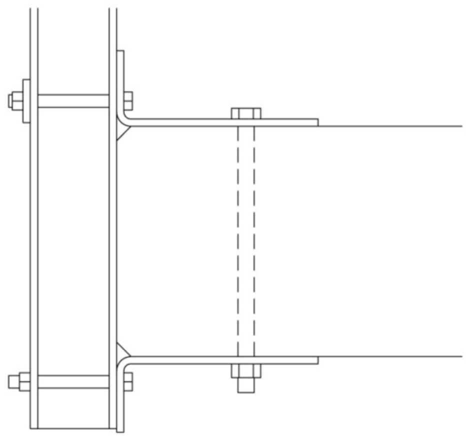

Figure 17. Top-Anchored Bent Plates Bolted to Post

Strengths of these concept variations were that they encroached minimally onto the bridge deck surface and used simple and economical hardware. Weakness was that the top anchorages, which did not extend onto the deck as far as the lateral plate tear-out connection, might still be damaged by snow plow operations. Welding the top anchorage to the post would also create an awkward section, as previously discussed. Bolting the post to the anchorages was not ideal either, as the combination of the narrow post flanges and relatively large bolt size would significantly reduce the post cross-section at its point of maximum bending moment.

3.1.2.7 Side-Mounted, Top-Anchored Socket

Another form of the side-mounted, top-anchored design used a socket that would be anchored to the top and bottom of the deck using a through-deck bolt. The socket would be a standard HSS shape, and the post would be supported by either a bolt that passed through the post and the socket, or a cap on the bottom of the socket. A shim would be used to snug the post inside the socket. Several variations of the anchorage system were developed. However, the final design consisted of a top strap that was welded to the socket and a bottom angle that was bolted to the socket, thereby allowing for variations in deck thickness. A sketch of this connection is shown in Figure 18.

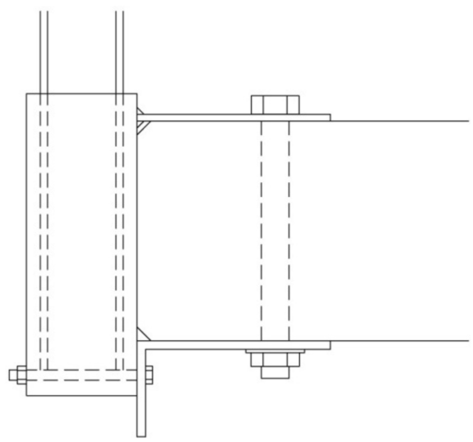

Figure 18. Side-Mounted, Top-Anchored Socket Concept

Strengths of this concept were that it did not encroach significantly onto the deck surface and that only the post would require replacement following an impact. Weaknesses were the somewhat awkward shape of the angle and mounting strap assembly and the expense of fabricating sockets for each post.

3.1.2.8 Selection of Design for Component Testing

Several concepts were thought to be viable, including the cast-in-place socket, the side-mounted bent plate socket, the top-anchored bent plates bolted to post, the top-anchored socket with lower angle, and the side-mounted post welded to base plate. The side-mounted bent plate socket was believed to be the most economical design, and thus it was selected for component testing.

Note that the ability of existing bridge decks to withstand loads imparted from both strong- and weak-post design concepts was unknown due to potential variations in bridge deck size, strength, and reinforcement layout. Thus, the ability of all design concepts to be retrofit to existing bridge decks was unknown.

3.2 Post-to-Rail Connection

The connection between the post and rail of a barrier plays an important role in system performance. The connection must be sufficiently strong such that it does not prematurely release downstream of the vehicle, which can allow the rail to drop and produce vehicle override. At the same time, the connection must be sufficiently weak such that it does not allow the rail to be pulled down by rotating posts, which may also produce vehicle override. This requirement is especially important in systems which do not utilize blockouts, which help maintain rail height during post rotation.

Thus, the post-to-rail connection design needed to (1) withstand forces caused by stress waves in the rail to prevent premature release, (2) fail consistently as the post rotated such that the rail would not be pulled downward, and (3) be economical. Ideally, the connection would utilize standard and readily available components. A variety of preliminary concepts for post-to-rail connections were developed which are described in the following sections.

3.2.1 Standard Weak-Post Guardrail (G2) Connection

The first design concept considered was the standard weak-post, W-beam guardrail (G2) connection. This utilized a $^{5}/_{16}$-in. (7.9-mm) diameter ASTM A307 Grade A bolt which passed through the rail and tension flange of the post, a nut, and a large square washer placed on the traffic-side face of the W-beam rail. This connection was originally designed to release during impact through fracture of the bolt, but more recent research suggested the connection might also fail by thread stripping in the nut and pull-through of the washer [47-48]. As the new bridge rail would have four times as many posts as the weak-post W-beam guardrail, shelf bolts would not be required to resist environmental loads and would therefore be omitted. A sketch of the standard G2 connection is shown in Figure 19.

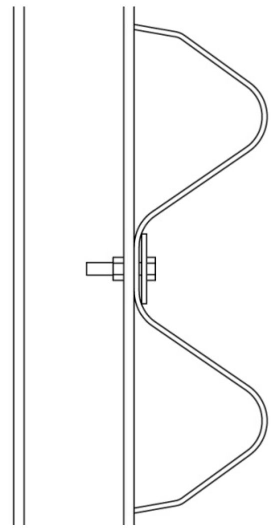

Figure 19. Standard G2 Connection

The greatest strength of this connection was its simplicity and low cost. Potential weakness was the possible inconsistency of failure. Position of the bolt and washer within the slot, the number of layers of guardrail at the connection (i.e., splice or non-splice), and the variability of material properties could greatly influence the failure mechanism and load. As bolt fracture was believed to require the greatest load, it represented an upper limit that could be tuned to the desired level.

3.2.2 TL-3 Weak-Post Guardrail Connection

A connection based on that of the TL-3 weak-post, W-beam guardrail was also considered. This connection would consist of a bolt, two washers, two nuts, and would rely solely upon the fracture of the bolt for rail release [47-48]. The two washers would have sufficient bending strength to prevent pull-through, while the two nuts would not allow the threads on either the nuts or the bolt to strip. A sketch of this connection is shown in Figure 20.

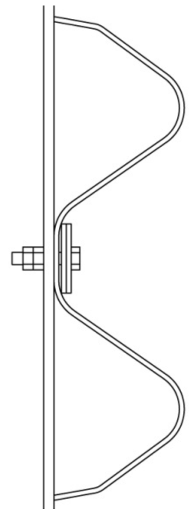

Figure 20. TL-3 Weak-Post W-beam Guardrail Connection

Strengths of this connection were its simplicity and low cost. A potential weakness was that the connection had little ductility and may not be able to absorb energy from stress waves in the guardrail, which could potentially lead to premature rail release from the posts.

3.2.3 Keyway Release Concept

Another design concept consisted of a keyway release mechanism located on the guardrail posts. The keyway would consist of a small diameter hole, through which the connection would be attached, positioned adjacent to a larger diameter hole such that as the post rotated, the bolt would slide from the smaller diameter hole to the larger diameter hole and release from the post. Sketches of the keyway concept are shown in Figure 21.

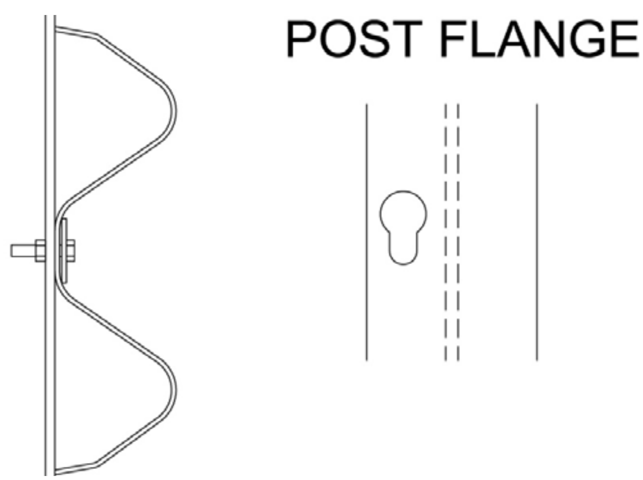

Figure 21. Keyway Connection Concept

Two major problems were identified for the keyway concept. First, initial bolt preload would cause friction between the rail and post that could potentially prevent the movement required for release. Second, post rotations in the upstream or downstream direction might not result in proper rail release.

3.2.4 Slotted Post Concept

Another concept utilized a slot in the post and a bolt to connect the post to the rail. Upon impact, the post would rotate, and as the rail deflected it would pull the bolt through the edge of the slot, releasing it from the post. The slot would either be positioned in the web or flange of the post; however, no connection mechanism was developed utilizing the web. A sketch of this concept is shown in Figure 22.

One problem identified with the slotted post concept was that it potentially conflicted with previously patented systems, including several cable barrier systems and the Nucor Nu-Guard guardrail system [57].

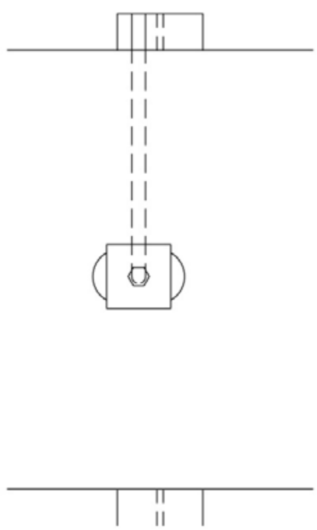

Figure 22. Slotted Post Concept

3.2.5 Hanger-Bracket Concept

Several variations of a hanger-bracket concept were considered during the development of the post-to-rail connection. The bracket would rest on top of the post and be connected to the rail with a bolt. As the post rotated, the bracket would slip off the edge of the post to release the rail.

One variation of this concept utilized two fingers that passed over the flange of the post on either side of the web to secure the hanger-bracket. The rail-connection bolt would be positioned with its head on the bracket side of the connection and the nut on the guardrail side of the connection, or backward from a standard connection, such that the bolt would not prevent the guardrail from laying flat against the post. Alternatively, the slot would be offset past the flange of the post such that the bolt could pass through the rail and hanger-bracket without contacting the post. Sketches of the backward bolt and offset slot variations are shown in Figure 23.

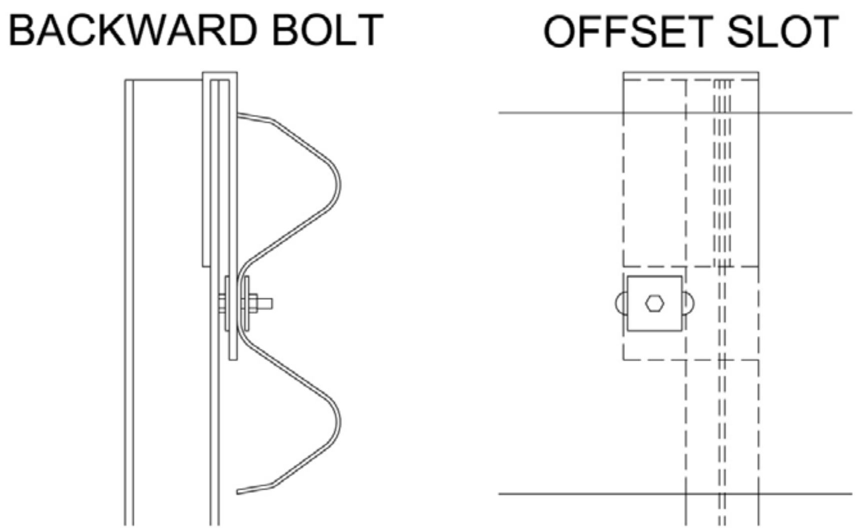

Figure 23. Hanger-Bracket Finger Concept

A variation of the hanger-bracket finger concept consisted of a bent plate that would pass over the entire post and rest outside both of the flanges. Bolts would be placed upstream and downstream of the post, immediately next to the flanges, to hold the bracket in place. The bracket would again be connected to the rail with either a backward bolt or an offset slot. A sketch of this concept is shown in Figure 24. Alternatively, the hanger-bracket could consist of a capped tube section that would fit around the top of the post and be attached to the rail or a bolt could be passed through the top of the tube to hold it in place on the post to eliminate the cap.

One problem with this hanger-bracket concept was that it might infringe on the patent of the King Block, a blockout which uses a similar support mechanism to aid in guardrail installation [59]. This connection would also be much more expensive than the other considered concepts.

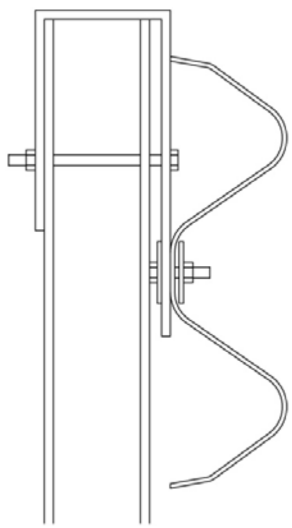

Figure 24. Hanger-Bracket Bolt Concept

3.2.6 Keyway Guardrail Slot

Another concept consisted of modification of the guardrail slot in an attempt to improve uniformity of bolt pullout forces. The modified guardrail slot would consist of larger diameter holes at both ends and a more slender region that connected the two. Overlap of the bolt head above and below the bolt would be greater in the center region than at the ends. In this way, the release loads at the edges of the slot would more closely match those at the center of the slot. A sketch of this concept is shown in Figure 25.

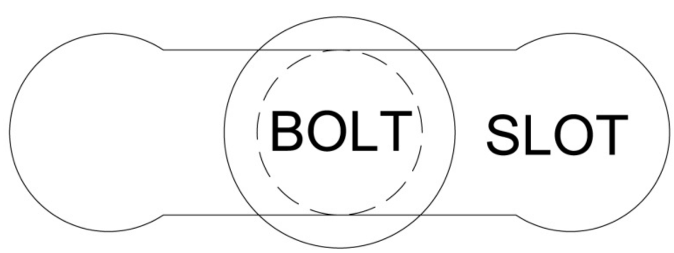

Figure 25. Keyway Guardrail Slot Concept

Shortcomings of this design were that the modified slot in the guardrail would require specially cut W-beam sections not used in other barrier designs and that the release loads at the center of the slot would be reduced due to its shape, thus, allowing potential premature release.

3.2.7 Selection of Design for Component Testing

While several of the concepts were believed to have the ability to function as desired, it was decided to use the standard weak-post W-beam (G2) system connection, which consisted of a $\frac{5}{16}$-in. (7.9-mm) diameter ASTM A307 Grade A bolt, a nut, and a 1¾-in. (44-mm) square washer. This connection was the simplest and most economical of the concepts and made from readily available standard parts. Complimentary failure mechanisms of bolt fracture, pull-through of the washer and guardrail slot, and stripping of bolt and nut threads would prevent the connection from developing excessive strength and pulling the rail down during post rotation. The ability of the washer and slot to deform would also give the connection ductility to absorb some of the impact energy, which would be important early in the event as stress waves passed through the W-beam rail. Although the connection was believed to fail prematurely in previous weak-post guardrail research [47-48], the new bridge rail would use four times as many posts. Thus, the rail would be supported in four times as many locations, and premature release was far less likely. For these reasons, the standard weak-post connection was selected as the primary design for the bridge rail.

4 COMPONENT TESTING

4.1 Purpose

Following the revision of the initial concepts, component tests were conducted to determine if the design concepts would perform as desired. Posts and post-to-deck attachments were dynamically tested to verify that appropriate resistive forces would be developed and sufficient energy would be absorbed by the system to safely redirect the vehicle. Static tests were performed on the connection between the W-beam rail and post to verify that the connection would release the rail at appropriate loads. Based on the results of the preliminary tests, the concepts were either further refined or abandoned. All static and dynamic tests were conducted at the MwRSF Proving Grounds in Lincoln, Nebraska.

4.2 Dynamic Testing

Seven dynamic bogie tests were conducted to explore the behavior of bridge rail posts and post-to-deck attachments. Two tests were used to examine the performance of the top-mounted lateral plate tear-out concept using W6x9 (W152x13.4) posts, and three tests were performed on the side-mounted tubular post tear-out concept using HSS6x4x⅛ (HSS152x102x3.2) posts. Finally, two tests were performed on S3x5.7 (S76x8.5) posts using two different deck attachments. Target impact conditions for the first six tests were a speed of 20 mph (32.2 km/h) and an angle of 90 degrees with respect to the longitudinal direction of the bridge rail. For the final test, the target speed was reduced to 15 mph (24.1 km/h). All posts were impacted 24⅞ in. (632 mm) above the ground line. The bogie test setup and tested concepts are shown in Figures 26 through 30. Full drawing sets for all tests are available in the project documentation but are not included in the report.

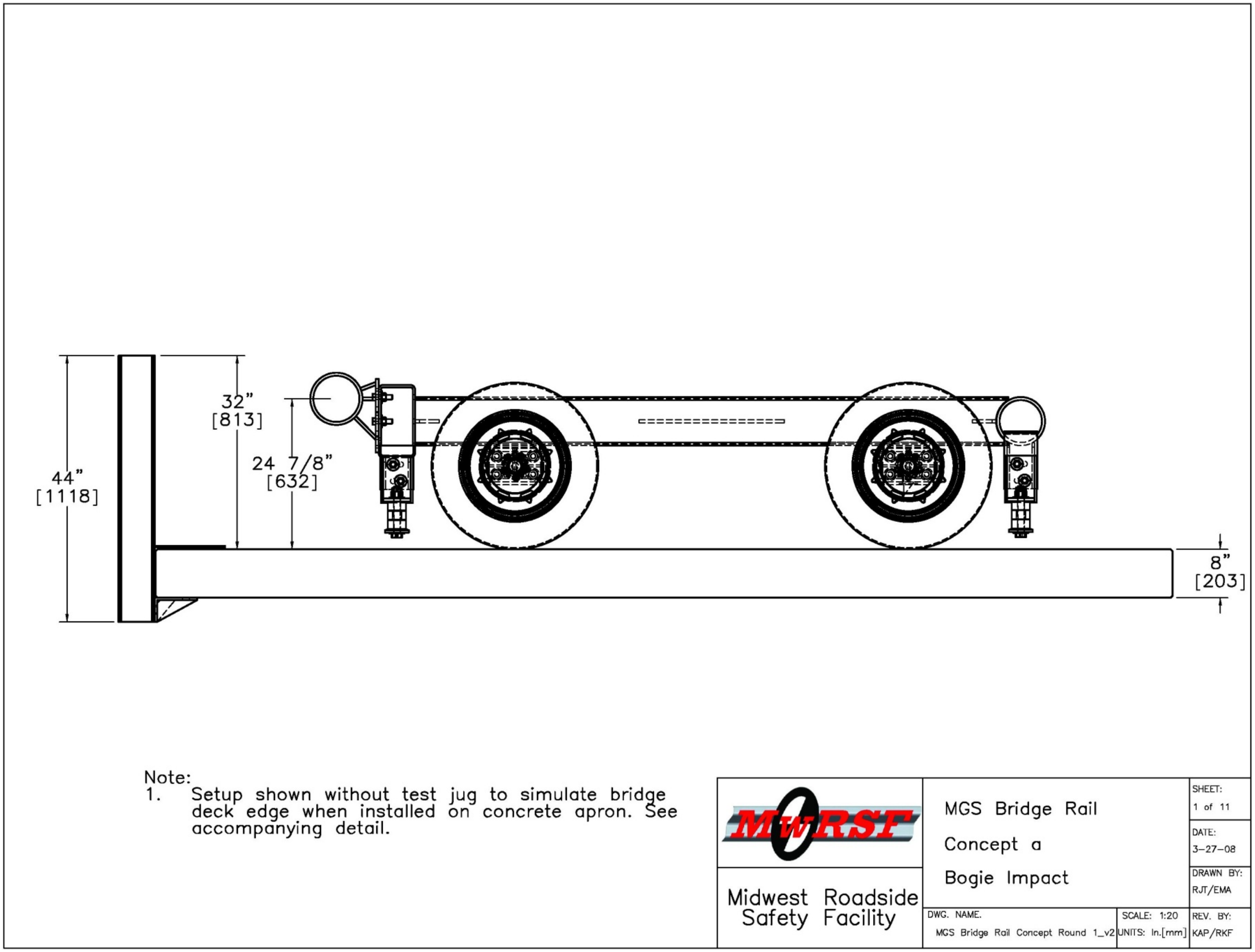

Figure 26. Bogie Testing Setup

MGS Bridge Rail – Concept A				
Item No.	QTY.	Description	Material Spec	Hardware Guide
a8	1	Concept A W6x9	A36 Steel	–
a9	1	Concept A Top Plate	A36 Steel	–
a10	2	Concept A Flats	A36 Steel	–

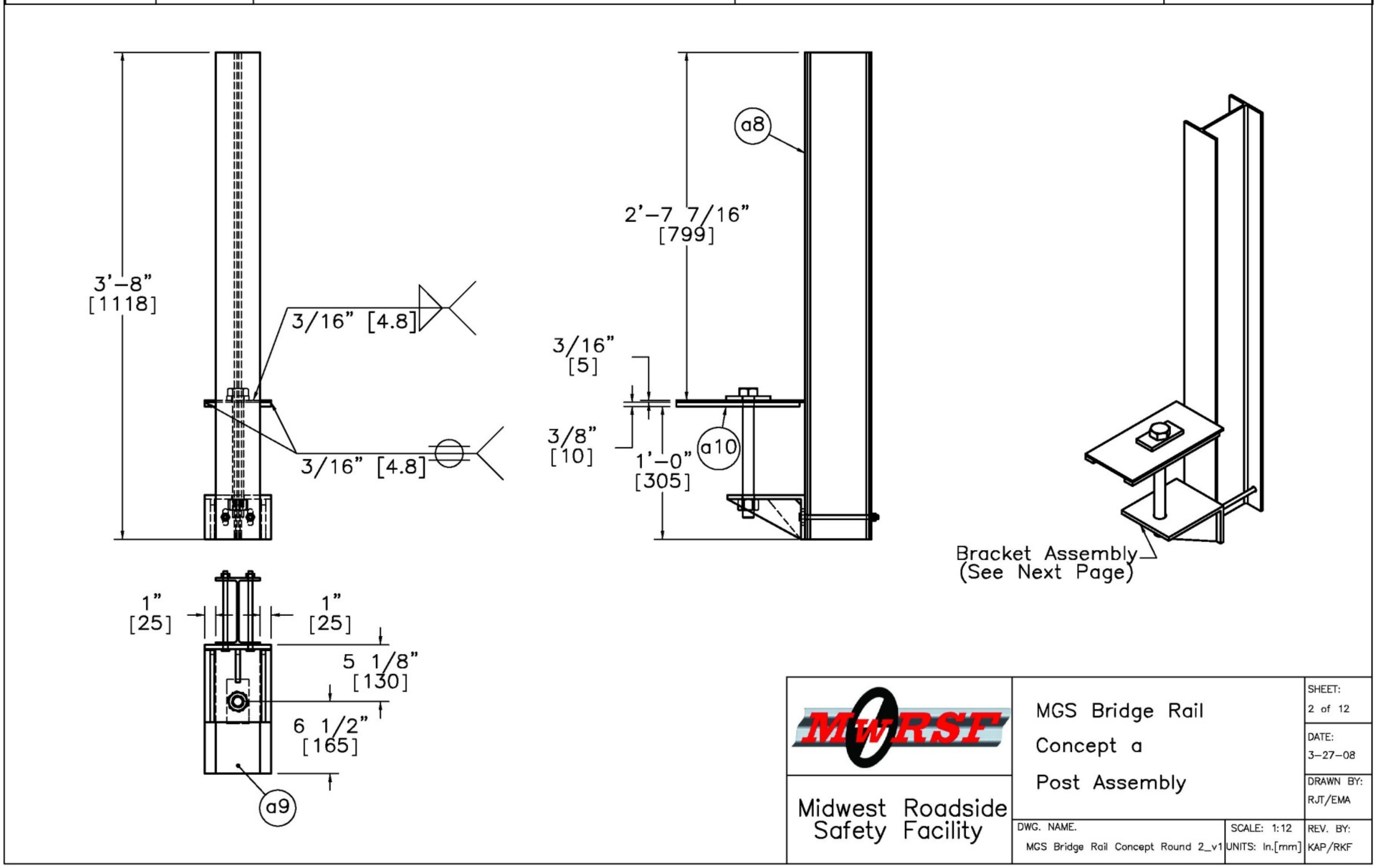

Figure 27. Top-Mounted Lateral Plate Tear-out Concept

MGS Bridge Rail – Concept B				
Item No.	QTY.	Description	Material Spec	Hardware Guide
b1	1	Concept B Base	–	–
b2	1	Concept B Post Assembly	–	–

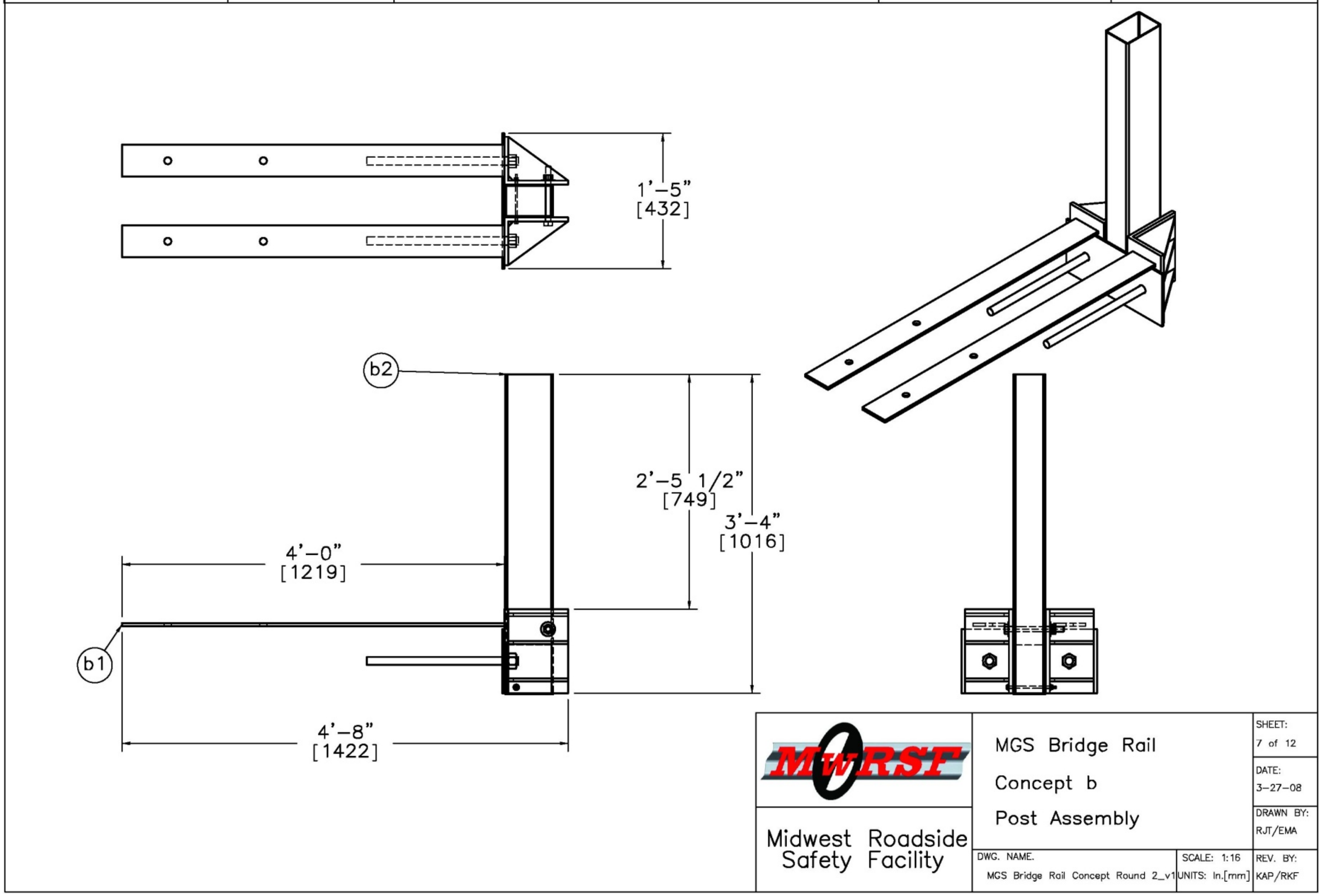

Figure 28. Side-Mounted Tubular Post Tear-out Concept

MGS Bridge Rail—Option 1			
Item No.	QTY.	Description	Material Specification
a1	1	1/4" thick Bent Plate Socket	ASTM A36
a2	1	1/4" Base Plate	ASTM A36
a3	2	ø 3/4"—10x16" Threaded Rod	ASTM A193—Grade B7
a4	2	ø 3/4" — 10 Heavy Hex Nut	ASTM A194 Grade 2H or ASTM A563DH
a5	1	8 x 2 x 1/8" thick Shim Plate	ASTM A36
a6	1	8 x 2 x 1/4" thick Shim Plate	ASTM A36
a7	1	8 x 2 x 3/8" thick Shim Plate	ASTM A36
a8	2	3/4" Washer	ASTM F436
a9	1	S3x5.7 by 40" Long	ASTM A36

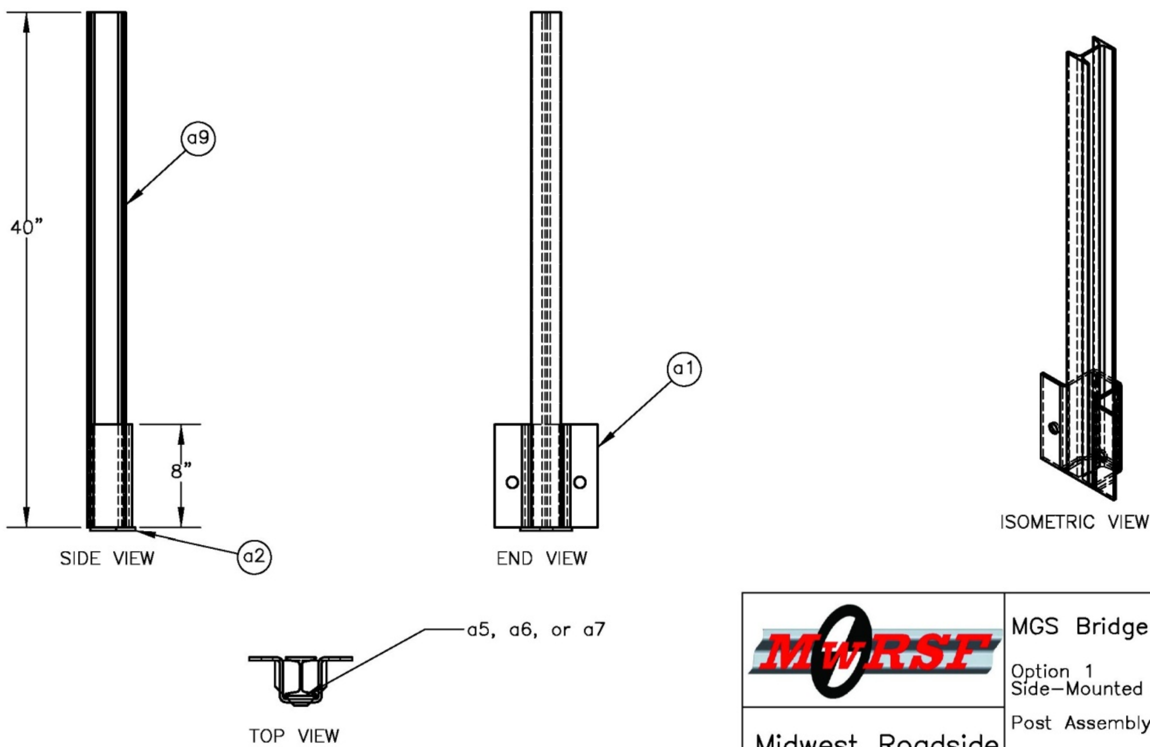

MwRSF Midwest Roadside Safety Facility	MGS Bridge Rail Option 1 Side—Mounted Bent Plate Socket Post Assembly	SHEET: 2 of 9 DATE: 10/24/08 DRAWN BY: MW
	DWG. NAME. MGS Bridge Rail Concept Round 3_v7	SCALE: 1:12 UNITS: Inches
		REV. BY: KP/RF

Figure 29. Side-Mounted Socket Concept

MGS Bridge Rail Round 2			
Item No.	QTY.	Description	Material Spec
a1	1	S3x5.7 Post	A36 Steel Galvanized
a2	4	S3x5.7 Post Standoff	A36 Steel Galvanized
a3	1	4x4x0.375 SQ Tube	A500 Grade B Steel Galvanized
a4	1	Top Mounting Plate	A572 Grade 50 Steel Galvanized
a5	1	Top Mounting Plate Gusset	A36 Steel Galvanized
a6	1	Heavy Hex Bolt 0.625–11x6x1.25	ASTM A325 Type 1 Galvanized
a7	1	Heavy Hex Nut 0.625–11	ASTM A563 DH Galvanized
a8	1	L7x4x0.375	A36 Steel Galvanized
a9	1	L7x4x0.375 Gusset	A36 Steel Galvanized
a10	1	Backside Retainer Plate	A36 Steel Galvanized
a11	2	1" Flat Washer	F436 Galvanized
a12	1	Heavy Hex Bolt 1–8x10.5x1.75	ASTM A325 Type 1 Galvanized
a13	1	Heavy Hex Nut 1–8	ASTM A563 DH Galvanized
a14	2	Heavy Hex Bolt 0.5–13x6x6	ASTM A325 Type 1 Galvanized
a15	2	Heavy Hex Nut 0.5–13	ASTM A563 DH Galvanized

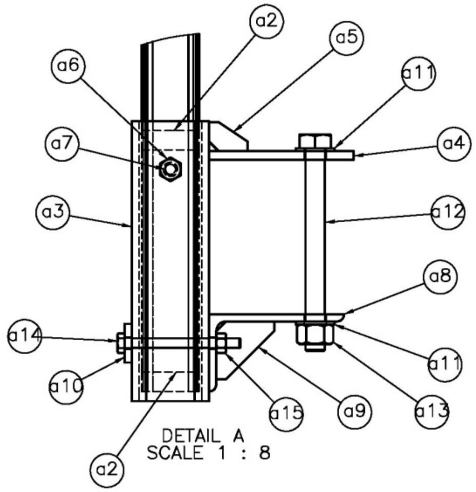

DETAIL A
SCALE 1 : 8

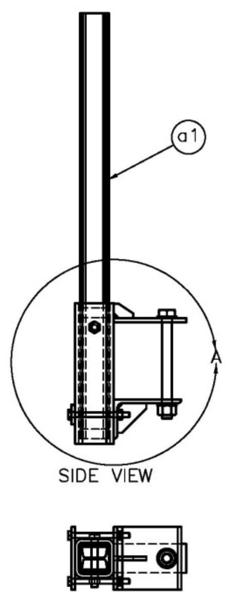

SIDE VIEW

TOP VIEW

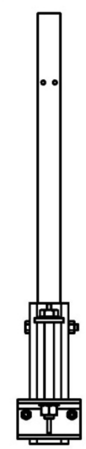

END VIEW

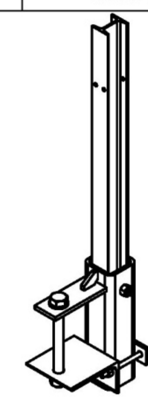

ISOMETRIC VIEW

MwRSF Midwest Roadside Safety Facility	MGSBRB–7 Post Mount Post Assembly	SHEET: 2 of 11 DATE: 12/4/08 DRAWN BY: MJW
	DWG. NAME. MGS Bridge Rail Round 2_v2 / SCALE: 1:16 UNITS: Inches	REV. BY: KAL

Figure 30. Side-Mounted, Top-Anchored Socket Concept

4.2.1 Dynamic Bogie Testing Equipment and Instrumentation

Equipment and instrumentation utilized to collect and record data during the dynamic bogie tests included a bogie, a test jig, accelerometers, pressure tape switches, as well as digital video and still cameras.

4.2.1.1 Bogie

A rigid-frame bogie was used to impact the posts. A variable-height, detachable impact head was constructed and used in the testing. The bogie head was constructed of 8-in. (203-mm) diameter, ½-in. (12.7-mm) thick standard steel pipe, with ¾-in. (19.1-mm) neoprene belting wrapped around the pipe. The neoprene cushioned the contact between the steel impact tube and the steel posts, which helped prevent overly large spikes in acceleration. The impact head was bolted to the bogie vehicle to create a rigid frame with an impact height of 24⅞ in. (632 mm). The bogie with the impact head is shown in Figure 31. The weight of the bogie with the addition of the mountable impact head was 1,841 lb (835 kg) for test nos. MGSBRB-1 through MGSBRB-3, 1,837 lb (833 kg) for test nos. MGSBRB-4 and MGSBRB-5, 1,797 lb (815 kg) for test no. MGSBRB-6, and 1,860 lb (844 kg) for test no. MGSBRB-7. The weight of the bogie varied due to changes in transducers mounted onboard and repairs made to the bogie vehicle following the damage that was sustained during testing.

For test nos. MGSBRB-1, MGSBRB-6, and MGSBRB-7, a pickup truck with a reverse cable tow system was used to propel the bogie. When the bogie reached the end of the guidance system, it was released from the tow cable, allowing it to be free rolling when it impacted the post. A remote braking system was installed on the bogie allowing it to be safely brought to a rest after the test.

Test nos. MGSBRB-2 through MGSBRB-5 were conducted using a steel corrugated beam guardrail to guide the tire of the bogie vehicle. A pickup truck was used to push the bogie vehicle to the required impact velocity. After reaching the target velocity, the push vehicle braked and allowed the bogie to roll ahead into the test article.

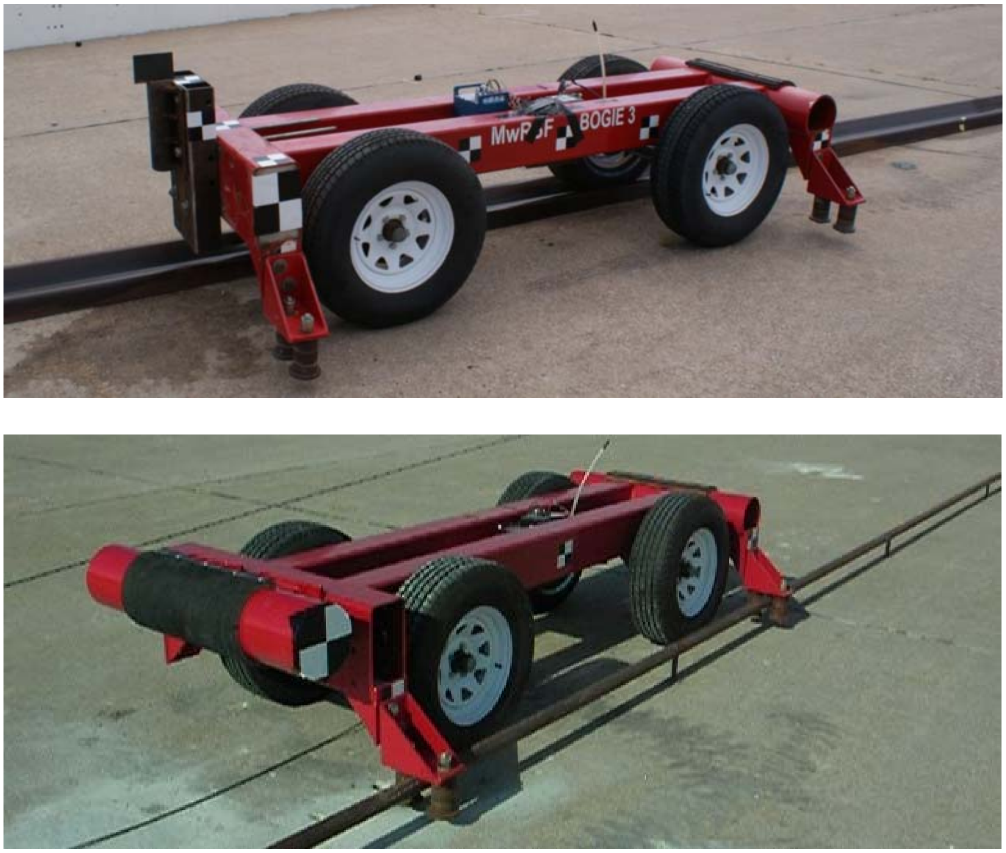

Figure 31. Rigid Frame Bogie on Guidance Tracks

4.2.1.2 Test Jig

Dynamic bogie tests were conducted on the rigid concrete pavement at the Lincoln Air Park. As the lateral plate tear-out concept was designed to be top-mounted to a bridge deck using vertical, through-deck bolts, it could not be directly mounted to the apron. A test jig was fabricated utilizing an 8-in. (203-mm) long, HSS6x4x¼ (HSS152x102x6.4) section that was filled with concrete. A conduit was placed vertically through the concrete to house the through-deck bolt for attaching the post to the jig. This conduit was positioned and supported by two lateral bolts. The tube section was welded to a ½-in. (12.7-mm) thick steel plate which was attached to the apron using 1-in. (25.4-mm) diameter threaded rods that were embedded in epoxy. Additional ½-in. (12.7-mm) thick steel gusset plates were welded to the mounting plate and tube to further reinforce the section. After preliminary tests demonstrated that the edge of the unreinforced deck was not capable of developing the required loads, two 4-ft (1.22-m) long steel straps were welded to the jig and used to further anchor it to the deck with drop-in anchors. A drawing of the test jig is shown in Figure 32. A full drawing set of the test jig is available in the project documentation but is not included in the report.

4.2.1.3 Accelerometers

Three environmental shock and vibration sensor/recorder systems were used to measure bogie vehicle accelerations in the longitudinal, lateral, and vertical directions. All of the accelerometers were mounted near the center of gravity of the bogie.

For test nos. MGSBRB-1 through MGSBRB-3, a two-arm piezoresistive accelerometer system was used that was developed by Endevco of San Juan Capistrano, California. Three accelerometers were used to measure each of the longitudinal, lateral, and vertical accelerations independently at a sample rate of 10,000 Hz. The accelerometers were configured and controlled using a system developed and manufactured by Diversified Technical Systems, Inc. (DTS) of Seal Beach, California. More specifically, data was collected using a DTS Sensor Input Module (SIM), Model TDAS3-SIM-16M. The SIM was configured with 16 MB SRAM memory and 8 sensor input channels with 250 kB SRAM/channel. The SIM was mounted on a TDAS3-R4 module rack. The module rack was configured with isolated power/event/communications, 10BaseT Ethernet and RS232 communication, and an internal backup battery. Both the SIM and module rack were crashworthy. The computer software program "DTS TDAS Control" and a customized Microsoft Excel worksheet were used to analyze and plot the accelerometer data.

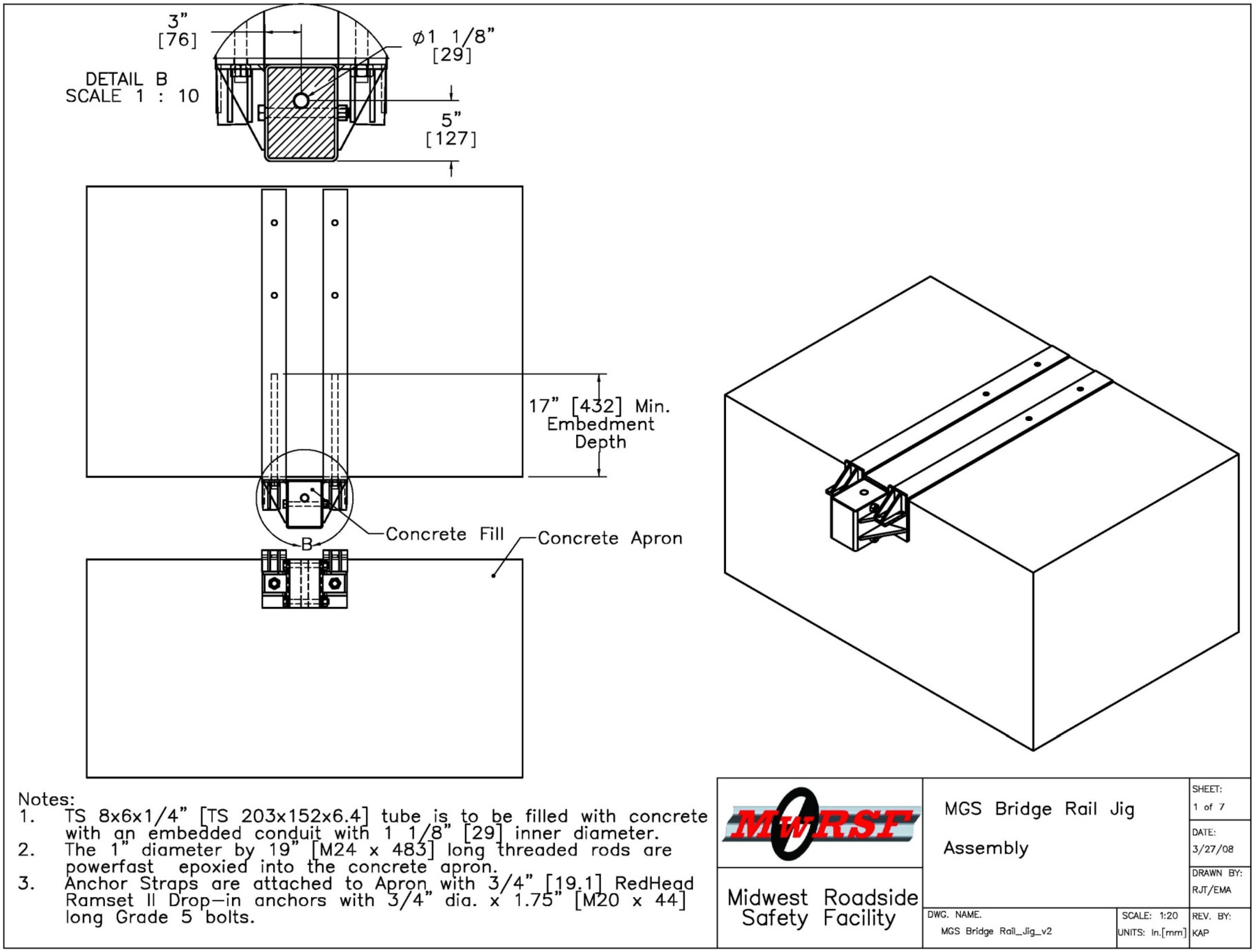

Figure 32. Lateral Plate Tear-out Concept Test Jig

A triaxial piezoresistive accelerometer system, Model EDR-4 6DOF-500/1200, was used for test nos. MGSBRB-4 through MGSBRB-7. This system was developed and manufactured by Instrumented Sensor Technology (IST) of Okemos, Michigan and includes three differential channels as well as three single-ended channels. The EDR-4 6DOF-500/1200 was configured with 24 MB of RAM memory, a range of ±500 g's, a sample rate of 10,000 Hz, and a 1,677 Hz anti-aliasing filter. "EDR4COM" and "DynaMap Suite" computer software programs and a customized Microsoft Excel worksheet were used to analyze and plot the accelerometer data.

For all seven bogie tests, a triaxial piezoresistive accelerometer system, Model EDR-3, also developed by IST of Okemos, Michigan was used. The EDR-3 was configured with 256 kB of RAM memory, a range of ±200 g's, a sample rate of 3,200 Hz, and a 1,120 Hz low-pass filter. The computer software program "DynaMax 1 (DM-1)" and a customized Microsoft Excel worksheet were used to analyze and plot the accelerometer data.

4.2.1.4 Pressure Tape Switches

Three pressure tape switches, spaced at 18-in. (457-mm) intervals and placed near the end of the bogie track, were used to determine the speed of the bogie just before impact. As the left-front or right-front tire of the bogie passed over each tape switch, a strobe light was fired sending an electronic timing signal to the data acquisition system. The system recorded the signals and the time each occurred. The speed was then calculated using the spacing between the sensors and the time between the signals. Strobe lights and high-speed video analysis are used only as a backup in the event that vehicle speeds cannot be determined from the electronic data.

4.2.1.5 Digital Video and Still Cameras

High-speed AOS VITcam digital video cameras and JVC digital video cameras were used to document each dynamic test. All high-speed AOS cameras had a frame rate of 500 frames per second and all JVC digital video cameras had a frame rate of 29.97 frames per second. A Nikon D50 digital still camera was also used to document pre- and post-test conditions for all tests.

For dynamic test no. MGSBRB-1, one AOS VITcam high-speed digital video camera was used to record video imagery of the dynamic testing. However, no high-speed footage was taken due to technical difficulties. Two JVC digital video cameras were also used, with one positioned to the side of the test apparatus and the other positioned downstream and to the side of the test apparatus.

For dynamic test nos. MGSBRB-2 through MGSBRB-5, one AOS VITcam and one AOS X-PRI high-speed digital video camera were used, with one positioned to the side of the test apparatus and zoomed-in on the tear-out region and the other positioned to the side of the test apparatus, but set to capture the entire bogie-post interaction. Two JVC digital video cameras were also used and were positioned to the side of the test apparatus with one camera placed on either side of the post.

For dynamic test no. MGSBRB-6, two AOS VITcam high-speed digital video cameras were used to record video imagery of the dynamic testing. However, no high-speed footage was taken due to technical difficulties. Two JVC digital video cameras were also used, with one positioned downstream and to the side of the test apparatus and the other positioned to the side of the test apparatus.

For dynamic test no. MGSBRB-7, two AOS X-PRI high-speed digital video cameras were used, with one positioned to the side of the test apparatus to record the action of the entire post and the other also positioned to the side of the test apparatus, but its zoom settings were set to focus on the base of the post. Three JVC digital video cameras were also used, with one positioned in-line and upstream of the bogie's path and the other two positioned to the side of the test apparatus with one camera placed on either side of the post.

4.2.2 End of Test Determination

During impact, the data acquisition systems record accelerations of the bogie, including vibrations of the vehicle before and after the event. Thus, the instruments continued to collect data beyond the failure of the post, and the end of the test requires definition.

In general, the end of test time was identified as the time that the vibration peaks in the acceleration trace subsided back toward zero and it was clear that the continued vibrations were not caused by interaction with the post. Additionally, test duration was limited by the bogie-post contact time so that there were no unreasonably long test durations.

4.2.3 Data Processing

The electronic accelerometer data obtained in dynamic testing was filtered using the SAE Class 60 Butterworth filter conforming to the SAE J211/1 specifications. The pertinent acceleration signal was extracted from the bulk of the data signals. The processed acceleration data was then multiplied by the mass of the bogie to get the impact force using Newton's Second Law. Next, the acceleration trace was integrated to find the change in velocity verses time. Initial velocity of the bogie, calculated from the pressure switch data, was then used to determine the bogie velocity, and the calculated velocity trace was integrated to find the bogie's displacement. This displacement is also the displacement of the post. Combining the previous results, a force vs. deflection curve was plotted for each test. Finally, integration of the force vs. deflection curve provided the energy vs. deflection curve for each test.

4.3 Strong-Post Dynamic Bogie Test Results

The information desired from the bogie tests was the relation between the force on the post and deflection of the post at the impact location. This data was then used to find total energy dissipated during each test, which was equal to the area under the force vs. deflection curve.

It should be noted that although the acceleration data was applied to the impact location, the data came from the center of gravity of the bogie. This added some error to the data, since the bogie was not perfectly rigid and vibrations in the bogie were recorded. The bogie may have also rotated during impact, causing differences in accelerations between the bogie center of mass and the bogie impact head. While these issues may affect the data, the data was still valid. Filtering procedures were applied to the data to smooth out vibrations, and rotations of the bogie during testing were minor. Significant pitch angles did develop late in some tests as the bogie overrode the post, however, these occurred after the post-bogie interaction of interest. One useful aspect of the accelerometer data was that it included influences of the post inertia on the reaction force. This was important as the mass of the post would affect barrier performance as well as bogie test results.

The accelerometer data for each test was processed in order to obtain acceleration, velocity, and displacement curves, as well as force vs. deflection and energy vs. deflection curves. The values described herein were calculated from the EDR-3 data curves. Although for most tests, the transducers produced similar results, the EDR-3 has historically provided accurate results, and was the only accelerometer used in all tests. Thus, these plots are included in the text. Test results for all transducers are provided in Appendix A.

For the bridge rail to have stiffness and strength similar to the approach guardrail, the bridge rail posts were required to have resistive forces similar to posts embedded in soil. Thus, it was desired that the strong-post concepts develop a resistive force of approximately 6 to 8 kips (26.7 to 35.6 kN) at the center of the guardrail for a deflection of 15 in. (381 mm). This behavior would result in total energy absorption, through 15 in. (381 mm) of deflection, of 90 to 120 kip-in. (10.1 to 13.6 kJ). Note that for the weak-post concepts, it was desired that the post resistive force and energy absorption be approximately one-half of the target values for the strong-post systems. A summary of all bogie testing results is shown in Table 1.

Table 1. Dynamic Testing Results

Test No.	Date	Post	Concept	Peak Force	Maximum Deflection	Energy (15 in.)	Failure Type
MGSBRB-1	4/21/2008	HSS6x4x1/8 (HSS152x102x3.2)	Tubular Post Tear-out	6.3 kips (27.9 kN)	34.2 in. (869 mm)	60.7 kip-in. (6.9 kJ)	Concrete failure due to threaded rod prying
MGSBRB-2	5/16/2008	W6x9 (W152x13.4)	Lateral Plate Tear-out	8.6 kips (38.2 kN)	11.8 in. (299 mm)	70.1 kip-in. (7.9 kJ)	Bolt head pulled out of tear-out plate
MGSBRB-3	5/16/2008	HSS6x4x1/8 (HSS152x102x3.2)	Tubular Post Tear-out	7.1 kips (31.5 kN)	43.9 in. (1,114 mm)	58.4 kip-in. (6.6 kJ)	Some post tearing, crushing of post base
MGSBRB-4	6/9/2008	W6x9 (W152x13.4)	Lateral Plate Tear-out	9.9 kips (44.1 kN)	41.9 in. (1,065 mm)	98.6 kip-in. (11.1 kJ)	Some plate tearing, post web buckling
MGSBRB-5	6/9/2008	HSS6x4x1/8 (HSS152x102x3.2)	Tubular Post Tear-out	8.1 kips (36.0 kN)	42.9 in. (1,090 mm)	74.9 kip-in. (8.5 kJ)	Tearing of post faces through entire post depth
MGSBRB-6	11/13/2008	S3x5.7 (S76x8.5)	Bent Plate Socket	4.6 kips (20.4 kN)	30.5 in. (774 mm)	48.6 kip-in. (5.5 kJ)	Bending of socket and threaded rod fracture
MGSBRB-7	1/20/2009	S3x5.7 (S76x8.5)	Top-Anchored Socket	6.7 kips (29.9 kN)	12.6 in. (319 mm)	31.4 kip-in. (3.5 kJ)	Concrete failure due to through-bolt pullout

4.3.1 Test No. MGSBRB-1

The first bogie test was performed on the side-mounted tubular post tear-out concept. An HSS6x4x⅛ (HSS152x102x3.2) post was mounted on the edge of the apron and impacted by the bogie travelling at a speed of 21.0 mph (33.7 km/h) perpendicular to the strong axis of the post. Upon impact of the bogie, the anchor rods bent downward and applied a prying force to the unreinforced concrete deck. This resulted in failure of the deck as the rods broke through the surface of a large section of concrete.

Inspection of the post after the test revealed that the bolt did not tear through the post as desired. However, local bearing damage, which was expected to precede tear-out, was found on both sides of the post. These failures caused deformations of ⅜ in. (9.5 mm) and ½ in. (12.7 mm) at the bolt holes on either side of the post.

No high-speed video footage was recorded due to technical difficulties with the equipment. However, the real-time video footage recorded by the digital cameras indicated that the concrete failed early in the event, after which the post rotated until it became braced against the edge of the deck. After becoming braced, the post provided continued resistance against the bogie's motion as it travelled up and over the post. Photographs of the system damage are shown in Figure 33. Force vs. deflection and energy vs. deflection curves for test no. MGSBRB-1 are shown in Figure 34.

4.3.2 Test No. MGSBRB-2

The second bogie test was conducted on the top-mounted lateral plate tear-out concept, which utilized a W6x9 (W152x13.4) post welded to a $^{3}\!/_{16}$-in. (4.8-mm) thick tear-out plate. As the anchorage of the test jig was originally designed to be the same as that of test no. MGSBRB-1, which failed, the system was redesigned. Two 48-in. x 4-in. x ⅜-in. (1,219-mm x 102-mm x 9.5-mm) strips of steel were welded to the back of the test jig that extended laterally above the deck. Each strap had holes through which ¾-in. (19.1-mm) diameter Red Head Multi-Set II Drop-In anchors were passed to anchor the straps to the concrete. These anchors were previously dynamically tested by MwRSF to determine their ultimate shear capacity [60]. Four drop-in anchors were used to anchor the bracket in addition to the previously-discussed threaded rods.

In the test, the bogie impacted the W6x9 (W152x13.4) post perpendicular to its strong axis at an initial velocity of 23.4 mph (37.6 km/h). The through-deck bolt bent, and the plate began tearing along two failure planes in out-of-plane shear. At the same time, the bottom angle plate bent in the region between its two gusset plates. After tearing through 1½ in. (38 mm) of the plate, the bolt head slipped through the opening in the plate. The post assembly then bent and was overridden by the bogie, after which the two bolts that anchored the bottom of the post fractured and completely released the post.

Figure 33. System Damage, Test No. MGSBRB-1

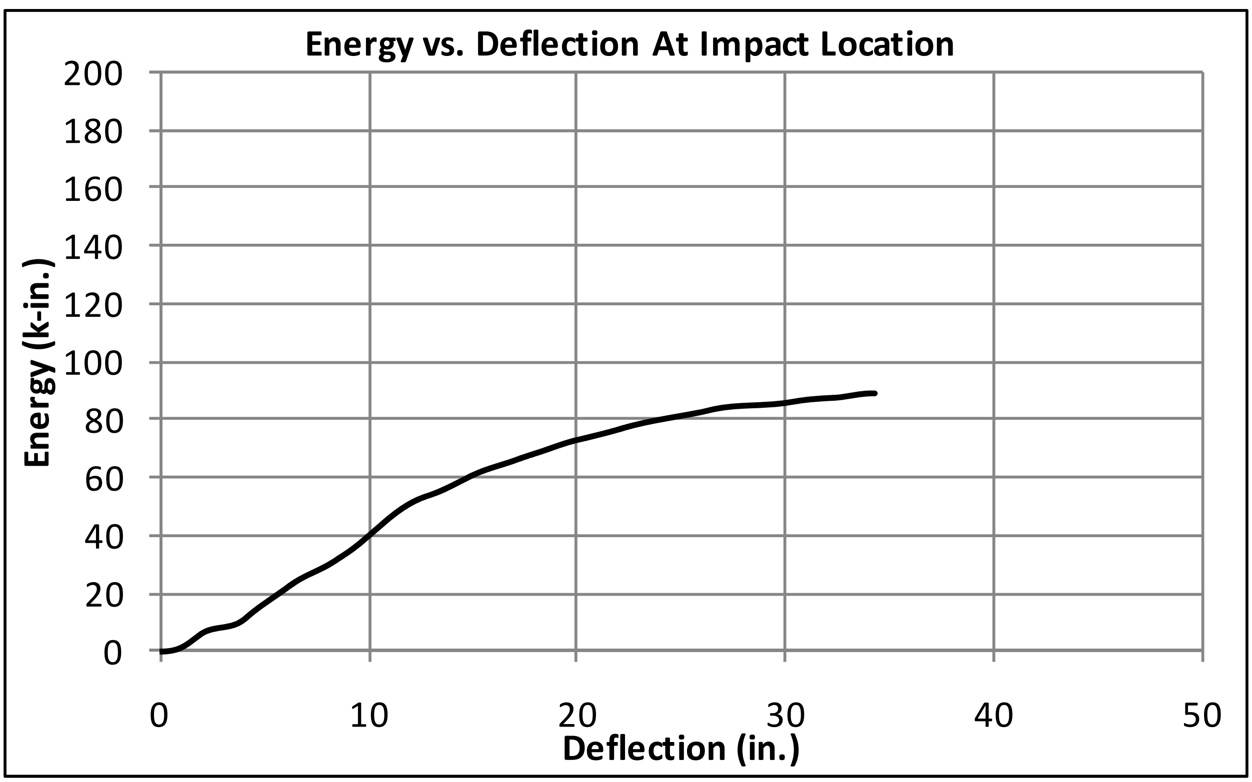

Figure 34. Transducer Data, Test No. MGSBRB-1 (EDR-3)

Although the tear-out mechanism was only partially successful, the developed forces were in the desired range. However, energy absorption was insufficient. Thus, the concept demonstrated that, with modification, it could provide the desired resistance to post rotation. Photographs of the system damage are shown in Figure 35. Force vs. deflection and energy vs. deflection curves for test no. MGSBRB-2 are shown in Figure 36.

4.3.3 Test No. MGSBRB-3

The third bogie test was performed on the side-mounted tubular post tear-out concept. As this concept's anchorage system failed during test no. MGSBRB-1, a revised anchorage system was developed. The new anchorage system was identical to that used for the test jig in test no. MGSBRB-2.

In this test, the bogie impacted the HSS6x4x⅛ (HSS152x102x3.2) post with an initial velocity of 20.4 mph (32.8 m/s) perpendicular to the strong axis of the post. Upon impact, the post rotated about its base, causing the ⅝-in. (15.9-mm) diameter bolt to tear through the walls of the post as desired. However, after the bolt tore through a distance of approximately 2 in. (51 mm), the base of the post collapsed and folded in on itself. This caused the tear-out to stop, and the center of rotation of the post moved from its base to the bolt. As rotation continued, the bottom of the post was further crushed as it was pressed against the mounting bracket. The post continued to provide resistance to the motion of the bogie as the post was never released from the bracket. Photographs of the system damage are shown in Figure 37. Force vs. deflection and energy vs. deflection curves for test no. MGSBRB-3 are shown in Figure 38.

The tear-out mechanism was only partially successful and developed a resistive force that was approximately one-half the desired level. However, the resistive force was higher early in the event when the tear-out mechanism was operating. This result indicated that the tear-out

Figure 35. System Damage, Test No. MGSBRB-2

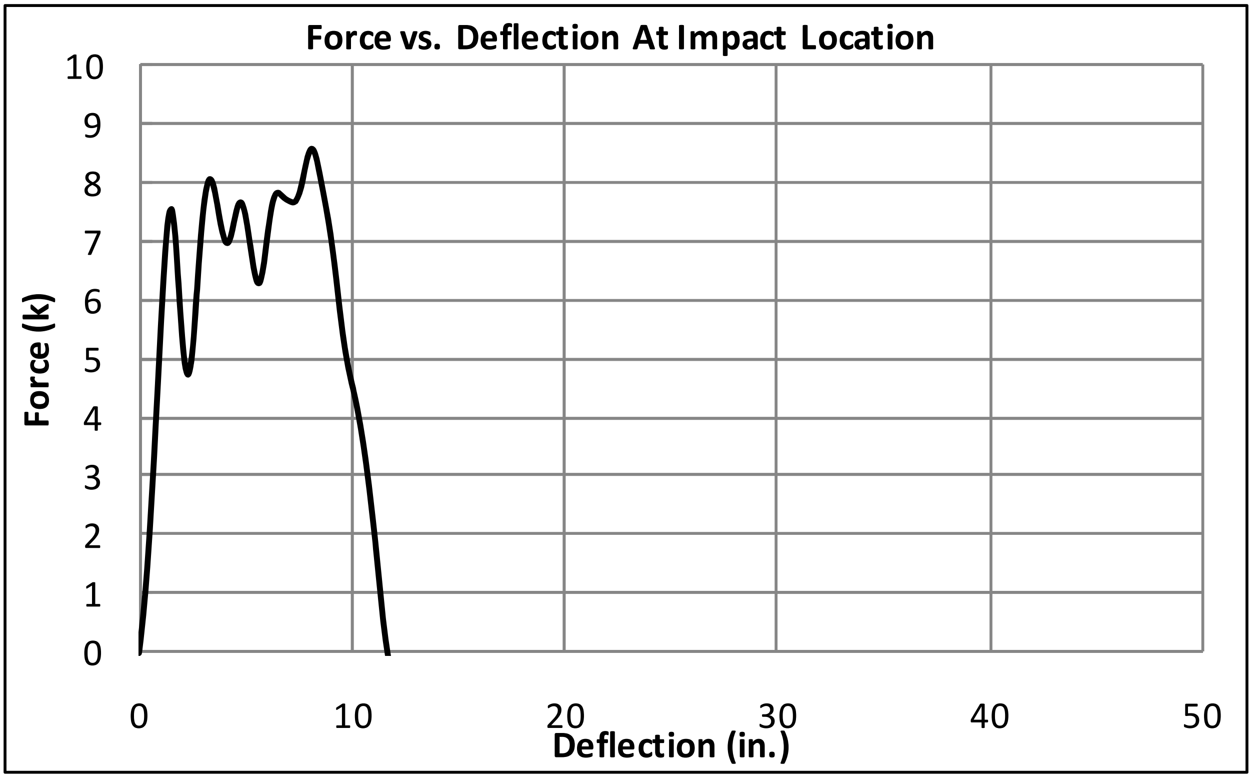

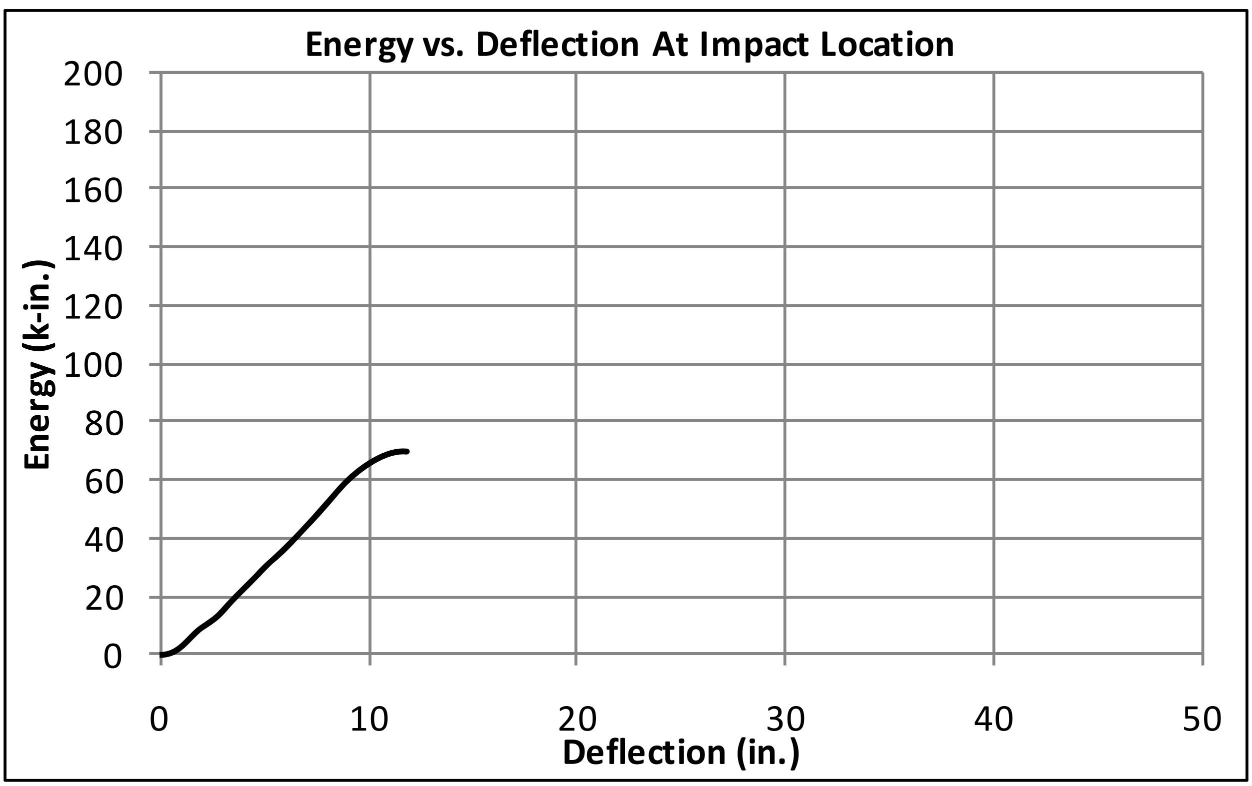

Figure 36. Transducer Data, Test No. MGSBRB-2 (EDR-3)

Figure 37. System Damage, Test No. MGSBRB-3

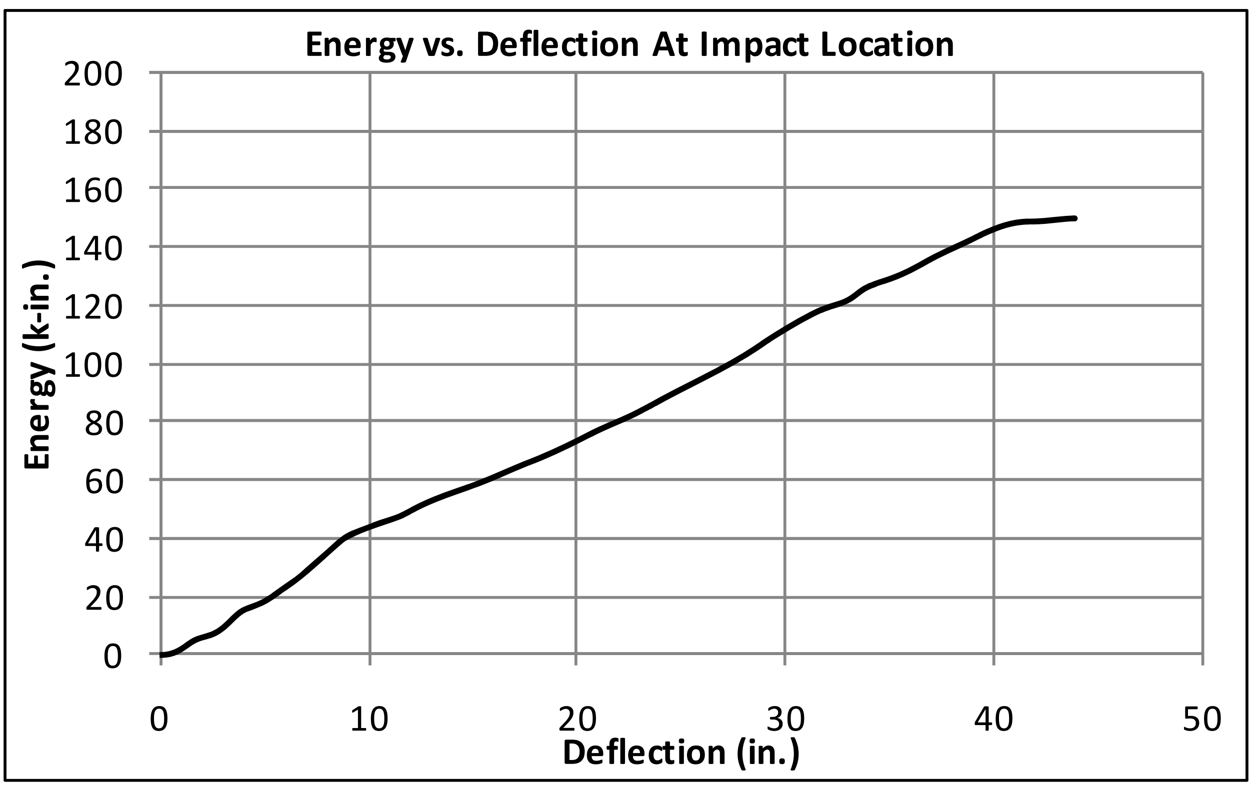

Figure 38. Transducer Data, Test No. MGSBRB-3 (EDR-3)

concept could likely create the desired resistive force. Thus, the concept required modification to isolate tear-out as the post failure mechanism.

4.3.4 Test No. MGSBRB-4

Following the unsatisfactory test results from test nos. MGSBRB-2 and MGSBRB-3, both strong-post concepts were modified in an attempt to improve performance and generate the desired behavior. Two modifications were made to the lateral plate tear-out concept. First, a plate washer was positioned between the tear-out plate and the bolt head to prevent the bolt head from slipping through the tear-out hole prematurely. A third gusset plate was also added at the center of the bottom angle plate to prevent the angle from yielding when loaded.

During the test, the bogie impacted the W6x9 (W152x13.4) post perpendicular to its strong axis with an initial velocity of 22.4 mph (36.1 km/h). Upon impact, the post began to rotate and initiated the desired tear-out failure in the lateral plate. However, during this rotation, the web of the post buckled as the post was pressed against the lower-gusseted angle plate. The angle did not yield due to the inclusion of the third gusset plate. As the web buckled, the post continued to rotate. However, the tear-out failure, which had progressed through approximately 2 in. (51 mm) of the plate, failed to continue. The web buckled, and the post rotated until the front and back flanges of the post nearly came into contact, at which point deformation ended. The bogie then overrode the post.

The developed resistive forces were near target levels through much of the event, and energy absorption was adequate. However, performance of the post was inconsistent as the tear-out mechanism stalled, and the web buckled. The post did not fully release from the deck as desired. Photographs of the system damage are shown in Figure 39. Force vs. deflection and energy vs. deflection curves for test no. MGSBRB-4 are shown in Figure 40.

Figure 39. System Damage, Test No. MGSBRB-4

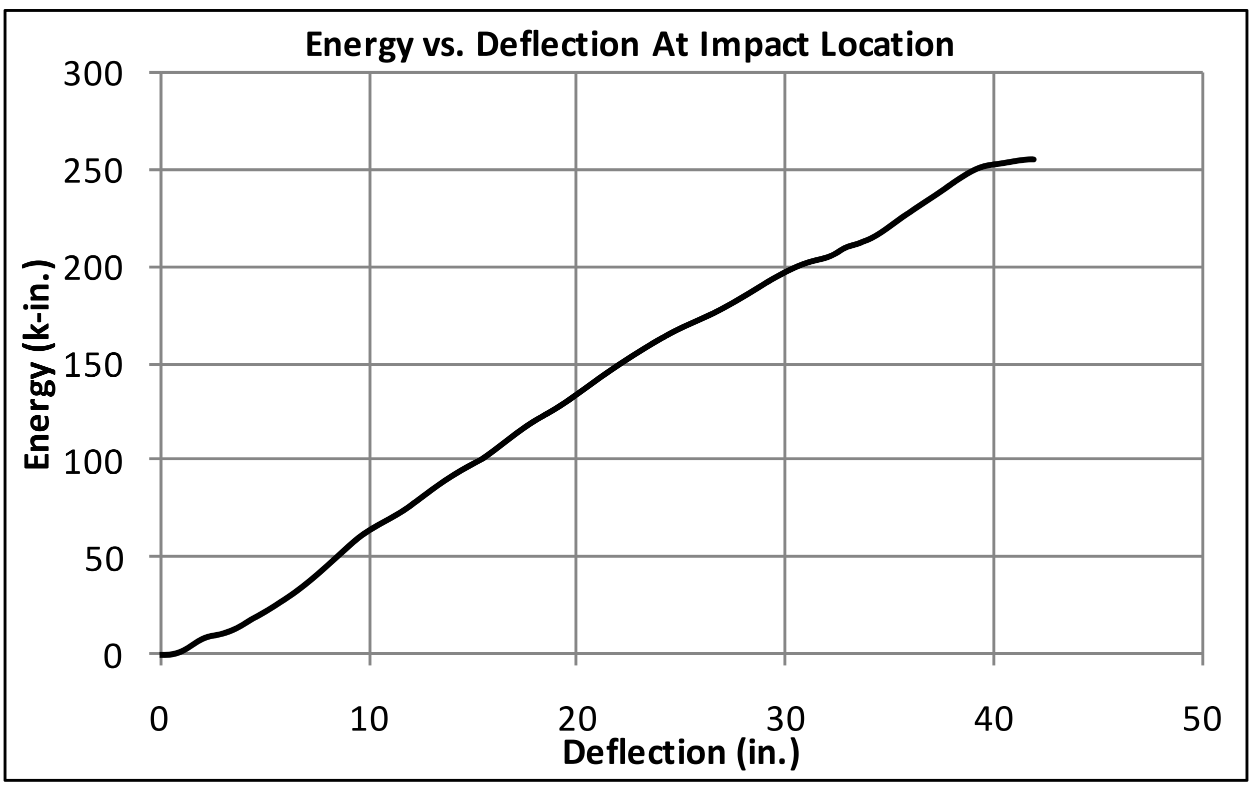

Figure 40. Transducer Data, Test No. MGSBRB-4 (EDR-3)

4.3.5 Test No. MGSBRB-5

For test no. MGSBRB-5, the tubular post tear-out concept was modified by welding a steel cap over the bottom end of an HSS6x4x⅛ (HSS152x102x3.2) post and filling the bottom 6 in. (152 mm) of the post with grout. The cap and grout were intended to prevent the post from crushing, forcing the bolt to tear through the tube faces.

During the test, the bogie impacted the HSS6x4x⅛ (HSS152x102x3.2) post perpendicular to its strong axis with an initial velocity of 23.0 mph (37.0 km/h). The post immediately began to rotate about its base and initiated the desired tear-out failure. As the base came under compression, the weld between the end-cap and the post failed, allowing the end-cap to separate from the post. The bottom portion of the post compressed and caused approximately 2 in. (51 mm) of grout at the bottom of the post to fail through crushing. In spite of this crushing, the post itself yielded minimally, and the tear-out failure proceeded across nearly the entire depth of the post. As the tear-out failure reached the back face of the post, the front and back faces of the post bent, offsetting the lower portion of the post from the top. Photographs of the system damage are shown in Figure 41. Force vs. deflection and energy vs. deflection curves for test no. MGSBRB-5 are shown in Figure 42.

Although the tear-out mechanism worked as desired, the resistive forces generated were smaller than the desired level of 6 to 8 kips (26.7 to 35.6 kN). A thicker post or different bolt location would be required to achieve the desired resistive force.

4.3.6 Discussion of Strong-Post Bogie Testing Results

The first five bogie tests demonstrated that the strong-post designs faced two major problems. First, it was difficult to obtain the desired behavior in the steel tear-out mechanism, thus requiring more elaborate and expensive systems than originally envisioned. Second, the load

Figure 41. System Damage, Test No. MGSBRB-5

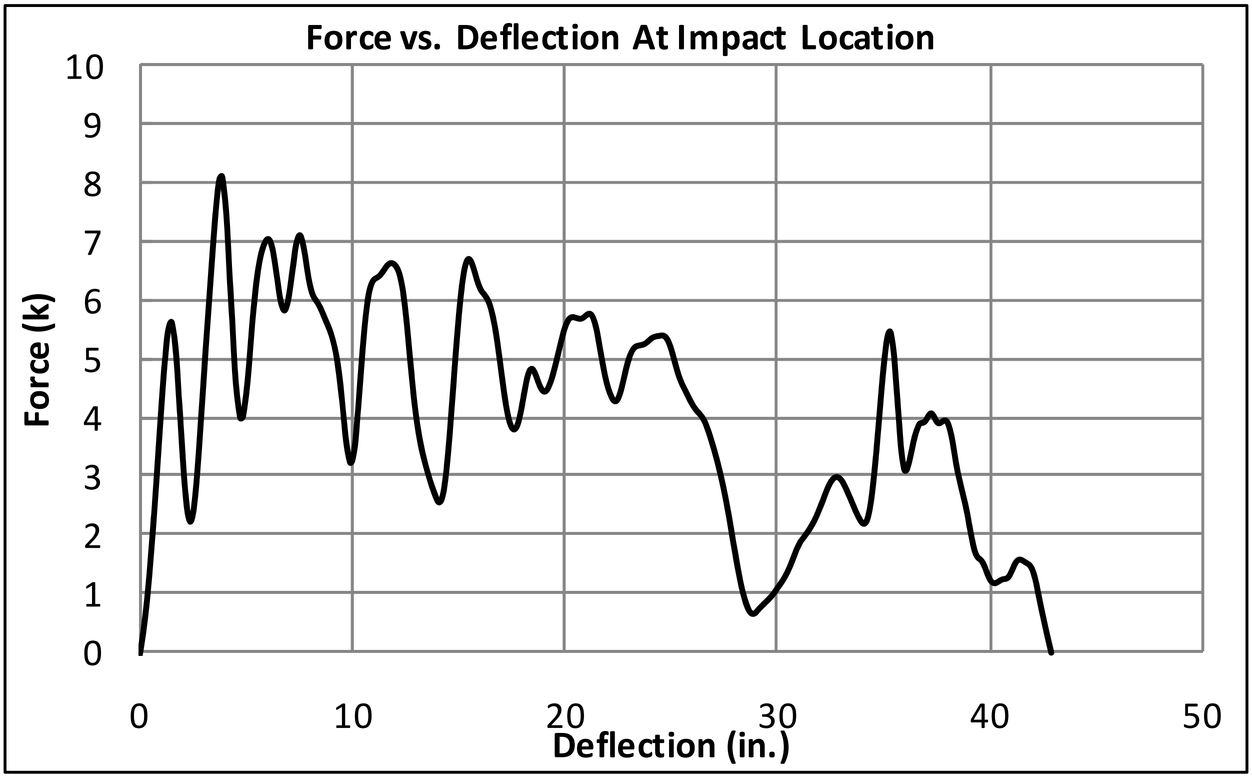

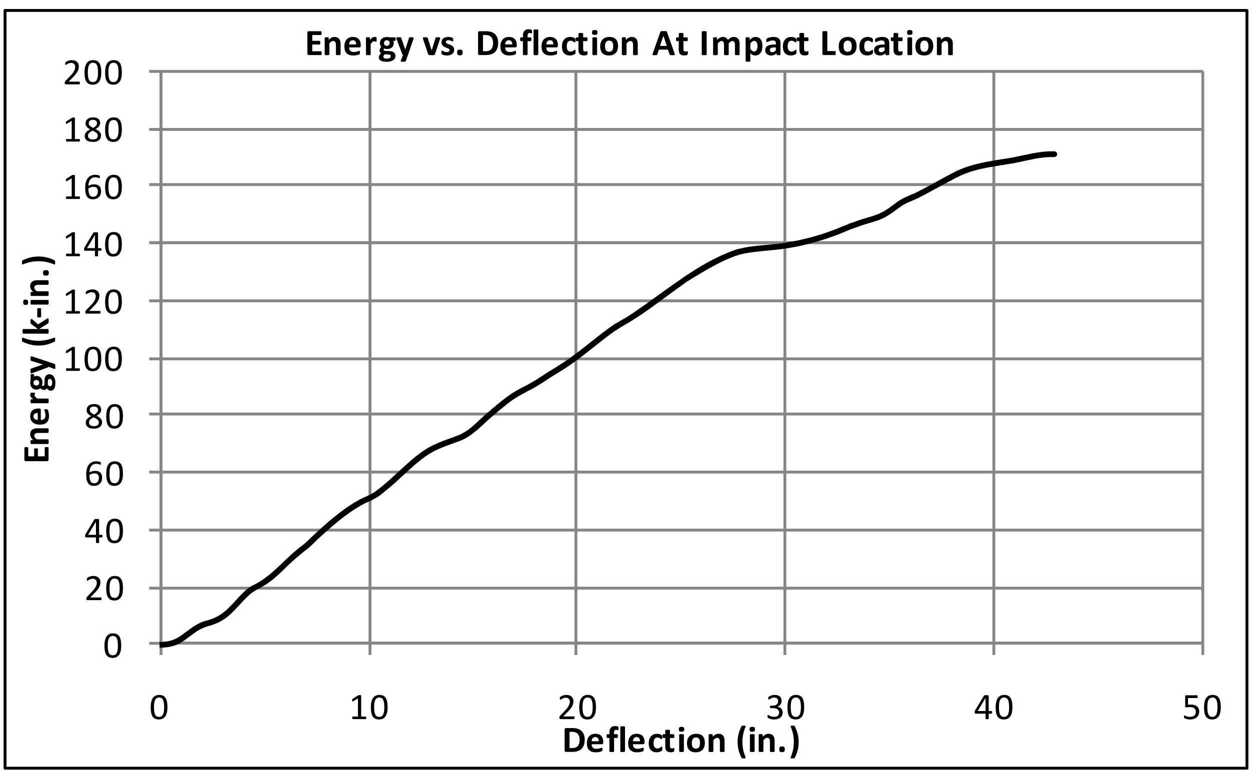

Figure 42. Transducer Data, Test No. MGSBRB-5 (EDR-3)

transmitted from the post into the deck was quite large and was believed to have the potential for damaging the bridge deck. Due to the flexible nature of the rail, the load would be localized to posts near the point of impact, rather than distributed to a larger number of posts as with a stiffer rail. To distribute the load through a larger portion of the deck, larger and more expensive post-to-deck connections would be required. For these reasons, the strong-post system was abandoned in favor of a weak-post bridge rail.

4.4 Weak-Post Bogie Test Results

Two bogie tests were performed on the weak-post concepts produced during preliminary design. These tests were performed with the concepts mounted on a 6-ft long x 4-ft wide x 8-in. thick (1.83-m x 1.22-m x 203-mm) test section of bridge deck which was constructed following the results of the strong-post bogie tests. Results for these tests are shown in the following sections.

4.4.1 Test No. MGSBRB-6

The first test on the weak-post concept utilized an S3x5.7 (S76x8.5) post housed in a ¼-in. (6.4-mm) thick bent-plate socket. Two ¾-in. (19.1-mm) threaded rods were embedded in epoxy in the side of the bridge deck and used to fasten the socket to the deck. A strap was welded across the bottom of the socket to hold the post in place, and holes were left around the edge of the strap to prevent water retention.

In the test, the bogie struck the post perpendicular to its strong axis with an initial velocity of 22.0 mph (35.3 km/h). As the post rotated, it bent the socket about an axis through the location of the threaded rods. Simultaneously, the socket was stretched away from the bridge deck due to movement of the post. This socket deformation caused bending in the threaded rods, one of which fractured approximately 0.08 seconds into the event. The second rod did not fracture, but initiated a shear failure in the socket, tearing out a section to the exterior of the rod.

Only a small amount of yielding occurred at the base of the post where it contacted the upper edge of the socket. Thus, most of the energy absorption was due to socket deformation. Accelerometer data for the event indicated the force of resistance generated was lower than desired. Some spalling occurred at the lower edge of the concrete test deck. Photographs of the system damage are shown in Figure 43. Force vs. deflection and energy vs. deflection curves for test no. MGSBRB-6 are shown in Figure 44.

4.4.2 Test No. MGSBRB-7

Following the failure of the side-anchored weak-post concept, a new side-mounted, top-anchored apparatus was developed that anchored to the deck with a vertical, through-deck bolt. This concept again utilized a socket to house the post, with a bolt passed through the web of the post and the socket to support the post and rail. Post standoff tabs were welded to the side of the post to help snug the post within the socket. A steel strap was welded to the top of the socket and reinforced with a gusset, and a steel angle-section was bolted to the bottom of the socket. This angle was also gusseted, and a bolt was passed through the top strap, the deck, and the bottom angle.

In this test, the bogie struck the post perpendicular to its strong axis with an initial velocity of 15.0 mph (24.2 km/h). Almost immediately, the concrete failed from the shear load, and large pieces were fractured off the edge. The longitudinal reinforcement in the deck prevented the bolt from pulling out completely, but it did not support the bolt under loading as the post had already rotated sufficiently and allowed the bogie to override the post. Photographs of the system damage are shown in Figure 45. Force vs. deflection and energy vs. deflection curves for test MGSBRB-7 are shown in Figure 46.

Figure 43. System Damage, Test No. MGSBRB-6

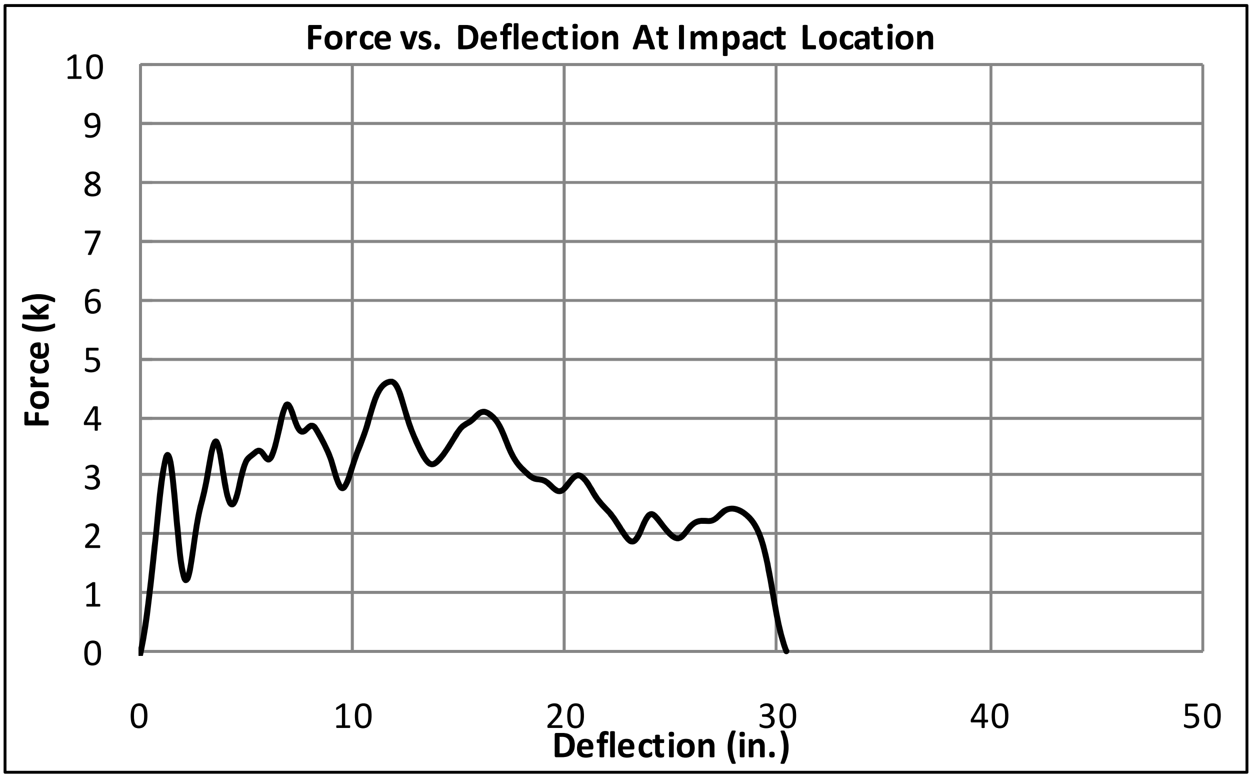

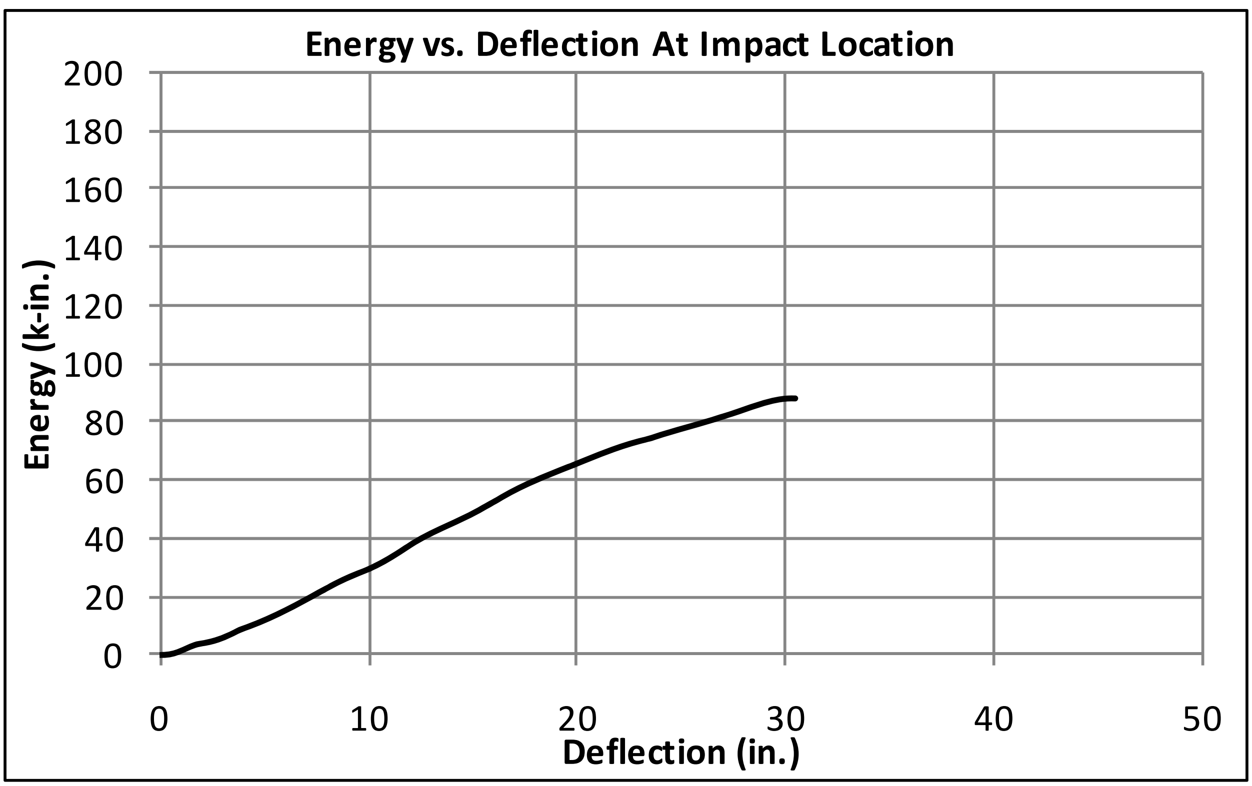

Figure 44. Transducer Data, Test No. MGSBRB-6 (EDR-3)

Figure 45. System Damage, Test No. MGSBRB-7

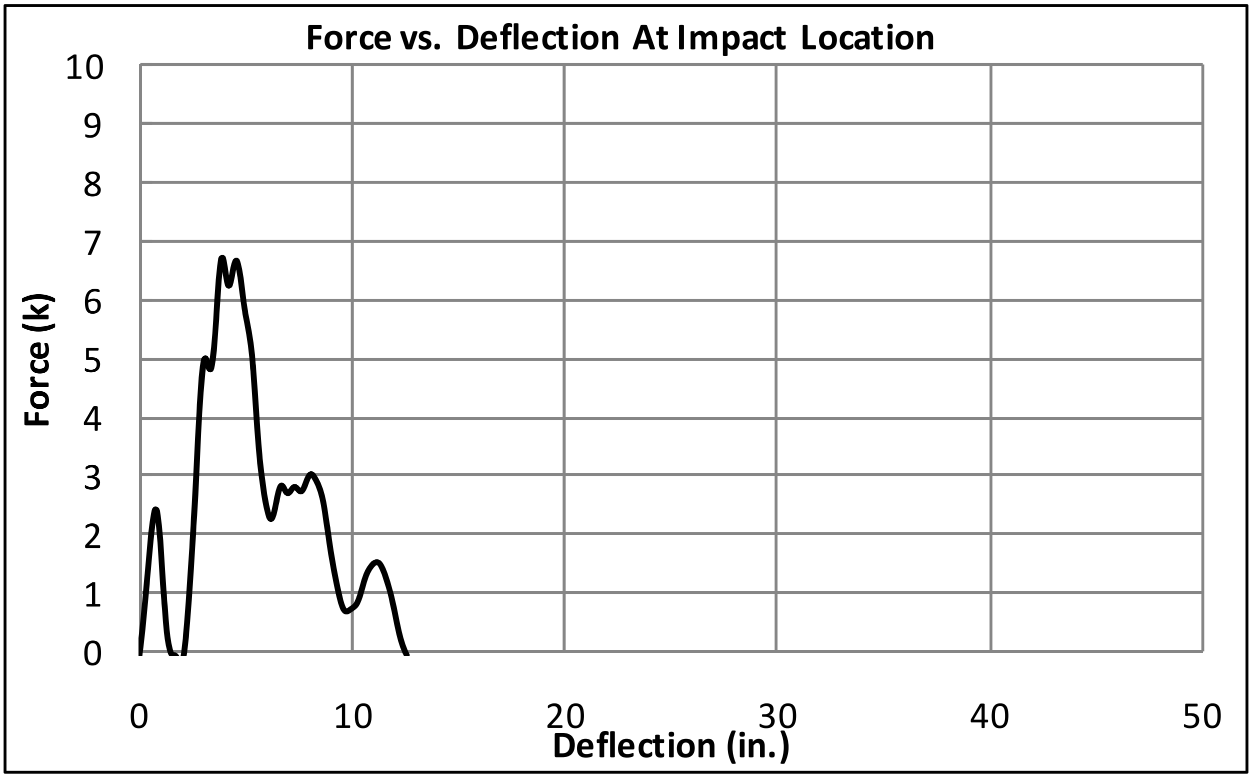

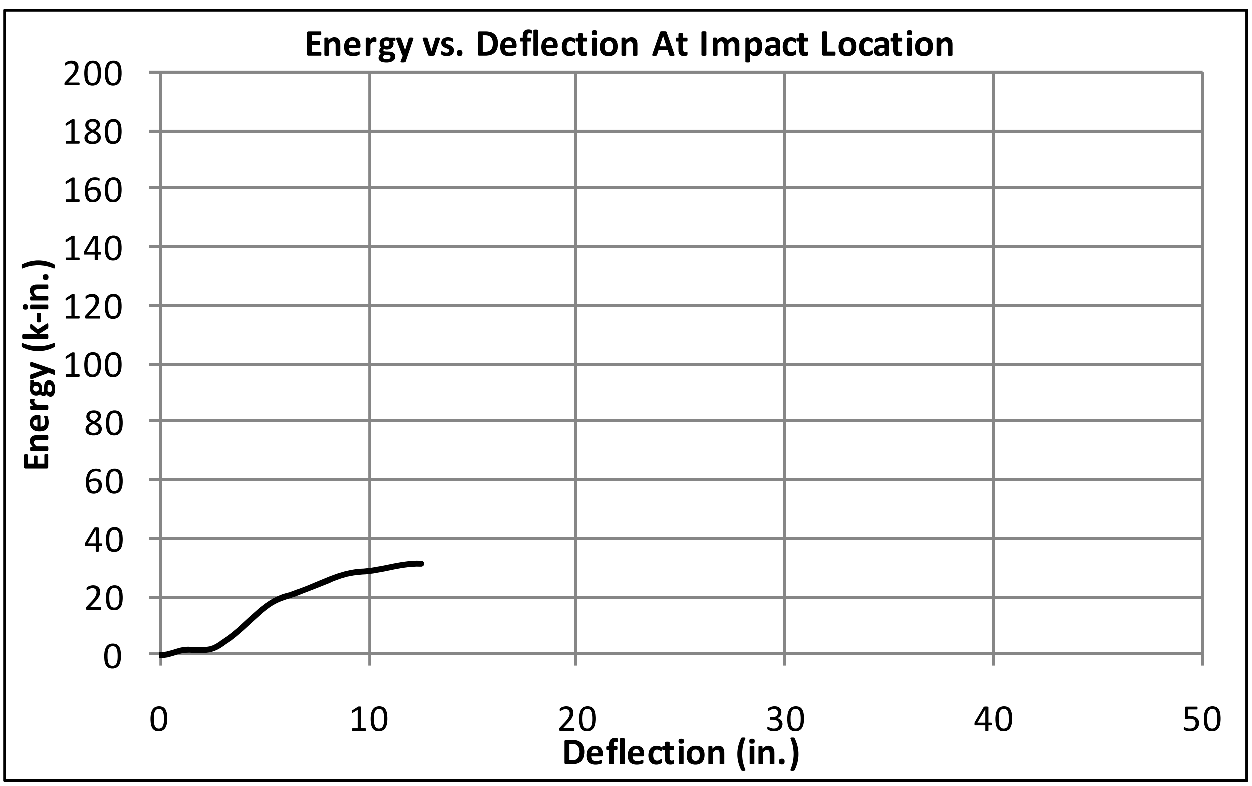

Figure 46. Transducer Data, Test No. MGSBRB-7 (EDR-3)

4.4.3 Discussion of Weak-Post Bogie Test Results

Despite the failed bogie tests, it was believed that the weak-post option represented the best design due to its inherently lower deck loads. It was also believed that a weak-post system would cause fewer wheel snag problems commonly seen in strong-post systems, and BARRIER VII computer simulation showed that the weak-post system with half-post spacing provided stiffness and strength very similar to the standard MGS guardrail and should not require a transition at the interface between the two systems.

Failure of the side-mounted concept was caused by insufficient moment arm of the anchors and flexibility of the socket. For slab-on-girder bridges, a deck thickness of approximately 8 in. (203 mm) is typical, and thicknesses of decks used on prestressed bridges can be even less. When considering concrete clear cover requirements, upper reinforcement of the deck, and tolerance for drilling holes to avoid damaging deck reinforcement, the maximum moment arm of the threaded rods about the base of the post is less than 4 in. (102 mm). This places the anchors under very large loads. Flexibility of the socket allowed bending to occur in the rods, which created high stresses that contributed to fracture. Significantly stiffening the side-mounted socket was considered expensive and might still result in rod fracture due to the small moment arm. Any rod fracture would be difficult and expensive to repair.

For these reasons, it was decided to use the side-mounted, top-anchored concept as the final design for the system. However, it was apparent that special reinforcement must be designed into the concrete bridge deck for the connection to have sufficient strength to resist loads from the post while not intruding significantly onto the deck. Thus, an effort to develop a connection that could be retrofitted to existing decks or attached to culvert headwalls was discontinued.

4.5 Static Testing

The connection between the bridge rail and posts was required to meet the design goals discussed in Section 3.2. To determine the desired force level at which the connection would fail, the W-beam guardrail was analyzed as a simply supported beam. The force at the center span of a simply supported beam for a given deflection can be found with the following equation:

$$P = \frac{48EI\Delta}{L^3}$$

where P = downward force at center span
E = beam modulus of elasticity
Δ = deflection
I = moment of inertia
L = span length

It was assumed that friction and interlock with the vehicle would support the rail at one end of the span. At the other end of the span, an undeformed guardrail post would also support the rail. In the center, a bending post would apply a downward load on the rail. Thus, the span of the beam was two post spaces, or 75 in. (1,905 mm). A sketch of the analysis layout is shown in Figure 47.

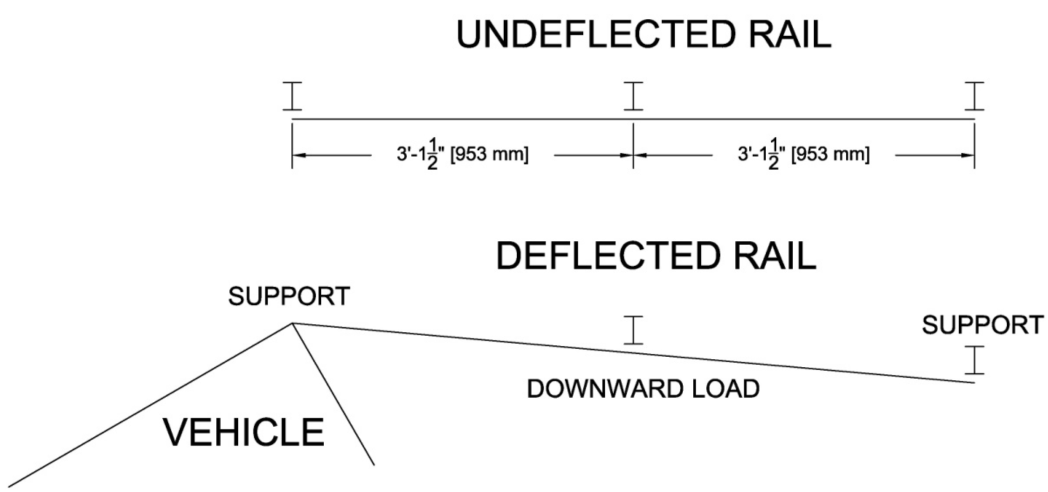

Figure 47. Post-to-Rail Connection Analysis Layout

To prevent the rail from being pulled under the vehicle, the downward force applied by the bending post must be limited. An acceptable angle of rotation of the post at which the post-to-rail connection would release was estimated. This angle was set to 10 degrees to ensure that the rail would be released before being pulled down significantly. If the post rotates perfectly about the base of the bridge deck, this corresponds to lateral and vertical deflections of approximately 4⅜ in. (111 mm) and ⅜ in. (10 mm), respectively. A sketch of the assumed release condition is shown in Figure 48.

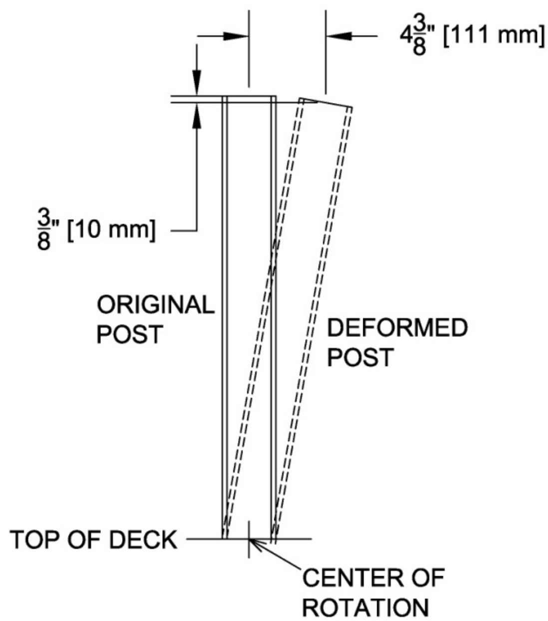

Figure 48. Post-to-Rail Connection Assumed Release Conditions

For simplicity, it was assumed that the W-beam rail would not twist during post rotation. Thus, the rail would bend about its strong axis. The strong-axis moment of inertia for 12-gauge (2.66-mm thick) W-beam rail is 30.5 in.^{4} (1.27x10^7 mm^4). A modulus of elasticity of steel of 29,000 ksi (200 GPa) was used in the calculation. Finally, a downward deflection of ⅜ in. (10 mm) and span length of 75 in. (1,905 mm) were also used, as discussed previously. With these values, the equation produced a downward force of 37.7 kips (167.8 kN).

The downward force can then be resolved into an axial force parallel to the post-to-rail connection bolt and a shear force along the post itself using trigonometric identities. It was assumed that all shear force is sustained by friction between the bottom of the rail and the post.

The axial force component therefore provides an upper limit to post-to-rail connection failure force. For a post rotation angle of 10 degrees, this analysis yielded an axial force component of 6.5 kips (28.9 kN). This load would act to pull the post bolt through the W-beam rail. Thus, this force represented the maximum acceptable axial failure force of the post-to-rail connection.

Three static tests were performed on the connection between the W-beam rail and system posts. All three tests were performed on variations of the standard G2 connection, which utilized a bolt, a square washer, and a nut. Bolt diameters of $^5/_{16}$ in. (7.9 mm) and ⅜ in. (9.5 in.) were tested under conditions which represented the extreme limits of system performance. Two tests investigated the maximum load the connection would develop, which would occur when the bolt and washer were positioned at the end of the guardrail slot at a splice location (i.e. 2 layers of guardrail). For one test, the bolt was positioned at the center of the guardrail slot of a single layer of guardrail to determine a lower bound for expected connection failure force. For all tests, the bolt was pulled at an angle normal to the W-beam, which should produce the maximum connection force, whereas a load applied at an angle would create bending stresses in the bolt and lead to fracture under a lower axial load. As such, the lower bound test would not determine the true minimum failure force. However, it was believed that this would provide a useful approximation for the minimum force. The static testing matrix and setup are shown in Figure 49. Complete drawings for the static tests and jig are available in the project documentation but are not included in the report

4.5.1 Static Testing Equipment and Instrumentation

Equipment and instrumentation utilized to collect and record data during the static tests included a winch, a test jig, load cells, and digital video and still cameras.

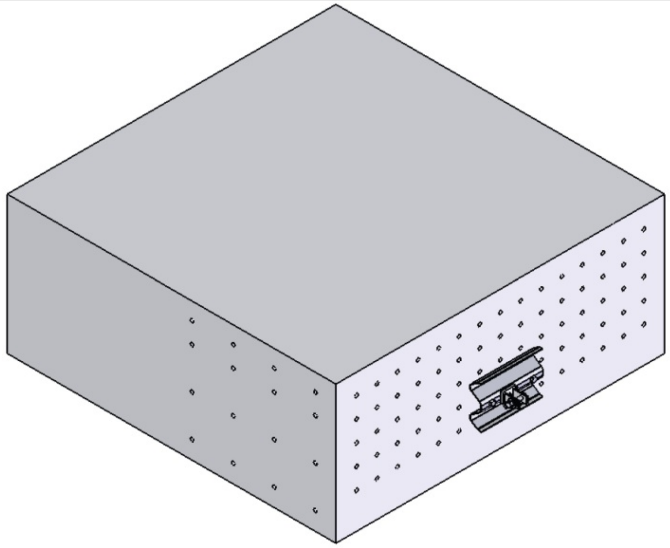

Static Test Matrix			
Test No.	Tested Bolt Diameter	Layers of Guardrail	Position of Tested Bolt in Slot
MGSBRS–1	5/16”	2	Edge of Slot
MGSBRS–2	5/16”	1	Center of Slot
MGSBRS–3	3/8”	2	Edge of Slot

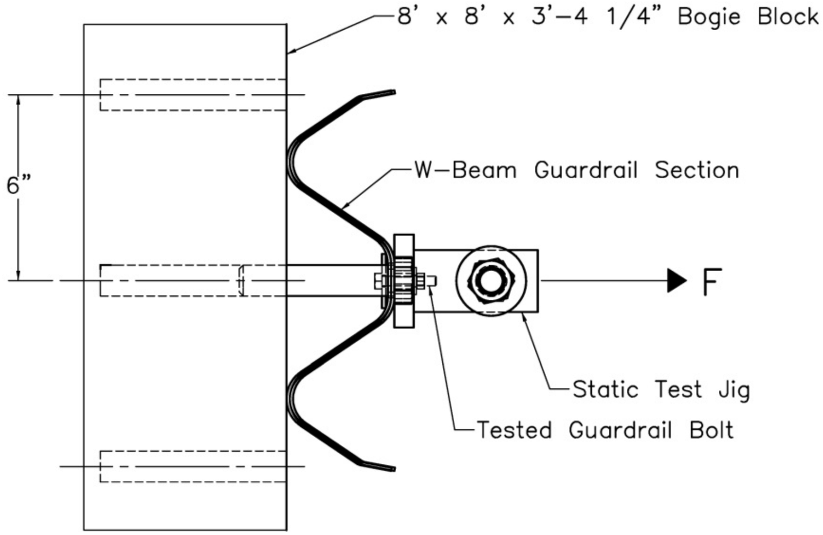

SCALE 1:5

NOTES: (1) Angle Between Winch Cable and Bogie Block is 90 Degrees.

(2) The Winch is Mounted at the Height of the Center of the W–Beam on the Bogie Block, 18” Above the Ground.

Midwest Roadside Safety Facility	MGS Bridge Rail Static Testing Matrix		SHEET: 1 of 9 DATE: 8/15/2008 DRAWN BY: CJS
	DWG. NAME. MGS Bridge Rail Static Test R2	SCALE: 1:32 UNITS: Inches	REV. BY: KAP

Figure 49. Static Test Matrix and Setup, Test Nos. MGSBRS-1 through MGSBRS-3

4.5.1.1 Winch

A winch, mounted on the rear of a pickup truck, was used to apply load to the connection. The winch was a Dayton 4YJ76 Electric Winch, and its cable was passed through a pulley and secured to the truck, creating a 2:1 pulley system for applying load to the connection. To further minimize the load rate, the winch was completely unwound at the start of testing to minimize the effective spindle size. A picture of the winch is shown in Figure 50.

4.5.1.2 Test Jig

For static post-to-rail connection testing, W-beam guardrail sections were bolted to a rigid reinforced concrete block such that the traffic side of the beam faced the block. The bolt that connected the post to the rail was then passed through the slot in the guardrail and secured with a standard 1¾-in. x 1¾-in. ⅛-in. (44-mm x 44-mm x 3.2-mm) square washer on the traffic side of the beam. The opposite end of the bolt was passed through a test jig that consisted of a base plate, two steel straps welded perpendicular to the base plate, and a bolt that passed through both straps. A picture of the test jig is shown in Figure 50.

4.5.1.3 Load Cells

Two load cells were installed in series with the cable and test jig and were used to measure the force sustained by the post-to-rail connection. A 50-kip (224-kN) load cell was placed outside the pulley system next to the test jig, while a 10-kip (44-kN) load cell was placed in the 2:1 pulley system, attached beneath the winch on the truck. Thus, the force measured by the 10-kip (44-kN) load cell was one-half of the force applied to the bolt.

The 50-kip (224-kN) load cell had a sample rate of 1,000 Hz, a 10V input voltage, a gain factor of 300, and a calibration factor of 2.995 mV/V. The 10-kip (44-kN) load cell had a sample rate of 1,000 Hz, a 10V input voltage, a gain factor of 400, and a calibration factor of 2.1524 mV/V. Pictures of both load cells are shown in Figure 51.

Figure 50. Static Testing Winch (Top) and Test Jig (Bottom)

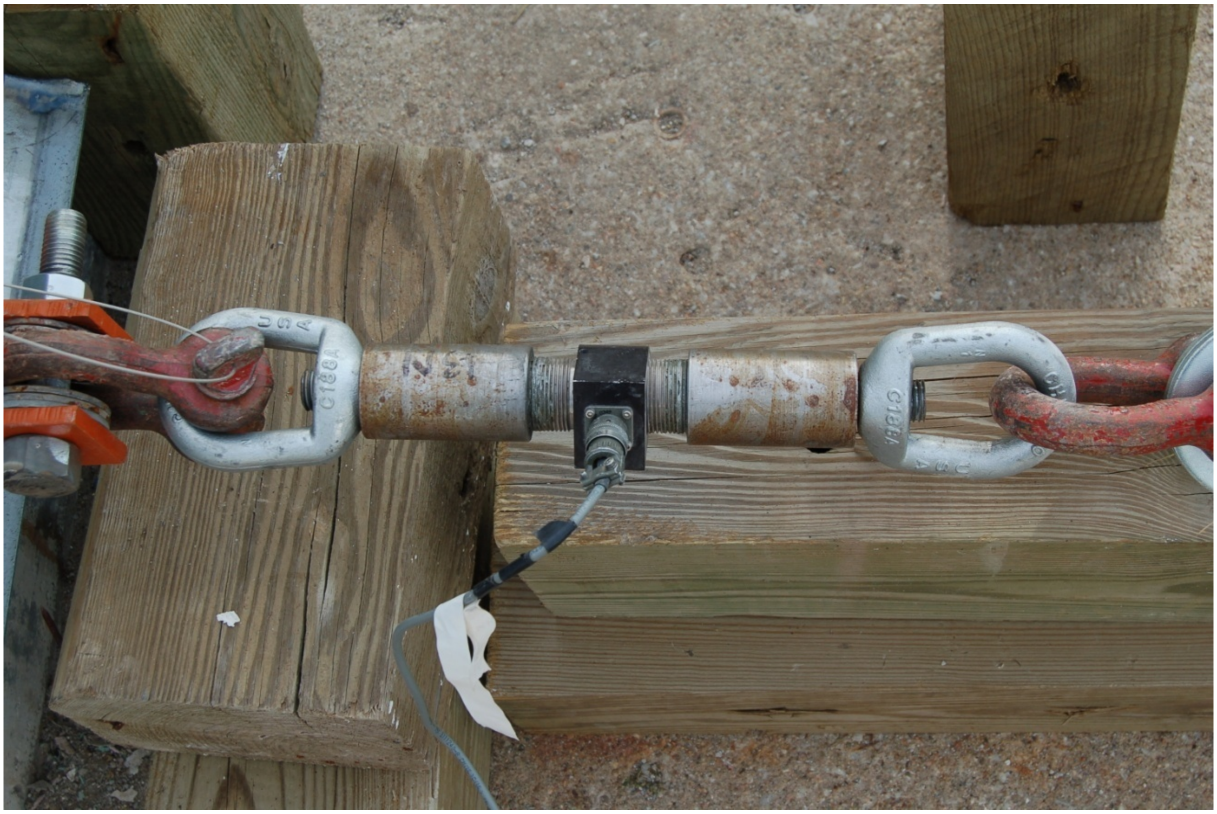

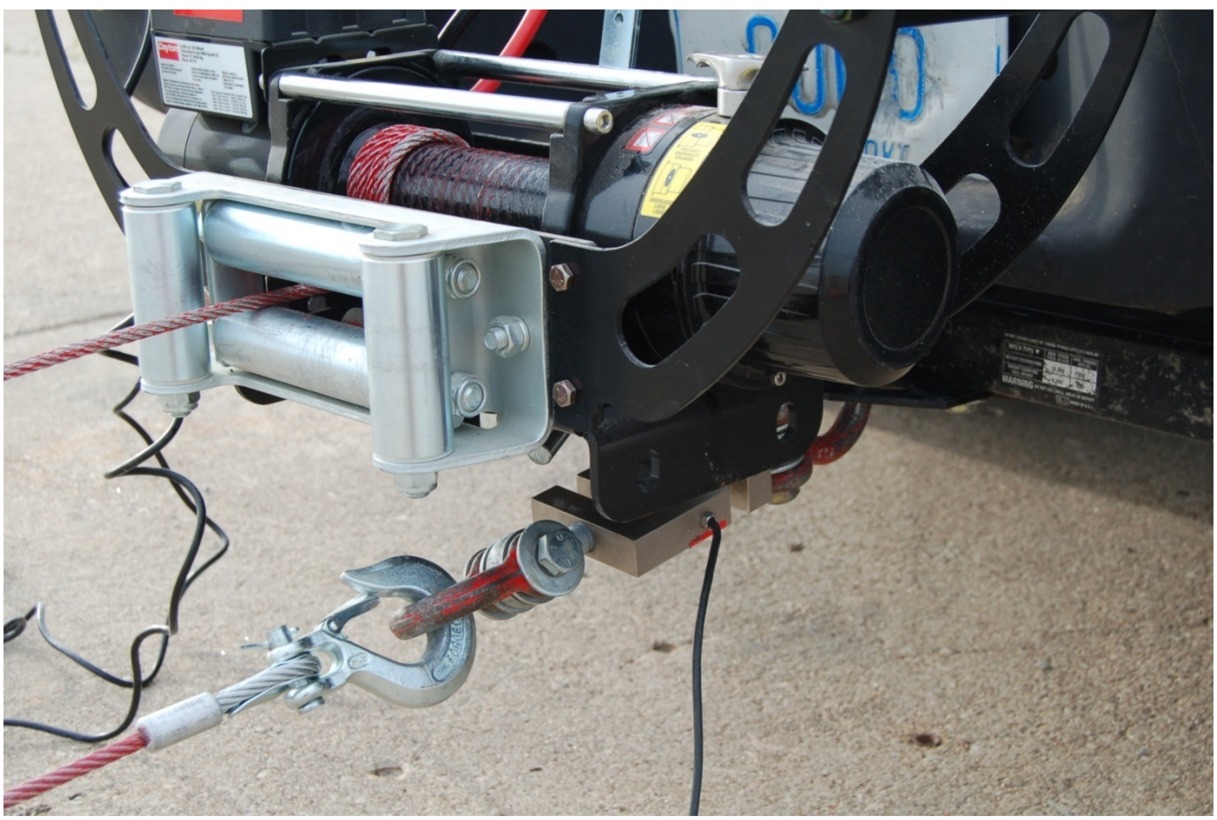

Figure 51. 50-kip (Top) and 10-kip (Bottom) Load Cells

4.5.2 End of Test Determination

For the static tests, an increasing force was applied to the post-to-rail connection until it failed and did not support any load. The test was deemed to be concluded when the bolt separated from the rail.

4.5.3 Data Processing

The electronic load cell data obtained in static testing was filtered using the SAE Class 60 Butterworth filter conforming to the SAE J211/1 specifications. Output voltage data was converted to force according to the system parameters of each load cell. A customized Microsoft Excel worksheet was used to analyze and plot the load cell data.

4.6 Static Post-to-Rail Test Results

Three static tests were performed on different configurations of the post-to-rail connection to determine its performance limits. The results of those tests are presented in the following sections, and a summary is shown Table 2.

Table 2. Static Testing Results

Test No.	Date	Concept	Bolt Diameter	Peak Force	Failure Type
MGSBRS-1	8/13/2008	G2 Post-to-Rail Connection	5/16 in. (7.9 mm)	4.3 kips (18.7 kN)	Bolt Fracture
MGSBRS-2	8/13/2008	G2 Post-to-Rail Connection	5/16 in. (7.9 mm)	2.8 kips (12.6 kN)	Washer Pull-Through
MGSBRS-3	8/13/2008	G2 Post-to-Rail Connection	3/8 in. (9.5 mm)	5.8 kips (25.7 kN)	Bolt Pull-Through

4.6.1 Test No. MGSBRS-1

The first static test featured a $^{5}/_{16}$-in. (7.9-mm) diameter, ASTM A307 Grade A bolt which was passed through two layers of 12-gauge (2.66-mm thick) W-beam guardrail. The head of the bolt was secured with a standard 1¾-in. x 1¾-in. x ⅛-in. (44-mm x 44-mm x 3.2-mm) square washer on the front face of the W-beam and a $^{5}/_{16}$-in. (7.9-mm) inner diameter round washer and nut on the side of the jig. The round washer was required as the hole in the test jig was sized to accommodate a ⅜-in. (9.5-mm) diameter bolt. For this test, the bolt was positioned at the edge of the slot to obtain the peak load that the connection could sustain by restraining the bending of the washer.

During the test, the $^{5}/_{16}$-in. (7.9-mm) diameter bolt fractured in tension with minimal deformation prior to failure. While there was some deformation in the square washer, no local deformation was present around the guardrail slot. The 50-kip (224-kN) load cell measured a maximum force of 4.2 kips (18.7 kN), while the 10-kip (44-kN) load cell measured a maximum force, when doubled to account for the 2:1 pulley system, of 4.3 kips (19.3 kN). A graph of force vs. time is shown in Figure 52, and post-test photographs of the connection components for test no. MGSBRS-1 are shown in Figure 53.

The 50-kip (224-kN) load cell was damaged during test no. MGSBRS-1 and was removed from the test apparatus for the remaining static tests.

4.6.2 Test No. MGSBRS-2

The second static test was performed on a $^{5}/_{16}$-in. (7.9-mm) diameter, ASTM A307 Grade A bolt that was passed through a single layer of 12-gauge (2.66-mm thick) W-beam. The bolt was positioned in the center of the guardrail slot, with the bolt head secured by a standard 1¾-in. x 1¾-in. x ⅛-in. (44-mm x 44-mm x 3.2-mm) square washer. A $^{5}/_{16}$-in. (7.9-mm) inner diameter round washer and nut were used to attach the bolt to the test jig. The round washer was required as the hole in the test jig was sized to accommodate a ⅜-in. (9.5-mm) diameter bolt. This test was intended to determine the minimum load that would cause the post-to-rail connection to fail. During the test, the square washer bent and pulled through the guardrail slot. The guardrail slot was deformed during the pull-through process. The measured peak force, when doubled to

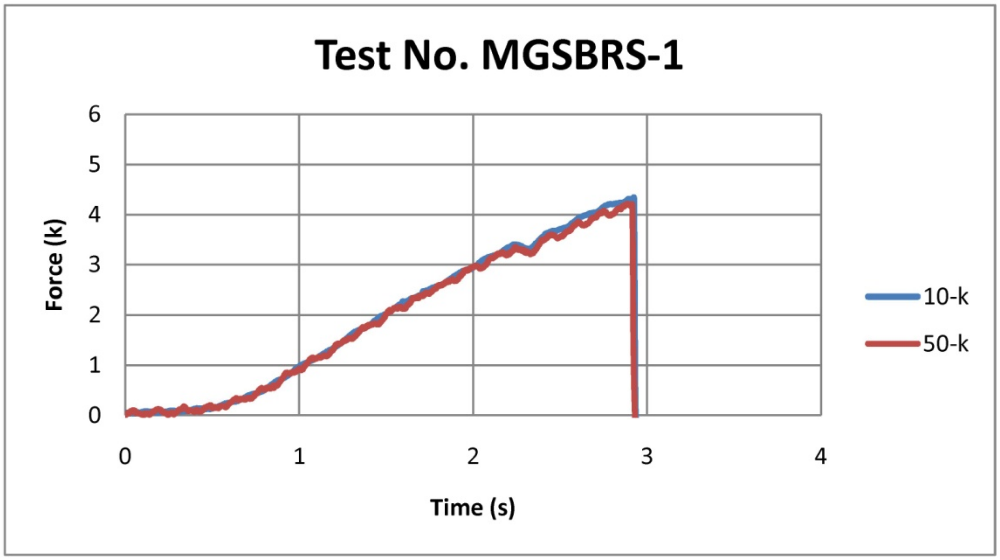

Figure 52. Load Cell Data, Test No. MGSBRS-1

Figure 53. System Damage, Test No. MGSBRS-1

account for the 2:1 pulley system, was 2.8 kips (12.6 kN). A graph of force vs. time is shown in Figure 54, and post-test photographs of the connection components for test no. MGSBRS-2 are shown in Figure 55.

4.6.3 Test No. MGSBRS-3

The final static test conducted was a repeat of the first test with a ⅜-in. (9.5-mm) diameter, ASTM A307 Grade A bolt. This bolt was secured to the guardrail using a standard 1¾-in. x 1¾-in. x ⅛-in. (44-mm x 44-mm x 3.2-mm) square washer. A ⅜-in. (9.5-mm) nut was used to secure the bolt to the test jig. The bolt was positioned at the edge of the guardrail slot to find the maximum expected load with this connection configuration.

During the test, the square washer bent significantly; however, it did not pass through the guardrail, and the slots in the rail did not deform. The connection failed as the bolt head pulled through the washer, leaving a hexagonal hole behind. This failure occurred at a measured peak force, when doubled to account for the 2:1 pulley system, of 5.8 kips (25.7 kN). A graph of force vs. time is shown in Figure 56, and post-test photographs of the connection components for test no. MGSBRS-3 are shown in Figure 57.

4.6.4 Discussion of Static Testing Results

Following the static testing, it was decided to use the tested concept with a $^5\!/_{16}$-in. (7.9-mm) diameter, ASTM A307 Grade A bolt. Worst-case loading conditions led to a maximum failure load of less than 4.5 kips (20.0 kN), at which point the bolt fractured. This relatively low failure load would ensure that the rail would be released from the post, thus preventing it from being pulled under the vehicle.

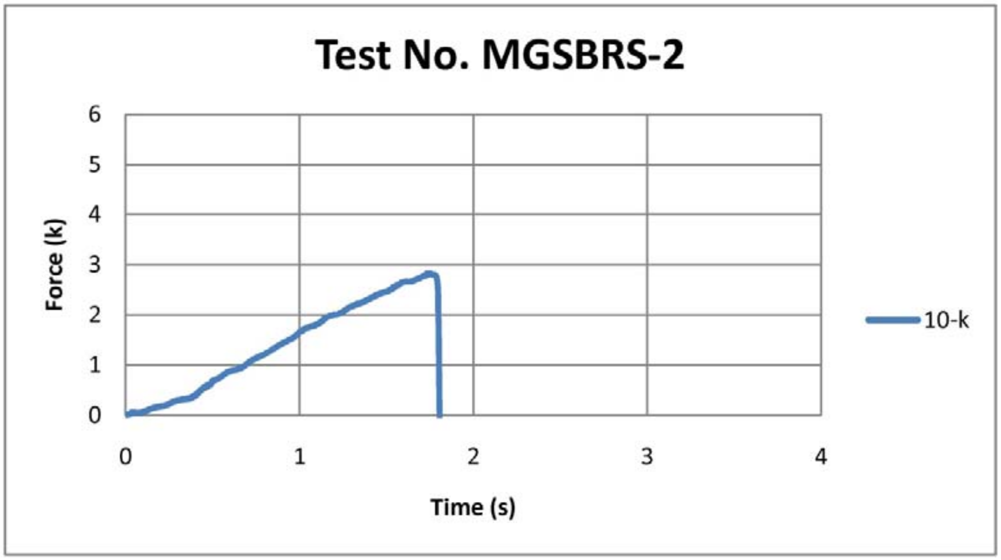

Figure 54. Load Cell Data, Test No. MGSBRS-2

Figure 55. System Damage, Test No. MGSBRS-2

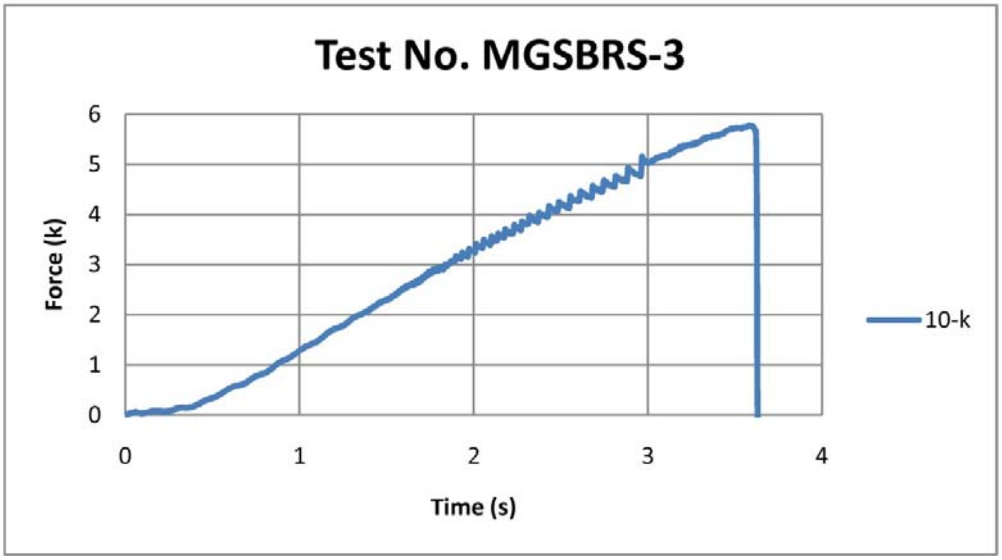

Figure 56. Load Cell Data, Test No. MGSBRS-3

Figure 57. System Damage, Test No. MGSBRS-3

While the connection showed the ability to fail under a load of less than 3.0 kips (13.4 kN), it was believed that this would not cause the rail to release prematurely, as was seen in previous weak-post W-beam guardrail testing [47]. Whereas the post spacing was 12 ft - 6 in. (3.81 m) in these previous guardrail tests, the new bridge rail utilized a post spacing of 3 ft - 1½ in. (0.95 m). Thus, the guardrail would be supported in four times as many locations, which decreased the likelihood that the rail would drop in front of the vehicle.

Recall that testing of weak-post W-beam guardrail exhibited rail rupture [46-48]. The rupture was attributed to small cuts or nicks in the guardrail produced by post flanges at non-splice posts. Two different options were considered to eliminate this potential problem. First, the splices could be moved to midspan locations between posts, and standard 12-in. (305-mm) long, W-beam backup plates could be placed between the bridge rail and each post. This would require specially punching the guardrail, with slots located every 1 ft - 6¾ in. (477 mm). Alternatively, the splices could be placed at the locations of the post, with a backup plate also placed behind the rail at every post. This would require installing a backup plate at splice locations. As the standard 12-in. (305-mm) long, W-beam backup plate does not fit between the splice bolts, 6-in. (152-mm) long backup plates would be used instead.

It was decided to place splices at posts and use 6-in. (152-mm) long, W-beam backup plates. This option was believed to be the most economical because it did not require special guardrail sections. For simplicity of construction, the same 6-in. (152-mm) long backup plate was used at both splice and non-splice locations. For the full-scale test, backup plates were created by cutting 3 in. (76 mm) of material off each end of standard backup plates, whereas for field applications the backup plate would be ordered to the correct length.

5 LS-DYNA SIMULATION

5.1 Introduction and Purpose

A finite element model of the side-mounted tubular post tear-out concept was created to better understand the behavior of this energy-absorbing post concept. The model was created with LS-DYNA software [61]. A model of this post system was considered important for future development of energy-absorbing hinge systems. Additionally, a working model would be useful in the event that this energy-absorbing post concept was selected for the new barrier.

5.2 Description of Physical Test

Test no. MGSBRB-5 was performed on the side-mounted tubular post tear-out concept, previously discussed in Section 4.3.5. In this test, a bogie vehicle impacted a tubular post which was fastened to a mounting bracket with a bolt that passed through the post and both sides of the bracket. Upon impact, the post rotated, causing the bolt to tear through both side faces, as shown in Figure 41.

5.3 Description of Simulation

The LS-DYNA model incorporated four basic components and included the post, the tear-through bolt, the mounting bracket, and the bogie. The modeling approach for each of these components is presented in the following sections. The finite element model and a photograph of the physical test specimen are shown in Figure 58.

5.3.1 Post

The HSS6x4x⅛ (HSS152x102x3.2) post was modeled using 4-node shell elements. Three different parts were defined for the post that were merged using coincident nodes at the interfaces between parts. Separate parts were defined for regions where tearing would occur, and one part was defined for the remainder of the post and the post cap. Type 16 (fully-integrated)

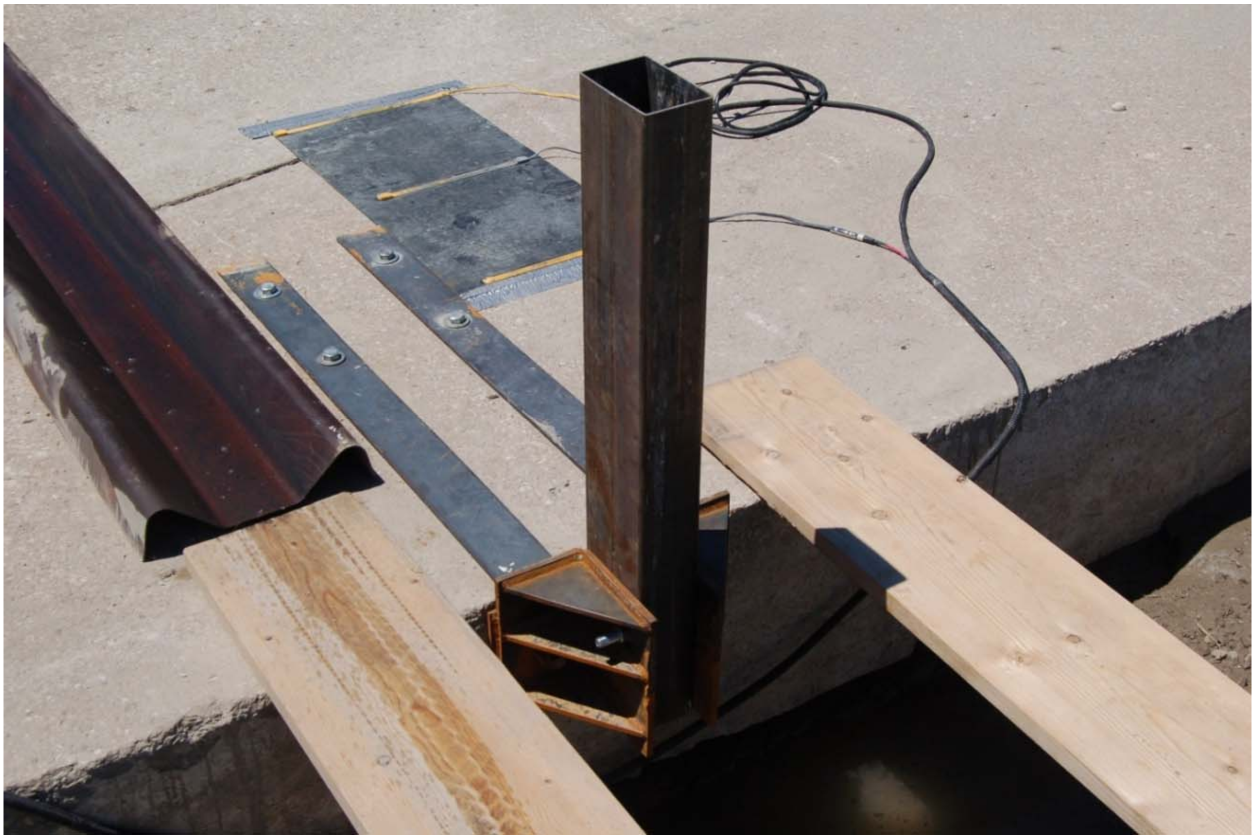

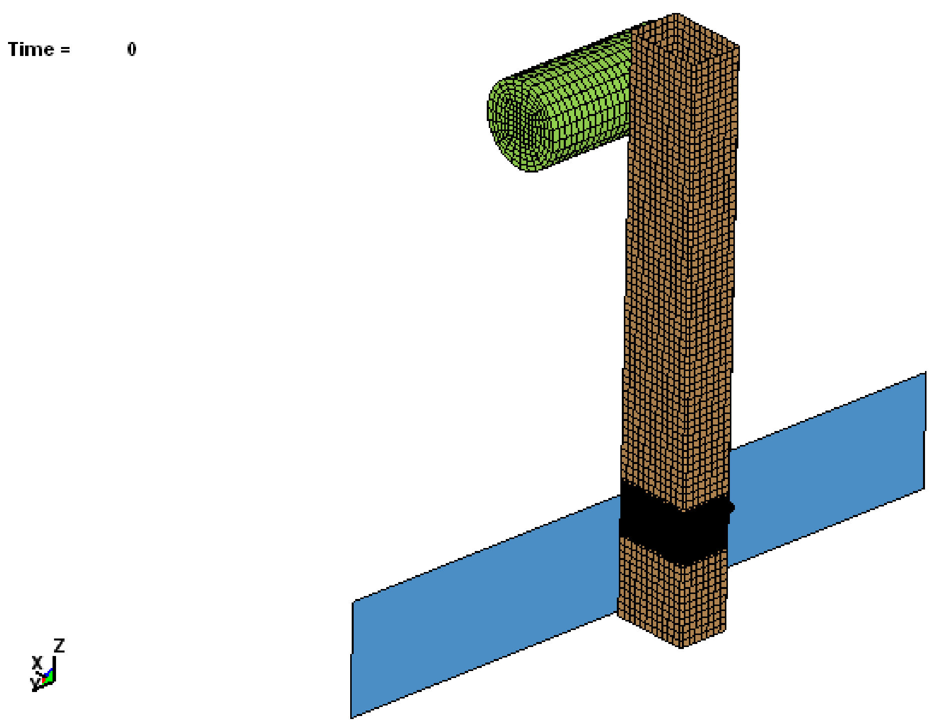

Figure 58. Physical and Simulated Models, Test No. MGSBRB-5

shell elements were used for the tear-out regions, and Type 2 (under-integrated) shell elements were used for the remainder of the post. A PIECEWISE_LINEAR_PLASTICITY material model, calibrated to a tensile test of a metal with similar yield and ultimate stresses, was used for the entire post. This material model used an effective plastic strain failure criterion, and elements were deleted upon reaching the limiting value of 1.2. The mesh was relatively fine in the tear-out regions, consisting of elements with approximately $^1/_{16}$-in. (1.6-mm) edge lengths, and relatively coarse elsewhere, consisting of elements with approximately ½-in. (12.7-mm) edge lengths. The grout used to prevent collapse of the bottom of the tube was not simulated, but its effects were retained through the bottom cap, which was not allowed to detach as its physical counterpart did during testing.

5.3.2 Bolt

A simulated bolt was created using rigid solid elements. Rigid material was deemed to be acceptable because no deformations were observed in the bolt after the test. As rigid elements do not add to computation cost, the bolt mesh was relatively fine. During the bogie test, the post was pushed away from the bridge deck, which made simulation of the ¼-in. (6.4-mm) diameter bolt, used for preventing motion toward the deck, unnecessary. Further, this bolt was located near the center of post rotation and was designed not to carry impact loads.

5.3.3 Mounting Bracket and Installation

A rigid wall was defined to simulate the edge of the deck and the base plate of the mounting bracket. The angles of the bracket were simulated using boundary conditions applied to the post. Displacement of the post nodes was constrained in the direction perpendicular to the angles (perpendicular to the path of the bogie) at three different heights of the post, which prevented lateral displacement of the post.

5.3.4 Bogie

The bogie was simulated using a rigid cylinder modeled with solid elements. The density of the material was adjusted to make the mass of the cylinder match the mass of the bogie.

5.3.5 Boundary and Initial Conditions

In addition to the boundary conditions applied to the post, boundary conditions were applied to the bolt elements to constrain all displacements and rotations. An initial velocity was applied to the simulated bogie to match that of the physical test.

5.3.6 Contact Definition

Contact was defined using the AUTOMATIC_SINGLE_SURFACE command. All parts of the post, the bolt, and the bogie head were included in the contact definition. The soft constraint formulation was used in defining forces between parts in contact. This formulation set contact stiffness as the maximum between the default penalty method stiffness and stiffness calculated using nodal masses and global time step size. Thus, this formulation caused contact stiffness to be at least that of the default penalty method.

5.4 Results

The simulation was performed for a duration of 100 milliseconds. Results are presented in the following sections. Data used to analyze the physical test was taken from accelerometers mounted near the center of gravity of the bogie vehicle. These accelerometers recorded raw accelerations, which were filtered using an SAE Class 60 Butterworth filter conforming to the SAE J211/1 specifications. This processed data was then used to develop force vs. deflection and energy vs. deflection criteria.

Simulated accelerations were taken from the center of gravity of the bogie impact head and were filtered using the same procedure as for the experimental data. Note that pitch and yaw angles of the bogie vehicle were both very low during physical testing. Therefore, the longitudinal accelerations measured on the physical bogie were not affected significantly by vehicle rotations. Hence, even though the accelerations were measured at different locations on the physical and simulated bogies, the results could still be reasonably compared and the longitudinal accelerations measured on the simulated impact head should accurately replicate accelerations measured at the center of the bogie during the crash test.

5.4.1 Qualitative Simulation Evaluation

The tear-out which occurred in the sides of the post during physical testing was due to a combination of Mode I and Mode III fracture. Sketches of both fracture modes are shown in Figure 59. Initially, the bolt bearing on the face of the post produced a local buckling of the face adjacent to the bolt. This local buckling produced out-of-plane tearing stresses on the post face and initiated tearing of the post. The out-of-plane (Mode III) tearing of the post then transitions as a crack opens up in advance of the bolt. As the bolt is pushed between the crack walls, it forces the crack to open wider and converts the crack growth from Mode III to Mode I. The cracking mode could convert back to Mode III any time the bolt came to bear directly on the crack tip itself. This condition can occur when the cracked portion of the post face buckles and the tension on the crack tip is reduced. Modes I and III occurred simultaneously in regions where a slight inward curve is visible on the face of the post, while Mode I failure occurred by itself in regions where this curve is absent.

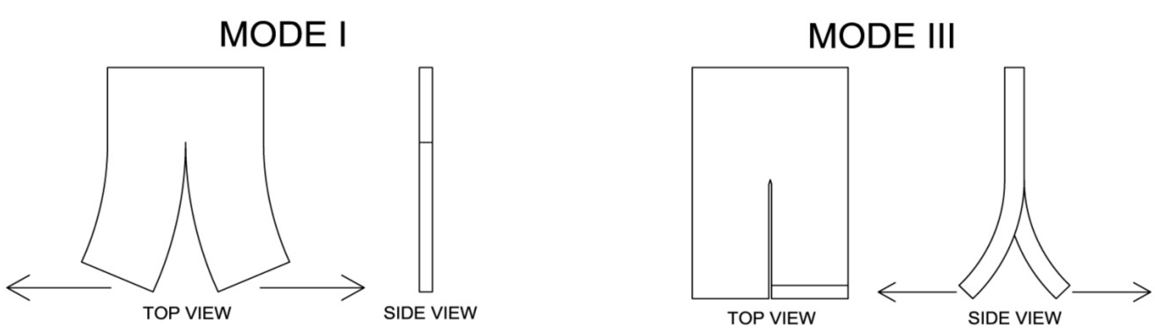

Figure 59. Mode I and Mode III Fracture

Unlike the physical test, the finite element material model was ideal and uniform throughout the post such that once tearing began, no variations in material were encountered which would cause the mechanism to change. Thus, similar tear-out continued through the entire depth of the post.

The out-of-plane nature of the tearing was exaggerated in the simulation when compared to the test. This behavior was to be expected, as the model discretized a continuous system. Whereas the physical model could deform at an infinite number of locations, the finite element model could only deform at each node. Thus, fewer opportunities for deformation existed. Extremely large, very localized strains caused failure in the physical test, whereas in the model these strains had to occur over a larger area (each element), which resulted in this behavior. Sequential images of the simulation are shown in Figures 60 through 63, and post-test photographs and simulation pictures of the post are shown in Figures 64 and 65.

5.4.2 Quantitative Simulation Evaluation

The finite element simulation of test no. MGSBRB-5 produced results that were substantially in agreement with the physical test data. The simulation produced smoother data without the larger variations seen in physical testing. This smoothness was due to the uniformity of the simulated material.

Results for the simulation were compared to the physical test using several graphs used to analyze results of bogie testing. These graphs included force vs. displacement, energy vs. displacement, bogie velocity vs. time, and post deflection vs. time. Graphs comparing the simulation data to that obtained from the EDR-3 and EDR-4 accelerometers used in physical testing are shown in Figures 66 and 67. As can be seen in the graphs, the results of the simulation closely matched the data taken from the EDR-4 and were in reasonable agreement with the data taken from the EDR-3.

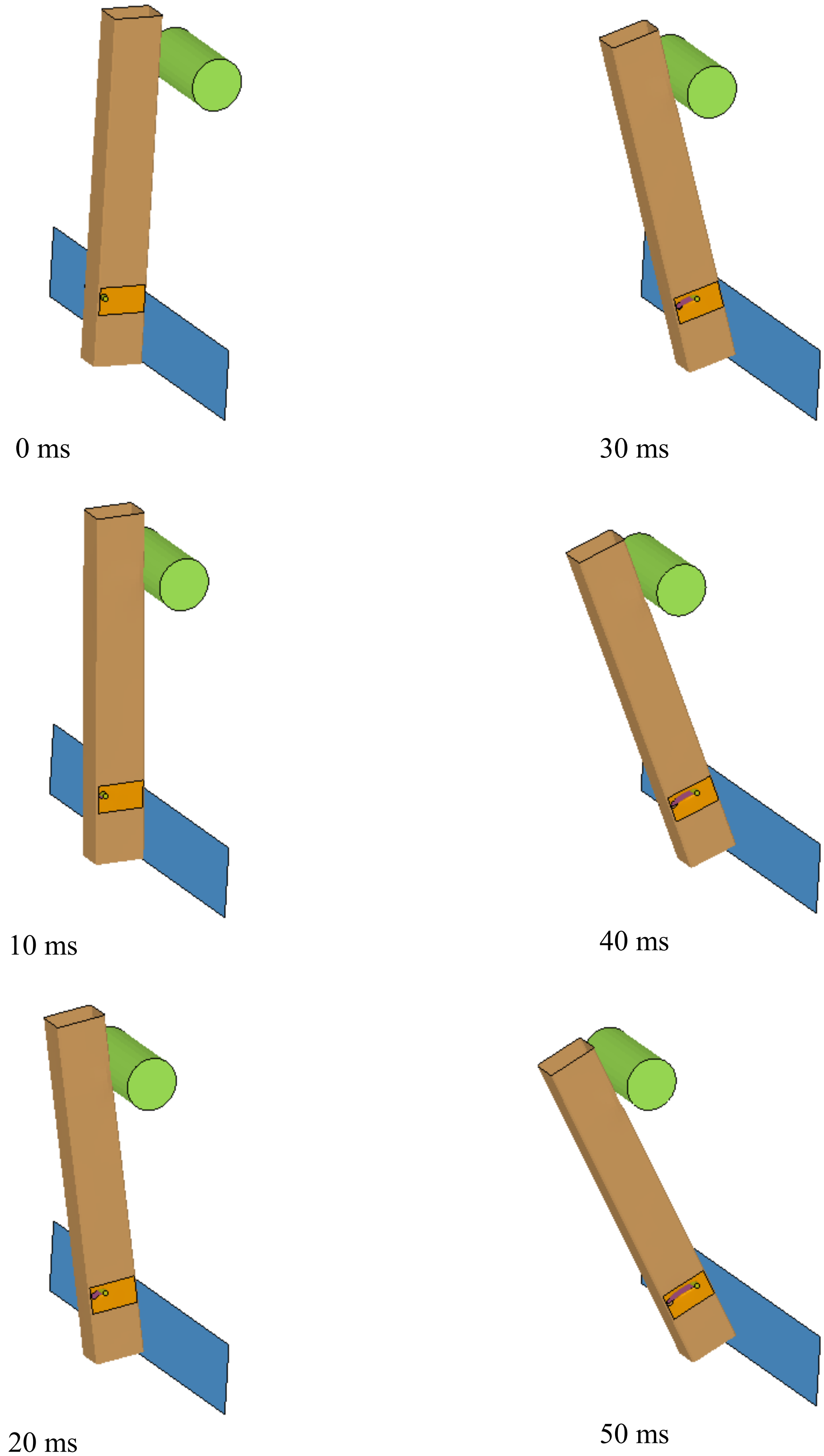

Figure 60. Sequential Pictures, Simulation of Test No. MGSBRB-5

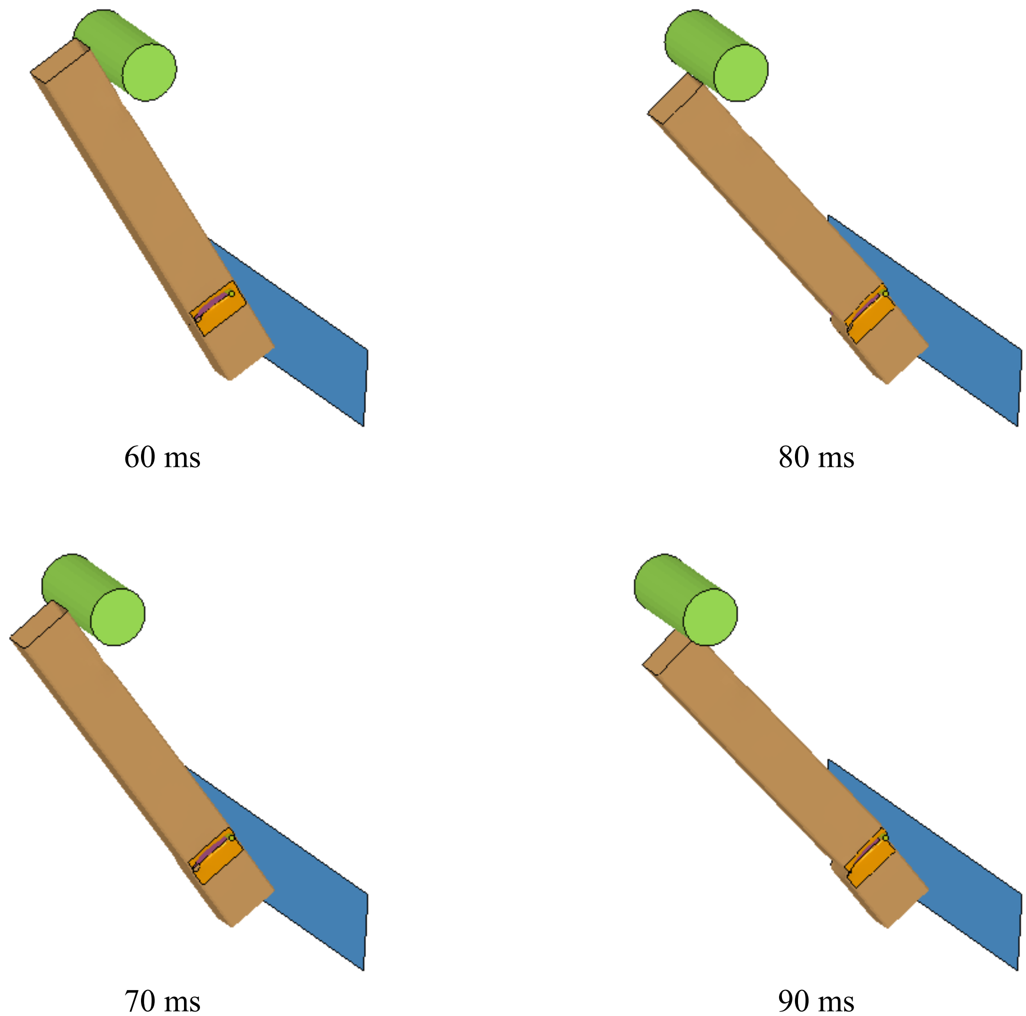

Figure 61. Sequential Pictures, Simulation of Test No. MGSBRB-5

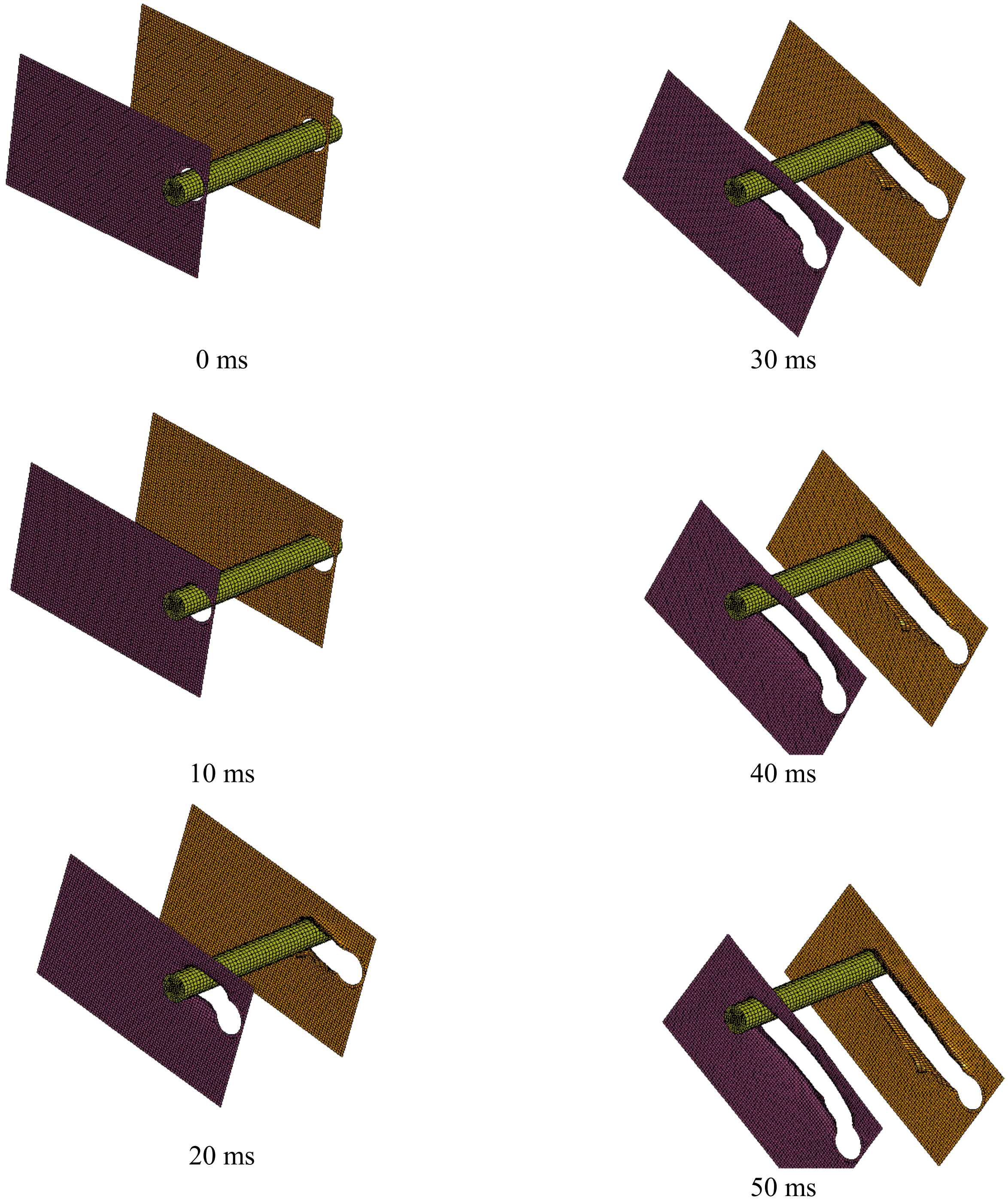

Figure 62. Sequential Pictures, Simulation of Test No. MGSBRB-5

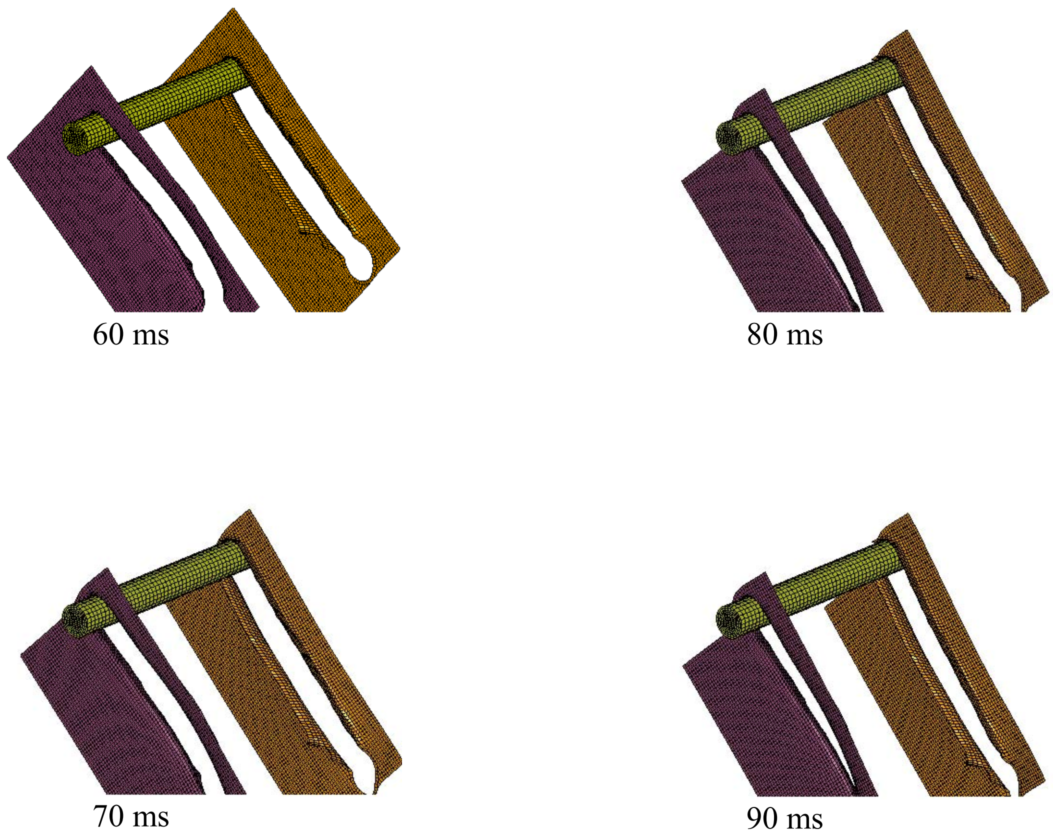

Figure 63. Sequential Pictures, Simulation of Test No. MGSBRB-5

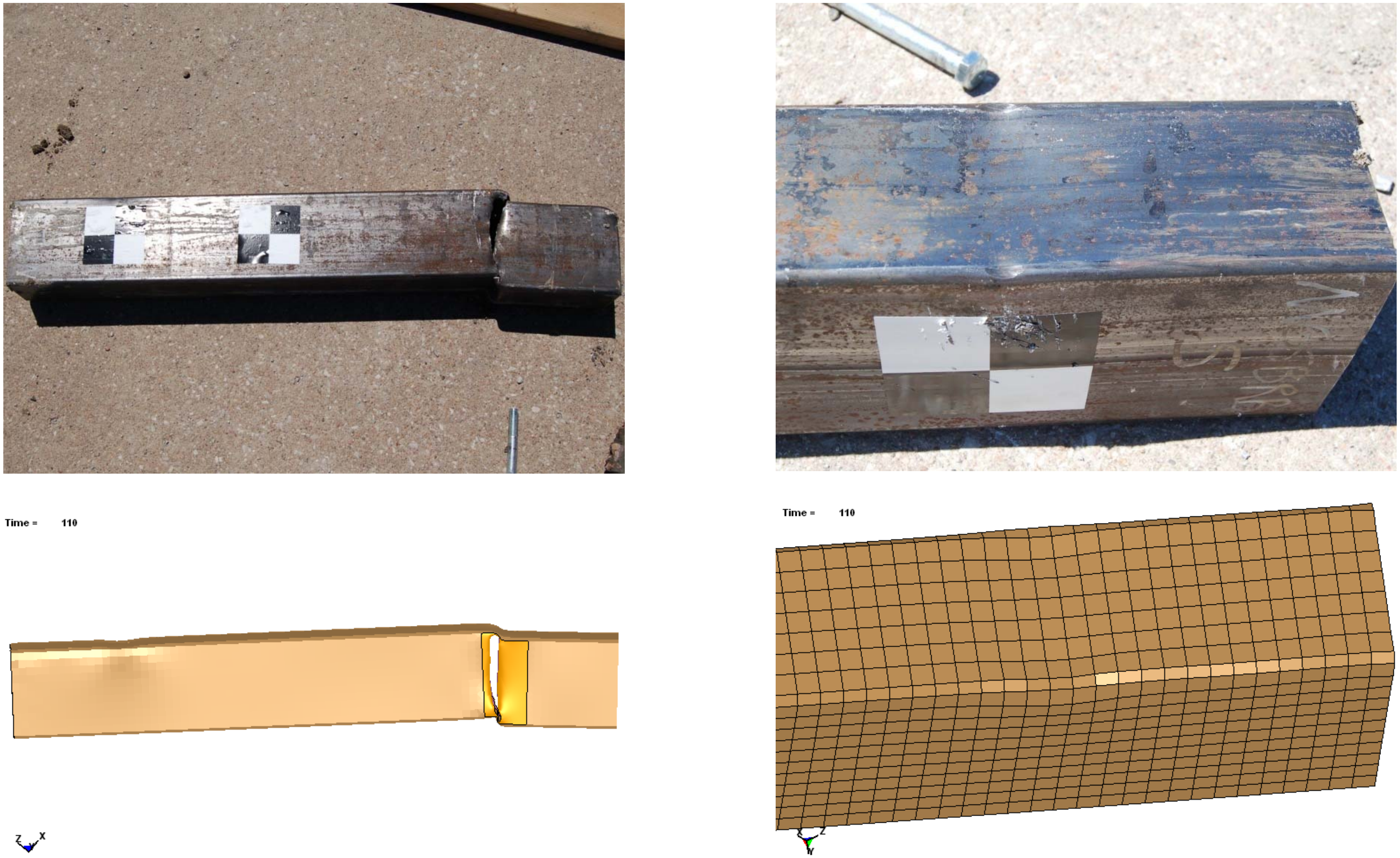

Figure 64. Simulation and Physical Test Results, Test No. MGSBRB-5

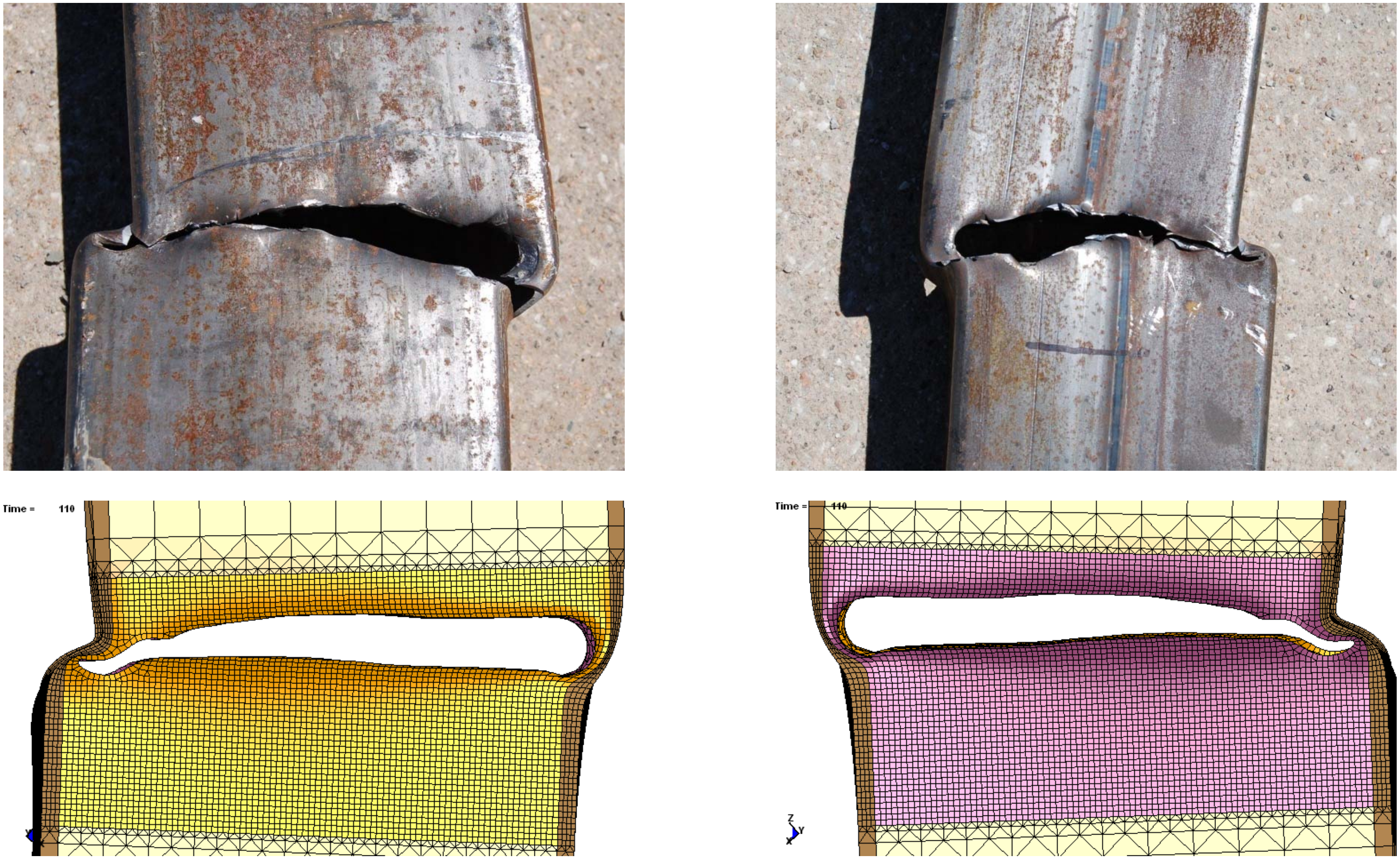

Figure 65. Simulation and Physical Test Results, Test No. MGSBRB-5

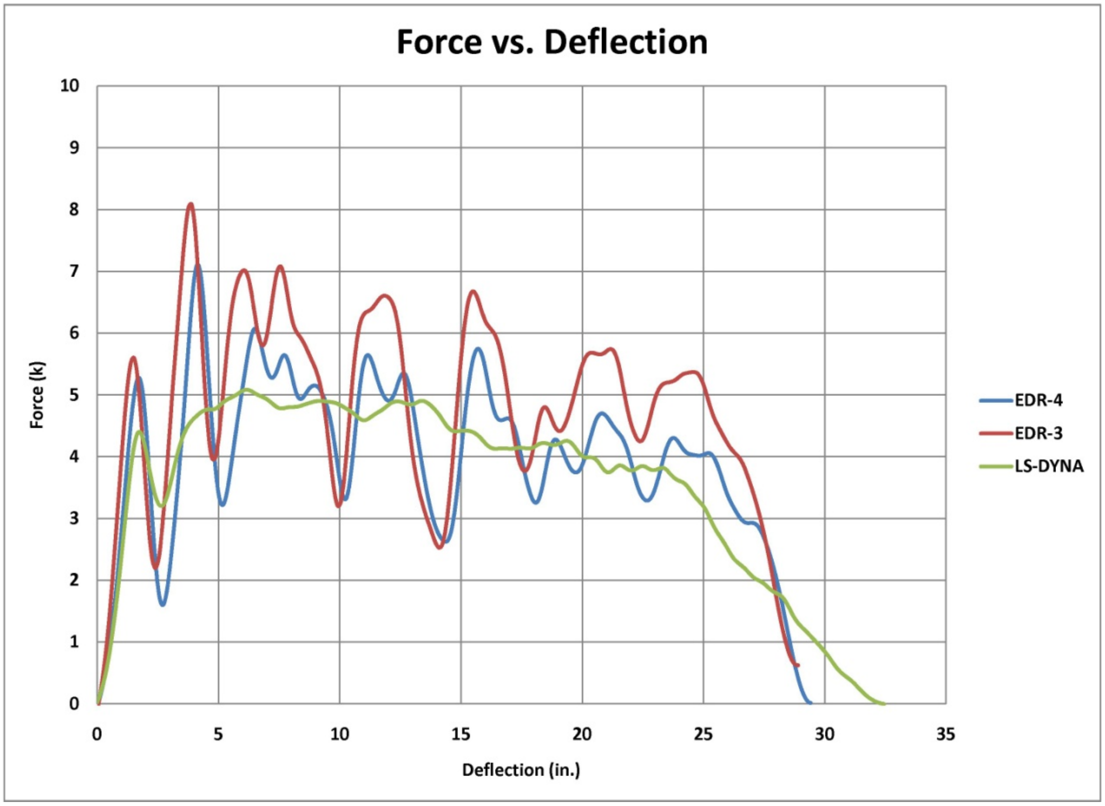

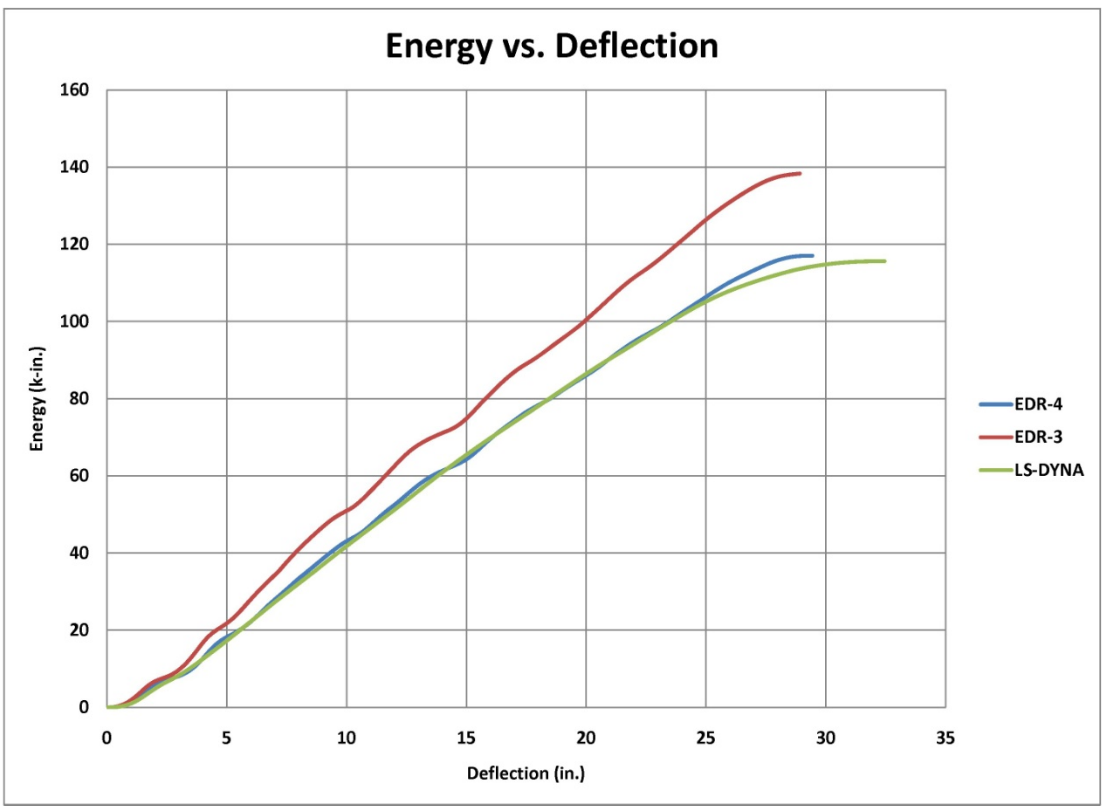

Figure 66. Simulation and Physical Test Results, Test No. MGSBRB-5

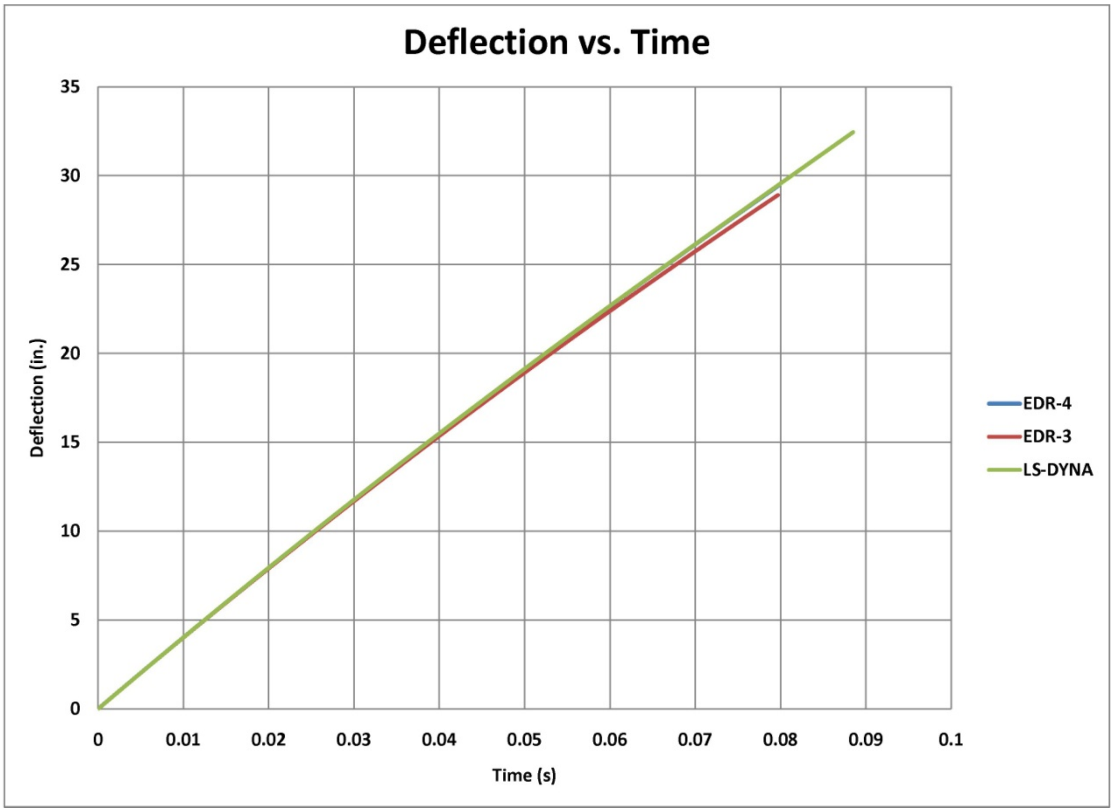

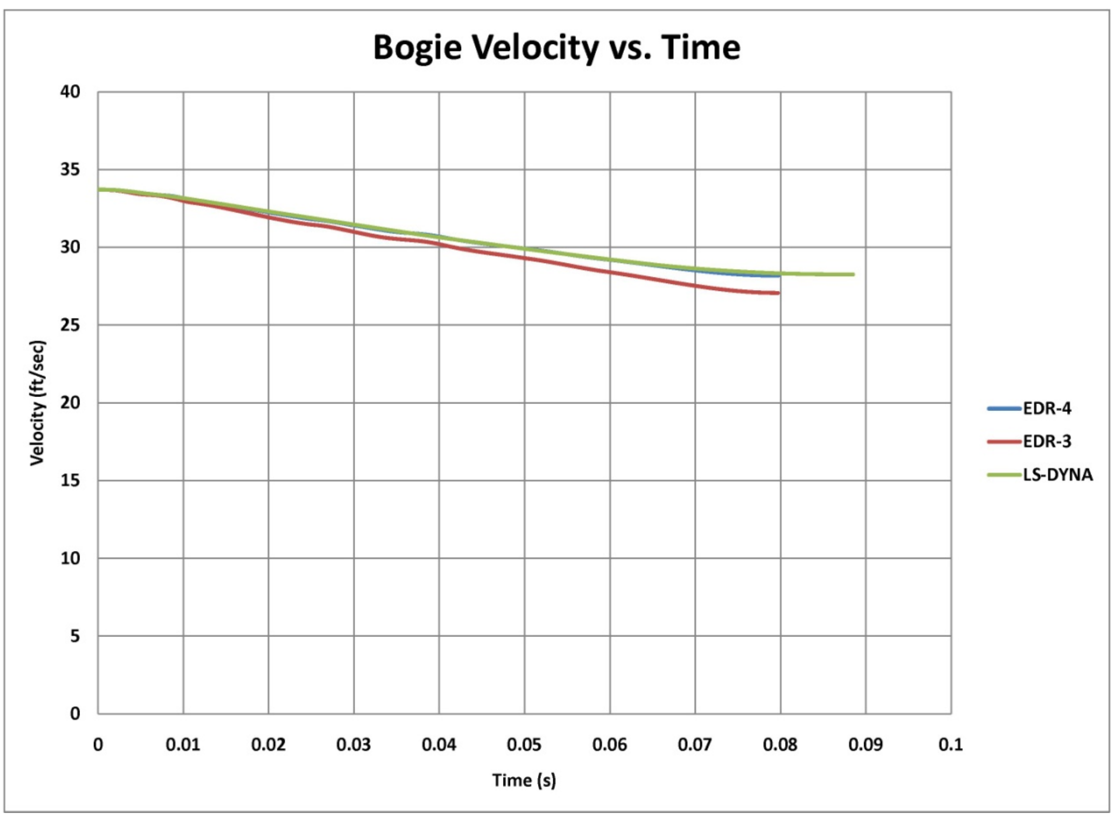

Figure 67. Simulation and Physical Test Results, Test No. MGSBRB-5

5.5 Testing of Other Modeling Components

After the working model was developed for test no. MGSBRB-5, several modeling parameters were evaluated to investigate their effect on model predictions. These parameters included alternate element formulations, material models, and meshes.

5.5.1 Alternate Element Formulations

Several different shell element formulations were tested in the tear-out region to determine if they would produce desirable results. These formulations included Types 1, 2, 6, 7, 8, 10, and 11. Comparison of the force vs. deflection and energy vs. deflection curves for the various element types, which are shown in Figures 68 and 69, revealed that all element formulations produced similar net effects on the bogie as long as they remained stable. However, inspection of the individual simulations shows that most of the element formulations displayed unrealistic behavior, primarily in the form of stable or unstable shooting nodes.

Type 1 (Hughes-Liu) elements remained stable throughout the simulation, but caused several stable shooting nodes to develop as the bolt was approximately halfway through the plates. Type 2 (Belytschko-Tsay) elements produced similar results. Type 6 (S/R Hughes-Liu) elements worked well until approximately one-quarter of the way through the simulation, at which point an unstable shooting node developed, the time step dropped dramatically, and the simulation effectively stalled. Type 7 (S/R Co-rotational Hughes-Liu) elements performed very well, producing neither shooting nodes nor any other analysis instabilities. Type 8 (Belytschko-Leviathan) elements did not produce shooting nodes, but did create odd variations in the tear-out mechanism. For example, the faces of the plate originally buckle inward, but later buckle outward during the simulation, and several elements detached from the post completely. Type 10 (Belytschko-Wong-Chiang) elements produced a large number of stable shooting nodes and

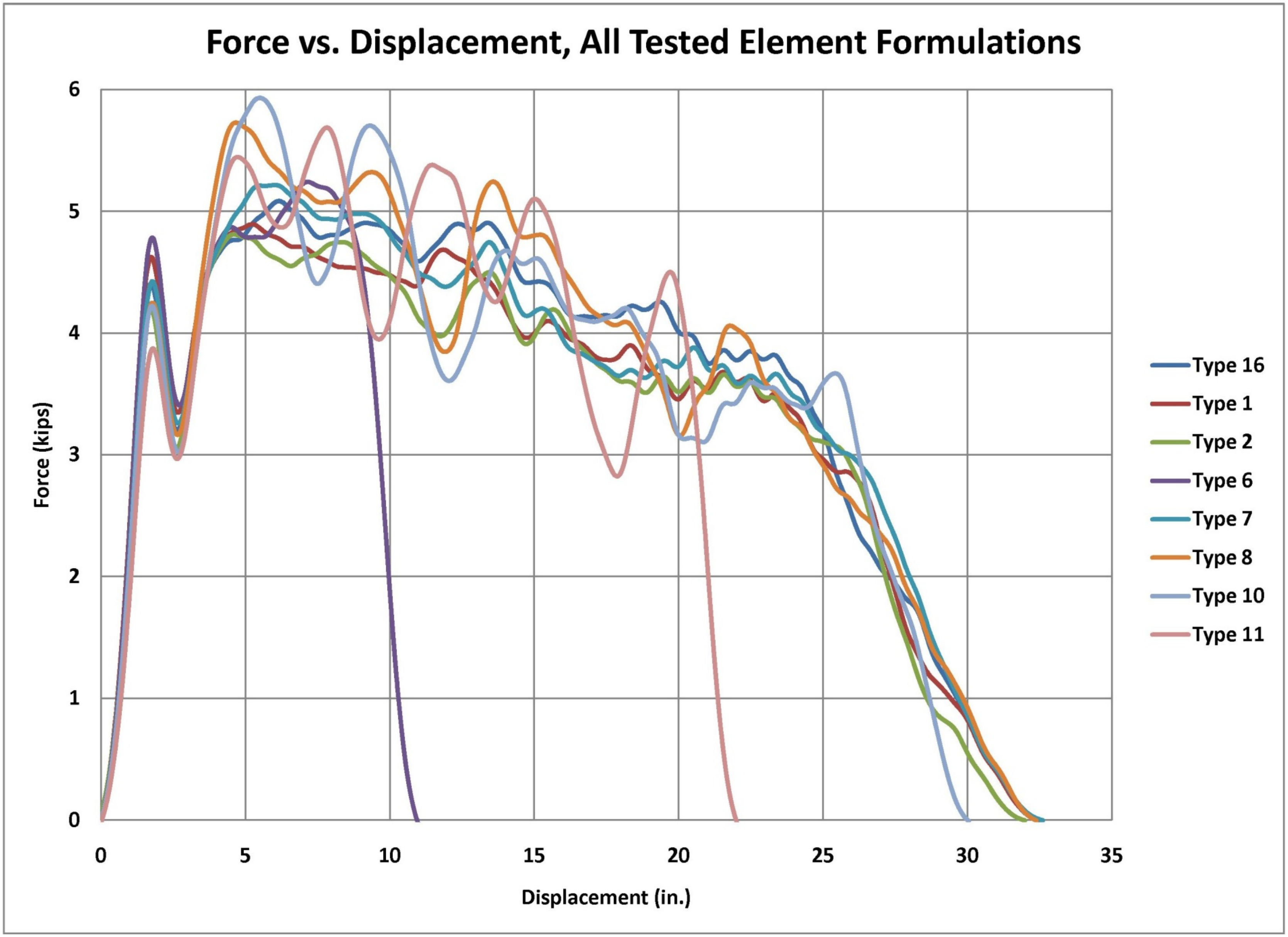

Figure 68. Force vs. Deflection Curves for Various Element Formulations

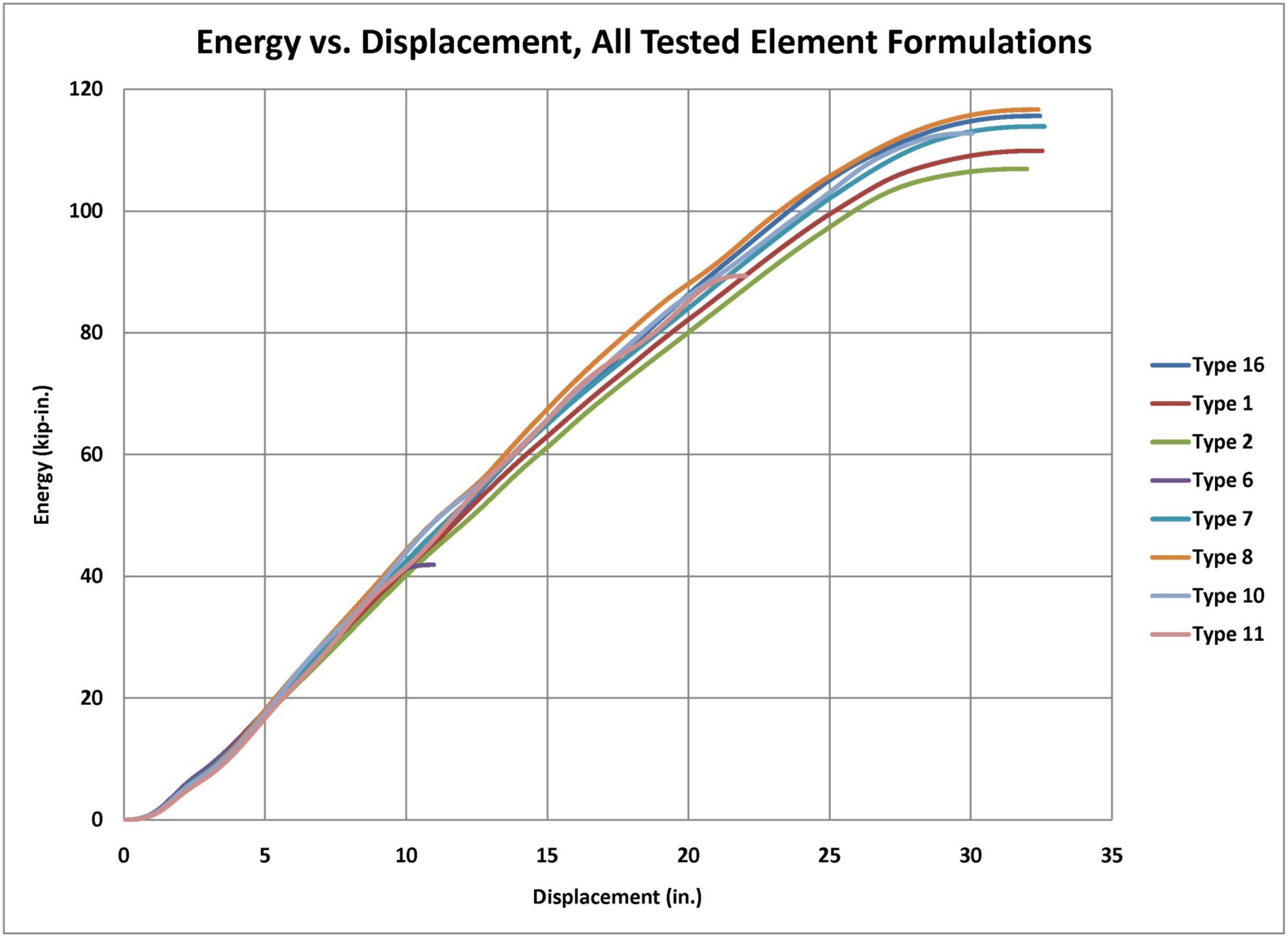

Figure 69. Energy vs. Deflection Curves for Various Element Formulations

bizarre element behavior until becoming unstable late in the event, at which point the time step decreased and progress effectively stopped. Finally, Type 11 (Fast Co-rotational Hughes-Liu) elements produced a large number of shooting nodes and also became unstable during the simulation. Thus, the Type 7 and Type 16 elements were the best formulations for the tear-out application and produced the most accurate results. Pictures of the simulation results for the various element types are shown in Figure 70.

Examination of the original simulation revealed that some hourglassing occurred in the post in the non-tear-out regions. The amount of hourglass energy was small when compared to the total energy absorbed through tear-out, but it was significant in comparison to the energy absorbed by the rest of the post. Thus, one additional simulation was run in which the entire post was composed of Type 16, fully-integrated shells. This change resulted in higher forces early in the event and lower forces later in the event. The total energy absorbed by the post changed minimally. As the hourglass energy in the original simulation was not large enough to cause concern and the effect of changing the element formulation was minimal, the original simulation was found to be acceptably accurate.

5.5.2 Alternate Material Models

Different material models were also substituted into the simulation to see how their use would affect results. A PLASTIC_KINEMATIC material model was used for the tear-out region of the post. Additionally, an elastic material model was used for the tear-out bolt to examine its effects on the tearing behavior. As the bolt did not yield during the physical test, no plastic material models were considered.

Whereas the PIECEWISE_LINEAR_PLASTICITY model allows a user to completely define a stress-strain curve for a material, the PLASTIC_KINEMATIC model is a bilinear

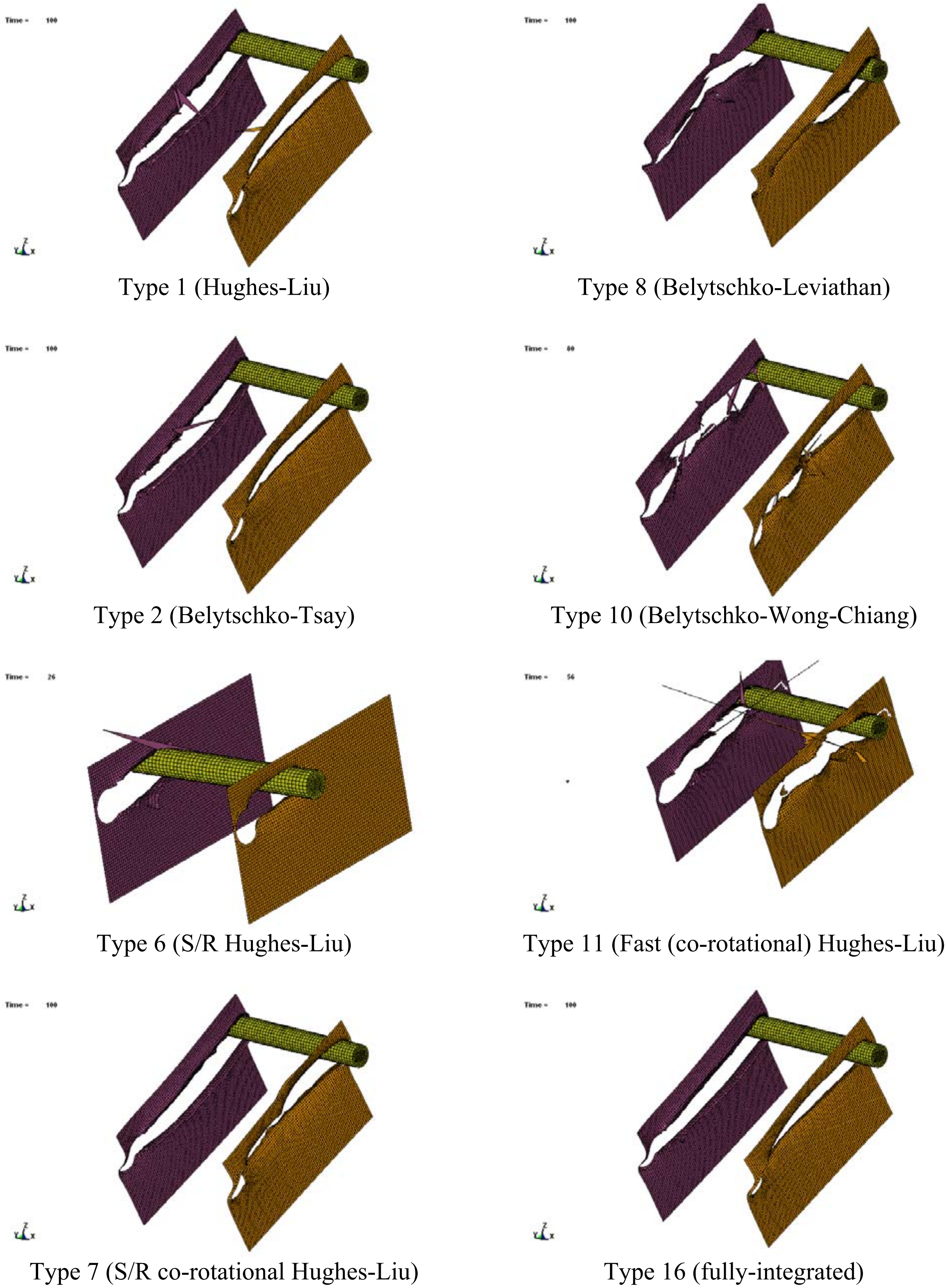

Type 1 (Hughes-Liu)

Type 8 (Belytschko-Leviathan)

Type 2 (Belytschko-Tsay)

Type 10 (Belytschko-Wong-Chiang)

Type 6 (S/R Hughes-Liu)

Type 11 (Fast (co-rotational) Hughes-Liu)

Type 7 (S/R co-rotational Hughes-Liu)

Type 16 (fully-integrated)

Figure 70. Element Formulations and Behavior

elastic, strain-hardening model. Isotropic or kinematic hardening can be defined for the material. The load on the post in the simulation was believed to not reverse, thus both types of hardening were expected to produce identical results. The PLASTIC_KINEMATIC material model also uses an effective plastic strain to define failure of the material. Note that a bilinear stress-strain curve can also be input into the PIECEWISE_LINEAR_PLASTICITY material model, and that this material model uses isotropic hardening. A sketch of isotropic and kinematic hardening behavior is shown in Figure 71.

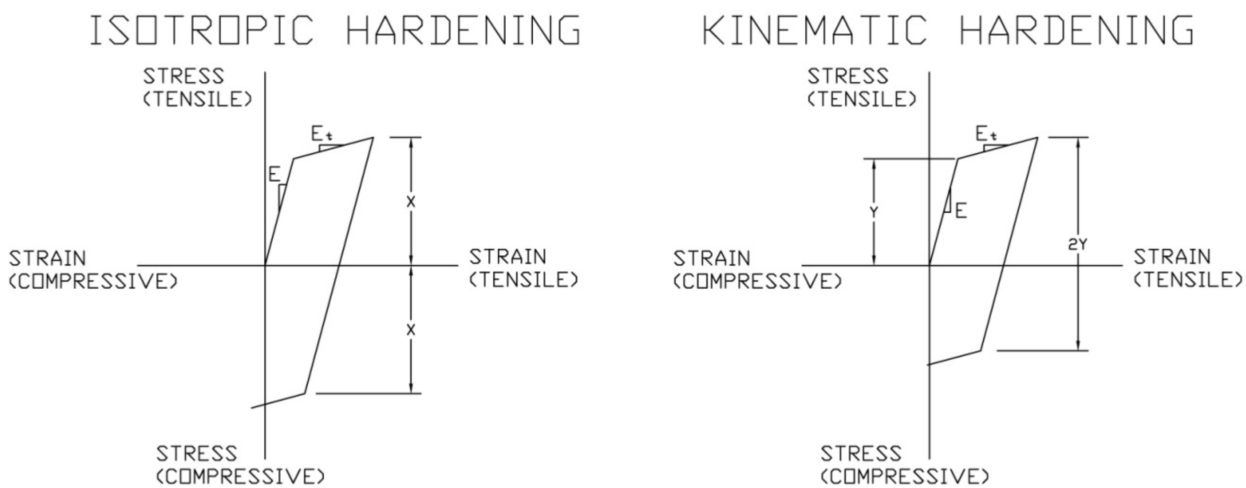

Figure 71. Isotropic and Kinematic Hardening

The new material model used an elastic modulus and ultimate strain equivalent to the original model. The yield stress and tangent modulus were then tuned to match the strain-energy density of the PIECEWISE model. The new material model was stable throughout the simulation, but it did produce some irregular element failures along the tear-out surface. Additionally, though resistance forces were similar for both models early in the event, the PLASTIC_KINEMATIC material model absorbed less energy than the original model and the physical test. A final picture of the simulation using the PLASTIC_KINEMATIC material model is shown in Figure 72, and a force vs. displacement curve is shown in Figure 73.

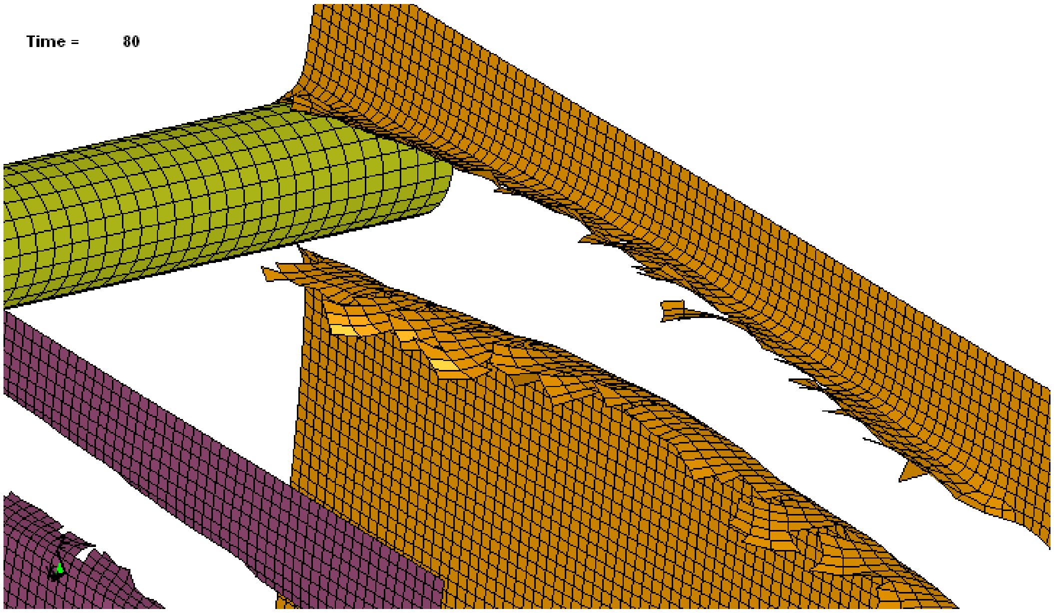

Figure 72. PLASTIC_KINEMATIC Material Model Simulated System Damage

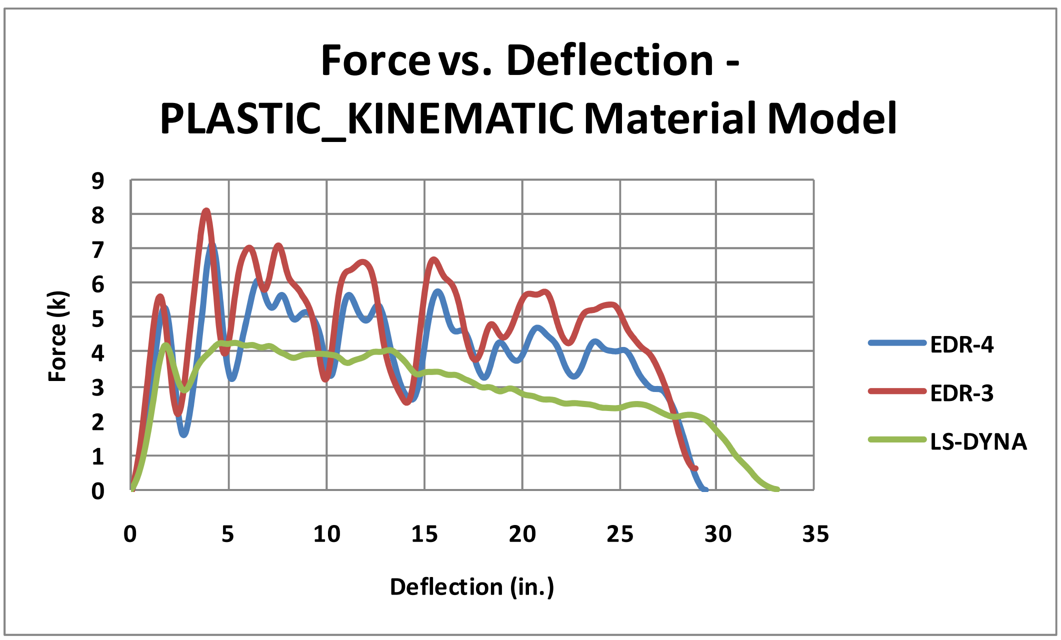

Figure 73. PLASTIC_KINEMATIC Material Model Results

Originally, the difference in energy absorption was attributed to the bilinear stress-strain curve. However, when an additional simulation was performed using a bilinear PIECEWISE_LINEAR_PLASTICITY material model, the simulation behaved similar to the original model. An additional simulation was performed using the PLASTIC_KINEMATIC material model with isotropic hardening. The results of this simulation matched the original simulation much more closely, indicating that the hardening behavior of the models created the difference.

In the simulation, the bolt causes compressive yielding in advance of the crack as the bolt bears against the face of the post. In the kinematic hardening model, this compressive yielding decreases the magnitude of the subsequent tensile yield stress of the material whereas in the isotropic model, this stress is increased. Thus, lower resistive forces are generated in the kinematic model through the tearing of the post, in which elements are loaded in tension, and less energy is absorbed. It is believed that the irregular element deletions along the crack of the kinematic model were also caused by this phenomenon. Elements near the crack surface that have yielded in compression subsequently yield at a lower tensile stress. Thus, more elements reach the effective plastic strain value required for element deletion. In isotropic hardening, these elements require a larger tensile stress to initiate yield. Thus, a smaller number of elements reach the effective plastic strain required for deletion, and the crack shape is smoother.

Type 1, under-integrated solid elements were used in the first simulation featuring the ELASTIC material model for the bolt. This resulted in very large amounts of hourglassing in the bolt, shown in Figure 74. Thus, the simulation was performed again with Type 2, fully-integrated solid elements. In this simulation, small indentations developed in the bolt that oscillated throughout the event. Similarly, the effective force on the bogie head oscillated more than was seen in the simulation with a rigid bolt. The average force and total energy absorbed were also lower than in the original simulation. As the elastic model allowed deformation, the bolt applied out-of-plane forces to the tear-out surfaces upon deflection, as shown in Figure 75. Thus, the force required to initiate and continue tearing was lower than in the original model, leading to a lower total energy absorbed.

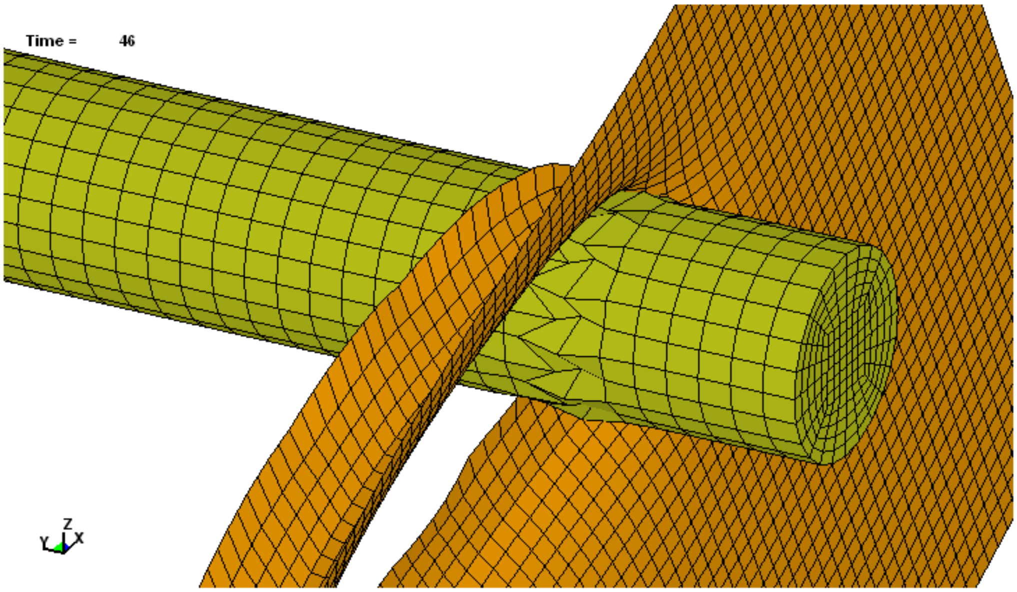

Figure 74. Under-Integrated, Elastic Bolt Modeling Effects

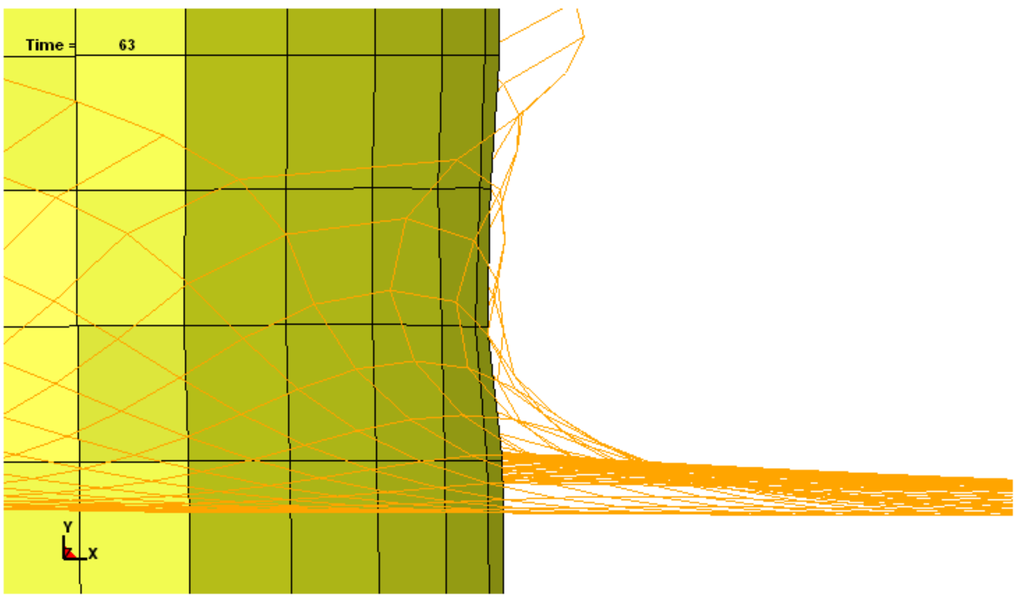

Figure 75. Fully-Integrated, Elastic Bolt Modeling Effects

While the elastic behavior was believed to be more realistic, use of fully-integrated solid elements greatly increased analysis time. The effect of this increase could be mitigated by not including the central portions of the bolt in the model, or splitting the bolt into different parts and using fully-integrated elements only in the contacted region. However, these options were not investigated. As the net effect on the model was not substantial, the original rigid bolt was found to be reasonably accurate.

5.5.3 Alternate Meshes

Finally, different mesh densities were used in the simulation to investigate their effect on the tear-out behavior. Two additional meshes were substituted into the model which utilized elements having edge lengths twice as long and one-half as long as the original mesh. These meshes are shown in Figures 76 and 77.

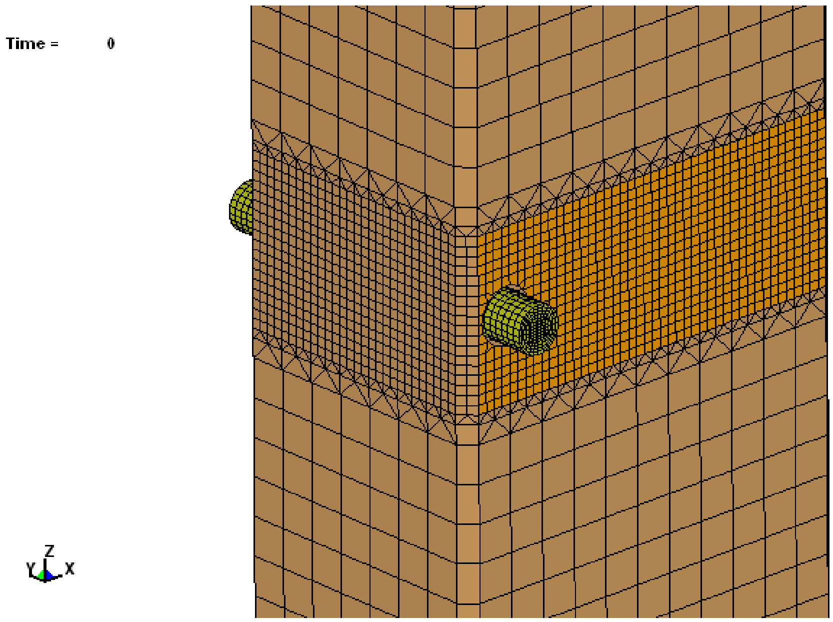

Figure 76. ⅛-in. (3.2-mm) Mesh

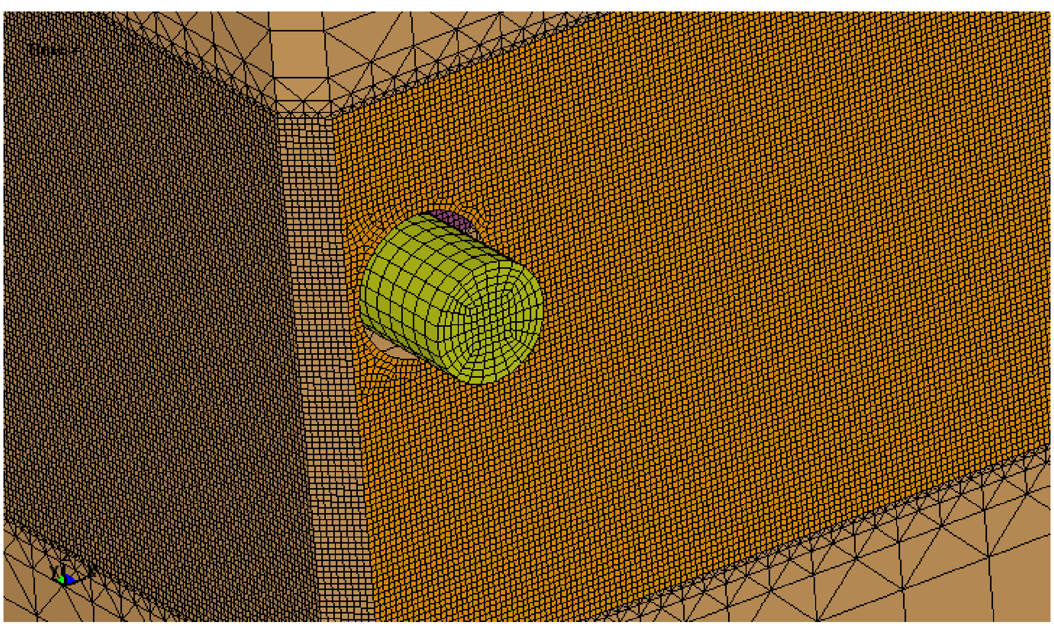

Figure 77. $^{1}/_{32}$-in. (0.8-mm) Mesh

The first mesh, which used ⅛-in. (3.2-mm) shell elements, proved stiffer than the original model. Tear-out proceeded across approximately 80 percent of the post face before stalling, at which point the post bent about the tear-out line and allowed the bogie to override it. The tearing force was increased significantly, and the total energy absorbed also increased. As the elements were larger, the strain required to fail an element was required to be spread over a larger area, resulting in greater forces. Some bizarre element behavior was observed, as several nodes began to shoot slightly and resulted in excessive element deformations. Final pictures of the model are shown in Figure 78, and a force vs. displacement curve is shown in Figure 79.

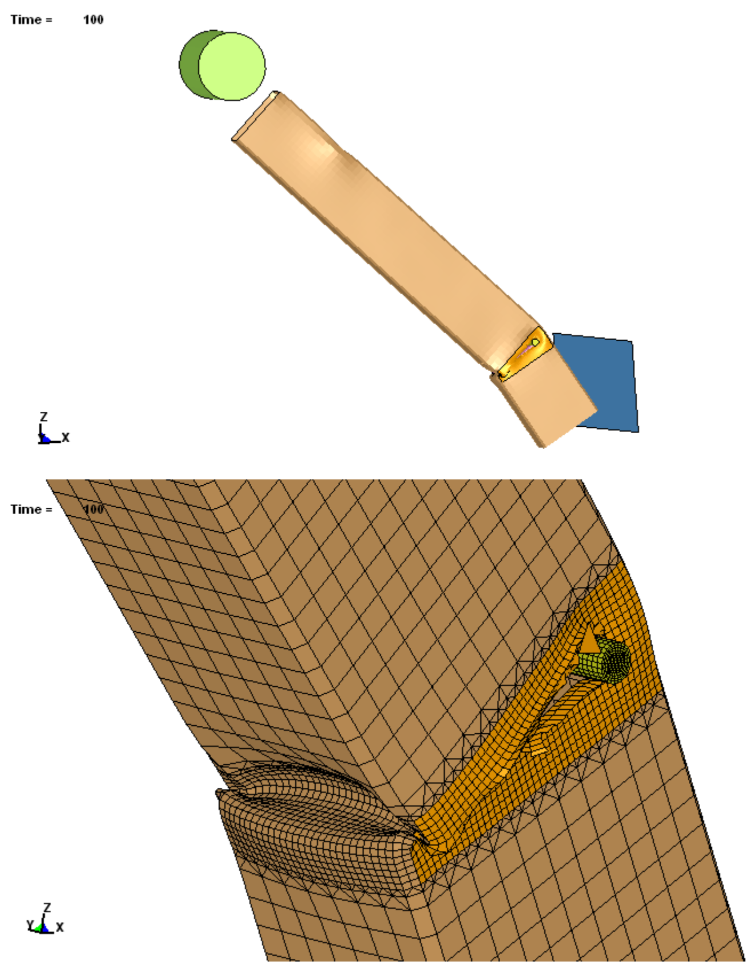

Figure 78. ⅛-in. (3.2-mm) Mesh Simulated System Damage

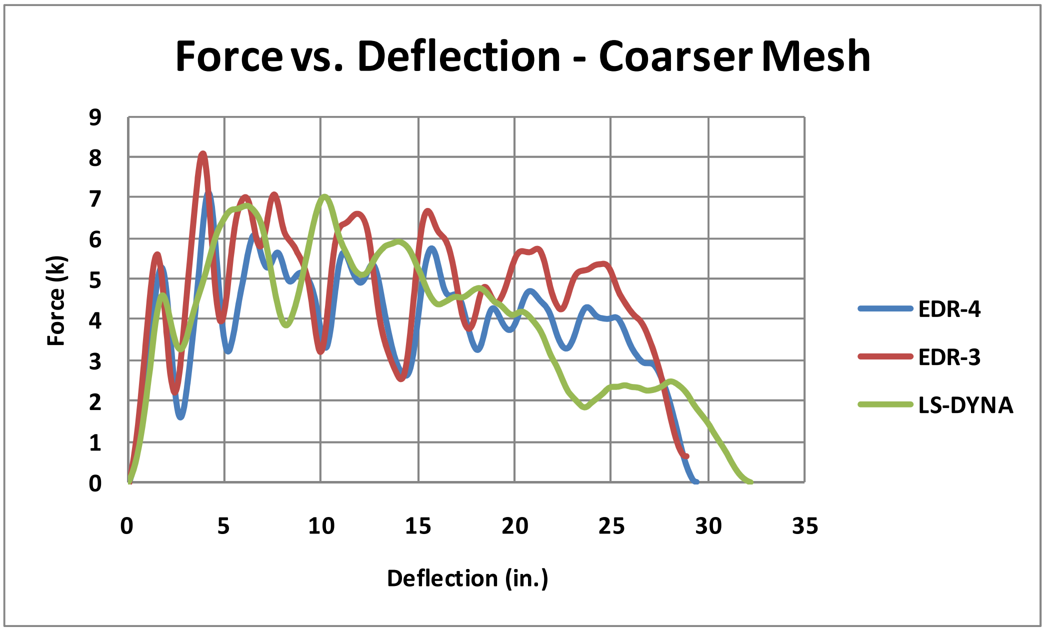

Figure 79. ⅛-in. (3.2-mm) Mesh Results

The second mesh, which used $^1/_{32}$ -in. (0.8-mm) shell elements, was more flexible than the original mesh. This mesh did capture the early force peak required to initiate tear-out. Once tear-out began, the average tearing force was less than that of the original mesh, and less energy was absorbed. The finer mesh allowed more out-of-plane deformation in the tear-out surface and more out-of-plane stress was applied to the elements, which facilitated failure. As previously discussed, the uniformity of the model did not allow the tear-out mechanism to fluctuate. Thus, tearing proceeded at this lower-force mechanism without the variation between failure modes seen in physical testing. Note that the finer mesh required more than eight times the analysis time of the original mesh. Computational cost could be reduced by further restricting the finer mesh to only areas where tearing will occur. However, this requires full knowledge of the tear-out path prior to simulation. Thus, the original mesh density was found to be best suited to simulating tearing. Final pictures of the simulation using the finest mesh are shown in Figure 80, and a force vs. displacement curve is shown in Figure 81. Force vs. displacement curves for all three mesh densities are shown in Figure 82.

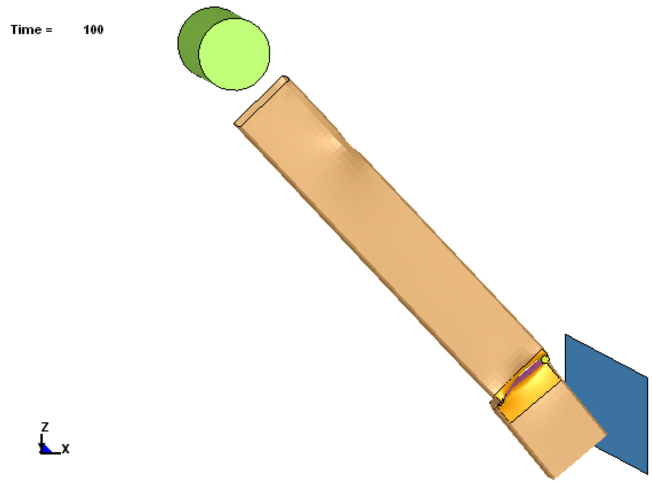

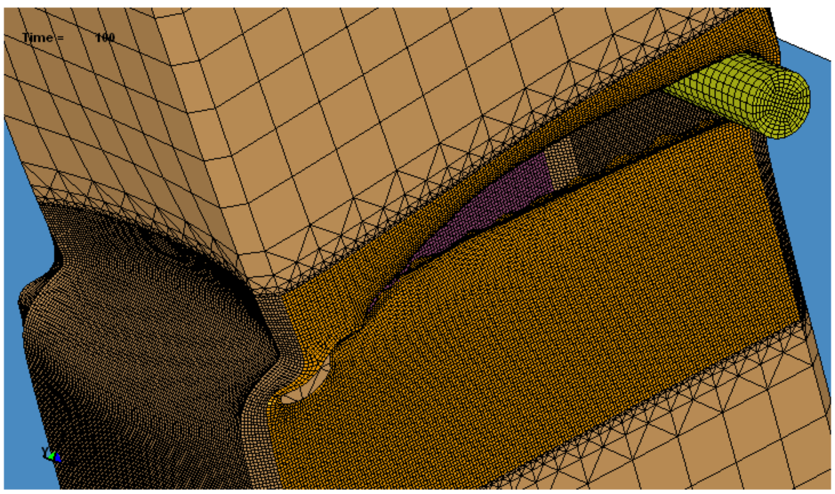

Figure 80. $^{1}/_{32}$-in. (0.8-mm) Mesh Simulated System Damage

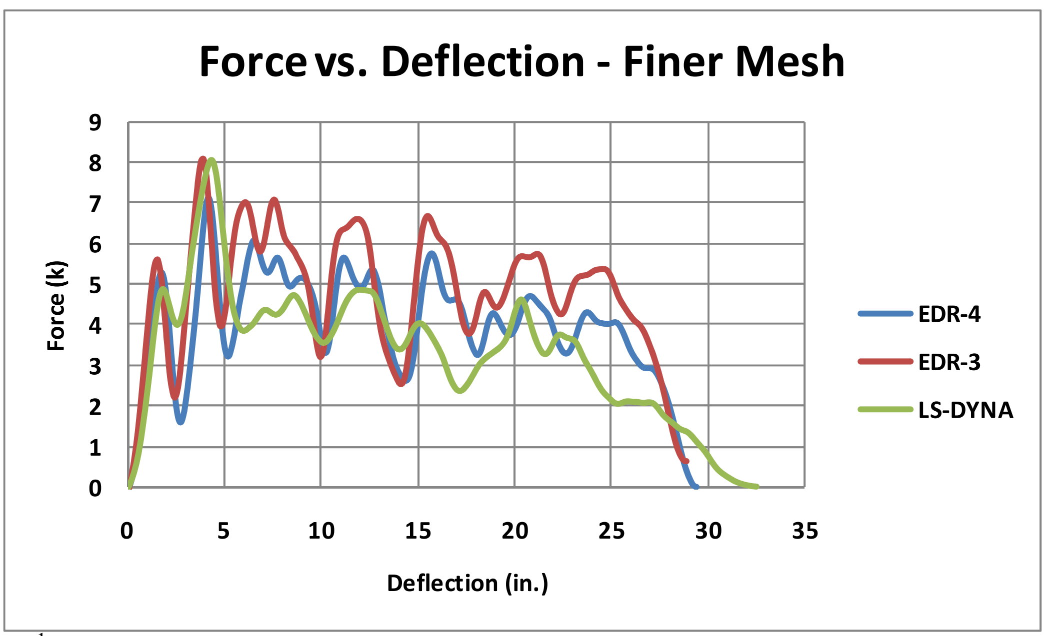

Figure 81. $^{1}/_{32}$-in. (0.8-mm) Mesh Results

Figure 82. Force vs. Deflection Curves for Various Mesh Densities

5.6 Findings

A finite element simulation was created of test no. MGSBRB-5 which was found to be in good agreement with the physical test. A variety of element and material formulations were evaluated to identify the most accurate modeling procedure for analysis of a bolt tear-out method for absorbing impact energy. Three element formulations were found to provide stable solutions, which were Type 7 (S/R co-rotational Hughes-Liu), Type 8 (Belytschko-Leviathan), and Type 16 (fully-integrated). The other tested formulations produced shooting nodes and other types of stability problems. As the Type 8 formulation produced some unrealistic behavior in the tear-out regions, Types 7 and 16 were the best formulations for simulating the tear-out.

PIECEWISE_LINEAR_PLASTICITY and PLASTIC_KINEMATIC material models were used in the simulation for the tear-out regions. Both material models produced results in good agreement with those of the physical test when isotropic hardening was used. Kinematic hardening, which could only be used in the PLASTIC_KINEMATIC material model, resulted in lower energy absorption levels and irregular tearing patterns in the post. Thus, isotropic hardening was better suited for modeling the tear-out behavior. Additionally, RIGID and ELASTIC material models were used to simulate the bolt. While the elastic model was believed to produce more realistic results, it required use of fully-integrated solid elements to prevent excessive hourglassing. Thus, the RIGID material model was found to be better suited for applications in which computational efficiency is important.

Finally, the original element edge length of $\frac{1}{16}$ in. (1.6 mm) was varied to investigate the effects of alternate mesh densities. These meshes consisted of shell elements with edge lengths twice as long and one-half as long as the original mesh. All meshes were able to model the tear-out mechanism; however, tear-out in the coarsest mesh stopped after proceeding through approximately 80 percent of the post face. The finer mesh accurately captured the original force peak of the physical test, although neither alternate mesh produced results as accurate as the original model. Additionally, the finer mesh took more than eight times as much analysis time. Thus, the original mesh density was found to be the best to simulate tearing.

However, the simulation for test no. MGSBRB-5 could be improved with the development of a more accurate material model for the post steel material. Several material models were investigated, which were calibrated to tensile tests of various specimens. As no models were available for the steel used in the post, a model with similar properties was used. A model that was developed based on the actual steel used in the post would provide superior results.

Additionally, the model could be improved through inclusion of a more complete bogie model. Due to contact and stability issues encountered when using a full model of the bogie, the bogie was modeled with a simple rigid cylinder. Since physical test data was obtained from an accelerometer mounted near the bogie's center of gravity, rotations would cause some disagreement between the physical and simulated data. While the bogie did not significantly rotate in the physical test, updating the model with a full bogie model would more accurately simulate these effects.

6 BARRIER VII ANALYSIS

6.1 Scope

BARRIER VII [62-63] simulations were used to evaluate the compatibility of the bridge rail with MGS to determine if an approach guardrail transition would be required between the two barriers. The primary safety concern associated with a connection between two barriers is that a vehicle striking the more flexible barrier can pocket behind the end of the stiffer downstream barrier. Pocketing occurs when a flexible barrier deflects sufficiently to allow the front of the vehicle to engage the blunt end of the stiffer barrier. The risk of a high-deceleration pocketing event has been correlated to the maximum angle between the deflected guardrail and the downstream section of rail [64]. Figure 83 illustrates how a pocketing angle is measured.

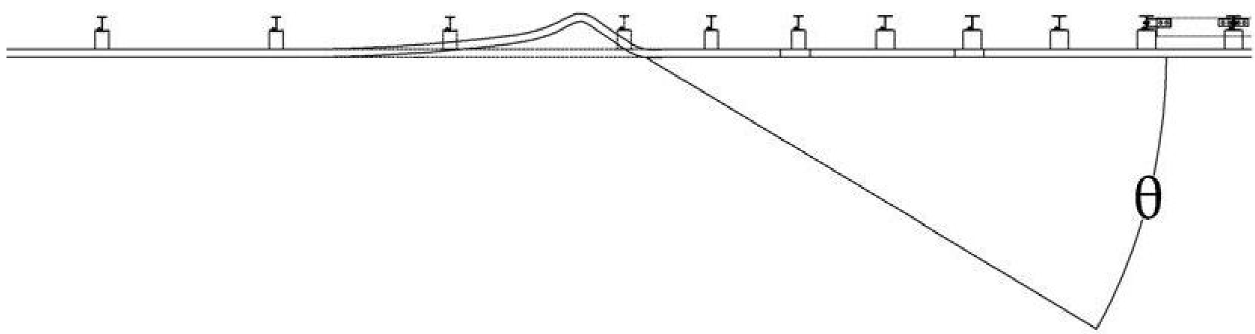

Figure 83. Pocketing Angle Measurement

BARRIER VII simulations were performed to determine if the weak-post bridge rail with half-post spacing would generate lateral stiffness, strength, and deflections comparable to those of the MGS with posts embedded in soil. This analysis was accomplished through two sets of simulations. First, impacts were simulated with separate systems comprised entirely of bridge rail or guardrail to determine if similar deflections resulted. Next, impacts in the transition region on both ends of a bridge were simulated to investigate deflections and to determine if vehicles could pocket at either the approach or departure interface.

Prior studies of transitions between barriers have indicated that it is desirable to limit the maximum guardrail pocketing angle to less than 30 degrees [64-65]. These angles were measured using the nodal displacements of the barrier in front of the vehicle. Linear regression was used to fit lines to both three and five consecutive nodes of the barrier, which corresponded to lengths of rail of 18¾ in. (476 mm) and 37½ in. (953 mm), respectively.

Wheel snag was not considered in this analysis. Prior testing has shown that severe wheel snag sufficient to remove the vehicle's wheel does not produce excessive deceleration nor vehicle instability during W-beam guardrail impacts. Further, the depth of blockouts used with the MGS guardrail has limited the degree of wheel snag during previous crash tests with standard MGS guardrail [1]. The weak, S3x5.7 (S76x8.5) post used in the bridge rail has also been widely used in unblocked out weak-post barrier systems, including weak-post W-beam and cable guardrails. Crash testing of these weak-post systems has proven that wheel snag on S3x5.7 (S76x8.5) posts is not a safety concern.

6.2 BARRIER VII Model

BARRIER VII is a 2-dimensional finite element program that uses a variety of ideal components to model real-world behavior. The program models post and beam systems using rail that yields only at nodal locations and elastic, perfectly plastic posts. Component models of S3x5.7 (S76x8.5) posts, W6x9 (W152x13.4) posts, anchor posts, and 12-gauge (2.66-mm thick) W-beam guardrail were required to perform the analysis. A summary of parameters used in BARRIER VII simulation is shown in Table 3.

6.2.1 S3x5.7 (S76x8.5) Post Models

The S3x5.7 (S76x8.5) post models used in analysis were created with data obtained from dynamic bogie tests performed previously by MwRSF [66]. In these bogie tests, posts were rigidly mounted in a steel tube that was encased in concrete. Wood spacers and steel plates were also inserted into the tube to orient the post at different angles to the path of the bogie. Tests were performed in which the bogie impacted posts at angles of 90, 75, and 60 degrees with respect to the strong axes of the posts at a height of 21.65 in. (550 mm) above the roadway. Force vs. deflection curves created from accelerometer data for these tests are shown in Figure 84.

Table 3. BARRIER VII Simulation Parameters

BARRIER VII Parameter			Input Value
90-deg Post	Kb - Strong Axis Stiffness	kip/in.	2.46
	Ma - Strong Axis Yield Moment	kip-in.	114.97
75-deg Post	Kb - Strong Axis Stiffness	kip/in.	2.08
	Ma - Strong Axis Yield Moment	kip-in.	94.27
60-deg Post	Kb - Strong Axis Stiffness	kip/in.	2.04
	Ma - Strong Axis Yield Moment	kip-in.	81.76
All BR Posts	Ka - Weak Axis Stiffness	kip/in.	2.53
	Mb - Weak Axis Yield Moment	kip-in.	25.74
	δf - Failure Displacement	in.	15
Rail	μk - Kinetic Friction Coefficient	Vehicle to Barrier	0.35
	Py - Yield Force in Tension	kips	99.5
	My - Yield Moment	kip-in.	68.5

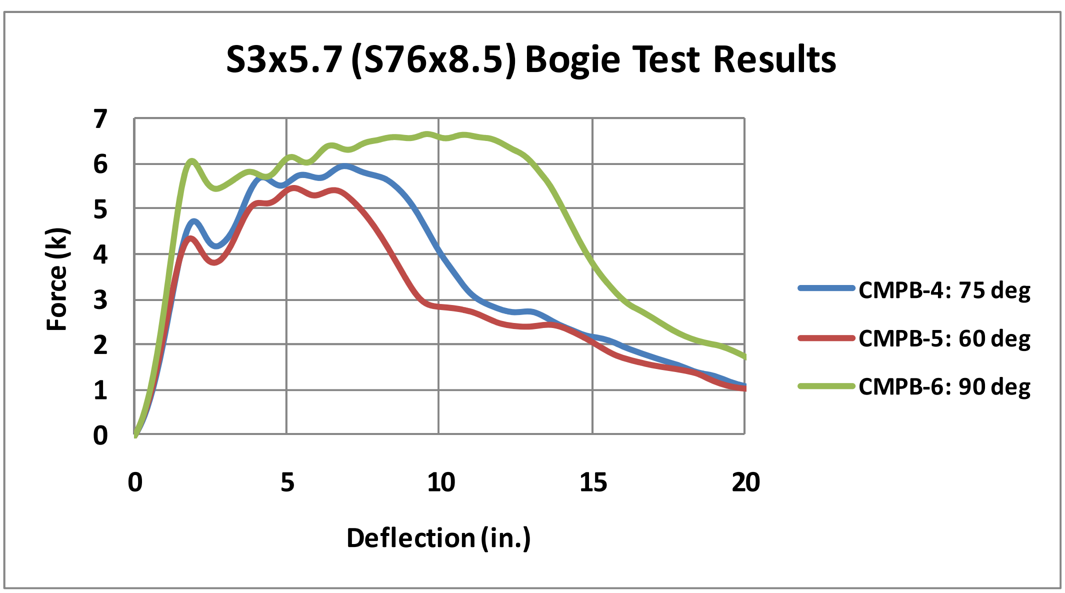

Figure 84. S3x5.7 (S76x8.5) Bogie Test Results

BARRIER VII post models behave as elastic, perfectly plastic elements. Elements develop linear force vs. deflection curves through a specified yield moment and then maintain constant bending moment until reaching a deflection at which the element fails. Upon failure, the resistive force of the member is reduced to zero over several time steps. The elastic stiffness, yield moments, and failure deflections for post members in axes both parallel and perpendicular to the barrier are required as input for the program. These values were obtained through analysis of the previous bogie tests.

Stiffness of the posts perpendicular to the barrier was obtained with the assumption that the initial peak resistive force of the post in each test marked the end of elastic behavior. This peak elastic force was divided by the corresponding deflection to determine stiffness. As the bridge rail system featured a higher guardrail mounting height than the prior tests, the stiffness value was reduced in proportion to this difference.

Yield moments perpendicular to the barrier for the post models were calculated by integrating the area beneath the force vs. deflection curves to find the energy absorbed by the post in each bogie test. Integration was performed from the onset of post yield, or the initial peak force, to the deflection at which the posts were considered to no longer contribute significant resistance to guardrail deflection. This distance was estimated to be 15 in. (381 mm), as it was believed that at this distance the guardrail would detach from and begin to override the post. Average yield forces were then obtained by dividing the total energy absorbed by the total amount of plastic deflection, which was found by subtracting the deflection corresponding to post yield from 15 in. (381 mm). A reduction factor of 0.875 was applied to the total energy absorbed and the linear stiffness for the data obtained from the strong-axis (90-degree) post test. This factor was an estimated parameter used to account for twist and subsequent reduction in strength of a post that would occur during a bridge rail impact, as the post would not be loaded perfectly along its strong axis. Note that this reduction factor was not applied to the data from the other two post tests. Finally, yield moments were obtained by multiplying the average yield force by the height of impact, 21.65 in. (550 mm). Graphical representations of the post model properties perpendicular to the barrier for an impact height of 24⅞ in. (632 mm) are shown in Figure 85.

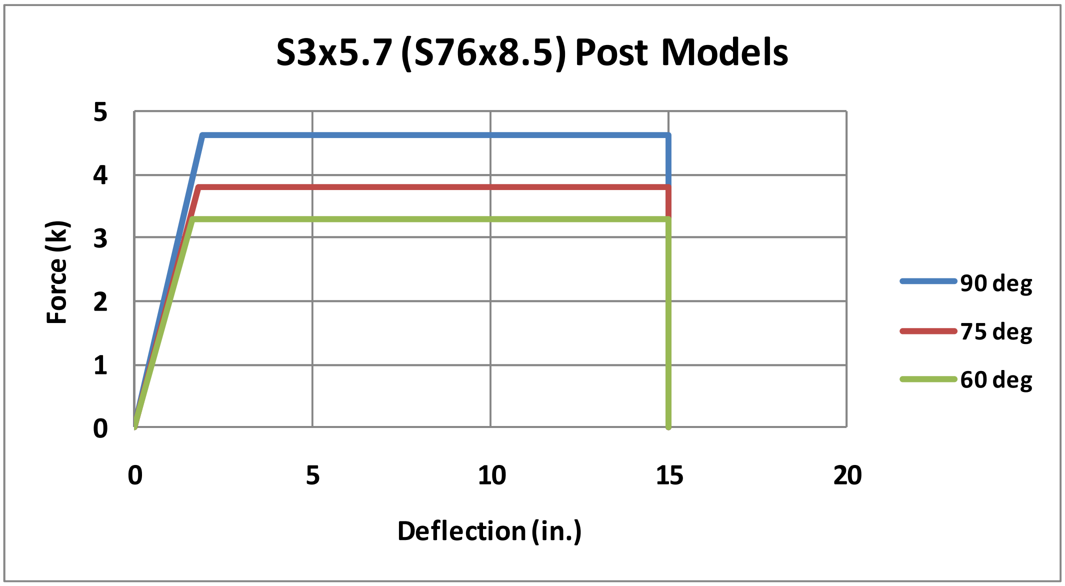

Figure 85. S3x5.7 (S76x8.5) BARRIER VII Post Models

Even with the reduction factor applied only to this load condition, the 90-degree post model was the strongest and stiffest post. The 75-degree post model had an intermediate strength and a stiffness that was slightly greater than that of the 60-degree model, which had the lowest strength.

Post properties parallel to the barrier, or perpendicular to the weak-axis of each post, were determined using elastic bending equations. As non-impacted posts would be loaded through tension in the rail, which is applied more slowly, no dynamic magnification factor was applied.

6.2.2 W6x8.5 (W152x12.6) Post Models

The post model used for the MGS W6x8.5 (W152x12.6) posts was taken from previously-developed BARRIER VII simulations calibrated to full-scale crash tests [1, 67-68]. This model simulated a 6-ft (1.83-m) long, W6x9 (W152x13.4) post embedded in soil. Resistance force perpendicular to the barrier at the height of the guardrail was approximately 5.8 kips (25.7 kN), and failure deflection was 15 in. (381 mm).

A stronger post model was developed based on the soil strength requirements stipulated in Appendix B of MASH, which state that a minimum average resistance force of 7.5 kips (33.4 kN) must be developed between deflections of 5 and 20 in. (127 and 508 mm) in strong-axis dynamic testing of W6x16 (W152x23.8) posts. These posts do not allow buckling that may occur with W6x9 (W152x13.4) guardrail posts, and as such represent an upper bound to the strength developed by the smaller post. A strong-axis resistive force of 8 kips (35.6 kN) was assumed for the stronger post model, and a reduction factor of 0.875 was applied to this value to account for twisting, buckling, or eccentric loading of the guardrail posts. Thus, yield force of the stronger posts was 7 kips (31.2 kN).

6.2.3 Anchor Post Models

Models for the anchor posts used in both the bridge rail and MGS guardrail simulations were based on modified breakaway cable terminal (BCT) post anchors that were used to replicate the tensile capacity of tangent guardrail installations. In full-scale testing, two of these posts are positioned at each end of the guardrail and housed in 6-ft (1.83-m) long foundation tubes. A ground line strut is positioned between the anchor posts, and a cable anchor is attached between the end post and the guardrail section. Previously-developed models for both the first and second BCT posts in the system were used for the BARRIER VII simulations [69].

6.2.4 W-Beam Guardrail Model

The W-beam guardrail model was based on the geometry and material properties of standard 12-gauge (2.66-mm thick) guardrail. Other required properties were determined using elastic bending equations.

6.2.5 Coefficient of Friction

Contact interfaces between the vehicle and barrier are defined within BARRIER VII with a coefficient of friction. Frictional force is applied along the edge of the vehicle in the simulation that resists vehicle redirection. Thus, it can be used to simulate the effects of wheel snag on posts, which create the same effect. Since no calibrated coefficient of friction was available for the bridge rail, a calibrated value from the MGS of 0.35 was initially used for both systems [1, 67].

6.2.6 Vehicle Models

Two different vehicle models were used in the simulations that corresponded with those prescribed for testing under MASH. These models were a truck with a mass of 5,000 lb (2,268 kg) denoted as the 2270P vehicle and a car with a mass of 2,425 lb (1,100 kg) denoted as the 1100C vehicle. These models were developed by MwRSF personnel as part of the NCHRP 22-14(2) project. For all simulations, each vehicle impacted the guardrail at a speed of 62.1 mph (100.0 km/h) and at an angle of 25 degrees in accordance with TL-3 criteria of MASH.

6.2.7 Mesh Density

A uniform mesh density was used across the entire length of all simulated systems. For the 175-ft (53.34-m) system, a total of 225 nodes were used, which resulted in a node spacing of $9\frac{3}{8}$ in. (238 mm). In later simulations, an increased mesh density of 449 nodes was used, with a resulting node spacing of $4\frac{11}{16}$ in. (119 mm).

6.3 BARRIER VII Simulation Results

As presented previously, a number of BARRIER VII input parameters had to be estimated. A parametric study was conducted to explore the possible effects of variations in these parameters.

6.3.1 Guardrail Simulation Results

The first systems analyzed consisted entirely of MGS guardrail and end anchor terminals to form a baseline for comparison. The total system length was 175 ft (53.34 m), which consisted of four anchor posts and twenty-five guardrail posts. Only the coarser (225-node) mesh was used in these simulations. Points of initial impact were selected such that the event was approximately centered in the system, with separate simulations performed for impact located at each node across one post spacing, for a total of 8 simulations. Maximum deflections and pocketing angles for these simulations are shown in Table 4. Note that these simulations were performed with the nominal test designation no. 3-11 impact severity of 115 kip-ft (156 kJ). Further note that maximum dynamic deflection of the MGS when tested under test designation no. 3-11 conditions with an impact severity of 122 k-ft (166 kJ) was 43.9 in. (1,114 mm), which compares favorably with the simulated values [67].

Table 4. Guardrail-Only and Bridge Rail-Only Results (225-Node)

System	Post Model	Vehicle	Maximum Barrier Deflection		Maximum 5-Node Pocketing	
			Deflection in. (mm)	Distance from Impact - ft (m)	Angle (deg)	Distance from Impact - ft (m)
Guardrail	**Weak**	2270P	43.4 (1,102)	15.6 (4.8)	16.0	10.9 (3.3)
Bridge Rail	**90-deg**	2270P	40.1 (1,019)	14.1 (4.3)	21.2	19.5 (5.9)
Bridge Rail	**75-deg**	2270P	43.5 (1,105)	15.6 (4.8)	19.4	21.1 (6.4)
Bridge Rail	**60-deg**	2270P	46.3 (1,175)	16.4 (5.0)	17.7	21.9 (6.7)
Guardrail	**Weak**	1100C	26.7 (678)	8.6 (2.6)	14.3	9.4 (2.9)
Bridge Rail	**90-deg**	1100C	23.7 (602)	7.8 (2.4)	15.9	10.2 (3.1)

6.3.2 Bridge Rail Simulation Results

Simulations were also performed on systems that consisted entirely of bridge rail and end anchor terminals using the coarser (225-node) mesh. Total system length was 175 ft (53.34 m), which consisted of four anchor posts and fifty-one bridge rail posts. Points of initial impact were selected such that the event was approximately centered in the system, with separate simulations performed for impact located at each node used in the guardrail simulations. All three of the previously-discussed models for S3x5.7 (S76x8.5) posts were used. Results of these simulations are also summarized in Table 4.

6.3.2.1 90-Degree Post Models

As the post model based on the 90-degree test was the strongest of the three, this simulated system displayed the lowest total deflection. Deflections of the system when impacted by the 1100C vehicle and 2270P vehicles were only 11 percent and 8 percent less, respectively, than that of the MGS. The maximum pocketing angle was the largest of all simulated systems, but it was still well within the recommended limit [64-65].

6.3.2.2 75-Degree Post Models

The 75-degree post model represented an intermediate post model, and its simulation results displayed intermediate performance. Deflection characteristics matched the MGS almost exactly. Maximum pocketing angle was also the intermediate value of the three bridge rail models.

6.3.2.3 60-Degree Post Models

As the weakest of the three, the 60-degree post model resulted in the greatest deflection of the bridge rail models. Deflection of this model was 7 percent greater than that found for the MGS when impacted by the pickup truck. Its maximum pocketing angle was also the lowest; however, it was still larger than that of the MGS.

6.3.3 Discussion of Preliminary Results

The results of the guardrail-only and bridge rail-only simulations indicated that the bridge rail would allow deflections similar to those of the MGS. Therefore, a transition should not be necessary between the two systems. Although pocketing angles were larger for the bridge rail models, they were well below recommended limits [64-65].

6.3.4 Bridge Rail with Approach Guardrail Results

Further investigation into the need for a transition section between the approach MGS and bridge rail was undertaken with simulations of systems comprised of 75 ft (22.86 m) of bridge rail positioned between two 50 ft (15.24 m) lengths of guardrail. Twenty-five bridge rail posts, twelve guardrail posts, and four anchor posts were used in the simulated systems. Inclusion of the MGS tended to decrease the deflections seen in the bridge rail. This reduction was due to the larger weak-axis strength of the guardrail posts. Although the guardrail possessed half as many posts as the bridge rail, the weak-axis capacity of each guardrail post was more than twice that of a bridge rail post, which resulted in greater overall resistance to rail movement along the barrier and lower loads on the anchor posts. For example, the predicted dynamic anchor movement at the height of the rail was reduced from 5.2 in. (132 mm) to 4.4 in. (112 mm) when the guardrail was added to the bridge rail.

Although many simulations were conducted, it was determined that four worst-case impact conditions defined the performance of the system. These included the largest pocketing angle in the approach interface (Case 1), the largest pocketing angle in the bridge rail system (Case 2), the largest pocketing angle in the departure interface (Case 3), and the largest deflection anywhere in the system (Case 4). All worst-case impact scenarios occurred in simulations with the 2270P vehicle. A summary of the BARRIER VII simulation results is shown in Table 5.

Table 5. Bridge Rail and Guardrail BARRIER VII Results with 2270P Vehicle

Combined Systems Results									
Case	GR Post	BR Post	Impact Location	# of Nodes	Deflections		Pocketing Angles (deg)		
					in. (mm)	Change	3-Node	5-Node	Change
1	Weak	90-deg	19.5 ft (6.0 m) upstream of first BR post	225	51.5 (1,308)	-	27.4	25.9	
				449	49.1 (1,247)	-4.7%	26.6	25.5	-6.7%
2	Weak	90-deg	0.8 ft (0.2 m) downstream of first BR Post	225	40.6 (1,031)		21.5	20.1	
				449	38.8 (986)	-4.5%	20.7	19.9	-7.5%
3	Strong	60-deg	3.1 ft (1.0 m) downstream of last BR post	225	45.3 (1,151)		19.7	19.5	
				449	42.6 (1,082)	-5.9%	19.5	18.5	-6.2%
4	Weak	60-deg	19.5 ft (6.0 m) upstream of first BR post	225	52.4 (1,331)	-	20.6	19.7	
				449	49.4 (1,255)	-5.7%	20.3	19.5	-5.1%

6.3.4.1 Largest Pocketing Angle, Approach Transition (Case 1)

The largest pocketing angles observed in the approach interface between the MGS and the bridge rail occurred in a model which used the weaker guardrail post and the 90-degree, or strongest, bridge rail post. Worst-case pocketing occurred when the simulated 2270P vehicle impacted the MGS just upstream of the third guardrail post before the bridge, or 19 ft - 6⅜ in. (5.95 m) upstream of the first bridge rail post. The largest guardrail pocketing angle measured across a distance of 5 nodes was 25.9 degrees. When compared with the recommended threshold value of 30 degrees, this pocketing angle cannot be considered to be a significant concern. Additionally, it was believed that the simulated angle was overestimated for two reasons. First, the bridge rail posts used in this simulation were the stiffest of the three post models. Worst-case pocketing angles across 5 nodes for the same impact using 75-degree and 60-degree post models, when used with the weaker guardrail post models, were 21.9 degrees and 19.8 degrees, respectively. Second, the guardrail post models used in this simulation represent the lower bound on post stiffness, as discussed previously. Although no simulations were performed with the stronger guardrail post models, deflections in the approach guardrail were generally larger than those in the bridge rail which utilized the stiffest posts. Therefore, smaller deflections in the approach guardrail would result in smaller pocketing angles in the bridge rail.

6.3.4.2 Largest Pocketing Angle, Bridge Rail System (Case 2)

The largest pocketing angle observed in the simulated bridge rail system was caused by an impact located 9⅜ in. (238 mm) downstream of the first bridge rail post. A maximum 5-node pocketing angle of 20.1 degrees occurred, which was well below recommended limits.

6.3.4.3 Largest Pocketing Angle, Departure Transition (Case 3)

Worst-case pocketing in the departure interface occurred in simulations using the 60-degree, or weakest, bridge rail post model and the stronger guardrail post model. A maximum pocketing angle of 19.5 degrees occurred in a simulation in which impact was located between the last bridge rail post and the first guardrail post, or 3 ft - 1½ in. downstream of the last bridge rail post. This pocketing angle, which was within acceptable limits, was exacerbated by the small number of guardrail posts downstream of impact. For points of impact which were located on the actual bridge rail, maximum pocketing angles were typically between 17 and 19 degrees. All of these pocketing angle values are well below recommended limits.

6.3.4.4 Largest Deflection of System (Case 4)

The largest deflection of the simulated bridge rail system occurred under the same impact conditions that caused the maximum pocketing angle in the upstream interface. The point of impact was 19 ft - 6⅜ in. (5.95 m) upstream of the first bridge rail post. Maximum deflection of 52.4 in. (1,331 mm) occurred in a simulated system featuring the weaker guardrail post and the weakest bridge rail post models. This relatively larger deflection was caused by the small number of upstream guardrail posts, which placed a larger load on the upstream anchors and allowed more longitudinal rail displacement. Inclusion of the 90-degree, or strongest, bridge rail post model reduced this deflection to 51.5 in. (1,308 mm). No simulations were performed with the stronger guardrail post models, but their inclusion would further decrease maximum deflection.

6.3.4.5 Increased Mesh Density

Following identification of the worst-case impact conditions, additional analyses were performed using a finer (449-node) mesh. These models had lower maximum deflections and pocketing angles than their coarser counterparts. For comparison of pocketing angles, 3-node angles from the coarser mesh were compared to 5-node angles of the finer mesh to result in the same length of rail. The decreased deflection and pocketing angles in the finer mesh were believed to have been caused by the additional number of bending points along the rail. The finer mesh had twice as many nodes, and bending at each node resulted in greater energy absorption through the entire system. Thus, deflection was reduced, which in turn reduced pocketing. However, the change in deflections between the coarser and finer meshes was very modest, which indicates that the simulation findings had converged.

6.3.5 Discussion of Results

The BARRIER VII simulations demonstrated good compatibility between the MGS and the bridge rail. Through varying the properties of both the guardrail and bridge rail posts, it was determined that pocketing angles and deflections were well below recommended limits, even under worst-case impact scenarios. Further, comparison between BARRIER VII results and prior MGS full-scale tests indicated that the BARRIER VII model produced accurate results. Thus, it is believed that no special transition section was required at the interface between the MGS and the bridge rail.

7 DESIGN DETAILS

The test installation consisted of 68 ft - 9 in. (21.0 m) of bridge rail installed between two approach sections of MGS measuring 50 ft (15.2 m) and 56 ft - 3 in. (17.1 m) in length, for a total system length of 175 ft (53.3 m). Standard 12-gauge (2.66-mm thick) W-beam guardrail was used throughout, and no approach guardrail transition sections were used at the guardrail-to-bridge rail interfaces. All lap-splice connections in the W-beam rail were configured to reduce vehicle snag at the splice during the test. Design details are shown in Figures 86 through 112, and photographs of the test installation are shown in Figures 113 through 118. Material specifications, mill certifications, and certificates of conformity for the system materials are shown in Appendix B.

The MGS was constructed in two sections with a total of seventeen guardrail posts. Post nos. 3 through 8 and 32 through 38 were galvanized ASTM A36 steel W6x8.5 (W152x12.6) sections measuring 72 in. (1,829 mm) long, as shown in Figures 86 through 88. Post nos. 1, 2, 39, and 40 were timber posts measuring 5½ in. wide x 7½ in. deep x 46 in. long (140 mm x 191 mm x 1,168 mm) and were placed in 72-in. (1,829-mm) long steel foundation tubes, as shown in Figures 90 and 99. The timber posts and foundation tubes are used on many tangent guardrail terminals.

Post nos. 1 through 8 and 32 through 40 were spaced 75 in. (1,905 mm) on center with a soil embedment depth of 40 in. (1,016 mm), as shown in Figures 86 through 88. The posts were placed in a compacted, coarse, crushed limestone material that met Grading B of AASHTO M147-65 (1990) as described in MASH. For post nos. 3 through 8 and 32 through 38, 6-in. wide x 12-in. deep x 14¼-in. long (152-mm x 305-mm x 362-mm) wood spacer blockouts were used to block the rail away from the front face of the steel posts, as shown in Figures 88 and 98.

Standard 12-gauge (2.66-mm thick) W-beam rails with post bolt slots at 75-in. (1,905-mm) intervals were placed between post nos. 1 through 8 and 32 through 40, as shown in Figures 86, 87, 89, and 102. The W-beam's top rail height was 31 in. (787 mm), with a 24⅞-in. (632-mm) center mounting height. Rail splices were located at the center of the guardrail span locations, as shown in Figures 86, 87, and 89.

The bridge rail was constructed with twenty-three guardrail posts. Post nos. 9 through 31 were ASTM A36 steel S3x5.7 (S76x8.5) sections measuring 44 in. (1,118 mm) long, as shown in Figures 86, 87, 88, and 97. Post nos. 9 through 31 were spaced 37½ in. (953 mm) on center and mounted in steel socket assemblies, as shown in Figures 86, 87, 88, and 92. A steel bolt was passed through the web of the post and both sides of the socket to support the bridge rail and posts. The sockets were anchored to the deck with a through-deck bolt that passed through the upper strap of the socket and a lower angle plate which was bolted to the socket, as shown in Figures 88 and 92.

Standard 12-gauge (2.66-mm thick) W-beam rails with post bolt slots at 37½-in. (953-mm) intervals were placed between post nos. 9 through 31, as shown in Figures 86, 87, 89, and 102. The W-beam's top rail height was 31 in. (787 mm), with a 24⅞-in. (632-mm) center mounting height. Rail splices were located at bridge rail post locations, as shown in Figures 86, 87, and 89. No blockouts were used with the bridge rail, and 6-in. (152-mm) long, 12-gauge (2.66-mm thick) W-beam backup plates were positioned between the bridge rail and bridge posts at both splice and non-splice locations. The rail was connected to the posts with ⁵⁄₁₆-in. (7.9-mm) diameter ASTM A307 Grade A bolts and nuts and 1¾-in. x 1¾-in. x ⅛-in. (44-mm x 44-mm x 3.2-mm) square washers that were positioned on the traffic-side face of the bridge rail.

A 75-ft long x 4-ft wide x 8-in. thick (22.86-m x 1.22-m x 203-mm) concrete bridge deck was designed and built for crash testing the bridge rail, as shown in Figures 103 through 108.

The thickness of the bridge deck was increased to 12 in. (305 mm) for a width of 12 in. (305 mm) adjacent to the rigid concrete surface and was anchored to the outer vertical edge of the rigid pavement. This deck was intended to simulate a slab-on-girder bridge deck. Anchorage consisted of bent no. 5 (16-mm diameter) upper dowels spaced 9 in. (229 mm) on center that were embedded in epoxy, as shown in Figure 106. Additional no. 4 (13-mm diameter) lower dowels were spaced 18 in. (457 mm) on center. All dowels and deck reinforcement were comprised of ASTM A615 steel.

The concrete deck was designed according to the Nebraska Department of Roads (NDOR) *Bridge Operations, Policies, and Procedures Manual* [70] and the empirical design guidelines presented in the *AASHTO LRFD Bridge Design Specifications* [11]. A deck thickness of 8 in. (203 mm) was used with concrete having a minimum specified 28-day compressive strength of 4,000 psi (27.6 MPa). Actual strength of the concrete is documented in Section 10.1. Longitudinal reinforcement consisted of upper no. 4 (13-mm diameter) bars on 12-in. (305-mm) centers and lower no. 5 (16-mm diameter) bars on 12-in. (305-mm) centers, with the upper reinforcement offset 6 in. (152 mm) from the lower reinforcement. Transverse reinforcement consisted of upper no. 4 (13-mm diameter) bars on 12-in. (305-mm) centers and lower no. 5 (16-mm diameter) bars on 12-in. (305-mm) centers, with the upper and lower layers also offset 6 in. (152 mm). Top concrete clear cover was 2½ in. (64 mm), edge concrete clear cover was 2 in. (51 mm), and bottom concrete clear cover was 1 in. (25 mm).

Two transverse no. 6 (19-mm diameter) bars were placed between each upper no. 4 (13-mm diameter) bar, which is standard practice in the cantilevered sections of the bridge deck in order to sustain loads from the bridge rail. At bridge rail post locations, a no. 6 (19-mm diameter) bar with a 5-in. (127-mm) diameter, 180-degree bend was looped around the location of the through-bolt to prevent the bolt from pulling out the side of the deck, as shown in Figure 104. At locations where the bent no. 6 (19-mm diameter) bars interfered with the straight bars, the straight bars were placed beneath the bent bars. At locations where the through-deck bolt sleeve assembly interfered with the straight bars, the straight bars were shifted sideways.

To aid with the installation of the bridge rail posts and minimize local deck damage, 2-in. x 2-in. x ¼-in. (51-mm x 51-mm x 6.4-mm) square bolt-sleeves were cast into the deck, as shown in Figures 104 and 110. These sleeves were 8 in. (203 mm) long, comprised of ASTM A500 Grade B steel, and housed the 1-in. (25.4-mm) diameter through-deck bolts which anchored the bridge posts. Number 3 (10-mm diameter) bars were tac-welded to the bolt sleeve and tied into the transverse deck reinforcement.

To further strengthen the deck, additional reinforcement was placed around each bolt-sleeve assembly, as is shown in Figures 104 and 105. Bent no. 4 (13-mm diameter) bars were placed above the upper reinforcement to the exterior of the bolt-sleeve assemblies. Longitudinal no. 6 (19-mm diameter) bars were placed to the interior of the bolt-sleeves, just above the lower transverse reinforcement, to prevent local crushing in the concrete in the lower portion of the deck.

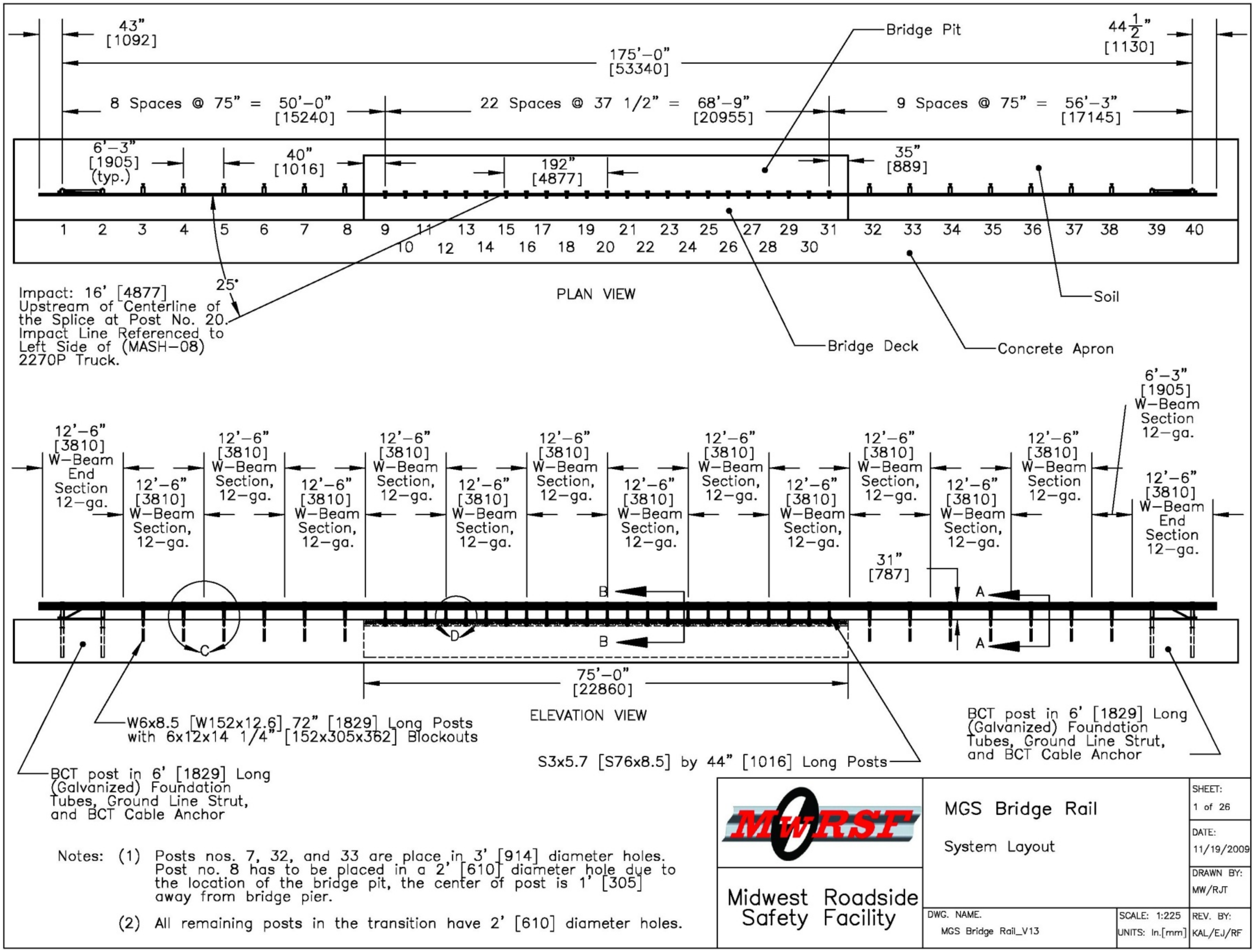

Figure 86. Test Installation Layout, Test No. MGSBR-1

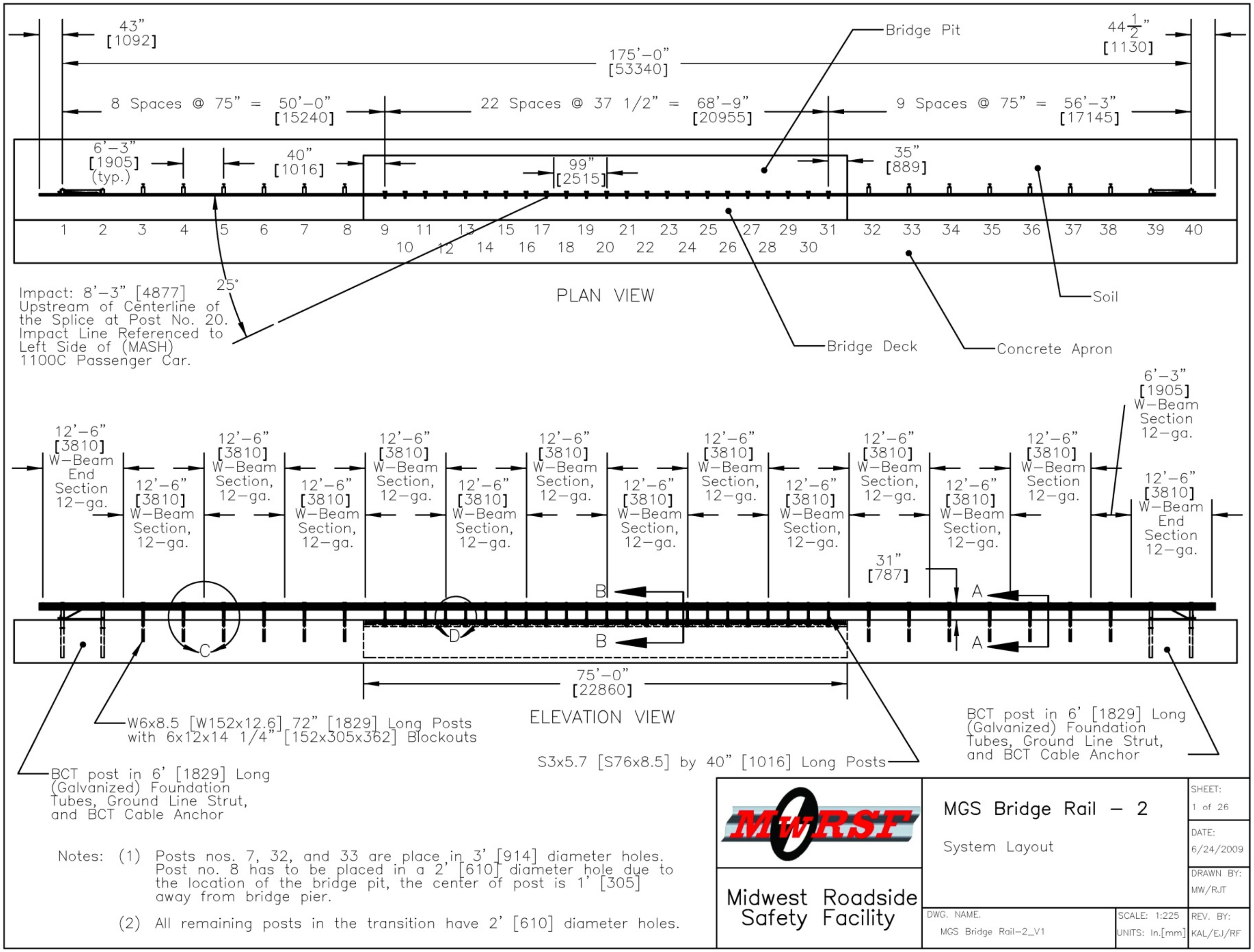

Figure 87. Test Installation Layout, Test No. MGSBR-2

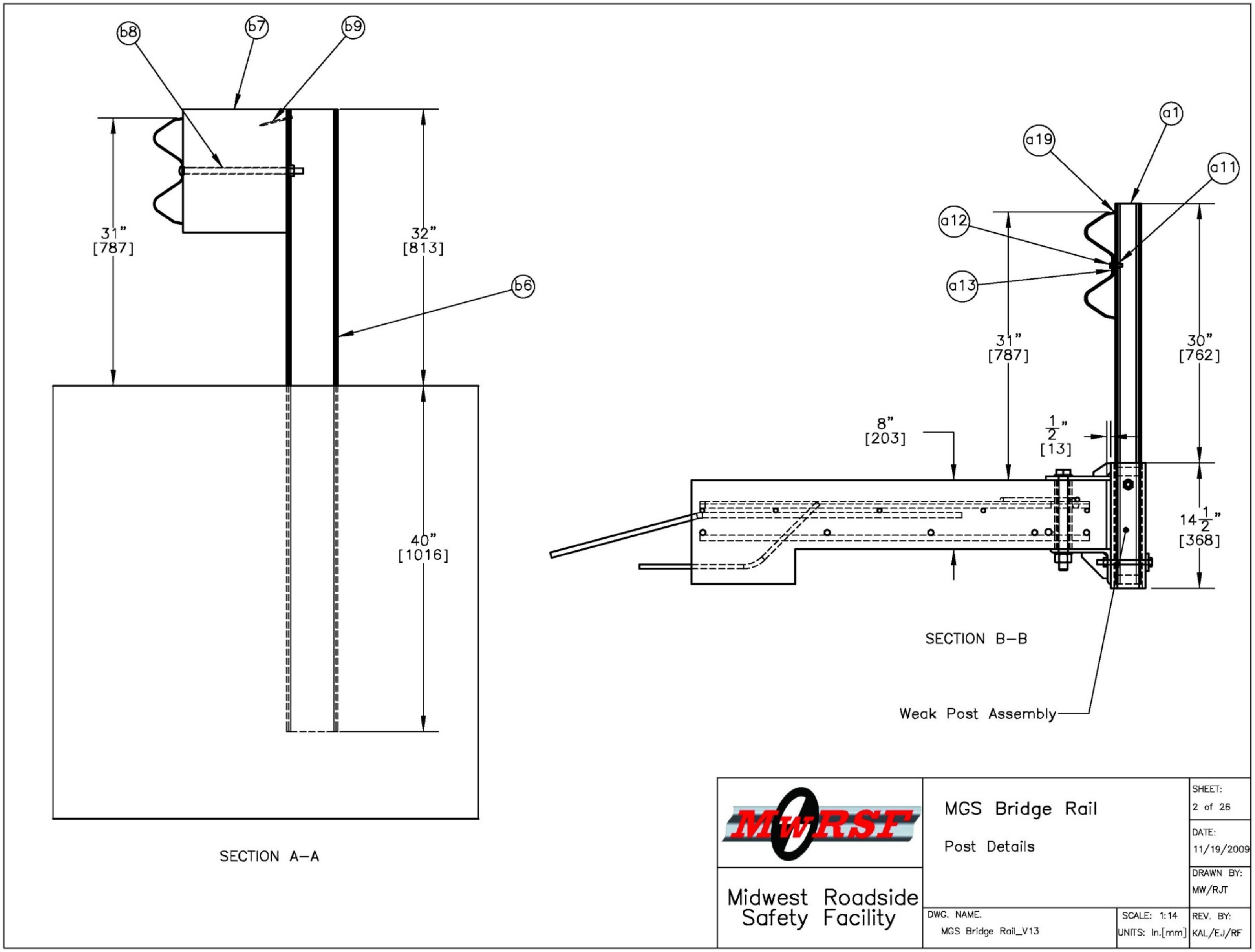

Figure 88. Post Details, Test Nos. MGSBR-1 and MGSBR-2

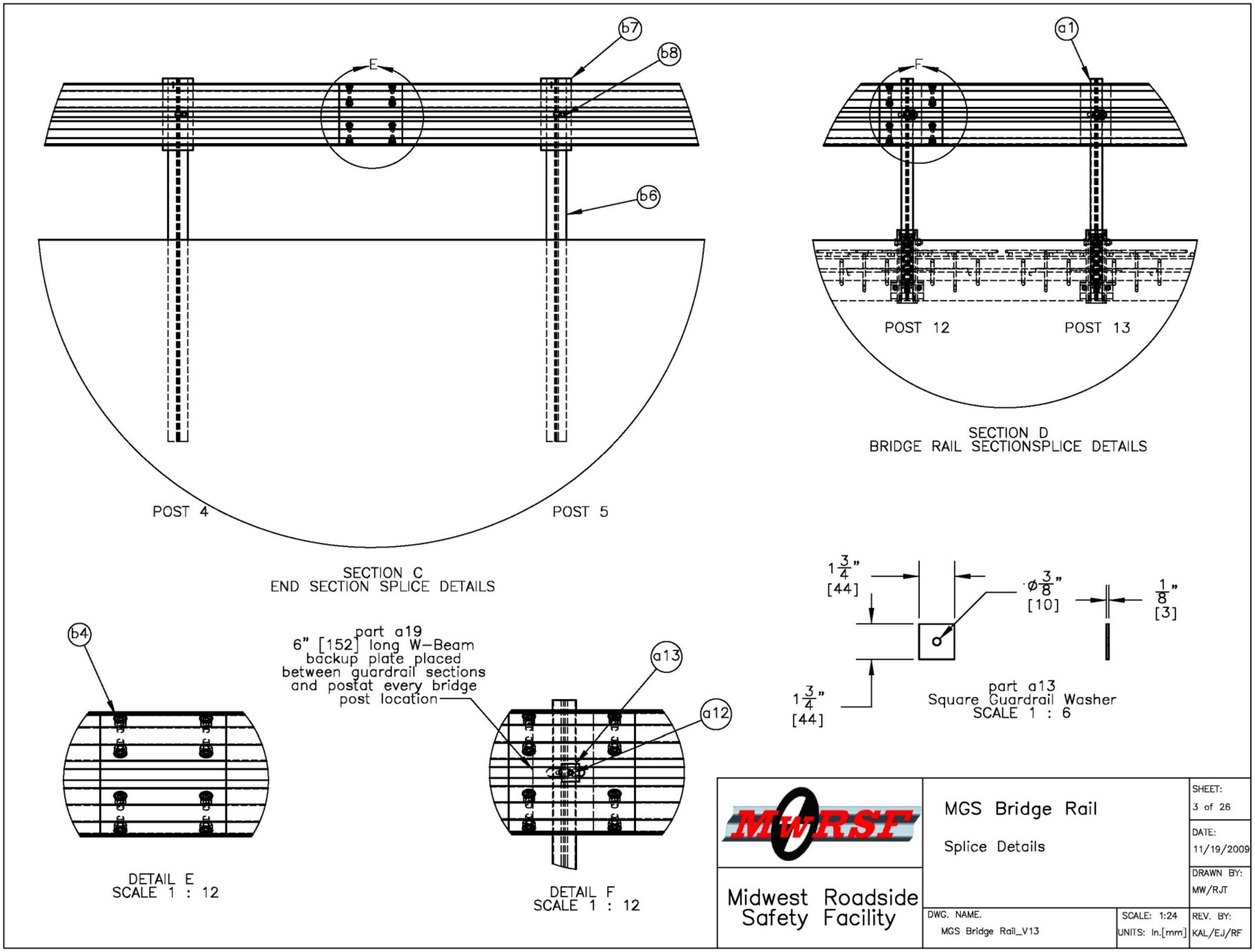

Figure 89. Splice Details, Test Nos. MGSBR-1 and MGSBR-2

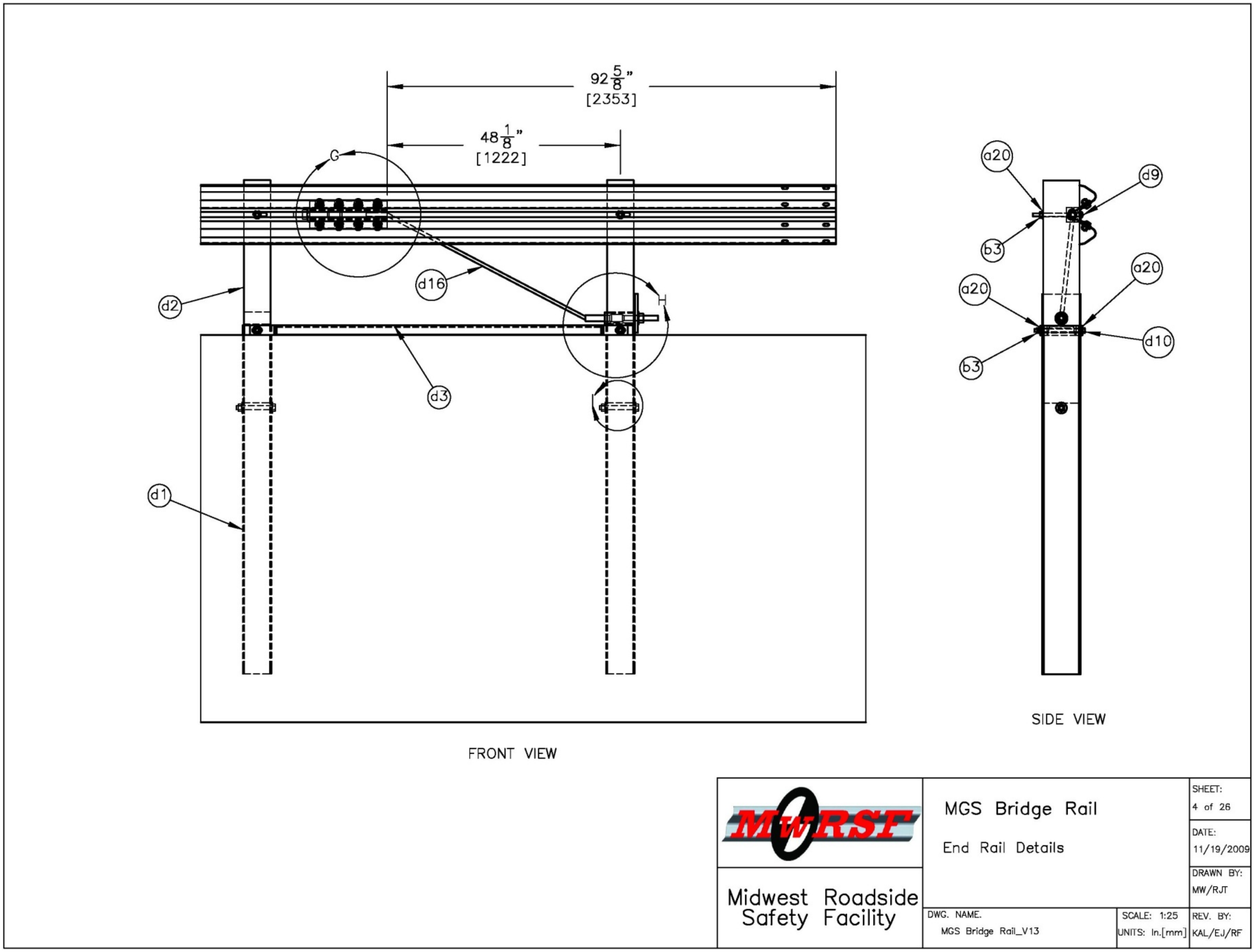

Figure 90. End Rail Details, Test Nos. MGSBR-1 and MGSBR-2

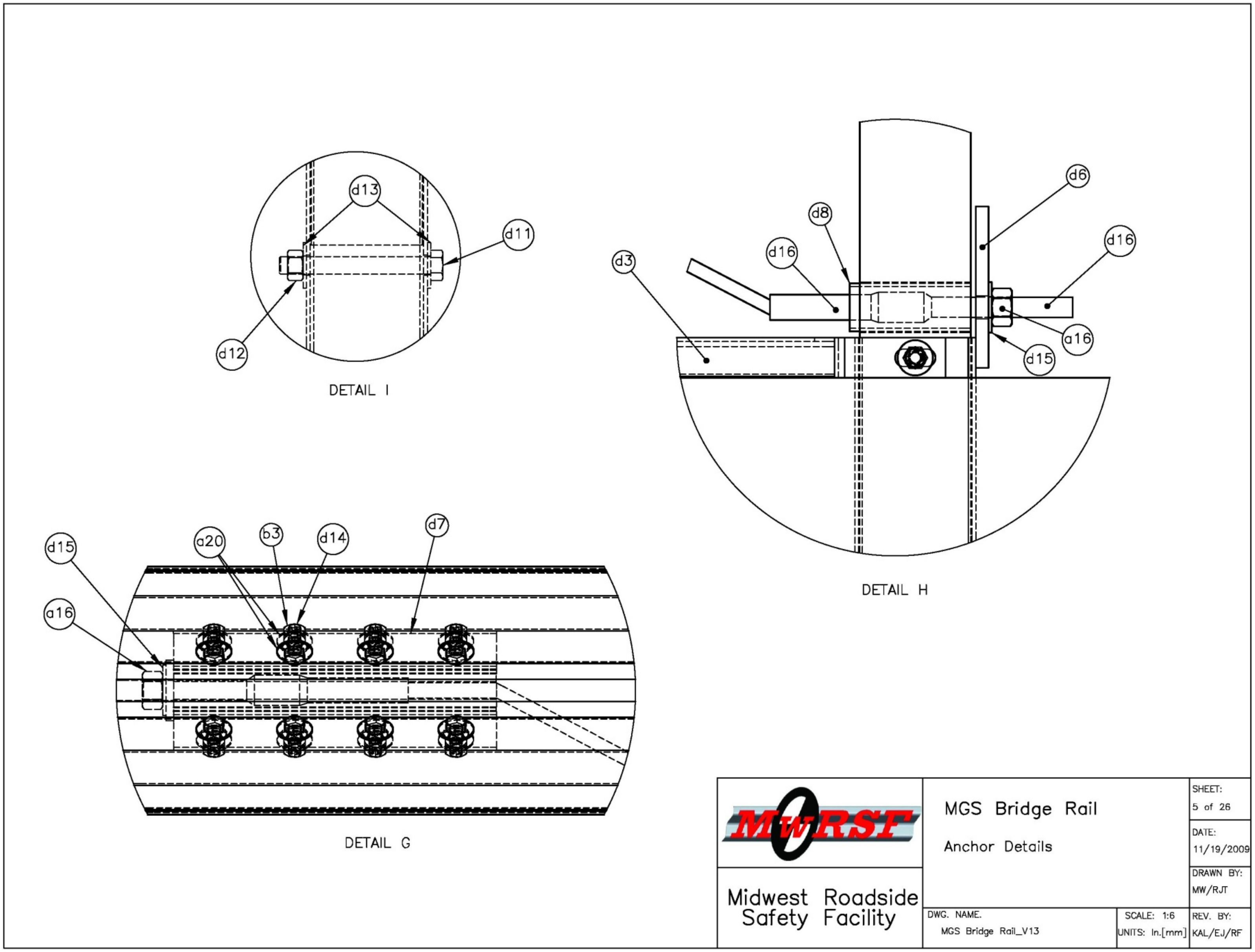

Figure 91. Anchor Details, Test Nos. MGSBR-1 and MGSBR-2

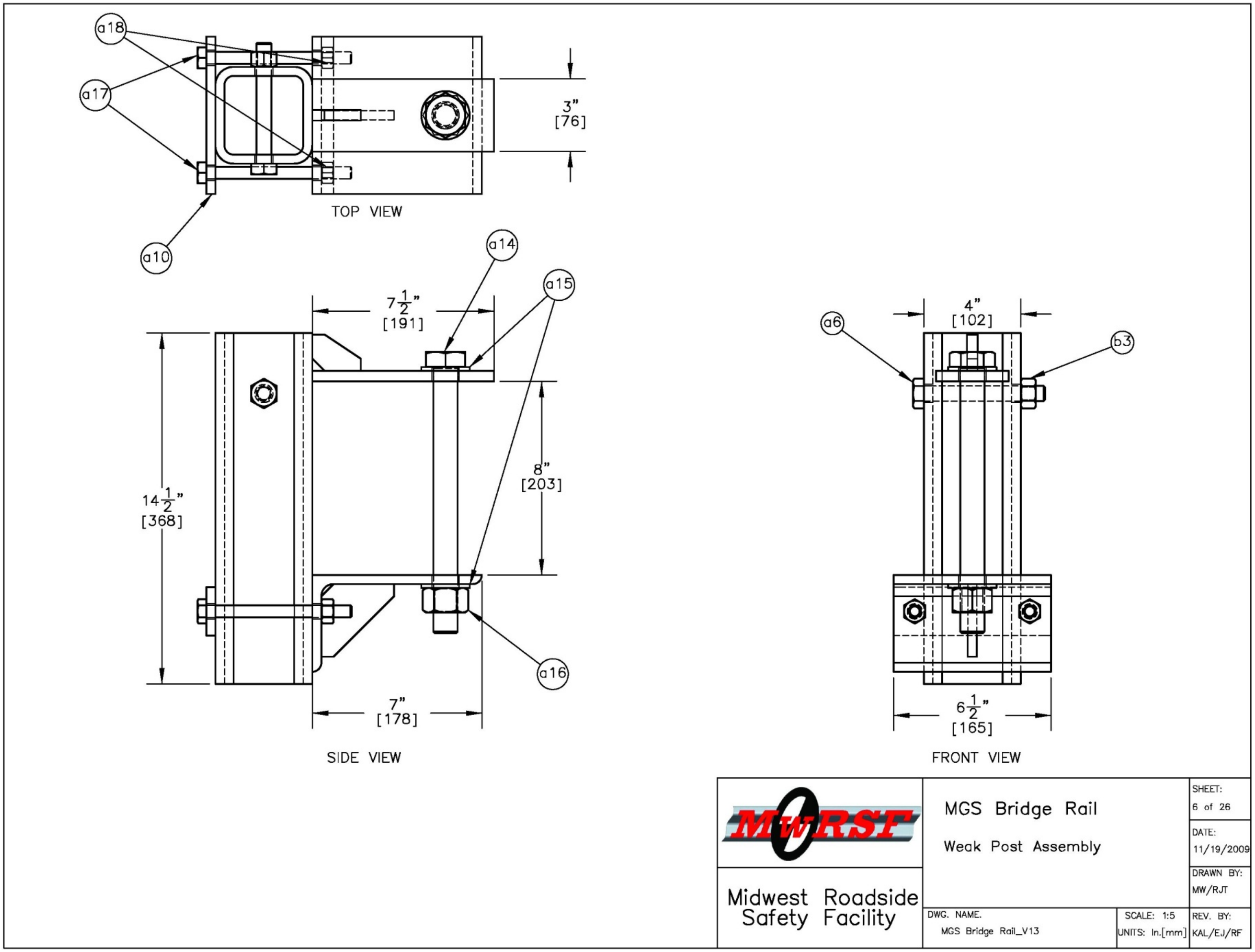

Figure 92. Mounting Bracket Assembly, Test Nos. MGSBR-1 and MGSBR-2

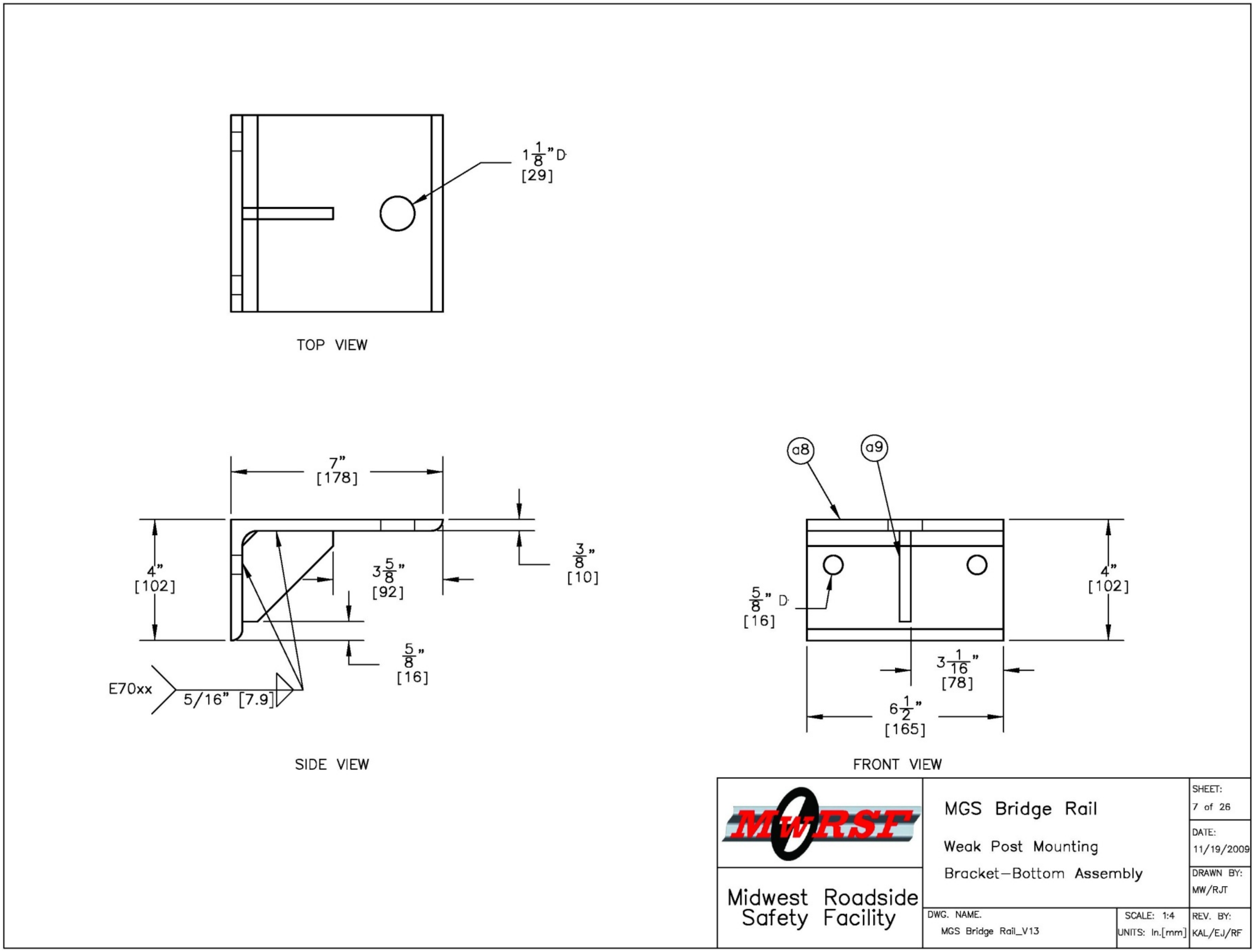

Figure 93. Mounting Bracket – Bottom Assembly, Test Nos. MGSBR-1 and MGSBR-2

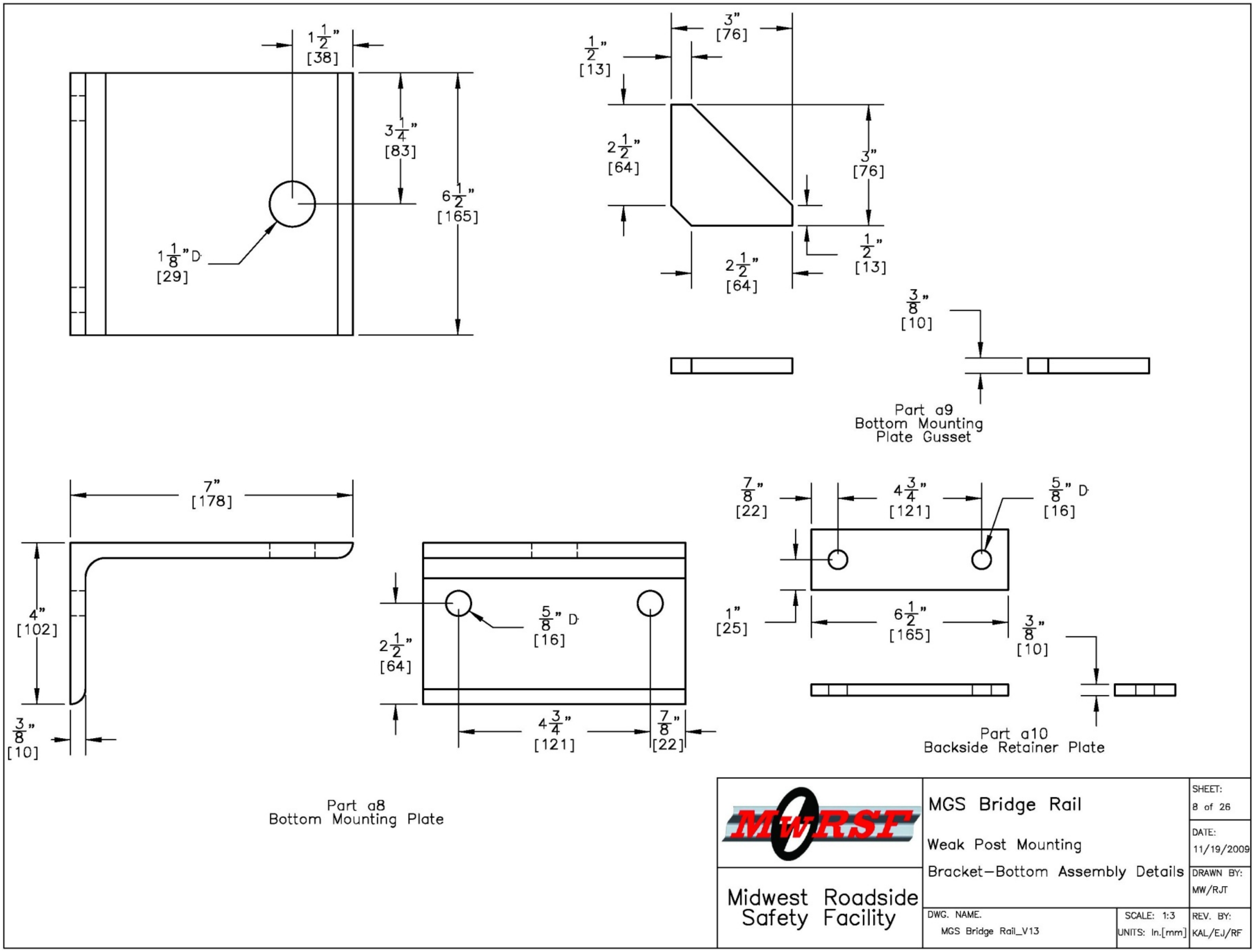

Figure 94. Mounting Bracket – Bottom Assembly Details, Test Nos. MGSBR-1 and MGSBR-2

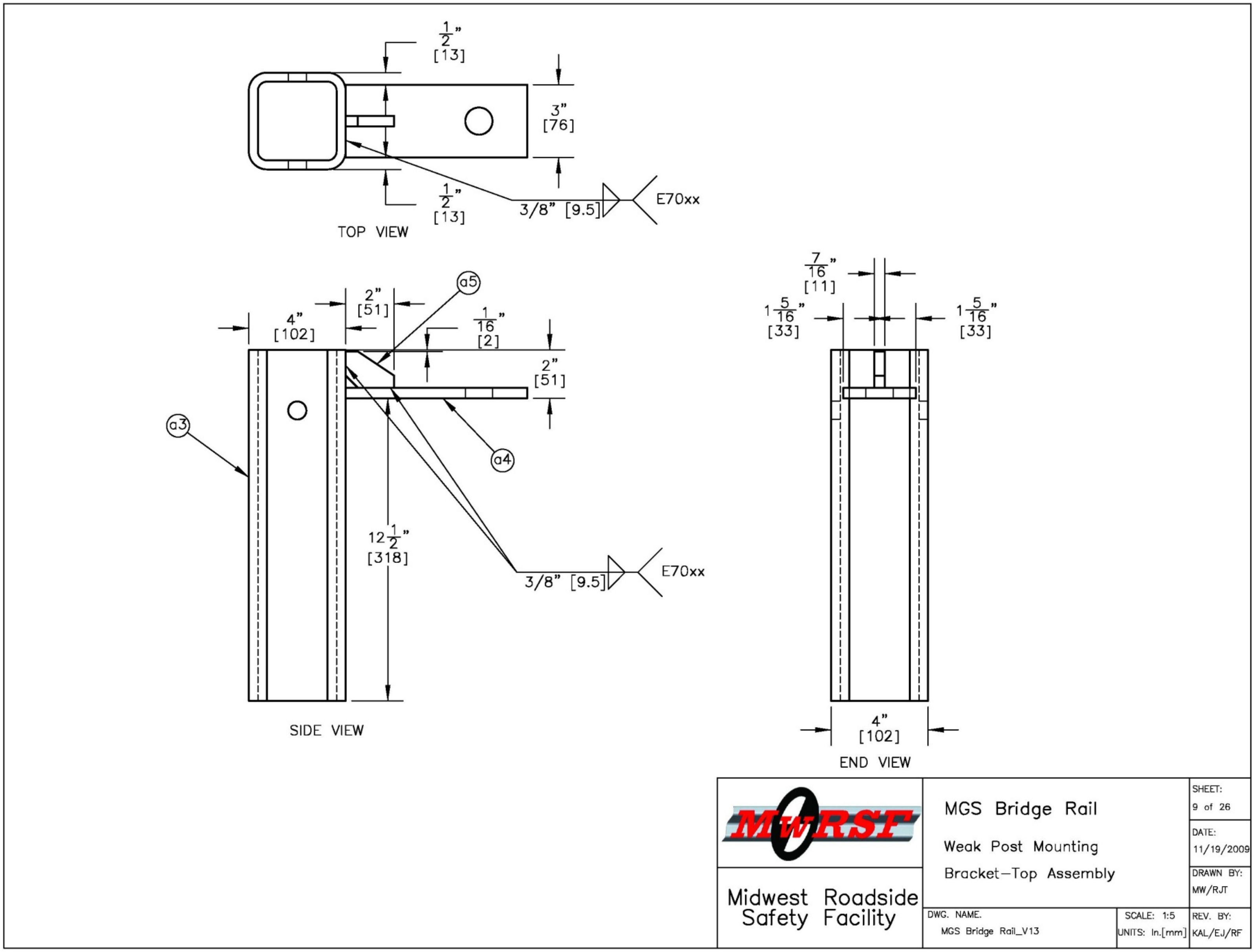

Figure 95. Mounting Bracket – Top Assembly, Test Nos. MGSBR-1 and MGSBR-2

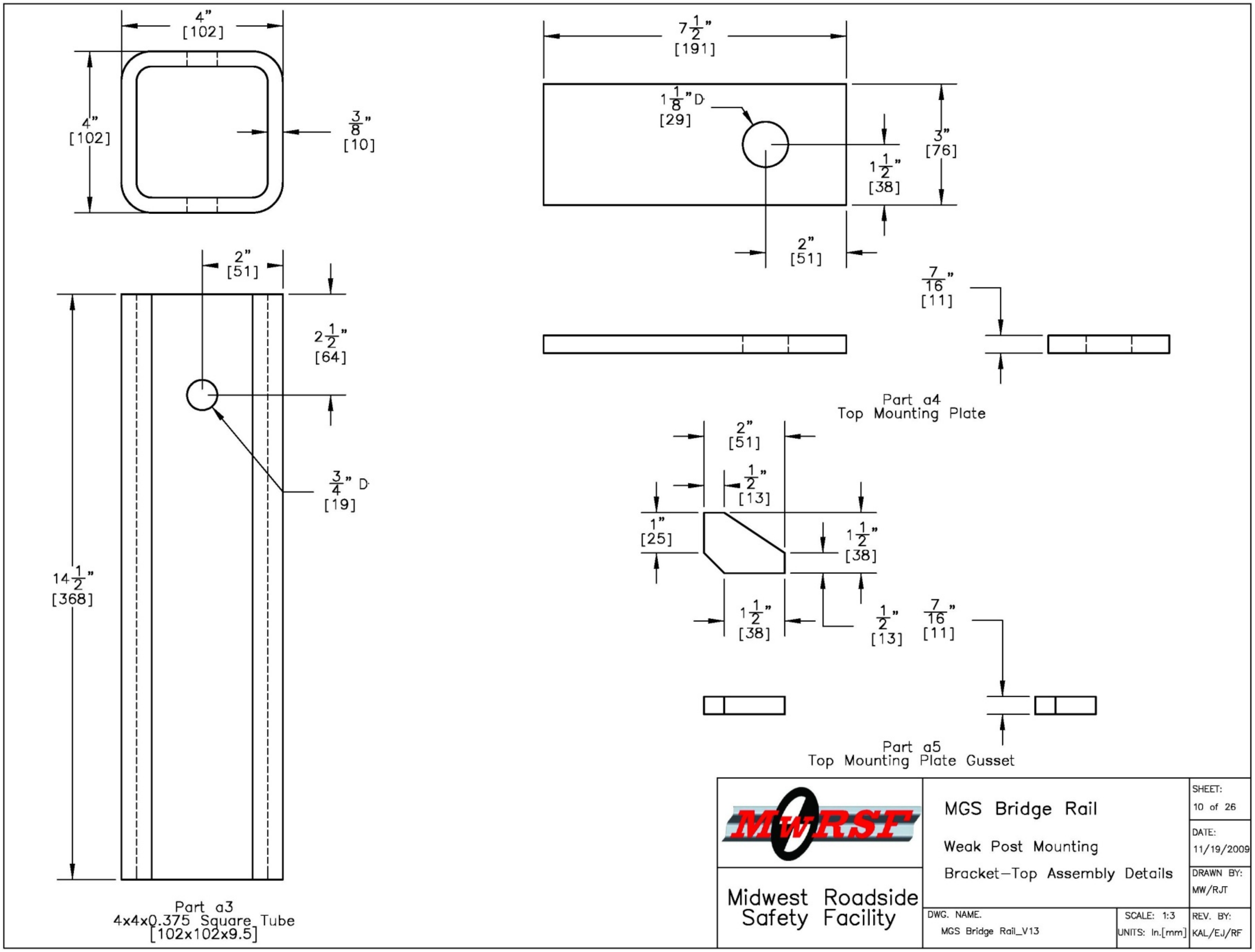

Figure 96. Mounting Bracket – Top Assembly Details, Test Nos. MGSBR-1 & MGSBR-2

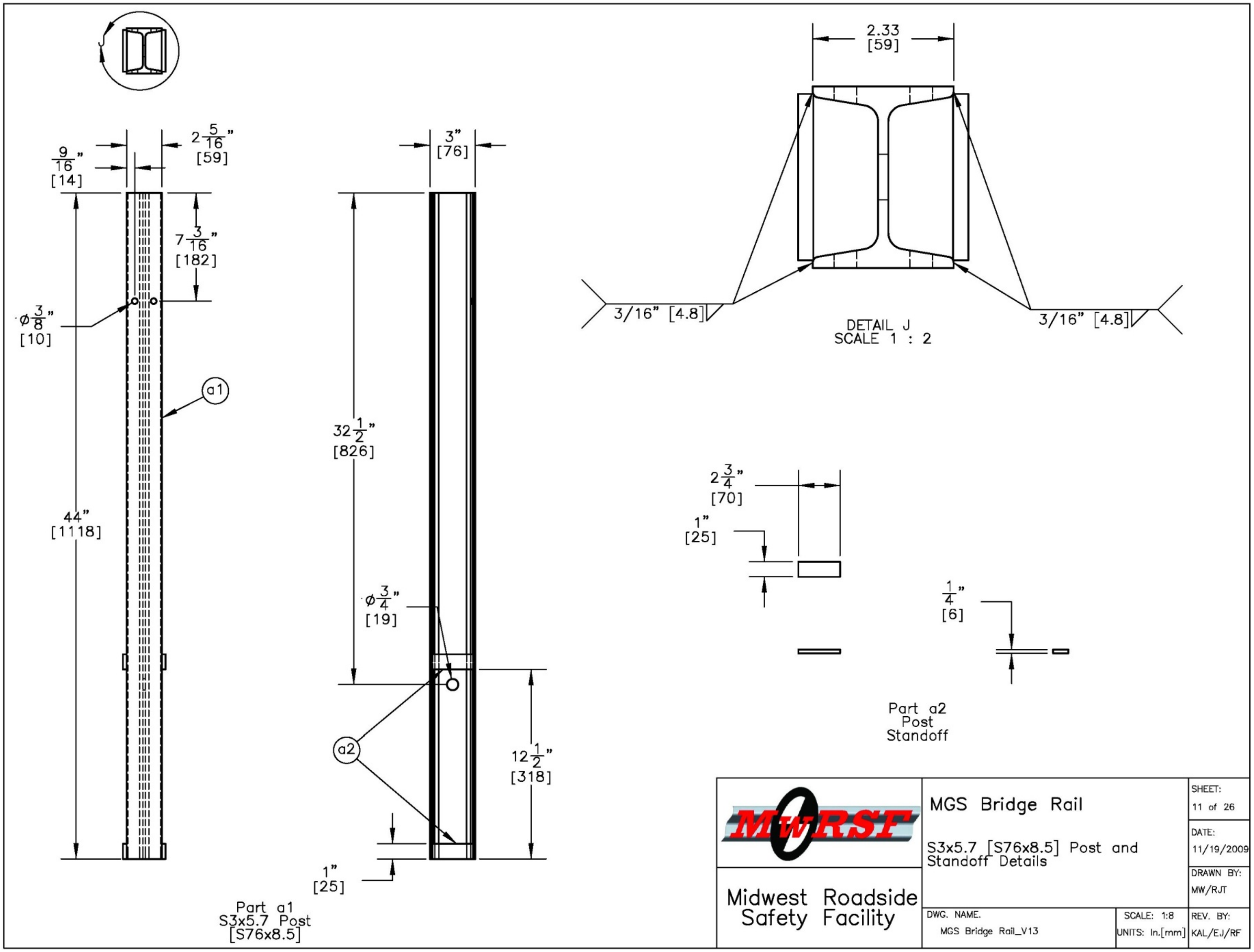

Figure 97. S3x5.7 (S76x8.5) Post and Standoff Details, Test Nos. MGSBR-1 & MGSBR-2

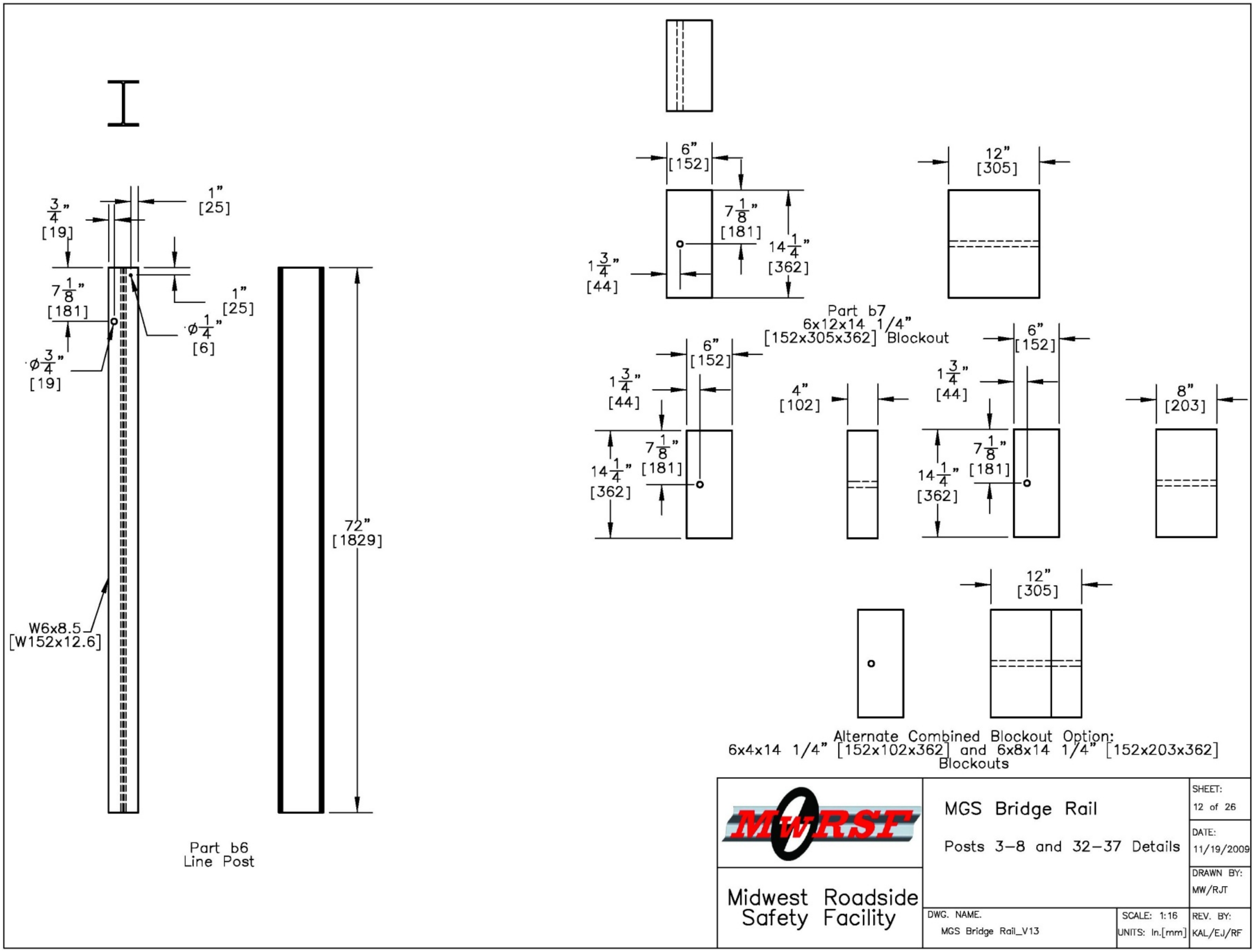

Figure 98. Posts 3-8 and 32-37 Details, Test Nos. MGSBR-1 and MGSBR-2

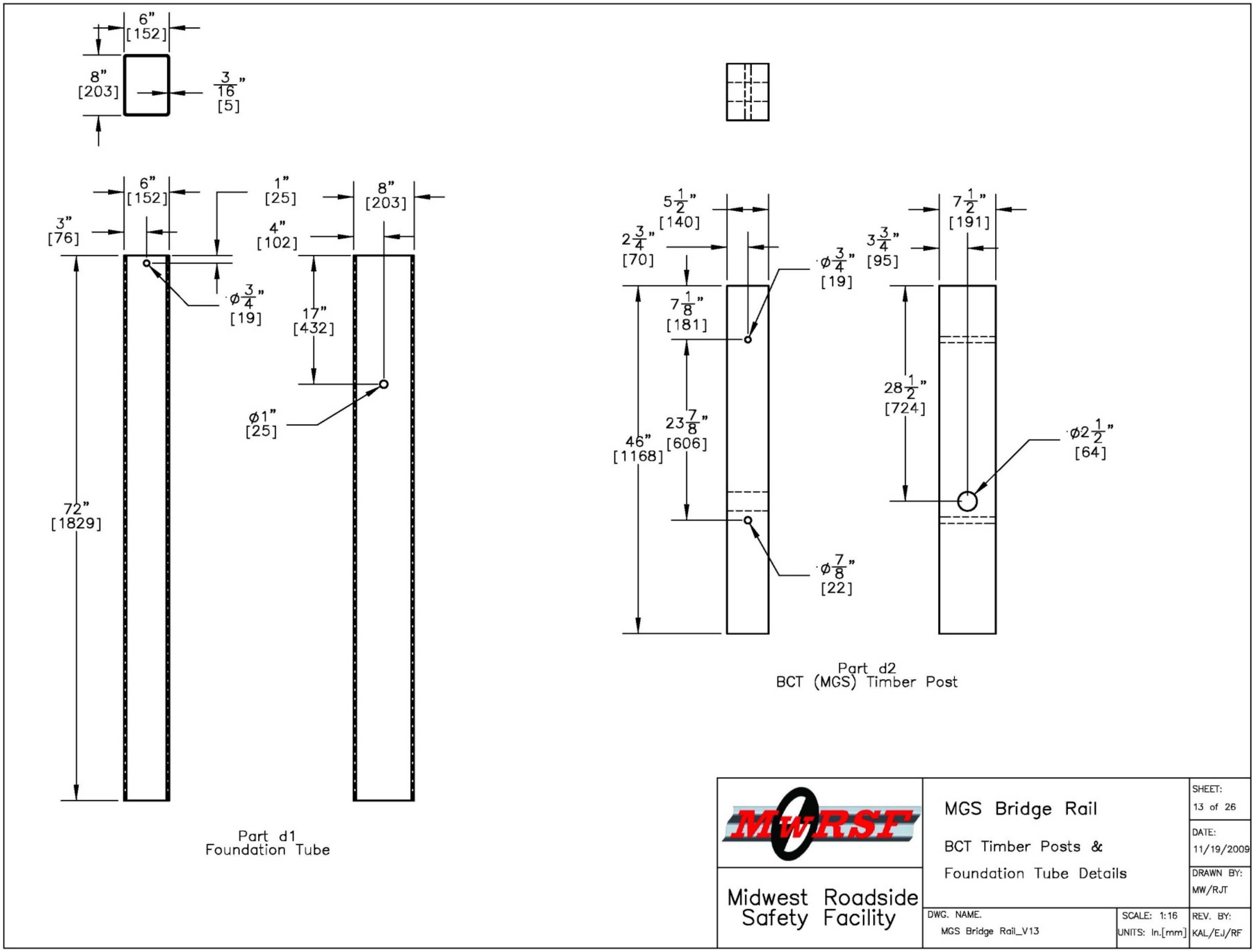

Figure 99. BCT Timber Posts & Foundation Tube Details, Test Nos. MGSBR-1 and MGSBR-2

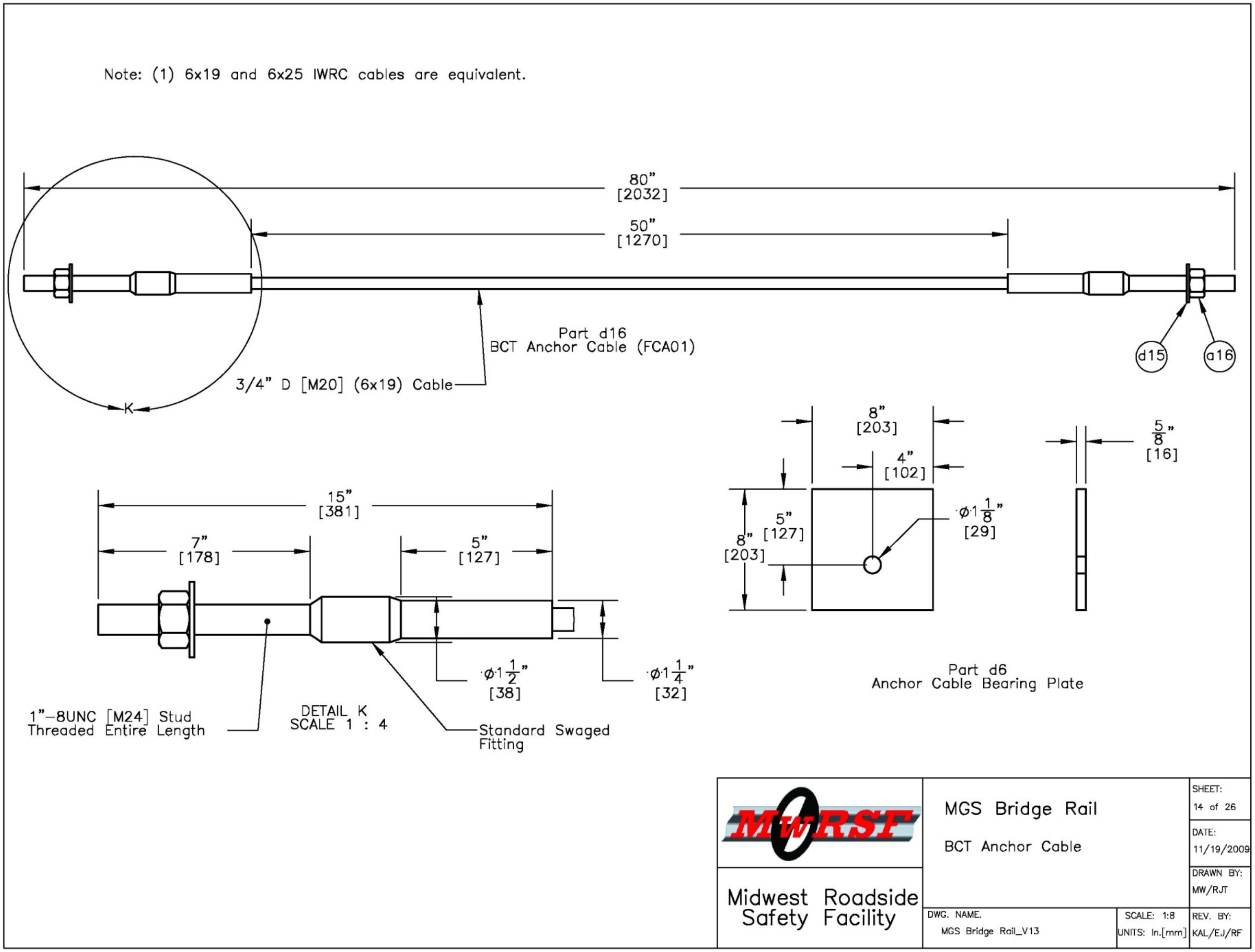

Figure 100. BCT Anchor Cable, Test Nos. MGSBR-1 and MGSBR-2

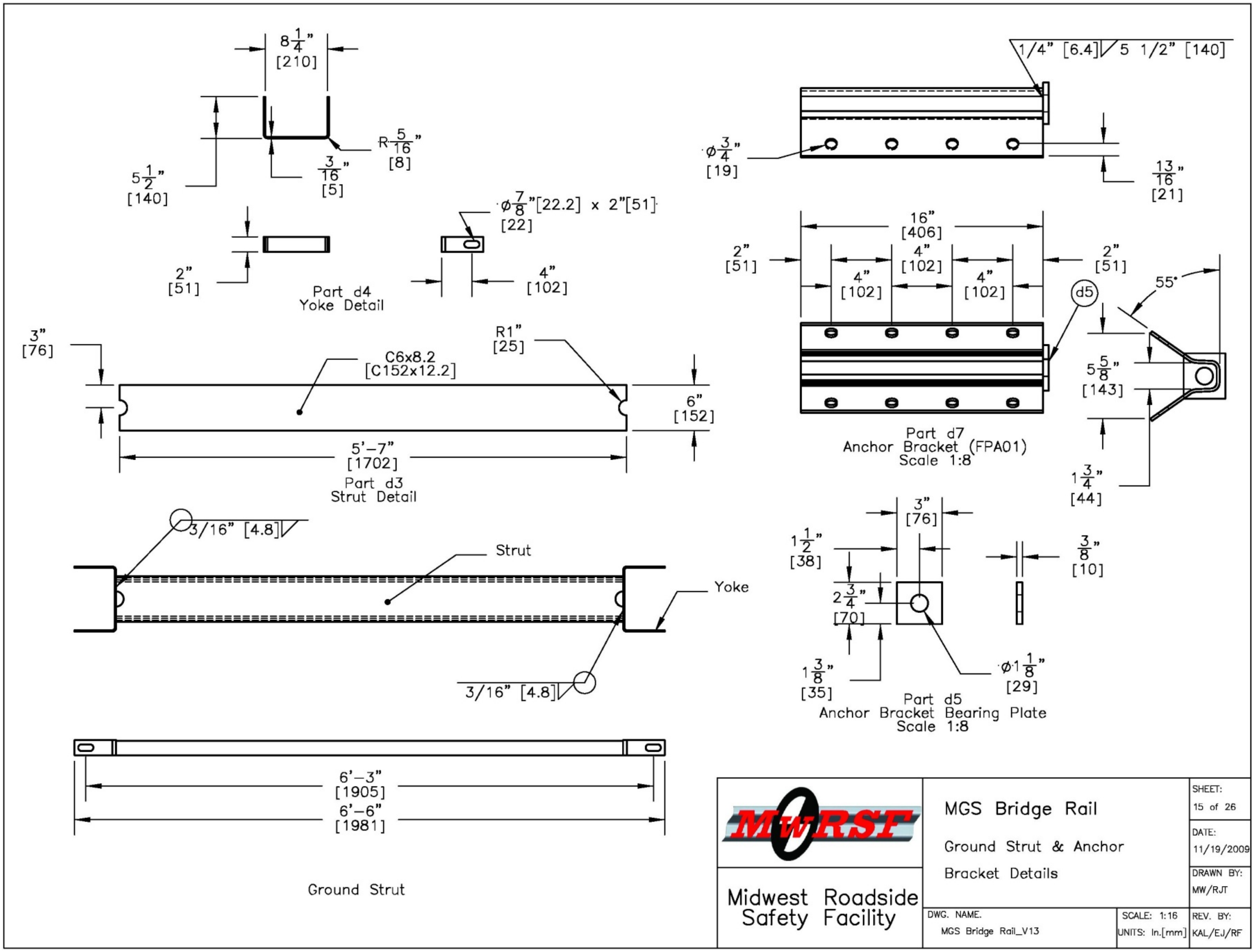

Figure 101. Ground Strut & Anchor Bracket Details, Test Nos. MGSBR-1 and MGSBR-2

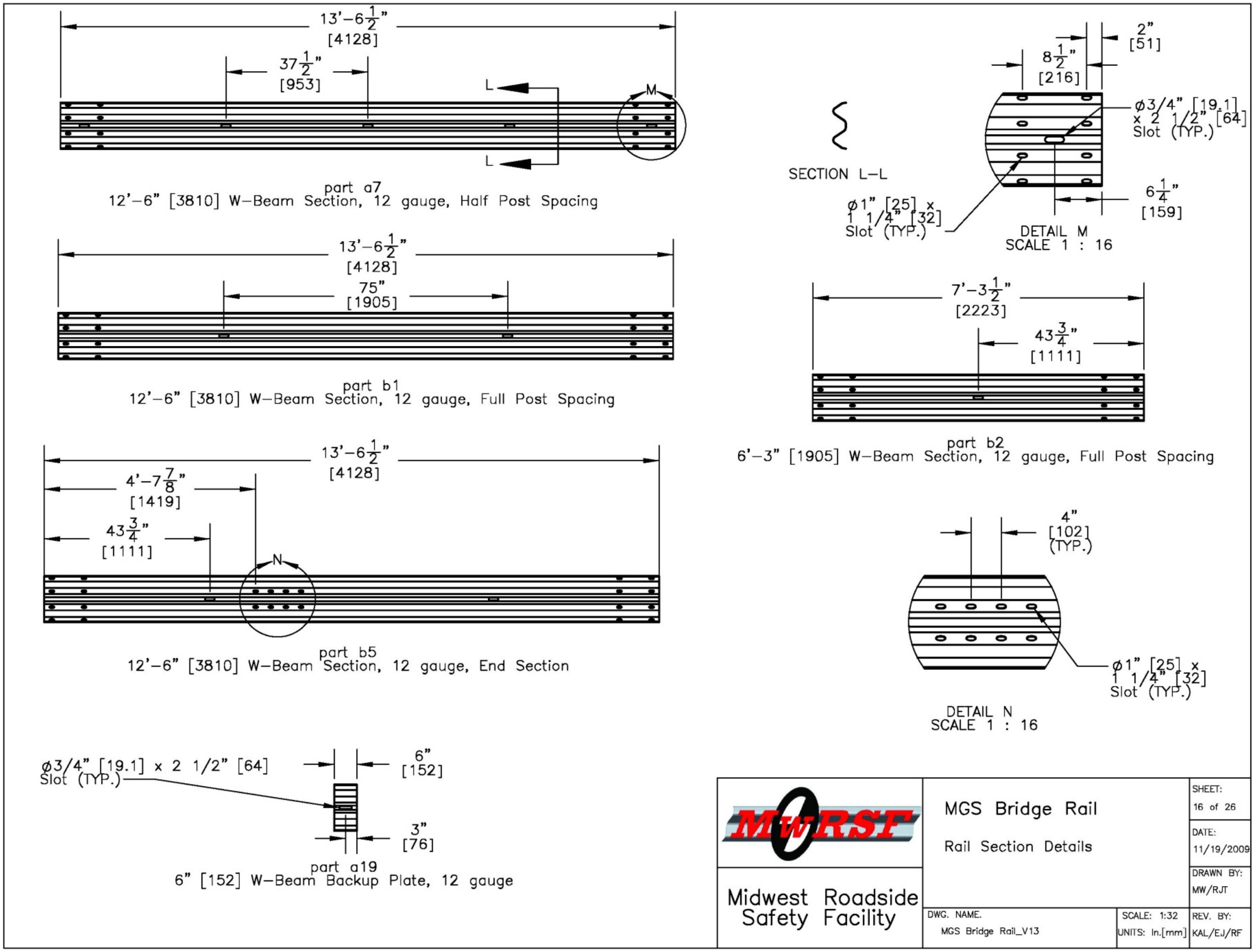

Figure 102. Rail Section Details, Test Nos. MGSBR-1 and MGSBR-2

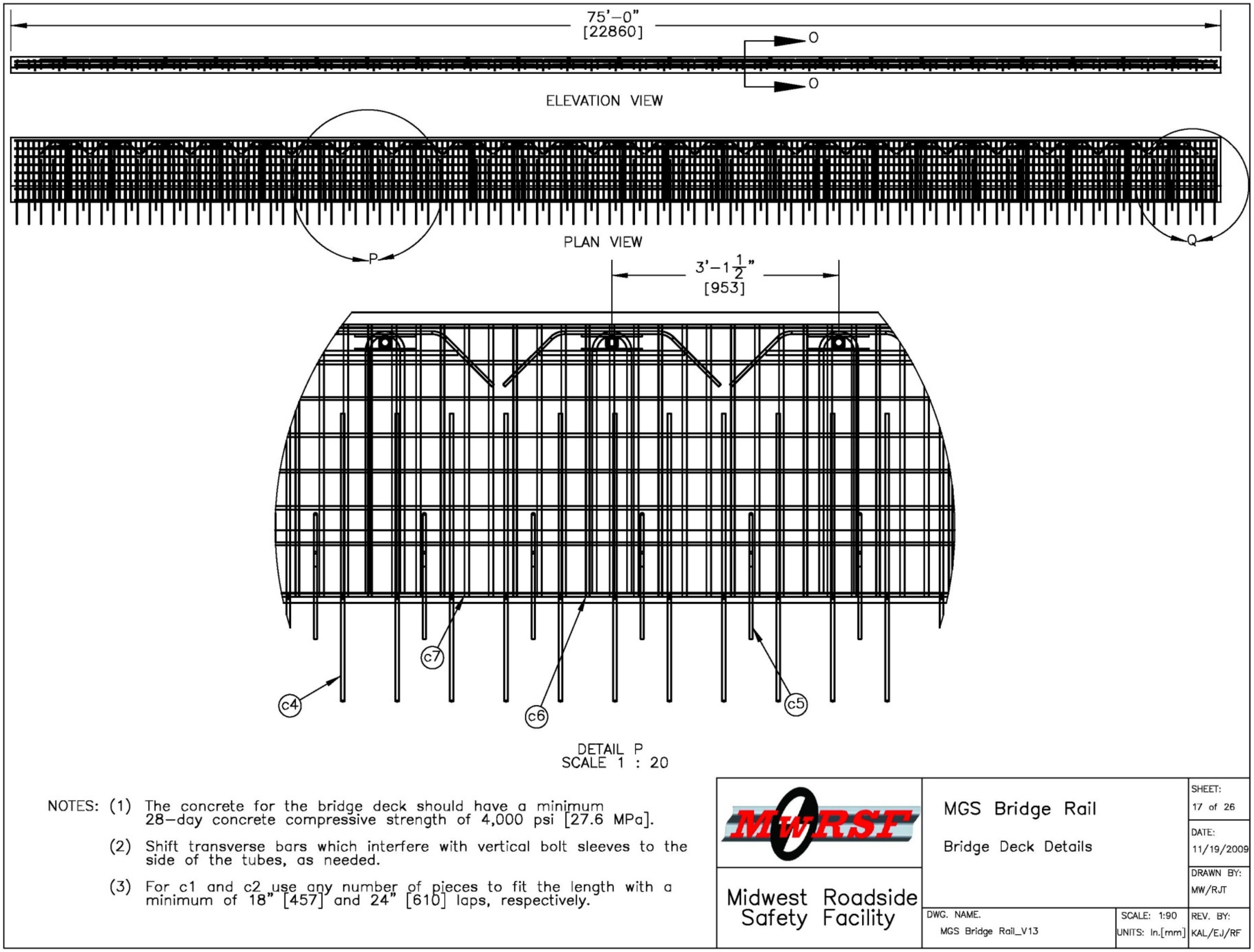

Figure 103. Bridge Deck Reinforcement Layout, Test Nos. MGSBR-1 and MGSBR-2

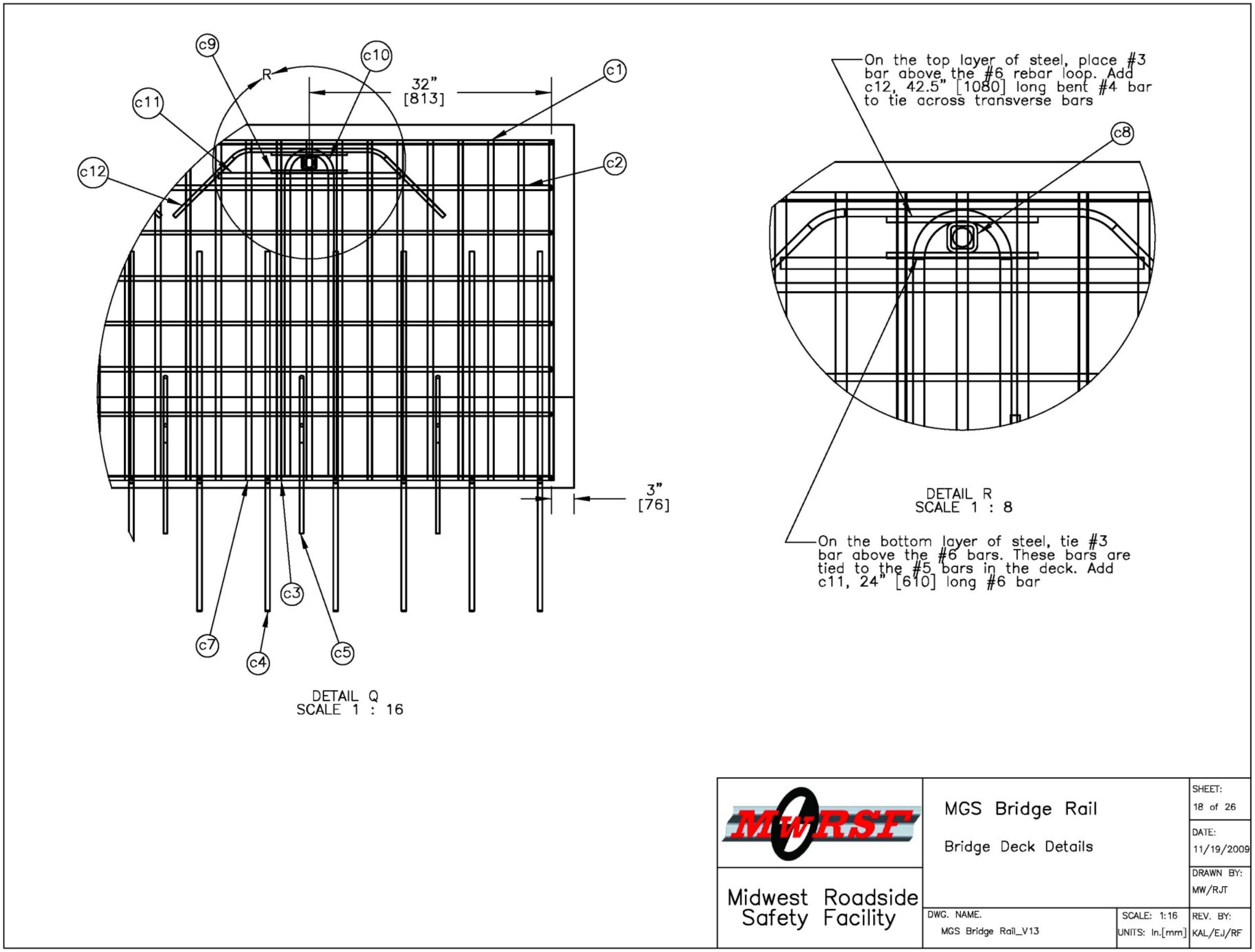

Figure 104. Bridge Deck Details, Test Nos. MGSBR-1 and MGSBR-2

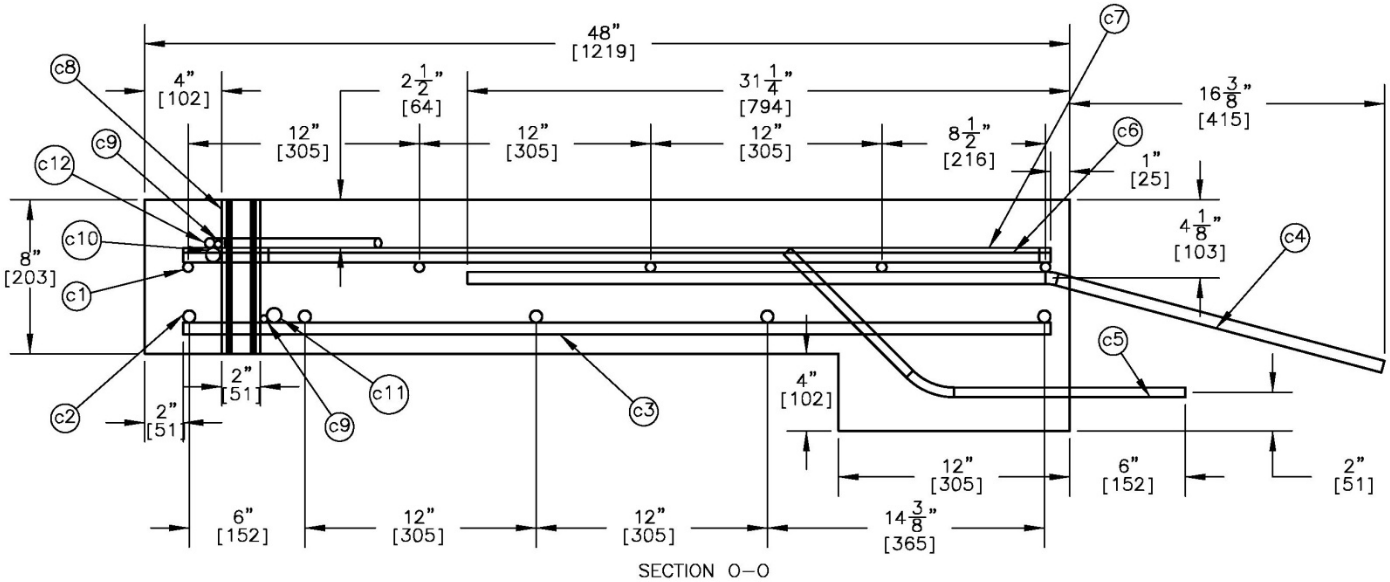

Notes: (1) Tie #4 and #6 bars to #3 bars after placement in the deck.

(2) The bottom of #4 and #6 bars are tied at the same plane as the bottom of the #3 bars. These bars are not centered.

(3) For c1 and c2 use any number of pieces to fit the length with a minimum of 18" [457] and 24" [610] laps, respectively.

Midwest Roadside Safety Facility	MGS Bridge Rail Bridge Deck Details	SHEET: 19 of 26
		DATE: 11/19/2009
		DRAWN BY: MW/RJT
	DWG. NAME. MGS Bridge Rail_V13 / SCALE: 1:8 / UNITS: In.[mm]	REV. BY: KAL/EJ/RF

Figure 105. Bridge Deck Section, Test Nos. MGSBR-1 and MGSBR-2

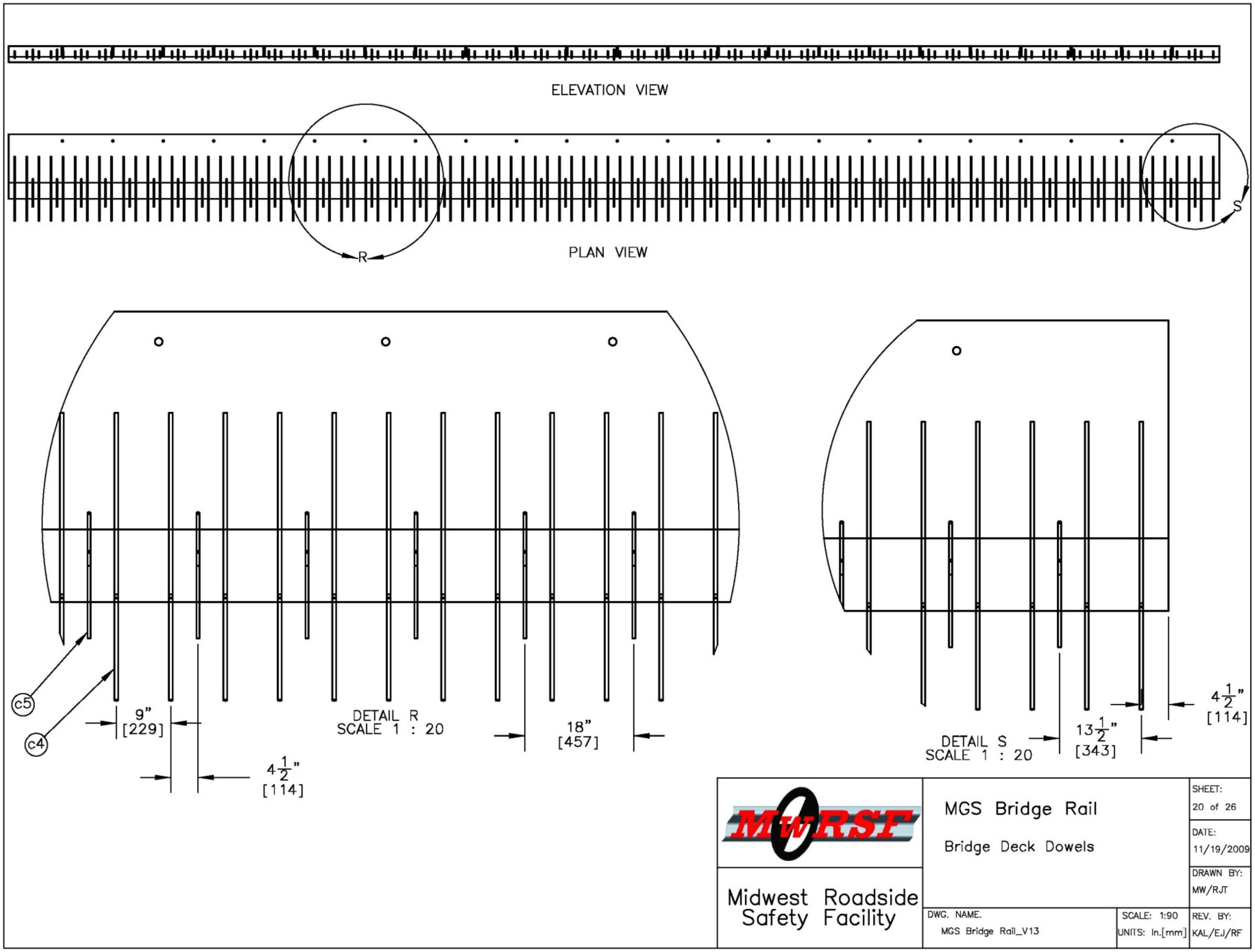

Figure 106. Bridge Deck Dowels, Test Nos. MGSBR-1 and MGSBR-2

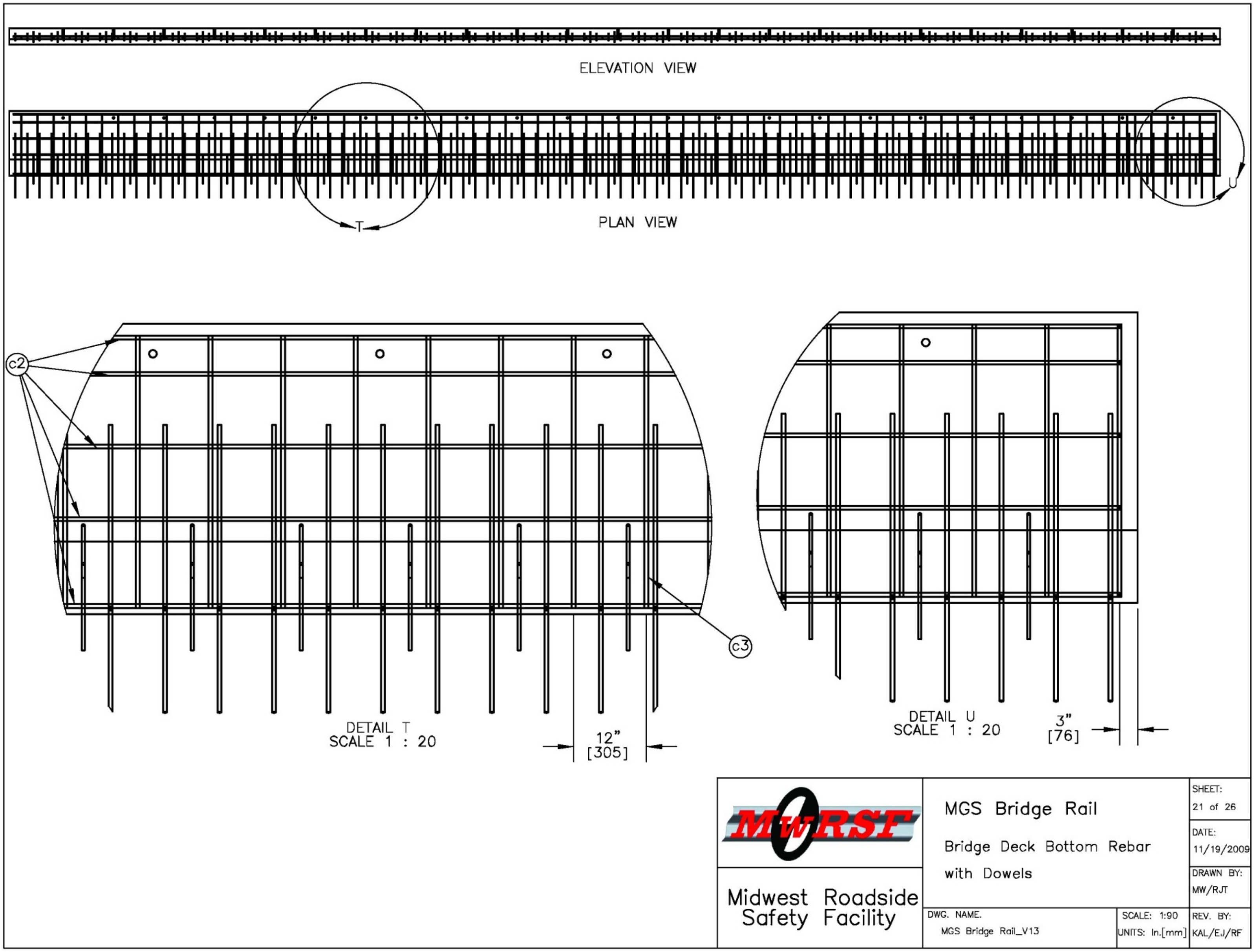

Figure 107. Bridge Deck Bottom Rebar and Dowels, Test Nos. MGSBR-1 and MGSBR-2

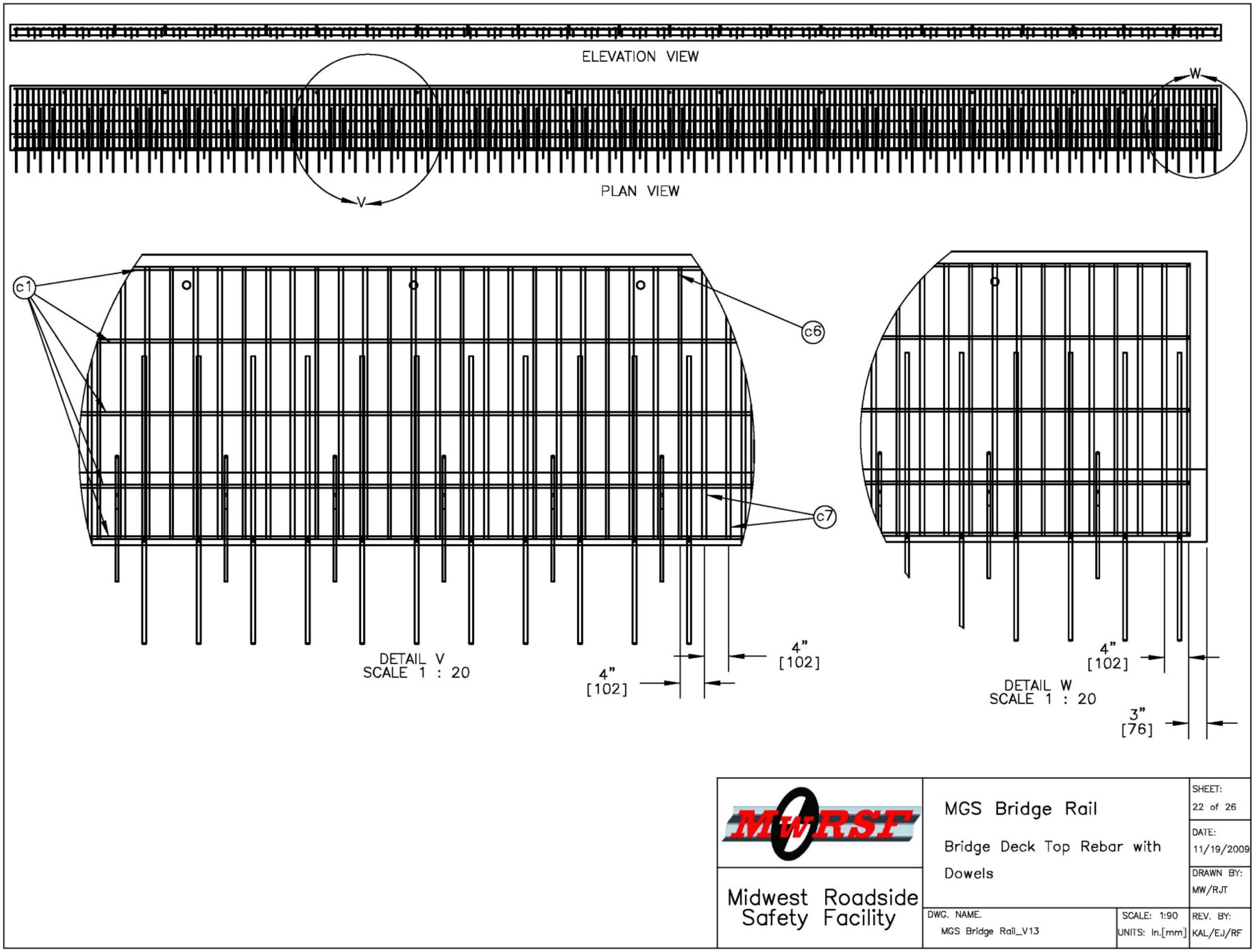

Figure 108. Bridge Deck Top Rebar and Dowels, Test Nos. MGSBR-1 and MGSBR-2

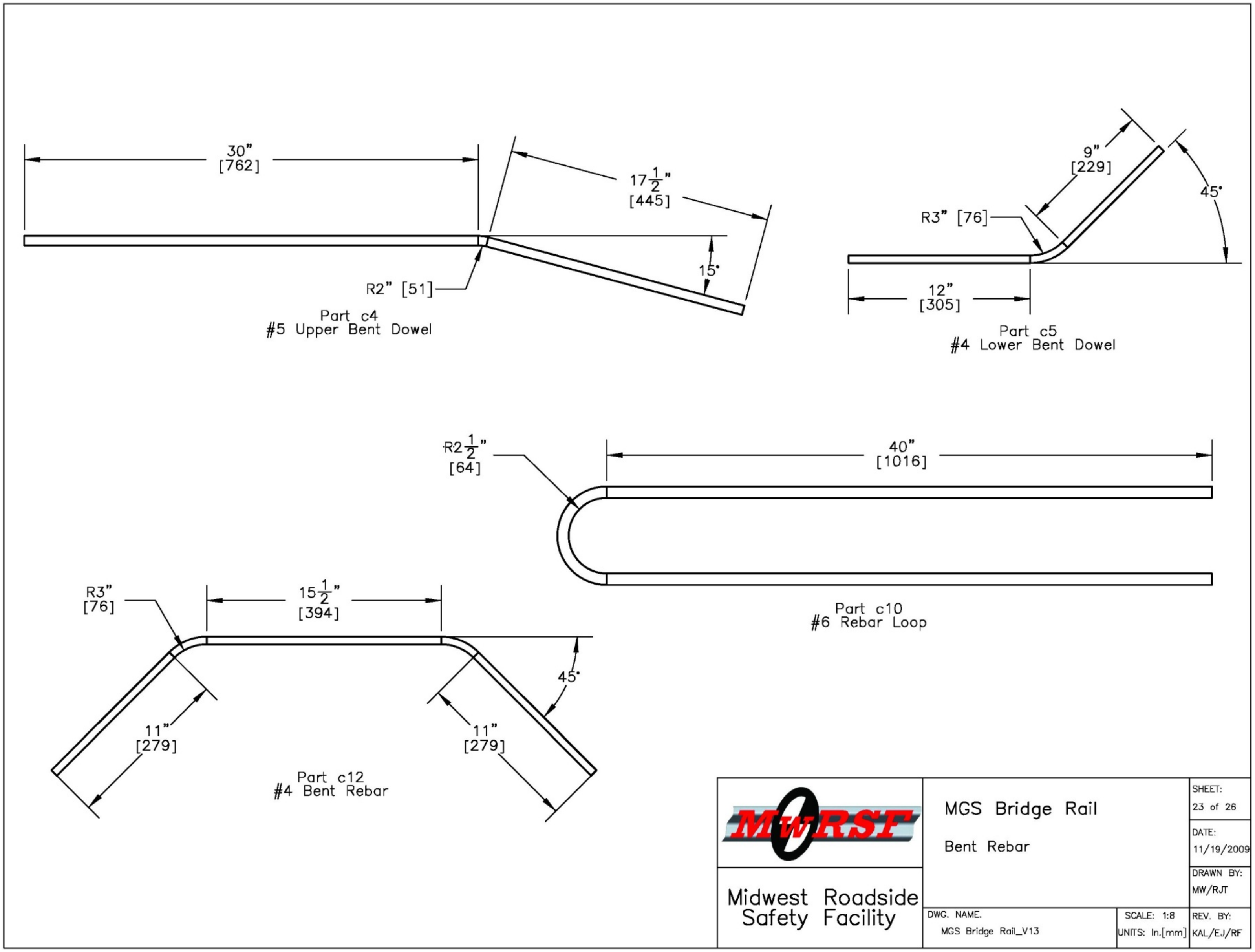

Figure 109. Bent Rebar, Test Nos. MGSBR-1 and MGSBR-2

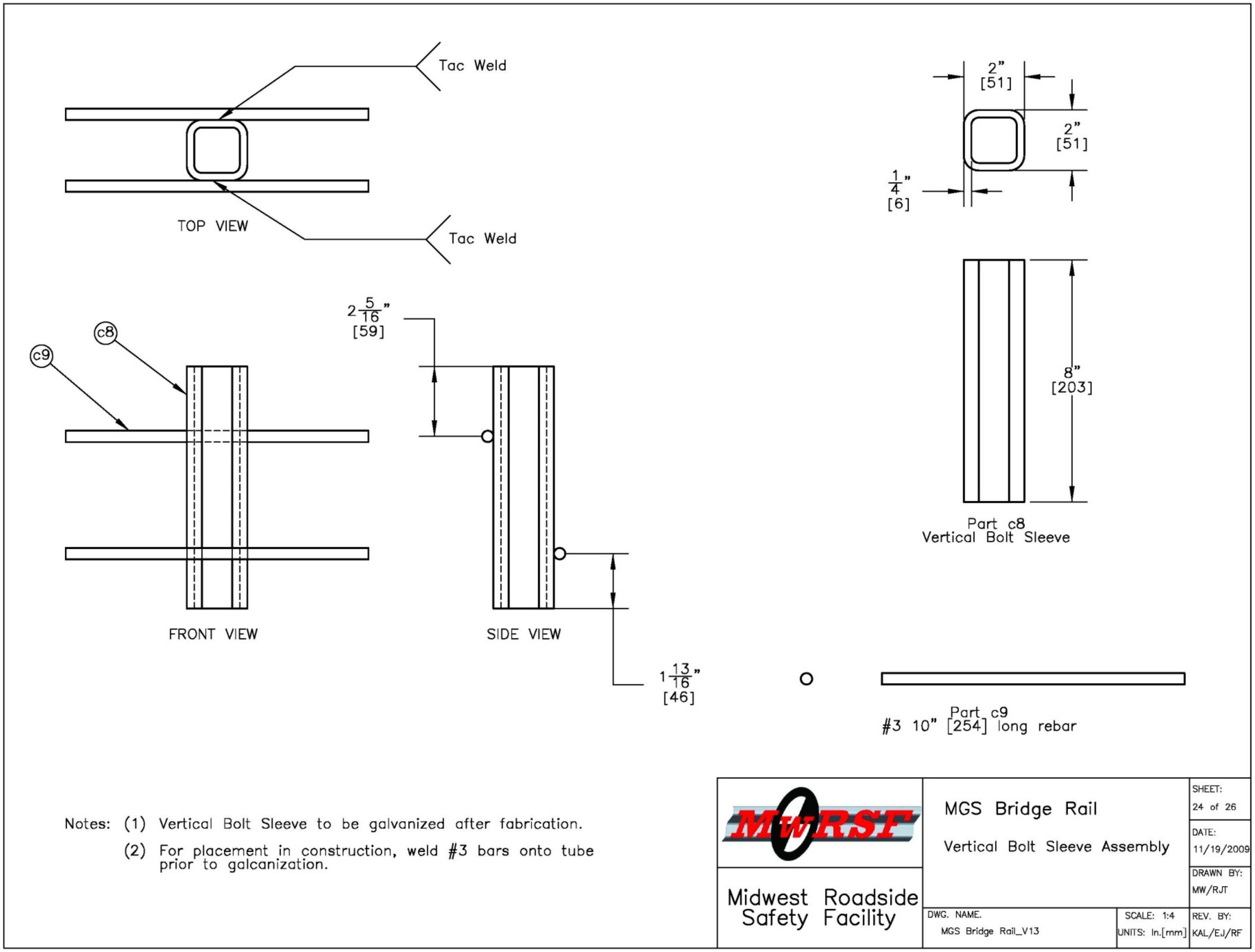

Figure 110. Vertical Bolt Sleeve Assembly, Test Nos. MGSBR-1 and MGSBR-2

MGS Bridge Rail System				
Item No.	QTY.	Description	Material Spec	Hardware Guide
a1	23	S3x5.7 by 44" long Post	A36 Steel Galvanized	–
a2	92	2.75"x1"x0.25" S3x5.7 Post Standoff	A36 Steel Galvanized	–
a3	23	4"x4"x0.375" by 14.5" Long SQ Tube	A500 Grade B Steel Galvanized	–
a4	23	7.5"x3"x0.4375" Top Mounting Plate	A572 Grade 50 Steel Galvanized	–
a5	23	Top Mounting Plate Gusset	A36 Steel Galvanized	–
a6	23	0.625"–11x5"x1.25" Hex Bolt	ASTM A325 Type 1 Galvanized	FBX16a
a7	6	12'–6" W–Beam MGS Section 1/2 Post Spacing	12 gauge AASHTO M180	–
a8	23	L7x4x0.375 Bottom Mounting Plate	A36 Steel Galvanized	–
a9	23	L7x4x0.375 Bottom Mounting Plate Gusset	A36 Steel Galvanized	–
a10	23	6.5"x2"x0.375" Backside Retainer Plate	A36 Steel Galvanized	–
a11	23	0.3125" Dia. Hex Nut	Grade 5	–
a12	23	0.3125"–18x1.25"x1.25" Hex Bolt	Grade A307	FBX08a
a13	23	1.75"x1.75"x0.125" Square Guardrail Washer	A36 Steel	RWR01
a14	23	1"–8x11"x2.5" Hex Bolt	Grade 5	
a15	46	1" Flat Washer	F436 Grade 1 Galvanized	–
a16	27	1" Dia. Hex Nut	ASTM A563 DH Galvanized	FBX24a
a17	46	0.5"–13x6"x6" Hex Bolt	ASTM A325 Type 1 Galvanized	FBX14a
a18	46	0.5" Dia. Hex Nut	ASTM A563 DH Galvanized	FBX14a
a19	23	6" W–Beam Backup Plate	12 gauge AASHTO M180	–
a20	44	0.625" Flat Washer	F436 Grade 1	FWC166
b1	6	12'–6" W–Beam MGS Section Full Post Spacing	12 gauge AASHTO M180	–
b2	1	6'–3" W–Beam MGS Section	12 gauge AASHTO M180	–
b3	47	0.625" Dia. Hex Nut	ASTM A563 DH Galvanized	FBX16a
b4	112	0.625"x1.5" Guardrail Bolt and Nut	Grade A307	FBB01
b5	2	12'–6" W–Beam MGS End Section	12 gauge AASHTO M180	RWM04a
b6	13	W6x8.5 by 72" long (W6x9 can be substituted)	A36 Steel	PWE06
b7	13	6"x12"x14 1/4" Blockout	SYP Grade No.1 or better	–
b8	13	0.625"x14" Guardrail Bolt and Nut	Grade A307	FBB06
b9	13	16D Double Head Nail	–	–
c1	5	#4 Straight Rebar, Total Length 74.5'	Grade 60	–
c2	5	#5 Straight Rebar, Total Length 74.5'	Grade 60	–
c3	76	#5 Straight Rebar, 45" long	Grade 60	–
c4	100	#5 Upper Bent dowel, total length unbent 42"	Grade 60	–
c5	49	#4 Lower Bent Dowel, total length unbent 23.5"	Grade 60	–
c6	75	#4 Transverse Bar, 45" long	Grade 60	–
c7	149	#6 Transverse Bar, 45" long	Grade 60	–
c8	23	2"x2"x1/4" by 8" Long Bolt Sleeves	ASTM A500 Grade B	–
c9	46	#3 Straight Rebar, 10" long	Grade 60	–

Midwest Roadside Safety Facility

MGS Bridge Rail

Bill of Materials

SHEET: 25 of 26
DATE: 11/19/2009
DRAWN BY: MW/RJT
DWG. NAME. MGS Bridge Rail_V13
SCALE: None
UNITS: In.[mm]
REV. BY: KAL/EJ/RF

Figure 111. Bill of Materials, Test Nos. MGSBR-1 and MGSBR-2

MGS Bridge Rail System				
Item No.	QTY.	Description	Material Spec	Hardware Guide
c10	23	#6 Rebar Loop, Total Length Unbent 89"	Grade 60	–
c11	23	#6 Straight Rebar, 24" long	Grade 60	–
c12	23	#4 Bent Rebar, Total Length Unbent 42.5"	Grade 60	–
c13	1	Concrete Deck	f'c = 4,000 psi	–
d1	4	72" Foundation Tube	ASTM A53 Grade B Schedule 40	PTE05
d2	4	BCT Timber Post –MGS Height	SYP Grade No. 1 or better	PDF01
d3	2	Straight Ground Strut 67" long	C6x8.2 Channel Section A36 Steel	PFP01
d4	4	Yoke	A36 Steel	PFP01
d5	2	Anchor Bracket End Plate	A36 Steel	FPA01
d6	2	5"x8"x0.625" Anchor Bearing Plate	A36 Steel	FPB01
d7	2	Anchor Bracket	A36 Steel	FPA01
d8	2	2" Schedule 10 x 6" long BCT Hole Insert	ASTM A53 Grade B	FMM02
d9	4	0.625"x10" Guardrail Bolt	Grade A307	FBB03
d10	4	0.625"x10" Hex Head Bolt	A307	FBX16a
d11	4	0.875"x7 1/2" Hex Head Bolt	Grade 5	FBX22a
d12	4	0.875" Dia. Hex Nut	Grade 5	FBX22a
d13	8	0.875" Flat Washer	Grade 5	FWC22a
d14	16	0.625"x1 1/2" Hex Head Bolt	Grade A307	FBX16a
d15	4	1" Flat Washer	Grade 5	FWC24a
d16	2	BCT Anchor Cable Assembely	ϕ0.75" 6x9 IWRC IPS Galvanized Wire Rope	FCA01–02

Midwest Roadside Safety Facility

MGS Bridge Rail

Bill of Materials Continued

SHEET: 26 of 26

DATE: 11/19/2009

DRAWN BY: MW/RJT

DWG. NAME. MGS Bridge Rail_V13

SCALE: None
UNITS: In.[mm]

REV. BY: KAL/EJ/RF

Figure 112. Bill of Materials, Test Nos. MGSBR-1 and MGSBR-2

Figure 113. Test Installation Photographs, Test No. MGSBR-1

Figure 114. Test Installation Photographs, Test No. MGSBR-1

Figure 115. Test Installation Photographs, Test No. MGSBR-1

Figure 116. Test Installation Photographs, Test No. MGSBR-1

Figure 117. Test Installation Photographs, Test No. MGSBR-1

Figure 118. Test Installation Photographs, Test No. MGSBR-1

8 TEST REQUIREMENTS AND EVALUATION CRITERIA

8.1 Test Requirements

Longitudinal barriers, such as W-beam bridge rails, must satisfy the impact safety standards provided in MASH in order to be accepted by the Federal Highway Administration (FHWA) for use on National Highway System (NHS) new construction projects or as a replacement for existing designs not meeting current safety standards. According to TL-3 of MASH, longitudinal barrier systems must be subjected to two full-scale vehicle crash tests. The two full-scale crash tests are as follows:

1. Test Designation 3-10 consisting of a 2,425-lb (1,100-kg) passenger car impacting the system at a nominal speed and angle of 62 mph (100 km/h) and 25 degrees, respectively.
2. Test Designation 3-11 consisting of a 5,000-lb (2,268-kg) 4-door, half-ton pickup truck impacting the system at a nominal speed and angle of 62 mph (100 km/h) and 25 degrees, respectively.

The test conditions of TL-3 longitudinal barriers are summarized in Table 6.

Table 6. MASH TL-3 Crash Test Conditions

Test Article	Test Designation	Test Vehicle	Impact Conditions			Evaluation Criteria [1]
			Speed		Angle (deg)	
			mph	km/h		
Longitudinal Barrier	3-10	1100C	62	100	25	A,D,F,H,I
	3-11	2270P	62	100	25	A,D,F,H,I

[1] Evaluation criteria explained in Table 7.

8.2 Evaluation Criteria

Evaluation criteria for full-scale vehicle crash testing are based on three appraisal areas: (1) structural adequacy; (2) occupant risk; and (3) vehicle trajectory after collision. Criteria for structural adequacy are intended to evaluate the ability of the barrier to contain and redirect impacting vehicles. Occupant risk evaluates the degree of hazard to occupants in the impacting vehicle. Vehicle trajectory after collision is a measure of the potential for the post-impact trajectory of the vehicle to cause secondary collisions with other vehicles or fixed objects. These evaluation criteria are summarized in Table 7 and defined in greater detail in MASH. Two full-scale vehicle crash tests were conducted and reported in accordance with the procedures provided in MASH.

In addition to the standard occupant risk measures, the Post-Impact Head Deceleration (PHD), the Theoretical Head Impact Velocity (THIV), and the Acceleration Severity Index (ASI) were determined and reported on the test summary sheet. Additional discussion on PHD, THIV and ASI is provided in Reference 4.

Table 7. MASH Evaluation Criteria for Longitudinal Barriers

<table>
<tr><td>Structural Adequacy</td><td colspan="4">A. Test article should contain and redirect the vehicle or bring the vehicle to a controlled stop; the vehicle should not penetrate, underride, or override the installation although controlled lateral deflection of the test article is acceptable.</td></tr>
<tr><td rowspan="11">Occupant Risk</td><td colspan="4">D. Detached elements, fragments or other debris from the test article should not penetrate or show potential for penetrating the occupant compartment, or present an undue hazard to other traffic, pedestrians, or personnel in a work zone. Deformations of, or intrusions into, the occupant compartment should not exceed limits set forth in Section 5.3 and Appendix E of MASH.</td></tr>
<tr><td colspan="4">F. The vehicle should remain upright during and after collision. The maximum roll and pitch angles are not to exceed 75 degrees.</td></tr>
<tr><td colspan="4">H. Occupant Impact Velocities (OIV) (see Appendix A, Section A5.3 of MASH for calculation procedure) should satisfy the following limits:</td></tr>
<tr><td rowspan="3"></td><td colspan="3">Occupant Impact Velocity Limits</td></tr>
<tr><td>Component</td><td>Preferred</td><td>Maximum</td></tr>
<tr><td>Longitudinal and Lateral</td><td>30 ft/s
(9.1 m/s)</td><td>40 ft/s
(12.2 m/s)</td></tr>
<tr><td colspan="4">I. The Occupant Ridedown Acceleration (ORA) (see Appendix A, Section A5.3 of MASH for calculation procedure) should satisfy the following limits:</td></tr>
<tr><td rowspan="3"></td><td colspan="3">Occupant Ridedown Acceleration Limits</td></tr>
<tr><td>Component</td><td>Preferred</td><td>Maximum</td></tr>
<tr><td>Longitudinal and Lateral</td><td>15.0 g’s</td><td>20.49 g’s</td></tr>
</table>

9 TEST CONDITIONS

9.1 Test Facility

The testing facility is located at the Lincoln Air Park on the northwest side of the Lincoln Municipal Airport and is approximately 5 miles (8.0 km) northwest of the University of Nebraska-Lincoln.

9.2 Vehicle Tow and Guidance System

A reverse cable tow system with a 1:2 mechanical advantage was used to propel the test vehicles. The distance traveled and the speed of the tow vehicle were one-half that of the test vehicles. The test vehicles were released from the tow cable before impact with the barrier system. A digital speedometer on the tow vehicle was used to control test vehicle speed.

A vehicle guidance system developed by Hinch [71] was used to steer the test vehicles. A guide-flag, attached to the right-front wheel and the guide cable, was sheared off before impact with the barrier system. The ⅜-in. (9.5-mm) diameter guide cable was tensioned to approximately 3,500 lbf (15.6 kN) and supported both laterally and vertically every 100 ft (30.48 m) by hinged stanchions. The hinged stanchions stood upright while holding up the guide cable, but as the vehicle was towed down the line, the guide-flag struck and knocked each stanchion to the ground. For test no. MGSBR-1 the vehicle guidance system was 1,093 ft (333 m) long, while for test no. MGSBR-2, the vehicle guidance system was 790 ft (241 m) long.

9.3 Test Vehicles

For test no. MGSBR-1, a 2004 Dodge Ram 1500 Quad Cab pickup truck was used as the test vehicle. The curb, test inertial, and gross static vehicle weights were 5,134 lb (2,329 kg), 5,005 lb (2,270 kg), and 5,174 lb (2,347 kg), respectively. The test vehicle is shown in Figure 119, and vehicle dimensions are shown in Figure 120.

Figure 119. Test Vehicle, Test No. MGSBR-1

Date: 6/18/2009 **Test Number:** MGSBR-1 **Model:** Ram 1500

Make: Dodge **Vehicle I.D.#:** 1D7HA18N44J194902

Tire Size: 265/70 R17 **Year:** 2004 **Odometer:** 68720

Tire Inflation Pressure: 35 psi

***(All Measurements Refer to Impacting Side)**

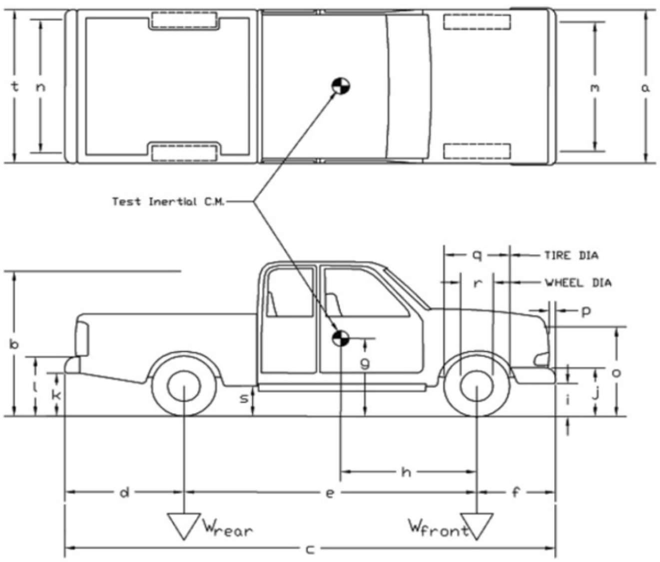

Vehicle Geometry -- in. (mm)

a	77.75	(1975)	b	73.5	(1867)
c	227.25	(5772)	d	45.5	(1156)
e	140.5	(3569)	f	41	(1041)
g	28.28	(718)	h	63.22	(1606)
i	14	(356)	j	26	(660)
k	19.5	(495)	l	27.75	(705)
m	68.125	(1730)	n	67.75	(1721)
o	44.5	(1130)	p	3	(76)
q	31.25	(794)	r	18.5	(470)
s	14.25	(362)	t	74.5	(1892)

Wheel Center Height Front	15.25	(387)
Wheel Center Height Rear	15.25	(387)
Wheel Well Clearance (F)	35	(889)
Wheel Well Clearance (R)	37.75	(959)
Frame Height (F)	17.5	(445)
Frame Height (R)	25.25	(641)
Engine Type	8cyl. Gas	
Engine Size	4.7L	

Transmition Type: Automatic Manual

FWD RWD 4WD

Mass Distribution

Gross Static	**LF**	1453	**RF**	1399
	LR	1154	**RR**	1168

Weights lbs (kg)	**Curb**	**Test Inertial**	**Gross Static**
W-front	2819 (1279)	2747 (1246)	2852 (1294)
W-rear	2315 (1050)	2258 (1024)	2322 (1053)
W-total	5134 (2329)	5005 (2270)	5174 (2347)

GVWR Ratings

Front	3650
Rear	3900
Total	6650

Dummy Data

Type: Hybrid II
Mass: 170 lbs
Seat Position: Driver

Note any damage prior to test: minor cosmetic

Figure 120. Vehicle Dimensions, Test No. MGSBR-1

For test no. MGSBR-2, a 2003 Kia Rio passenger car was used as the test vehicle. The curb, test inertial, and gross static vehicle weights were 2,408 lb (1,092 kg), 2,416 lb (1,096 kg), and 2,585 lb (1,173 kg), respectively. The test vehicle is shown in Figure 121, and vehicle dimensions are shown in Figure 122.

The longitudinal component of the center of gravity (c.g.) was determined using the measured axle weights. The Suspension Method [72] was used to determine the vertical component of the c.g. for the 2270P vehicle. This method is based on the principle that the c.g. of any freely suspended body is in the vertical plane through the point of suspension. The 2270P vehicle was suspended successively in three positions, and the respective planes containing the c.g. were established. The intersection of these planes pinpointed the final c.g. location for the test inertial condition. The c.g. height of the 1100C vehicle was estimated based on historical c.g. height measurements. The locations of the final c.g. for each vehicle are shown in Figures 119 through 124. Data used to calculate the location of the c.g. for each vehicle and ballast information are shown in Appendix C.

Square black and white-checkered targets were placed on the vehicles to aid in the analysis of the high-speed videos, as shown in Figures 123 and 124. Round, checkered targets were placed at the center of gravity on the left-side door, the right-side door, and the roof of each vehicle. The remaining targets were located for references so that they could be viewed from the high-speed cameras for video analysis.

The front wheels of the test vehicles were aligned for camber, caster, and toe-in values of zero so that the vehicles would track properly along the guide cable. A 5B flash bulb was mounted on the left-side of each vehicle's dash and was fired by a pressure tape switch mounted at the impact corner of the bumper. The flash bulb was fired upon initial impact with the test

Figure 121. Test Vehicle, Test No. MGSBR-2

Date: 6/26/2009 **Test Number:** MGSBR-2 **Model:** Rio Sedan

Make: KIA **Vehicle I.D.#:** KNADC125136221497

Tire Size: 175/65 R14 **Year:** 2003 **Odometer:** 50464

Tire Inflation Pressure: 30 psi

***(All Measurements Refer to Impacting Side)**

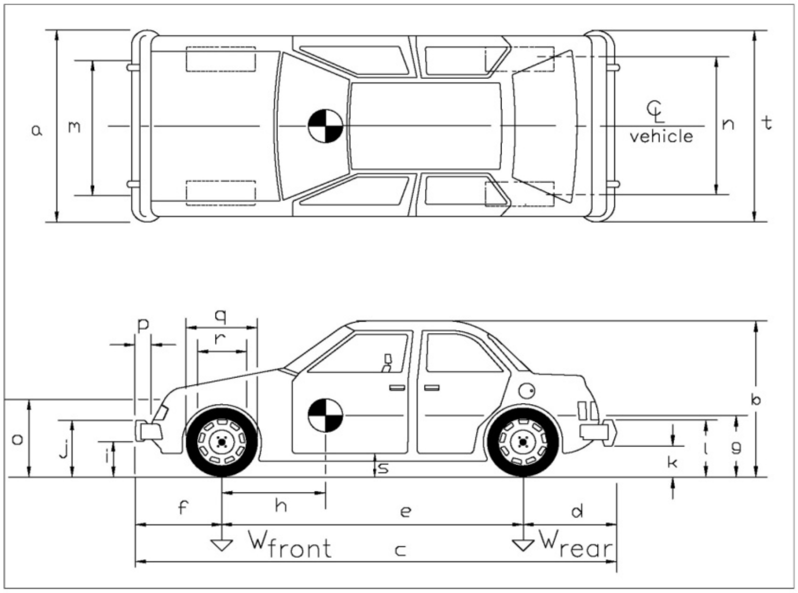

Vehicle Geometry -- in. (mm)

a	64.75	(1645)	b	56.25	(1429)
c	166.5	(4229)	d	39.25	(997)
e	95.25	(2419)	f	32	(813)
g	18	(457)	h	36.02	(915)
i	9	(229)	j	22.5	(572)
k	11.5	(292)	l	22.5	(572)
m	56.25	(1429)	n	56.75	(1441)
o	27	(686)	p	3	(76)
q	15.5	(394)	r	23	(584)
s	7.25	(184)	t	64.25	(1632)

Wheel Center Height Front	10.5	(267)
Wheel Center Height Rear	11	(279)
Wheel Well Clearance (F)	24.25	(616)
Wheel Well Clearance (R)	24.25	(616)
Frame Height (F)	9.5	(241)
Frame Height (R)	16.5	(419)
Engine Type	4cyl. Gas	
Engine Size	1.4L	

Transmition Type: Automatic Manual

FWD RWD 4WD

Mass Distribution

Gross Static	**LF**	799	**RF**	781
	LR	518	**RR**	487

Weights lbs (kg)	**Curb**	**Test Inertial**	**Gross Static**
W-front	1536 (697)	1492 (677)	1580 (717)
W-rear	872 (396)	923 (419)	1005 (456)
W-total	2408 (1092)	2416 (1096)	2585 (1173)

GVWR Ratings

Front	1808
Rear	1742
Total	3379

Dummy Data

Type: Hybrid 1

Mass: 170 lbs.

Seat Position: Driver's side

Note any damage prior to test: None

Figure 122. Vehicle Dimensions, Test No. MGSBR-2

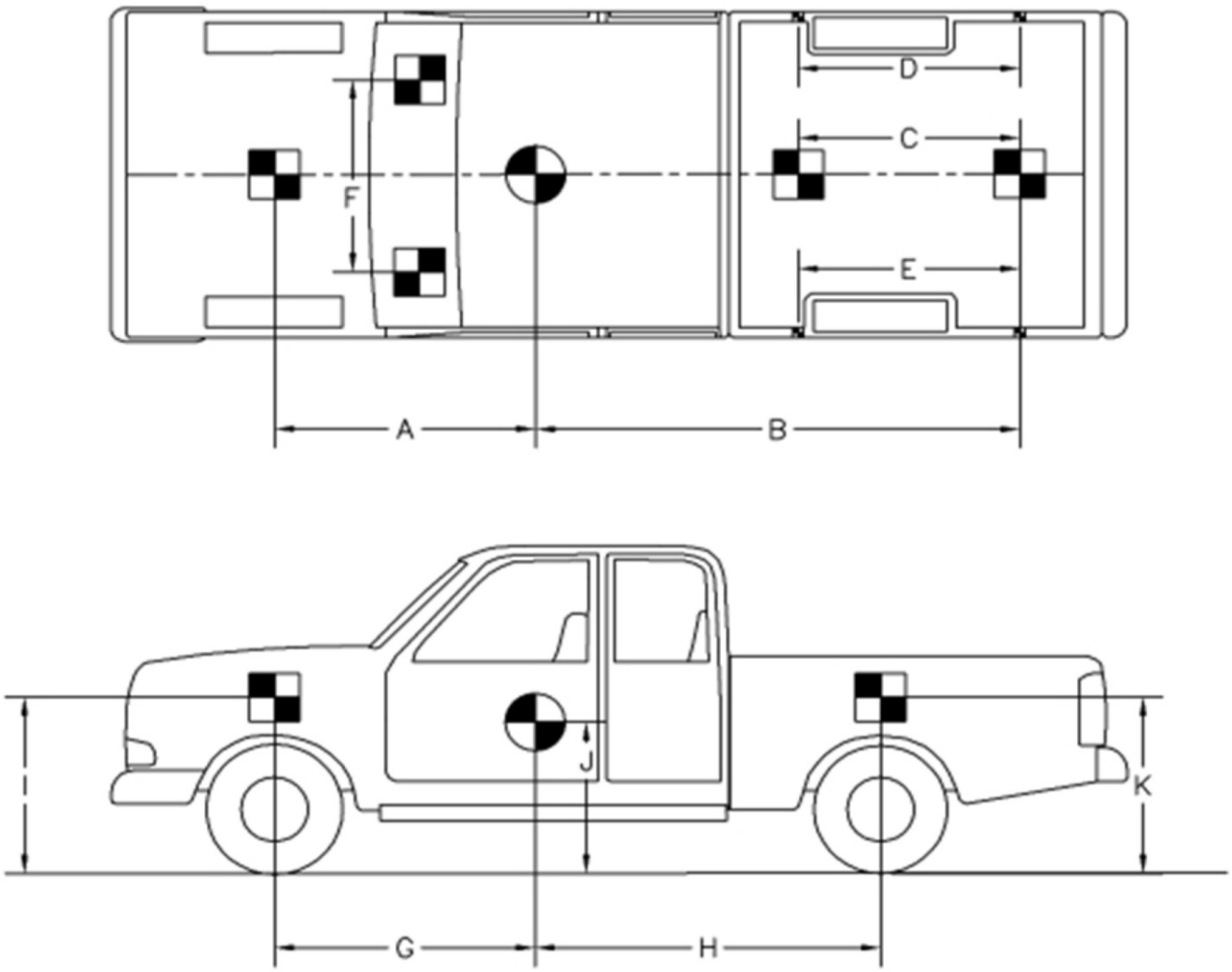

TEST #: MGSBR-1

TARGET GEOMETRY-- in. (mm)

A	**75.75**	**(1924)**	**E**	**70.5**	**(1791)**	**I**	**39.75**	**(1010)**
B	**103**	**(2616)**	**F**	**46.25**	**(1175)**	**J**	**28.25**	**(718)**
C	**47.5**	**(1207)**	**G**	**63.25**	**(1607)**	**K**	**42**	**(1067)**
D	**70.5**	**(1791)**	**H**	**77.25**	**(1962)**			

Note: K is measured from the ground to the windshield target

Figure 123. Target Geometry, Test No. MGSBR-1

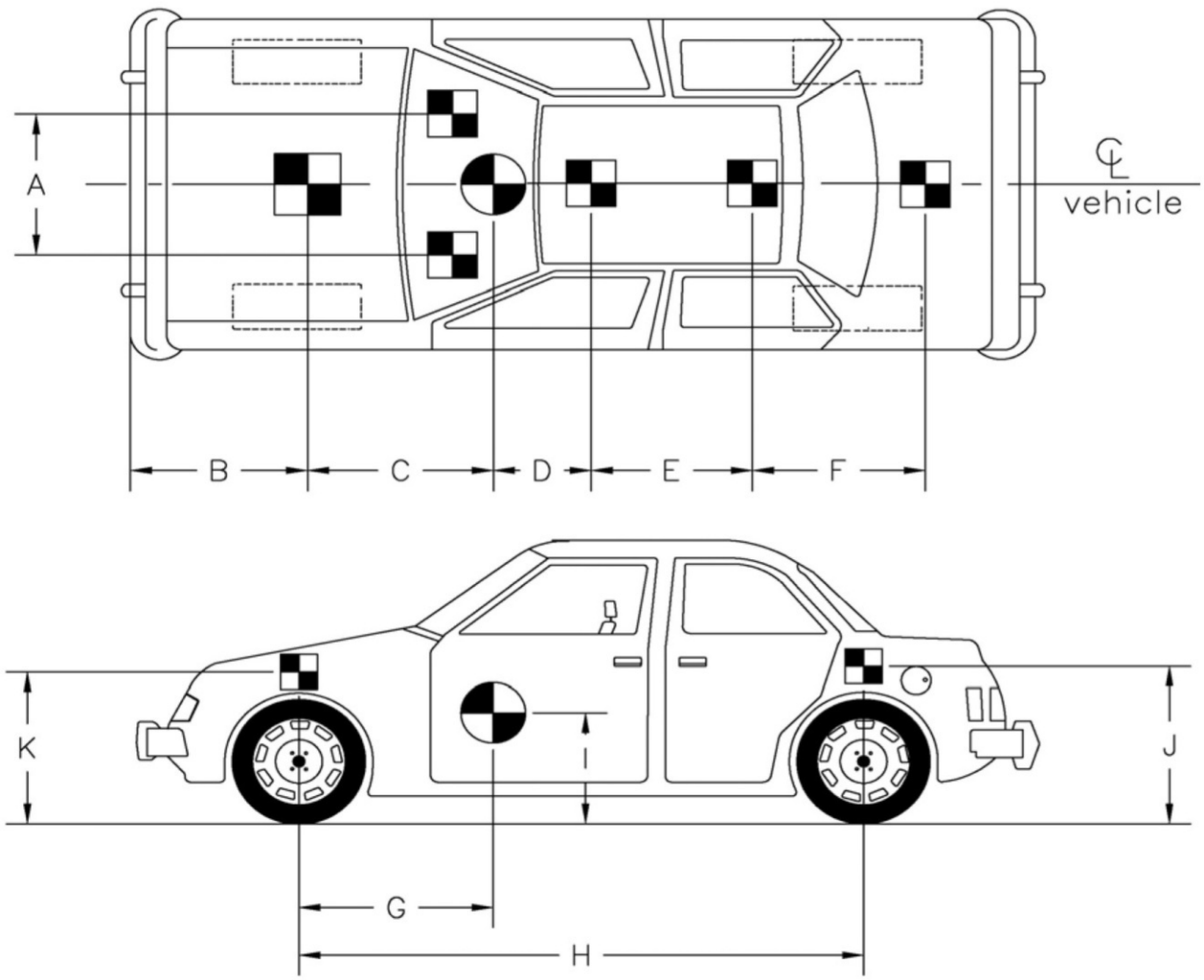

TEST #: MGSBR-2

TARGET GEOMETRY-- in. (mm)

A	**23.375**	**(594)**	**E**	**25.375**	**(645)**	**I**	**18**	**(457)**
B	**25.25**	**(641)**	**F**	**37.25**	**(946)**	**J**	**28.5**	**(724)**
C	**43**	**(1092)**	**G**	**63**	**(1600)**	**K**	**28.25**	**(718)**
D	**24**	**(610)**	**H**	**95.25**	**(2419)**			

Figure 124. Target Geometry, Test No. MGSBR-2

article to create a visual indicator of the precise time of impact on the high-speed videos. A remote controlled brake system was installed in each test vehicle so the vehicles could be brought safely to a stop after the tests.

9.4 Simulated Occupant

A Hybrid II 50th Percentile Adult Male Test Dummy, equipped with clothing and footwear, was placed in the right-front seat of the test vehicle with the seat belt fastened. The dummy, which had a final weight of 170 lb (77 kg), was represented by model no. 572, serial no. 451, and was manufactured by Android Systems of Carson, California. As recommended by MASH, the dummy was not included in calculating the c.g. location.

9.5 Data Acquisition Systems

9.5.1 Accelerometers

Three environmental shock and vibration sensor/recorder systems were used to measure the accelerations in the longitudinal, lateral, and vertical directions. All of the accelerometers were mounted near the center of gravity of the test vehicles.

One triaxial piezoresistive accelerometer system, Model EDR-4 6DOF-500/1200, was developed and manufactured by Instrumented Sensor Technology (IST) of Okemos, Michigan and includes three differential channels as well as three single-ended channels. The EDR-4 6DOF-500/1200 was configured with 24 MB of RAM memory, a range of ±500 g's, a sample rate of 10,000 Hz, and a 1,677 Hz anti-aliasing filter. The "EDR4COM" and "DynaMap Suite" computer software programs and a customized Microsoft Excel worksheet were used to analyze and plot the accelerometer data.

The second system was a two-arm piezoresistive accelerometer system developed by Endevco of San Juan Capistrano, California. Three accelerometers were used to measure each of the longitudinal, lateral, and vertical accelerations independently at a sample rate of 10,000 Hz.

The accelerometers were configured and controlled using a system developed and manufactured by Diversified Technical Systems, Inc. (DTS) of Seal Beach, California. More specifically, data was collected using a DTS Sensor Input Module (SIM), Model TDAS3-SIM-16M. The SIM was configured with 16 MB SRAM memory and 8 sensor input channels with 250 kB SRAM/channel. The SIM was mounted on a TDAS3-R4 module rack. The module rack was configured with isolated power/event/communications, 10BaseT Ethernet and RS232 communication, and an internal backup battery. Both the SIM and module rack were crashworthy. The computer software program "DTS TDAS Control" and a customized Microsoft Excel worksheet were used to analyze and plot the accelerometer data.

The third system, Model EDR-3, was a triaxial piezoresistive accelerometer system developed and manufactured by IST of Okemos, Michigan. The EDR-3 was configured with 256 kB of RAM memory, a range of ±200 g's, a sample rate of 3,200 Hz, and a 1,120 Hz low-pass filter. The computer software program "DynaMax 1 (DM-1)" and a customized Microsoft Excel worksheet were used to analyzed and plot the accelerometer data.

9.5.2 Rate Transducers

An Analog Systems 3-axis rate transducer with a range of 1,200 degrees/sec in each of the three directions (roll, pitch, and yaw) was used to measure the rates of motion of the test vehicles. The rate transducer was mounted inside the body of the EDR-4 6DOF-500/1200 and recorded data at 10,000 Hz to a second data acquisition board inside the EDR-4 6DOF-500/1200 housing. The raw data measurements were then downloaded, converted to the appropriate Euler angles for analysis, and plotted. The computer software programs "EDR4Com" and "DynaMax Suite" and a customized Microsoft Excel spreadsheet were used to analyze and plot the rate transducer data.

An additional angle rate sensor, the ARS-1500, with a range of 1,500 degrees/sec in each of the three directions (roll, pitch, and yaw) was used to measure the rates of rotation of the test vehicles. The angular rate sensor was mounted on an aluminum block inside the test vehicles near the center of gravity and recorded data at 10,000 Hz to the SIM. The raw data measurements were then downloaded, converted to the proper Euler angles for analysis, and plotted. The computer software program "DTS TDAS Control" and a customized Microsoft Excel worksheet were used to analyze and plot the angular rate sensor data.

9.5.3 Pressure Tape Switches

For test nos. MGSBR-1 and MGSBR-2, five pressure-activated tape switches spaced at 6.56 ft (2 m) intervals were used to determine the speed of each vehicle before impact. Each tape switch fired a strobe light which sent an electronic timing signal to the data acquisition system as the left-front tire of the test vehicle passed over it. Test vehicle speeds were determined from electronic timing mark data recorded using TestPoint and LabVIEW computer software programs. Strobe lights and high-speed video analysis are used only as a backup in the event that vehicle speeds cannot be determined from the electronic data.

9.5.4 Digital Photography

For test no. MGSBR-1, three AOS VITcam high-speed digital video cameras, three AOS X-PRI high-speed digital video cameras, four JVC digital video cameras, and two Canon digital video cameras were used to film the crash test. Camera details, camera operating speeds, lens information, and a schematic of the camera locations are shown in Figure 125.

For test no. MGSBR-2, three AOS VITcam high-speed digital video cameras, three AOS X-PRI high-speed digital video cameras, three JVC digital video cameras, and two Canon digital video cameras were used to film the crash test. Camera details, camera operating speeds, lens information, and a schematic of the camera locations are shown in Figure 126.

The high-speed videos were analyzed using ImageExpress MotionPlus and RedLake MotionScope software. Actual camera speed and camera divergence factors were considered in the analysis of the high-speed videos.

	No.	Type	Operating Speed (frames/sec)	Lens	Lens Setting
High-Speed Video	2	AOS Vitcam CTM	500	Sigma 12.5 mm Fixed	-
	3	AOS Vitcam CTM	500	Sigma 24 - 70 mm	42 mm
	4	AOS Vitcam CTM	500	Tamron 100 - 300 mm	200 mm
	5	AOS X-PRI	500	Sigma 24 - 135 mm	35 mm
	6	AOS X-PRI	500	Fujinon 50 mm Fixed	-
	7	AOS X-PRI	500	Sigma 50 mm Fixed	-
Digital Video	1	JVC - GZ-MC500 (Everio)	29.97		
	2	JVC - GZ-MG27u (Everio)	29.97		
	3	JVC - GZ-MG27u (Everio)	29.97		
	4	JVC - GZ-MG27u (Everio)	29.97		
	1	Canon-ZR90	29.97		
	2	Canon-ZR10	29.97		

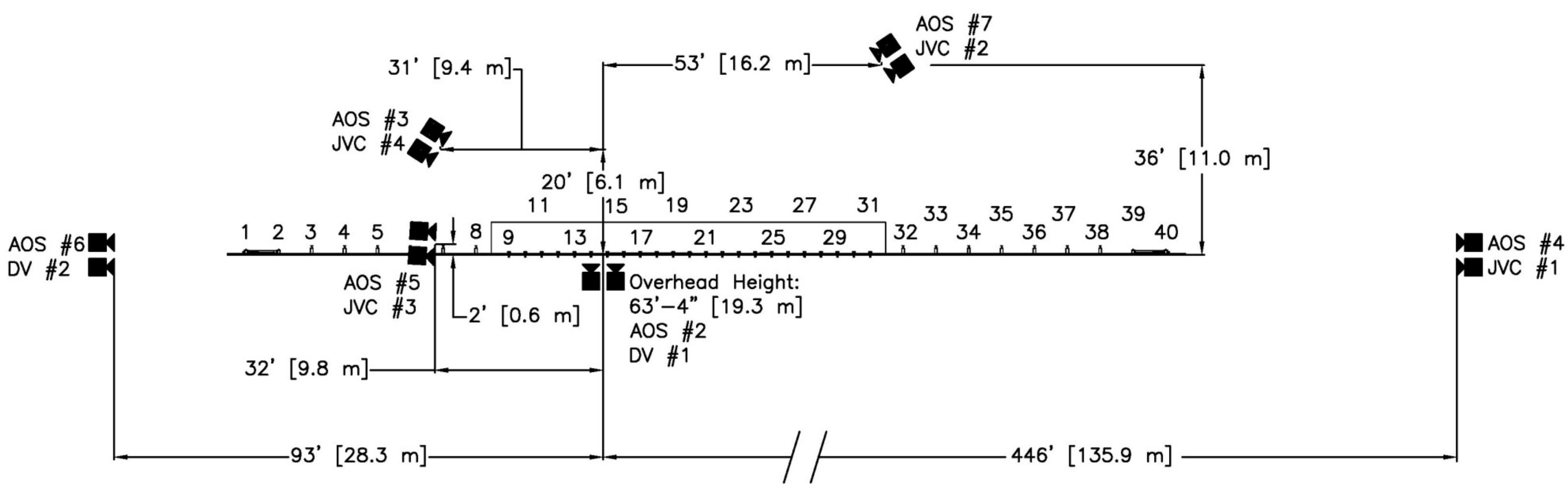

Figure 125. Camera Locations, Speeds, and Lens Settings, Test No. MGSBR-1

	No.	Type	Operating Speed (frames/sec)	Lens	Lens Setting
High-Speed Video	2	AOS Vitcam CTM	500	Sigma 12.5 mm Fixed	-
	3	AOS Vitcam CTM	500	Sigma 24 - 70 mm	50 mm
	4	AOS Vitcam CTM	500	Tamron 100 - 300 mm	135 mm
	5	AOS X-PRI	500	Fujinon 50 mm Fixed	-
	6	AOS X-PRI	500	Sigma 24 - 135 mm	35 mm
	7	AOS X-PRI	500	Sigma 50 mm Fixed	-
Digital Video	2	JVC - GZ-MG27u (Everio)	29.97		
	3	JVC - GZ-MG27u (Everio)	29.97		
	4	JVC - GZ-MG27u (Everio)	29.97		
	1	Canon-ZR90	29.97		
	2	Canon-ZR10	29.97		

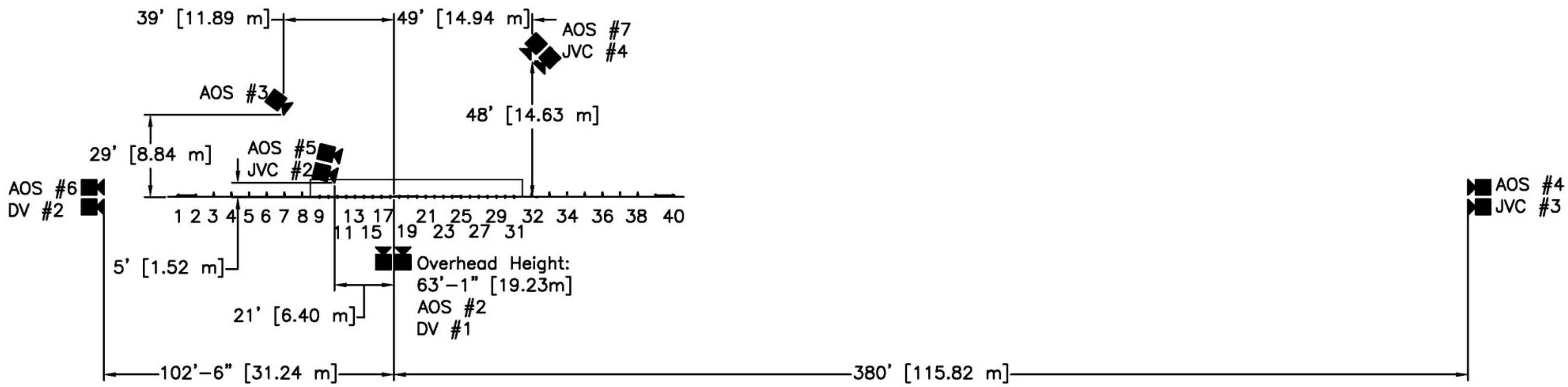

Figure 126. Camera Locations, Speeds, and Lens Settings, Test No. MGSBR-2

10 FULL-SCALE CRASH TEST NO. MGSBR-1

10.1 Concrete Cylinder Compression Tests

The strength of the concrete bridge deck was evaluated using compression testing of concrete cylinders before full-scale testing was begun. Three 6-in. (152-mm) diameter, 12-in. (305-mm) long concrete cylinders were cast in accordance with ASTM C31 [73] and tested in accordance with ASTM C39 [74]. Two cylinders were tested 20 days after casting, and one cylinder was tested 28 days after casting. For all three cylinders, the strength exceeded the specified minimum compressive strength of 4,000 psi (27.6 MPa). Thus, the barrier system was approved for full-scale crash testing. Results for the concrete cylinder compressive tests are shown in Table 8.

Table 8. Results from Concrete Cylinder Compression Testing

Test	Date Cast	Date Tested	Defects	Max. Force	Max. Stress (psi)	Fracture
1	5/14/2009	6/3/2009	None	136.9 kips (608.9 kN)	4,842 psi (33.4 MPa)	Partial Cone
2	5/14/2009	6/3/2009	None	135.8 kips (604.2 kN)	4,804 psi (33.1 MPa)	Partial Cone
3	5/14/2009	6/11/2009	None	141.2 kips (628.0 kN)	4,993 psi (34.4 MPa)	Cone

10.2 Test No. MGSBR-1

During test no. MGSBR-1, a 5,174-lb (2,347-kg) pickup truck, with a dummy placed in the left-front seat, impacted the bridge rail at a speed of 61.9 mph (99.6 km/h) and at an angle of 24.9 degrees. A summary of the test results and sequential photographs are shown in Figure 127. Additional sequential photographs are shown in Figures 128 through 130. Documentary photographs of the crash test are shown in Figures 131 through 133.

10.3 Weather Conditions

Test no. MGSBR-1 was conducted on June 18, 2009, at approximately 2:20 pm. The weather conditions as per the National Oceanic and Atmospheric Administration (station 14939/LNK) were reported as shown in Table 9.

Table 9. Weather Conditions, Test No. MGSBR-1

Temperature	93° F
Humidity	38%
Wind Speed	18 mph
Wind Direction	230° from True North
Sky Conditions	Sunny
Visibility	10 Statute Miles
Pavement Surface	Dry
Previous 3-Day Precipitation	0.29 in.
Previous 7-Day Precipitation	0.70 in.

10.4 Test Description

The targeted point of impact was 16 ft (4.88 m) upstream of the centerline of the splice at post no. 20, as shown in Figure 134. The actual point of impact was 15 ft - 9½ in. (4.81 m) upstream of the centerline of the splice at post no. 20. A sequential description of the impact events is contained in Table 10. The vehicle came to rest 241 ft (73.5 m) downstream from impact and 43 ft - 7 in. (13.3 m) laterally behind the edge of the bridge deck, where it struck a temporary concrete barrier. The vehicle trajectory and final position are shown in Figure 135.

Table 10. Sequential Description of Impact Events, Test No. MGSBR-1

TIME (sec)	EVENT
0.000	Left-front bumper corner impacted the bridge rail upstream of post no. 15
0.036	Left-front tire underrode the rail and the tire rotation slowed
0.038	Rail disengaged from post no. 15
0.040	Rail disengaged from post no. 14
0.044	Vehicle began to redirect
0.046	Left-front tire became airborne, and rail disengaged from post no. 16
0.048	Rail disengaged from post no. 17

0.052	Left-front tire contacted post no. 16
0.058	Left-front bumper corner contacted post no. 17
0.072	Top of vehicle rolled toward left side, and rail disengaged from post no. 18
0.088	Undercarriage contacted post no. 17, and rail disengaged from post no. 19
0.092	Left-front tire contacted post no. 18
0.094	Front bumper contacted post no. 18, and rail disengaged from post no. 20
0.102	Left-front wheel assembly contacted post no. 17
0.120	Undercarriage contacted the top of post no. 18
0.124	Front bumper contacted post no. 19
0.128	Rail disengaged from post no. 21
0.136	Front axle contacted post no. 18, and rail disengaged from post no. 22
0.140	Rail disengaged from post no. 23
0.150	Rail disengaged from post no. 24
0.160	Undercarriage contacted top of post no. 19
0.180	Front bumper contacted post no. 20, and front axle contacted post no. 19
0.196	Left-rear tire became airborne as it lost contact with the bridge deck
0.200	Right-front tire became airborne
0.210	Left-rear bumper corner struck rail between post nos. 15 and 16
0.224	Front axle contacted post no. 20
0.226	Front bumper contacted post no. 21
0.266	Front axle contacted post no. 21
0.280	Vehicle became parallel to the system at a speed of 44.9 mph (72.3 km/h)
0.310	Right-rear tire became airborne
0.414	Top of vehicle rolled toward the right side
0.456	Left-front tire contacted post no. 24, left-front tire disengaged from the vehicle, and rail disengaged from post no. 25
0.632	Right-rear tire contacted the ground
0.648	Vehicle exited system at a speed of 34.5 mph (55.5 km/h) and at an angle of 20.4 degrees as left side lost contact with the rail at post no. 25
0.700	Right-front tire contacted the ground

10.5 Barrier Damage

Damage to the barrier was moderate, as shown in Figures 136 through 147. System damage consisted of bridge deck cracking and spalling, one failed post mounting bracket, deformed guardrail posts, disengaged post-to-rail connections, and contact marks on and deformation of the W-beam rail. The length of vehicle contact along the system was approximately 34 ft - 3⅞ in. (10.5 m), which spanned from 2 in. (51 mm) upstream of post no. 15 to 2⅝ in. (67 mm) upstream of post no. 26.

Through-deck cracking was found at post nos. 14 and 16. Minor punching shear cracks were developed on the outside edge of the bridge deck at post no. 14. These cracks were caused by downward deflection of the top mounting plate as the post and mounting bracket created prying action about the vertical, through-deck bolt. More serious cracking occurred at post no. 16, where several cracks extended from the through-deck bolt toward the deck edge and down the side of the deck. Cracks on the top surface of the deck at post no. 16 were caused by vehicle snag on the post near the top of the mounting bracket assembly. This applied a downstream and lateral pullout load to the through-deck bolt. Note that these cracks were narrow and that no rebar was exposed, and that the through-deck bolt and steel insert sleeve were not displaced.

Spalling occurred on the edge of the deck at 12 posts, nos. 14 through 24 and 26. Most was very minor, but more significant spalling occurred at post nos. 24 and 26. Spalling at the top of the deck was caused by downward deflection of the top mounting plate due to the prying action of the post and mounting bracket assembly about the through-deck bolt. Edge of deck spalling was caused by vehicle snag on system posts. This snag caused the mounting brackets to twist downstream and impact the deck edge.

Damage to most mounting brackets was minimal, consisting of minor bending of the backside retainer plates and bolts. The bracket at post no. 24 failed as the weld between the tube, top mounting plate, and gusset fractured. This failure was caused by wheel snag on the mounting bracket as the pickup was redirected back onto the deck.

Post nos. 12 through 25 posts showed varying degrees of damage. Nine posts, nos. 16 through 24, completely failed through bending and twisting. The flanges of post nos. 16, 17, 21, and 22 partially ruptured. Scrapes and/or gouges were found on the flanges of post nos. 18 through 24.

Post nos. 14 through 25 were disengaged from the rail due to fracture of the post-to-rail connection bolts. Post nos. 32 through 38 were disengaged due to deformation of the slot in the W-beam rail and bolt pullout. The W-beam backup plates at post nos. 15 through 25 were also disengaged from the system. The splices at post nos. 12, 16, 20, and 24 showed evidence of slipping from ⅛ in. (3 mm) to ¼ in. (6 mm) due to membrane action of the W-beam rail.

General deformation and flattening of the W-beam rail occurred from 4 in. (102 mm) upstream of post no. 15 to post no. 25, with some additional flattening at post no. 14. Contact marks were visible on the guardrail beginning 2 in. (51 mm) upstream of post no. 15 to 2⅝ in. (67 mm) upstream of post no. 26. Slight buckling occurred near post nos. 13 through 15 and 26. More severe buckling occurred at post no. 25. Deformations in the bottom of the W-beam rail due to contact with the posts occurred near post nos. 16 through 18 and 20 through 23.

A ½-in. (13-mm) soil gap was present at the upstream edge of post no. 1, and a ⅜-in. (10-mm) soil gap was present on the downstream edge of post no. 2. Soil gaps of ½ in. (13 mm) and 1⅜ in. (35 mm) were present at the downstream edges of post nos. 39 and 40, respectively.

The permanent set of the barrier system is shown in Figures 136 and 137. The maximum permanent set rail and post deflections were 31⅞ in. (810 mm) at post no. 20 and 24¾ in. (629 mm) at post no. 24, respectively, as measured in the field. The maximum lateral dynamic rail and post deflections were 48.9 in. (1,242 mm) at post no. 19 and 28.0 in. (711 mm) at post no. 18, respectively, as determined from high-speed digital video analysis. The working width of the system was 53.2 in. (1,351 mm), also determined from high-speed digital video analysis.

10.6 Vehicle Damage

The damage to the vehicle was moderate, as shown in Figures 148 through 151. The maximum occupant compartment deformations are listed in Table 11 with the deformation limits established in MASH for various areas of the occupant compartment. It should be noted that none of the MASH established deformation limits were violated. Complete occupant compartment and vehicle deformations and the corresponding locations are provided in Appendix D.

Table 11. Maximum Occupant Compartment Deformations by Location

LOCATION	MAXIMUM DEFORMATION in. (mm)	MASH ALLOWABLE DEFORMATION in. (mm)
Wheel Well & Toe Pan	¾ (19)	≤ 9 (229)
Floor Pan & Transmission Tunnel	½ (13)	≤ 12 (305)
Side Front Panel (in Front of A-Pillar)	1¾ (44)	≤ 12 (305)
Side Door (Above Seat)	¾ (19)	≤ 9 (229)
Side Door (Below Seat)	½ (13)	≤ 12 (305)
Roof	¼ (6)	≤ 4 (102)
Windshield	0	≤ 3 (76)

The front bumper was pushed inward and had heavy scraping along its left end. The grill was cracked, and the hood was pushed back and upward. A small crack was found at the lower-left corner of the windshield. The front of the left-front quarter panel was deformed inward and pulled out around the wheel well and its back end was deformed inward. The left-front wheel was disengaged from the vehicle and its brake line was severed. The left-front door was deformed inward and bent slightly out of the frame. Scrapes and scuffs were found along the entire left side of the vehicle and on the left-rear tire. A gap was found between the tailgate and the left-rear quarter panel.

Inspection of the vehicle undercarriage revealed that a top frame member sustained significant deformation. The vehicle frame was bent near its connection to the left-front lower control arm. The vertical stabilizer bar was bent but still attached, and the sway bar was shifted.

10.7 Occupant Risk

The calculated occupant impact velocities (OIVs) and maximum 0.010-sec occupant ridedown accelerations (ORAs) in both the longitudinal and lateral directions are shown in Table 12. All OIVs and ORAs were within the suggested limits provided in MASH. The calculated THIV, PHD, and ASI values are also shown in Table 12. The results of the occupant risk analysis, as determined from the accelerometer data, are summarized in Figure 127. The recorded data from the accelerometers and the rate transducers are shown graphically in Appendix E. It was noted that the DTS accelerometer displayed non-realistic behavior as the vehicle lost contact with the barrier. However, as the occupant risk measurements occurred early in the event, this behavior was not believed to have influenced the data.

Table 12. Summary of OIV, ORA, THIV, PHD, and ASI Values, Test No. MGSBR-1

Evaluation Criteria		Transducer			MASH Limits
		EDR-4	**DTS**	**EDR-3**	
OIV ft/s (m/s)	Longitudinal	-16.94 (-5.16)	-16.86 (-5.14)	-18.84 (-5.74)	≤ 40 (12.2)
	Lateral	13.27 (4.04)	14.23 (4.34)	14.18 (4.32)	≤40 (12.2)
ORA g's	Longitudinal	-10.61	-10.44	-12.55	≤ 20.49
	Lateral	5.42	6.33	5.61	≤ 20.49
THIV ft/s (m/s)		20.66 (6.30)	21.03 (6.41)		not required
PHD g's		10.64	10.50		not required
ASI		0.53	0.57	0.64	not required

10.8 Discussion

The analysis of the test results for test no. MGSBR-1 showed that the bridge rail adequately contained and redirected the vehicle. There were no detached elements nor fragments which showed potential for penetrating the occupant compartment nor presented undue hazard to other traffic. The deformation of, or intrusion into, the occupant compartment was minimal and did not pose a threat to cause serious injury. The test vehicle did not penetrate nor ride over the barrier and remained upright during and after the collision. Vehicle roll, pitch, and yaw angular displacements, as shown in Appendix E, were well below the limit of 75 degrees recommended by MASH. After impact, the vehicle exited the barrier at an angle of 20.4 degrees, and its trajectory did not violate the bounds of the exit box. Therefore, test no. MGSBR-1 was determined to be acceptable according to the TL-3 safety performance criteria found in MASH for test designation no. 3-11.

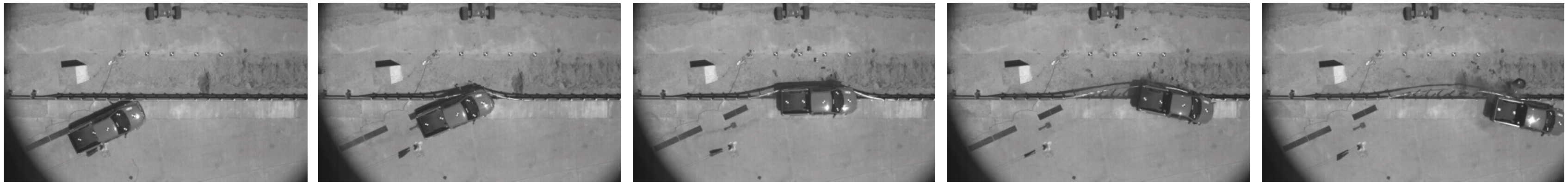

0.000 sec 0.106 sec 0.280 sec 0.456 sec 0.648 sec

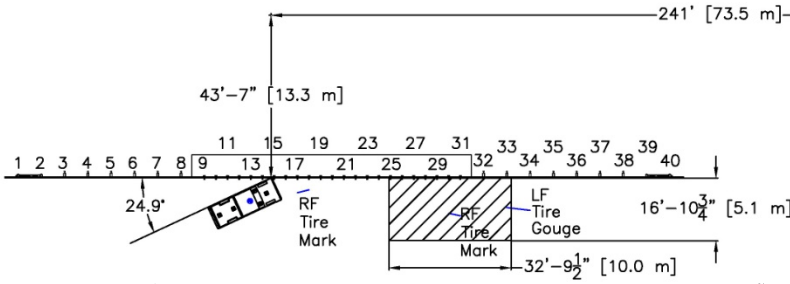

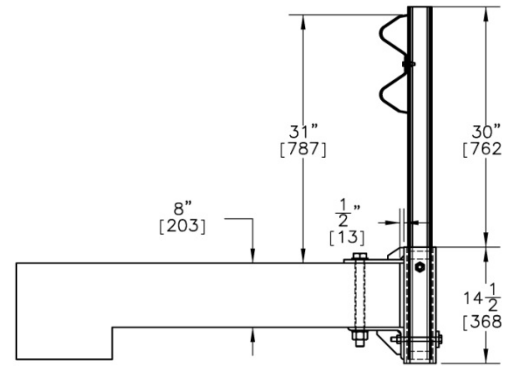

- Test Agency .... MwRSF
- Test Number MGSBR-1
- Date 6/18/2009
- MASH Test Designation 3-11
- Test Article .... MGS Bridge Rail with approach MGS Guardrails
- Total Length .... 175 ft (53.3 m)
- Key Component – MGS Bridge Rail
  - Post Type S3x5.7 (S76x8.5)
  - Post Spacing .... 3 ft - 1½ in. (953 mm)
  - Post-to-Rail Connection .... ⁵⁄₁₆-in. (7.9-mm) dia. ASTM A307A Bolt
- Key Component – Simulated Bridge Deck
  - Thickness (outer edge) .... 8 in. (203 mm)
  - Concrete Strength (minimum) .... 4,000 psi (27.6 MPa)
- Vehicle Model .... 2004 Dodge Ram 1500 Quad Cab Pickup Truck
  - Curb .... 5,134 lb (2,329 kg)
  - Test Inertial .... 5,005 lb (2,270 kg)
  - Gross Static .... 5,174 lb (2,347 kg)
- Impact Conditions
  - Speed .... 61.9 mph (99.6 km/h)
  - Angle .... 24.9 degrees
  - Impact Location .... 15 ft - 9½ in. (4.81 m) US of post no. 20 splice
- Exit Conditions
  - Speed .... 34.5 mph (55.5 km/h)
  - Angle .... 20.4 degrees
  - Exit Box .... Pass
- Vehicle Stability .... Satisfactory
- Vehicle Stopping Distance .... 241 ft (73.5 m) downstream
  43 ft - 7 in. (13.3 m) behind edge of bridge deck
- Vehicle Damage .... Moderate
  - VDS[75] 11-LFQ-3
  - CDC[76] 11-LYEW-4
  - Maximum Interior Deformation .... 1¾ in. (44 mm), left side panel
- Test Article Damage .... Moderate
- Test Article Deflections
  - Permanent Set .... 31⅞ in. (810 mm)
  - Dynamic .... 48.9 in. (1,242 mm)
  - Working Width .... 53.2 in. (1,351 mm)
- Angular Displacements (EDR-4)
  - Roll .... -15.3 degrees
  - Pitch .... -5.6 degrees
  - Yaw .... 37.8 degrees
- Angular Displacements (DTS)
  - Roll .... -14.0 degrees
  - Pitch .... -5.4 degrees
  - Yaw .... 39.8 degrees
- Transducer Data

Evaluation Criteria		Transducer			MASH Limit
		EDR-4	DTS	EDR-3	
OIV ft/s (m/s)	Longitudinal	-16.94 ft/s (-5.16 m/s)	-16.86 ft/s (-5.14 m/s)	-18.84 ft/s (-5.74 m/s)	≤ 40 (12.2)
	Lateral	13.27 ft/s (4.04 m/s)	14.23 ft/s (4.34 m/s)	14.18 ft/s (4.32 m/s)	≤ 40 (12.2)
ORA g's	Longitudinal	-10.61	-10.44	-12.55	≤ 20.49
	Lateral	5.42	6.33	5.61	≤ 20.49
THIV – ft/s (m/s)		20.66 ft/s (6.30 m/s)	21.03 ft/s (6.41 m/s)		not required
PHD – g's		10.64	10.50		not required
ASI		0.53	0.57	0.64	not required

Figure 127. Summary of Test Results and Photographs, Test No. MGSBR-1


0.000 sec


0.072 sec


0.110 sec


0.278 sec


0.426 sec


0.648 sec


0.000 sec


0.138 sec


0.282 sec


0.414 sec


0.648 sec


0.792 sec

Figure 128. Additional Sequential Photographs, Test No. MGSBR-1

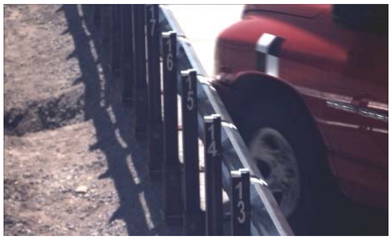
0.000 sec


0.046 sec

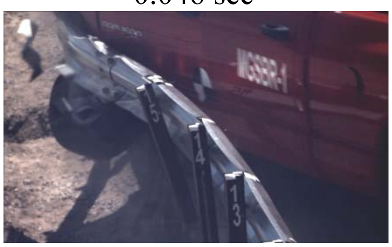

0.088 sec


0.156 sec

0.210 sec

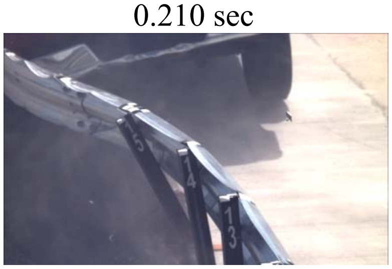
0.310 sec


0.000 sec


0.088 sec

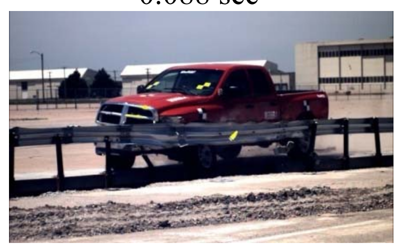
0.160 sec


0.226 sec


0.298 sec


0.404 sec

Figure 129. Additional Sequential Photographs, Test No. MGSBR-1


0.000 sec


0.094 sec

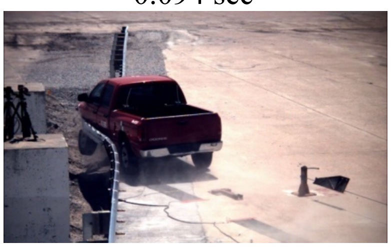
0.160 sec

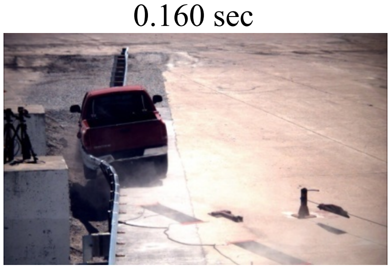
0.274 sec


0.310 sec

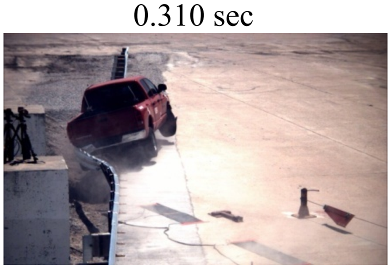
0.386 sec


0.456 sec


0.522 sec

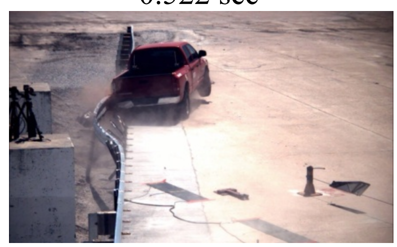
0.632 sec

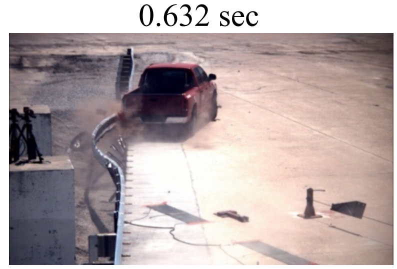
0.700 sec

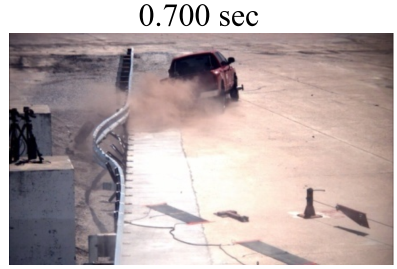
1.040 sec

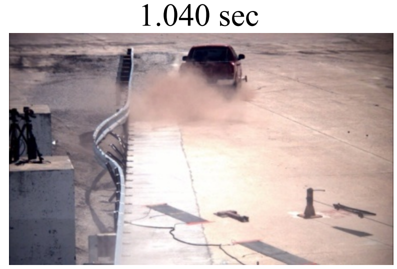
1.318 sec

Figure 130. Additional Sequential Photographs, Test No. MGSBR-1

Figure 131. Documentary Photographs, Test No. MGSBR-1

Figure 132. Documentary Photographs, Test No. MGSBR-1

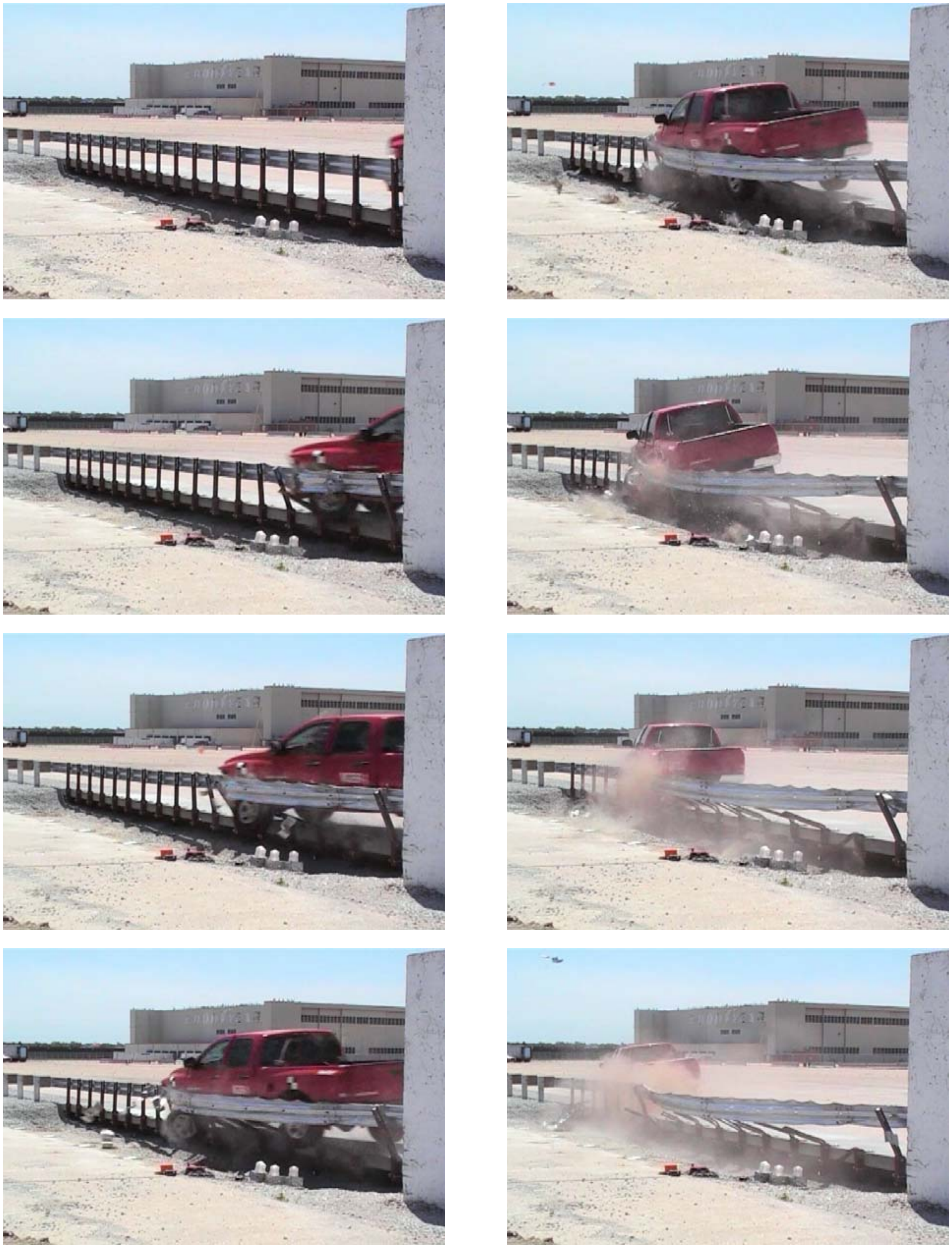

Figure 133. Documentary Photographs, Test No. MGSBR-1

Figure 134. Impact Location, Test No. MGSBR-1

Figure 135. Vehicle Final Position and Trajectory Marks, Test No. MGSBR-1

Figure 136. System Damage, Test No. MGSBR-1

Figure 137. Permanent Set, Test No. MGSBR-1

Figure 138. Typical Splice Damage, Post 20, Test No. MGSBR-1

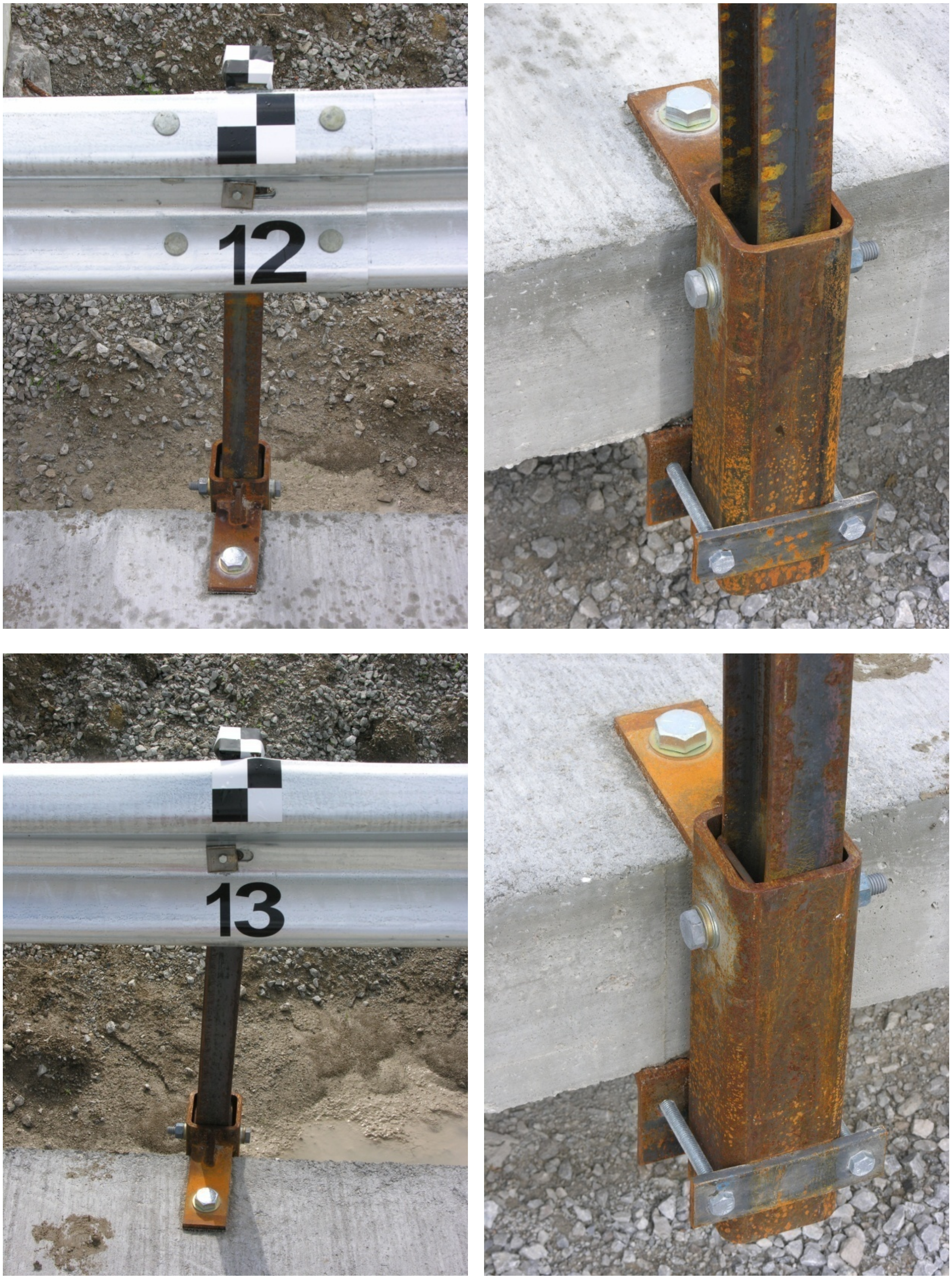

Figure 139. Post Nos. 12 and 13 Damage, Test No. MGSBR-1

Figure 140. Post Nos. 14 and 15 Damage, Test No. MGSBR-1

Figure 141. Post Nos. 16 and 17 Damage, Test No. MGSBR-1

Figure 142. Post Nos. 18 and 19 Damage, Test No. MGSBR-1

Figure 143. Post Nos. 20 and 21 Damage, Test No. MGSBR-1

Figure 144. Post Nos. 22 and 23 Damage, Test No. MGSBR-1

Figure 145. Post No. 24 Damage, Test No. MGSBR-1

Figure 146. Post Nos. 25 and 26 Damage, Test No. MGSBR-1

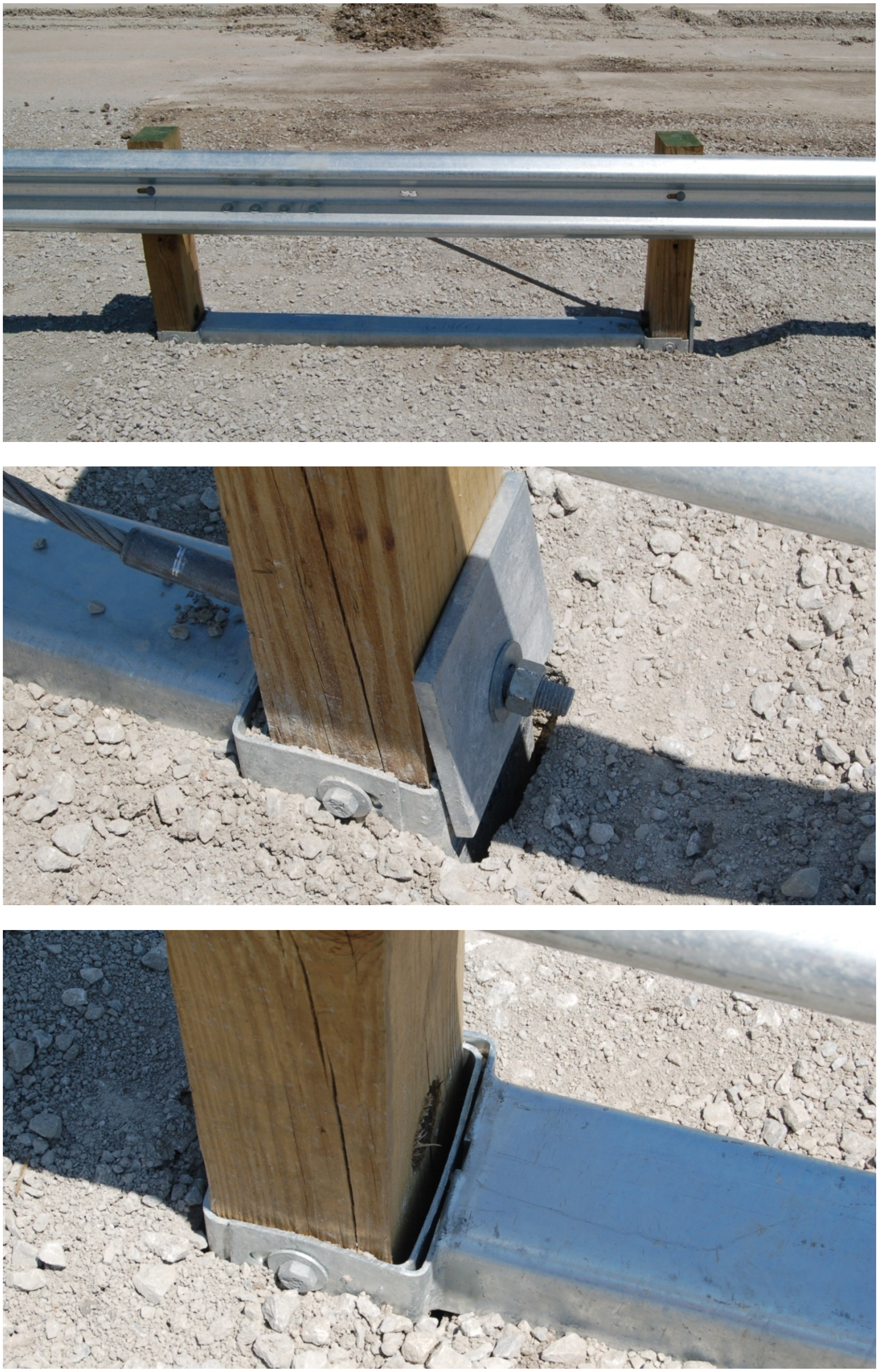

Figure 147. Downstream Anchorage Damage, Test No. MGSBR-1

Figure 148. Vehicle Damage, Test No. MGSBR-1

Figure 149. Vehicle Damage, Test No. MGSBR-1

Figure 150. Undercarriage Damage, Test No. MGSBR-1

Figure 151. Occupant Compartment Deformation, Test No. MGSBR-1

11 FULL-SCALE CRASH TEST NO. MGSBR-2

11.1 Test No. MGSBR-2

In test no. MGSBR-2, a 2,585-lb (1,173-kg) small car, with a dummy in the left-front seat, impacted the bridge rail at a speed of 62.3 mph (100.2 km/h) and at an angle of 24.9 degrees. A summary of the test results and sequential photographs are shown in Figure 152. Additional sequential photographs are shown in Figures 153 through 155. Documentary photographs of the crash test are shown in Figures 156 through 158.

11.2 Weather Conditions

Test no. MGSBR-2 was conducted on June 26, 2009 at approximately 12:15 pm. The weather conditions as per the National Oceanic and Atmospheric Administration (station 14939/LNK) were reported as shown in Table 13.

Table 13. Weather Conditions, Test No. MGSBR-2

Temperature	87° F
Humidity	59%
Wind Speed	14 mph
Wind Direction	120° from True North
Sky Conditions	Overcast
Visibility	10 Statute Miles
Pavement Surface	Dry
Previous 3-Day Precipitation	0.01 in.
Previous 7-Day Precipitation	2.48 in.

11.3 Test Description

The target impact point was 8 ft - 3 in. (2.51 m) upstream of the centerline of the splice at post no. 20, as shown in Figure 159. The actual point of impact was 7 ft - 9 in. (2.36 m) upstream of the centerline of the splice at post no. 20. A sequential description of the impact events is contained in Table 14. The vehicle came to rest 116 ft - 5¾ in. (35.50 m) downstream from targeted impact and 4 ft - 5 in. (1.34 m) laterally behind the front face of the guardrail. Vehicle trajectory and final position are shown in Figure 160.

Table 14. Sequential Description of Impact Events, Test No. MGSBR-2

TIME (sec)	EVENT
0.000	Left-front bumper corner contacted the rail between post nos. 17 and 18
0.012	Left-front bumper corner contacted post no. 18
0.020	Left-front bumper corner underrode the rail downstream of post no. 18
0.026	Left-front tire contacted post no. 18
0.032	Rail disengaged from post no. 18
0.038	Left side of front bumper contacted post no. 19
0.042	Left-front tire became airborne
0.044	Rail disengaged from post no. 19
0.048	Top of vehicle rolled to the right side
0.078	Center of front bumper contacted post no. 20, and front bumper disengaged from the vehicle
0.080	Rail disengaged from post no. 20
0.118	Center of front bumper contacted post no. 21
0.120	Rail disengaged from post no. 21
0.166	Left-rear tire became airborne
0.172	Rail disengaged from post no. 22
0.184	Rail disengaged from post no. 23
0.218	Rail disengaged from post no. 24
0.226	Left-front bumper corner contacted post no. 23
0.278	Rail disengaged from post no. 25
0.282	Rail disengaged from post no. 26
0.298	Vehicle was parallel to the system at a speed of 31.2 mph (50.3 km/h)
0.306	Rail disengaged from post no. 27
0.358	Left-front tire contacted the deck edge between post nos. 24 and 25
0.436	Left-rear tire contacted the deck edge between post nos. 23 and 24
0.582	Vehicle exited system at a speed of 27.7 mph (44.6 km/h) and at an angle of 10.9 degrees as left-rear quarter panel lost contact with the rail between post nos. 24 and 25

11.4 Barrier Damage

Damage to the barrier was moderate, as shown in Figures 161 through 171. Barrier damage consisted of bridge deck cracking and spalling, deformed guardrail posts, disengaged post-to-rail connections, and contact marks on and deformation of the W-beam rail. The length of vehicle contact along the system was approximately 22 ft - 8 in. (6.91 m), which spanned from 19½ in. (495 mm) downstream of post no. 17 to 8½ in. (216 mm) upstream of post no. 25.

Through-deck cracking occurred at post nos. 18, 20 through 22, and 24. These cracks were minor at post nos. 20 and 24, while cracks were more significant at post nos. 18 and 22. Severe cracking occurred at post no. 21, where several pieces of concrete separated from the deck and left rebar exposed. The through-deck bolt and bolt sleeve were not displaced. Cracks in the deck were again caused by a combination of lateral shear due to bolt pullout loads and punching shear due to downward loads. The bolt pullout loads were caused by downstream and lateral forces on the posts and mounting brackets and resulted in cracks on the top surface of the deck. Punching shear cracks were formed in the vertical edge of the deck that were caused by downward vehicle loads and prying action of the post and mounting bracket assembly about the through-deck bolt.

Spalling of the edge of the concrete deck occurred at post nos. 16 through 22, 24, and 25. Most of this spalling was minor, but the spalling at post no. 24 was severe. Note that significant spalling damage previously occurred at post nos. 24 and 26 during test no. MGSBR-1. Spalling was again caused by downward deflection of the top mounting bracket plate due to the prying action and impact of the mounting bracket against the edge of the deck as it rotated about the vertical through-deck bolt.

Minor damage was sustained by the mounting brackets, consisting of slightly bent backside retainer plates and lower bracket connection bolts. Post nos. 17 through 26 showed varying degrees of damage. Eight posts, nos. 18 through 25, completely failed through bending and twisting. The front flanges of post nos. 18 and 19 were completely ruptured, and the front flanges of post nos. 20 through 24 were partially ruptured. Scrapes and/or gouges were found on post nos. 18 through 25.

Post nos. 18 through 27 were disengaged from the rail due to fracture of the post-to-rail connection bolts. The W-beam backup plates at post nos. 18 through 26 were also disengaged from the system. The splices at post nos. 12, 20, 24, and 28 showed evidence of slipping from $^1/_{16}$ in. (2 mm) to $^3/_{16}$ in. (5 mm) due to membrane action of the W-beam rail.

General deformation and flattening of the W-beam rail occurred from post no. 18 to a location 8 in. (203 mm) upstream of post no. 25. Contact marks were visible on the guardrail from 19½ in. (495 mm) downstream of post no. 17 to 8½ in. (216 mm) upstream of post no. 25, with additional contact marks from 8 in. (203 mm) downstream of post no. 26 to 15 in. (381 mm) downstream of post no. 26 and from 13 in. (330 mm) upstream of post no. 27 to 2 in. (51 mm) upstream of post no. 27. Slight buckling occurred near post nos. 16, 17, 25, 26, and 28. Deformation to the bottom of the W-beam due to contact with the post occurred near post no. 26.

A ½-in. (13-mm) soil gap was found on the upstream edge of post no. 1 and ⅛-in. (3-mm) and $^1/_{16}$-in. (2-mm) soil gaps were found on the upstream and downstream edges of post no. 2, respectively. Additionally, a ⅛-in. (3-mm) soil gap was found on the downstream side of post no. 38, and soil gaps of ½ in. (13 mm) were found on the downstream edges of post nos. 39 and 40.

The permanent set of the barrier system is shown in Figures 161 and 162. The maximum permanent set rail and post deflections were 20 in. (508 mm) at post no. 21 and 13½ in. (343 mm) at post no. 20, respectively, as measured in the field. The maximum lateral dynamic rail and post deflections were 28.0 in. (712 mm) at post no. 21 and 18.4 in. (468 mm) at post no. 18, respectively, as determined from high-speed digital video analysis. The working width of the system was determined to be 33.8 in. (859 mm), also determined from high-speed digital video analysis.

11.5 Vehicle Damage

The damage to the vehicle was moderate, as shown in Figures 172 and 173. The maximum occupant compartment deformations are listed in Table 11 with the deformation limits established in MASH for various areas of the occupant compartment. It should be noted that none of the MASH established deformation limits were violated. Complete occupant compartment and vehicle deformations and the corresponding locations are provided in Appendix D.

Table 15. Maximum Occupant Compartment Deformations by Location

LOCATION	MAXIMUM DEFORMATION in. (mm)	MASH ALLOWABLE DEFORMATION in. (mm)
Wheel Well & Toe Pan	1¼ (32)	≤ 9 (229)
Floor Pan & Transmission Tunnel	¼ (6)	≤ 12 (305)
Side Front Panel (in Front of A-Pillar)	¼ (6)	≤ 12 (305)
Side Door (Above Seat)	½ (13)	≤ 9 (229)
Side Door (Below Seat)	¼ (6)	≤ 12 (305)
Roof	½ (13)	≤ 4 (102)
Windshield	0	≤ 3 (76)

The front bumper was disengaged and came to rest on the traffic-side face of the barrier. The hood was ajar, and the grill was crushed inward at its center. The left-front corner of the hood and body were deformed inward. The windshield had several cracks near its lower left-front corner. The left-front tire was flat, and the left-front rim was deformed. The left-front brake fluid container was punctured. The left-front quarter panel was deformed and scraped along its length. This scraping continued along both left doors and part of the left-rear quarter panel of the vehicle. The left-front door was slightly ajar. Contact marks were found on the left-rear hubcap.

Inspection of the vehicle undercarriage revealed that the skid plate, radiator mounting brackets, and the transmission oil pan were damaged. The left-front suspension links were bent, and the exhaust pipe was disengaged at the rear of the catalytic converter. The unibody was significantly damaged at the connection to the left-front lower control arm.

11.6 Occupant Risk

The calculated occupant impact velocities (OIVs) and maximum 0.010-sec occupant ridedown accelerations (ORAs) in both the longitudinal and lateral directions are shown in Table 16. It is noted that the OIVs and ORAs were well below recommended limits provided in MASH. The calculated THIV, PHD, and ASI values are also shown in Table 16. The results of the occupant risk analysis, as determined from the accelerometer data, are summarized in Figure 152. The recorded data from the accelerometers and the rate transducers are shown graphically in Appendix F. It was noted that the DTS accelerometer displayed non-realistic behavior as the vehicle lost contact with the barrier. However, as the occupant risk measurements occurred early in the event, this behavior was not believed to have influenced the data.

Table 16. Summary of OIV, ORA, THIV, PHD, and ASI Values, Test No. MGSBR-2

Evaluation Criteria		**Transducer**			**MASH Limits**
		EDR-4	**DTS**	**EDR-3**	
OIV ft/s (m/s)	Longitudinal	-24.40 (-7.44)	-22.90 (-6.98)	-25.29 (-7.71)	≤ 40 (12.2)
	Lateral	16.54 (5.04)	16.38 (4.99)	17.94 (5.47)	≤40 (12.2)
ORA g's	Longitudinal	-7.69	-7.41	-8.65	≤ 20.49
	Lateral	6.58	7.34	7.39	≤ 20.49
THIV ft/s (m/s)		28.50 (8.69)	28.04 (8.55)		not required
PHD g's		9.93	9.90		not required
ASI		0.79	0.78	0.88	not required

11.7 Discussion

The analysis of the test results for test no. MGSBR-2 showed that the bridge rail adequately contained and redirected the vehicle. There were no detached elements nor fragments which showed potential for penetrating the occupant compartment nor presented undue hazard to other traffic. The deformation of, or intrusion into, the occupant compartment was minimal and did not pose a threat to cause serious injury. The test vehicle did not penetrate nor ride over the barrier and remained upright during and after the collision. Vehicle roll, pitch, and yaw angular displacements, shown in Appendix F, were well below the limit of 75 degrees recommended by MASH. After impact, the vehicle exited the barrier at an angle of 10.9 degrees, and its trajectory did not violate the bounds of the exit box. Therefore, test no. MGSBR-2 was determined to be acceptable according to the TL-3 safety performance criteria found in MASH for test designation no. 3-10.

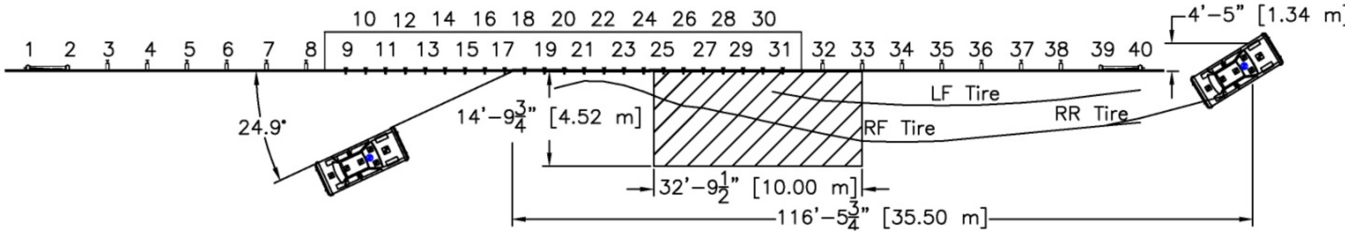

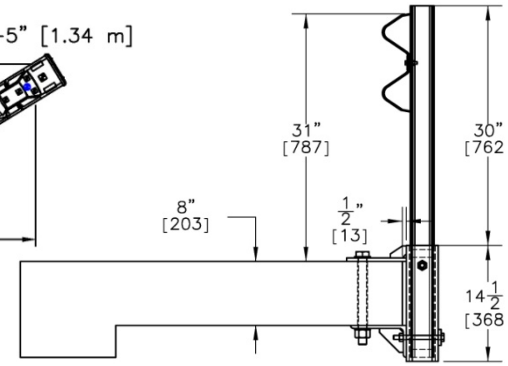

- Test Agency ....MwRSF
- Test Number MGSBR-2
- Date 6/26/2009
- MASH Test Designation 3-10
- Test Article ....MGS Bridge Rail with approach MGS Guardrails
- Total Length ....175 ft (53.3 m)
- Key Component – MGS Bridge Rail
  - Post Type S3x5.7 (S76x8.5)
  - Post Spacing ....3 ft - 1½ in. (953 mm)
  - Post-to-rail Connection ....5⁄16-in. (7.9-mm) dia. ASTM A307A Bolt
- Key Component – Simulated Bridge Deck
  - Thickness (outer edge) ....8 in. (203 mm)
  - Concrete Strength (minimum) ....4,000 psi (27.6 MPa)
- Vehicle Model ....2003 Kia Rio Passenger Car
  - Curb ....2,408 lb (1,092 kg)
  - Test Inertial ....2,416 lb (1,096 kg)
  - Gross Static ....2,585 lb (1,173 kg)
- Impact Conditions
  - Speed ....62.3 mph (100.2 km/h)
  - Angle ....24.9 degrees
  - Impact Location ....7 ft - 9 in. (2.36 m) US of the splice at post no. 20
- Exit Conditions
  - Speed ....27.7 mph (44.6 km/h)
  - Angle ....10.9 degrees
  - Exit Box ....Pass
- Vehicle Stability ....Satisfactory
- Vehicle Stopping Distance ....116 ft - 5¾ in. (35.5 m) downstream
  4 ft - 5 in. (1.3 m) behind front face of guardrail
- Vehicle Damage ....Moderate
  - VDS[75] 11-LFQ-4
  - CDC[76] 11-LYEW-5
  - Maximum Interior Deformation .... 1¼ in. (32 mm), front of floor pan
- Test Article Damage ....Moderate
- Test Article Deflections
  - Permanent Set ....20 in. (508 mm)
  - Dynamic ....28.0 in. (712 mm)
  - Working Width ....33.8 in. (859 mm)
- Angular Displacements (EDR-4)
  - Roll ....-8.7 degrees
  - Pitch ....-8.2 degrees
  - Yaw ....34.7 degrees
- Angular Displacements (DTS)
  - Roll ....-12.7 degrees
  - Pitch ....-5.0 degrees
  - Yaw ....35.1 degrees
- Transducer Data

Evaluation Criteria		Transducer			MASH Limit
		EDR-4	DTS	EDR-3	
OIV ft/s (m/s)	Longitudinal	-24.40 ft/s (-7.44 m/s)	-22.90 ft/s (-6.98 m/s)	-25.29 ft/s (-7.71 m/s)	≤ 40 (12.2)
	Lateral	16.54 ft/s (5.04 m/s)	16.38 ft/s (4.99 m/s)	17.94 ft/s (5.47 m/s)	≤ 40 (12.2)
ORA g's	Longitudinal	-7.69	-7.41	-8.65	≤ 20.49
	Lateral	6.58	7.34	7.39	≤ 20.49
THIV – ft/s (m/s)		28.50 ft/s (8.69 m/s)	28.04 ft/s (8.55 m/s)		not required
PHD – g's		9.93	9.90		not required
ASI		0.79	0.78	0.88	not required

Figure 152. Summary of Test Results and Photographs, Test No. MGSBR-2


0.000 sec


0.042 sec


0.084 sec

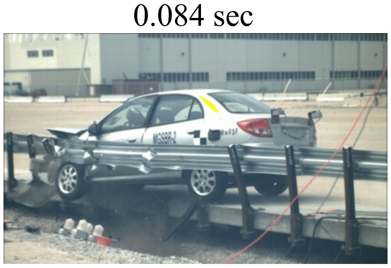
0.140 sec

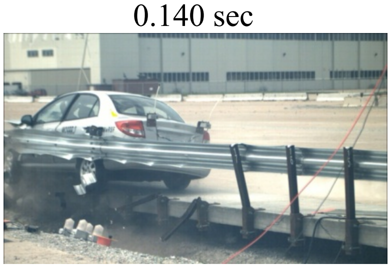
0.256 sec


0.418 sec


0.000 sec


0.078 sec


0.162 sec


0.282 sec


0.398 sec


0.582 sec

Figure 153. Additional Sequential Photographs, Test No. MGSBR-2

0.000 sec


0.000 sec

0.026 sec


0.064 sec

0.038 sec


0.118 sec

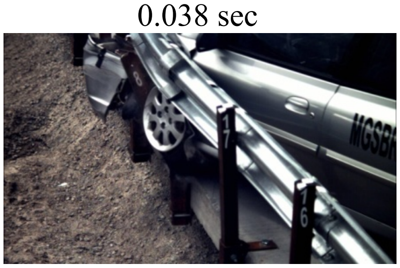

0.048 sec


0.142 sec

0.074 sec


0.184 sec

0.134 sec


0.286 sec

Figure 154. Additional Sequential Photographs, Test No. MGSBR-2

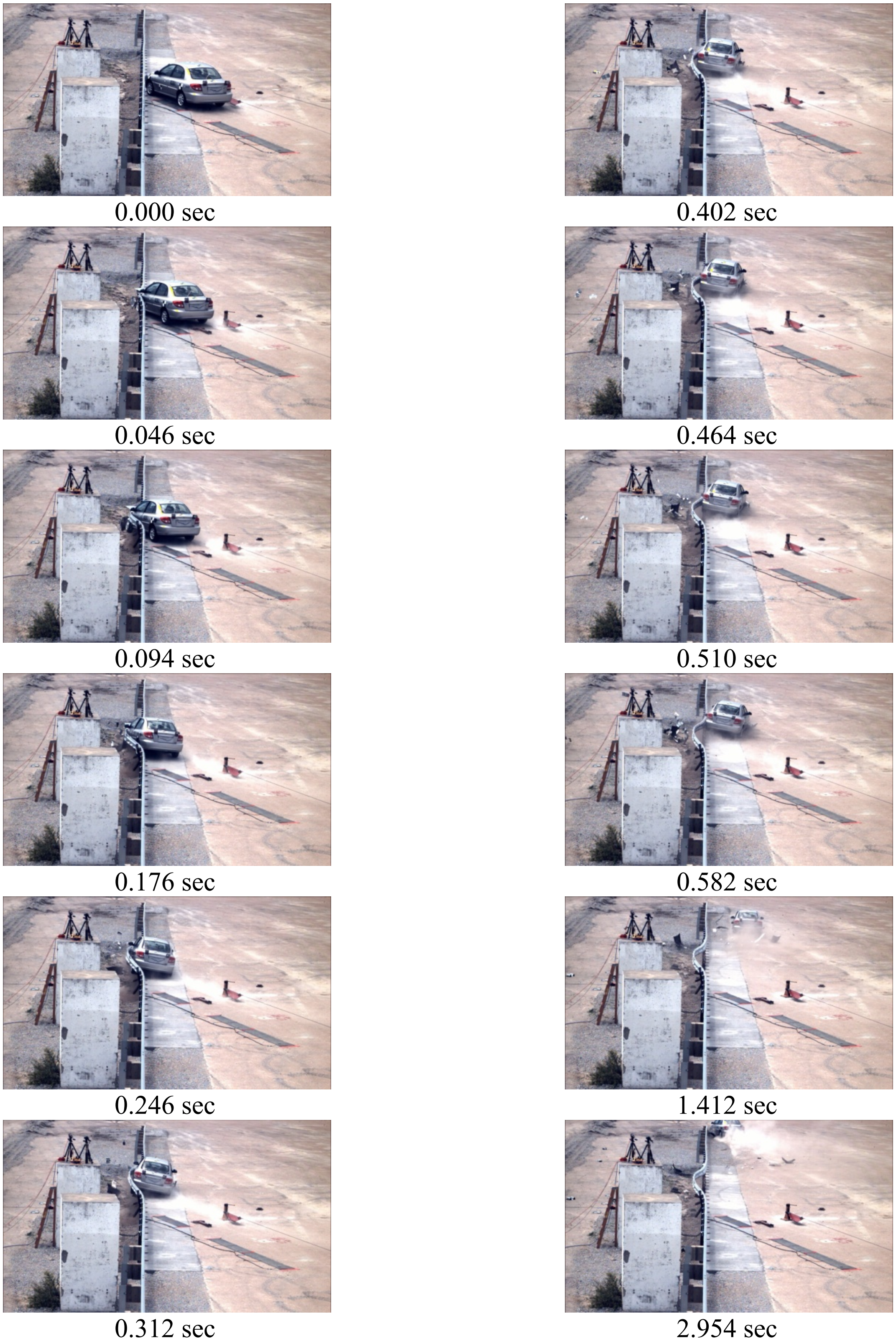

Figure 155. Additional Sequential Photographs, Test No. MGSBR-2

Figure 156. Documentary Photographs, Test No. MGSBR-2

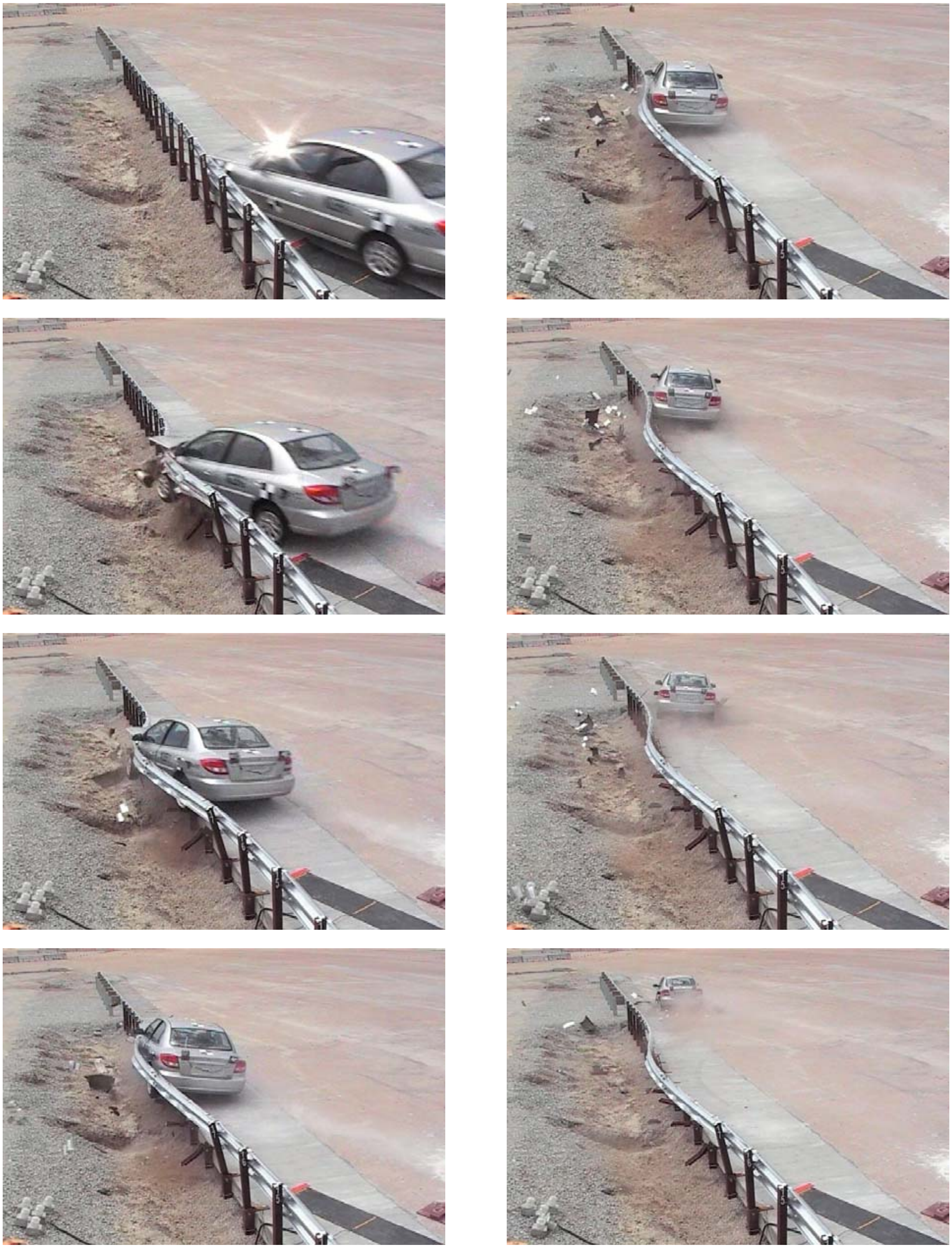

Figure 157. Documentary Photographs, Test No. MGSBR-2

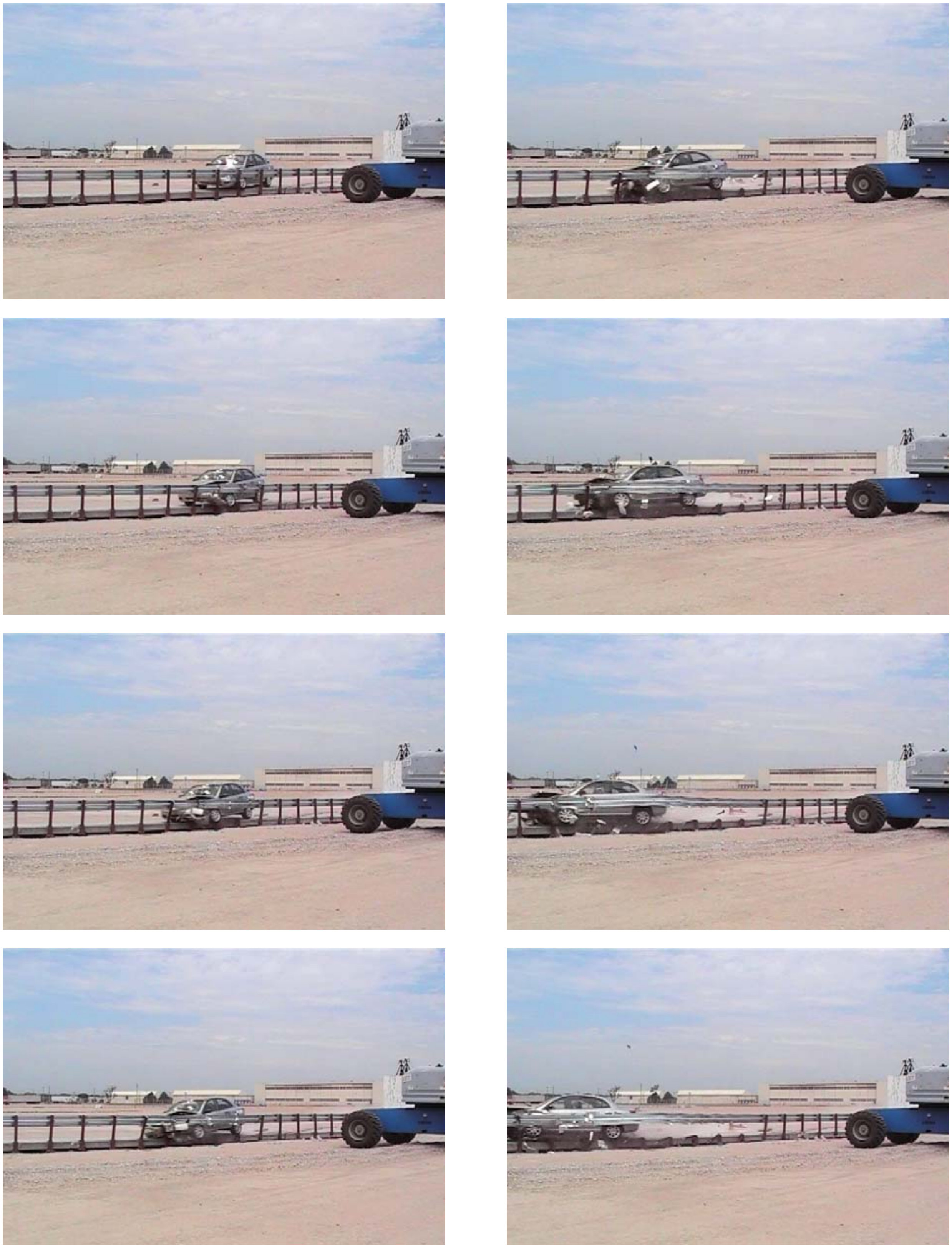

Figure 158. Documentary Photographs, Test No. MGSBR-2

Figure 159. Impact Location, Test No. MGSBR-2

Figure 160. Vehicle Final Position and Trajectory Marks, Test No. MGSBR-2

Figure 161. System Damage, Test No. MGSBR-2

Figure 162. Permanent Set, Test No. MGSBR-2

Figure 163. Rail Damage, Test No. MGSBR-2

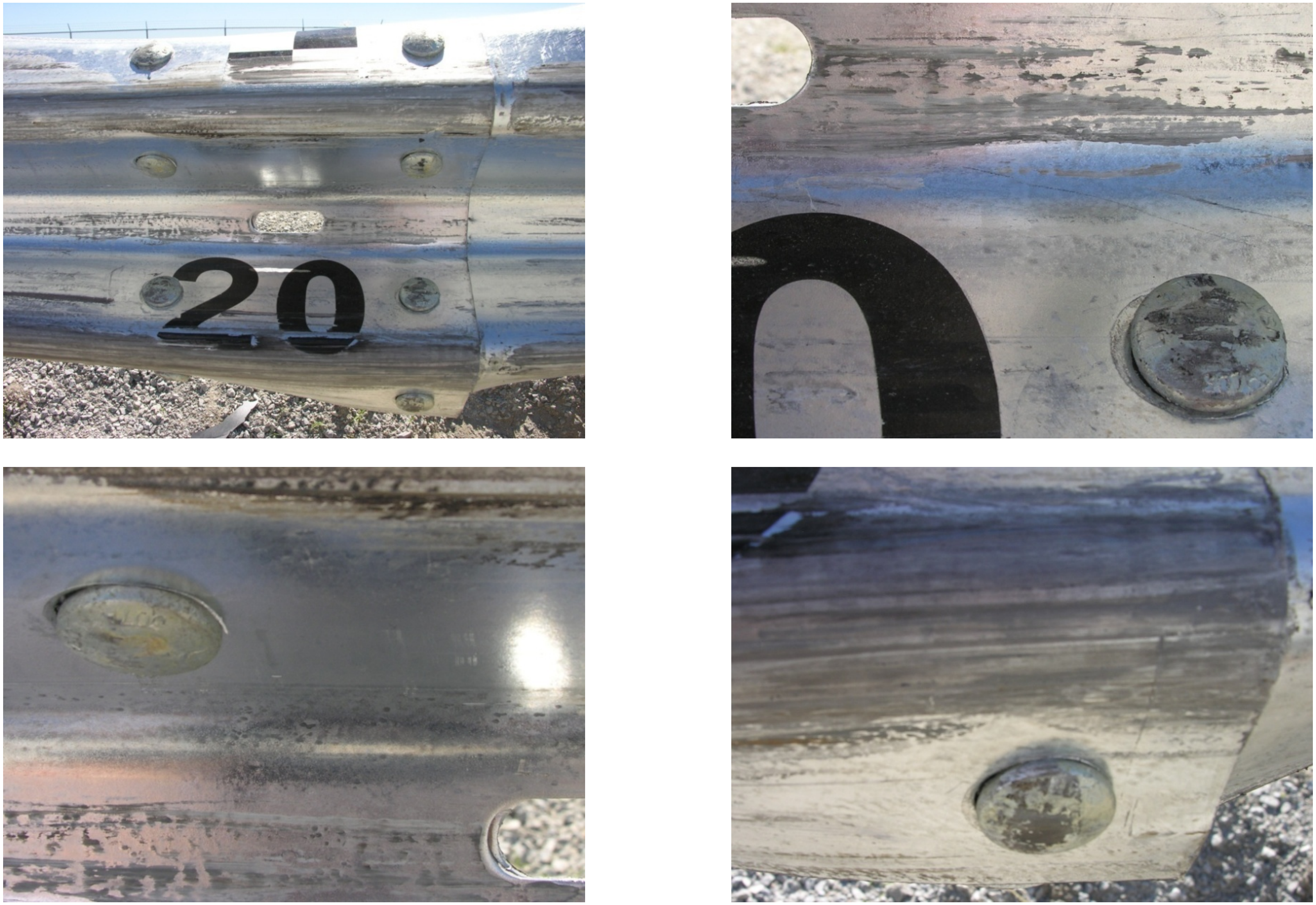

Figure 164. Typical Splice Damage, Post 20, Test No. MGSBR-2

*Note that through-deck cracking occurred at post no. 16 during test no. MGSBR-1

Figure 165. Post Nos. 16 and 17 Damage, Test No. MGSBR-2

Figure 166. Post Nos. 18 and 19 Damage, Test No. MGSBR-2

Figure 167. Post Nos. 20 and 21 Damage, Test No. MGSBR-2

Figure 168. Post Nos. 22 and 23 Damage, Test No. MGSBR-2

*Note that significant spalling occurred at post no. 24 during test no. MGSBR-1.

Figure 169. Post Nos. 24 and 25 Damage, Test No. MGSBR-2

*Note that significant spalling occurred at post no. 26 during test no. MGSBR-1

Figure 170. Post Nos. 26 and 27 Damage, Test No. MGSBR-2

Figure 171. Upstream Anchorage Damage, Test No. MGSBR-2

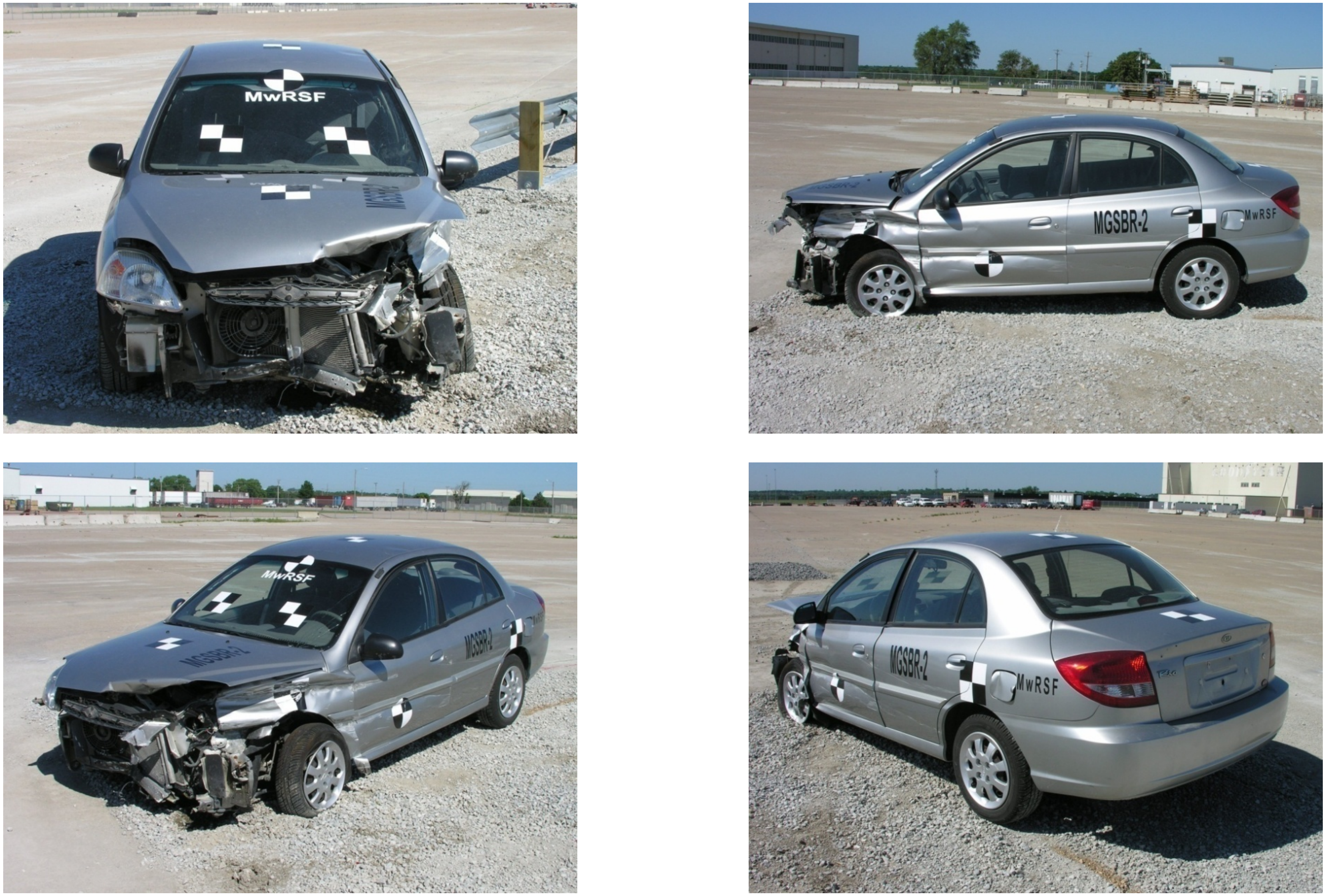

Figure 172. Vehicle Damage, Test No. MGSBR-2

Figure 173. Occupant Compartment Deformation, Test No. MGSBR-2

12 BARRIER VII VALIDATION AND ADDITIONAL ANALYSIS

12.1 Purpose and Scope

Following the full-scale crash tests, additional BARRIER VII modeling was required to validate the results of the pre-test simulations. These analyses had been performed to demonstrate that a transition section would not be required between the bridge rail and approach MGS.

Two sets of simulations were performed. First, the BARRIER VII models were calibrated to match the results of the full-scale crash tests. Calibrated BARRIER VII input files for both full-scale crash tests are shown in Appendix G. Additional simulations were then performed to more thoroughly explore the need for a transition section between the MGS and the bridge rail.

12.2 Calibration of BARRIER VII Models

Following full-scale test nos. MGSBR-1 and 2, it was necessary to compare the results of the physical tests to those predicted by the BARRIER VII models as well as to calibrate the models to improve model accuracy. Analyses were performed using the previously-developed barrier model with impact conditions matching those of the full-scale tests. Impact locations, speeds, angles, and vehicle weights were updated, and the barrier model was modified to include one additional guardrail post and two fewer bridge rail posts to match the as-built barrier specifications.

Both simulations were calibrated with 225-node barrier models. Following calibration with the 225-node models, the same parameters were used in 449-node models to investigate the effects of mesh density on model predictions.

Two parameters of the models required calibration. These parameters were the stiffness and strength of the bridge rail posts and the coefficient of friction between the vehicle and the bridge rail. Three different post models were used in the pre-test modeling, which were created using data from three dynamic bogie tests. In these tests, a bogie struck three S3x5.7 (S76x8.5) posts at angles of 90 degrees, 75 degrees, and 60 degrees with respect to the strong axis of each post [66]. In development of the post models, a reduction factor of 0.875 was applied to the 90-degree post data to account for post twisting and subsequent loss of strength that would occur in a rail impact. Simulations of both full-scale tests demonstrated that post models based on an S3x5.7 (S76x8.5) post impacted at an angle of 60 degrees to its strong axis, the weakest of the 3 post models, provided the most accurate results.

The coefficient of friction between the vehicle and the barrier also required calibration. While BARRIER VII does not include the effects of wheel snag in its analysis, the effect of this phenomenon on vehicle trajectory can be simulated by adjusting the coefficient of friction. When a vehicle's wheel snags on a post, a force is applied near the edge of the vehicle, which creates a moment that resists redirection of the vehicle. This affect can be simulated in BARRIER VII by increasing the coefficient of friction between the vehicle and the barrier. This approach is most accurate when the snag occurs near the edge of a vehicle. Previously, a coefficient of friction of 0.35 was used, which was created through calibration of an MGS model. Differences in snag characteristics between the guardrail and bridge rail warranted calibration of this value. As the pickup and small car also have different snag characteristics, separate coefficients of friction were required for each test.

Three different contact interfaces were specified in the updated BARRIER VII models. Two contact interfaces were defined for the approach guardrails using the previous coefficient of friction of 0.35, and one contact interface was defined for the bridge rail. This value was calibrated to produce results similar to findings from each of the full-scale tests, as described in the following sections.

12.2.1 Simulation of Test No. MGSBR-1

Test no. MGSBR-1 was simulated using coefficients of friction varying from 0.20 to 0.35. The final coefficient of friction used in the simulation was 0.23. This value was considerably lower than that of the MGS, but it was thought to be sufficiently accurate due to the different nature of the snag.

Many of the bridge rail posts snagged on the pickup truck near the center of its front bumper, whereas in guardrail snag occurs closer to the edge of a vehicle. This difference was caused by several factors. First, the approach guardrail uses blockouts, whereas the bridge rail does not. Additionally, while the center of rotation of guardrail posts is beneath the ground surface, the bridge rail posts bend at the top of the bridge deck. Deflections in both systems are similar, thus the vehicle overrides posts to a greater extent in the bridge rail. This allows for snag to occur near the vehicle's center, which does not apply a moment to resist vehicle redirection, whereas in the guardrail, post snag does resist redirection. Thus, a lower coefficient of friction was used for the bridge rail.

A comparison of simulation and physical test results for test no. MGSBR-1 is shown in Table 17. Note that dynamic deflection was predicted to within 10 percent of the true value, and predicted parallel time, length of contact, and permanent set deflections were nearly identical to those of the full-scale test.

Graphical comparisons of the 225-node simulated and actual barrier deflections are shown in Figures 174 through 177. As shown in the figures, the model predicted a reasonably accurate deflected shape of the barrier. Deflections were slightly underestimated around the point of vehicle contact, and slightly overestimated upstream and downstream of vehicle contact. The largest difference in deflected shape occurred after the rear of the vehicle contacted the guardrail.

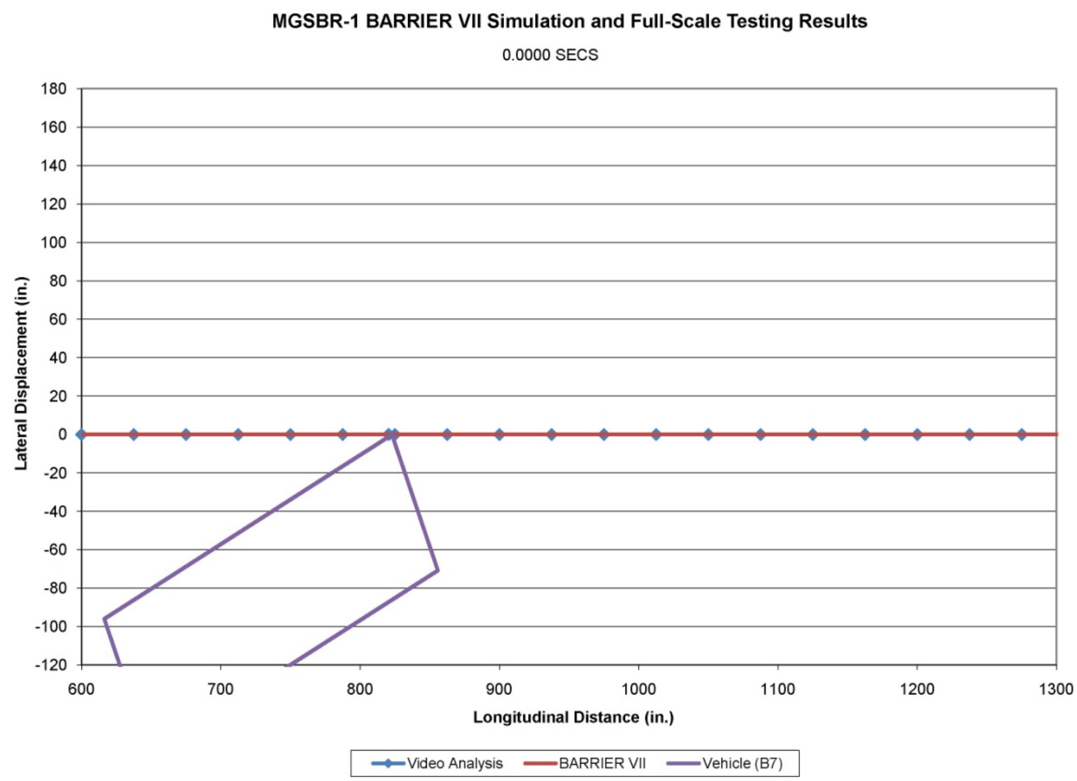

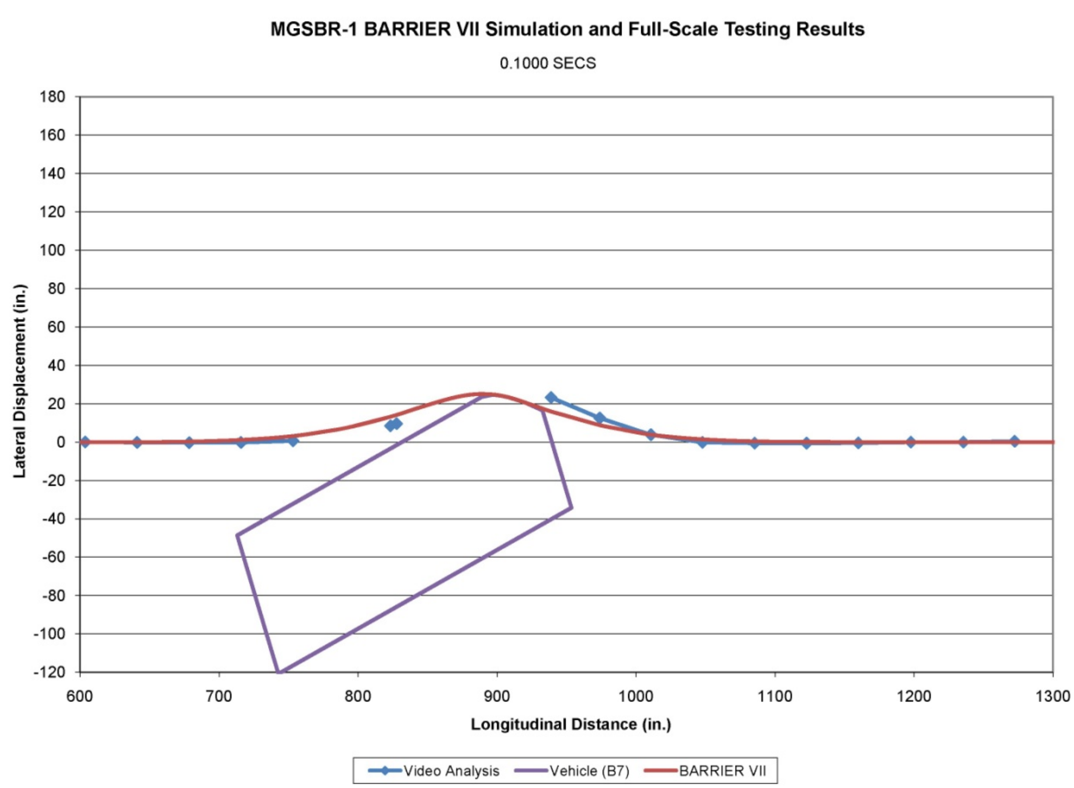

Figure 174. Sequential Figures from BARRIER VII Simulation of MGSBR-1

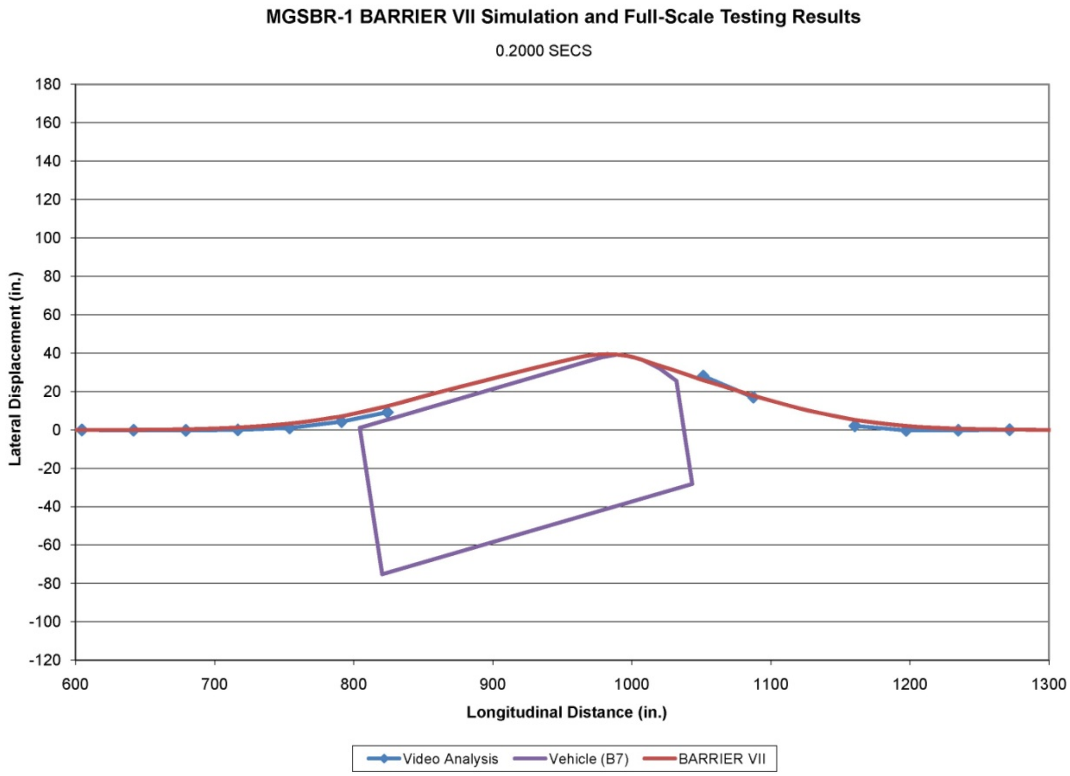

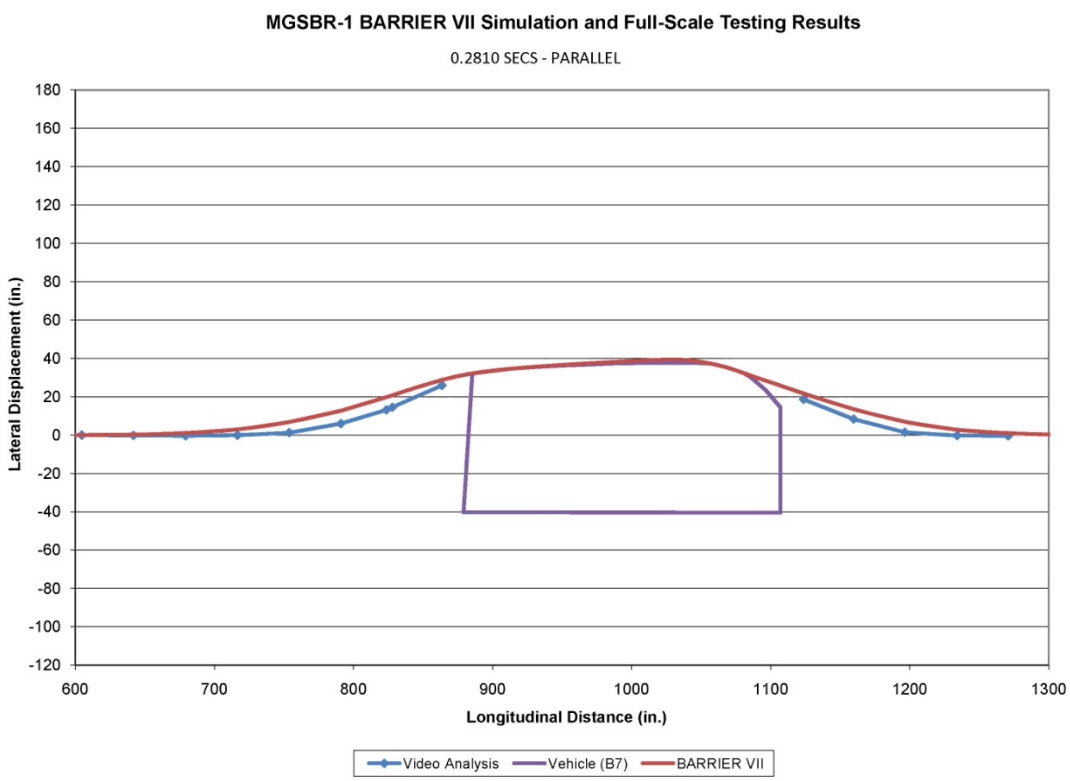

Figure 175. Sequential Figures from BARRIER VII Simulation of MGSBR-1

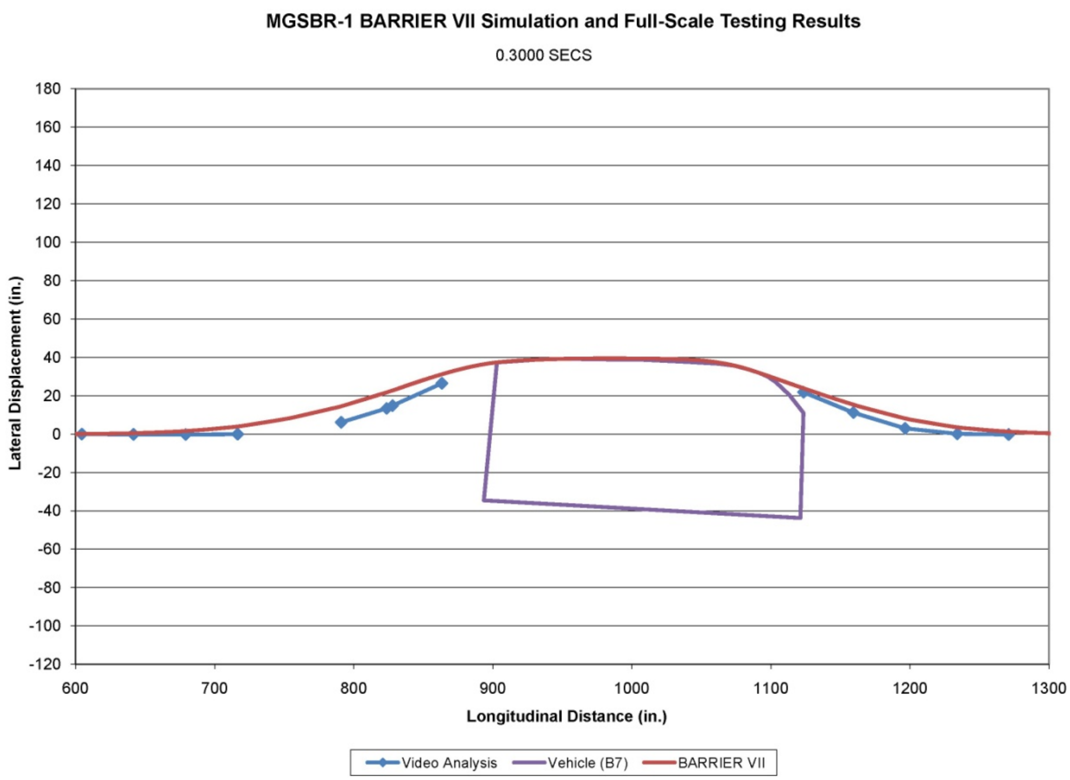

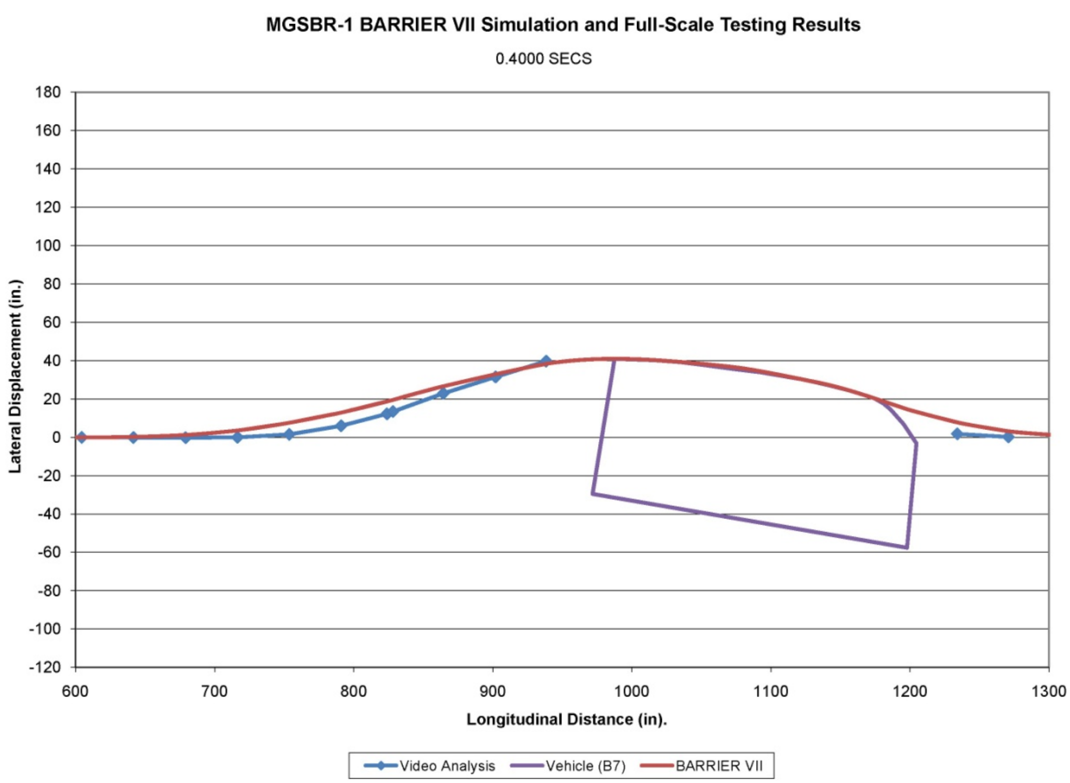

Figure 176. Sequential Figures from BARRIER VII Simulation of MGSBR-1

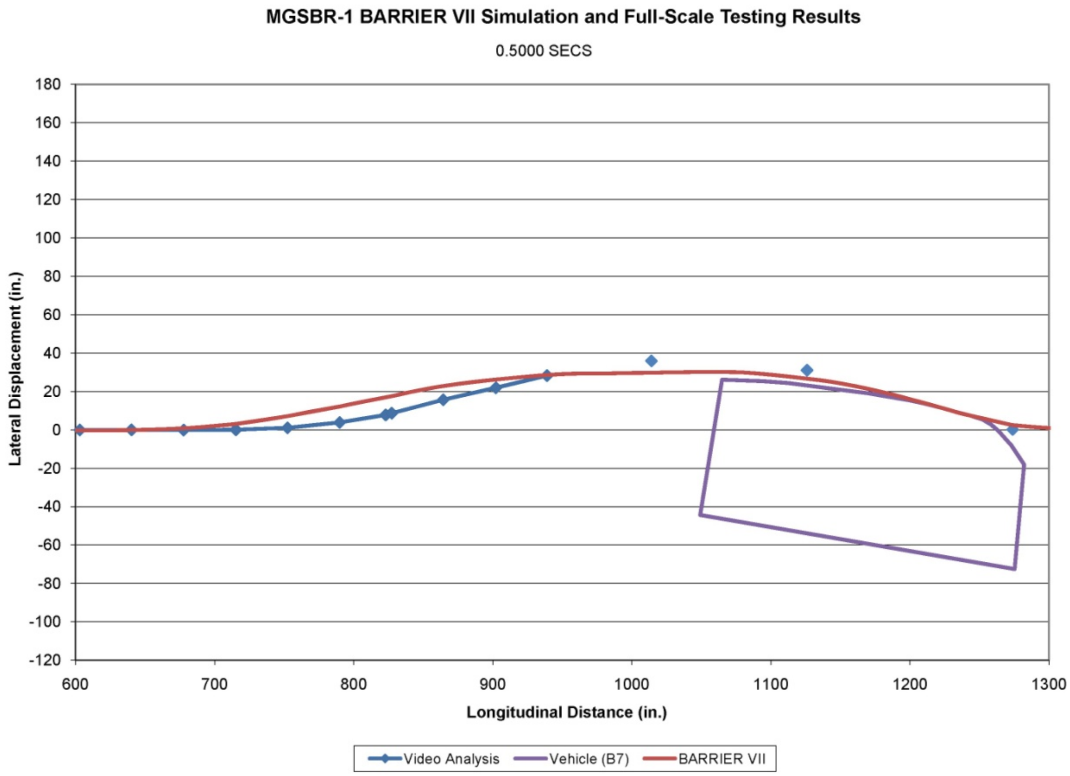

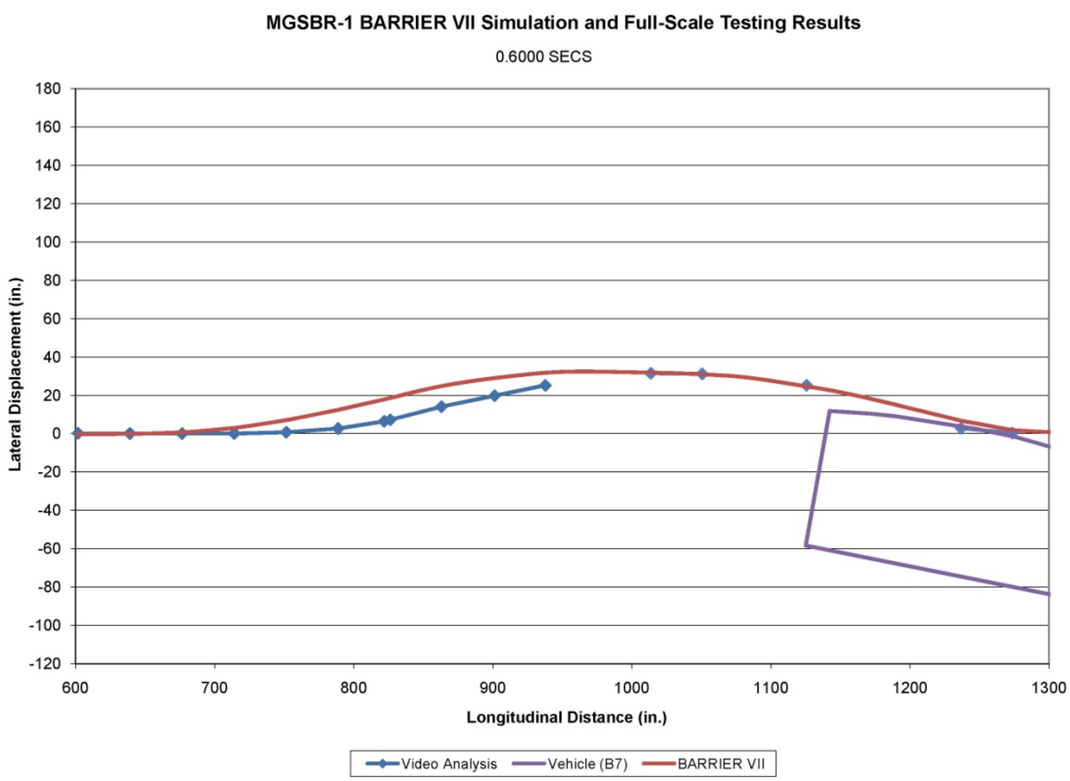

Figure 177. Sequential Figures from BARRIER VII Simulation of MGSBR-1

This generated larger deflections in the simulated rail upstream of the vehicle than occurred in the physical test.

Table 17. Calibrated BARRIER VII Simulation Results, Test No. MGSBR-1

Evaluation Criteria	Physical Test Results	BARRIER VII Simulation Results			
		225-Node	Error	449-Node	Error
Dynamic Deflection - in. (mm)	48.9 (1,242)	44.0 (1,118)	-10.0%	43.3 (1,100)	-11.5%
Permanent Set Deflections - in. (mm)	31.9 (810)	32.2 (818)	0.9%	32.2 (818)	0.9%
Length of Contact - in. (mm)	411.9 (10,462)	409.3 (10,396)	-0.6%	355.1 (9,020)	-13.8%
Failed Posts (>15 in. rail deflection)	16-24	15-25	2 posts	15-25	2 posts
Parallel Time - msec	280	281	0.4%	276	-1.4%
Parallel Speed - mph (km/h)	44.9 (72.3)	47.7 (76.8)	6.2%	47.0 (75.6)	4.7%
Exit Time - msec	648	544	-16.0%	518	-20.1%
Exit Speed - mph (km/h)	34.5 (55.5)	44.4 (71.5)	28.7%	43.7 (70.3)	26.7%

The model showed significant error in predicting vehicle speeds due to limitations of the BARRIER VII analysis, which did not include energy-absorbing effects unique to this test. In the full-scale test, the pickup truck overrode approximately nine posts as it was overhanging the edge of the deck. The pickup impacted these posts at low heights, near the tops of the mounting brackets, which allowed the posts to absorb significant amounts of energy as they yielded despite their small weak-axis section modulus. As many of these posts contacted the vehicle near its center, the vehicle was decelerated without affecting redirection. Thus, this phenomenon could not be simulated using the coefficient of friction. Additionally, the left-front wheel of the vehicle was detached from the vehicle, and the vehicle itself had to be pulled back above the deck by the barrier after overhanging the edge, both of which would require significant amounts of energy. Thus, the ability of BARRIER VII to accurately predict velocity of the pickup truck was limited. This effect also produced error in the predicted exit times.

Some error was also present in the simulated number of failed posts. BARRIER VII deletes post elements when the system deflects beyond a designated failure deflection. For these models, this deflection was set to 15 in. (381 mm). The posts and rails are attached and move as one unit, whereas in the physical system, the posts detach and can move independently of the rail. Therefore, to determine a comparable number of failed posts from the physical test, dynamic rail deflections were examined at post locations.

Any dynamic deflection greater than 15 in. (381 mm) was considered to fail the post. Rail deflection exceeded this value at only nine posts in the physical test, whereas BARRIER VII predicted eleven failed posts. However, in the physical test, post nos. 15 and 25 deflected 14.9 in. (378 mm) and 6.1 in. (155 mm), respectively, which demonstrates better agreement between the simulation and the test. Additionally, energy was absorbed as the pickup truck snagged on and yielded the bridge rail posts in the physical test. BARRIER VII could not account for this energy dissipation, as discussed previously; therefore, the kinetic energy of the simulated pickup truck was greater than that of the physical pickup truck throughout the impact. This allowed the simulated pickup truck to deflect the downstream guardrail to a greater extent than in the full-scale test, thus predicting a greater number of failed posts. Note that for test no. MGSBR-1, the number of posts that failed through all mechanisms, including snag, was equivalent to the number that deflected greater than 15 in. (381 mm).

Following analysis with the 225-node model, a 449-node model was used to further investigate mesh sensitivity of the model. While the results of the finer mesh displayed some differences, they were very similar to those of the coarser mesh, indicating the results had converged. Thus, the 225-node model was used for further analysis.

12.2.2 Calibration of Test No. MGSBR-2

Test no. MGSBR-2 was simulated using coefficients of friction varying from 0.35 to 0.55. The simulation predicted the most accurate results with a coefficient of friction of 0.525. With this value, the model produced excellent results for all parameters except number of failed posts and length of contact. The coefficient of friction was much higher for the small car than for the pickup due to the nature of the snag on the posts. The small car did not deflect the system as much as the pickup truck; thus, the snag on the posts was closer to the edge of the vehicle. This applied a moment to the car that delayed redirection, resulting in a higher calibrated coefficient of friction. The rail also deformed the left-front corner of the small car inward to a greater extent than that of the pickup truck. This allowed the rail itself to apply greater friction force to the small car due to the increased interlock between the vehicle and the rail. Thus, the calibrated friction force between the rail and the small car was greater than in the pickup truck test.

A comparison of simulation and physical test results for test no. MGSBR-2 is shown in Table 18. Note that predicted dynamic deflection, permanent set deflection, and parallel time were nearly identical to the values from the full-scale test. Graphical comparisons of the 225-node simulated and actual barrier deflections are shown in Figures 178 through 181. The simulation predicted excellent results for the deformed shape of the barrier, as shown in the figures.

Table 18. Calibrated BARRIER VII Simulation Results, Test No. MGSBR-2

Evaluation Criteria	Physical Test Results	BARRIER VII Simulation Results			
		225-Node	Error	449-Node	Error
Dynamic Deflection - in. (mm)	28.0 (711)	27.9 (709)	-0.4%	27.0 (686)	-3.6%
Permanent Set Deflections - in. (mm)	20.0 (508)	21.0 (533)	5.0%	19.9 (505)	-0.5%
Length of Contact - in. (mm)	272.0 (6,909)	203.4 (5,166)	-25.2%	200.9 (5,103)	-26.1%
Failed Posts (>15 in. rail deflection)	18-22	19-22	1 post	18-22	0 posts
Parallel Time - msec	298	298	0.0%	302	1.3%
Parallel Speed - mph (km/h)	31.2 (50.3)	31.9 (51.3)	2.2%	31.6 (50.9)	1.3%
Exit Time - msec	582	493	-15.3%	498	-14.4%
Exit Speed - mph (km/h)	27.7 (44.6)	30.4 (48.9)	9.7%	30.1 (48.4)	8.7%

As discussed previously, the difference in number of failed posts was due to the method BARRIER VII uses to fail a post. In the full-scale test, wheel snag caused many post failures,

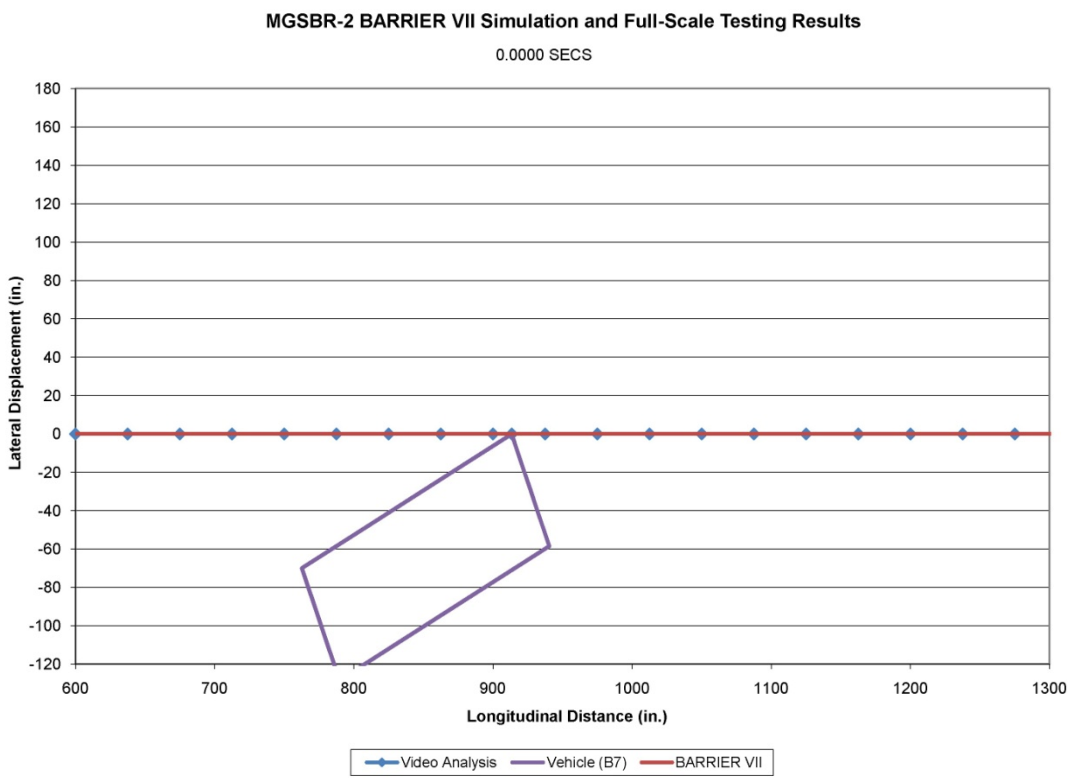

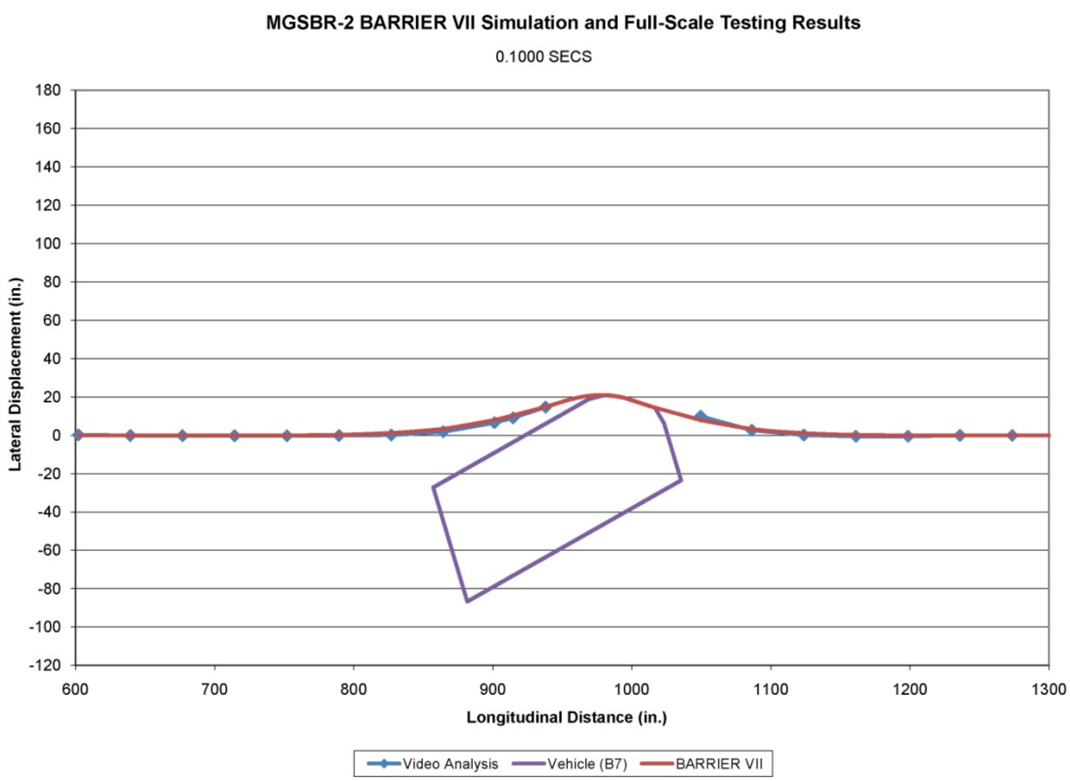

Figure 178. Sequential Figures from BARRIER VII Simulation of MGSBR-2

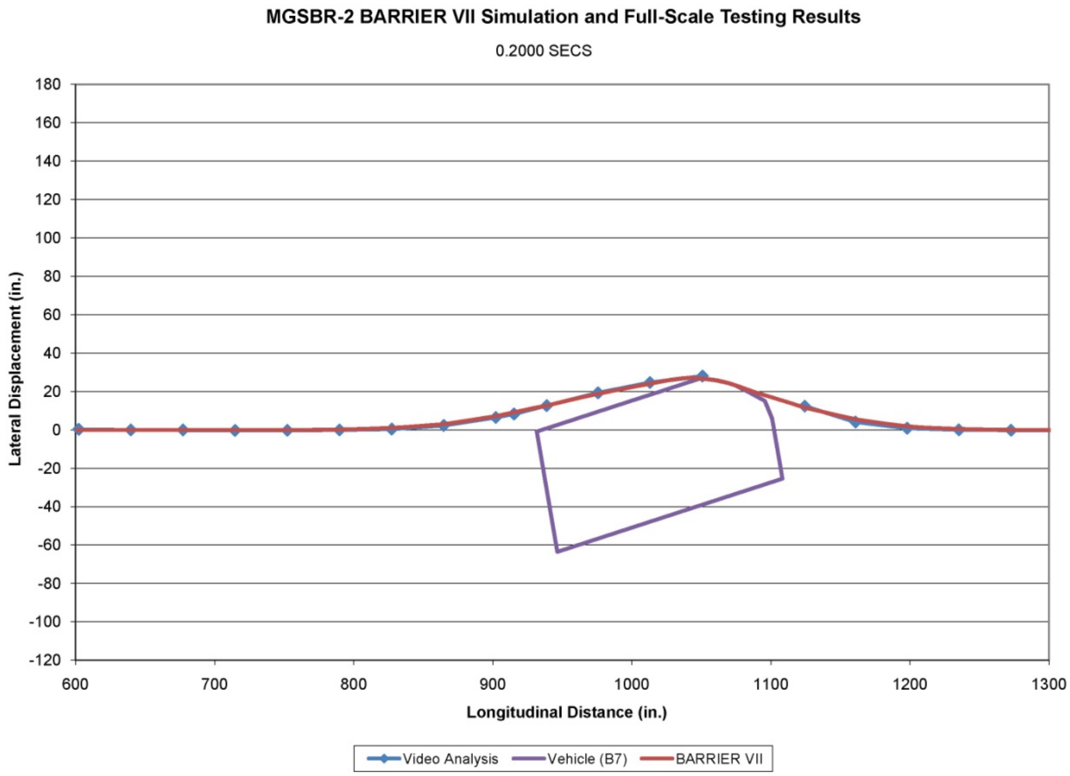

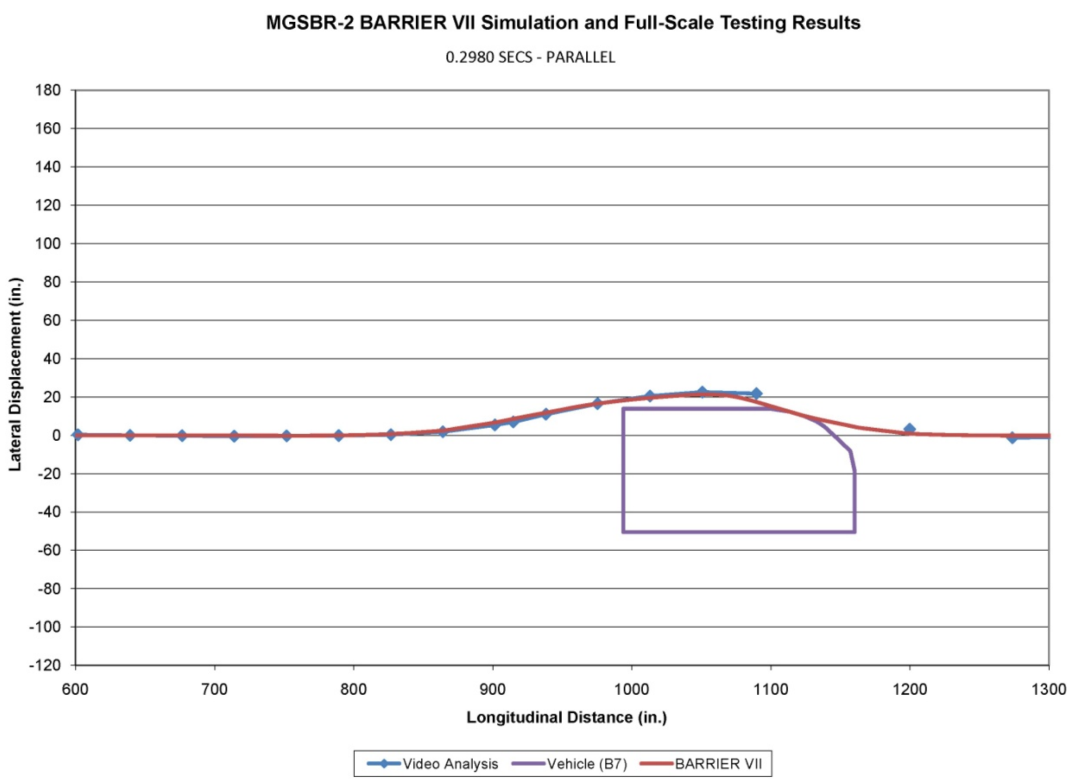

Figure 179. Sequential Figures from BARRIER VII Simulation of MGSBR-2

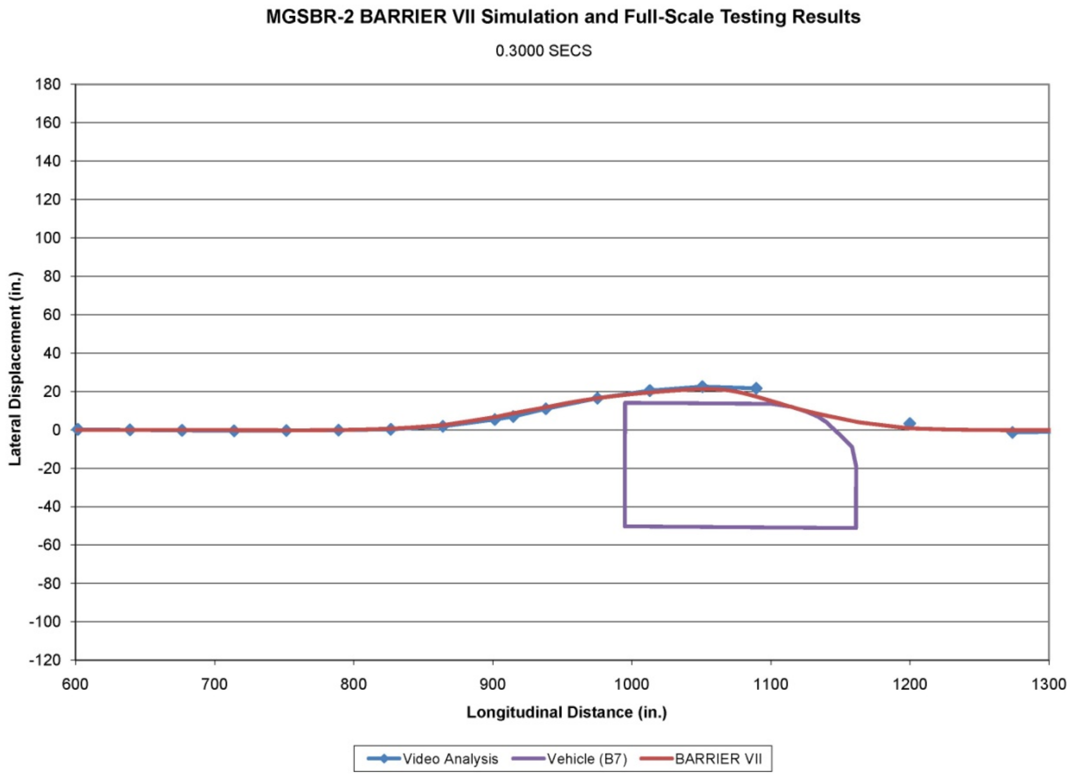

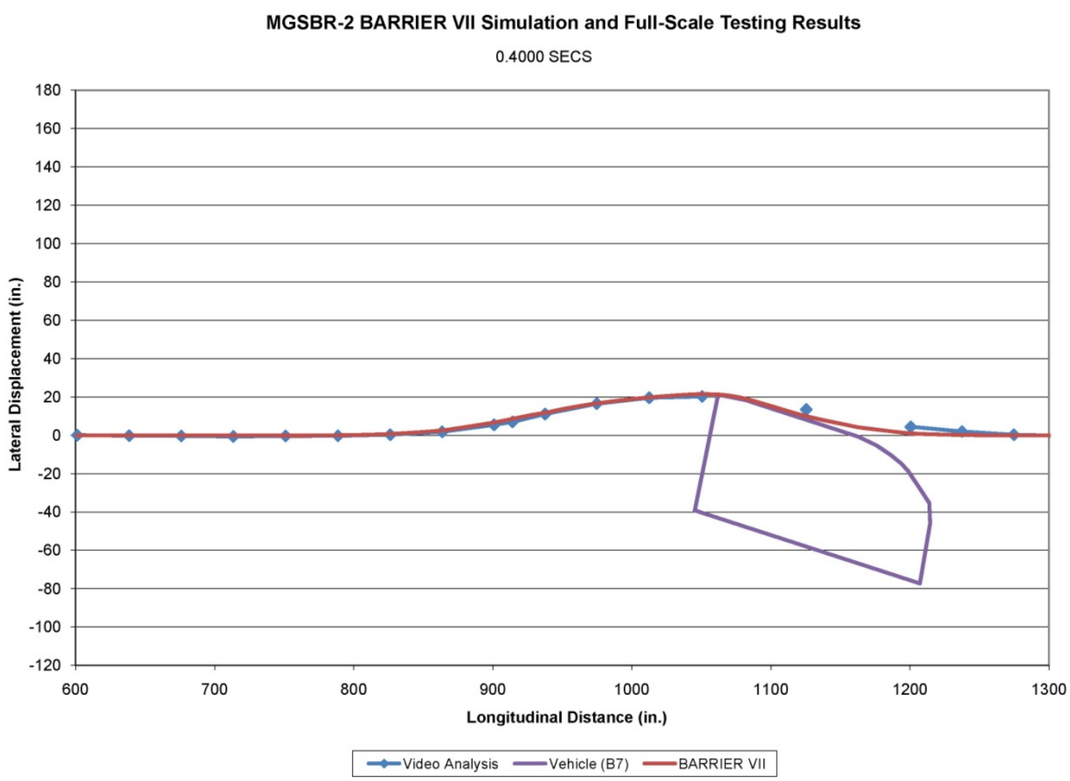

Figure 180. Sequential Figures from BARRIER VII Simulation of MGSBR-2

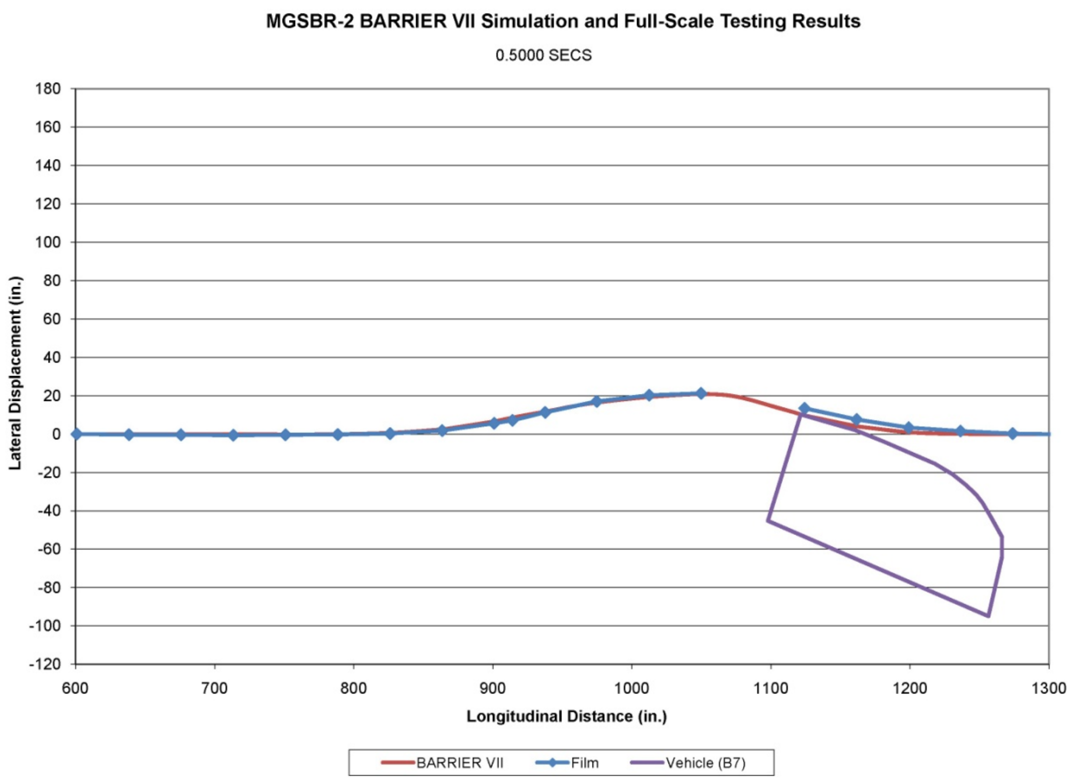

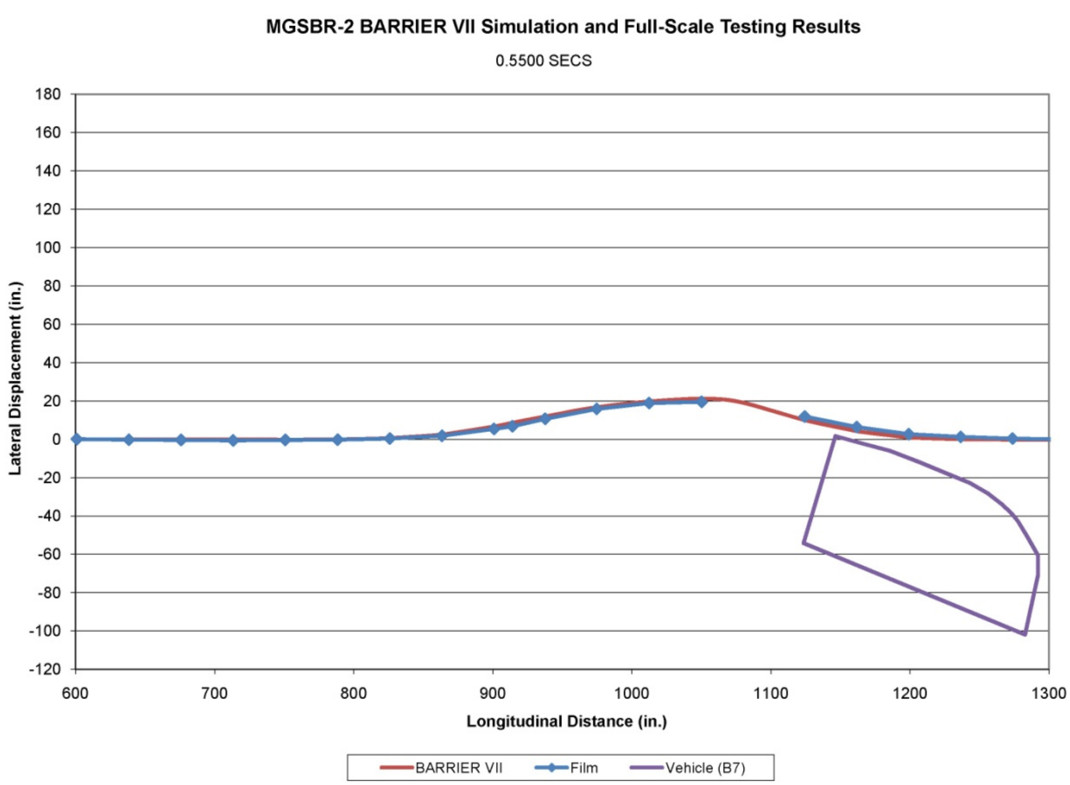

Figure 181. Sequential Figures from BARRIER VII Simulation of MGSBR-2

whereas BARRIER VII only considered post failure to occur when the rail deflection exceeded 15 in. (381 mm) at a post location. Note that eight posts, nos. 18 through 25, failed during testing. Dynamic deflection data for the rail, obtained from high-speed video analysis, demonstrated that the rail deflected more than 15 in. (381 mm) at only five post locations, nos. 18 through 22. Thus, the BARRIER VII prediction of four failed posts, nos. 19 through 22, matches the full-scale test results much more closely when compared with this criterion.

While the length of contact differed between the computer simulation and the actual crash test, the deflected shape of the rail matched very well. Some of the contact observed in the physical test was due to the vehicle overhang off the bridge deck, which caused the car to roll toward and contact the rail even after it was redirected. This affect could not be simulated in BARRIER VII.

12.2.3 Discussion of Calibration Results

The BARRIER VII results for simulations of test nos. MGSBR-1 and MGSBR-2 were found to be reasonably accurate when the post stiffness of the 60-degree impact orientation was incorporated. While simulated vehicle speeds for test no. MGSBR-1 displayed significant error, BARRIER VII was incapable of simulating several energy-absorbing mechanisms observed in the test. However, deflected rail shapes and pocketing angles, which were the primary measurements of interest, were not affected by this limitation. Thus, the models should be useful for evaluating the need for a transition between the MGS and bridge rail.

12.3 Bridge Rail-to-Guardrail Interface Analysis

Transition sections are required when a more flexible barrier connects to a less flexible barrier and allows a vehicle to pocket behind the stiffer barrier, thus generating dangerous accelerations and/or vehicle instability. As the bridge rail proved to be more flexible than the MGS, the potential for vehicle pocketing existed for impacts originating on the bridge rail and continuing into the guardrail. However, the relative flexibility of the bridge rail ensured that impacts which originated in the approach guardrail and continued into the bridge rail would not experience unacceptable pocketing angles. Thus, only the bridge rail-to-guardrail interface required additional investigation.

Pocketing angles were only a concern for the pickup truck, as the small car did not deflect the system sufficiently to become pocketed. Thus, additional analyses were only performed with the pickup truck model. While the calibrated barrier model for test no. MGSBR-1 produced good results, it underestimated deflection by approximately 10 percent. Vehicle deflections into the upstream barrier were considered critical to accurately evaluate pocketing in the downstream barrier. Underestimating deflection could lead to an underestimation of pocketing angles and produce unacceptable results. To avoid this problem, the BARRIER VII post models for the bridge rail were weakened to provide better correlation between simulated and measured deflection for test no. MGSBR-1. The yield moment of the bridge rail posts was reduced from 82 kip-in. (9.26 kN-m) to 74.5 kip-in. (8.42 kN-m). These post models were then used to investigate the potential for pocketing at the bridge rail-to-guardrail interface. A comparison of the weakened model predictions and test results is shown in Table 19.

Table 19. Weakened Post BARRIER VII Results, Test No. MGSBR-1

Evaluation Criteria	Physical Test Results	BARRIER VII Results	Error
Dynamic Deflection - in. (mm)	48.9 (1,242)	49.0 (1,245)	0.2%
Permanent Set Deflections - in. (mm)	31.9 (810)	33.9 (861)	6.3%
Length of Contact - in. (mm)	411.9 (10,462)	455.9 (11,580)	10.7%
Failed Posts (>15 in. deflection)	16-24	14-26	4 posts
Parallel Time (msec)	280	286	2.1%
Parallel Speed - mph (km/h)	44.9 (72.3)	48.1 (77.4)	7.1%
Exit Time - msec	648	571	-11.9%
Exit Speed - mph (km/h)	34.5 (55.5)	44.4 (71.5)	28.7%

Simulations were performed in which the 2270P pickup truck model impacted the barrier at 33 different points along the bridge rail-to-guardrail interface using a 225-node barrier model. Impacts were simulated at each node beginning six post spaces from the end of the bridge rail through the first guardrail post. These impacts were spaced 9⅜ in. (238 mm) along the bridge rail. Then, the simulation predicting the largest pocketing angle was performed using a 449-node model to ensure that mesh density was not adversely affecting analysis results.

The effects of snag were not considered in the analysis for several reasons. First, the MGS has been previously tested with flare rates as high as 5:1 [77]. During these tests, the pickup truck deflected the system over 75 in. (1,905 mm). Such large deflections ensure interaction between the vehicle wheels and the posts. In these tests, snag was not found to be problematic. As the peak deflection of the bridge rail was approximately 48.9 in. (1242 mm), snag on MGS posts would not adversely affect performance. Additionally, the left-front wheel of the pickup truck was detached during test no. MGSBR-1. Similar behavior was expected for impacts throughout the bridge rail. Detachment of this wheel from the pickup truck would make wheel snag on a guardrail post impossible.

Pocketing angles were therefore the primary measure of system performance. These angles were measured using the nodal displacements of the barrier in front of the vehicle. Linear regression was used to fit lines to both three and five consecutive nodes of the barrier, which corresponded to lengths of rail of 18¾ in. (476 mm) and 37½ in. (953 mm), respectively. Peak pocketing angles were found and compared against the maximum tolerable angle of 30 degrees.

12.4 Results

BARRIER VII simulations demonstrated that pocketing angles of the pickup truck in the bridge rail-to-guardrail interface were not sufficiently large to be problematic. The peak simulated pocketing angle occurred when the pickup truck impacted at the midspan between the last bridge rail post and the first guardrail post. This produced maximum 3-node and 5-node pocketing angles of 19.6 degrees and 19.5 degrees, respectively, which were well within the suggested limit of 30 degrees.

Following successful performance of the 225-node model, the worst-case impact condition was simulated using a 449-node model. Impact occurred at the midspan between the last bridge rail post and the first guardrail post. Maximum simulated 3-node and 5-node pocketing angles were 19.1 degrees and 18.4 degrees, respectively. These were both smaller values than were generated by the 225-node simulation. Additionally, as the node spacing was one-half that of the previous 225-node model, pocketing angles were measured across half as much rail length. Measuring across smaller distances necessarily increases measured angles. However, the finer mesh produced decreased pocketing angles. Therefore, the 225-node model may have estimated higher pocketing angles in all previous simulations, and therefore provided more conservative results.

Note that the impact condition that produced maximum pocketing was essentially an impact on the guardrail itself. This BARRIER VII analysis indicates that pocketing angles for impacts in the downstream MGS are greater than for impacts in the transition section. All impacts which began before the last bridge rail posts generated maximum 3-node and 5-node pocketing angles of less than 18.2 degrees and 17.5 degrees, respectively. Impacts which began further into the bridge rail tended to generate even lower pocketing angles. Further, all predicted values of pocketing angles were well below recommended values. Therefore, the bridge rail was believed to perform adequately with a direct attachment to the MGS, and a transition section was not needed.

13 SUMMARY

The goal of the research project was to develop a low-cost bridge railing system that would satisfy the TL-3 safety performance criteria outlined in MASH without requiring the use of an approach guardrail transition when used with the MGS. This new bridge rail, designated the MGS Bridge Rail, was required to exhibit lateral stiffness and strength comparable to that exhibited by the MGS with posts embedded in soil. It was also desired to minimize rail intrusion onto the bridge deck surface by attaching posts to the edge of the bridge deck or culvert headwall and to prevent damage to the bridge deck during most impacts.

The research project began with an extensive literature review of existing bridge rail and guardrail systems. Bridge rails that were flexible or utilized post-to-deck connection hardware that intruded minimally onto the deck surface were reviewed. A review of weak-post W-beam guardrail testing and post-to-rail connections for various guardrail systems was also performed.

Brainstorming sessions were then conducted to develop concepts for post-to-deck attachment hardware that would absorb impact energy through various means. Design concepts were also created for post-to-rail attachment hardware. Conceptual designs were evaluated analytically and through both static and dynamic component testing.

The first design approach for the post-to-deck connection was to develop a strong-post bridge rail system that absorbed energy by tearing or rupturing steel. Five dynamic bogie tests were performed to evaluate two of these concepts. A finite element model of one strong-post concept was created and simulated in LS-DYNA and calibrated to match the results of the dynamic bogie test. This concept utilized a tubular post and a tear-out bolt that passed through both sides of the post, thus rupturing the steel upon post rotation. A working model was developed, and several different element formulations, material models, and meshes were used to investigate the effects on the performance of the model.

Dynamic testing demonstrated that the strong-post concepts could work as desired, although the costs were higher than the weak-post alternatives. These strong-post systems could also potentially cause vehicle snag and damage bridge to decks due to the higher forces generated by the strong posts.

The strong-post concepts were therefore abandoned in favor of weak-post concepts. Two dynamic tests were performed on two weak-post concepts which demonstrated that post loads were large enough to cause catastrophic damage to the concrete deck. Thus, special reinforcement was designed into the concrete bridge deck to prevent damage, and attempts to retrofit the barrier to existing bridge decks or attach it to culvert headwalls were abandoned.

The standard G2 guardrail post-to-rail connection was subjected to three static tests to determine if it would perform as desired in the bridge rail. Based on the failure loads obtained, the standard connection was found to be acceptable for use in the bridge rail. Backup plates were added at every post, including splice locations, to prevent the guardrail rupture from initiating on the sharp edges of post flanges.

Finite element simulation was also performed using BARRIER VII to investigate the viability of a weak-post, W-beam bridge rail system. Models were developed for the new bridge rail system based on prior dynamic bogie testing which enveloped the potential range of performance of the barrier. These bridge rail models were then combined with previously-created and calibrated models of the MGS to investigate the compatibility of the systems. The primary data of interest were the maximum deflections and pocketing angles created in either the bridge rail or the interface with the guardrail. To prevent abrupt deceleration and vehicle instability, it was desired that maximum pocketing angles be less than 30 degrees. Preliminary analysis indicated that the new bridge rail should sustain comparable deflections to standard MGS while generating pocketing angles within acceptable levels.

A final design was created for the bridge rail that was then constructed and subjected to two full-scale crash tests according to the TL-3 criteria presented in MASH. Test no. MGSBR-1 featured a 5,174-lb (2,347-kg) pickup truck that impacted the barrier at a speed of 61.9 mph (99.6 km/h) and at an angle of 24.9 degrees. The bridge rail successfully redirected the vehicle while meeting all required safety criteria and sustaining a maximum deflection of 48.9 in. (1,242 mm), compared to 43.9 in. (1,114 mm) for MGS testing under similar impact conditions [67].

In test no. MGSBR-2, a 2,585-lb (1,173-kg) small car impacted the barrier at a speed of 62.3 mph (100.2 km/h) and at an angle of 24.9 degrees. The barrier again successfully redirected the vehicle while meeting all required safety criteria and sustaining a maximum deflection of 28.0 in. (712 mm). This deflection was very similar to the 35.9-in. (913-mm) deflection measured during testing of the MGS under similar impact conditions [78]. A summary of the tests and performance criteria is shown in Table 20.

BARRIER VII models of the bridge rail were then calibrated to match the results of the full-scale tests. With these calibrated models, further investigation was performed to determine if a transition was necessary between the bridge rail and approach guardrail. As the bridge rail proved more flexible than the MGS in the 2270P test, pocketing was a concern only for impacts beginning in the bridge rail and progressing to the guardrail. The results of these simulations, together with those of the full-scale crash tests, demonstrated that the MGS Bridge Rail should perform acceptably without requiring a transition section when attached directly to approach MGS guardrails.

The new bridge rail should provide a low-cost alternative to traditional bridge rails. System cost was estimated using a price obtained from a local steel fabricator of $1.30/lb ($2.87/kg) for mounting bracket fabrication and galvanization. It was estimated that installation of each bracket would require one-half hour of labor at a cost of $50/hr. Costs of additional reinforcing steel in the bridge deck were estimated at \$0.80/lb (\$1.76/kg). Fabrication costs of standard barrier hardware in the bridge rail were obtained from a guardrail supplier. An estimated installation cost of \$10.55/ft (\$34.61/m) was calculated by subtracting these costs from the total cost of strong-post W-beam guardrail of \$21/ft (\$69/m), obtained from Washington and Illinois statewide bid averages. Finally, an estimated cost of \$100/ft^2 (\$1,037/m^2) was used for the required bridge deck area due to barrier encroachment. The new bridge rail would overlap onto the bridge 3 in. (76 mm) for bridges with a wearing surface and 7 in. (178 mm) for bridges without a wearing surface. This difference is due to extension of the top mounting plate beyond the front face of the W-beam rail, which would be covered by a wearing surface. Note that if there is no wearing surface, a blockout would be needed to protect the top mounting plate from snow plows. The estimated total costs of the bridge rail were \$73/ft (\$240/m) and \$106/ft (\$348/m) for decks with and without wearing surfaces, respectively.

For comparison, a total cost of the Nebraska Open Concrete Rail was also estimated. Total costs of \$81.25/yd^3 (\$106.26/m^3) for concrete and \$1.02/lb (\$2.25/kg) for reinforcing steel fabrication and installation for the barrier were previously obtained from contractors throughout the Midwest [79]. With these values, the cost of the barrier itself was estimated at \$18/ft (\$59/m), which is believed to be lower than the actual cost. To find the total system cost, the cost of the required area of bridge deck was added to this value. Finally, the cost of fabrication and installation of transition sections was obtained from a guardrail supplier. The total cost of W-beam guardrail for this same length was subtracted from the total transition cost to find the additional expense of using transition sections. This additional cost was divided out over an assumed bridge length of 75 ft (22.9 m) to determine the added cost per foot of barrier. The final estimated price of the system with an open concrete rail and transition was \$160/ft (\$525/m).

This analysis indicates that the cost savings of the new bridge rail should be significant when compared to a concrete barrier. The MGS Bridge Rail is estimated to save approximately \$87/ft (\$285/m) on decks with a wearing surface and \$54/ft (\$117/m) on decks without a wearing surface. For an assumed bridge length of 75 ft (22.9 m), total cost savings are approximately \$13,000 and \$8,000, respectively.

Table 20. Summary of Safety Performance Evaluation Results

<table>
<tr><th>Evaluation Factors</th><th colspan="4">Evaluation Criteria</th><th>Test No. MGSBR-1</th><th>Test No. MGSBR-2</th></tr>
<tr><td>Structural Adequacy</td><td>A.</td><td colspan="3">Test article should contain and redirect the vehicle or bring the vehicle to a controlled stop; the vehicle should not penetrate, underride, or override the installation although controlled lateral deflection of the test article is acceptable.</td><td>S</td><td>S</td></tr>
<tr><td rowspan="11">Occupant Risk</td><td>D.</td><td colspan="3">Detached elements, fragments or other debris from the test article should not penetrate or show potential for penetrating the occupant compartment, or present an undue hazard to other traffic, pedestrians, or personnel in a work zone. Deformations of, or intrusions into, the occupant compartment should not exceed limits set forth in Section 5.3 and Appendix E of MASH.</td><td>S</td><td>S</td></tr>
<tr><td>F.</td><td colspan="3">The vehicle should remain upright during and after collision. The maximum roll and pitch angles are not to exceed 75 degrees.</td><td>S</td><td>S</td></tr>
<tr><td rowspan="4">H.</td><td colspan="3">Occupant Impact Velocities (OIV) (see Appendix A, Section A5.3 of MASH for calculation procedure) should satisfy the following limits:</td><td rowspan="4">S</td><td rowspan="4">S</td></tr>
<tr><td colspan="3">Occupant Impact Velocity Limits</td></tr>
<tr><td>Component</td><td>Preferred</td><td>Maximum</td></tr>
<tr><td>Longitudinal and Lateral</td><td>30 ft/s (9.1 m/s)</td><td>40 ft/s (12.2 m/s)</td></tr>
<tr><td rowspan="4">I.</td><td colspan="3">The Occupant Ridedown Acceleration (ORA) (see Appendix A, Section A5.3 of MASH for calculation procedure) should satisfy the following limits:</td><td rowspan="4">S</td><td rowspan="4">S</td></tr>
<tr><td colspan="3">Occupant Ridedown Acceleration Limits</td></tr>
<tr><td>Component</td><td>Preferred</td><td>Maximum</td></tr>
<tr><td>Longitudinal and Lateral</td><td>15.0 g’s</td><td>20.49 g’s</td></tr>
</table>

S – Satisfactory U – Unsatisfactory NA - Not Applicable

14 RECOMMENDATIONS

The new bridge rail successfully met all safety performance criteria recommended by MASH during full-scale crash testing. However, there are opportunities to improve the performance of the bridge rail. Although the bridge deck cracking and spalling sustained during testing would not affect the structural integrity of the repaired barrier, some users may wish to eliminate such damage. One mounting bracket was also destroyed during the full-scale testing. Minor changes in the socket design may prevent this damage as well. Finally, available evidence indicates that the W-beam backup plates used in the final design of the bridge rail may not be necessary.

Through-deck cracking was observed at several system posts following full-scale testing. This cracking was caused by a combination of lateral shear and downward or punching shear. Lateral shear toward the exterior of the bridge deck occurred as the through-deck bolt was loaded by the top mounting plate during impact. This created cracks in the top surface of the deck, as shown in Figure 182. Downward or punching shear was caused by downward loading of the mounting bracket due to vehicle override of the posts and the prying action of the posts and mounting bracket about the through-deck bolt. This created cracks in the vertical face of the deck, as shown in Figure 183.

Figure 182. Lateral Shear Cracking, Test No. MGSBR-1

Figure 183. Vertical Shear Cracking, Test No. MGSBR-1

As the through-deck bolts and mounting sleeves were not permanently displaced during either test, yielding in deck reinforcement was minimal or non-existent. Thus, structural adequacy of the bridge rail and deck were maintained. Further, most of the observed cracks were developed only after the second test. As each test represented worst-case impacts, it is unlikely that field installations on low-volume roads would be subjected to very many impacts of this magnitude. In such cases, field repair of the damaged bridge would only be required to cover exposed rebar in the deck. However, if necessary, the extent of cracking can be reduced through several methods. First, the use of higher strength concrete and a thicker bridge deck should reduce the likelihood of cracking due to both vertical and lateral shear. Additional methods are addressed separately for lateral shear cracking and vertical or punching shear cracking.

Lateral shear cracking can be mitigated by locating the through-deck bolt and bolt sleeve farther inward on the deck. Many bridge rail posts yielded during both full-scale crash tests, but cracks only occurred at certain post locations. This suggests that the current design is nearly adequate for resisting deck cracks.

Bending of bridge rail posts creates a shear force on the deck that is transmitted by the through-deck bolt and bolt sleeve. A simple analysis of the deck shear capacity can be concluded by treating the deck as a beam under shear loading using Equation 11-3 of ACI 318 [80]:

$$V_c = 2\sqrt{f'_c} b_w d$$

where V_c = concrete shear capacity
f_c' = concrete 28-day compression strength (psi)
b_w = beam width
d = depth of reinforcement

This equation is based upon the concept that the bolt rotates in the concrete due to the moment of the rail force about the concrete deck. As the applied shear at the top of the deck is greater than that at the bottom of the deck, it is assumed that the top 6 in. (152 mm) of the deck resists the shear load. This value is used for the width of the beam, b_w. Edge distance of the bolt sleeve, 4 in. (102 mm), is used for beam depth, d. Note that the shear capacity of the transverse deck steel is omitted from the calculation as the steel to the exterior of the crack is not fully developed. A sketch illustrating the deck and beam analogy is shown in Figure 184.

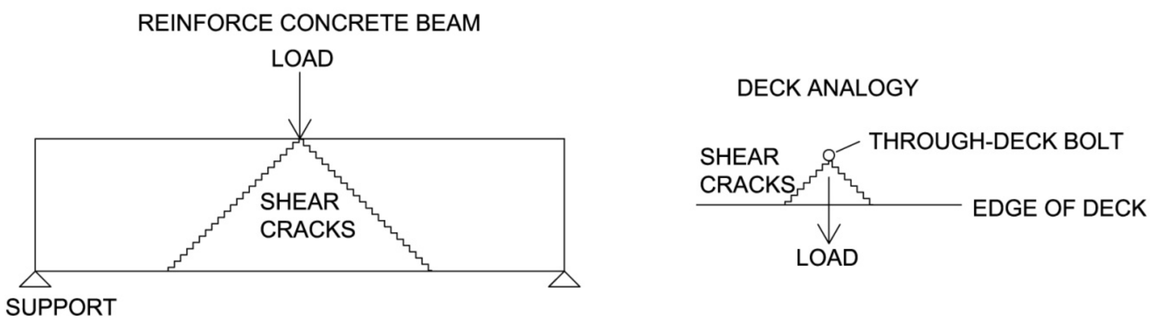

Figure 184. Beam Analysis of Deck Shear Support Capacity

Predicted deck shear capacity is then doubled to account for two shear cracks extending from the through-deck bolt. Using an estimated actual concrete strength of 4,500 psi (31.0 MPa), the formula predicts a shear capacity of the current deck of approximately 6.5 kips (28.9 kN).

This force can be compared to the nominal capacity of the post in bending. Perpendicular to its strong axis of bending, an S3x5.7 (S76x8.5) post has an elastic bending moment of 60 kip-in. (6.8 kN-m) for a yield stress of 36 ksi (248 MPa). Assuming the post is supported at the top of the mounting bracket, a force of approximately 2.6 kips (11.6 kN) at the center height of the rail is required to yield the post. If the post rotates about the bottom of the deck, the deck must develop resistive force of approximately 10.7 kips (47.7 kN) at its top surface.

The estimated deck resistance and applied force are somewhat similar in magnitude, which further suggests the deck capacity is nearly adequate to resist the applied load. Thus, small increases in mounting-tube edge distance may mitigate deck cracking. Note that the reinforcement that supports the bolt sleeve was designed for significantly higher forces obtained through dynamic bogie testing [66].

Lateral shear cracking might be further reduced by designing the deck reinforcement to more quickly develop resistive forces. The tested design utilized a rebar loop with a 5-in. (127-mm) inner diameter bend placed around the 2-in. (51-mm) wide bolt sleeve. As such, some stretching of the loop was required to develop resistive forces in the steel. Note that the minimum diameter bend of a no. 6 (19-mm diameter) bar is 4½ in. (114 mm), but a 5-in. (127-mm) bend was used due to fabrication limitations of the rebar supplier. Thus, the current design will be slightly improved in field applications. However, performance might be further improved by replacing each no. 6 (19-mm diameter) rebar loop with two no. 4 (13-mm diameter) rebar loops. This would allow for a tighter loop with approximately a 10 percent reduction in reinforcing area and a slight decrease in moment arm length. This steel should develop resistance more quickly in response to the applied load, potentially reducing crack width. However, additional analysis or testing may be required to ensure adequate capacity to resist the applied loads. Alternatively, straight bars can be welded to the sides of the bolt sleeve. These bars would develop resistance in the steel even faster upon bolt sleeve loading.

Vertical or punching shear cracks can be mitigated and resisted through several options. First, the top mounting plate could be widened to apply the downward load over a greater area of the bridge deck. A thicker plate may be required to ensure adequate stiffness to distribute the load. Deck reinforcement may also be altered to improve deck resistance to punching shear. Larger upper and lower longitudinal bars at the exterior edge of the bridge deck would help resist the effects of punching shear. Use of U-shaped transverse reinforcement, such that the upper and lower transverse bars are one continuous piece, could provide vertical reinforcement to resist these cracks as well. However, the tested bridge deck utilized staggered transverse reinforcement, which may prevent the installation of U-shaped reinforcement.

Spalling of the bridge deck edge was observed during testing due to two different mechanisms. First, the prying action of the mounting bracket caused the top mounting plate to deflect downward, spalling off the top edge of the deck. Second, the exterior post mounting tube rotated about the through-deck bolt and impacted the side of the deck, which created cracks that led to spalling. Both behaviors may be reduced through the elimination or reduction of the ½-in. (13-mm) gap between the deck edge and the mounting bracket. Eliminating the gap may cause the tube to bear against the lower edge of the deck instead of prying about the bolt, which should reduce the downward deflection of the top mounting plate. Additionally, elimination of the gap will prevent the mounting tube from rotating and impacting the edge of the deck. Alternatively, a bearing pad can be placed in the gap to distribute the impact force over a greater area of the deck edge. However, elimination of the gap is the more economical option. Note that elimination of the gap would also reduce extension of the top mounting plate past the face of the W-beam rail. Finally, the edges of the simulated bridge deck were not chamfered like those found in actual field installations. This might also reduce deck spalling due to top mounting plate deflection.

One mounting bracket was destroyed during the first full-scale test due to fracture of the weld between the mounting tube and top mounting plate. This failure was caused by wheel snag on the mounting tube as the pickup was being redirected back onto the bridge deck. As only one mounting bracket was destroyed during two worst-case impacts, it is believed this damage is acceptable. However, this failure may be avoided by increasing the size of the welds between the mounting tube and the top mounting plate and gusset. Total weld area can also be increased by adding a second gusset plate, thickening the top mounting plate, or extending the top mounting plate around both sides of the mounting tube. Alternatively, the socket could be cast into the deck, as discussed in Section 3.1.2.3. This modification should prevent any socket damage.

Backup W-beam plates were included in the post-to-rail connection of the new bridge rail at both splice and non-splice locations. These plates were intended to prevent the rail from contacting the sharp edge of the S3x5.7 (S76x8.5) post flange, which has initiated rail rupture in prior weak-post, W-beam guardrail testing [46-48]. Results of the full-scale crash tests indicated that these backup plates might not be necessary in the new bridge rail.

In test no. MGSBR-1, evidence of contact between bridge rail posts and the rail was found near post nos. 16 through 18 and 20 through 23. All areas of rail damage were found more than 3 in. (76 mm) away from the centerline of their respective posts. As the 6-in. (152-mm) long backup plates extended only 3 in. (76 mm) to either side of the centerline of the post, all post contact areas were beyond the reach of the backup plates. Thus, the backup plates could not have prevented this damage. Additionally, most areas of contact were found more than 6 in. (152 mm) away from their respective posts, indicating that 12-in. (305-mm) long backup plates would not prevent this damage either. A photograph of damage at the bottom of the rail due to post contact is shown in Figure 185.

Review of high-speed digital video revealed that the posts were not twisted at the time of contact with the rail. Thus, the post flange contacted the rail with its flat edge, not the sharp corner of the flange. A photograph taken from high-speed digital video for test no. MGSBR-1 is shown in Figure 186. The backup plates were deformed, but they did not exhibit sharp nicks indicative of contact with the edge of the flange that would be expected to initiate rail rupture. Photographs of W-beam backup plates from test no. MGSBR-1 are shown in Figure 187.

Figure 185. Rail Damage from Post Contact, Test No. MGSBR-1

Figure 186. Post Contact with Rail, Test No. MGSBR-1

Figure 187. Typical Backup Plate Damage, Test No. MGSBR-1

No rail damage due to post contact was found following test no. MGSBR-2. Review of high-speed digital video revealed that posts remained in contact with the W-beam backup plates until being snagged by the vehicle. A photograph taken from high-speed digital video for test no. MGSBR-2 is shown in Figure 188. Additionally, twisting of the posts was minimal prior to vehicle snag, indicating that the sharp edge of the post flange did not contact the rail. The backup plates themselves were deformed, but they did not exhibit the type of sharp nicks that initiate rail rupture.

Figure 188. Post Contact with Rail, Test No. MGSBR-2

The reduction in twisting of the bridge rail posts when compared to weak-post, W-beam guardrail may be due to the difference in deflection between the systems. Maximum dynamic deflection under conditions corresponding to test designation no. 3-11 for the weak-post, W-beam guardrail system was 83.5 in. (2,120 mm) [51], which was significantly greater than the 48.9 in. (1,242 mm) sustained by the new bridge rail. The smaller deflection of the bridge rail reduces the tendency of the rail to pull posts upstream or downstream, which in turn reduces the twisting of posts. Additionally, the posts of the weak-post guardrail system are embedded in soil, whereas those of the bridge rail are placed in steel tubes. Thus, the bridge rail posts are better supported to resist twisting loads. This combination of decreased rail deflection and stronger mounting conditions may reduce twisting in the bridge rail posts, which prevents the edge of the post flange from contacting the rail. Therefore, the W-beam backup plates appear to be unnecessary for the bridge rail. However, additional research may be required before this modification can be safely used.

For the bridge rail to be safely used on alternate bridge decks, retrofit to existing structures, or attached to culvert headwalls, users must ensure that the connection hardware and concrete deck have adequate capacity to resist the imparted rail loads. The tested system was designed for a peak post force of 6.3 kips (28.0 kN) at the center height of the rail, or 24⅞ in. (632 mm) above the roadway. Anchorage of the mounting bracket and internal reinforcement of the concrete must be designed to resist such a force or an equivalent system of forces and moments, as shown in Figure 189. Note that the bolt sleeve was also designed to resist bending and prevent local damage to the top of the concrete deck. Further analysis and/or testing should be performed to verify that any new designs are capable of withstanding the imparted loads.

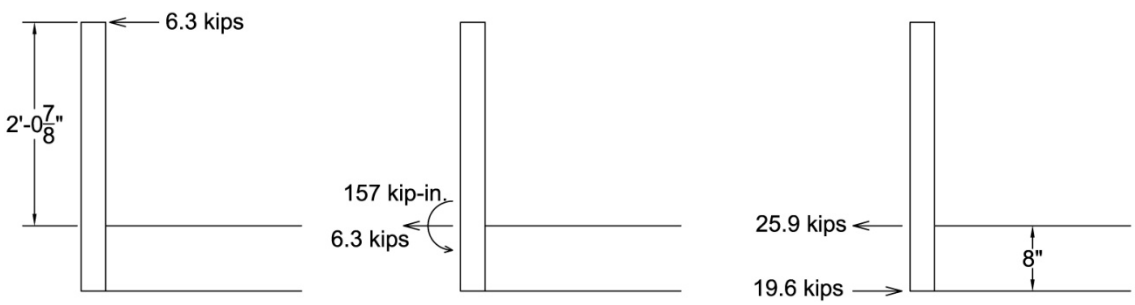

Figure 189. Design Loads for Bridge Deck

Designers should also be aware that other significant loads are imparted into the system. As discussed previously, significant downward loads are applied due to the prying action of the mounting brackets and vehicle override of bridge rail posts. Further, vehicle snag on posts may occur at relatively low heights above the top of the mounting bracket, which applies large lateral shear loads. Though these loads cannot be accurately quantified at this time, designers should be aware of these forces and design connecting hardware and bridge decks or culverts accordingly.

Full-scale testing was performed on a simulated 8-in. (203-mm) thick bridge deck without a wearing surface. Should the bridge rail be desired for use on decks with such a wearing surface poured above the top mounting plate, post length should be modified accordingly. Additionally, the length of the mounting tubes must be increased above the top mounting plate to ensure similar resistive forces are developed by the posts.

The top mounting plate of the new bridge rail extends beyond the front face of the W-beam rail. Thus, the top mounting plate and through-deck bolt would be susceptible to damage from snow-plow operations on bridge decks without a wearing surface. This problem could be eliminated by using a 4-in. (102-mm) deep blockout between the W-beam rail and system posts. However, additional analysis or testing is required before alternate rail mounting details can be recommended.

Finally, users should ensure that actual installation conditions for the new bridge rail are reflective of the assumptions used in design. Specifically, post models used to analyze the MGS were based on bogie testing performed on posts installed in level, compacted soil. Thus, the approach guardrail posts, particularly near the ends of the bridge rail, should be installed with a 2-ft (0.61-m) slope grading. Alternatively, users may install the MGS posts using the 2:1 slope installation details where slopes are present near the ends of a bridge deck.

15 CONCLUSIONS

A new, weak-post bridge rail was developed that satisfies the TL-3 performance criteria presented in MASH. This bridge rail has a lateral stiffness and strength close to that of the MGS. Therefore, the bridge rail system may be directly connected to the MGS without the use of an approach guardrail transition section. As such, the additional post and rail elements typically required by transition sections are eliminated, and barrier cost and complexity are reduced. Since the new bridge rail utilizes posts mounted on the side of the deck and does not require blockouts, encroachment of the bridge rail onto the bridge deck is minimized. Repair of the new bridge rail is simple and should typically require replacement of only steel posts, W-beam rail, and post-to-rail connection hardware. Damage caused to the deck during testing is believed to be acceptable and can be further mitigated through the implementation of recommended design revisions. The post-to-deck attachment can also be revised to reduce mounting bracket damage or allow the bridge posts to be installed in the deck itself. The new bridge rail will provide a low-cost alternative for use on low- and medium-volume bridges. Further, the new bridge rail will provide a safer alternative than many bridge rail designs now in use on local roads and streets across the nation.

16 REFERENCES

1. Polivka, K.A, Faller, R.K., Sicking, D.L., Reid, J.D., Rohde, J.R., Holloway, J.C., Bielenberg, R.W., and Kuipers, B.D., *Development of the Midwest Guardrail System (MGS) for Standard and Reduced Post Spacing and in Combination with Curbs*, Final Report to the Midwest States Regional Pooled Fund Program, MwRSF Research Report No. TRP-03-139-04, Project No. SPR-3(017)-Years 10 and 12-13, Project Codes RPFP-00-02, 02-01, and 03-05, Midwest Roadside Safety Facility, University of Nebraska-Lincoln, Lincoln, Nebraska, September 1, 2004.

2. Ross, H.E., Sicking, D.L., Zimmer, R.A., and Michie, J.D., *Recommended Procedures for the Safety Performance Evaluation of Highway Features*, National Cooperative Highway Research Program (NCHRP) Report 350, Transportation Research Board, Washington, D.C., 1993.

3. Bielenberg, R.W., Faller, R.K., Rohde, J.R., Reid, J.D., Sicking, D.L., Holloway, J.C., Allison, E.M., and Polivka, K.A., *Midwest Guardrail System for Long-Span Culvert Applications,* Final Report to the Midwest States Regional Pooled Fund Program, MwRSF Research Report No. TRP-03-187-07, Project No. SPR-3(017)-Year 15, Project Code RPFP-05-04, Midwest Roadside Safety Facility, University of Nebraska-Lincoln, Lincoln, Nebraska, November 16, 2007.

4. *Manual for Assessing Safety Hardware (MASH),* American Association of State and Highway Transportation Officials (AASHTO), Washington, D.C., 2009.

5. *Standard Specifications for Highway Bridges, Twelfth Edition*, American Association of State Highway and Transportation Officials (AASHTO), Washington, D.C., 1977.

6. *Recommended Procedures for Vehicle Crash Testing of Highway Appurtenances,* Transportation Research Circular (TRC) 191, Transportation Research Board, Washington, D.C., 1978.

7. Michie, J.D., *Recommended Procedures for the Safety Performance Evaluation of Highway Appurtenances*, National Cooperative Highway Research Program (NCHRP) Report 230, Transportation Research Board, Washington, D.C., March 1981.

8. *Guide Specifications for Bridge Railings,* American Association of State Highway and Transportation Officials (AASHTO), Washington, D.C., 1989.

9. Horne, D.A., *Crash Testing of Bridge Railings,* Memorandum to Regional Administrators and Federal Lands Highway Program Administrator, Federal Highway Administration, May 30, 1997.

10. Wright, F.G., *Bridge Rail Analysis*, Memorandum to Resource Center Directors and Division Administrators, Federal Highway Administration, May 16, 2000.

11. *AASHTO LRFD Bridge Design Specifications, 3th Edition*, American Association of State Highway and Transportation Officials (AASHTO), Washington, D.C., 2004.

12. Stoker, J.R., Hackett, R.P., Doty, R.N., Pelkey, R.A., and Nordlin, E.F., *Dynamic Tests of the California Type 15 Bridge Barrier Rail Series XXV*, Report No. 656496, State of California – Materials and Research Department, Sacramento, California, June 1971.

13. Hirsch, T.J., Panak, J.J., and Buth, C.E., *Tubular W-Beam Bridge Rail*, Research Report No. FHWATX78-230-1, Prepared for the Texas State Department of Highways and Public Transportation, Texas Transportation Institute, Texas A&M University, College Station, Texas, October 1978.

14. Buth, C.E., Bligh, R.P., and Menges, W.L., *NCHRP Report 350 Test 3-11 of the Texas Type T6 Bridge Rail*, Report No. FHWA/TX-98/1804-4, Letter Report 1804-4, Texas Transportation Institute, Texas A&M University, College Station, Texas, July 1998.

15. Buth, C.E., Williams, W.F., Bligh, R.P., and Menges, W.L., *Test 3 – NCHRP Report 350 Test 3-11 of the Texas Type T6 Bridge Rail on Bridge Deck*, Report No. FHWA/TX-99/1804-3, Letter Report 1804-3, Texas Transportation Institute, Texas A&M University, College Station, Texas, October 1998.

16. Bullard, D.L., Menges, W.L., and Alberson, D.C., *NCHRP Report 350 Compliance Test 3-11 of the Modified G4(1S) Guardrail with Timber Blockouts*, Report No. FHWA-RD-96-175, Project No. 405421-1, Texas Transportation Institute, Texas A&M University, College Station, Texas, January 1996.

17. Bligh, R.P., and Menges, W.L., *Testing and Evaluation of a Modified Steel Post W-Beam Guardrail System with Recycled Polyethylene Blockouts*, Report No. 400001-MPT, Sponsored by Mondo Polymer Technologies, Performed by Texas Transportation Institute, Texas A&M University, College Station, Texas, February 1997.

18. Mak, K.K., Bligh, R.P., and Menges, W.L., *Testing of State Roadside Safety Systems Volume XI: Appendix J – Crash Testing and Evaluation of Existing Guardrail Systems*, Report No. FHWA-RD-95, Texas Transportation Institute, Texas A&M University, College Station, Texas, December 1995.

19. Buth, C.E., Williams, W.F., Bligh, R.P., and Menges, W.L., *NCHRP Report 350 Test 3-11 of the Modified Texas Type T6 Bridge Rail on Bridge Deck*, Report No. FHWA/TX-00/1804-10, Texas Transportation Institute, Texas A&M University, College Station, Texas, February 2000.

20. Bligh, R.P., Abu-Odeh, A.Y., Hamilton, M.E., and Seckinger, N.R., *Evaluation of Roadside Safety Devices Using Finite Element Analysis*, Report No. FHWA/TX-04/0-1816-1, Texas Transportation Institute, Texas A&M University, College Station, Texas, August 2004.

21. Bligh, R.P., Abu-Odeh, A.Y., Williams, W.F., and Menges, W.L., *Analysis of a Flexible Bridge Rail System for High-Speed Roadways*, Report No. FHWA/TX-08/0-5210-4, Texas Transportation Institute, Texas A&M University, College Station, Texas, December 2008.

22. Williams, W.F., Bligh, R.P., and Menges, W.L., *Crash Testing and Evaluation of the TXDOT Type T8 Bridge Rail*, Report No. 407049-1, Texas Transportation Institute, Texas A&M University, College Station, Texas, March 2008.

23. Bligh, R.P., Williams, W.F., Menges, W.L., *NCHRP Report 350 Test 3-11 of the Modified T8 Bridge Rail*, Report No. FHWA/TX-09/0-5210-6, Texas Transportation Institute, Texas A&M University, College Station, Texas, April 2009.

24. Hirsch, T.J. and Beggs, D., *Use of Guardrails on Low Fill Bridge Length Culverts*, Submitted to the 67th Annual Meeting of the Transportation Research Board, Paper No. 870265, Texas Transportation Institute, Texas A&M University, College Station, Texas, August 6, 1987.

25. Pfeifer, B.G. and Luedke, J.K., *Safety Performance Evaluation of a Nested W-Beam with Half-Post Spacing Over a Low-Fill Culvert*, Final Report to Kansas Department of Transportation, MwRSF Research Report No. TRP-03-36-92, Midwest Roadside Safety Facility, University of Nebraska-Lincoln, Lincoln, Nebraska, March 1993.

26. Bligh, R.P., Mak, K.K., and Hirsch, T.J., *Evaluation of Tennessee Bridge Rail Designs*, Research Report No. RF 7199-1, Texas Transportation Institute, Texas A&M University, College Station, Texas, May 1994.

27. Faller, R.K., Rosson, B.T., and Fowler, M.D., *Top-Mounted W-Beam Bridge Railing for Longitudinal Glulam Timber Decks Located on Low-Volume Roads*, Submitted to Forest Products Laboratory, MwRSF Research Report No. TRP-03-61-96, Midwest Roadside Safety Facility, University of Nebraska-Lincoln, Lincoln, Nebraska, September 1996.

28. Faller, R.K. and Rosson, B.T., *Development of a Flexible Bridge Railing for Longitudinal Timber Decks*, Submitted to Forest Products Laboratory, MwRSF Research Report No. TRP-03-62-96, Midwest Roadside Safety Facility, University of Nebraska-Lincoln, Lincoln, Nebraska June 1997.

29. Polivka, K.A., Faller, R.K., Sicking, D.L., Rohde, J.R., Reid, J.D., and Holloway, J.C., *NCHRP 350 Development and Testing of a Guardrail Connection to Low-Fill Culverts*, Final Report to the Midwest States Regional Pooled Fund Program, MwRSF Research Report No. TRP-03-114-02, Project No. SPR-3(017)-Year 10, Project Code RPFP-00-04, Midwest Roadside Safety Facility, University of Nebraska-Lincoln, Lincoln, Nebraska, November 1, 2002.

30. *Roadside Design Guide*, 3rd Edition 2006, with updated Chapter 6, American Association of State Highway and Transportation Officials (AASHTO), Washington, D.C., 2006.

31. Williams, W.F., Bligh, R.P., Bullard, D.L., Menges, W.L., *Crash Testing and Evaluation of W-Beam Guardrail on Box Culvert,* Report No. 405160-5-1, Texas Transportation Institute, Texas A&M University, College Station, Texas, August 2008.

32. American Association of State and Highway Transportation Officials (AASHTO) Associated General Contractors (AGC) American Road and Transportation Builders Association (ARTBA), Meeting Minutes, Hershey, Pennsylvania, May 5-6, 2008.

33. Buth, C.E., Arnold, A., Campise, W.L., Hirsch, T.J., Ivey, D.L., and Noel, J.S., *Safer Bridge Railings Volume 1: Summary Report*, Report No. FHWA/RD-82/072, Texas Transportation Institute, Texas A&M University, College Station, Texas, June 1984.

34. Arnold, A. and Hirsch, T.J., *Bridge Deck Designs for Railing Impacts*, Report No. FHWA/TX-85/ 17 +295-1F, Texas Transportation Institute, Texas A&M University, College Station, Texas, August 1985.

35. Bronstad, M.E., Michie, J.D., Calcote, L.R., Hancock, K.L., and Mayer Jr., J.B., *Bridge Rail Designs and Performance Standards Volume 1: Research Report*, Submitted to the Safety Design Division, Federal Highway Administration, Report No. FHWA/RD-87/049, Southwest Research Institute, San Antonio, Texas, February 1987.

36. Plaxico, C.A., Kennedy, J.C., and Miele, C.R., *Evaluation and Design of ODOT's Type 5 Guardrail with Tubular Backup*, Submitted to the Ohio Department of Transportation, Report No. FHWA/OH-2006/4, Battelle Memorial Institute, Columbus, Ohio, February 2006.

37. Bronstad, M.E. and Michie, J.D., *Multiple-Service-Level Highway Bridge Railing Selection Procedures*, National Cooperative Highway Research Program (NCHRP) Report 239, Transportation Research Board, National Research Council, Washington, D.C., November 1981.

38. Jewell, J., Glauz, D., Stoughton, R., Crozier, W., and Folsom, J.J., *Vehicle Crash Tests of Steel Bridge Barrier Rail Systems for Use on Secondary Highways*, Report No. FHWA/CA/TL-93/01, Division of New Technology, Materials & Research, California Department of Transportation, Sacramento, California, March 1993.

39. Buth, C.E., Hirsch, T.J., and Menges, W.L., *Testing of New Bridge Rail and Transition Designs, Volume 1: Technical Report*, Report No. FHWA-RD-93-058, Texas Transportation Institute, Texas A&M University, College Station, Texas, June 1997.

40. Polivka, K.A., Faller, R.K., Ritter, M.A., and Rosson, B.T., *Development of the TBC-8000 Bridge Railing*, Submitted to the U.S. Department of Agriculture, MwRSF Research Report No. TRP-03-30-93, Midwest Roadside Safety Facility, University of Nebraska-Lincoln, Lincoln, Nebraska, September 5, 2000.

41. Polivka, K.A., Faller, R.K., Ritter, M.A., Rosson, B.T., Fowler, M.D., and Keller, E.A., *Two Test Level 4 Bridge Railing and Transition Systems for Transverse Glue-Laminated Timber Decks*, Submitted to the U.S. Department of Agriculture, MwRSF Research Report No. TRP-03-71-01, Midwest Roadside Safety Facility, University of Nebraska-Lincoln, Lincoln, Nebraska, January 30, 2002.

42. Polivka, K.A., Faller, R.K., Ritter, M.A., Rosson, B.T., Rohde, J.R., and Keller, E.A., *Two Test Level 2 Bridge Railing and Transition Systems for Transverse Glue-Laminated Timber Decks*, Submitted to the U.S. Department of Agriculture, MwRSF Research Report No. TRP-03-125-03, Midwest Roadside Safety Facility, University of Nebraska-Lincoln, Lincoln, Nebraska, March 11, 2003.

43. Stoughton, R.L., Stoker, J.R., Nagai, I., Hale Jr., P., Bishop, R.W., *Vehicle Impact tests of a See-Through Collapsing Ring, Structural Steel Tube, Bridge Barrier Railing*, Report No. FHWA/CA/TL-83/05, Office of Transportation Laboratory, California Department of Transportation, Sacramento, California, June 1983.

44. Federal Highway Administration, Bridge Rail Guide 2005, Available: <http://www.fhwa.dot.gov/bridge/bridgerail/>, [February 24, 2010].

45. Ray, M.H. and McGinnis, R.G., *Guardrail and Median Barrier Crashworthiness*, National Cooperative Highway Research Program (NCHRP) Synthesis No. 244, Transportation Research Board, Washington, D.C., 1997.

46. Kilareski, W.P., El-Gindy, M., St. John, B.D., and Pecheux, B., *Type 2 Weak Post Guiderail Testing*, Submitted to Pennsylvania Department of Transportation, Report No. PTI 9925, Agreement No. 359704, Work Order 20, Pennsylvania Transportation Institute, Penn State University, University Park, Pennsylvania, February 1999.

47. Engstrand, K.E., Improvements to the Weak-Post W-Beam Guardrail, Thesis, Worcester Polytechnic Institute, Worcester, Massachusetts, June 2000.

48. Ray, M.H., Engstrand, K., Plaxico, C.A., and McGinnis, R.G., *Improvements to the Weak-Post W-Beam Guardrail,* Transportation Research Record 1743, Transportation Research Board, Washington, D.C., 2001.

49. Buth, C.E., Menges, W.L., and Schoeneman, S.K., *NCHRP Report 350 Test 3-11 on the Modified PennDOT Type 2 Guide Rail,* Project No. RF473750-1, Texas Transportation Institute, Texas A&M University, College Station, Texas, January 2000.

50. Buth, C.E., Menges, W.L., and Schoeneman, S.K., *NCHRP Report 350 Test 3-11 on the Modified PennDOT Type 2 Guide Rail – Test 2,* Project No. RF473750-2, Texas Transportation Institute, Texas A&M University, College Station, Texas, February 2000.

51. Buth, C.E., Menges, W.L., Williams, W.F., and Schoeneman, S.K., *NCHRP Report 350 Test 3-11 on the Modified PennDOT Type 2 Guide Rail – Test 3,* Project No. RF473750-3, Texas Transportation Institute, Texas A&M University, College Station, Texas, June 2000.

52. Buth, C.E., Menges, W.L., Williams, W.F., and Schoeneman, S.K., *NCHRP Report 350 Test 3-10 on the Modified PennDOT Type 2 Guide Rail – Test 4,* Project No. RF473750-4, Texas Transportation Institute, Texas A&M University, College Station, Texas, July 2000.

53. Akram, A., Menges, W.L., and Haug, R.R., *NCHRP Report 350 Test 3-11 of the New York DOT W-Beam on Light Post Median Barrier,* Project No. 400611-1, Texas Transportation Institute, Texas A&M University, College Station, Texas, February 2003.

54. Plaxico, C.A., Mozzarelli, F., and Ray, M.H., *Tests and Simulation of a W-Beam Rail-to-Post Connection*, Paper No. 02-2549, Published in the Compendium of Papers CD-ROM, Transportation Research Board, Washington, D.C., January 2002.

55. Bligh, R.P., Buth, C.E., Bullard, D.L., and Alberson, D.C., *An Increased Capacity, Strong-Post Guardrail System with Reduced Offset*, Paper No. 07-3124, Published in the Compendium of Papers CD-ROM, Transportation Research Board, Washington, D.C., January 2007.

56. Ochoa, C.M., *GMS Guardrail Mini Spacer Releasable Fastener: Improving Performance and Reliability of Conventional Strong-Post Guardrail*, Paper No. 08-0811, Published in the Compendium of Papers CD-ROM, Transportation Research Board, Washington, D.C., January 2008.

57. Rice, G.E., FHWA NCHRP Report 350 approval letter HSSD/B-162 of the Nucor Nu-Guard Guardrail, to Rick Mauer, Nucor Steel Marion Inc., Marion, Ohio, September 11, 2007.

58. Bielenberg, R.W., Faller, R.K., Holloway, J.C., Reid, J.D., Rohde, J.R., and Sicking, D.L., *Performance Evaluation of the SKT-MGS End Terminal – NCHRP 350 Test 3-31*, Final Report to Safety By Design, MwRSF Research Report No. TRP-03-144-03, Midwest Roadside Safety Facility, University of Nebraska-Lincoln, Lincoln, Nebraska, December 18, 2003.

59. Wright, F.G., FHWA NCHRP Report 350 approval letter HSA/B-85 of the King Block Blockout, to Rodney A. Boyd, Trinity Industries, Dallas, Texas, June 1, 2001.

60. Bielenberg, R.W., *Letter Report Documenting Dynamic Component Testing of Potential Alternative Anchors for the F-Shape Temporary Concrete Barrier Steel Strap Tie-Down System,* Final Report to the Midwest States Regional Pooled Fund Program, Midwest Report No. TRP-03-182-07, Project No. SPR-3(017)-Year 16, Project Code RPFP-06-06, Midwest Roadside Safety Facility, University of Nebraska-Lincoln, Lincoln, Nebraska, April 9, 2007.

61. Halquist, J.O., *LS-DYNA Keyword User's Manual*, Version 971, Livermore Software Technology Corporation, Livermore, California, May 2007.

62. Powell, G.H., *Computer Evaluation of Automobile Barrier Systems,* Report No. FHWA-RD-73-73, Department of Civil Engineering, University of California, Berkeley, California, August 1970.

63. Powell, G.H., *Barrier VII: A Computer Program for Evaluation of Automobile Barrier Systems,* Report No. FHWA-RD-73-51, Department of Civil Engineering, University of California, Berkeley, California, April 1973.

64. Eller, C.M., Polivka, K.A., Faller, R.K., Sicking, D.L., Rohde, J.R., Reid, J.D., Bielenberg, R.W., and Allison, E.M., *Development of the Midwest Guardrail System (MGS) W-Beam to Thrie Beam Transition Element*, Final Report to the Midwest States Regional Pooled Fund Program, MwRSF Research Report No. TRP-03-167-07, SPR-3(017)-Years 11-12 and 16, Project Codes RPFP-01-04, 02-05, and 06-04, Midwest Roadside Safety Facility, University of Nebraska-Lincoln, Lincoln, Nebraska, November 26, 2007.

65. Rosenbaugh, S.K., Lechtenberg, K.A., Faller, R.K., Sicking, D.L., Reid, J.D., and Bielenberg, R.W., *Development of the MGS Approach Guardrail Transition Using Steel and Wood Standardized Posts,* Final Report to the Midwest States Regional Pooled Fund Program, MwRSF Research Report No. TRP-03-210-10, Project No. SPR-3(017)-Years 18-19, Project Code RPFP-08-05, Midwest Roadside Safety Facility, University of Nebraska-Lincoln, Lincoln, Nebraska, In Progress.

66. Kuipers, B.D. and Reid, J.D., *Testing of M203x9.7 (M8x6.5) and S76x8.5 (S3x5.7) Steel Posts – Post Comparison Study for the Cable Median Barrier,* Final Report to the Midwest States Regional Pooled Fund Program, MwRSF Report No. TRP-03-143-03, Project No. SPR-3(017)-Year 12, Project Code RPFP-01-05, Midwest Roadside Safety Facility, University of Nebraska-Lincoln, Lincoln, Nebraska, October 2003.

67. Polivka, K.A., Faller, R.K., Sicking, D.L., Rohde, J.R., Bielenberg, B.W., and Reid, J.D., *Performance Evaluation of the Midwest Guardrail System – Updated to NCHRP 350 Test No. 3-11 with 28" C.G. Height (2214MG-2)*, Final Report to the National Cooperative Highway Research Program, MwRSF Research Report No. TRP-03-171-06, Midwest Roadside Safety Facility, University of Nebraska-Lincoln, Lincoln, Nebraska, October 11, 2006.

68. Kuipers, B.D., and Reid, J.D., *Testing of W152x23.8 (W6x16) Steel Posts – Soil Embedment Depth Study for the Midwest Guardrail System*, Final Report to the Midwest States Regional Pooled Fund Program, MwRSF Research Report No. TRP-03-136-03, Project No. SPR-3(017)-Years 10 and 12-13, Project Codes RPFP-00-02, 02-01, and 03-05, Midwest Roadside Safety Facility, University of Nebraska-Lincoln, Lincoln, Nebraska, June 12, 2003.

69. Kuipers, B.D., Faller, R.K., and Reid, J.D., *Critical Flare Rates for W-Beam Guardrail – Determining Maximum Capacity Using Computer Simulation*, Final Report to the Midwest States Regional Pooled Fund Program, MwRSF Research Report No. TRP-03-136-03, Project No. SPR-3(017)-Years 14-15, Project Codes RPFP-04-03 and 05-05, Midwest Roadside Safety Facility, University of Nebraska-Lincoln, Lincoln, Nebraska, January 24, 2005.

70. *Bridge Operations, Policies, and Procedures*, Nebraska Department of Roads, Bridge Division, Lincoln, Nebraska, August 12, 2005.

71. Hinch, J., Yang, T.L., and Owings, R., *Guidance Systems for Vehicle Testing,* ENSCO, Inc., Springfield, Virginia, 1986.

72. *Center of Gravity Test Code - SAE J874 March 1981,* SAE Handbook Vol. 4, Society of Automotive Engineers, Inc., Warrendale, Pennsylvania, 1986.

73. ASTM Standard C31/C31M 2009, "Standard Practice for Making and Curing Concrete Test Specimens in the Field," ASTM International, West Conshohocken, Pennsylvania, 2009, DOI: 10.1520/C0031_C0031M-09, <www.astm.org>.

74. ASTM Standard C39/C39M 2009, "Standard Test Method for Compressive Strength of Cylindrical Concrete Specimens," ASTM International, West Conshohocken, Pennsylvania, 2009, DOI: 10.1520/C0039_C0039M-09A, <www.astm.org>.

75. *Vehicle Damage Scale for Traffic Investigators*, Second Edition, Technical Bulletin No. 1, Traffic Accident Data (TAD) Project, National Safety Council, Chicago, Illinois, 1971.

76. *Collision Deformation Classification – Recommended Practice J224 March 1980*, Handbook Volume 4, Society of Automotive Engineers (SAE), Warrendale, Pennsylvania, 1985.

77. Stolle, C.S., Polivka, K.A., Reid, J.D., Faller, R.K., Sicking, D.L., Bielenberg, R.W., and Rohde, J.R., *Evaluation of Critical Flare Rates for the Midwest Guardrail System (MGS)*, Final Report to the Midwest States Regional Pooled Fund Program, MwRSF Report No. TRP-03-191-08, Project No. SPR-3(017)-Years 14-15, Project Codes RPFP-04-03 and 05-05, Midwest Roadside Safety Facility, University of Nebraska-Lincoln, Lincoln, Nebraska, July 15, 2008.

78. Polivka, K.A., Faller, R.K., Sicking, D.L., Rohde, J.R., Bielenberg, R.W., and Reid, J.D., *Performance Evaluation of the Midwest Guardrail System - Update to NCHRP 350 Test No. 3-10 (2214MG-3)*, Final Report to the National Cooperative Highway Research Program (NCHRP), MwRSF Research Report No. TRP-03-172-06, Midwest Roadside Safety Facility, University of Nebraska-Lincoln, Lincoln, Nebraska, October 11, 2006.

79. Rosenbaugh, S.K., Development of a TL-5 Vertical-Faced Concrete Median Barrier Incorporating Head Ejection Criteria, Thesis, University of Nebraska-Lincoln, Lincoln, Nebraska, September 2007.

80. *Building Code Requirements for Structural Concrete (ACI 318-08) and Commentary*, American Concrete Institute, Farmington Hills, Michigan, June 2008.

17 APPENDICES

Appendix A. Component Testing Results

MIDWEST ROADSIDE SAFETY FACILITY

Bogie Test Summary

Test Information	MGS Bridge Rail	
Test Number:	MGSBRB-1	
Test Date:	21-Apr-2008	
Failure Type:	Concrete Failure	
Post Properties		
Post Type:	Side-Mounted Tube Tearout	
Post Size:	HSS6x4x1/8	HSS152x102x3
Post Length:	40 in.	101.6 cm
Embedment Depth:	NA in.	NA cm
Orientation:	Strong Axis, Centered	
Soil Properties		
Gradation:	NA	
Moisture Content:	NA	
Compaction Method:	NA	
Soil Density, γd:	NA	
Bogie Properties		
Impact Velocity:	20.96 mph (30.7 fps)	9.37 m/s
Impact Height:	24.875 in.	63.2 cm
Bogie Mass:	1841 lbs	835.1 kg
Data Acquired		
Acceleration Data:	DTS	
Camera Data:	High Speed Camera Malfunctioned	

Test Results Summary		
Max. Deflection:	39.0	in.
Peak Force:	10.3	k
Initial Linear Stiffness:	4.2	k/in.
Total Energy:	108.9	k-in.

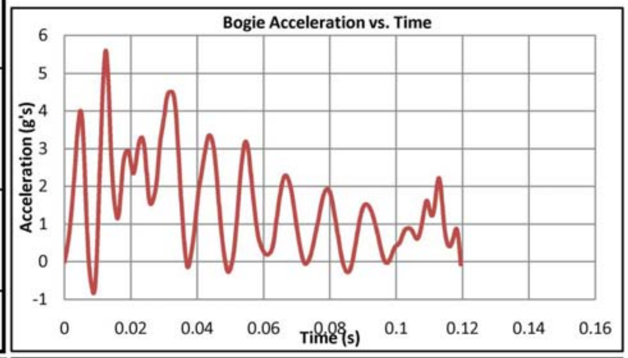

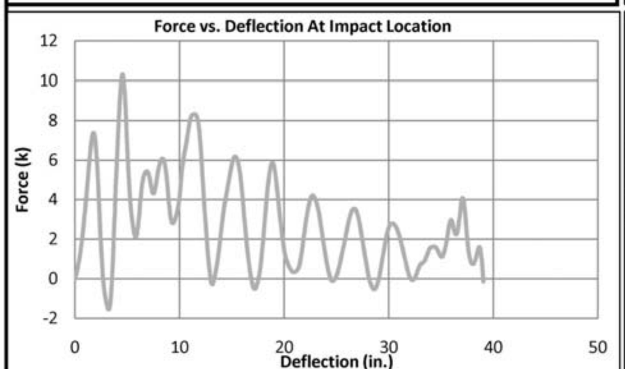

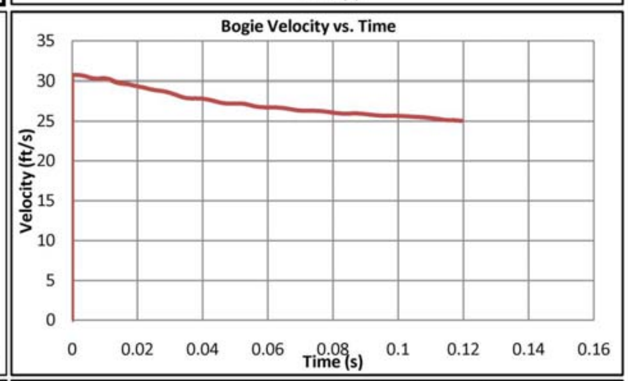

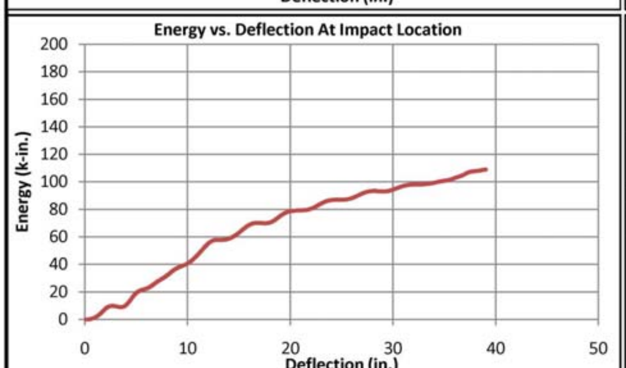

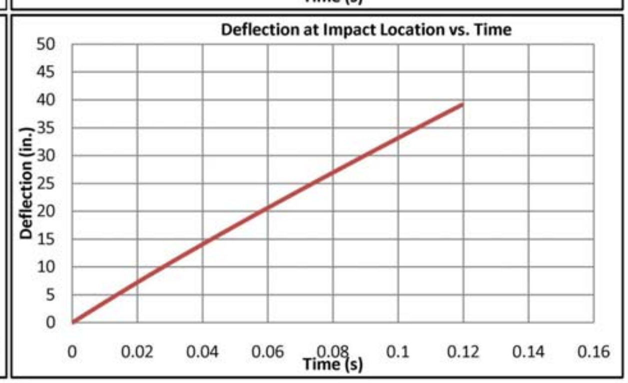

Figure A-1. Test No. MGSBRB-1 Results (DTS)

MIDWEST ROADSIDE SAFETY FACILITY

Bogie Test Summary

Test Information	MGS Bridge Rail	
Test Number:	MGSBRB-1	
Test Date:	21-Apr-2008	
Failure Type:	Concrete Failure	
Post Properties		
Post Type:	Side-Mounted Tube Tearout	
Post Size:	HSS6x4x1/8	HSS152x102x3
Post Length:	40 in.	101.6 cm
Embedment Depth:	NA in.	NA cm
Orientation:	Strong Axis, Centered	
Soil Properties		
Gradation:	NA	
Moisture Content:	NA	
Compaction Method:	NA	
Soil Density, γd:	NA	
Bogie Properties		
Impact Velocity:	20.96 mph (30.7 fps)	9.37 m/s
Impact Height:	24.875 in.	63.2 cm
Bogie Mass:	1841 lbs	835.1 kg
Data Acquired		
Acceleration Data:	EDR-3	
Camera Data:	High Speed Camera Malfunctioned	

Test Results Summary		
Max. Deflection:	34.2	in.
Peak Force:	6.3	k
Initial Linear Stiffness:	3.3	k/in.
Total Energy:	88.6	k-in.

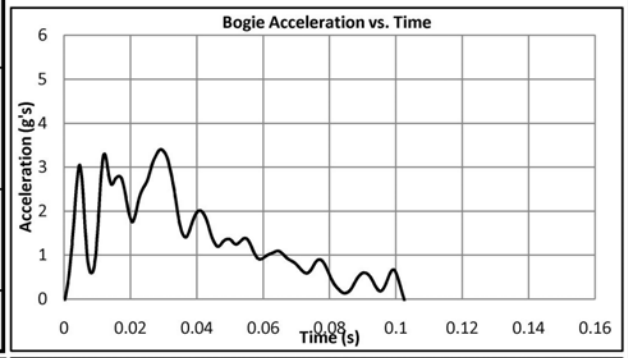

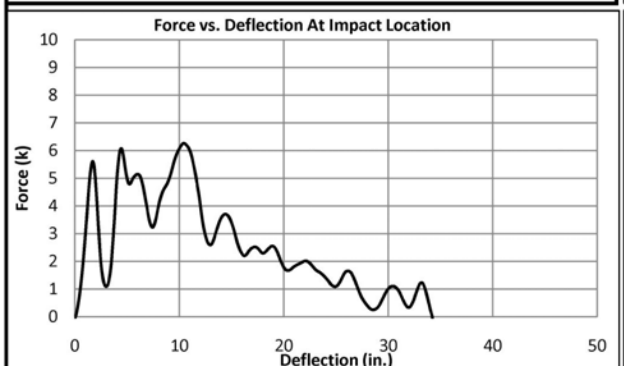

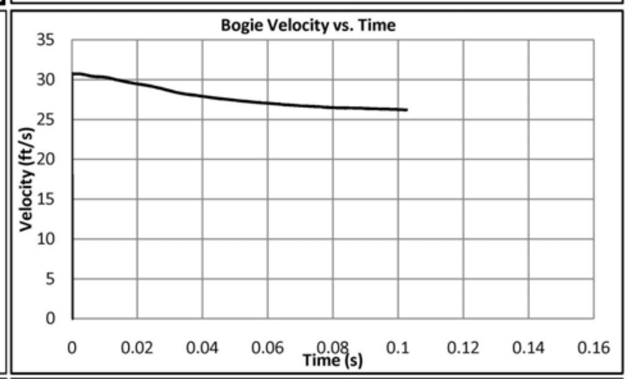

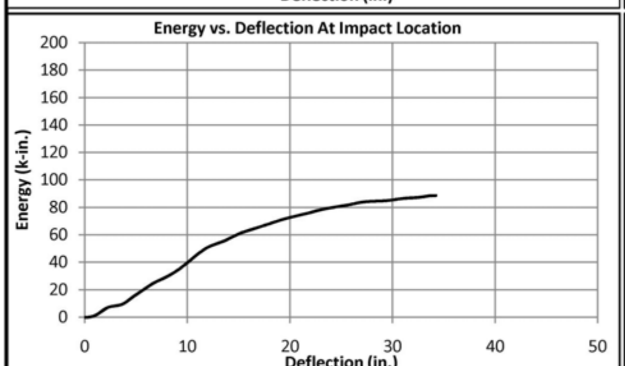

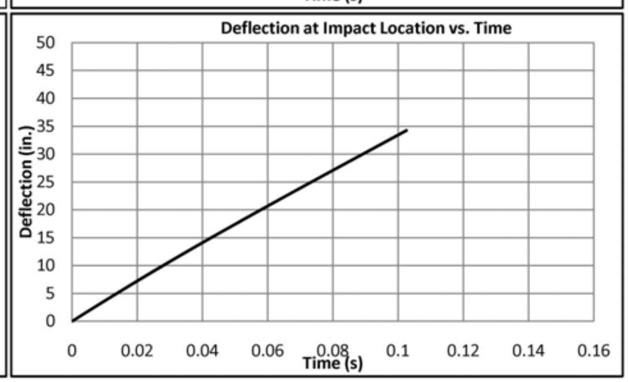

Figure A-2. Test No. MGSBRB-1 Results (EDR-3)

MIDWEST ROADSIDE SAFETY FACILITY

Bogie Test Summary

Test Information	MGS Bridge Rail	
Test Number:	MGSBRB-2	
Test Date:	16-May-2008	
Failure Type:	Bolt Pulled Out of Plate	
Post Properties		
Post Type:	Top-Mounted Bolt Tearout	
Post Size:	W6x9	W152x13.4
Post Length:	44 in.	111.8 cm
Embedment Depth:	NA in.	NA cm
Orientation:	Strong Axis, Centered	
Soil Properties		
Gradation:	NA	
Moisture Content:	NA	
Compaction Method:	NA	
Soil Density, γd:	NA	
Bogie Properties		
Impact Velocity:	23.38 mph (34.3 fps)	10.45 m/s
Impact Height:	24.875 in.	63.2 cm
Bogie Mass:	1841 lbs	835.1 kg
Data Acquired		
Acceleration Data:	DTS	
Camera Data:	AOS-5 Perpendicular - 20'-1"	

Test Results Summary		
Max. Deflection:	11.7	in.
Peak Force:	8.3	k
Initial Linear Stiffness:	5.1	k/in.
Total Energy:	40.9	k-in.

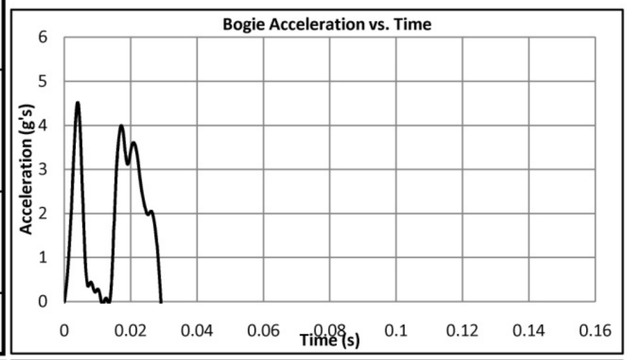

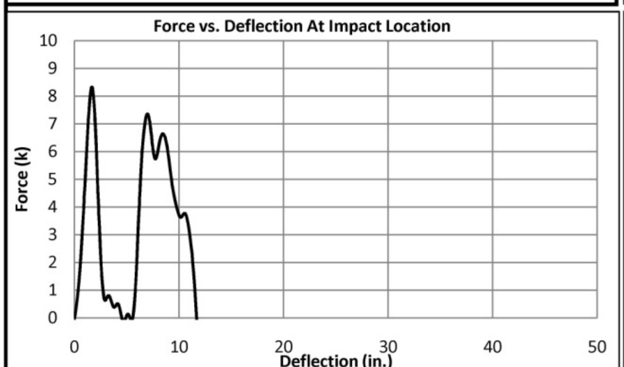

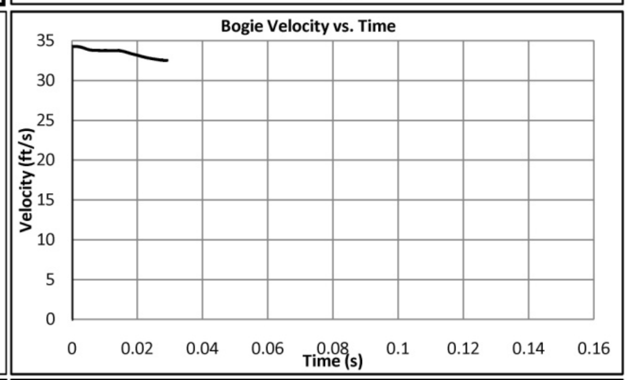

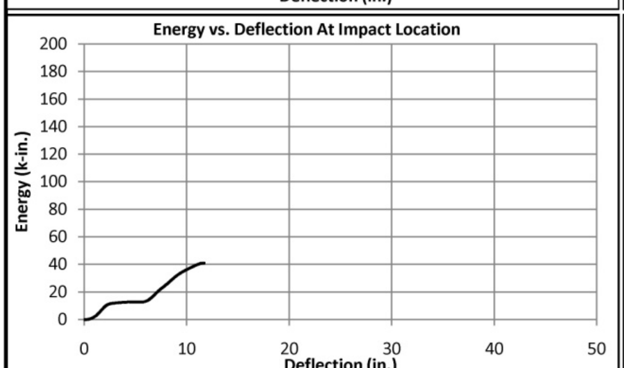

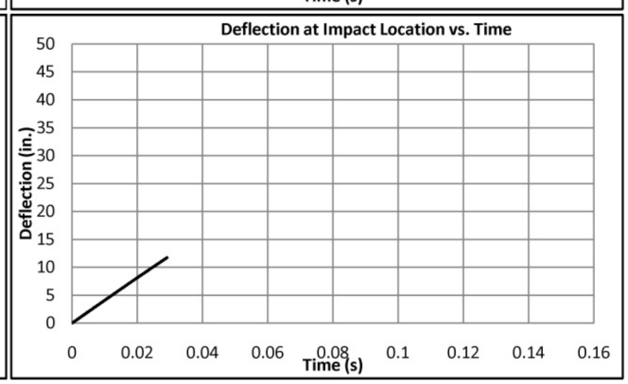

Figure A-3. Test No. MGSBRB-2 Results (DTS)

MIDWEST ROADSIDE SAFETY FACILITY

Bogie Test Summary

Test Information	MGS Bridge Rail	
Test Number:	MGSBRB-2	
Test Date:	16-May-2008	
Failure Type:	Bolt Head Pulled Out of Plate	
Post Properties		
Post Type:	Top-Mounted Bolt Tearout	
Post Size:	W6x9	W152X13.4
Post Length:	44 in.	111.8 cm
Embedment Depth:	NA in.	NA cm
Orientation:	Strong Axis, Centered	
Soil Properties		
Gradation:	NA	
Moisture Content:	NA	
Compaction Method:	NA	
Soil Density, γd:	NA	
Bogie Properties		
Impact Velocity:	23.38 mph (34.3 fps)	10.45 m/s
Impact Height:	24.875 in.	63.2 cm
Bogie Mass:	1841 lbs	835.1 kg
Data Acquired		
Acceleration Data:	EDR-3	
Camera Data:	AOS-5 Perpendicular - 20'-1"	

Test Results Summary		
Max. Deflection:	11.8	in.
Peak Force:	8.6	k
Initial Linear Stiffness:	4.9	k/in.
Total Energy:	70.1	k-in.

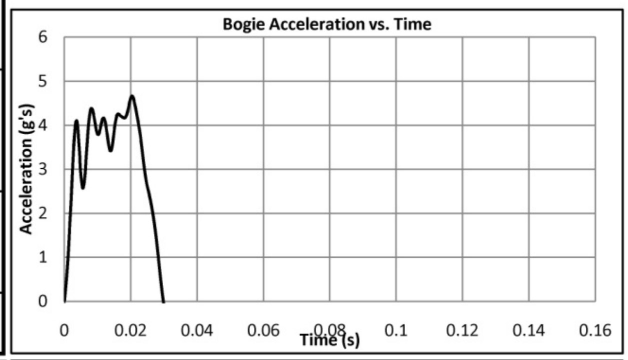

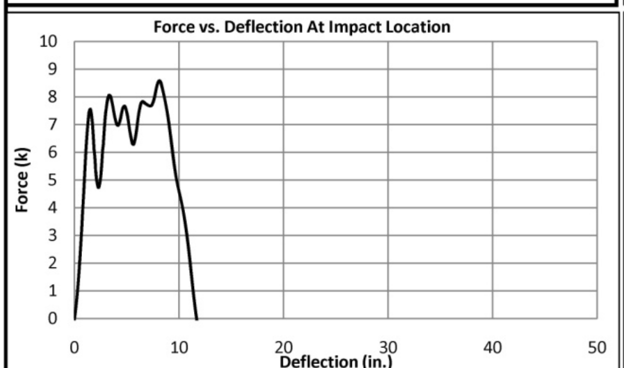

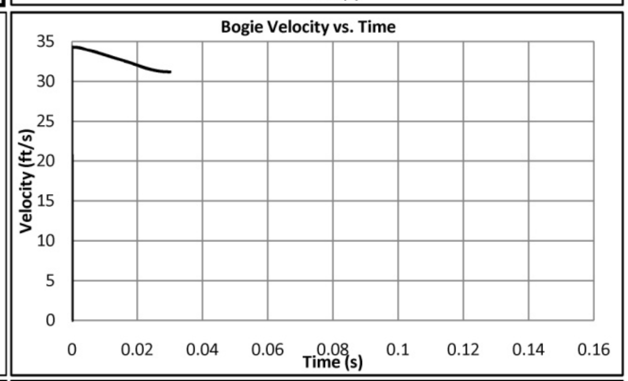

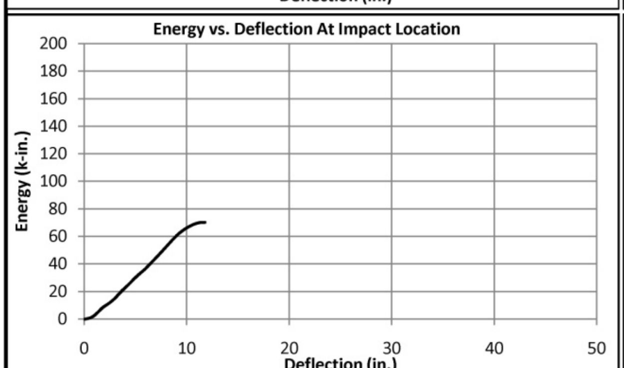

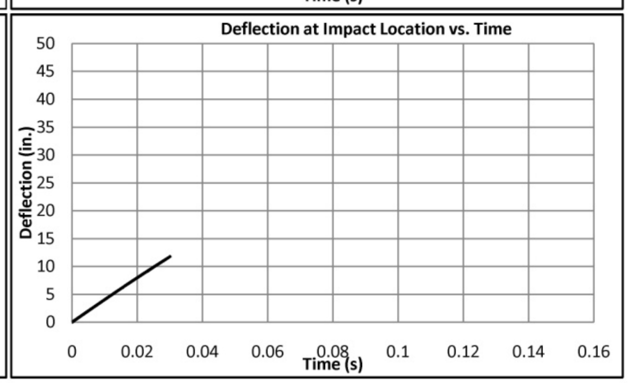

Figure A-4. Test No. MGSBRB-2 Results (EDR-3)

MIDWEST ROADSIDE SAFETY FACILITY

Bogie Test Summary

Test Information	MGS Bridge Rail	
Test Number:	MGSBRB-3	
Test Date:	16-May-2008	
Failure Type:	Bolt Tearout and Post Crush	
Post Properties		
Post Type:	Side-Mounted Tube Tearout	
Post Size:	HSS6x4x1/8	HSS152x102x3
Post Length:	40 in.	101.6 cm
Embedment Depth:	NA in.	NA cm
Orientation:	Strong Axis, Centered	
Soil Properties		
Gradation:	NA	
Moisture Content:	NA	
Compaction Method:	NA	
Soil Density, γd:	NA	
Bogie Properties		
Impact Velocity:	20.36 mph (29.9 fps)	9.1 m/s
Impact Height:	24.875 in.	63.2 cm
Bogie Mass:	1841 lbs	835.1 kg
Data Acquired		
Acceleration Data:	DTS	
Camera Data:	AOS-5 Perpendicular - 20'-1"	

Test Results Summary		
Max. Deflection:	44.9	in.
Peak Force:	7.7	k
Initial Linear Stiffness:	3.8	k/in.
Total Energy:	134.6	k-in.

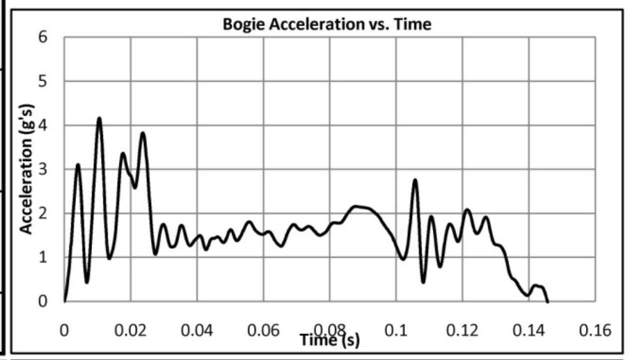

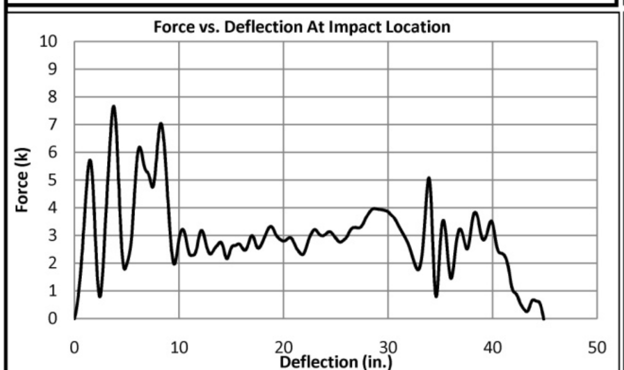

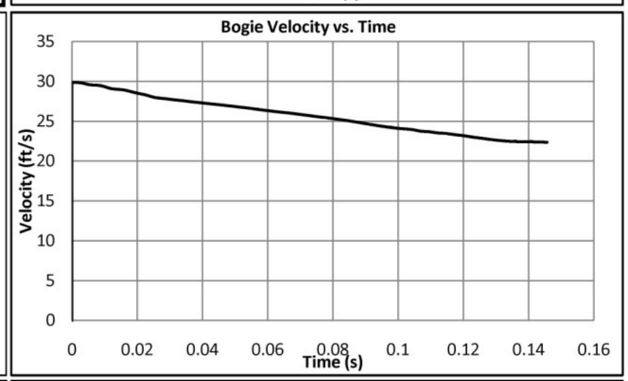

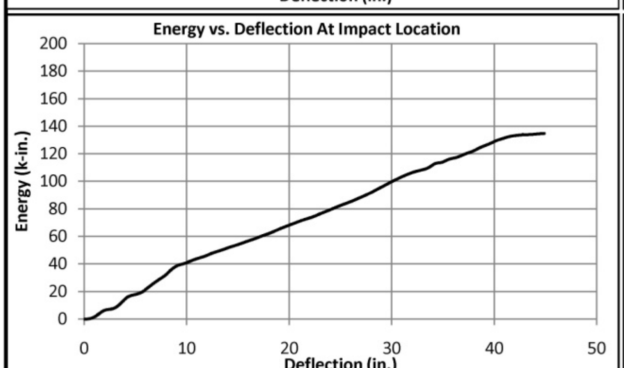

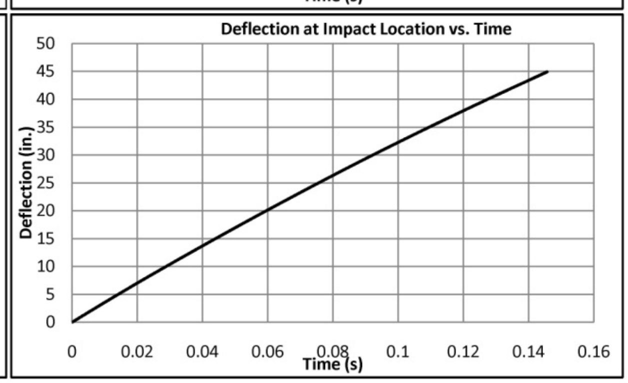

Figure A-5. Test No. MGSBRB-3 Results (DTS)

MIDWEST ROADSIDE SAFETY FACILITY

Bogie Test Summary

Test Information	MGS Bridge Rail	
Test Number:	MGSBRB-3	
Test Date:	16-May-2008	
Failure Type:	Bolt Tearout and Post Crush	
Post Properties		
Post Type:	Side-Mounted Tube Tearout	
Post Size:	HSS6x4x1/8	HSS152x102x3
Post Length:	40 in.	101.6 cm
Embedment Depth:	NA in.	NA cm
Orientation:	Strong Axis, Centered	
Soil Properties		
Gradation:	NA	
Moisture Content:	NA	
Compaction Method:	NA	
Soil Density, γd:	NA	
Bogie Properties		
Impact Velocity:	20.36 mph (29.9 fps)	9.1 m/s
Impact Height:	24.875 in.	63.2 cm
Bogie Mass:	1841 lbs	835.1 kg
Data Acquired		
Acceleration Data:	EDR-3	
Camera Data:	AOS-5 Perpendicular - 20'-1"	

Test Results Summary		
Max. Deflection:	43.9	in.
Peak Force:	7.1	k
Initial Linear Stiffness:	3.8	k/in.
Total Energy:	149.9	k-in.

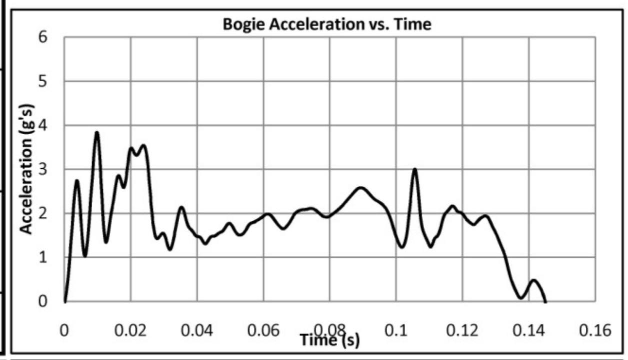

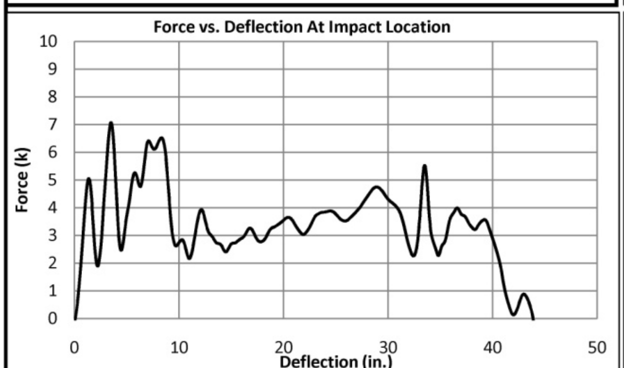

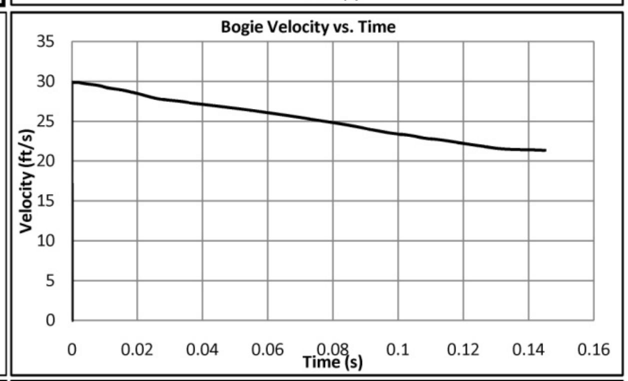

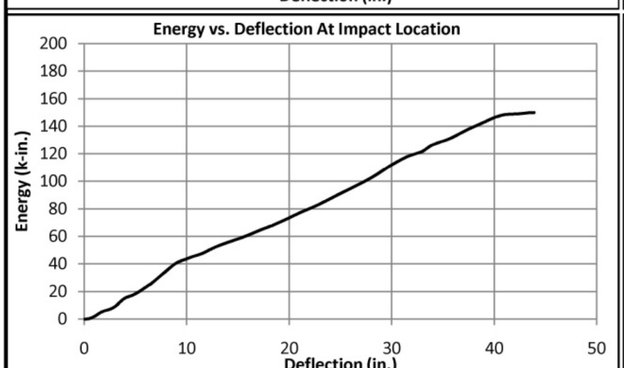

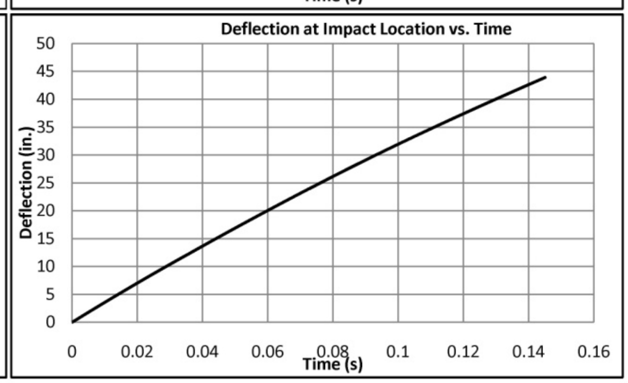

Figure A-6. Test No. MGSBRB-3 Results (EDR-3)

MIDWEST ROADSIDE SAFETY FACILITY

Bogie Test Summary

Test Information	MGS Bridge Rail	
Test Number:	MGSBRB-4	
Test Date:	9-Jun-2008	
Failure Type:	Plate Tearing, Web Buckling	
Post Properties		
Post Type:	Top-Mounted Bolt Tearout	
Post Size:	W6x9	W152x13.4
Post Length:	44 in.	111.8 cm
Embedment Depth:	NA in.	NA cm
Orientation:	Strong Axis, Centered	
Soil Properties		
Gradation:	NA	
Moisture Content:	NA	
Compaction Method:	NA	
Soil Density, γd:	NA	
Bogie Properties		
Impact Velocity:	22.41 mph (32.9 fps)	10.02 m/s
Impact Height:	24.875 in.	63.2 cm
Bogie Mass:	1837 lbs	833.2 kg
Data Acquired		
Acceleration Data:	EDR-4	
Camera Data:	AOS-2 Perpendicular - 19'-6"	

Test Results Summary		
Max. Deflection:	42.9	in.
Peak Force:	8.3	k
Initial Linear Stiffness:	3.8	k/in.
Total Energy:	187.2	k-in.

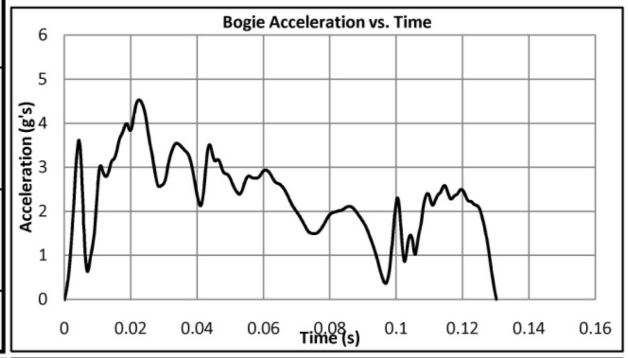

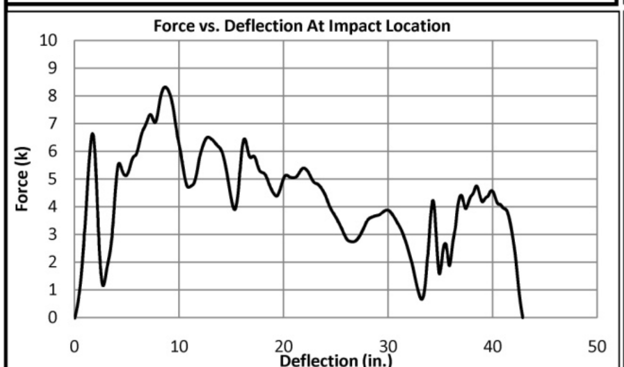

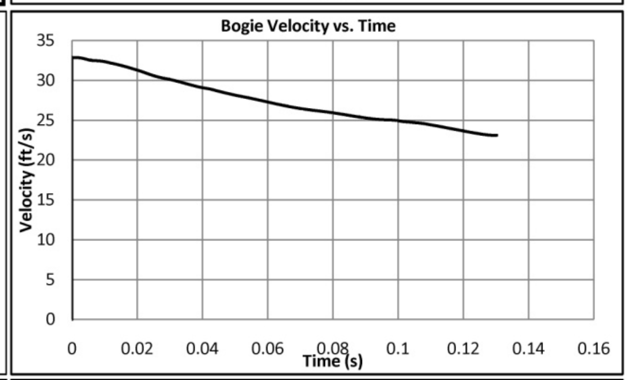

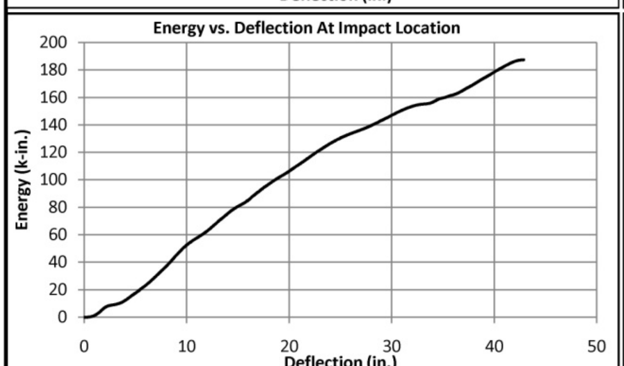

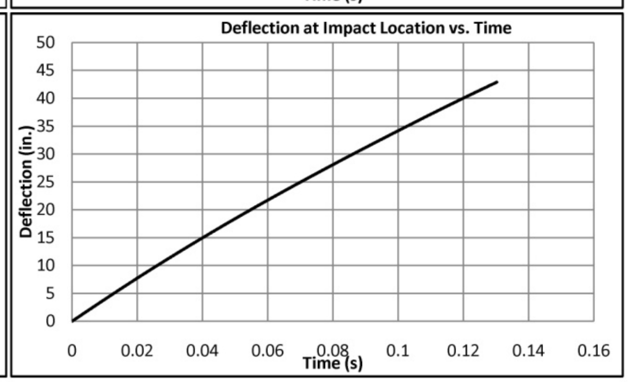

Figure A-7. Test No. MGSBRB-4 Results (EDR-4)

MIDWEST ROADSIDE SAFETY FACILITY

Bogie Test Summary

Test Information	MGS Bridge Rail	
Test Number:	MGSBRB-4	
Test Date:	9-Jun-2008	
Failure Type:	Plate Tearing, Web Buckling	
Post Properties		
Post Type:	Top-Mounted Bolt Tearout	
Post Size:	W6x9	W152x13.4
Post Length:	44 in.	111.8 cm
Embedment Depth:	NA in.	NA cm
Orientation:	Strong Axis, Centered	
Soil Properties		
Gradation:	NA	
Moisture Content:	NA	
Compaction Method:	NA	
Soil Density, γd:	NA	
Bogie Properties		
Impact Velocity:	22.41 mph (32.9 fps)	10.02 m/s
Impact Height:	24.875 in.	63.2 cm
Bogie Mass:	1837 lbs	833.2 kg
Data Acquired		
Acceleration Data:	EDR-3	
Camera Data:	AOS-2 Perpendicular - 19'-6"	

Test Results Summary		
Max. Deflection:	41.9	in.
Peak Force:	9.9	k
Initial Linear Stiffness:	4.3	k/in.
Total Energy:	254.9	k-in.

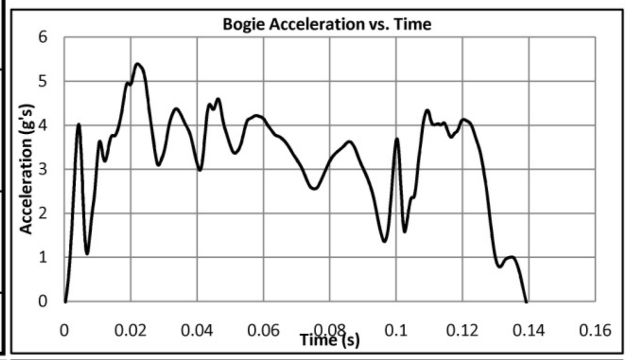

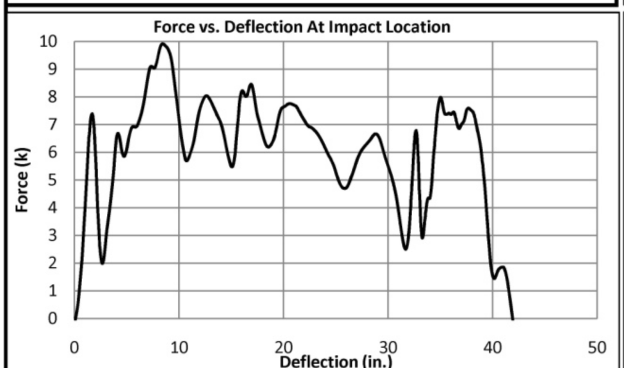

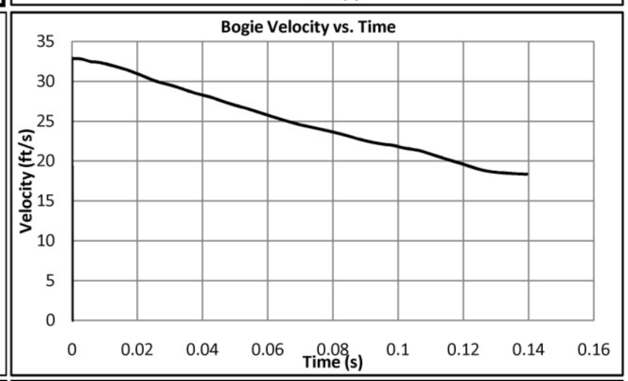

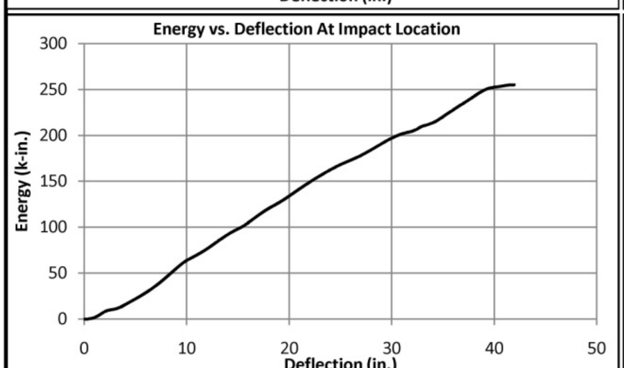

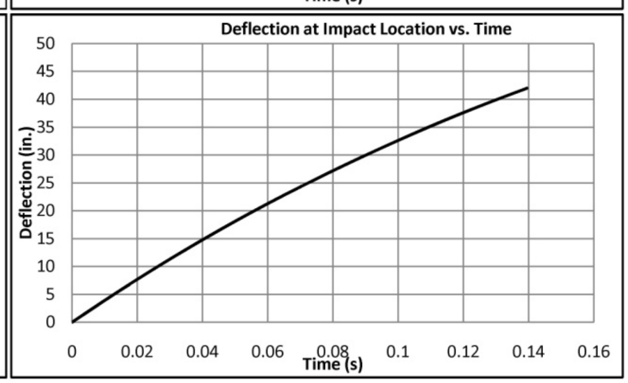

Figure A-8. Test No. MGSBRB-4 Results (EDR-3)

MIDWEST ROADSIDE SAFETY FACILITY

Bogie Test Summary

Test Information	MGS Bridge Rail	
Test Number:	MGSBRB-5	
Test Date:	9-Jun-2008	
Failure Type:	Bolt Tearout Through Post	
Post Properties		
Post Type:	Side-Mounted Tube Tearout	
Post Size:	HSS6x4x1/8	HSS152x102x3
Post Length:	40 in.	101.6 cm
Embedment Depth:	NA in.	NA cm
Orientation:	Strong Axis, Centered	
Soil Properties		
Gradation:	NA	
Moisture Content:	NA	
Compaction Method:	NA	
Soil Density, γd:	NA	
Bogie Properties		
Impact Velocity:	22.97 mph (33.7 fps)	10.27 m/s
Impact Height:	24.875 in.	63.2 cm
Bogie Mass:	1837 lbs	833.2 kg
Data Acquired		
Acceleration Data:	EDR-4	
Camera Data:	AOS-2 Perpendicular - 19'-6"	

Test Results Summary		
Max. Deflection:	43.8	in.
Peak Force:	7.1	k
Initial Linear Stiffness:	3.1	k/in.
Total Energy:	134.2	k-in.

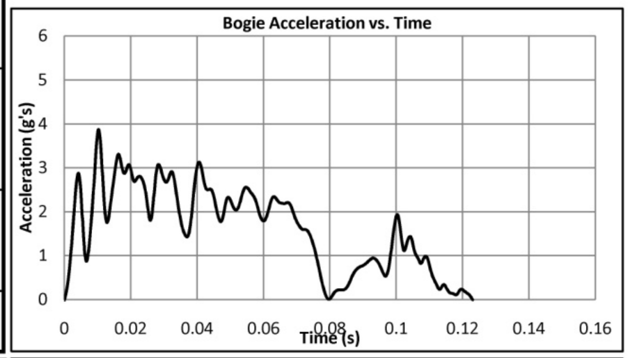

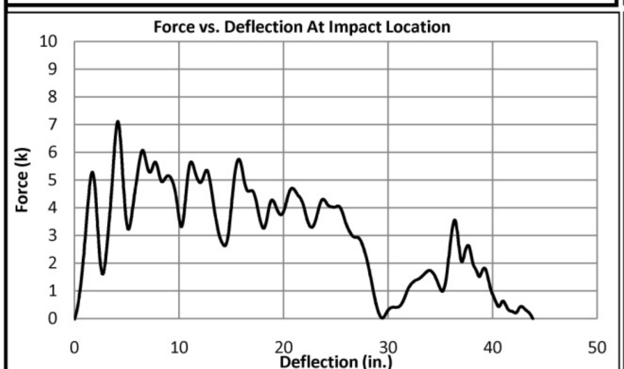

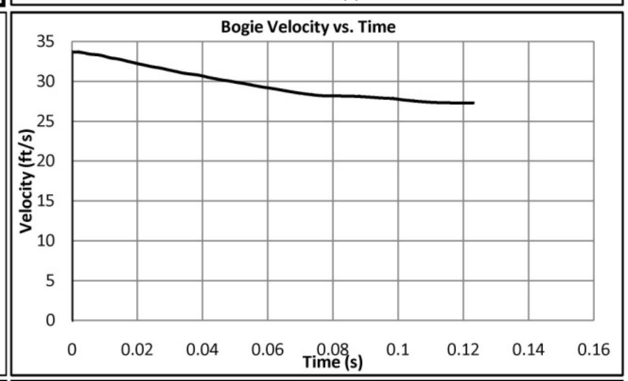

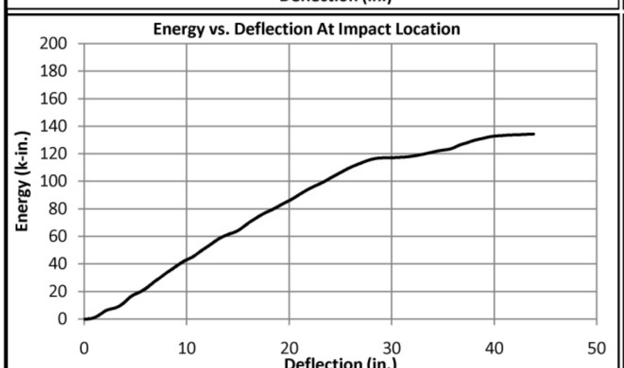

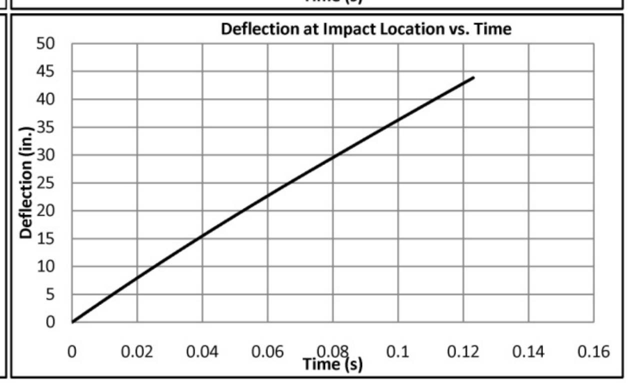

Figure A-9. Test No. MGSBRB-5 Results (EDR-4)

MIDWEST ROADSIDE SAFETY FACILITY

Bogie Test Summary

Test Information	MGS Bridge Rail	
Test Number:	MGSBRB-5	
Test Date:	9-Jun-2008	
Failure Type:	Bolt Tearout Through Post	
Post Properties		
Post Type:	Side-Mounted Tube Tearout	
Post Size:	HSS6x4x1/8	HSS152x102x3
Post Length:	40 in.	101.6 cm
Embedment Depth:	NA in.	NA cm
Orientation:	Strong Axis, Centered	
Soil Properties		
Gradation:	NA	
Moisture Content:	NA	
Compaction Method:	NA	
Soil Density, γd:	NA	
Bogie Properties		
Impact Velocity:	22.97 mph (33.7 fps)	10.27 m/s
Impact Height:	24.875 in.	63.2 cm
Bogie Mass:	1837 lbs	833.2 kg
Data Acquired		
Acceleration Data:	EDR-3	
Camera Data:	AOS-2 Perpendicular - 19'-6"	

Test Results Summary		
Max. Deflection:	42.9	in.
Peak Force:	8.1	k
Initial Linear Stiffness:	3.7	k/in.
Total Energy:	171.2	k-in.

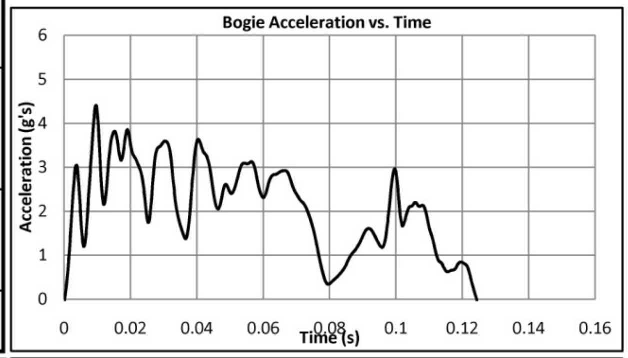

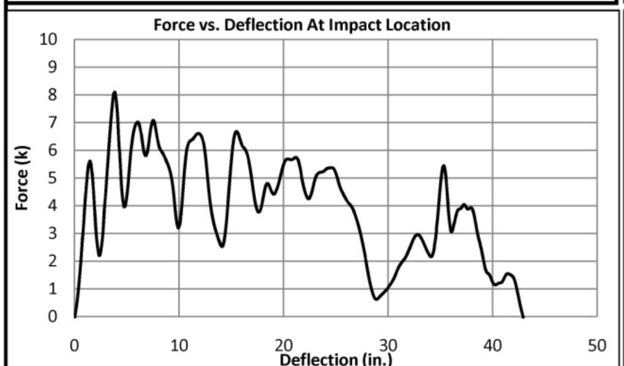

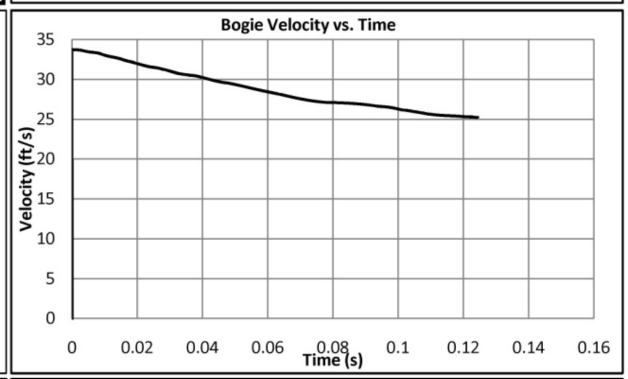

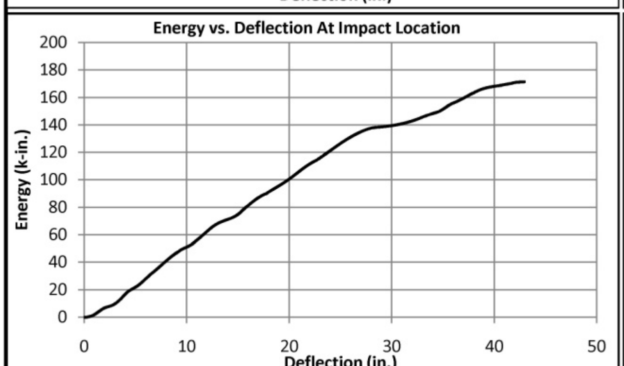

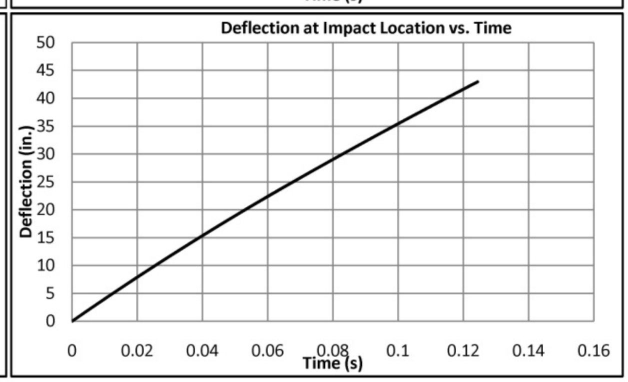

Figure A-10. Test No. MGSBRB-5 Results (EDR-3)

MIDWEST ROADSIDE SAFETY FACILITY

Bogie Test Summary

Test Information	MGS Bridge Rail	
Test Number:	MGSBRB-6	
Test Date:	13-Nov-2009	
Failure Type:	Threaded Rod Fracture	
Post Properties		
Post Type:	Side-Mounted Weak Post Socket	
Post Size:	S3x5.7	S76x8.5
Post Length:	40 in.	101.6 cm
Embedment Depth:	NA in.	NA cm
Orientation:	Strong Axis, Centered	
Soil Properties		
Gradation:	NA	
Moisture Content:	NA	
Compaction Method:	NA	
Soil Density, γd:	NA	
Bogie Properties		
Impact Velocity:	21.94 mph (32.2 fps)	9.81 m/s
Impact Height:	24.875 in.	63.2 cm
Bogie Mass:	1797 lbs	815.1 kg
Data Acquired		
Acceleration Data:	EDR-4	
Camera Data:	High Speed Camera Malfunctioned	

Test Results Summary		
Max. Deflection:	30.6	in.
Peak Force:	4.0	k
Initial Linear Stiffness:	2.3	k/in.
Total Energy:	82.9	k-in.

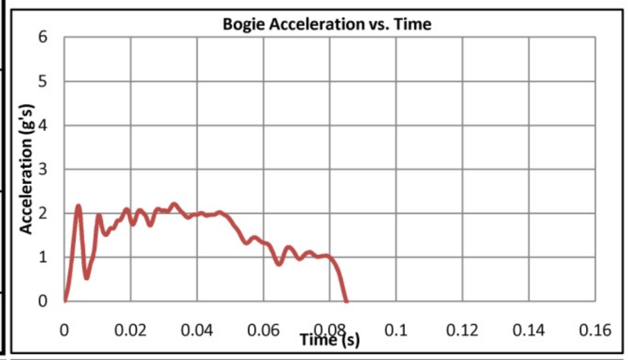

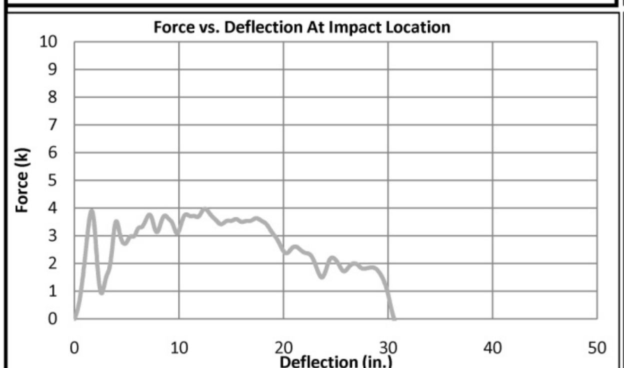

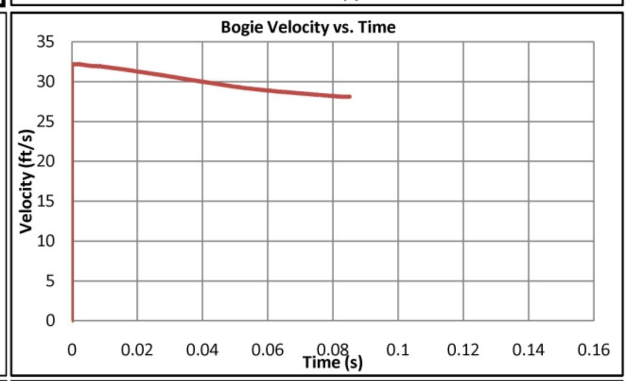

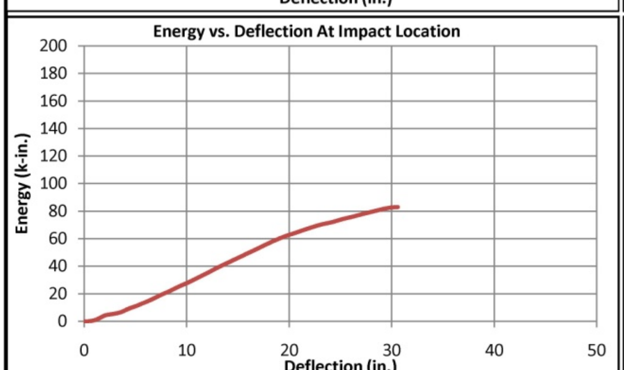

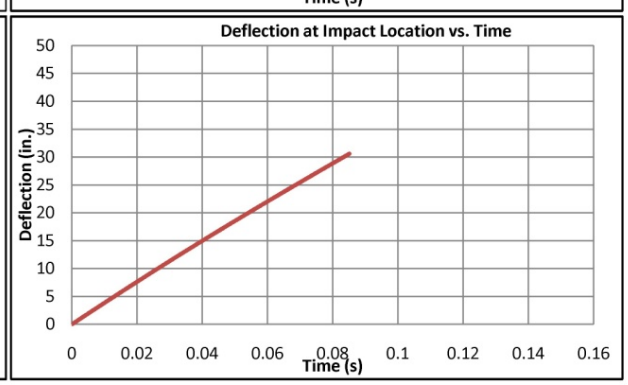

Figure A-11. Test No. MGSBRB-6 Results (EDR-4)

MIDWEST ROADSIDE SAFETY FACILITY

Bogie Test Summary

Test Information	MGS Bridge Rail	
Test Number:	MGSBRB-6	
Test Date:	13-Nov-2009	
Failure Type:	Threaded Rod Fracture	
Post Properties		
Post Type:	Side-Mounted Weak Post Socket	
Post Size:	S3x5.7	S76x8.5
Post Length:	40 in.	101.6 cm
Embedment Depth:	NA in.	NA cm
Orientation:	Strong Axis, Centered	
Soil Properties		
Gradation:	NA	
Moisture Content:	NA	
Compaction Method:	NA	
Soil Density, γd:	NA	
Bogie Properties		
Impact Velocity:	21.94 mph (32.2 fps)	9.81 m/s
Impact Height:	24.875 in.	63.2 cm
Bogie Mass:	1797 lbs	815.1 kg
Data Acquired		
Acceleration Data:	EDR-3	
Camera Data:	High Speed Camera Malfunctioned	

Test Results Summary		
Max. Deflection:	30.5	in.
Peak Force:	4.6	k
Initial Linear Stiffness:	2.5	k/in.
Total Energy:	87.6	k-in.

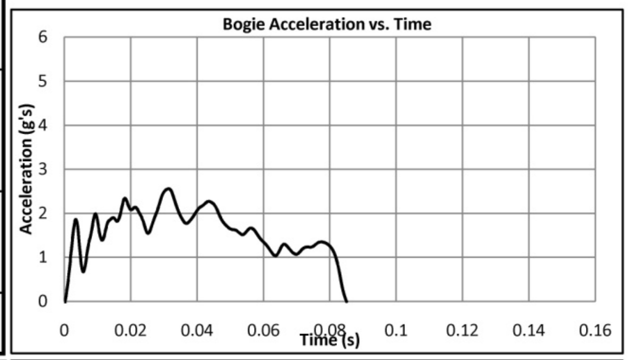

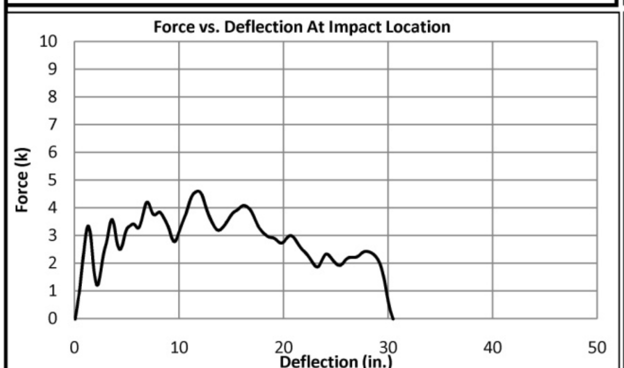

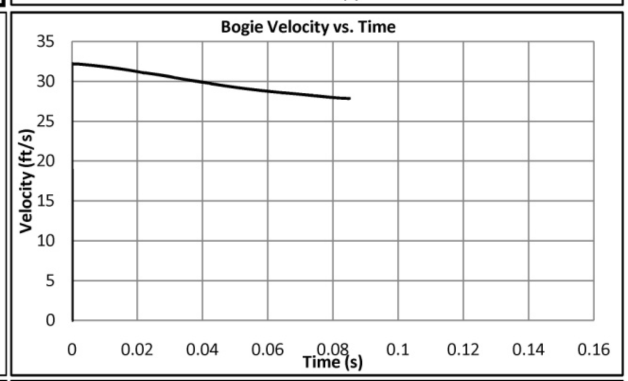

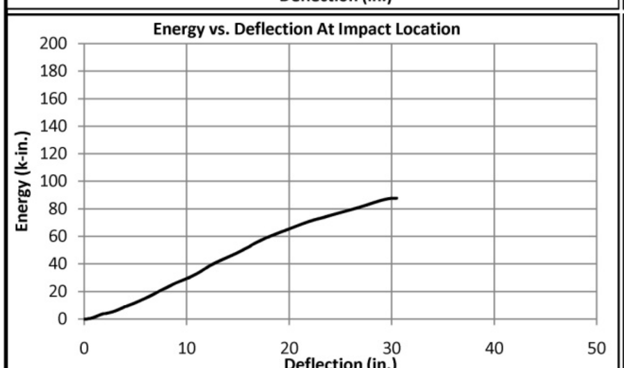

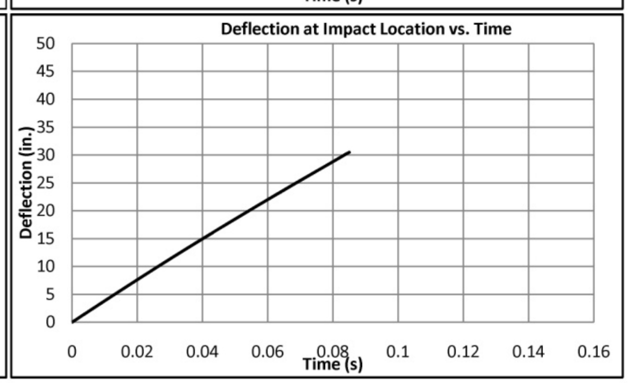

Figure A-12. Test No. MGSBRB-6 Results (EDR-3)

MIDWEST ROADSIDE SAFETY FACILITY

Bogie Test Summary

Test Information	MGSBRB-7	
Test Number:	MGSBRB-7	
Test Date:	20-Jan-2009	
Failure Type:	Concrete Shear Failure	
Post Properties		
Post Type:	Top-Mounted Weak Post in Socket	
Post Size:	S3x5.7	S76x8.5
Post Length:	44 in.	111.8 cm
Embedment Depth:	NA in.	NA cm
Orientation:	Strong Axis, Centered	
Soil Properties		
Gradation:	NA	
Moisture Content:	NA	
Compaction Method:	NA	
Soil Density, γd:	NA	
Bogie Properties		
Impact Velocity:	15.01 mph (22 fps)	6.71 m/s
Impact Height:	24.875 in.	63.2 cm
Bogie Mass:	1860 lbs	843.7 kg
Data Acquired		
Acceleration Data:	EDR-4	
Camera Data:	AOS-6 Perpendicular - 31'	

Test Results Summary		
Max. Deflection:	24.6	in.
Peak Force:	6.6	k
Initial Linear Stiffness:	3.1	k/in.
Total Energy:	35.5	k-in.

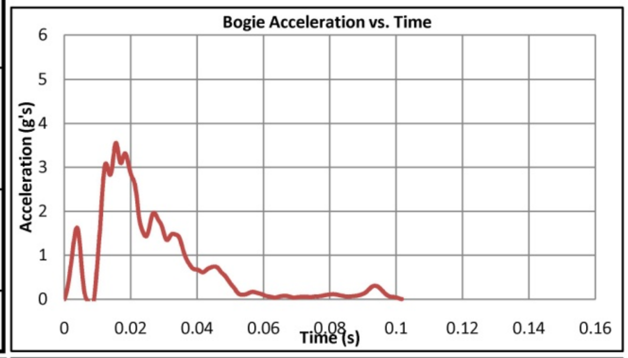

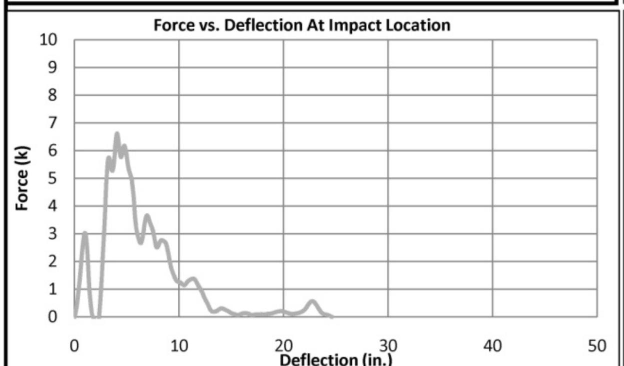

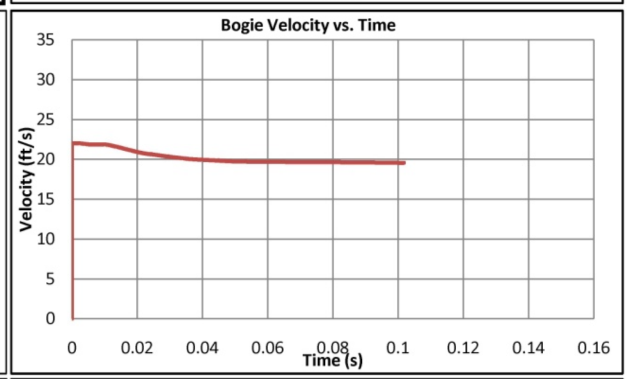

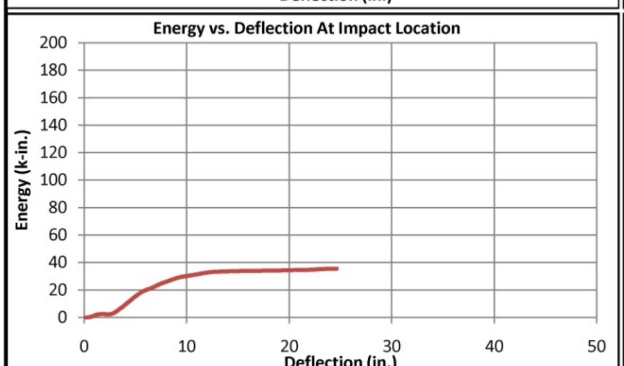

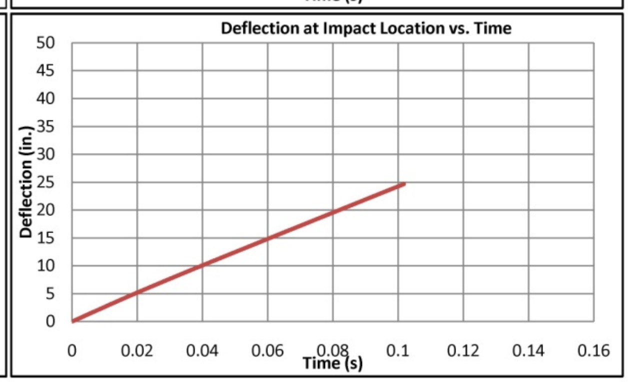

Figure A-13. Test No. MGSBRB-7 Results (EDR-4)

MIDWEST ROADSIDE SAFETY FACILITY

Bogie Test Summary

Test Information	MGSBRB-7	
Test Number:	MGSBRB-7	
Test Date:	20-Jan-2009	
Failure Type:	Concrete Shear Failure	
Post Properties		
Post Type:	Top-Mounted Weak Post in Socket	
Post Size:	S3x5.7	S76x8.5
Post Length:	44 in.	111.8 cm
Embedment Depth:	NA in.	NA cm
Orientation:	Strong Axis, Centered	
Soil Properties		
Gradation:	NA	
Moisture Content:	NA	
Compaction Method:	NA	
Soil Density, γd:	NA	
Bogie Properties		
Impact Velocity:	15.01 mph (22 fps)	6.71 m/s
Impact Height:	24.875 in.	63.2 cm
Bogie Mass:	1860 lbs	843.7 kg
Data Acquired		
Acceleration Data:	EDR-3	
Camera Data:	AOS-6 Perpendicular - 31'	

Test Results Summary		
Max. Deflection:	12.6	in.
Peak Force:	6.7	k
Initial Linear Stiffness:	3.3	k/in.
Total Energy:	31.4	k-in.

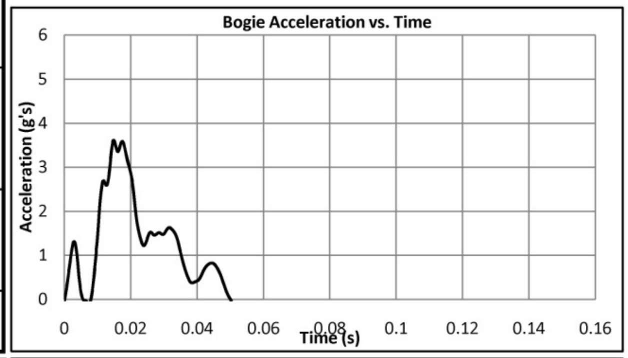

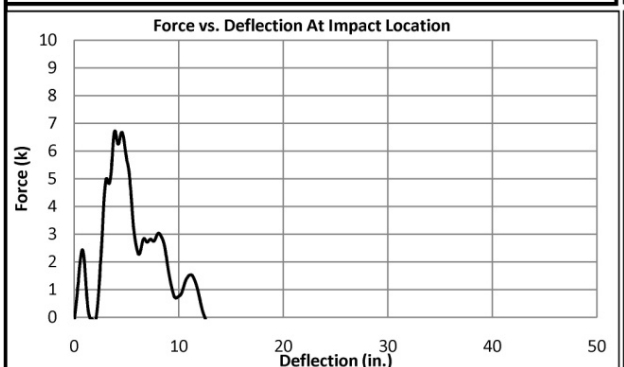

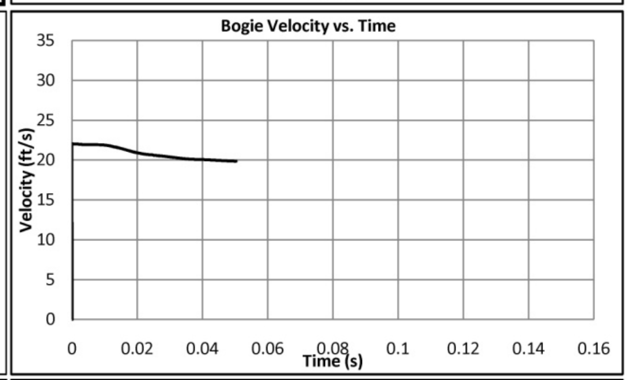

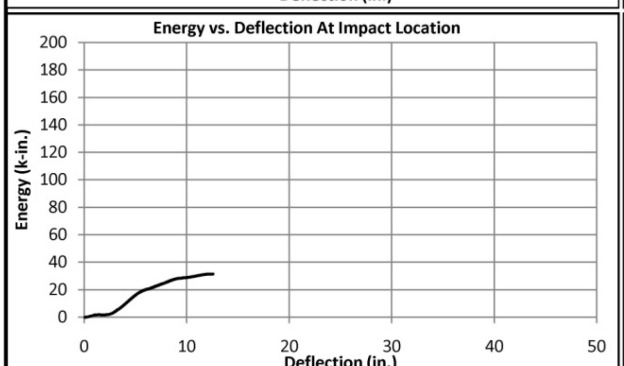

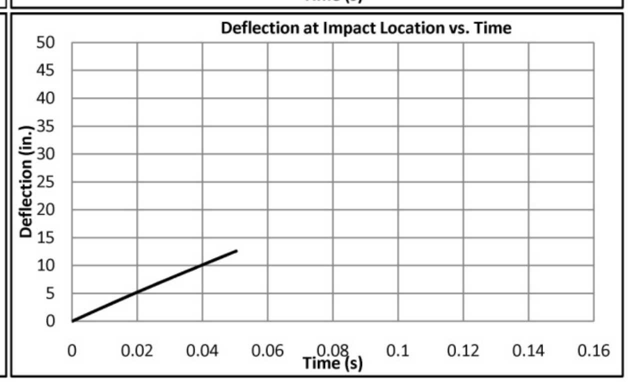

Figure A-14. Test No. MGSBRB-7 Results (EDR-3)

Appendix B. Material Specifications

3" 5.7#

GERDAU AMERISTEEL

CARTERSVILLE STEEL MILL
384 OLD GRASSDALE RD NE
CARTERSVILLE GA 30121 USA
(770) 387-3300

Chemical and Physical Test Report

MADE IN UNITED STATES

G-110068

PRODUCED IN: CARTERSVILLE

SHIP TO	INVOICE TO	SHIP DATE
STATE STEEL 13433 CENTECH RD P.O. BOX 390745 OMAHA, NE 68139	STATE STEEL SUPPLY CO INC/SC/I PO BOX 3224 SIOUX CITY, IA 51102	02/19/08 CUST. ACCOUNT NO 60005758

SHAPE + SIZE	GRADE	SPECIFICATION	SALES ORDER	CUST P.O. NUMBER
W3 X 5.7# S-BEAM	A57250/992	ASTM A572 GR50-07, ASTM A992 -06A	8020438-04	P80218JT051-04

HEAT I.D.	C	Mn	P	S	Si	Cu	Ni	Cr	Mo	V	Nb	B	N	Sn	Al	Ti	Ca	Zn	C Eqv
G800884	.14	.90	.009	.020	.20	.30	.10	.03	.020	.015	.002	.0003	.0091	.009	.001	.00100	.00090	.00440	.33

Mechanical Test: Yield 52900 PSI, 364.73 MPA Tensile: 72100 PSI, 497.11 MPA %El: 23.5/8in, 23.5/200MM Std Dev:0 Idl Diam: .457
Customer Requirements CASTING: STRAND CAST
Mechanical Test: Yield 55300 PSI, 381.28 MPA Tensile: 71300 PSI, 491.6 MPA %El: 23.4/8in, 23.4/200MM Std Dev:0 Id Diam: .457
Customer Requirements CASTING: STRAND CAST

This material, including the billets, was produced and manufactured in the United States of America

Bhaskar Yalamanchili
Quality Director
Gerdau Ameristeel

THE ABOVE FIGURES ARE CERTIFIED EXTRACTS FROM THE ORIGINAL CHEMICAL AND PHYSICAL TEST RECORDS AS CONTAINED IN THE PERMANENT RECORDS OF COMPANY.

Mgr. Metallurg. Svcs.
CARTERSVILLE STEEL MILL

Seller warrants that all material furnished shall comply with specifications subject to standard published manufacturing variations. NO OTHER WARRANTIES, EXPRESSED OR IMPLIED, ARE MADE BY THE SELLER, AND SPECIFICALLY EXCLUDED ARE WARRANTIES OF MERCHANTABILITY AND FITNESS FOR A PARTICULAR PURPOSE.
In no event shall seller be liable for indirect, consequential or punitive damages arising out of or related to the materials furnished by seller.
Any claim for damages for materials that do not conform to specifications must be made from buyer to seller immediately after delivery of same in order to allow the seller the opportunity to inspect the material in question.

Figure B-1. S3x5.7 Posts Mill Certification, Test Nos. MGSBR-1 and MGSBR-2

**LAND 15
NUCOR STEEL - BERKELEY
P.O. Box 2259
Mt. Pleasant, S.C. 29464
Phone: (843) 336-6000

CERTIFIED MILL TEST REPORT

6/10/09 18:19:43
100% MELTED AND MANUFACTURED IN THE USA
All beams produced by Nucor-Berkeley are cast and rolled to a fully killed and fine grain practice.

Sold To: STEEL & PIPE SUPPLY CO., INC.
PO BOX 1688

MANHATTAN, KS 66505

Ship To: LONGVIEW WAREHOUSE
4750 WEST MARSHALL AVE

LONGVIEW, TX 75604

Customer #.: 472 - 14
Customer PO: 4500121839
B.O.L. #...: 754168

SPECIFICATIONS: Tested in accordance with ASTM specification A6/A6M and A370.
AASHTO : M270-50-05
ASTM : A992-06a:A36-08/A529-05-50/A572-07-50/A709-0950S/A709-345M

Description	Heat# Grade(s) Test	Yield/ Tensile Ratio	Yield (PSI) (MPa)	Tensile (PSI) (MPa)	Elong %	C Cr ******	Mn Mo ******	P Sn ******	S B ******	Si V N	Cu Nb ******	Ni ****** CI	CE1 CE2 Pcm
M6X4.4	2804339	.91	70300	77400	24.98	.06	.83	.008	.023	.24	.08	.03	.22
040' 00.00"	A529-05-50		485	534		.03	.01	.0053	.0015	.004	.027		.2706
M152X6.5		.90	69800	77800	25.24					.0045		2.59	.1321
012.1920m			481	536		30 Piece(s)						Inv#:	0
M8X6.5	2809489	.88	67500	77000	23.89	.06	.84	.009	.038	.22	.14	.04	.23
040' 00.00"	A529-05-50		465	531		.03	.01	.0076	.0005	.002	.015		.2732
M200X9.7		.86	65500	76100	25.91					.0043		3.72	.1324
012.1920m			452	525		20 Piece(s)						Inv#:	0
S3X5.7	1901346	.80	56000	69800	27.70	.06	.94	.014	.019	.25	.19	.05	.26
040' 00.00"	A992-06a		386	481		.07	.01	.0087	.0003	.005	.015		.3069
S75X8.5		.81	56200	69500	27.88					.0056		4.69	.1422
012.1920m			387	479		35 Piece(s)						Inv#:	0
W5X16	2814371	.81	55000	67500	26.99	.06	.83	.007	.025	.20	.18	.05	.23
040' 00.00"	A992-06a		379	465		.04	.01	.0085	.0004	.002	.025		.2739
W130X23.8		.82	55100	67300	26.86					.0046		4.21	.1321
012.1920m			380	464		12 Piece(s)						Inv#:	0

Elongation based on 8" (20.32cm) gauge length. 'No Weld Repair' was pefomed.
CI = 26.01Cu+3.88Ni+1.20Cr+1.49Si+17.28P-(7.29Cu*Ni)-(9.10Ni*P)-33.39(Cu*Cu)
Pcm = C+(Si/30)+(Mn/20)+(Cu/20)+(Ni/60)+(Cr/20)+(Mo/15)+(V/10)+5B

Hg free and no contact with Hg during manufacture.
CE1= C+(Mn/6)+((Cr+Mo+V)/5)+((Ni+Cu)/15)
CE2 = C+((Mn+Si)/6)+((Cr+Mo+V+Cb)/5)+((Ni+Cu)/15)

I hereby certify that the contents of this report are accurate and correct. All test results and operations performed by the material manufacturer are in compliance with material specifications, and when designated by the Purchaser, meet applicable specifications.

Bruce A. Work
Metallurgist

Figure B-2. S3x5.7 Posts Mill Certification, Test No. MGSBR-2

BL#-0294755 P.O.-4500106488

Date: 7/07/08

Nucor Corporation

Heat Number: 748735

Nucor Steel Division
Post Office Box 309 Norfolk, Nebraska 68702 Phone (402) 644-0200
Mill Certification

A2LA ACCREDITED
Chemical Testing
Certificate: 0780-01
Expires: 11/30/08

*Chemical Analysis

Test conform to ASTM A29-05, ASTM E415 and ASTM E1019-resulphurized grades
Spec: A36 ASTM A36-08 Size: 1/4 X 1 Flats
ASME SA-36 E04

C	.17	P	.02	Mo	.02
Mn	.70	Cu	.24	V	.001
Si	.20	Cr	.08	Nb	.001
S	.03	Ni	.09		

Physical Properties

	Imperial			Metric		
Yield	50,389	51,184	psi	347	353	MPA
Tensile	71,407	71,310	psi	492	492	MPA
% Elongation	25	27	% in 8"	25	27	% in 203.3 mm

Strand Cast

Reduction Ratio: 176:1

STEEL & PIPE SUPPLY
555 POYNTZ AVE.
MANHATTAN, KS 66502

Jim Hill Division Metallurgist

All Manufacturing processes, including melting have been performed in the U.S.A. Mercury, in any form, has not been used in the production or testing of this material. Welding or weld repair was not performed on this material. This material conforms to the specifications described on this document and may not be reproduced except in full, without written approval of Nucor Corporation. This product is NAFTA certified under Paragraph "B" of the NAFTA rules of origin.

FORM: 10F002 *Within Our A2LA Accreditation Scope HT3000R

1066488

Figure B-3. Post Standoff Mill Certification, Test Nos. MGSBR-1 and MGSBR-2

NY

4x4x3/8

Certification 918592 6/10/08 1

Submitted By: Hanna Steel Corporation
Tuscaloosa Division
1701 Boone Blvd
P O Box 428
Northport AL 35476

Cust P.O.: P80606SS001
Date Shipped: 6/10/08
Load Tally 5-20961
Invoice # 000000

Send To: State Steel of Omaha
13433 CENTECH ROAD
P O Box 390745
Omaha NE 68139

Ship To: State Steel of Omaha
13433 CENTECH ROAD
P O Box 390745
Omaha NE 68139

No Item	Heat #	ASTM	Year		GradeClass		Yield	Tens	Elong	Rock
01 4500212		4 SQ 3/8		HRA500	24.000FT					
3666790	B74033	A500	2003a		B	1	64,000	71,500	25.3	B85

Total Weight 6,217

Heat #	C	Mn	P	S	Si	Al	Cb	Cr	Cu	Mo	Ni	V
B74033	.180	.770	.010	.010	.011	.029	.000	.030	.050	.010	.020	.001

N .0045 Ti .0020 B .0001

Heat# B74033 was melted and manufactured in the USA

Figure B-4. 4x4x⅜ Mounting Tube Mill Certification, Test Nos. MGSBR-1 and MGSBR-2

EMJ

7/16×3

CERTIFICATE OF TEST

Page 01 of 01

Certification Date
15-DEC-2008

CUSTOMER ORDER NUMBER
29288

CUSTOMER PART NUMBER
0001

EARLE M. JORGENSEN COMPANY
1800 N UNIVERSAL AVENUE
KANSAS CITY MO 64120

Invoice Number
T627516

SOLD TO: RIVERS METAL PRODUCTS
3100 N 38TH
LINCOLN NE 68504

SHIP TO: RIVERS METAL PRODUCTS
3100 NORTH 38TH
LINCOLN NE 68504

Description: 1018 CF BAR ASTM A108
7/16 X 3 FLATS X 12' R/L
HEAT: 0716363 ITEM: 502898

Line Total: 56 LB

Specifications:
ASTM A108 03

CHEMICAL ANALYSIS

C	MN	P	S	SI	CU	NI	CR
0.19	0.85	0.01	0.027	0.16	0.17	0.07	0.11

MO	V	SN	TI
0.03	0.006	0.008	0.001

RCPT: R475956
MILL : NUCOR WISCONSIN COLD FINISH COUNTRY OF ORIGIN : USA

STRAND CAST REDUCTION RATIO 17.8 TO 1
MATERIAL IS FREE FROM MERCURY CONTAMINATION

COMMENTS
melt source ameristeel usa
coarse grain
ACCEPTED FOR 1E0065B FOR ALL PF PARTS PER JFG 5-22-08

The above data were transcribed from the manufacturer's Certificate of Test after verification for completeness and specification requirements of the information on the certificate. All test results remain on file subject to examination.

We hereby certify that the material covered by this report will meet the applicable requirements described herein, including any specification forming a part of the description.

The willful recording of false, fictitious, or fraudulent statements in connection with test results may be punishable as a felony under federal statutes.

Material did not come in contact with mercury while in our possession.

LARRY BUSICK

Larry A Busick

Manager, Quality Assurance

Figure B-5. Top Mounting Plate, Gusset Mill Certification, Test Nos. MGSBR-1 and MGSBR-2

GREGORY HIGHWAY PRODUCTS, INC.
4100 13th St. P.O. Box 80508
Canton, Ohio 44708

Test Report

Customer: UNIVERSITY OF NEBRASKA-LINCOLN
401 CANFIELD ADMIN BLDG
P O BOX 880439
LINCOLN, NE. 68588-0439

B.O.L. # 39963 DATE SHIPPED: 05/07/09
Customer P.O. 4500204081/ 04/06/2009
Shipped to: UNIVERSITY OF NEBRASKA-LINCOLN
Project : TEST PANELS
GHP Order No 105271

HT # code	C.	Mn.	P.	S.	Si.	Tensile	Yield	Elong.	Quantity	Class	Type	Description
4614	0.21	0.84	0.011	0.003	0.03	89432	67993	19.8	160	A	2	12GA 12FT6IN/3FT1 1/2IN WB T2

Bolts comply with ASTM A-307 specifications and are galvanized in accordance with ASTM A-153, unless otherwise stated.
Nuts comply with ASTM A-563 specifications and are galvanized in accordance with ASTM A-153, unless otherwise stated.
All other galvanized material conforms with ASTM-123 & ASTM-525
All steel used in the manufacture is of Domestic Origin, "Made and Melted in the United States"
All Guardrail and Terminal Sections meets AASHTO M-180, All structural steel meets AASHTO M-183 & M270
All Bolts and Nuts are of Domestic Origin
All material fabricated in accordance with Nebraska Department of Transportation
All controlled oxidized/corrosion resistant Guardrail and terminal sections meet ASTM A606, Type 4.

By: ____________________
Andrew Artar
Vice President of Sales & Marketing
Gregory Highway Products, Inc.

STATE OF OHIO: COUNTY OF STARK
Sworn to and subscribed before me, a Notary Public, by Andrew Artar this 8th day of May, 2009.

Cynthia K Crawford
Notary Public, State of Ohio

NOTARIAL SEAL
STATE OF OHIO

CYNTHIA K. CRAWFORD
Notary Public, State of Ohio
My Commission Expires 09-16-2012

Figure B-6. W-Beam, Backup Plates Mill Certification, Test Nos. MGSBR-1 & MGSBR-2

Name: Gerdau Ameristeel AutoFax System Ph: ID: #227483 Page 4 of 7 03/24/2007 Sat 09:45

7x4x3/16

GERDAU AMERISTEEL

CALVERT CITY STEEL MILL
1035 SHAR-CAL ROAD
CALVERT CITY KY 42029 USA
(270) 395-3100

Chemical and Physical Test Report

MADE IN UNITED STATES

Y-029353

PRODUCED IN: CALVERT CITY

SHIP TO	INVOICE TO	SHIP DATE
STATE STEEL 13433 CENTECH RD P.O. BOX 390745 OMAHA, NE 68139	STATE STEEL SUPPLY CO INC/SC/I PO BOX 3224 SIOUX CITY, IA 51102	03/24/07 **CUST. ACCOUNT NO** 60005758

SHAPE + SIZE	GRADE	SPECIFICATION	SALES ORDER	CUST P.O. NUMBER
A7 X 4 X 3/8	A36	A36/44W A36/44W ASTM A36-05, ASTM A709 GR36	6110268-01	P61020DE001-01

HEAT I.D.	C	Mn	P	S	Si	Cu	Ni	Cr	Mo	V	Nb	B	N	Sn	Al	Ti	C Eqv
Y700399	.14	.71	.015	.032	.23	.31	.10	.05	.025	.001	<.008	.0005	.0085	.012	.001	.00100	.339

Mechanical Test: Yield 50000 PSI, 344.74 MPA Tensile: 69000 PSI, 475.74 MPA %El: 27.0/8in, 27.0/203.2mm Std Dev:0
Customer Requirements CASTING: STRAND CAST
Mechanical Test: Yield 50000 PSI, 344.74 MPA Tensile: 69000 PSI, 475.74 MPA %El: 23.0/8in, 23.0/203.2mm Std Dev:0
Customer Requirements CASTING: STRAND CAST

SHAPE + SIZE	GRADE	SPECIFICATION	SALES ORDER	CUST P.O. NUMBER
A8 X 6 X 1/2	A36	A36/44/572 A36/44/572 ASTM A36-05, A709 GR36, A572-50, A709 GR50/345	6076635-01	P60629DE011-01

HEAT I.D.	C	Mn	P	S	Si	Cu	Ni	Cr	Mo	V	Nb	B	N	Sn	Al	Ti	C Eqv
Y701324	.17	.86	.017	.019	.28	.30	.09	.08	.022	.019	<.008	.0005	.0092	.011	.001	.00100	.41

Mechanical Test: Yield 54000 PSI, 372.32 MPA Tensile: 76000 PSI, 524 MPA %El: 21.0/8in, 21.0/203.2mm Std Dev:0
Customer Requirements CASTING: STRAND CAST
Mechanical Test: Yield 54000 PSI, 372.32 MPA Tensile: 76000 PSI, 524 MPA %El: 23.0/8in, 23.0/203.2mm Std Dev:0
Customer Requirements CASTING: STRAND CAST
CUST ITEM NUMBER: 2/24

This material, including the billets, was melted and manufactured in the United States of America

Bhaskar Yalamanchili
Quality Director
Gerdau Ameristeel

THE ABOVE FIGURES ARE CERTIFIED EXTRACTS FROM THE ORIGINAL CHEMICAL AND PHYSICAL TEST RECORD AS CONTAINED IN THE PERMANENT RECORDS OF COMPANY.

Mgr. Metallurg. Svcs.
CALVERT CITY STEEL MILL

Figure B-7. Bottom Mounting Plate Mill Certification, Test Nos. MGSBR-1 and MGSBR-2

THE STEEL WORKS, L.L.C.
P.O. BOX 366 • 1020 NIEDRINGHAUS
GRANITE CITY, ILLINOIS 62040
PHONE 618-452-2833
FAX 618-452-2904

CHEMICAL CERTIFICATION

VENDOR
THE STEEL WORKS, L.L.C.
P.O. BOX 366
1020 NIEDRINGHAUS BLDG.4
GRANITE CITY IL 62040

BILL OF LADING NO. 127025
DATE SHIPPED 04/29/09
SHIPPER NO.
INVOICE NUMBER
INVOICE DATE / /
PURCHASE ORDER NO.
SALES ORD. NO. 99141808

SOLD TO
STEEL & PIPE SUPPLY CO. INC.
P.O. BOX 1688
MANHATTAN, KS 66502

SHIP TO
CUSTOMER WILL CALL

TSW COIL NO.	DESCRIPTION	YIELD	TENSILE	% ELONG	BEND	R.W.	OLSON
586549	HR FL A36 H/T # 190085 0.1250 X 2.0000 Length: 240.0000	38200	57700	35.			

TSW COIL NO.	C	MN	P	S	SI	AL	CB	V	CU	NI	CR	MO
586549	.040	0.180	.009	.002	.030	.030		.001	.080	0.040	0.04	.008
	SN	N	B	TI								
	.006	.008	.006	.001								
TSW COIL NO.												
TSW COIL NO.												

MELTED & ROLLED IN THE U.S.A.

WE HEREBY CERTIFY THE ABOVE IS CORRECT AS CONTAINED IN THE RECORDS OF THE CORPORATION.

Mary Macko

119031

Figure B-8. Square Washers Mill Certification, Test Nos. MGSBR-1 and MGSBR-2

RECEIVED
OCT 05 2005
UNL FMP

03/09/2009 14:21 4024722022

GREGORY HIGHWAY PRODUCTS, INC.
4100 13th St. P.O. Box 80508
Canton, Ohio 44708

Test Report

Customer:	UNIVERSITY OF NEBRASKA-LINCOLN 401 CANFIELD ADMIN BLDG P O BOX 880439 LINCOLN, NE. 68588-0439
B.O.L. #	15808
DATE SHIPPED:	09/27/05
Customer P.O.:	VERBAL JOHN ROHDE
Shipped to:	UNIVERSITY OF NEBRASKA-LINCOLN
Project:	STOCK
GHP Order No.:	44822

HEAT #	C.	Mn.	P.	S.	Si.	Tensile	Yield	Elong.	Quantity	Class	Type	Description
3390	0.21	0.8	0.013	0.007	0.01	81660	62520	20.76	160		2	12GA 12FT6IN/3FT1 1/2IN WB T2

MWRSF

Bolts comply with ASTM A-307 specifications and are galvanized in accordance with ASTM A-153, unless otherwise stated.
Nuts comply with ASTM A-563 specifications and are galvanized in accordance with ASTM A-153, unless otherwise stated.
All other galvanized material conforms with ASTM-123 & ASTM-525
All steel used in the manufacture is of Domestic Origin, "Made and Melted in the United States"
All Guardrail and Terminal Sections meets AASHTO M-180, All structural steel meets AASHTO M-183 & M270
All Bolts and Nuts are of Domestic Origin

UNL ACCOUNTING
RECEIVED
OCT - 3 2005

By: [signature]
Andrew Artar
Vice President of Sales and Marketing
Gregory Highway Products, Inc.

STATE OF OHIO: COUNTY OF STARK
Sworn to and subscribed before me, a Notary Public, by Andrew Artar this 28th day of September, 2005
[signature]
Dawn R. Batton
Notary Public, State of Ohio
My Commission Expires February 24, 2008

PAGE 01

Figure B-9. W-Beam Backup Plates Mill Certification, Test Nos. MGSBR-1 & MGSBR-2

Certified Test Report

NORTH STAR BLUESCOPE STEEL LLC
6767 County Road 9
Delta, Ohio 43515
Telephone: (888) 822-2112

Customer:
Lawson Steel, Inc.
3238 E. 82nd St.
Cleveland, OH 44104
Customer P.O.: 021336
Cust. Ref/Part # n/a

Order Number	171137	**Ordered Width (mm/in)**	1454.150 / 57.250
Line Item Number	1	**Ordered Gauge (mm/in)**	2.438 / 0.096
Heat Number	111813	**Material Description**	ASTM A568, 1018 CQ Modified
Coil Number	842536	**Production Date/Time**	Mar 1 2008 5:41PM

Heat Chemical Analysis (wt%)

Type	C	Mn	P	S	Si	Al	Cu	Cr	Ni	Mo	Sn	N	B	V	Nb	Ti	Ca
Heat	0.19	0.73	0.012	0.003	0.03	0.02	0.09	0.04	0.03	0.01	0.00	0.005	0.0000	0.000	0.000	0.002	0.002

Mechanical Test Report

All mechanical tests are performed on a sample from the tail of a coil.

Yield Strength	Tensile Strength	% Elongation in 2 inches
64,860 psi	83,230 psi	23.5%

This material has been produced and tested in accordance with each of the following applicable standards: ASTM E 1806-96, ASTM E 415-99a, ASTM A 751-01, ASTM A 370-03a, JIS Z2201:1998, JIS Z 2241:1998. This report certifies that the above test results are representative of those contained in the records of North Star BlueScope Steel LLC for the material identified in this test report and is intended to comply with the requirements of the material description. North Star BlueScope Steel LLC is not responsible for the inability of this material to meet specific applications. Any modifications to this certification as provided negates the validity of this test report. All reproductions must have the written approval of North Star BlueScope Steel. This product was manufactured, melted, cast, and hot-rolled (min. 3:1 reduction ratio), entirely within the U.S.A at North Star BlueScope Steel LLC, Delta, Ohio. This material was not exposed to Mercury or any alloy which is liquid at ambient temperature during processing or while in North Star BlueScope Steel LLC possession. Test equipment calibration certificates are available upon request. NIST traceability is established through test equipment calibration certificates which are available upon request. Uncertainty calculations are calculated in accordance with NIST standards and are maintained at a 4:1 ratio in accordance with NIST standards. Uncertainty data is available upon request.

Tim Mitchell — **Manager Quality Assurance and Technology**

Date Issued: Mar 12, 2008 11:00:32
Revision#: 01

Figure B-10. 6-ft 3-in. W-beam Rail Mill Certification, Test Nos. MGSBR-1 & MGSBR-2

06/04/2009 16:36 402-761-3288 MIDWEST MACHINERY

TRINITY HIGHWAY PRODUCTS, LLC.
Plant #55
425 E. O' CONNOR AVENUE
Lima, OH 45801
419-227-1296

MATERIAL CERTIFICATION

CUSTOMER: STOCK	DATE: March 10, 2009
	INVOICE #
	LOT NUMBER: 081128B
PART NUMBER: 3360G	QUANTITY: 107,458
DESCRIPTION: 5/8"x 1 ¼" GR BOLT	DATE SHIPPED:
SPECIFICATIONS: ASTM A307-A /A153	HEAT#: 7366484,7262312

MATERIAL CHEMISTRY

C	MN	P	S	SI	NI	CR	MO	CU	SN	V	AL	N	B	TI	NB
.13	.38	.007	.002	.18	.04	.06	.02	.03	.001	.002	.037	.004	.000	.000	.000
.15	.48	.006	.007	.06	.02	.04	.02	.02	.001	.002	.024	.0039	.000	.000	.000

PLATING AND/OR PROTECTIVE COATING

HOT DIP GALVANIZED (OZ. PER SQ. FT.)		1.25 Avg.

****THIS PRODUCT WAS MANUFACTURED IN THE UNITED STATES OF AMERICA****

THE MATERIAL USED IN THIS PRODUCT WAS MELTED AND MANUFACTURED IN THE U.S.A

WE HEREBY CERTIFY THAT TO THE BEST OF OUR KNOWLEDGE ALL INFORMATION CONTAINED HEREIN IS CORRECT.

TRINITY HIGHWAY PRODUCTS, LLC.

STATE OF OHIO, COUNTY OF ALLEN
SWORN AND SUBSCRIBED BEFORE ME
THIS 10TH DAY OF MARCH, 2009

NOTARY PUBLIC

425 E. O 'CONNOR AVENUE LIMA, OH 45801 419-227-1296

Figure B-11. ⅝-in. Guardrail Bolts Mill Certification, Test Nos. MGSBR-1 & MGSBR-2

GREGORY HIGHWAY PRODUCTS, INC.
4100 13th St. P.O. Box 80508
Canton, Ohio 44708

Customer: MIDWEST MACHINERY & SUPPLY CO.
2200 Y STREET

LINCOLN, NE. 68501

Test Report
B.O.L. # 33981
Customer P.O. 2042
Shipped to: MIDWEST MACHINERY & SUPPLY CO.
Project: STOCK
GHP Order No 2456AA

DATE SHIPPED: 06/10/08

HT # code	C.	Mn.	P.	S.	Si.	Tensile	Yield	Elong.	Quantity	Class	Type	Description
25835	0.13	0.66	0.013	0.019	0.25	70000	48000	24.3	750	A		6IN WF AT 8.5 X 6FT 0IN GR POST
25834	0.13	0.7	0.014	0.022	0.26	68000	48000	26.7				
44260	0.13	0.72	0.007	0.024	0.22	66000	45000	24.2				
25840	0.14	0.66	0.015	0.024	0.22	68000	47000	24.7				
13716	0.13	0.81	0.022	0.028	0.22	69000	47000	25.9				

Bolts comply with ASTM A-307 specifications and are galvanized in accordance with ASTM A-153, unless otherwise stated.
Nuts comply with ASTM A-563 specifications and are galvanized in accordance with ASTM A-153, unless otherwise stated.
All other galvanized material conforms with ASTM-123 & ASTM-525
All steel used in the manufacture is of Domestic Origin, "Made and Melted in the United States"
All Guardrail and Terminal Sections meets AASHTO M-180, All structural steel meets AASHTO M-183 & M270
All Bolts and Nuts are of Domestic Origin
All material fabricated in accordance with Nebraska Department of Transportation

By: Andrew Artar
Andrew Artar
Vice President of Sales and Marketing
Gregory Highway Products, Inc.

STATE OF OHIO: COUNTY OF STARK
Sworn to and subscribed before me, a Notary Public, by Andrew Artar this 11th day of June, 2008.

Notary Public, State of Ohio

DAWN R. BATTON
NOTARY PUBLIC
STATE OF OHIO
Comm. Expires
March 03, 2013
Recorded in
Portage County

SEAL
STATE OF OHIO

Figure B-12. W6x8.5 Posts Mill Certification, Test Nos. MGSBR-1 and MGSBR-2

06/04/2009 16:36 402-761-3288 MIDWEST MACHINERY PAGE 15/52

04/14/2009 10:14 FAX 740 681 4433 MID WEST FAB: ROCKMILL 002

35406

MID WEST
FABRICATING CO.

CERTIFICATE OF COMPLIANCE

WE CERTIFY THAT ALL BOLTS ARE MADE AND MANUFACTURED IN THE USA.

TO: TRINITY INDUSTRIES INC.
Plant #55
550 East Robb Ave. 419-222-7398
Lima, Ohio 45801
SHIP DATE: 4/13/2009
MANUFACTURER: MID WEST FABRICATING CO.
ASTM: A307A
GALVANIZERS: Bristol/Pilot/Columbus TO A-153 CLASS C

QTY	PART NO.	HEAT NO.	LOT NO.	P.O.NO.
5,250	5/8 X 10-6"	20060370	95055	130236BR25
2,625	5/8 X 10-6"	20060370	95052	130236BR25
28,500	5/8 X14-6"	7366618	85199	126266BR114

Signature D. Smith D. Smith
TITLE: QUALITY CONTROL
DATE: 4/13/2009

313 North Johns Street • Amanda, Ohio 43102 • 740/969-4411 • FAX: 740/969-4433

Figure B-13. ⅝x14-6 in. Bolts Certificate of Compliance, Test Nos. MGSBR-1 and MGSBR-2

GERDAU AMERISTEEL

ST PAUL STEEL MILL
1678 RED ROCK ROAD
ST PAUL MN 55119 USA

Chemical and Physical Test Report

MADE IN UNITED STATES

SHAPE + SIZE	GRADE	SPECIFICATION	SALES ORDER	CUST P.O. NUMBER
X13MM REBAR (# 4)	420 (60)	A615/A615M-07 Grade 60/420 A6/A6M-07		

HEAT I.D.	C	Mn	P	S	Si	Cu	Ni	Cr	Mo	V	Nb	N	Sn	Al	Ti	Ca	Zn	Co
M644029	.44	1.05	.021	.039	.22	.29	.13	.21	.041	.002	.001	.0115	.014	.002	.00200	.00140	.00100	.008

Mechanical Test: Yield 73500 PSI, 506.76 MPA Tensile: 113000 PSI, 779.11 MPA %El: 12.8/8in, 12.8/203.2mm Bend: OK Red R 155.69 Std Dev:0 Idl Diam: 2.176

Customer Requirements SOURCE: GA-STP CASTING: STRAND CAST

Comment: Steel not exposed to mercury, no weld repairment performed.
melt shop heat 81508M

SHAPE + SIZE	GRADE	SPECIFICATION	SALES ORDER	CUST P.O. NUMBER
X13MM REBAR (# 4)	420 (60)	A615/A615M-07 Grade 60/420 A6/A6M-07		

HEAT I.D.	C	Mn	P	S	Si	Cu	Ni	Cr	Mo	V	Nb	N	Sn	Al	Ti	Ca	Zn	Co
M644030	.44	1.08	.017	.041	.20	.29	.11	.19	.034	.001	.001	.0079	.018	.001	.00100	.00120	.00100	.006

Mechanical Test: Yield 70000 PSI, 482.63 MPA Tensile: 108000 PSI, 744.63 MPA %El: 15.6/8in, 15.6/203.2mm Bend: OK Red R 155.69 Std Dev:0 Idl Diam: 2.102

Customer Requirements SOURCE: GA-STP CASTING: STRAND CAST

Comment: Steel not exposed to mercury, no weld repairment performed.
melt shop heat 81500M

This material, including the billets, was produced and manufactured in the United States of America

Bhaskar Yalamanchili
Quality Director
Gerdau Ameristeel

THE ABOVE FIGURES ARE CERTIFIED EXTRACTS FROM THE ORIGINAL CHEMICAL AND PHYSICAL TEST RECORDS AS CONTAINED IN THE PERMANENT RECORDS OF COMPANY.

Mgr. Metallurg. Svcs.
ST PAUL STEEL MILL

Figure B-14. No. 4 Rebar Mill Certification, Test Nos. MGSBR-1 and MGSBR-2

B/L# 442174

NUCOR STEEL
A Division of NUCOR Corporation
JEWETT, TEXAS 75846 PH (903) 626-4461

CERTIFIED MILL TEST REPORT

00000
REGAL METALS INTERNATIONAL
106 SENTRY DRIVE

MANSFIELD TX 76063

43065
REGAL METALS INTERNATIONAL

TX

SIZE GRADE	HEAT #	C	Mn	Si	S	P	V	Nb	Cu	Cr	Ni	Mo	Sn	Bend Test
NO.5 REBAR / 16 MM METRIC	403-0645	.410	1.070	.220	.053	.012	.004	.001	.370	.140	.130	.038	.013	OK

ASTM A615-06/GR60/420MPA
PO# - 35949

Tensile 1: 100800 Yield 1: 66100 Elong% 1: 13
Tensile 2: 103100 Yield 2: 66000 Elong% 2: 13

ELONGATION IN 8 INCH SCALE
MELTED AND MANUFACTURED IN U.S.A.

ALL MATERIAL STRAND CAST

CHIEF METALLURGIST
Ben Cave
By CARMELA

Figure B-15. No. 5 Rebar Mill Certification, Test Nos. MGSBR-1 and MGSBR-2

Rocky Mountain Steel Mills

P.O. Box 316
Pueblo, CO 81002 USA

MATERIAL TEST REPORT

Date Printed: 30–AUG–08

Date Shipped: 30–AUG–08 **Product:** DEF 13mm #4 **Specification:** ASTM–A–615M–07 GR420 / ASTM–A–706M–0

FWIP: 52815322 **Customer:** CONCRETE INDUSTRIES INC **Cust. PO:** 72784

CHEMICAL ANALYSIS (Heat chemistry entered 08/08/08)

Heat Number	C	Mn	P	S	Si	Cu	Ni	Cr	Mo	Al	V	B	Cb	Sn	N	Ti
111283	0.27	1.20	0.019	0.035	0.22	0.26	0.08	0.11	0.024	0.004	0.045		0.010	0.013		

MECHANICAL PROPERTIES

Heat Number	Sample No.	Yield (Psi)	Ultimate (Psi)	Elongation (%)	Reduction (%)	Bend	Wt/ft
111283	01	65706	99250	15.4		ok	0.670
111283	02	65796	98410	14.9		ok	0.669

ALL MELTING AND MANUFACTURING PROCESSES OF THE MATERIAL SUBJECT TO THIS TEST CERTIFICATE OCCURRED IN THE UNITED STATES OF AMERICA.

THIS MATERIAL HAS BEEN PRODUCED AND TESTED IN ACCORDANCE WITH THE REQUIREMENTS OF THE APPLICABLE SPECIFICATIONS. WE HEREBY CERTIFY THAT THE ABOVE TEST RESULTS REPRESENT THOSE CONTAINED IN THE RECORDS OF THE COMPANY.

Mark Espanel

Quality Assurance Department

Figure B-16. No. 4 Dowels Mill Certification, Test Nos. MGSBR-1 and MGSBR-2

GERDAU AMERISTEEL

SAND SPRINGS STEEL MILL
P.O. BOX 218
SAND SPRINGS OK 74063 USA
(918) 245-1335

Chemical and Physical Test Report

MADE IN UNITED STATES

OK-032242

SHIP TO	INVOICE TO	SHIP DATE
NEBCO, INC. STEEL DIVISION HAVELOCK, NE 68521	CONCRETE INDUSTRIES INC PO BOX 29529 LINCOLN, NE 68529-0529	08/14/08 CUST. ACCOUNT NO 60052172

PRODUCED IN: SAND SPRINGS

SHAPE + SIZE	GRADE	SPECIFICATION	SALES ORDER	CUST P.O. NUMBER
X19MM REBAR (# 6)	420 (60)	ASTM A615/A615M AASHTO M31	8088414-01	72546-01

HEAT I.D.	C	Mn	P	S	Si	Cu	Ni	Cr	Mo	V	Nb	N	Sn
0819460	.37	1.13	.013	.028	.18	.27	.12	.20	.060	.006	.002	.0110	.012

Mechanical Test: Yield 70100 PSI, 483.32 MPA Tensile: 107900 PSI, 743.94 MPA %El: 12.0/8in, 12.0/203.2mm Bend: OK

PRODUCED IN: SAND SPRINGS

SHAPE + SIZE	GRADE	SPECIFICATION	SALES ORDER	CUST P.O. NUMBER
X19MM REBAR (# 6)	420 (60)	ASTM A615/A615M AASHTO M31	8088414-01	72546-01

HEAT I.D.	C	Mn	P	S	Si	Cu	Ni	Cr	Mo	V	Nb	N	Sn
0826506	.38	1.17	.015	.028	.22	.27	.13	.15	.040	.005	.001	.0113	.013

Mechanical Test: Yield 64900 PSI, 447.47 MPA Tensile: 103300 PSI, 712.23 MPA %El: 11.0/8in, 11.0/203.2mm Bend: OK

This material, including the billets, was produced and manufactured in the United States of America

Bhaskar Yalamanchili
Quality Director
Gerdau Ameristeel

THE ABOVE FIGURES ARE CERTIFIED EXTRACTS FROM THE ORIGINAL CHEMICAL AND PHYSICAL TEST RECORDS AS CONTAINED IN THE PERMANENT RECORDS OF COMPANY.

Mgr. Metallurg. Svcs.
SAND SPRINGS STEEL MILL

Seller warrants that all material furnished shall comply with specifications subject to standard published manufacturing variations. NO OTHER WARRANTIES, EXPRESSED OR IMPLIED, ARE MADE BY THE SELLER, AND SPECIFICALLY EXCLUDED ARE WARRANTIES OF MERCHANTABILITY AND FITNESS FOR A PARTICULAR PURPOSE.
In no event shall seller be liable for indirect, consequential or punitive damages arising out of or related to the materials furnished by seller.
Any claim for damages for materials that do not conform to specifications must be made from buyer to seller immediately after delivery of same in order to allow the seller the opportunity to inspect the material in question.

Figure B-17. No. 6 Rebar Mill Certification, Test Nos. MGSBR-1 and MGSBR-2

Atlas ABC Corp (Atlas Tube Chicago)
1855 East 122nd Street
Chicago, Illinois, USA
60633
Tel: 773-646-4500
Fax: 773-646-6128

Ref.B/L: 80238779
Date: 05.16.2007
Customer: 179

TUBE

MATERIAL TEST REPORT

Sold to

Steel & Pipe Supply Compan
PO Box 1688
MANHATTAN KS 66505
USA

Shipped to

Steel & Pipe Supply Compan
401 New Century Parkway
NEW CENTURY KS 66031
USA

Material: 2.0x2.0x188x20'0"0(10x5). **Material No:** 200201882000 **Made in:** USA
Melted & Manufactured in USA
Sales order: 303317 **Purchase Order:** C450001188 **Cust Material #:** 6520018820

Heat No	C	Mn	P	S	Si	Al	Cu	Cb	Mo	Ni	Cr	V
D40221	0.150	0.460	0.012	0.009	0.007	0.035	0.010	0.001	0.002	0.010	0.020	0.001

Bundle No	Yield	Tensile	Eln.2in	Certification
M600021778	068030 Psi	070270 Psi	42 %	ASTM A500-03A GRADE C & B

Material Note:
Sales Or.Note:

Material: 2.0x2.0x250x24'0"0(10x5). **Material No:** 200202502400 **Made in:** USA
Melted & Manufactured in USA
Sales order: 303315 **Purchase Order:** C450001188 **Cust Material #:** 6520025024

Heat No	C	Mn	P	S	Si	Al	Cu	Cb	Mo	Ni	Cr	V
T42158	0.200	0.720	0.010	0.008	0.022	0.041	0.030	0.001	0.004	0.010	0.040	0.001

Bundle No	Yield	Tensile	Eln.2in	Certification
M700038748	061600 Psi	074400 Psi	33 %	ASTM A500-03A GRADE C & B

Material Note:
Sales Or.Note:

Material: 4.0x4.0x375x24'0"0(5x3). **Material No:** 400403752400 **Made in:** USA
Sales order: 303006 **Purchase Order:** C450001184 **Cust Material #:** 6540037524

Heat No	C	Mn	P	S	Si	Al	Cu	Cb	Mo	Ni	Cr	V
1566G	0.200	0.820	0.006	0.006	0.030	0.027	0.030	0.001	0.010	0.010	0.020	0.005

Bundle No	Yield	Tensile	Eln.2in	Certification
0001654992	000000 Psi	000000 Psi	%	ASTM A500-03A GRADE C & B

Material Note:
Sales Or.Note:

received 4/28/09

Authorized by Quality Assurance: Greg Dardarine

Page : 1 Of 3

Steel Tube Institute OF NORTH AMERICA

Metals Service Center Institute

Figure B-18. Tube Housing Mill Certification, Test Nos. MGSBR-1 and MGSBR-2

Bill To: REGAL METALS INTRNATIONAL INC 207 SENTRY DRIVE MANSFIELD TX 76063 US	Ship To: 1 REGAL METALS INTERNATIONAL, IN 207 Sentry Drive MANSFIELD TX 76017 US	Order Date:12/19/2008 PO No:38023 Mill Order No:3560836 Load No:1234864 Manifest No:1939387	**CERTIFIED MATERIAL TEST REPORT** **GERDAU AMERISTEEL** GERDAU AMERISTEEL Midlothian Mill 300 Ward Road Midlothian, TX 76065 (972)775-8241

SPECIFICATIONS	SIZE	GRADE	LENGTH	PRODUCT
ASTM A615/A615M-06	# 3 REBAR/10 MM / 10 MM	60/420	20 FT / 6.096 M	REBAR

HEAT NO: 11833790

CHEMICAL ANALYSIS

C	Mn	P	S	Si	Cu	Ni	Cr	Mo	Sn	V	Al	Nb
.44	.90	.010	.030	.30	.19	.08	.10	.027	.007	.003	.003	.016

PHYSICAL PROPERTIES

Yield Strength		Tensile Strength		Specimen Area		Elongation			Bend Test		ROA
KSI	MPa	KSI	MPa	Sq In	Sq cm	%	Gage Length		Dia.	Result	%
67.5	465.4	99.3	684.6	0.106	0.68	13.9	8 In	200 mm	3.5	PASS	

All manufacturing processes of this product, including electric arc MELTING and continuous CASTING, occurred in the U.S.A.
CMTR complies with EN 10204 3.1

"I hereby certify that the contents of this report are correct and accurate. All tests and operations performed by this material manufacturer or its sub-contractors, when applicable, are in compliance with the requirements of the material specifications and applicable purchaser designated requirements."

Signed: Tom L. Harrington Date: Dec. 22, 2008 Signed: ____________ Date: ________
Tom L. Harrington: Quality Assurance Manager Notary Public (if applicable)

Page: 1 of 1

Figure B-19. No. 3 Rebar Mill Certification, Test Nos. MGSBR-1 and MGSBR-2

CAUTION
FRESH CONCRETE

Body and or eye contact with fresh (moist) concrete should be avoided because it contains alkali and is caustic.

Ready Mixed Concrete Company

6200 Cornhusker Highway, P.O. Box 29288
Lincoln, Nebraska 68529
Telephone 402-434-1844

ANT	MIX CODE	YARDS	TRUCK	DRIVER	DESTINATION	CLASS	TIME	DATE	TICKET
4	24013000	8.00	0115		NTE		02:42PM	05/14/09	4102189

JSTOMER	JOB	CUSTOMER NAME	TAX CODE	PARTIAL	NIGHT R.	LOADS
00003		COD---MIDWEST ROADSIDE				1

ELIVERY ADDRESS	SPECIAL INSTRUCTIONS	P.O. NUMBER
4800 NW 35TH	N/ OF THE NO. GOODYEAR HANGER INSIDE FENCE	450-6250

LOAD QUANTITY	CUMULATIVE QUANTITY	ORDERED QUANTITY	PRODUCT CODE	PRODUCT DESCRIPTION		UNIT PRICE	AMOUNT
8.00	8.00	8.00	24013000	L-4000	4.00	91.25	730.00

SUBTOTAL	730.00
TAX	730.00
TOTAL	730.00

ATER ADDED ON JOB
CUSTOMER'S REQUEST 6 GAL. RECEIVED BY

TRUCK	USER LOGIN	DISP TICKET NUM	TICKET NUM	TICKET ID	TIME	DATE
0115	USER	4102189	122426	130355	14:42	05/14/2009

LOAD SIZE	MIX CODE	SEQ	LOAD ID
8.00 yd	24013000	W	131634

MATERIAL	DESIGN QTY	REQUIRED	BATCHED	VAR	% VAR	%MOISTURE	ACTUAL WAT
G47B	2098.0 lb	17186. lb	17140.	-46.0	-.27%	2.40 E	48.14 gl
L47B	913.0 lb	7340.5 lb	7320.0	-20.5	-.28%	0.50 M	4.36 gl
CEM1	611.0 lb	4888.0 lb	4875.0	-13.0	-.27%		
PROT	4.3 oz	34.4 oz	34.0	-0.4	-1.16%		
WATER	32.0 gl	211.4 gl	210.9	-0.5	-.24%		210.90 gl
WATER2	0.0 gl #	0.0 gl	0.0	0.0	0.00%		

NON-SIMULATED NUM BATCHES: 1
LOAD TOTAL: 31097 lb DESIGN W/C: 0.437 WATER/CEMENT: 0.451A DESIGN WATER: 256.0 gl , ACTUAL WATER: 263.4 gl
SLUMP: 4.00 "# WATER IN TRUCK: 0.0 gl

Figure B-20. Deck Concrete Material Certification, Test Nos. MGSBR-1 and MGSBR-2

Certified Analysis

Trinity Highway Products , LLC
425 E. O'Connor
Lima, OH
Customer: MIDWEST MACH.& SUPPLY CO.
P. O. BOX 81097

LINCOLN, NE 68501-1097
Project: STOCK

Order Number: 1108107
Customer PO: 2132
BOL Number: 48341
Document #: 1
Shipped To: NE
Use State: KS

As of: 5/22/09

Qty	Part#	Description	Spec	CL	TY	Heat Code/ Heat #	Yield	TS	Elg	C	Mn	P	S	Si	Cu	Cb	Cr	Vn	ACW
			M-180	A	2	C49037	64,600	88,600	21.2	0.210	0.880	0.010	0.000	0.030	0.080	0.000	0.060	0.010	4
25	736G	5'/TUBE SL/.188"X6"X8"FLA	A-500			Y85912	56,500	72,980	37.0	0.210	0.770	0.009	0.006	0.016	0.010	0.00	0.020	0.001	4
6	742G	6'0 TUBE SL/.188X8X6	A-500			Y85912	56,500	72,980	37.0	0.210	0.770	0.009	0.006	0.016	0.010	0.00	0.020	0.001	4
26	764G	1/4"X24"X24"SOIL PLATE	A-36			120039	46,660	73,630	26.9	0.190	0.520	0.012	0.003	0.020	0.090	0.00	0.040	0.000	4
12	923G	BRONSTAD 98" W/O	M-180	A	2	122209	63,590	82,010	26.6	0.190	0.730	0.015	0.004	0.020	0.110	0.00	0.040	0.000	4
4	927G	10/END SHOE/EXT	M-180	B	2	A814375	59,770	78,641	27.4	0.210	0.750	0.017	0.005	0.030	0.090	0.00	0.030	0.002	4

Upon delivery, all materials subject to Trinity Highway Products , LLC Storage Stain Policy No. LG-002.

ALL STEEL USED WAS MELTED AND MANUFACTURED IN USA AND COMPLIES WITH THE BUY AMERICA ACT.
ALL GUARDRAIL MEETS AASHTO M-180, ALL STRUCTURAL STEEL MEETS ASTM A36
ALL GALVANIZED MATERIAL CONFORMS WITH ASTM-123, UNLESS OTHERWISE STATED.
BOLTS COMPLY WITH ASTM A-307 SPECIFICATIONS AND ARE GALVANIZED IN ACCORDANCE WITH ASTM A-153, UNLESS OTHERWISE STATED.
NUTS COMPLY WITH ASTM A-563 SPECIFICATIONS AND ARE GALVANIZED IN ACCORDANCE WITH ASTM A-153, UNLESS OTHERWISE STATED.

3/4" DIA CABLE 6X19 ZINC COATED SWAGED END AISI C-1035 STEEL ANNEALED STUD 1" DIA ASTM 449 AASHTO M30, TYPE II BREAKING STRENGTH -- 49100 LB

State of Ohio, County of Allen. Sworn and subscribed before me this 22nd day of May, 2009
Notary Public: Sun Q Hanlins
Commission Expires 11 28 2012

Trinity Highway Products , LLC
Certified By:
Quality Assurance

4 of 7

MIDWEST MACHINERY

06/04/2009 16:35 402-751-3288

Figure B-21. Foundation Tubes Mill Certification, Test Nos. MGSBR-1 and MGSBR-2

S.L. Storey
LUMBER COMPANY, INC.

CERTIFICATE OF COMPLIANCE

SEPTEMBER 5, 2008

MIDWEST MACHINERY
MILFORD, NE

THE FOLLOWING MATERIAL DELIVERED ON 9/5/08 ON BILL OF LADING NUMBER 18805 HAS BEEN INSPECTED BEFORE AND AFTER TREATMENT AND IS IN FULL COMPLIANCE WITH APPLICABLE NEBRASKA DEPARTMENT OF ROADS REQUIREMENTS FOR SOUTHERN YELLOW PINE TIMBER GUARDRAIL COMPONENTS, PRESERVATIVE TREATED WITH CHROMATED-COPPER-ARSENATE (CCA-C) TO A MINIMUM RETENTION OF .60 LBS/CU.FT. THE ACCEPTANCE OF EACH PIECE BY COMPANY QUALITY CONTROL IS INDICATED BY A HAMMER BRAND ON THE END OF EACH PIECE.

MATERIAL	CHARGE #	DATE	RETENTION	QUANTITY
51/2x71/2-46" TB Bullnose	08-608	8/28/08	0.72	48

THIS CERTIFICATE APPLIES TO MATERIAL ORDERED FOR your order no.: 2066

FOR ANY INQUIRIES, PLEASE RETAIN THIS DOCUMENT FOR FUTURE REFERENCE.

THANK YOU FOR YOUR ORDER.

SINCERELY,

Karen L Story

Karen Storey

SIGNED BEFORE ME THIS 5 DAY OF SEPTEMBER 2008.

Notary: William S. Houston
Notary Public Floyd County Georgia
My Commission Expires Oct. 18, 2010

WILLIAM S. HOUSTON
NOTARY
PUBLIC
Exp. Oct. 18, 2010
FLOYD COUNTY, GA

Phone: 706-234-1605 P.O. Box 99, Armuchee, GA 30105 Fax: 706-235-8132

Figure B-22. BCT Posts Certificate of Compliance, Test Nos. MGSBR-1 and MGSBR-2

ıarge Report

ıt No. : 1

Address

. Storey Lumber Co.
5 Sike Storey Rd.
nuchee, GA 30105
: 706 234-1605
c706 235-8132

A Reg. No. 3008-36

Charge : 608
Treatment : Guardrail Type 1
Date : 8/28/08 8:49:33AM
Chemical : CCA
Target Retention : .60
Cylinder : 1 (9,090)
Tank : 3
Operator : Richard
Total Time : 2:06:57
Turn Around Time (min) : 1,017
Time/Date Off Drip Pad : 9:20 9/2

Total Board Ft : 5,030
Total Cubic Ft : 381
Total Treatable Cubic Ft : 381
Displaced Volume In : 502
Displaced Volume Out : 571
Volume Start : 8,606
Volume Finish : 7,605
Volume Used : 1,001
Penetration Sampled : 0
Penetration Failed : 0
Treat By Tally : True

Step	Time Min	Time Max	Time Act	Pressure Min	Pressure Max	Pressure Act	Injection Min	Injection Max	Injection Act	Retention Min	Retention Max	Retention Act	Flow Rate Min	Flow Rate Max	Flow Rate Act	Time Ramp	Time Start	Time End	Volume End	Reason
Initial Vacuum	0	17	17	0	-23	-23	0.00	0.00	0.00	.00	.00	.00	0.00	0.00	0.00	0	8:49:33	9:06:35	8,601	Time
Fill	0	10	7	0	-23	6	0.00	0.00	0.00	.00	.00	.00	0.00	0.00	0.00	0	9:06:35	9:13:16	3,271	Full
Raise Press	0	2	1	0	75	78	0.00	0.00	0.00	.00	.00	.00	0.00	0.00	0.00	0	9:13:16	9:13:55	2,974	PSI
Pressure	1	45	45	75	140	120	0.00	3.20	0.00	.00	.00	.00	0.00	0.00	0.01	1	9:13:56	9:58:58	2,239	Time
Press Relief	0	1	1	0	25	18	0.00	0.00	0.00	.00	.00	.00	0.00	0.00	0.00	1	9:58:58	9:59:56	2,282	PSI
Empty	0	10	7	0	0	-1	0.00	0.00	4.17	.00	.00	.70	0.00	0.00	0.00	0	9:59:57	10:07:21	7,102	Empty
Final Vacuum	0	45	45	0	-29	-26	0.00	1.75	2.79	.00	.00	.47	0.00	0.00	0.01	0	10:07:21	10:52:23	7,598	Time
Final Empty	0	1	2	-1	-1	-1	0.00	0.00	2.78	.00	.00	.46	0.00	0.00	0.00	0	10:52:23	10:54:27	7,603	Empty
Finish	0	1	1	0	-1	0	0.00	0.00	2.77	.00	.00	.46	0.00	0.00	0.00	0	10:54:28	10:55:30	7,605	Time

Chemical	Solution Percent Start	Solution Percent Finish	Lbs. Per Gallon Start	Lbs. Per Gallon Finish	Lbs. Per Gallon Absorbed	Total Lbs. Gauge	Total Lbs. Absorbed	Retention Gauge	Retention Absorbed	Assay Min Retn	Assay Wood
CCA	1.95 %	1.95 %	.1668	.1668	.1670	167	167	.483	.483	-	-
Totals :	1.95 %	1.95 %	.1668	.1668	.1670	167	167	.483	.483	.60	-

Additive List

Additives	Solution %

Automatic Mix Information

Chemical	Current Value	Target Value	Required	Actual	Difference
Water	7,518 Gals.	- Gals.	1,055 Gals.	1,046 Gals.	-9 Gals.
CCA	1.95 %	1.95 %	27 Gals.	27 Gals.	- Gals.

1 021.001044.60 Pieces: 84 Packs/Size : 2 @ 42 Desc: 6 x 8 x 6-6 Line Post S4S Kansas BF: 2,184 CF: 168 HW: - % Moist. Cont.: - %
Std.: .60 Mill: Cust Num: None Retreat?: False Chg#: 0 Species: SYP Rem1: None

2 021.001009.60 Pieces: 168 Packs/Size : 1 @ 168 Desc: 6 x 8 x 0-14 Blockout S4S BF: 780 CF: 67 HW: - % Moist. Cont.: - %
Std.: .60 Mill: Cust Num: None Retreat?: False Chg#: 0 Species: SYP Rem1: None

3 9999 Pieces: 168 Packs/Size : 1 @ 168 Desc: 6 x 8 x 0-23 Rub Block S4S CD - Kansas BF: 1,269 CF: 97 ... Moist. Cont.: - %
Std.: .60 Mill: Cust Num: None Retreat?: False Chg#: 0 Species: SYP

4 9999 Pieces: 48 Packs/Size : 1 @ 48 Desc: 5-1/2 x 7-1/2 x 0-46 TB Bullnose NE BF: 768 C
Std.: .60 Mill: Cust Num: None Retreat?: False Chg#: 0 Species: SYP

ANALYSIS REPORT

RETENTION

CR03 = 0.35 pcf
CU0 = 0.13 pcf
AS205 = 0.24 pcf

TOTAL RETENTION
0.72 pcf

ınted on: 9/2/08 8:37:36AM Plant Number : 1 Charge Number : 608

Figure B-23. BCT Posts Certificate of Compliance, Test Nos. MGSBR-1 and MGSBR-2

425 E. O'Connor
Lima, OH

Customer: MIDWEST MACH.& SUPPLY CO.
P. O. BOX 81097

LINCOLN, NE 68501-1097

Sales Order: 1093497
Customer PO: 2030
BOL # 43073
Document # 1

Print Date: 6/30/08
Project: RESALE
Shipped To: NE
Use State: KS

Trinity Highway Products. LLC

Certificate Of Compliance For Trinity Industries, Inc. ** SLOTTED RAIL TERMINAL **

NCHRP Report 350 Compliant

Pieces	Description
64	5/8"X10" GR BOLT A307
192	5/8"X18" GR BOLT A307
32	1" ROUND WASHER F844
64	1" HEX NUT A563
192	WD 6'0 POST 6X8 CRT
192	WD BLK 6X8X14 DR
64	NAIL 16d SRT
64	WD 3'9 POST 5.5X7.5 BAND
32	STRUT & YOKE ASSY
128	SLOT GUARD '98
32	3/8 X 3 X 4 PL WASHER

MGSBR

Ground Strut

090453-8

Upon delivery, all materials subject to Trinity Highway Products , LLC Storage Stain Policy No. LG-002.

ALL STEEL USED WAS MELTED AND MANUFACTURED IN USA AND COMPLIES WITH THE BUY AMERICA ACT
ALL GUARDRAIL MEETS AASHTO M-180, ALL STRUCTURAL STEEL MEETS ASTM A36
ALL OTHER GALVANIZED MATERIAL CONFORMS WITH ASTM-123.
BOLTS COMPLY WITH ASTM A-307 SPECIFICATIONS AND ARE GALVANIZED IN ACCORDANCE WITH ASTM A-153, UNLESS OTHERWISE STATED.
NUTS COMPLY WITH ASTM A-563 SPECIFICATIONS AND ARE GALVANIZED IN ACCORDANCE WITH ASTM A-153, UNLESS OTHERWISE STATED.
3/4" DIA CABLE 6X19 ZINC COATED SWAGED END AISI C-1035 STEEL ANNEALED STUD 1" DIA ASTM 449 AASHTO M30, TYPE II BREAKING STRENGTH – 49100 LB

State of Ohio, County of Allen. Sworn and Subscribed before me this 30th day of June, 2008

Notary Public:
Commission Expires

Trinity Highway Products, LLC
Certified By:

2 of 4

06/04/2009 16:36 402-761-3288

Figure B-24. Strut Assembly Certificate of Compliance, Test Nos. MGSBR-1 & MGSBR-2

Certified Analysis

Trinity Highway Products , LLC
2548 N.E. 28th St.
Ft Worth, TX
Customer: MIDWEST MACH.& SUPPLY CO.
P. O. BOX 81097

LINCOLN, NE 68501-1097

Project: RESALE

Order Number: 1095199
Customer PO: 2041
BOL Number: 24481
Document #: 1
Shipped To: NE
Use State: KS

As of: 6/20/08

Qty	Part#	Description	Spec	CL	TY	Heat Code/ Heat #	Yield	TS	Elg	C	Mn	P	S	Si	Cu	Cb	Cr	Vn	ACW
25	6G	12/6'3/S	M-180	A		84964	64,230	81,300	25.4	0.180	0.720	0.012	0.001	0.040	0.080	0.000	0.060	0.000	4
20	701A	.25X11.75X16 CAB ANC	A-36			4153095	44,900	60,800	34.0	0.240	0.750	0.012	0.003	0.020	0.020	0.000	0.040	0.002	4
10	742G	6'0 TUBE SL/.188X8X6	A-500			A8P1160	74,000	87,000	25.2	0.050	0.670	0.013	0.005	0.030	0.220	0.000	0.060	0.021	4
20	782G	5/8"X8"X8" BEAR PL/OF	A-36			6106195	46,700	69,900	23.5	0.180	0.830	0.010	0.005	0.020	0.230	0.000	0.070	0.006	4
40	907G	12/BUFFER/ROLLED	M-180	A		L0049	54,200	73,500	25.0	0.160	0.700	0.011	0.008	0.020	0.200	0.000	0.100	0.000	4

Upon delivery, all materials subject to Trinity Highway Products , LLC Storage Stain Policy No. LG-002.

ALL STEEL USED WAS MELTED AND MANUFACTURED IN USA AND COMPLIES WITH THE BUY AMERICA ACT.
ALL GUARDRAIL MEETS AASHTO M-180, ALL STRUCTURAL STEEL MEETS ASTM A36
ALL OTHER GALVANIZED MATERIAL CONFORMS WITH ASTM-123.
BOLTS COMPLY WITH ASTM A-307 SPECIFICATIONS AND ARE GALVANIZED IN ACCORDANCE WITH ASTM A-153, UNLESS OTHERWISE STATED.
NUTS COMPLY WITH ASTM A-563 SPECIFICATIONS AND ARE GALVANIZED IN ACCORDANCE WITH ASTM A-153, UNLESS OTHERWISE STATED.

3/4" DIA CABLE 6X19 ZINC COATED SWAGED END AISI C-1035 STEEL ANNEALED STUD 1" DIA ASTM 449 AASHTO M30, TYPE II BREAKING STRENGTH – 49100 LB

State of Texas, County of Tarrant. Sworn and subscribed before me this 20th day of June, 2008

Notary Public:
Commission Expires

RACHEL R. MEDINA
Notary Public
State of Texas
My Commission Expires

Trinity Highway Products , LLC
Certified By:

Stefanie Onnol.a

Figure B-25. Anchor Bracket Assembly Mill Certification, Test Nos. MGSBR-1 and MGSBR-2

EXLTUBE

905 ATLANTIC STREET, NORTH KANSAS CITY, MO 64116 1-816-474-5210 TOLL FREE 1-800-892-TUBE

STEEL VENTURES, LLC dba EXLTUBE

CERTIFIED TEST REPORT

Customer:	Size:	Spec No:	Date:
SPS - New Century 401 New Century Parkway New Century KS 66031	02.375	ASTM A500-07, A53E-07	05/22/2008
	Gauge: .154	Grade: A500B,C, A53BNT	Customer Order No: 4500104158
			S/L No: 81162893

SLEEVE MAT
CRT

Heat No	Yield P.S.I.	Tensile P.S.I.	Elongation % 2 Inch
280638	61,500	66,400	23.00

Heat No	C	MN	P	S	SI	CU	NI	CR	MO	V
280638	0.040	0.330	0.010	0.000	0.034	0.088	0.039	0.042	0.015	0.003

We hereby certify that the above material was manufactured in the U.S.A and that all test results shown in this report are correct as contained in the records of our company. All testing and manufacturing is in accordance to A.S.T.M. parameters encompassed within the scope of the specifications denoted in the specification and grade tiles above.

BNT=Grade B not tested - meets tensile properties ONLY.

STEEL VENTURES, LLC dba EXLTUBE

Steve Frerichs
Quality Assurance Manager

104158

Figure B-26. BCT Hole Insert Mill Certification, Test Nos. MGSBR-1 and MGSBR-2

06/04/2009 16:36 402-761-3288 MIDWEST MACHINERY PAGE 08/32

MID WEST
FABRICATING CO.

CERTIFICATE OF COMPLIANCE

WE CERTIFY THAT ALL BOLTS ARE MADE AND MANUFACTURED IN THE USA.

TO: TRINITY INDUSTRIES INC.
Plant #55
425 E. O'Connor 419-222-7398
Lima,Ohio 45801
SHIP DATE:.11/6/2008
MANUFACTURER: MID WEST FABRICATING CO.
ASTM: A307A
GALVANIZERS: Columbus/Piolt TO A-153 CLASS C

QTY	PART NO.	HEAT NO.	LOT NO.	P.O.NO.
3,524	5/8 X 10-6"	7261134	85204	126266BR80
1,076	5/8 X 10-6"	7261134	85204	126266BR78
8,900	5/8 X 10-6"	7261134	85204	126266BR74
YIG 4,500	5/8 X 10-6"	7261611 X	85217	126266BR74
2,550	5/8 X 10W-6"	7261286	85180	126266BR84
4,500	5/8 X 14-6"	7366618	85199	126266BR68
6,000	5/8 X 18-6"	7366618	85157	126266BR84
1,536	5/8 X 18-6"	7366618	85157	126266BR74
130	5/8 X 18-6"	7366618	85156	126266BR74
2,964	5/8 X 18-6"	7366618	85149	126266BR74
4,370	5/8 X 18-6"	7261611	85146	126266BR74
400	5/8 X 3.5"	5978691	85016	126266BR82

Signature D. Smith D. Smith
TITLE: QUALITY CONTROL
DATE: 11/6/2008

313 North Johns Street • Amanda, Ohio 43102 • 740/969-4411 • FAX: 740/969-4433

Figure B-27. Guardrail Bolts Certificate of Compliance, Test Nos. MGSBR-1 & MGSBR-2

425 E. O'Connor
Lima, OH

Customer: MIDWEST MACH.& SUPPLY CO.
P. O. BOX 81097

LINCOLN, NE 68501-1097

Sales Order: 1093497
Customer PO: 2030
BOL # 43073
Document # 1

Print Date: 6/30/08
Project: RESALE
Shipped To: NE
Use State: KS

Trinity Highway Products. LLC

Certificate Of Compliance For Trinity Industries, Inc. ** SLOTTED RAIL TERMINAL **

NCHRP Report 350 Compliant

Pieces	Description
32	12/12'6/S SRT-1
32	12/25'0/SPEC/S SRT-2
32	3/16X12.5X16 CAB ANC BRKT
32	2" X 5 1/2" PIPE (LONG)
64	6'0 TUBE SL/.188X8X6
32	5/8 X 6 X 8 BEARING PLATE
32	12/BUFFER/ROLLED
32	CBL 3/4X6'6/DBL SWG/NOHWD
640	5/8" RD WASHER 1 3/4 OD
1,728	5/8" GR HEX NUT
1,152	5/8"X1.25" GR BOLT
256	5/8"X1.5" HEX BOLT A307
64	5/8"X9.5" HEX BOLT A307

MGSBR

5/8" x 9.5" Hex bolt A307
090453-11

5/8" washer 1 3/4" OD
090453-15

[redacted]

Upon delivery, all materials subject to Trinity Highway Products, LLC Storage Stain Policy No. LG-002.

ALL STEEL USED WAS MELTED AND MANUFACTURED IN USA AND COMPLIES WITH THE BUY AMERICA ACT
ALL GUARDRAIL MEETS AASHTO M-180, ALL STRUCTURAL STEEL MEETS ASTM A36
ALL OTHER GALVANIZED MATERIAL CONFORMS WITH ASTM-123.
BOLTS COMPLY WITH ASTM A-307 SPECIFICATIONS AND ARE GALVANIZED IN ACCORDANCE WITH ASTM A-153, UNLESS OTHERWISE STATED.
NUTS COMPLY WITH ASTM A-563 SPECIFICATIONS AND ARE GALVANIZED IN ACCORDANCE WITH ASTM A-153, UNLESS OTHERWISE STATED.
3/4" DIA CABLE 6X19 ZINC COATED SWAGED END AISI C-1035 STEEL ANNEALED STUD 1" DIA ASTM 449 AASHTO M30, TYPE II BREAKING STRENGTH - 49100 LB
State of Ohio, County of Allen. Sworn and Subscribed before me this 30th day of June, 2008

Notary Public:
Commission Expires

Trinity Highway Products, LLC
Certified By:

Figure B-28. Terminal Certificate of Compliance, Test Nos. MGSBR-1 and MGSBR-2

06/04/2009 16:36 402-761-3288 MIDWEST MACHINERY PAGE 32/32

TRINITY HIGHWAY PRODUCTS, LLC.
425 E. O'CONNOR AVENUE
LIMA, OHIO 45801
419-227-1296

MATERIAL CERTIFICATION

CUSTOMER: STOCK	DATE: JANUARY 2, 2008 INVOICE #: LOT #: 061229B
PART NUMBER: 3380G	QUANTITY: 103,182
DESCRIPTION: 5/8" X 1 ½ HH BOLT	DATE SHIPPED:
SPECIFICATIONS: ASTM A307-A/A153	HEAT #: 443270 & 446650

MATERIAL CHEMISTY

C	MN	P	S	SI	CU	NI	CR	MO	AL	V	N	CB	SN	B	TI	NB
.09	.38	.006	.009	.100	.09	.06	.06	.02	.032	.001	.0060	.000	.005	.0001	.001	.001
.09	.39	.007	.010	.090	.08	.05	.07	.02	.023	.001	.0070	.000	.006	.0001	.001	.001

PLATING AND/OR PROTECTIVE COATING

HOT DIP GALVANIZING (OZ. PER SQ. FT.)	1.25 AVG.

****THIS PRODUCT WAS MANUFACTURED IN THE UNITED STATES OF AMERICA***

THE MATERIAL USED IN THIS PRODUCT WAS MELTED AND MANUFACTURED IN THE U.S.A.

WE HEREBY CERTIFY THAT TO THE BEST OF OUR KNOWLEDGE ALL INFORMATION CONTAINED HEREIN IS CORRECT.

TRINITY HIGHWAY PRODUCTS, LLC.

STATE OF OHIO, COUNTY OF ALLEN
SWORN AND SUBSCRIBED BEFORE ME
THIS 2ND DAY OF JANUARY, 2008

NOTARY PUBLIC

425 E. O'CONNOR AVENUE LIMA, OHIO 45801 419-227-1296

Figure B-29. ⅝-in. Hex Head Bolts Mill Certification, Test Nos. MGSBR-1 and MGSBR-2

WireCo
WorldGroup

April 2, 2008

Order No. 1596192

CERTIFICATION OF COMPLIANCE

This is to certify that the diameter, strand construction, minimum breaking strength, and wire coating weights for RP122260 3/4 6x19W RR A741 CL-A SC-US produced on SJR2227 are in accordance with ASTM A741-98(2003) titled "Standard Specification for Zinc Coated Steel Wire Rope and Fittings for Highway Guard Rail".

All wire and rope manufacturing processes occurred in the United States.
All steel used was melted and manufactured in the United States.

ACTUAL TEST DATA

MEASURED ROPE DIAMETER:	.750		
STRAND CONSTRUCTION:	19 WARRINGTON 1-6-(6+6)		
BREAKING STRENGTH:	69,000 pounds		Req'd. 42,800 pounds
ZINC COATING WEIGHTS (Class A):	Wire Dia.	Min. Oz/ft^2	Avg. Oz/ft^2
	.395"	N/A	.42
	.460"	.40	.43
	.540"	.40	.63
	.610"	.40	.45

WIRE ROPE CORPORATION OF AMERICA, INC.

Gilbert Smith
Administrator Engineering Information

12200 NW Ambassador Drive, Kansas City, MO 64163-1244
T 816-270-4700 F 816-270-4707 www.WireCoWorldGroup.com

AUG.12. 2008 6:34PM TRINITY SHIPPING 419 227 0019 NO.881
08/12/2008 16:59 402-761-3288 MIDWEST MACHINERY

Figure B-30. Anchor Cable Certificate of Compliance, Test Nos. MGSBR-1 and MGSBR-2

Appendix C. Vehicle Center of Gravity Determination

	MGSBR-1		Vehicle:	Ram 1500		
			Vehicle CG Determination			
VEHICLE	Equipment	Weight	Long CG	Vert CG	HOR M	Vert M
+	Unbalasted Truck(Curb)	5134	63.36414	28.1418	325311.5	144480
+	Brake receivers/wires	9	108	52.5	972	472.5
+	Brake Frame	5	36	24.5	180	122.5
+	Brake Cylinder (Nitrogen)	29	73	25	2117	725
+	Strobe/Brake Battery	4	67.5	29	270	116
+	Hub	20	0	15	0	300
+	CG Plate (EDRs)	8	72	29.5	576	236
-	Battery	-30	-8	39.5	240	-1185
-	Oil	-11	5.5	27	-60.5	-297
-	Interior	-81	52.5	23	-4252.5	-1863
-	Fuel	-164	114.5	19.5	-18778	-3198
-	Coolant	-4	-17.25	32.5	69	-130
-	Washer fluid	0	-18	32.5	0	0
BALLAST	Water	81	114.5	19.5	9274.5	1579.5
	Misc.	25	71	30	1775	750
	Misc.				0	0
					317694	142108.5
	TOTAL WEIGHT	5025			63.22269	28.2803

wheel base 140.5

Calculated Test Inertial Weight			
MASH Targets	Targets	CURRENT	Difference
Test Inertial Weight	5000	5025	25.0
Long CG	62	63.22	1.22269
Vert CG	28	28.28	0.28030

Note, Long. CG is measured from front axle of test vehicle

Curb Weight	Left	Right
Front	1444	1375
Rear	1145	1170
FRONT	2819	
REAR	2315	
TOTAL	5134	

Actual test inertial weight (from scales)	Left	Right
Front	1362	1385
Rear	1116	1142
FRONT	2747	
REAR	2258	
TOTAL	5005	

Figure C-1. Vehicle Mass Distribution, Test No. MGSBR-1

Test: **MGSBR-2** Vehicle: **Rio Sedan**

Vehicle CG Determination

VEHICLE	Equipment	Weight	Long CG	HOR M
+	Unbalasted Car	2408	34.49	83058
+	Brake receivers/wires	5	126	630
+	Brake Frame	6	21	126
+	Brake Cylinder	29	61	1769
+	Strobe Battery	6	60	360
+	Hub	15	0	0
+	CG Plate (EDRs)	10	37	370
+	DTS	25	61	1525
-	Battery	-27	-8	216
-	Oil	-6	-4.5	27
-	Interior	-50	41	-2050
-	Fuel	-8	73	-584
-	Coolant	-9	-17	153
-	Washer fluid	-4	-17	68
BALLAST	Water	21	73	1533
	Misc.			0
	Misc.			0
				87201
	TOTAL WEIGHT	2421		36.01859

wheel base 95.25

MASH targets		CURRENT	Difference
Test Inertial Weight	2420 (+/-)55	2421	1.0
Long CG	39 (+/-)4	36.02	-2.98141

Note, Long. CG is measured from front axle of test vehicle

Dummy = 166lbs.

Curb Weight	Left	Right
Front	766	770
Rear	431	441
FRONT	1536	
REAR	872	
TOTAL	2408	

Actual test inertial weight (from scales)

	Left	Right
Front	730	762
Rear	462	461
FRONT	1492	
REAR	923	
TOTAL	2415	

Figure C-2. Vehicle Mass Distribution, Test No. MGSBR-2

Appendix D. Vehicle Deformation Records

VEHICLE PRE/POST CRUSH
FLOORPAN - SET 1

TEST: MGSBR-1
VEHICLE: Ram 1500

Note: If impact is on driver side need to enter negative number for Y

POINT	X	Y	Z	X'	Y'	Z'	DEL X	DEL Y	DEL Z
1	30.25	-26	0	30.25	-26	0	0	0	0
2	32.75	-22.5	-0.25	32.75	-22	-0.25	0	0.5	0
3	34	-18	0.25	34	-18	0.25	0	0	0
4	32	-12.5	0	32	-12.25	0	0	0.25	0
5	29.25	-9	-0.25	29.5	-9.5	-0.25	0.25	-0.5	0
6	27.75	-27.5	-2.5	27.75	-27.5	-2.75	0	0	-0.25
7	29.5	-23	-3	29.5	-23.75	-3.25	0	-0.75	-0.25
8	29	-18.25	-3.5	29	-18.5	-3.75	0	-0.25	-0.25
9	28.25	-13	-4	28	-13	-4	-0.25	0	0
10	25.5	-8.25	-2.5	25.75	-8	-2.5	0.25	0.25	0
11	24.25	-27.75	-5.5	24	-28	-5.75	-0.25	-0.25	-0.25
12	23.75	-22.25	-6	23.75	-23	-6	0	-0.75	0
13	23.5	-14.25	-6.5	23.5	-14.75	-6.75	0	-0.5	-0.25
14	20.25	-8	-4	20	-8.5	-4	-0.25	-0.5	0
15	17.25	-27.25	-7.25	17.25	-28	-7.75	0	-0.75	-0.5
16	17.25	-17.5	-8	17	-18.25	-8	-0.25	-0.75	0
17	15.5	-9.25	-6	15.5	-9.5	-6	0	-0.25	0
18	13.75	-5.25	-1.5	13.75	-5	-1.5	0	0.25	0
19	11	-24.5	-7.5	11	-24.5	-7.75	0	0	-0.25
20	11	-15.75	-8	10.5	-15.5	-8	-0.5	0.25	0
21	8.5	-8.25	-2.75	8.5	-8	-2.75	0	0.25	0
22	7	-20.25	-8	6.75	-20.25	-8.25	-0.25	0	-0.25
23	4.75	-2.5	-3	4.75	-2.5	-3	0	0	0
24	0.75	-27	-3.5	0.75	-26.5	-3.75	0	0.5	-0.25
25	0.5	-20.75	-4	0.5	-20.5	-4.25	0	0.25	-0.25
26	0.5	-15	-4.25	0.5	-15	-4.5	0	0	-0.25
27	0.75	-6	-2.25	0.75	-6	-2.25	0	0	0
28							0	0	0
29							0	0	0
30							0	0	0
31							0	0	0

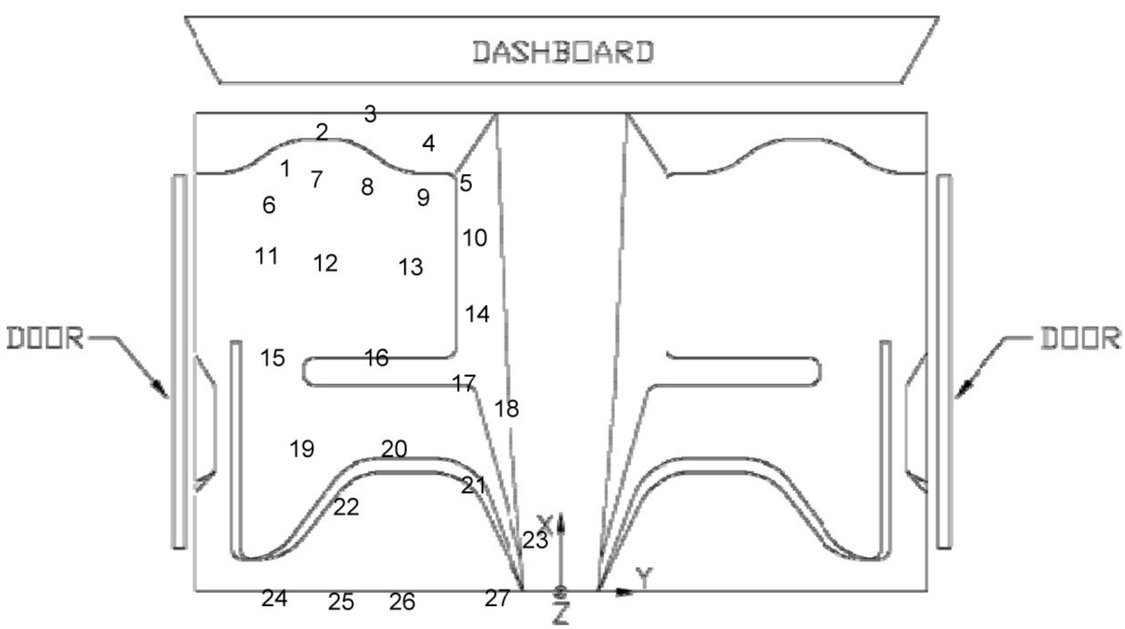

Figure D-1. Floor Pan Deformation Data – Set 1, Test No. MGSBR-1

VEHICLE PRE/POST CRUSH
FLOOR PAN - SET 2

TEST: MGSBR-1
VEHICLE: Ram 1500

Note: If impact is on driver side need to enter negative number for Y

POINT	X	Y	Z	X'	Y'	Z'	DEL X	DEL Y	DEL Z
1	NA	NA	-2.75	NA	NA	-2.5	#VALUE!	#VALUE!	0.25
2	NA	NA	-2.25	NA	NA	-2	#VALUE!	#VALUE!	0.25
3	NA	NA	-1.25	NA	NA	-1	#VALUE!	#VALUE!	0.25
4	NA	NA	-1	NA	NA	-0.5	#VALUE!	#VALUE!	0.5
5	NA	NA	-0.5	NA	NA	-0.25	#VALUE!	#VALUE!	0.25
6	NA	NA	-5.25	NA	NA	-5	#VALUE!	#VALUE!	0.25
7	NA	NA	-5.25	NA	NA	-5	#VALUE!	#VALUE!	0.25
8	NA	NA	-5.25	NA	NA	-4.75	#VALUE!	#VALUE!	0.5
9	NA	NA	-4.75	NA	NA	-4.25	#VALUE!	#VALUE!	0.5
10	NA	NA	-2.75	NA	NA	-2.5	#VALUE!	#VALUE!	0.25
11	NA	NA	-8.5	NA	NA	-8.25	#VALUE!	#VALUE!	0.25
12	NA	NA	-8	NA	NA	-7.75	#VALUE!	#VALUE!	0.25
13	NA	NA	-7.5	NA	NA	-7	#VALUE!	#VALUE!	0.5
14	NA	NA	-4.25	NA	NA	-4	#VALUE!	#VALUE!	0.25
15	NA	NA	-10.25	NA	NA	-10	#VALUE!	#VALUE!	0.25
16	NA	NA	-9.25	NA	NA	-9	#VALUE!	#VALUE!	0.25
17	NA	NA	-6	NA	NA	-5.75	#VALUE!	#VALUE!	0.25
18	NA	NA	-1.25	NA	NA	-1	#VALUE!	#VALUE!	0.25
19	NA	NA	-9.75	NA	NA	-9.5	#VALUE!	#VALUE!	0.25
20	NA	NA	-9	NA	NA	-8.75	#VALUE!	#VALUE!	0.25
21	NA	NA	-2.75	NA	NA	-2.5	#VALUE!	#VALUE!	0.25
22	NA	NA	-9.5	NA	NA	-9.25	#VALUE!	#VALUE!	0.25
23	NA	NA	-2	NA	NA	-2	#VALUE!	#VALUE!	0
24	NA	NA	-6	NA	NA	-6	#VALUE!	#VALUE!	0
25	NA	NA	-5.5	NA	NA	-5.5	#VALUE!	#VALUE!	0
26	NA	NA	-5	NA	NA	-5	#VALUE!	#VALUE!	0
27	NA	NA	-1.75	NA	NA	-1.5	#VALUE!	#VALUE!	0.25
28							0	0	0
29							0	0	0
30							0	0	0
31							0	0	0

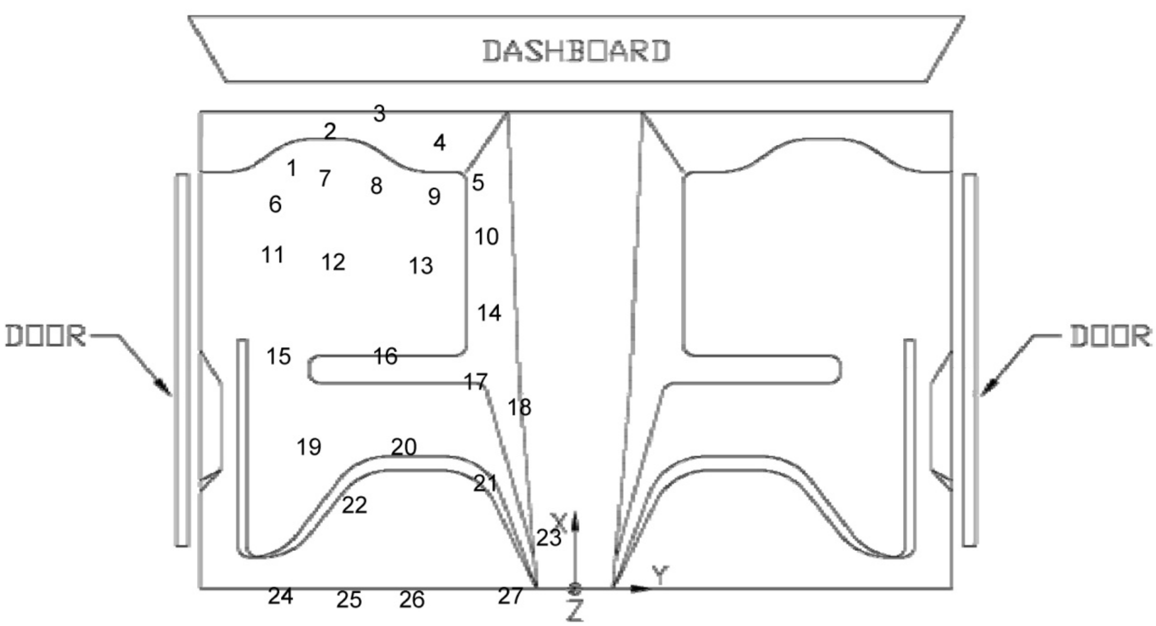

Figure D-2. Floor Pan Deformation Data – Set 2, Test No. MGSBR-1

VEHICLE PRE/POST CRUSH
INTERIOR CRUSH - SET 1

TEST: MGSBR-1
VEHICLE: Ram 1500

Note: If impact is on driver side need to enter negative number for Y

	POINT	X	Y	Z	X'	Y'	Z'	DEL X	DEL Y	DEL Z
DASH	A1	84.75	-15.75	-2.25	84.5	-15.25	-2.25	-0.25	0.5	0
	A2	86.5	-0.25	-1	86.5	-0.25	-1	0	0	0
	A3	84.75	14	-0.5	85	14	-0.25	0.25	0	0.25
	A4	70.75	-21.75	-0.75	70.5	-21.75	-0.75	-0.25	0	0
	A5	72.5	-1.25	-0.25	72.75	-1.25	-0.25	0.25	0	0
	A6	73.5	18.5	-1.5	74	18.5	1.5	0.5	0	3
SIDE PANEL	B1	25	-30.25	3	25	-32	2.75	0	-1.75	-0.25
	B2	21.5	-30.25	1.5	21.25	-32	1	-0.25	-1.75	-0.5
	B3	23	-30.25	-2	23.25	-32	-2.25	0.25	-1.75	-0.25
IMPACT SIDE DOOR	C1	-6	-40.25	19.75	-6.25	-40.5	19.5	-0.25	-0.25	-0.25
	C2	6.75	-40	19.25	6.25	-40.25	19	-0.5	-0.25	-0.25
	C3	1	-37.5	13.75	1	-38.25	13.5	0	-0.75	-0.25
	C4	-11.25	-36	8.25	-11.25	-36.5	8.25	0	-0.5	0
	C5	4	-35.5	8.5	4	-35.75	8.25	0	-0.25	-0.25
	C6	1.5	-34	0.75	1.5	-33.75	0.75	0	0.25	0
ROOF	D1	47.5	-20.5	8	47.5	-20.5	8	0	0	0
	D2	49.25	-10.5	8.5	49.5	-10.5	8.5	0.25	0	0
	D3	49.25	0	8.25	49.5	0	8.5	0.25	0	0.25
	D4	49	10.5	7.5	49.25	10.25	7.5	0.25	-0.25	0
	D5	47.25	20.75	6	47.5	20.75	6	0.25	0	0
	D6	37.5	-13.5	10.5	37.5	-13.5	10.75	0	0	0.25
	D7	37.25	-6	10.75	37.25	-6	11	0	0	0.25
	D8	37	0	10.5	37.25	0	10.75	0.25	0	0.25
	D9	35.75	13	9.5	36.5	13	9.5	0.75	0	0
	D10	26.25	-9.5	9	26.25	-9.5	9.25	0	0	0.25
	D11	26	-0.25	9	26.25	-0.25	9.25	0.25	0	0.25
	D12	25.75	9	8.5	26	9	8.75	0.25	0	0.25
	D13	10	-12	8.25	10	-12	8.25	0	0	0
	D14	9.25	-1.5	8.75	9.25	-1.5	8.75	0	0	0
	D15	10.75	13.25	8	11	13.5	8	0.25	0.25	0

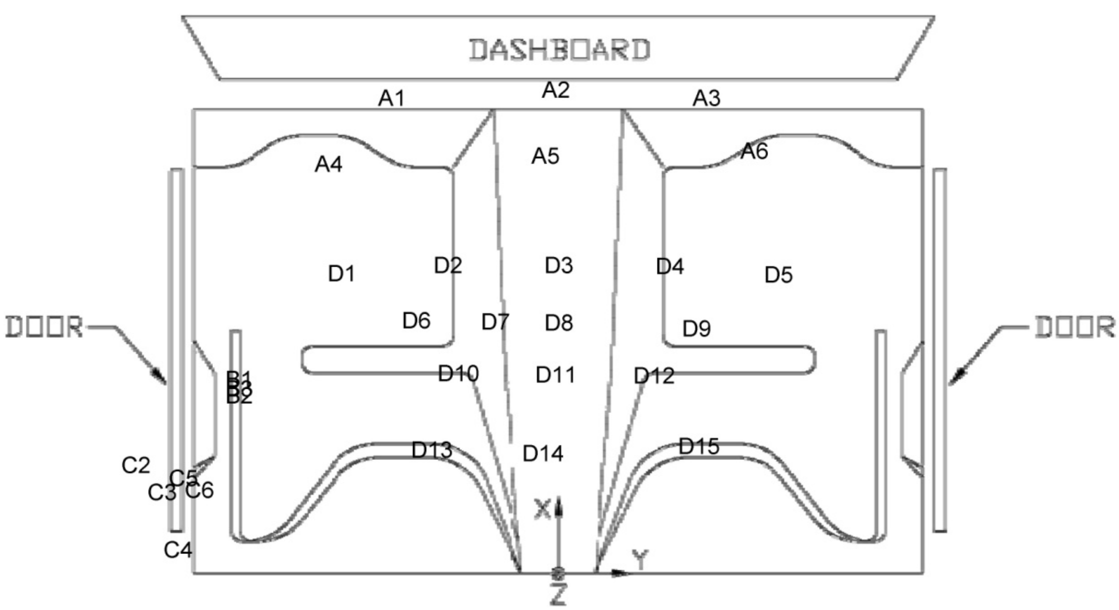

Figure D-3. Occupant Compartment Deformation Data – Set 1, Test No. MGSBR-1

VEHICLE PRE/POST CRUSH
INTERIOR CRUSH - SET 2

TEST: MGSBR-1
VEHICLE: Ram 1500

Note: If impact is on driver side need to enter negative number for Y

	POINT	X	Y	Z	X'	Y'	Z'	DEL X	DEL Y	DEL Z
DASH	A1	84.75	-15.75	NA	NA	NA	NA	#VALUE!	#VALUE!	#VALUE!
	A2	86.5	-0.25	NA	NA	NA	NA	#VALUE!	#VALUE!	#VALUE!
	A3	84.75	14	NA	NA	NA	NA	#VALUE!	#VALUE!	#VALUE!
	A4	70.75	-21.75	NA	NA	NA	NA	#VALUE!	#VALUE!	#VALUE!
	A5	72.5	-1.25	NA	NA	NA	NA	#VALUE!	#VALUE!	#VALUE!
	A6	73.5	18.5	NA	NA	NA	NA	#VALUE!	#VALUE!	#VALUE!
SIDE PANEL	B1	25	-30.25	-0.5	NA	NA	0	#VALUE!	#VALUE!	0.5
	B2	21.5	-30.25	-2.25	NA	NA	-1.5	#VALUE!	#VALUE!	0.75
	B3	23	-30.25	-5.5	NA	NA	-5.5	#VALUE!	#VALUE!	0
IMPACT SIDE DOOR	C1	-6	-40.25	16.25	NA	NA	16.5	#VALUE!	#VALUE!	0.25
	C2	6.75	-40	16	NA	NA	16	#VALUE!	#VALUE!	0
	C3	1	-37.5	10.25	NA	NA	10.5	#VALUE!	#VALUE!	0.25
	C4	-11.25	-36	5	NA	NA	5.25	#VALUE!	#VALUE!	0.25
	C5	4	-35.5	5	NA	NA	5.25	#VALUE!	#VALUE!	0.25
	C6	1.5	-34	-2.5	NA	NA	-2.25	#VALUE!	#VALUE!	0.25
ROOF	D1	47.5	-20.5	5.25	NA	NA	5.25	#VALUE!	#VALUE!	0
	D2	49.25	-10.5	6.25	NA	NA	6.25	#VALUE!	#VALUE!	0
	D3	49.25	0	6.75	NA	NA	6.5	#VALUE!	#VALUE!	-0.25
	D4	49	10.5	6.75	NA	NA	6.75	#VALUE!	#VALUE!	0
	D5	47.25	20.75	6.25	NA	NA	6.25	#VALUE!	#VALUE!	0
	D6	37.5	-13.5	8.5	NA	NA	8.25	#VALUE!	#VALUE!	-0.25
	D7	37.25	-6	9.25	NA	NA	9.25	#VALUE!	#VALUE!	0
	D8	37	0	9.25	NA	NA	9	#VALUE!	#VALUE!	-0.25
	D9	35.75	13	9	NA	NA	9	#VALUE!	#VALUE!	0
	D10	26.25	-9.5	7.75	NA	NA	7.75	#VALUE!	#VALUE!	0
	D11	26	-0.25	8.25	NA	NA	8.25	#VALUE!	#VALUE!	0
	D12	25.75	9	8	NA	NA	8	#VALUE!	#VALUE!	0
	D13	10	-12	7.75	NA	NA	8	#VALUE!	#VALUE!	0.25
	D14	9.25	-1.5	8	NA	NA	8	#VALUE!	#VALUE!	0
	D15	10.75	13.25	7.75	NA	NA	7.75	#VALUE!	#VALUE!	0

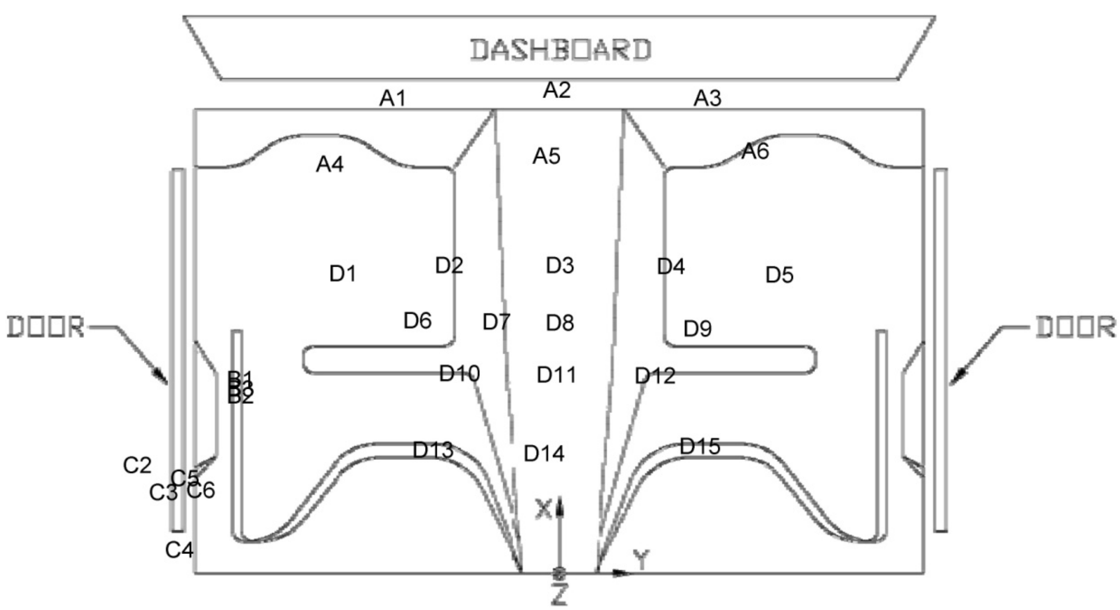

Figure D-4. Occupant Compartment Deformation Data – Set 2, Test No. MGSBR-1

Date:	6/23/2009	**Test Number:**	MGSBR-1		
Make:	Dodge	**Model:**	Ram 1500	**Year:**	2004

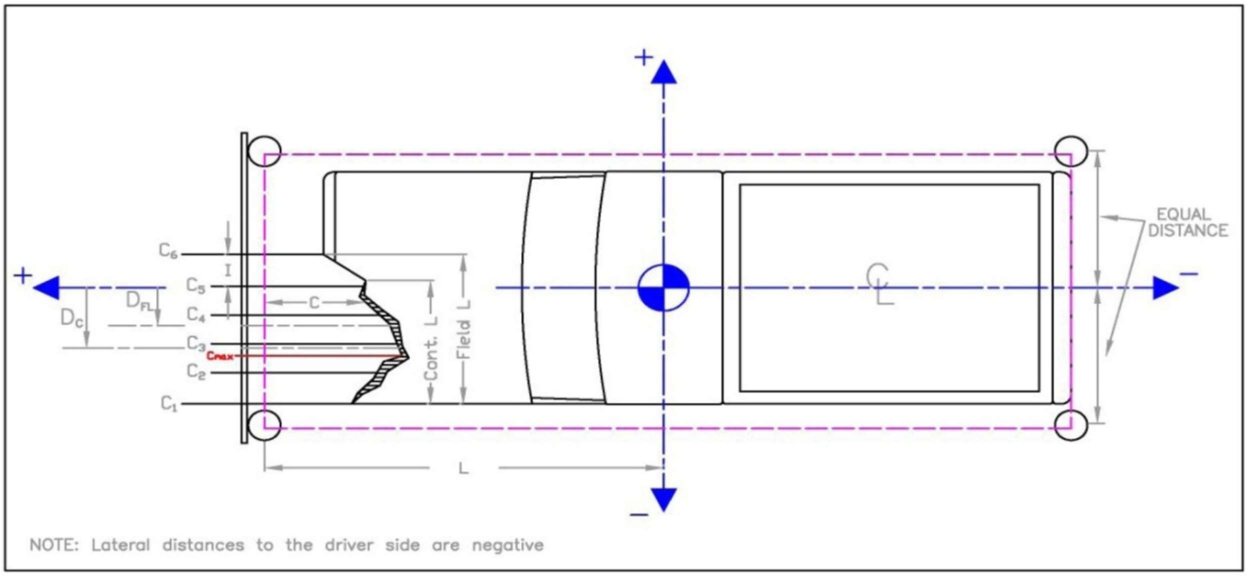

	in.	(mm)
Distance from C.G. to reference line - L_{REF}:	116.25	(2953)
Width of contact and induced crush - Field L:	55.875	(1419)
Crush measurement spacing interval (L/5) - I:	11.175	(284)
Distance from center of vehicle to center of Field L - D_{FL}:	-10.938	-(278)
Width of Contact Damage:	38.875	(987)
Distance from center of vehicle to center of contect damage - D_C:	19.4375	(494)

	Crush Measurement		Lateral Location		Original Profile Measurement		Dist. Between Ref. Lines		Actual Crush	
	in.	(mm)	in.	(mm)	in.	(mm)	in.	(mm)	in.	(mm)
C_1	NA	#######	-38.875	-(987)	29	(737)	3.52731	(90)	#######	#######
C_2	39.25	(997)	-27.7	-(704)	15.1563	(385)			20.5664	(522)
C_3	22.5	(572)	-16.525	-(420)	11.8906	(302)			7.08206	(180)
C_4	19.5	(495)	-5.35	-(136)	10.3438	(263)			5.62894	(143)
C_5	17	(432)	5.825	(148)	10.3594	(263)			3.11331	(79)
C_6	15.75	(400)	17	(432)	11.9375	(303)			0.28519	(7)
C_{MAX}	39.25	(997)	-27.7	-(704)	15.1563	(385)			20.5664	(522)

Figure D-5. Exterior Vehicle Crush (NASS) - Front, Test No. MGSBR-1

Date:	6/23/2009	**Test Number:**	MGSBR-1		
Make:	Dodge	**Model:**	Ram 1500	**Year:**	2004

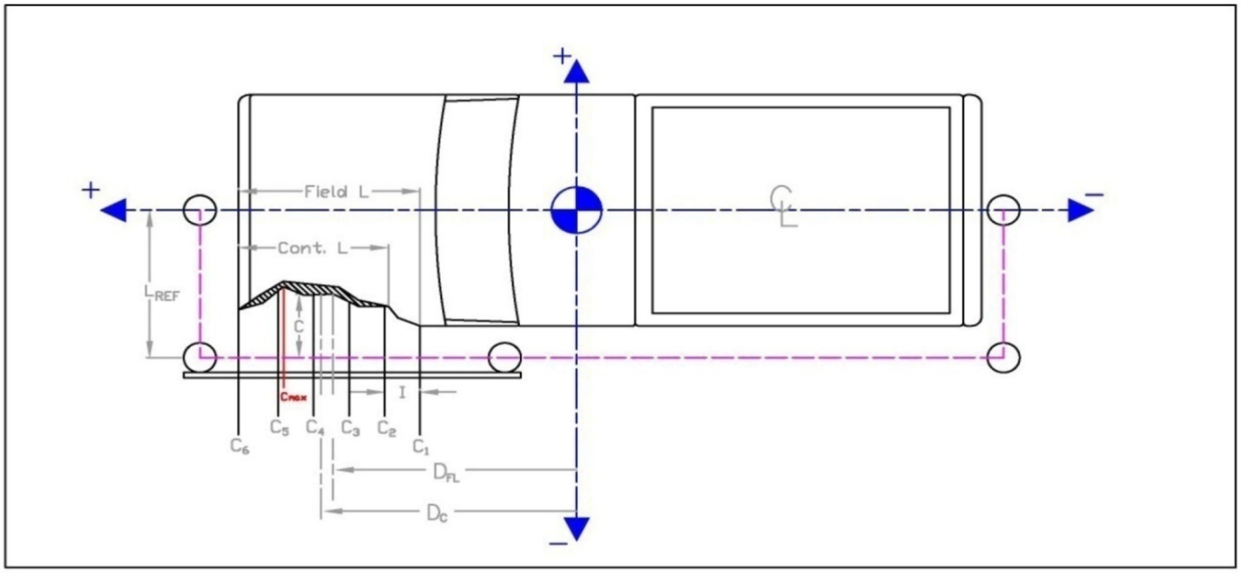

	in.	(mm)
Distance from centerline to reference line - L_{REF}:	47.75	(1213)
Width of contact and induced crush - Field L:	227.25	(5772)
Crush measurement spacing interval (L/5) - I:	45.45	(1154)
Distance from vehicle c.g. to center of Field L - D_{FL}:	-9.405	-(239)
Width of Contact Damage:	227.25	(5772)
Distance from vehicle c.g. to center of contect damage - D_C:	9.4	(239)

	Crush Measurement		Longitudinal Location		Original Profile Measurement		Dist. Between Ref. Lines		Actual	Crush
	in.	(mm)	in.	(mm)	in.	(mm)	in.	(mm)	in.	(mm)
C_1	14.5	(368)	-123.03	-(3125)	15.375	(391)	-2.25	-(57)	1.375	(35)
C_2	10.5	(267)	-77.58	-(1971)	10.5	(267)			2.25	(57)
C_3	8.25	(210)	-32.13	-(816)	11.6042	(295)			-1.1042	-(28)
C_4	9.5	(241)	13.32	(338)	11.25	(286)			0.5	(13)
C_5	NA	########	58.77	(1493)	10.5	(267)			#######	########
C_6	NA	########	104.22	(2647)	36.125	(918)			#######	########
C_{MAX}	20.5	(521)	71.5	(1816)	10.5	(267)			12.25	(311)

Figure D-6. Exterior Vehicle Crush (NASS) - Side, Test No. MGSBR-1

VEHICLE PRE/POST CRUSH
FLOORPAN - SET 1

TEST: MGSBR-2
VEHICLE: Rio Sedan

Note: If impact is on driver side need to enter negative number for Y

POINT	X	Y	Z	X'	Y'	Z'	DEL X	DEL Y	DEL Z
1	24.75	-23	-1.5	24	-22.75	-1.5	-0.75	0.25	0
2	27.5	-18.25	-1	26.75	-18.5	-1	-0.75	-0.25	0
3	30.5	-11	0	31	-10.75	0	0.5	0.25	0
4	30.5	-7.25	-2.25	30.75	-7.5	-2.25	0.25	-0.25	0
5	24.75	-22	-3.5	24.25	-21.5	-3.5	-0.5	0.5	0
6	26.75	-18.5	-3.75	26.5	-17.25	-4	-0.25	1.25	-0.25
7	28	-10	-5.25	28	-9.5	-5.5	0	0.5	-0.25
8	22.75	-22.5	-6.5	22.5	-21.75	-6.5	-0.25	0.75	0
9	24.5	-19	-6.75	24.25	-18.75	-7	-0.25	0.25	-0.25
10	25.75	-14	-7	25.5	-14	-7	-0.25	0	0
11	26.25	-10	-7	26.25	-10	-7	0	0	0
12	26.25	-6.5	-7.25	26.25	-6	-7.5	0	0.5	-0.25
13	20	-21.25	-8	20	-21	-8	0	0.25	0
14	20.5	-14.25	-8	20.25	-14	-8.25	-0.25	0.25	-0.25
15	20	-7.5	-9	20.25	-7.25	-9	0.25	0.25	0
16	16.75	-19.75	-8.25	16.5	-19.25	-8.25	-0.25	0.5	0
17	16.75	-14.5	-8.25	16.75	-14.25	-8.25	0	0.25	0
18	17.25	-10	-9	17.25	-10	-9	0	0	0
19	17	-5.25	-8.75	16.75	-5.5	-9	-0.25	-0.25	-0.25
20	11	-22	-7.5	10.75	-22.25	-7.5	-0.25	-0.25	0
21	11	-16.25	-7.75	11	-16	-8	0	0.25	-0.25
22	11.5	-10.5	-8.75	11.5	-10	-8.75	0	0.5	0
23	9.75	-2.25	-5.75	9.75	-2	-6	0	0.25	-0.25
24	5.75	-20	-7.75	5.5	-20	-8	-0.25	0	-0.25
25	6.25	-9	-8.5	6.25	-8.75	-8.5	0	0.25	0
26	5.5	-2.25	-5.25	5.5	-2.25	-5.5	0	0	-0.25
27	0.5	-19	-4.75	0.5	-19	-4.75	0	0	0
28	0.25	-11.5	-5.5	0.25	-11.25	-5.5	0	0.25	0
29							0	0	0
30							0	0	0
31							0	0	0

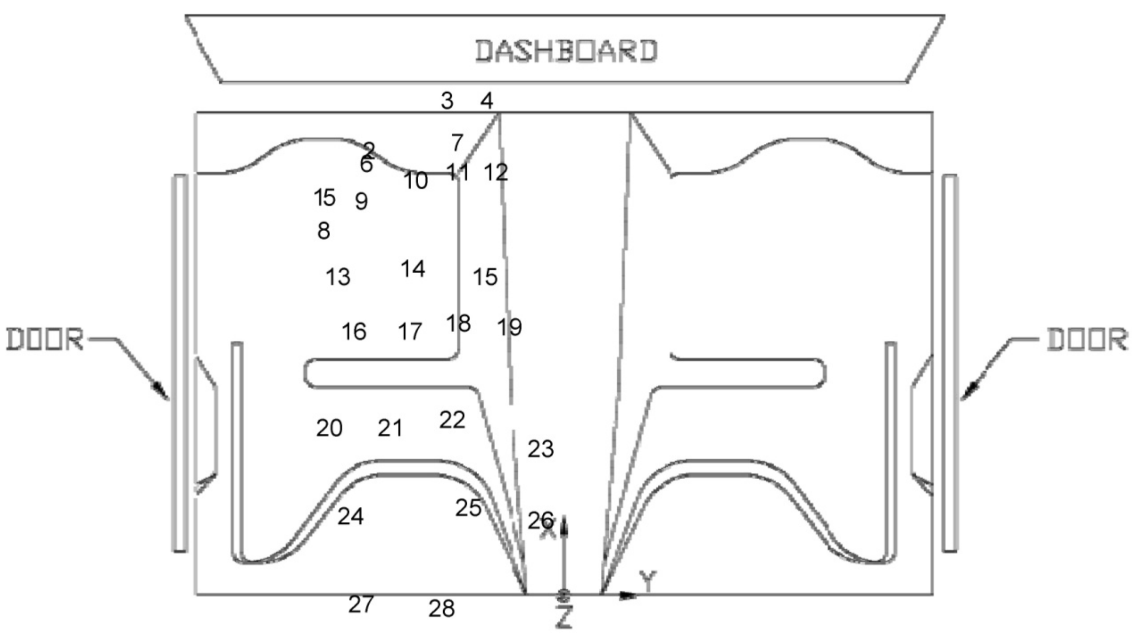

Figure D-7. Floor Pan Deformation Data – Set 1, Test No. MGSBR-2

VEHICLE PRE/POST CRUSH
FLOORPAN - SET 2

TEST: MGSBR-2
VEHICLE: Rio Sedan

Note: If impact is on driver side need to enter negative number for Y

POINT	X	Y	Z	X'	Y'	Z'	DEL X	DEL Y	DEL Z
1	24.75	-23	-2.5	NA	NA	-2.5	#VALUE!	#VALUE!	0
2	27.5	-18.25	-2	NA	NA	-2	#VALUE!	#VALUE!	0
3	30.5	-11	-0.5	NA	NA	-0.5	#VALUE!	#VALUE!	0
4	30.5	-7.25	-2.75	NA	NA	-3	#VALUE!	#VALUE!	-0.25
5	24.75	-22	-4.25	NA	NA	-4.5	#VALUE!	#VALUE!	-0.25
6	26.75	-18.5	-4.75	NA	NA	-4.75	#VALUE!	#VALUE!	0
7	28	-10	-5.75	NA	NA	-5.75	#VALUE!	#VALUE!	0
8	22.75	-22.5	-7.25	NA	NA	-7.5	#VALUE!	#VALUE!	-0.25
9	24.5	-19	-7.5	NA	NA	-7.75	#VALUE!	#VALUE!	-0.25
10	25.75	-14	-7.25	NA	NA	-7.5	#VALUE!	#VALUE!	-0.25
11	26.25	-10	-7.25	NA	NA	-7.5	#VALUE!	#VALUE!	-0.25
12	26.25	-6.5	-7.75	NA	NA	-8	#VALUE!	#VALUE!	-0.25
13	20	-21.25	-8.5	NA	NA	-8.75	#VALUE!	#VALUE!	-0.25
14	20.5	-14.25	-8.5	NA	NA	-8.75	#VALUE!	#VALUE!	-0.25
15	20	-7.5	-9	NA	NA	-9	#VALUE!	#VALUE!	0
16	16.75	-19.75	-8.75	NA	NA	-8.75	#VALUE!	#VALUE!	0
17	16.75	-14.5	-8.5	NA	NA	-8.75	#VALUE!	#VALUE!	-0.25
18	17.25	-10	-9	NA	NA	-9.25	#VALUE!	#VALUE!	-0.25
19	17	-5.25	-9	NA	NA	-9	#VALUE!	#VALUE!	0
20	11	-22	-8	NA	NA	-8	#VALUE!	#VALUE!	0
21	11	-16.25	-8	NA	NA	-8.25	#VALUE!	#VALUE!	-0.25
22	11.5	-10.5	-8.75	NA	NA	-9	#VALUE!	#VALUE!	-0.25
23	9.75	-2.25	-5.5	NA	NA	-5.5	#VALUE!	#VALUE!	0
24	5.75	-20	-8	NA	NA	-8.25	#VALUE!	#VALUE!	-0.25
25	6.25	-9	-8.25	NA	NA	-8.25	#VALUE!	#VALUE!	0
26	5.5	-2.25	-5	NA	NA	-5	#VALUE!	#VALUE!	0
27	0.5	-19	-4.75	NA	NA	-4.75	#VALUE!	#VALUE!	0
28	0.25	-11.5	-5	NA	NA	-5	#VALUE!	#VALUE!	0
29	NA	NA	NA	NA	NA	NA	#VALUE!	#VALUE!	#VALUE!
30	NA	NA	NA	NA	NA	NA	#VALUE!	#VALUE!	#VALUE!
31	NA	NA	NA	NA	NA	NA	#VALUE!	#VALUE!	#VALUE!

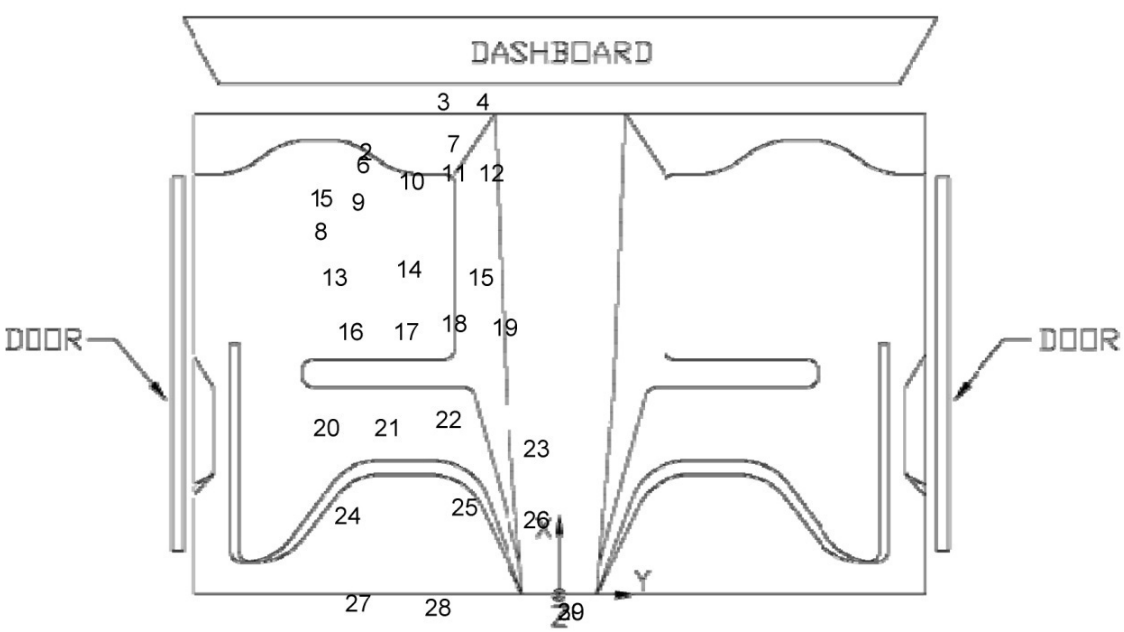

Figure D-8. Floor Pan Deformation Data – Set 2, Test No. MGSBR-2

VEHICLE PRE/POST CRUSH
INTERIOR CRUSH - SET 1

TEST: MGSBR-2
VEHICLE: Rio Sedan

Note: If impact is on driver side need to enter negative number for Y

	POINT	X	Y	Z	X'	Y'	Z'	DEL X	DEL Y	DEL Z
DASH	A1	60.5	-19	21.25	60.75	-19	21.75	0.25	0	0.5
	A2	62.25	-0.75	21	62.25	-0.75	21.5	0	0	0.5
	A3	62	13.25	19	62	13.5	18.75	0	0.25	-0.25
	A4	54.5	-18	21.75	54.5	-17.75	21.75	0	0.25	0
	A5	56.5	1.5	20.5	56.5	1.5	20.5	0	0	0
	A6	57.25	13.5	18.5	57.25	13.5	18.5	0	0	0
SIDE PANEL	B1	19.25	-25.5	2	19.25	-25.75	2.25	0	-0.25	0.25
	B2	23.5	-24.5	-2.75	23.25	-24.25	-2.75	-0.25	0.25	0
	B3	19	-23.5	-4.25	19	-23.5	-4.25	0	0	0
IMPACT SIDE DOOR	C1	-7.25	-34	18	-7.5	-34.5	17.75	-0.25	-0.5	-0.25
	C2	0.25	-33.5	16	0.5	-33.75	15.75	0.25	-0.25	-0.25
	C3	8.75	-33	15.75	8.5	-33	15.75	-0.25	0	0
	C4	0.5	-30	9.25	0.25	-30.25	9.25	-0.25	-0.25	0
	C5	-10.75	-28.25	5.25	-10.5	-28.5	5	0.25	-0.25	-0.25
	C6	6.5	-28.25	4.5	6	-28.25	4.5	-0.5	0	0
ROOF	D1	44.5	-14.75	22.25	44.5	-14.5	22	0	0.25	-0.25
	D2	44.5	-8.75	22	44.75	-8.75	22	0.25	0	0
	D3	45.75	-0.25	21.5	45.5	-0.25	21.25	-0.25	0	-0.25
	D4	44.75	7.5	21.25	44.5	7.25	21.25	-0.25	-0.25	0
	D5	44.25	14.25	20.5	44.25	14.25	20.75	0	0	0.25
	D6	33.75	-12	25.5	33.5	-12	25.5	-0.25	0	0
	D7	31.75	6	25	31.5	6	25	-0.25	0	0
	D8	24.5	-12.5	25.5	24.25	-12.5	25.25	-0.25	0	-0.25
	D9	24.5	-0.25	26	24.5	-0.25	26	0	0	0
	D10	24.25	12.5	24.25	24.5	12.5	24	0.25	0	-0.25
	D11	14.75	-13.25	26.5	14.75	-13	27	0	0.25	0.5
	D12	14.75	-0.5	26.5	15	-0.5	26.75	0.25	0	0.25
	D13	15.5	9.75	25.5	15.75	9.5	25.75	0.25	-0.25	0.25
	D14	1.5	-11.75	26	1.5	-11.75	26	0	0	0
	D15	1	4.75	26	1	4.75	25.5	0	0	-0.5

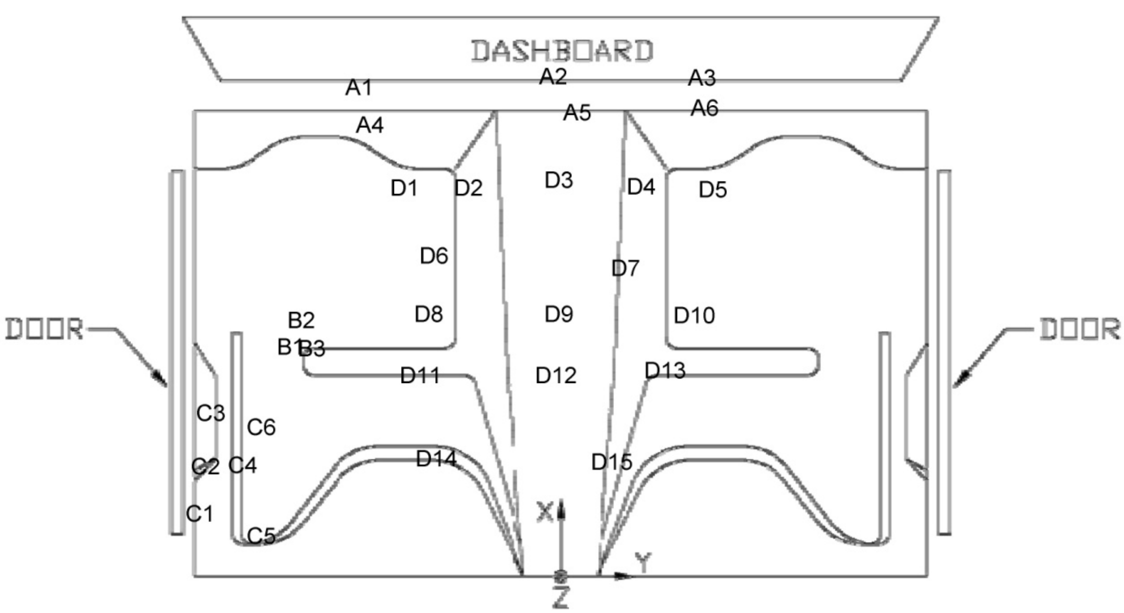

Figure D-9. Occupant Compartment Deformation Data – Set 1, Test No. MGSBR-2

VEHICLE PRE/POST CRUSH
INTERIOR CRUSH - SET 2

TEST: MGSBR-2
VEHICLE: Rio Sedan

Note: If impact is on driver side need to enter negative number for Y

	POINT	X	Y	Z	X'	Y'	Z'	DEL X	DEL Y	DEL Z
DASH	A1	60.5	-19	21.5	NA	NA	21.25	#VALUE!	#VALUE!	-0.25
	A2	62.25	-0.75	21.75	NA	NA	22	#VALUE!	#VALUE!	0.25
	A3	62	13.25	20.75	NA	NA	20.25	#VALUE!	#VALUE!	-0.5
	A4	54.5	-18	21.5	NA	NA	21.5	#VALUE!	#VALUE!	0
	A5	56.5	1.5	21	NA	NA	20.75	#VALUE!	#VALUE!	-0.25
	A6	57.25	13.5	19.5	NA	NA	20	#VALUE!	#VALUE!	0.5
SIDE PANEL	B1	19.25	-25.5	1.25	NA	NA	1.25	#VALUE!	#VALUE!	0
	B2	23.5	-24.5	-3.75	NA	NA	-3.75	#VALUE!	#VALUE!	0
	B3	19	-23.5	-5	NA	NA	-5	#VALUE!	#VALUE!	0
IMPACT SIDE DOOR	C1	-7.25	-34	17.75	NA	NA	18	#VALUE!	#VALUE!	0.25
	C2	0.25	-33.5	15.75	NA	NA	15.5	#VALUE!	#VALUE!	-0.25
	C3	8.75	-33	15.25	NA	NA	15.25	#VALUE!	#VALUE!	0
	C4	0.5	-30	9	NA	NA	9	#VALUE!	#VALUE!	0
	C5	-10.75	-28.25	5.25	NA	NA	5.25	#VALUE!	#VALUE!	0
	C6	6.5	-28.25	4	NA	NA	4	#VALUE!	#VALUE!	0
ROOF	D1	NA	NA	NA	NA	NA	NA	#VALUE!	#VALUE!	#VALUE!
	D2	NA	NA	NA	NA	NA	NA	#VALUE!	#VALUE!	#VALUE!
	D3	NA	NA	NA	NA	NA	NA	#VALUE!	#VALUE!	#VALUE!
	D4	NA	NA	NA	NA	NA	NA	#VALUE!	#VALUE!	#VALUE!
	D5	NA	NA	NA	NA	NA	NA	#VALUE!	#VALUE!	#VALUE!
	D6	NA	NA	NA	NA	NA	NA	#VALUE!	#VALUE!	#VALUE!
	D7	NA	NA	NA	NA	NA	NA	#VALUE!	#VALUE!	#VALUE!
	D8	NA	NA	NA	NA	NA	NA	#VALUE!	#VALUE!	#VALUE!
	D9	NA	NA	NA	NA	NA	NA	#VALUE!	#VALUE!	#VALUE!
	D10	NA	NA	NA	NA	NA	NA	#VALUE!	#VALUE!	#VALUE!
	D11	NA	NA	NA	NA	NA	NA	#VALUE!	#VALUE!	#VALUE!
	D12	NA	NA	NA	NA	NA	NA	#VALUE!	#VALUE!	#VALUE!
	D13	NA	NA	NA	NA	NA	NA	#VALUE!	#VALUE!	#VALUE!
	D14	NA	NA	NA	NA	NA	NA	#VALUE!	#VALUE!	#VALUE!
	D15	NA	NA	NA	NA	NA	NA	#VALUE!	#VALUE!	#VALUE!

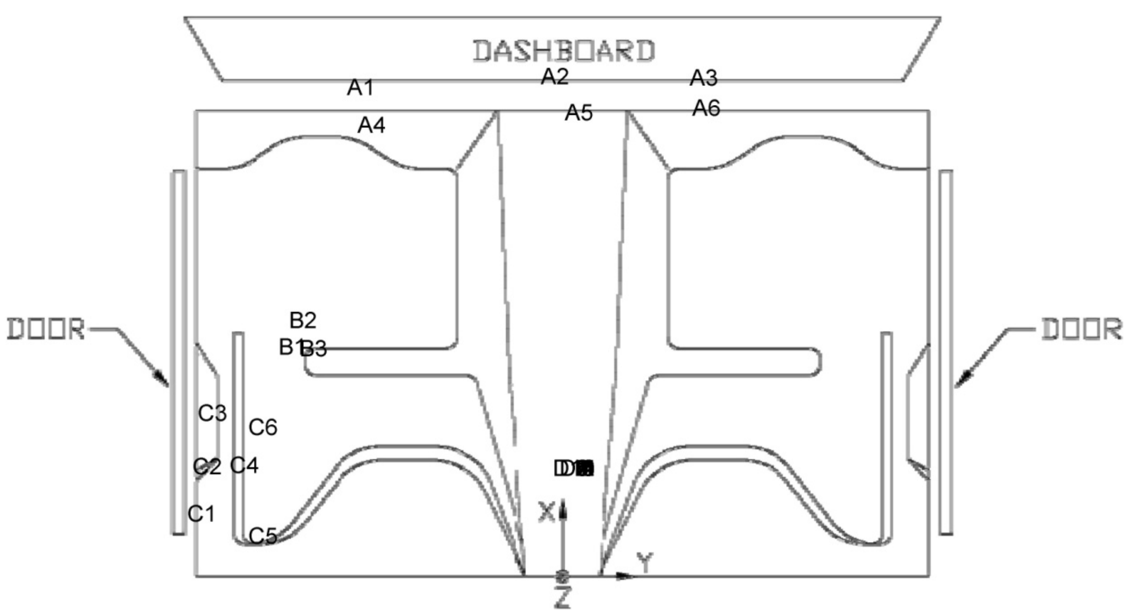

Figure D-10. Occupant Compartment Deformation Data – Set 2, Test No. MGSBR-2

Date: 6/26/2009 **Test Number:** MGSBR-2

Make: KIA **Model:** Rio Sedan **Year:** 2003

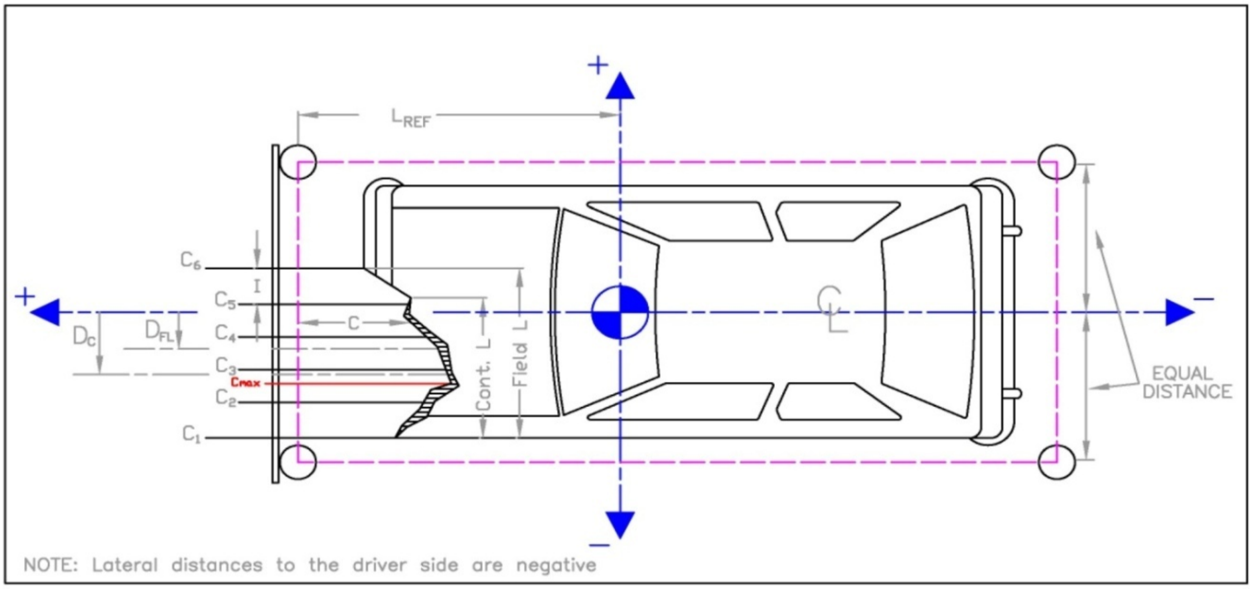

	in.	(mm)
Distance from C.G. to reference line - L_{REF}:	78.5	(1994)
Width of contact and induced crush - Field L:	64.75	(1645)
Crush measurement spacing interval (L/5) - I:	12.95	(329)
Distance from center of vehicle to center of Field L - D_{FL}:	0	()
Width of Contact Damage:	36.875	(937)
Distance from center of vehicle to center of contect damage - D_C:	13.9375	(354)

	Crush Measurement		Lateral Location		Original Profile Measurement		Dist. Between Ref. Lines		Actual	Crush
	in.	(mm)	in.	(mm)	in.	(mm)	in.	(mm)	in.	(mm)
C_1	NA	#######	-32.375	-(822)	30.625	(778)	-0.2686	-(7)	#######	#######
C_2	19	(483)	-19.425	-(493)	10.0938	(256)			9.17484	(233)
C_3	20	(508)	-6.475	-(164)	7.75	(197)			12.5186	(318)
C_4	20.25	(514)	6.475	(164)	7.75	(197)			12.7686	(324)
C_5	18.5	(470)	19.425	(493)	10.0156	(254)			8.75296	(222)
C_6	28	(711)	32.375	(822)	30.625	(778)			-2.3564	-(60)
C_{MAX}	22	(559)	4	(102)	7.5	(191)			14.7686	(375)

Figure D-11. Exterior Vehicle Crush (NASS) - Front, Test No. MGSBR-2

Date:	39990	**Test Number:**	MGSBR-2		
Make:	KIA	**Model:**	Rio Sedan	**Year:**	2003

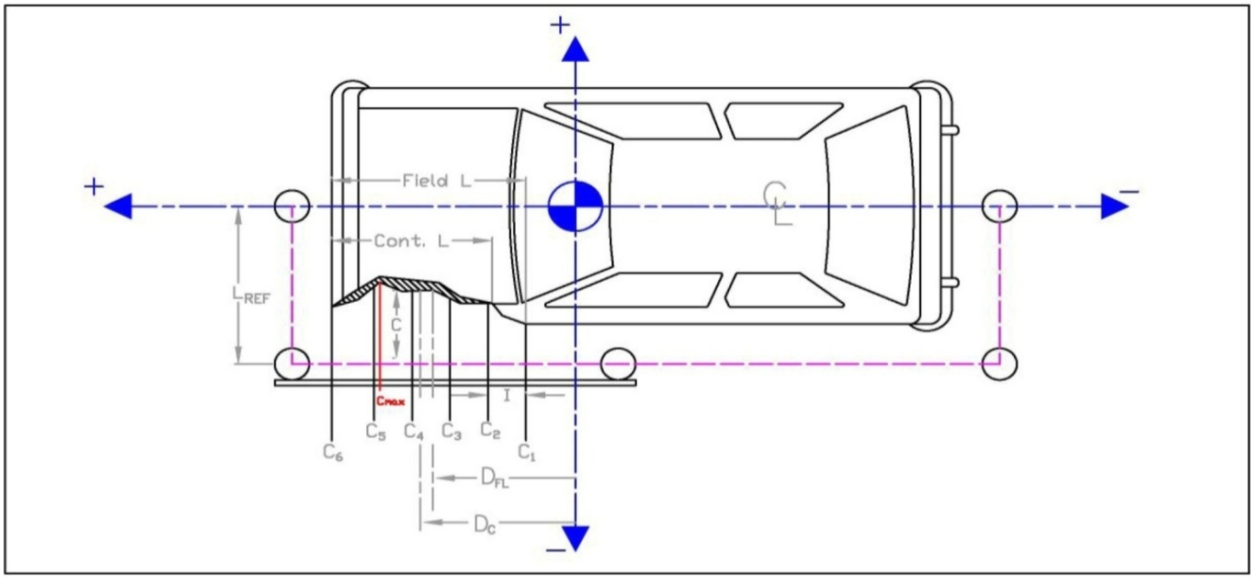

	in.	(mm)
Distance from centerline to reference line - L_{REF}:	40.5	(1029)
Width of contact and induced crush - Field L:	89	(2261)
Crush measurement spacing interval (L/5) - I:	17.8	(452)
Distance from vehicle c.g. to center of Field L - D_{FL}:	23.5	(597)
Width of Contact Damage:	89	(2261)
Distance from vehicle c.g. to center of contect damage - D_C:	57.5	(1461)

	Crush Measurement		Longitudinal Location		Original Profile Measurement		Dist. Between Ref. Lines		Actual	Crush
	in.	(mm)	in.	(mm)	in.	(mm)	in.	(mm)	in.	(mm)
C_1	8	(203)	-21	-(533)	3.25	(83)	4.5	(114)	0.25	(6)
C_2	9	(229)	-3.2	-(81)	3.25	(83)			1.25	(32)
C_3	9.5	(241)	14.6	(371)	3.25	(83)			1.75	(44)
C_4	9.5	(241)	32.4	(823)	4.5	(114)			0.5	(13)
C_5	12.5	(318)	50.2	(1275)	4.25	(108)			3.75	(95)
C_6	NA	#######	68	(1727)	23.375	(594)			#######	#######
C_{MAX}	18	(457)	58	(1473)	6.75	(171)			6.75	(171)

Figure D-12. Exterior Vehicle Crush (NASS) - Side, Test No. MGSBR-2

Appendix E. Accelerometer and Rate Transducer Plots, Test No. MGSBR-1

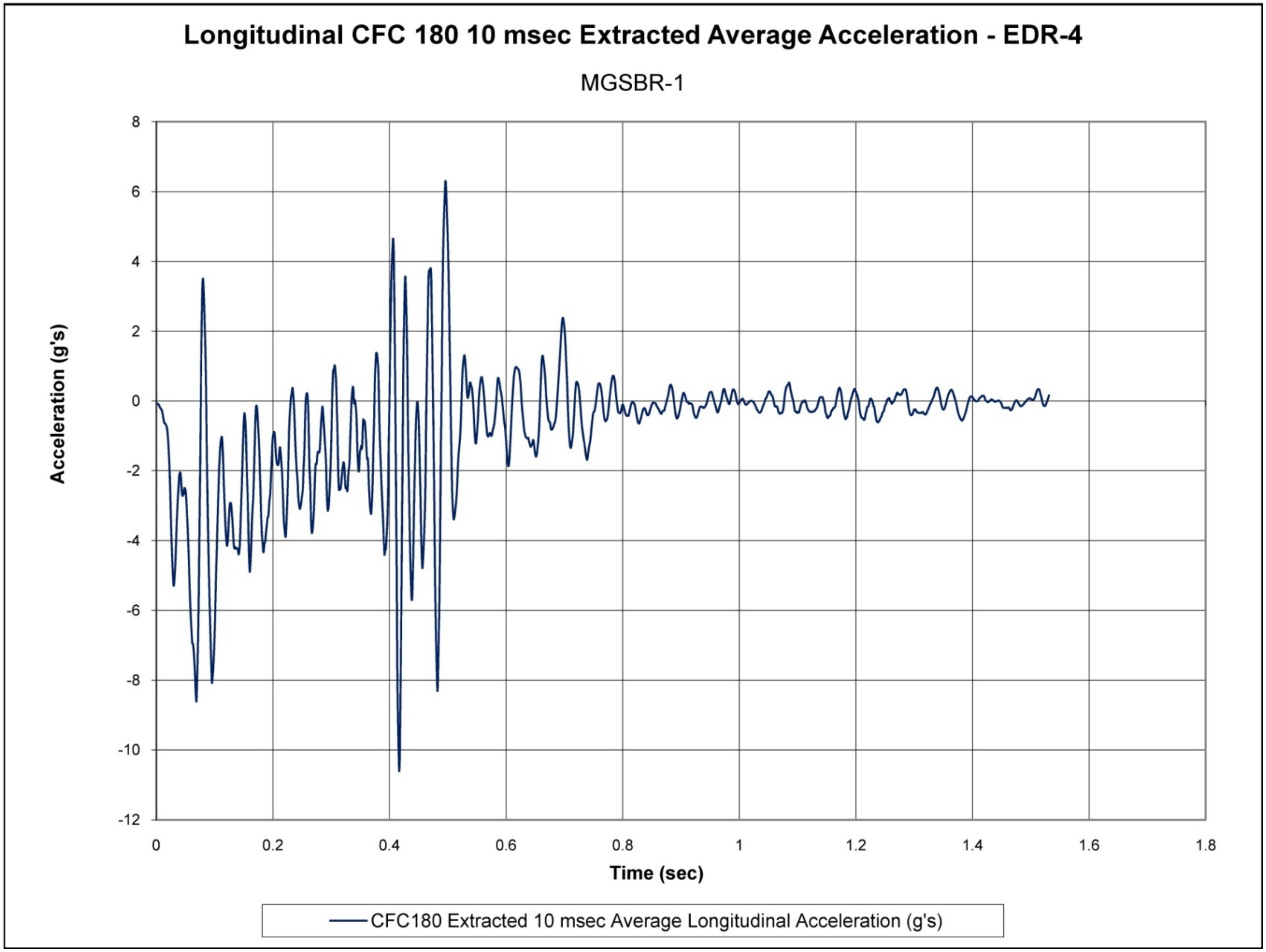

Figure E-1. 10-ms Average Longitudinal Deceleration (EDR-4), Test No. MGSBR-1

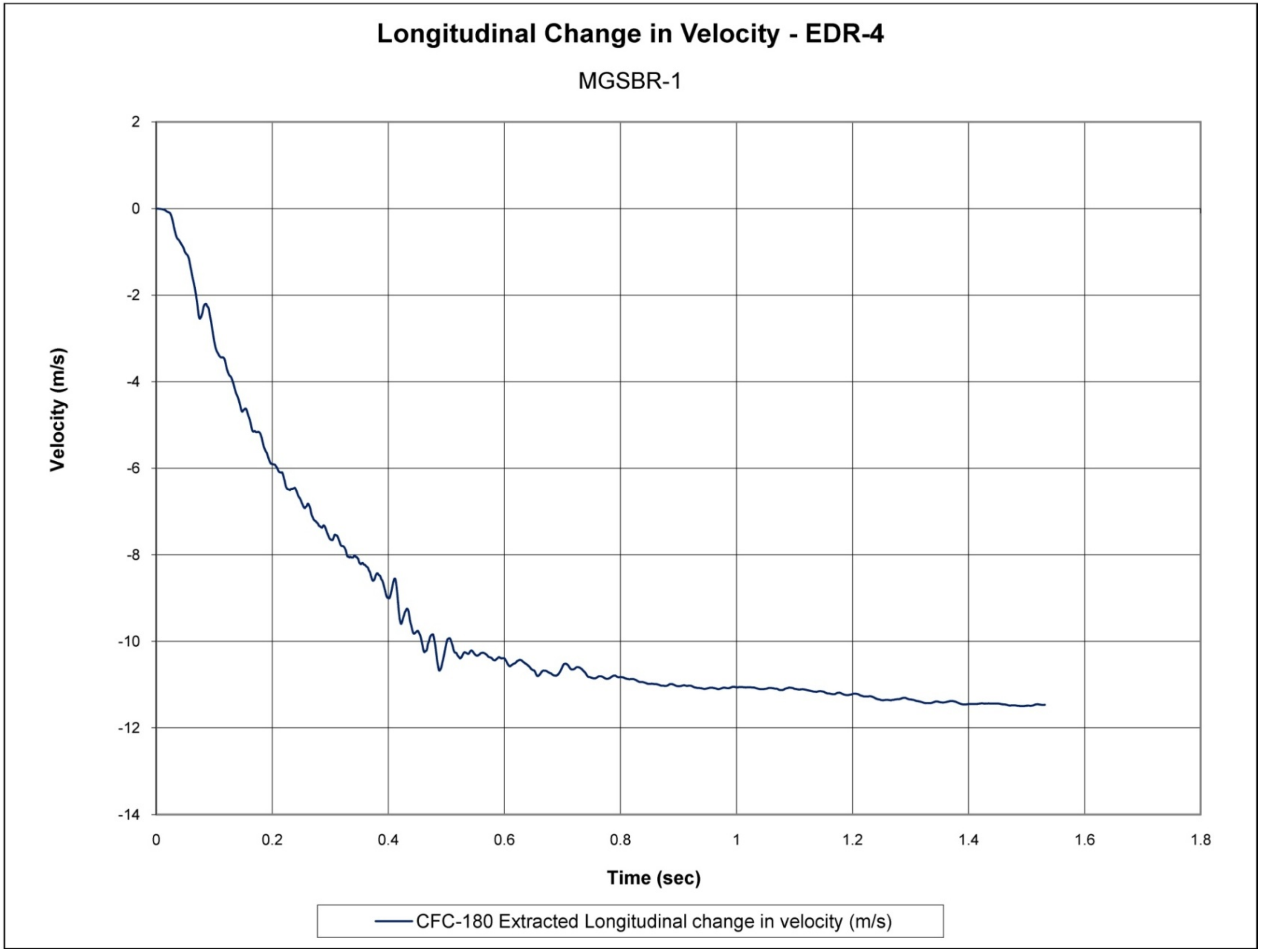

Figure E-2. Longitudinal Occupant Impact Velocity (EDR-4), Test No. MGSBR-1

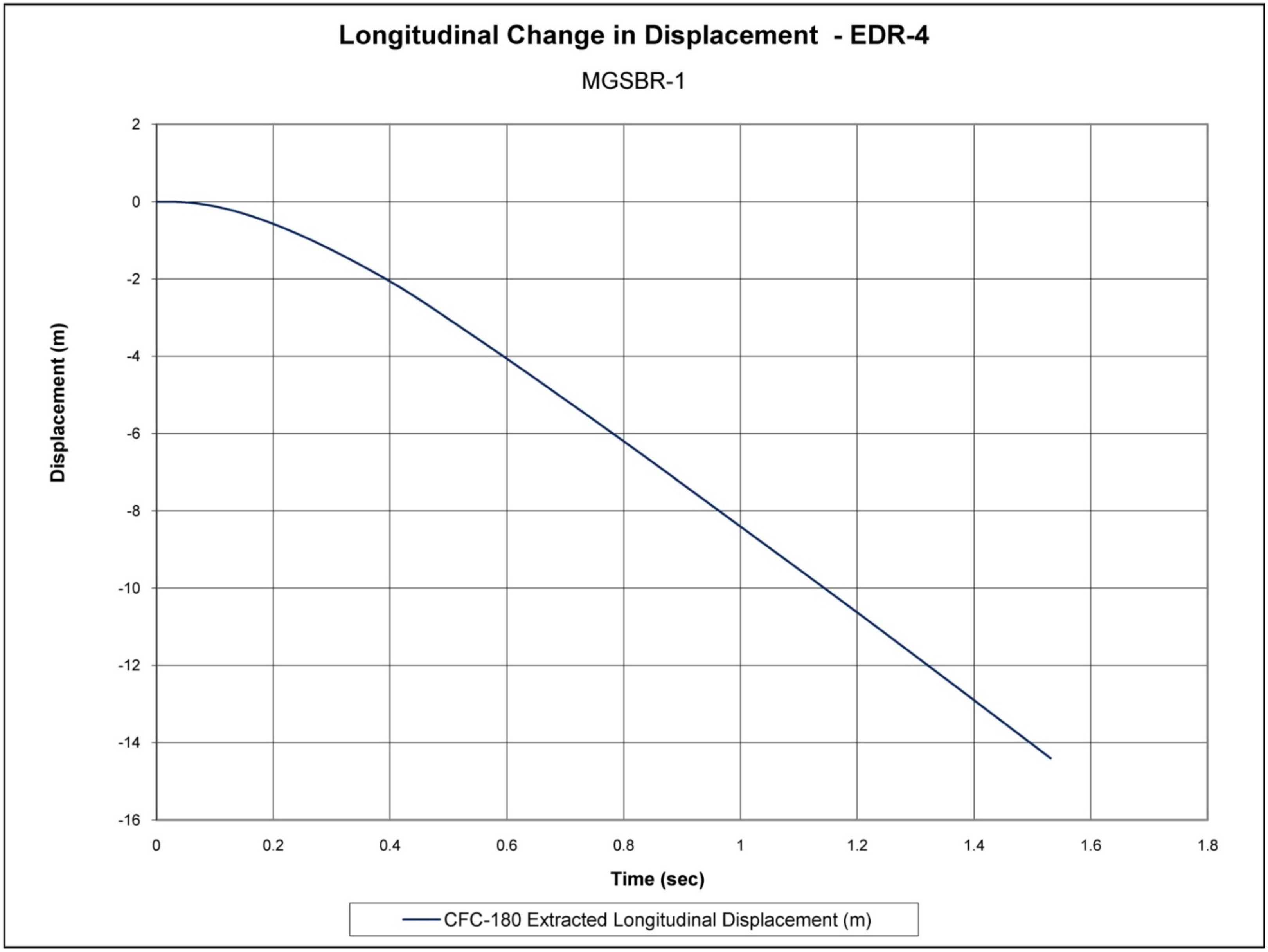

Figure E-3. Longitudinal Occupant Displacement (EDR-4), Test No. MGSBR-1

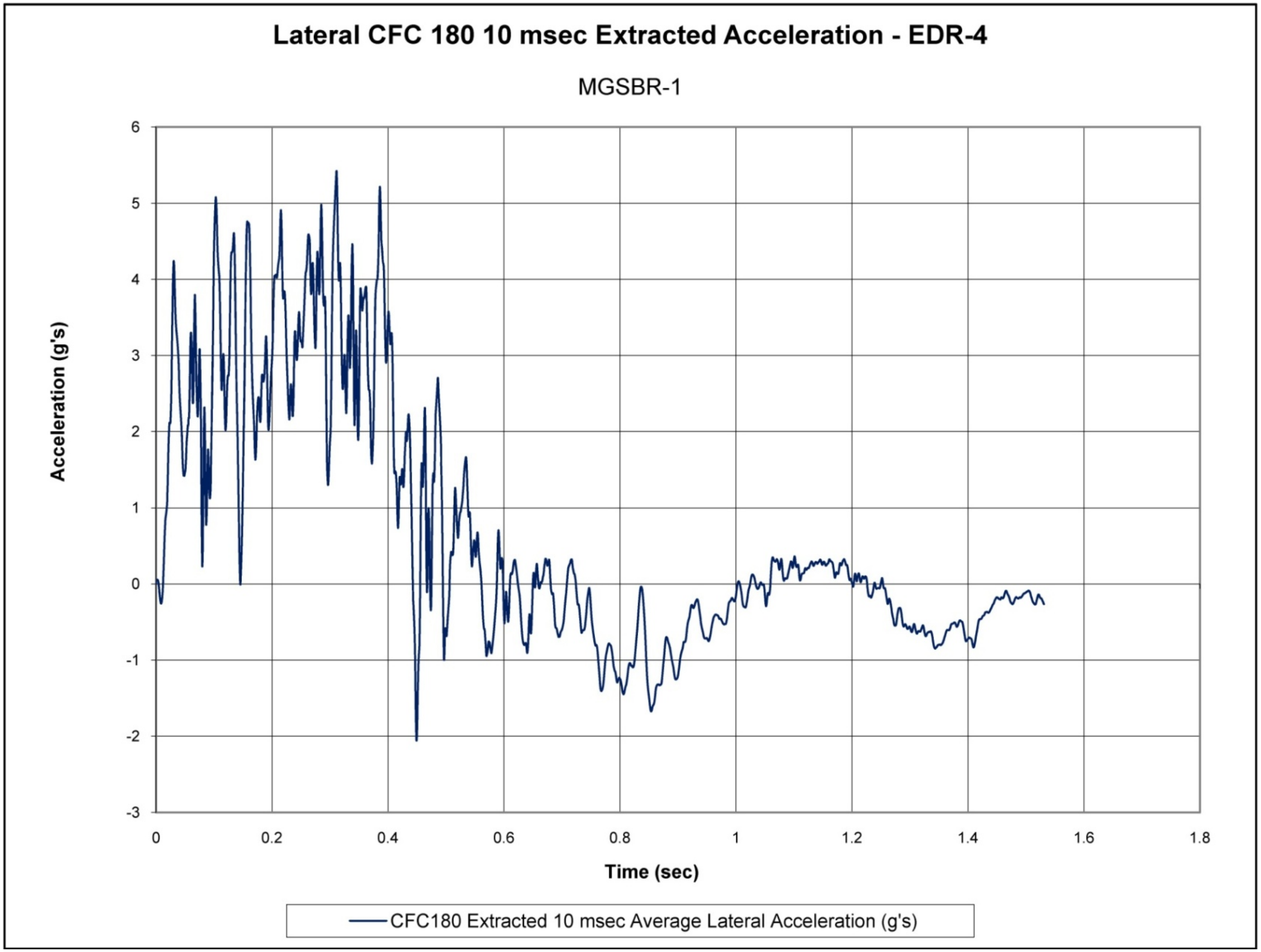

Figure E-4. 10-ms Average Lateral Deceleration (EDR-4), Test No. MGSBR-1

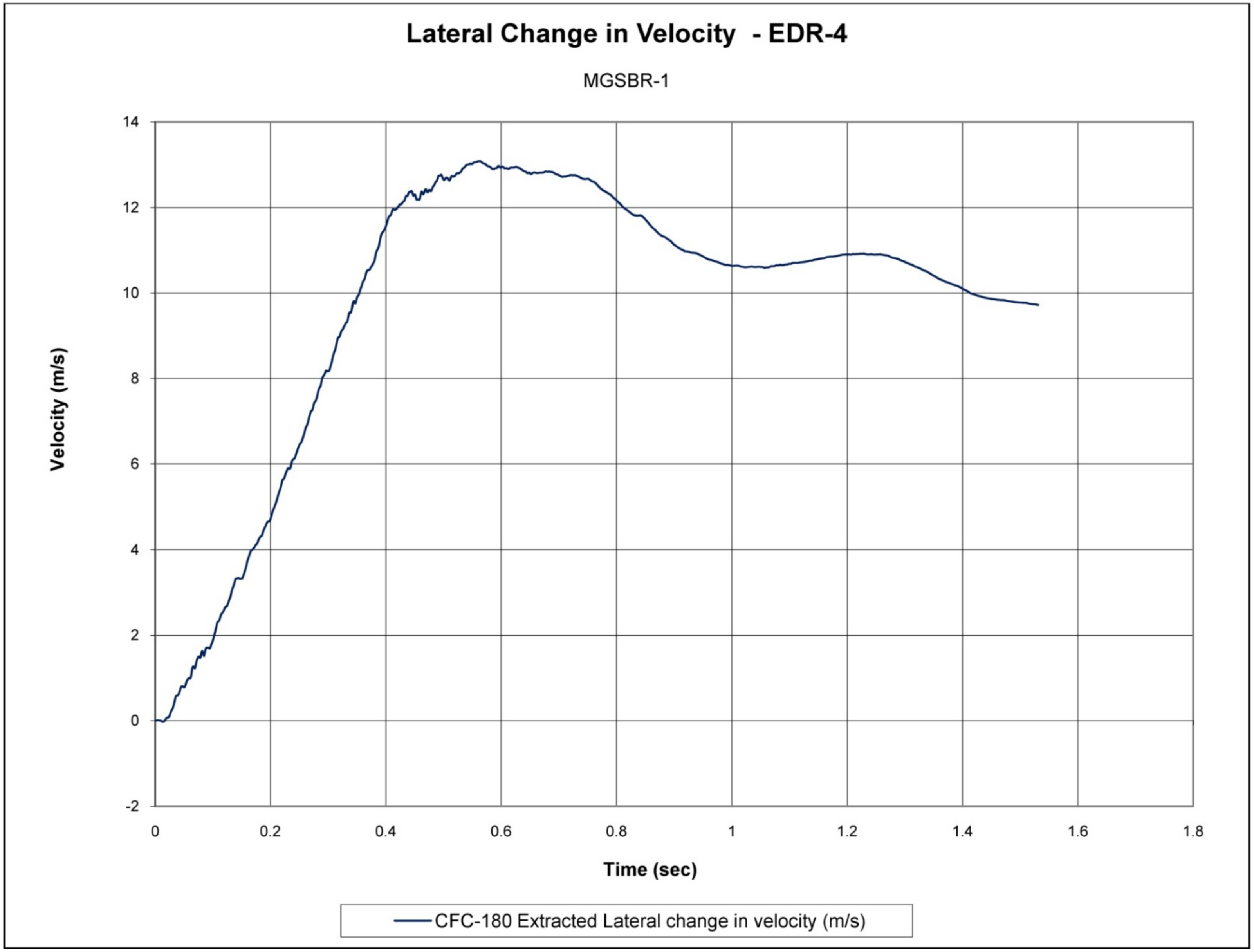

Figure E-5. Lateral Occupant Impact Velocity (EDR-4), Test No. MGSBR-1

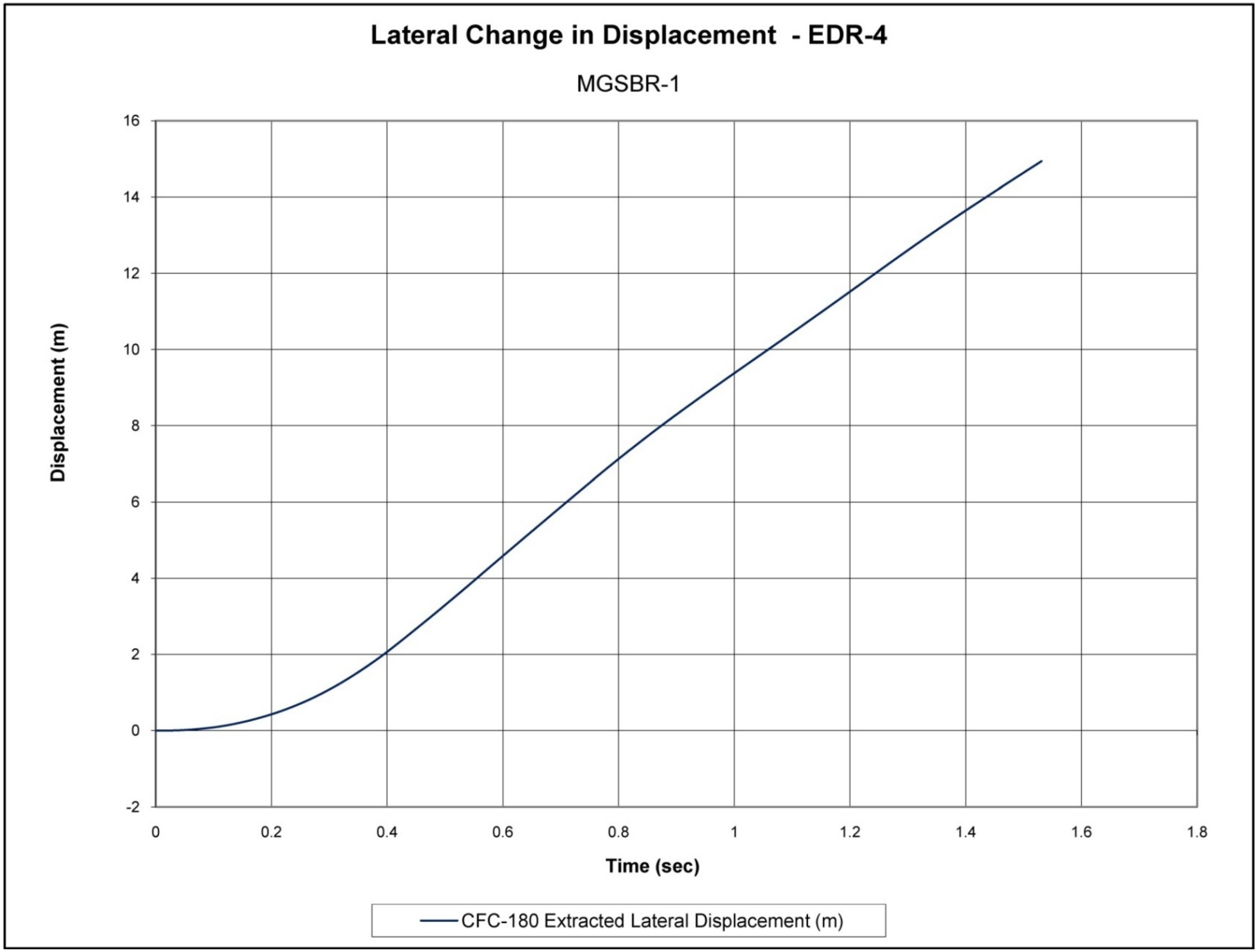

Figure E-6. Lateral Occupant Displacement (EDR-4), Test No. MGSBR-1

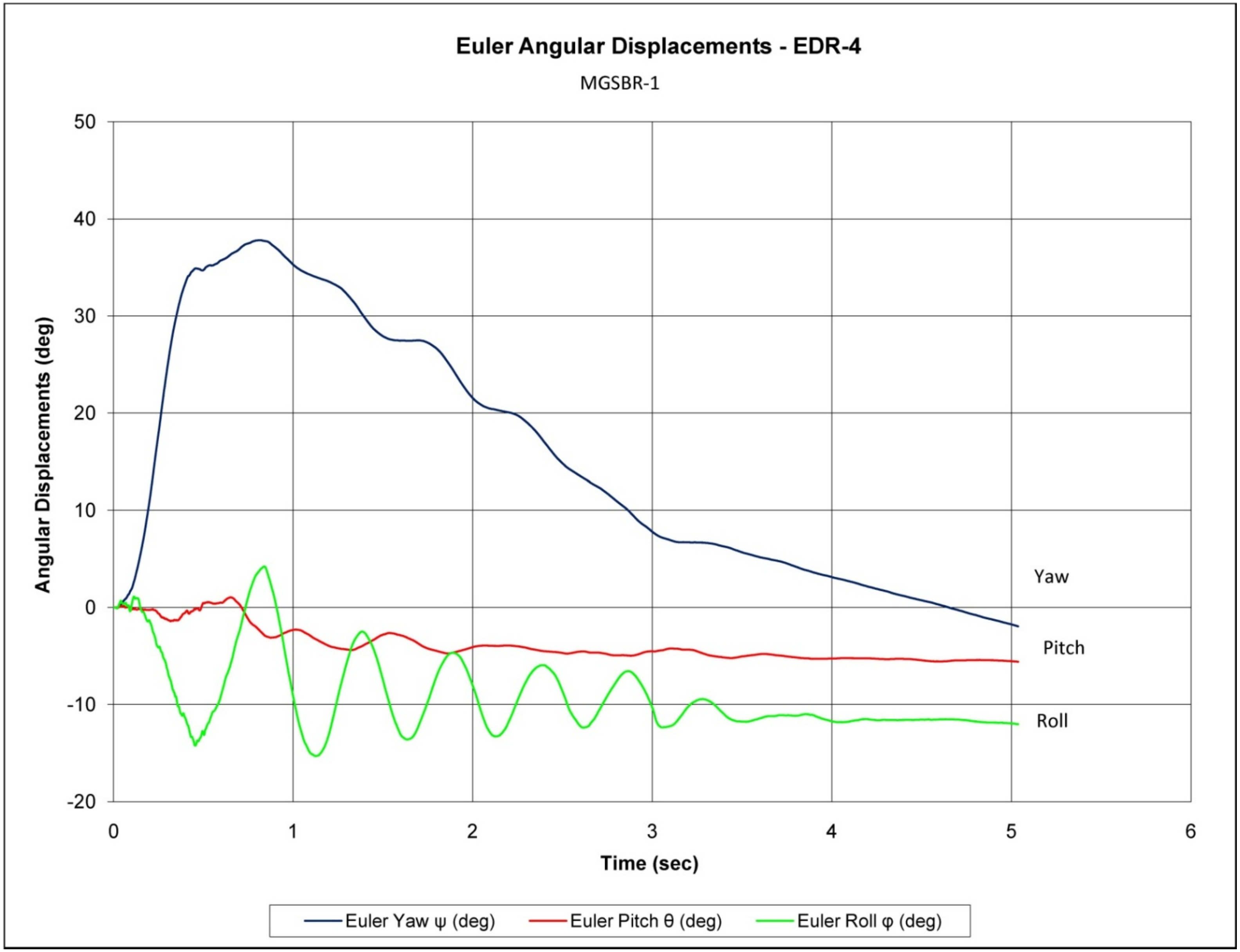

Figure E-7. Vehicle Angular Displacements (EDR-4), Test No. MGSBR-1

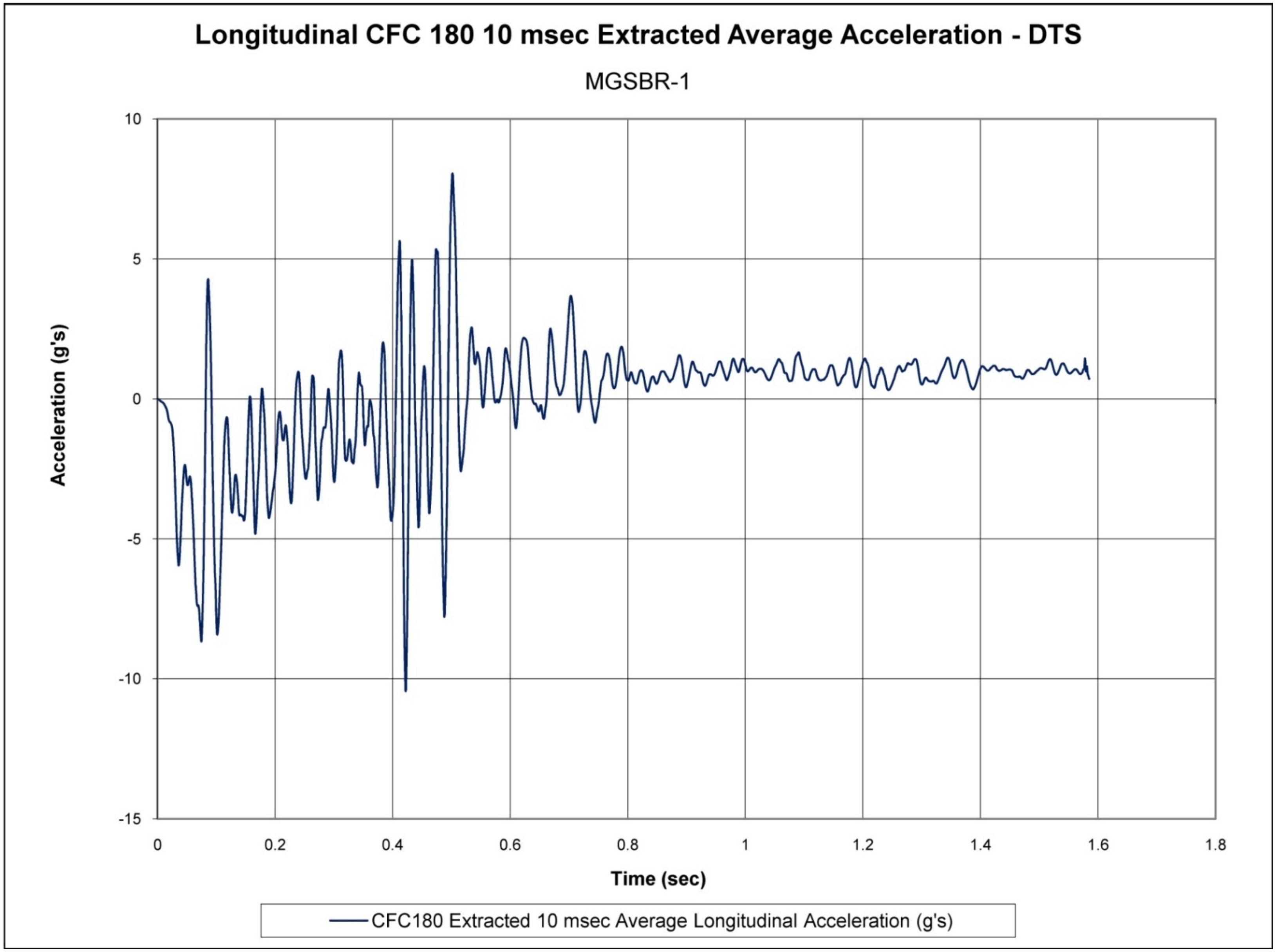

Figure E-8. 10-ms Average Longitudinal Deceleration (DTS), Test No. MGSBR-1

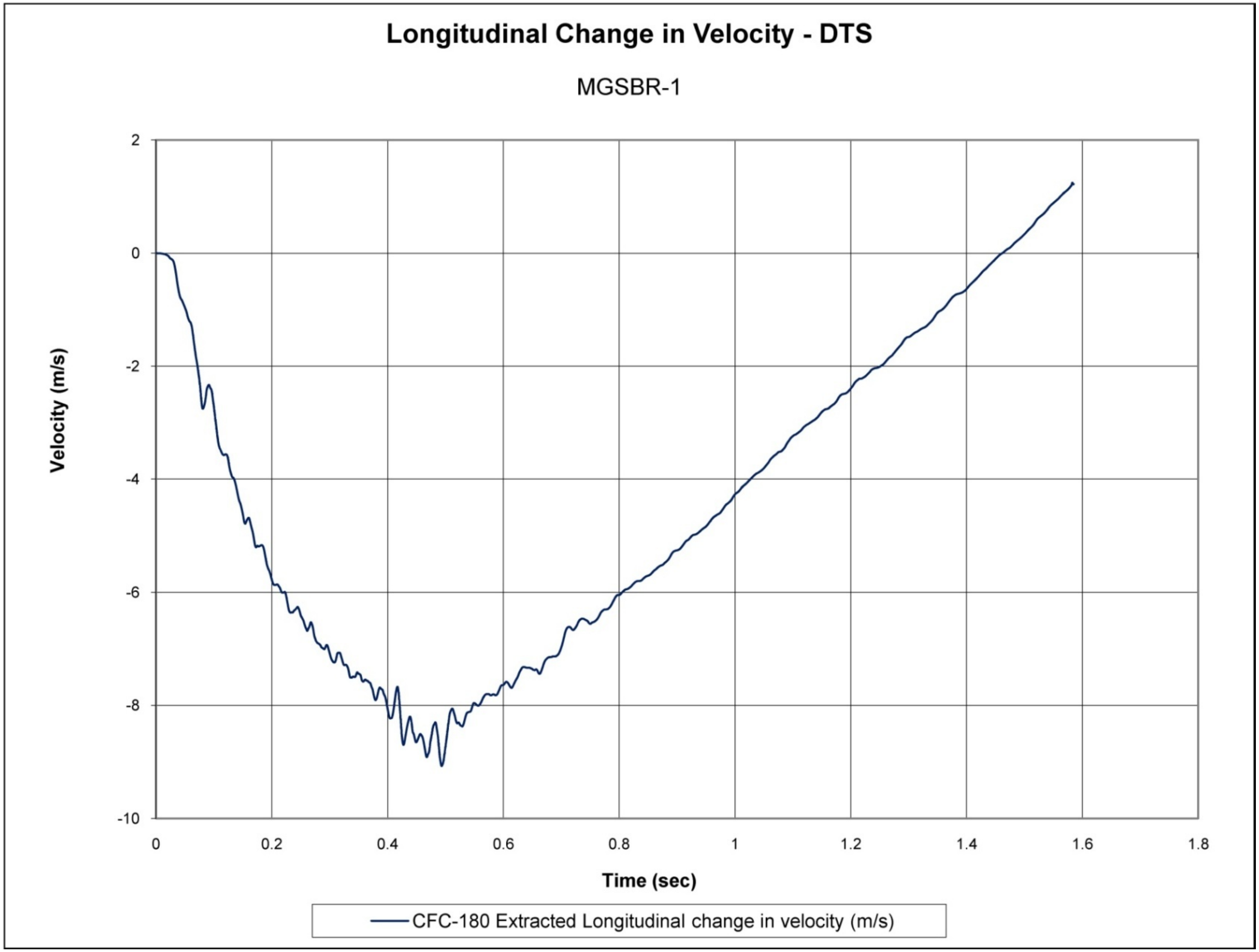

Figure E-9. Longitudinal Occupant Impact Velocity (DTS), Test No. MGSBR-1

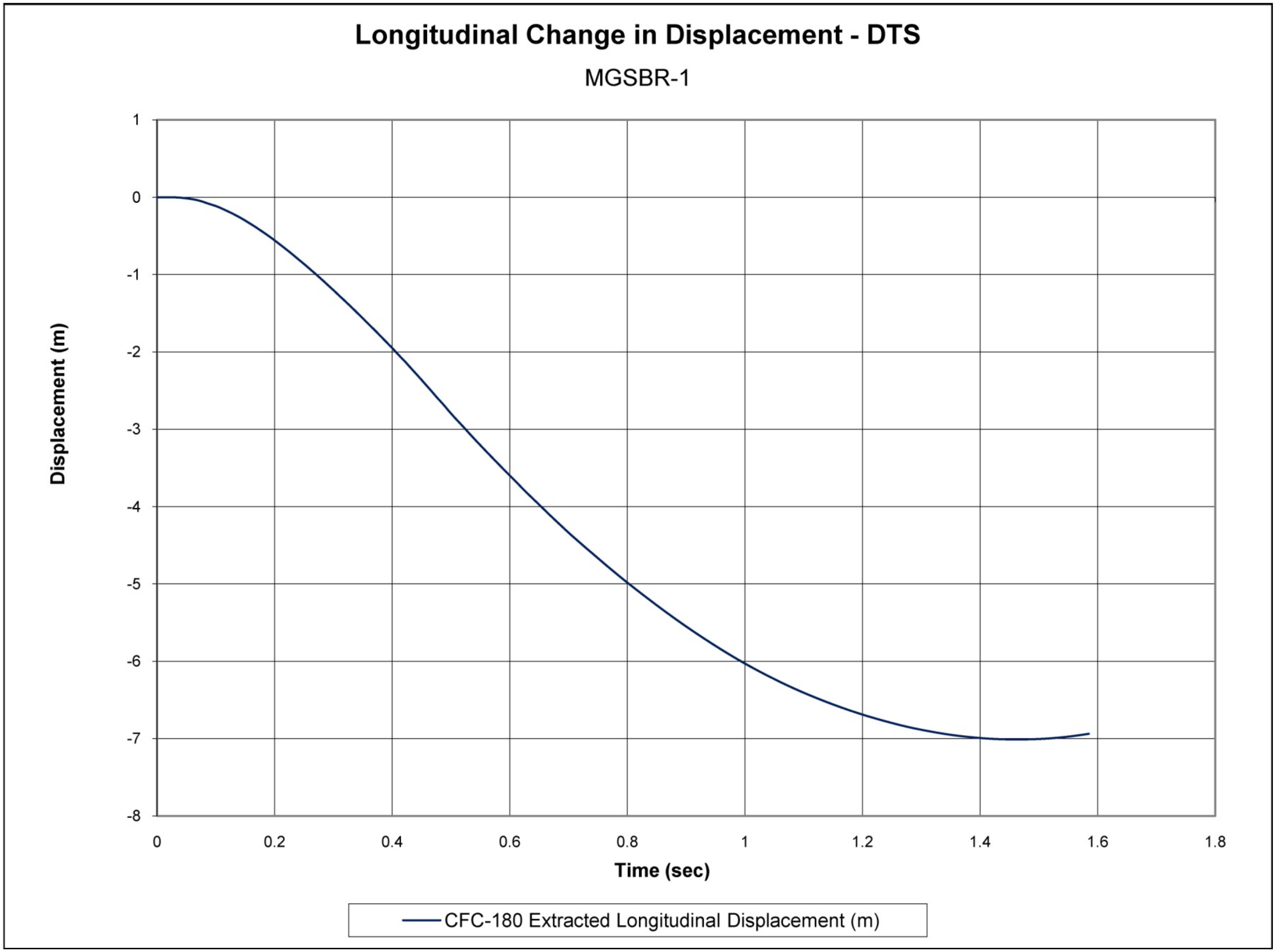

Figure E-10. Longitudinal Occupant Displacement (DTS), Test No. MGSBR-1

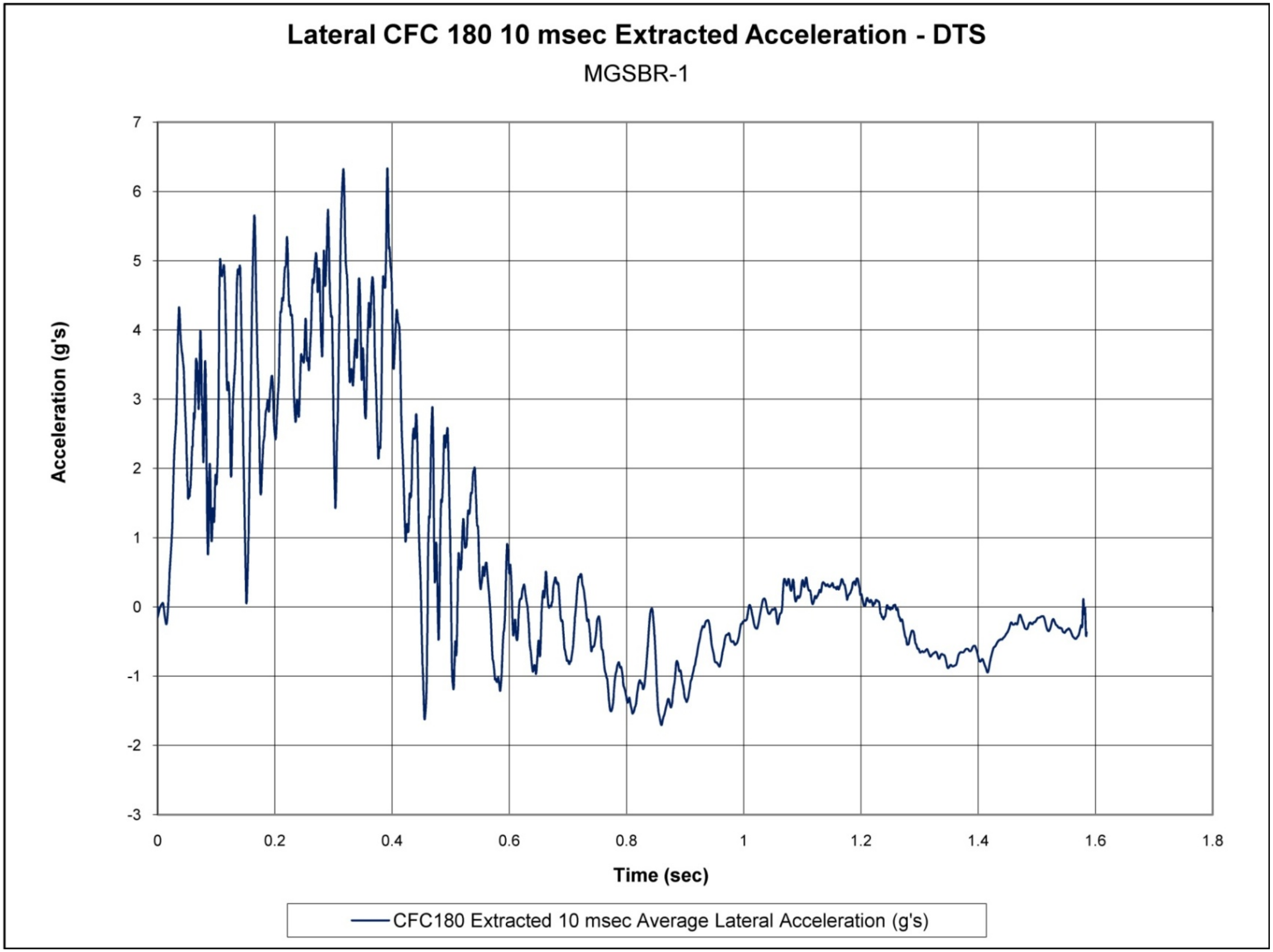

Figure E-11. 10-ms Average Lateral Deceleration (DTS), Test No. MGSBR-1

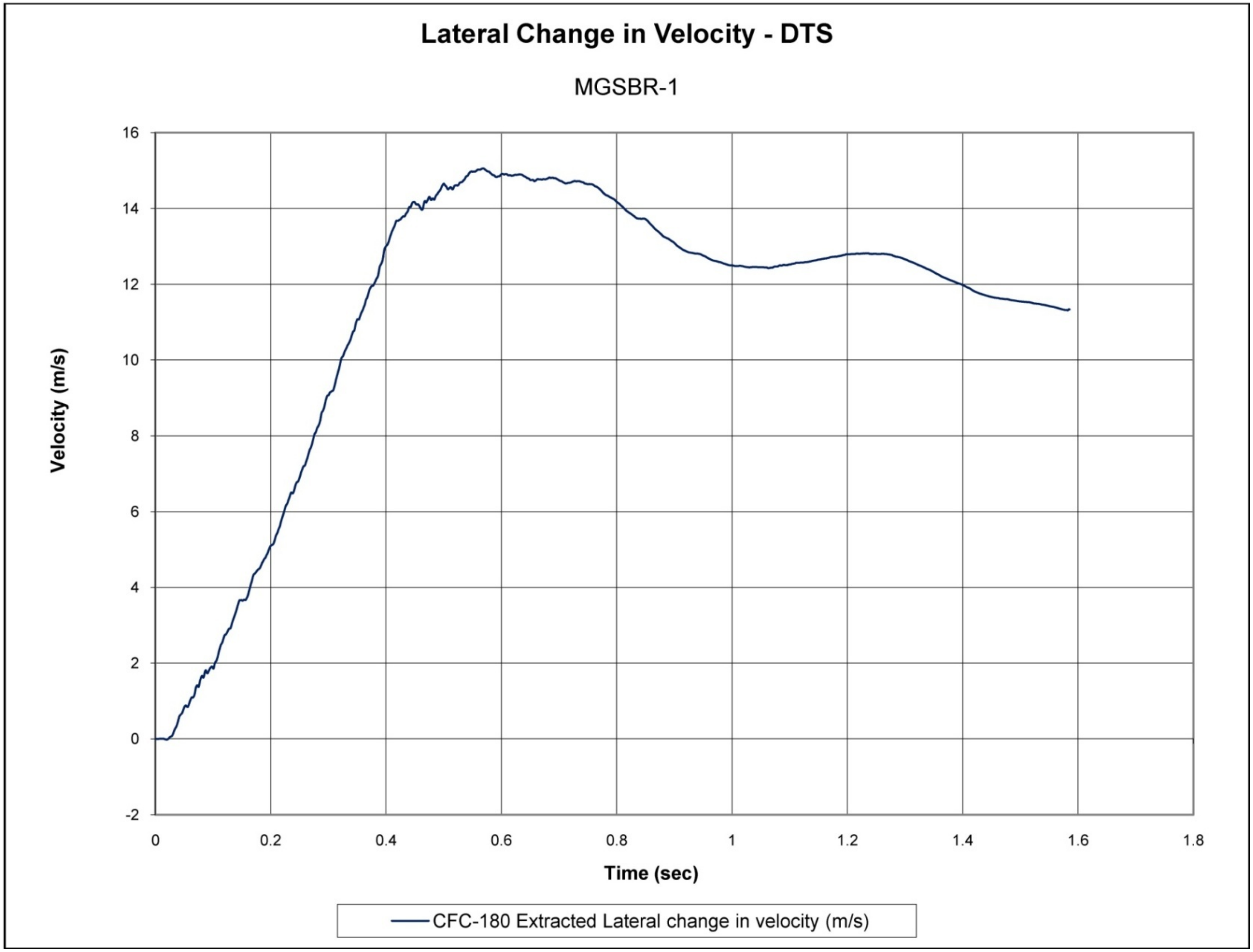

Figure E-12. Lateral Occupant Impact Velocity (DTS), Test No. MGSBR-1

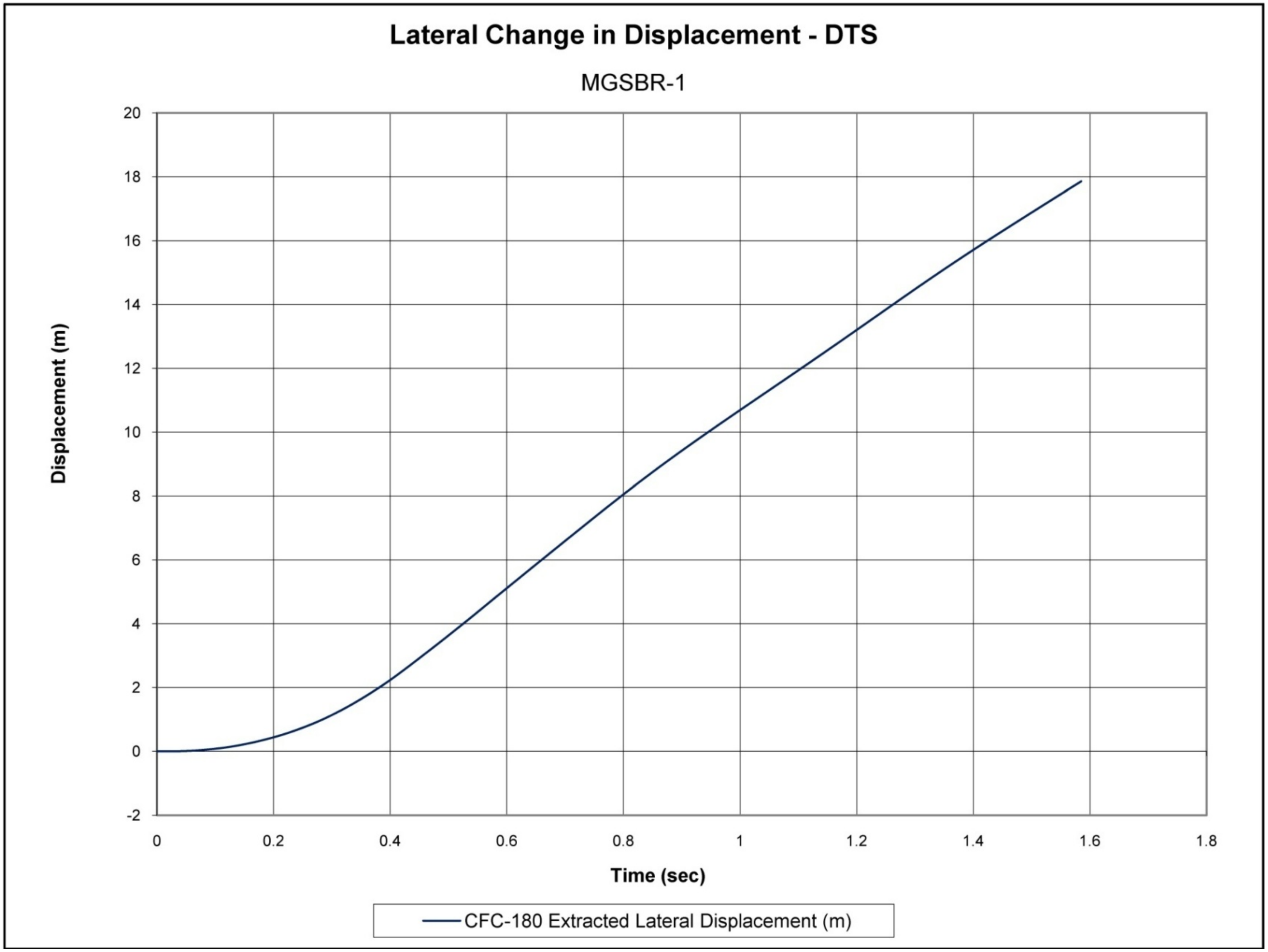

Figure E-13. Lateral Occupant Displacement (DTS), Test No. MGSBR-1

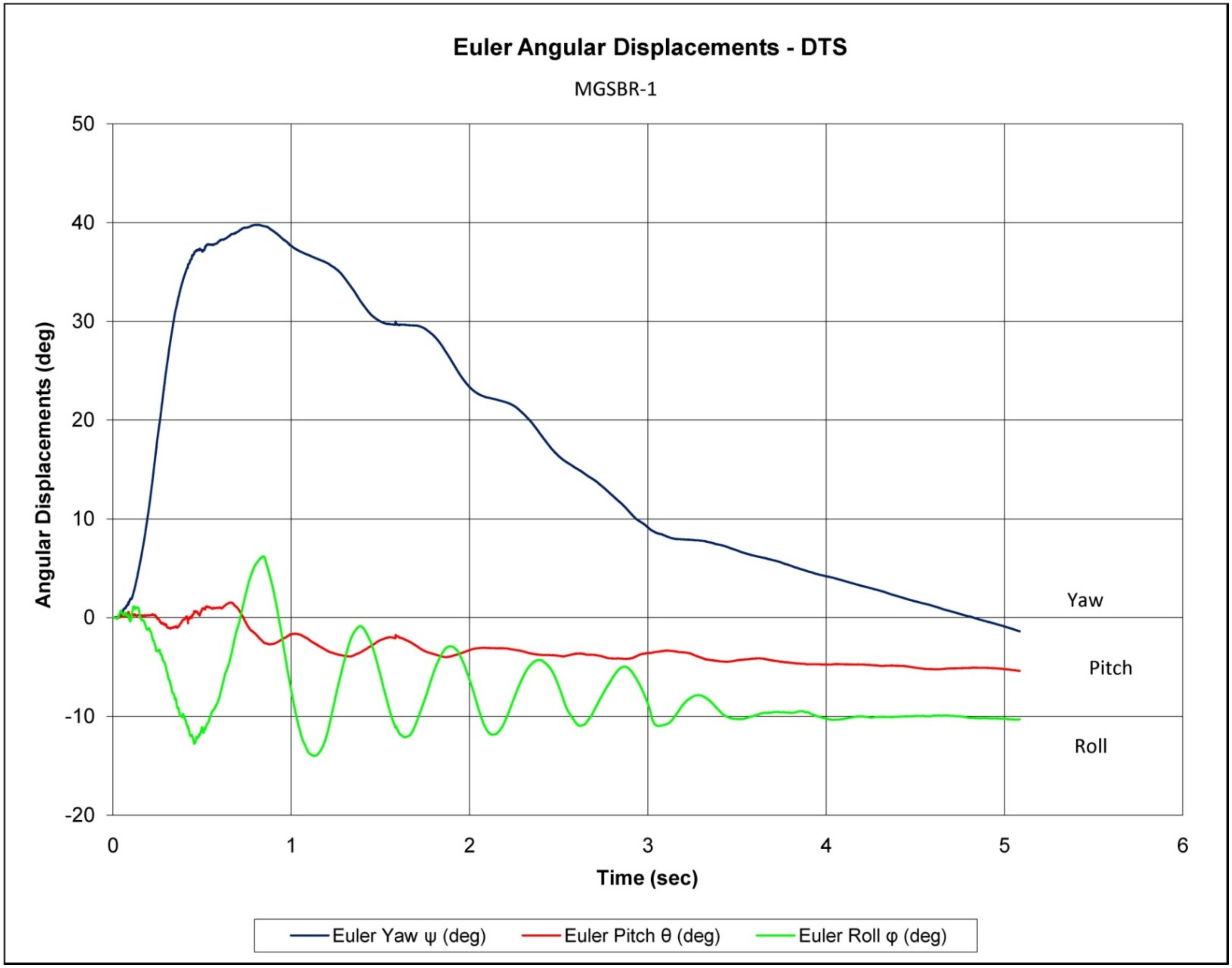

Figure E-14. Vehicle Angular Displacements (DTS), Test No. MGSBR-1

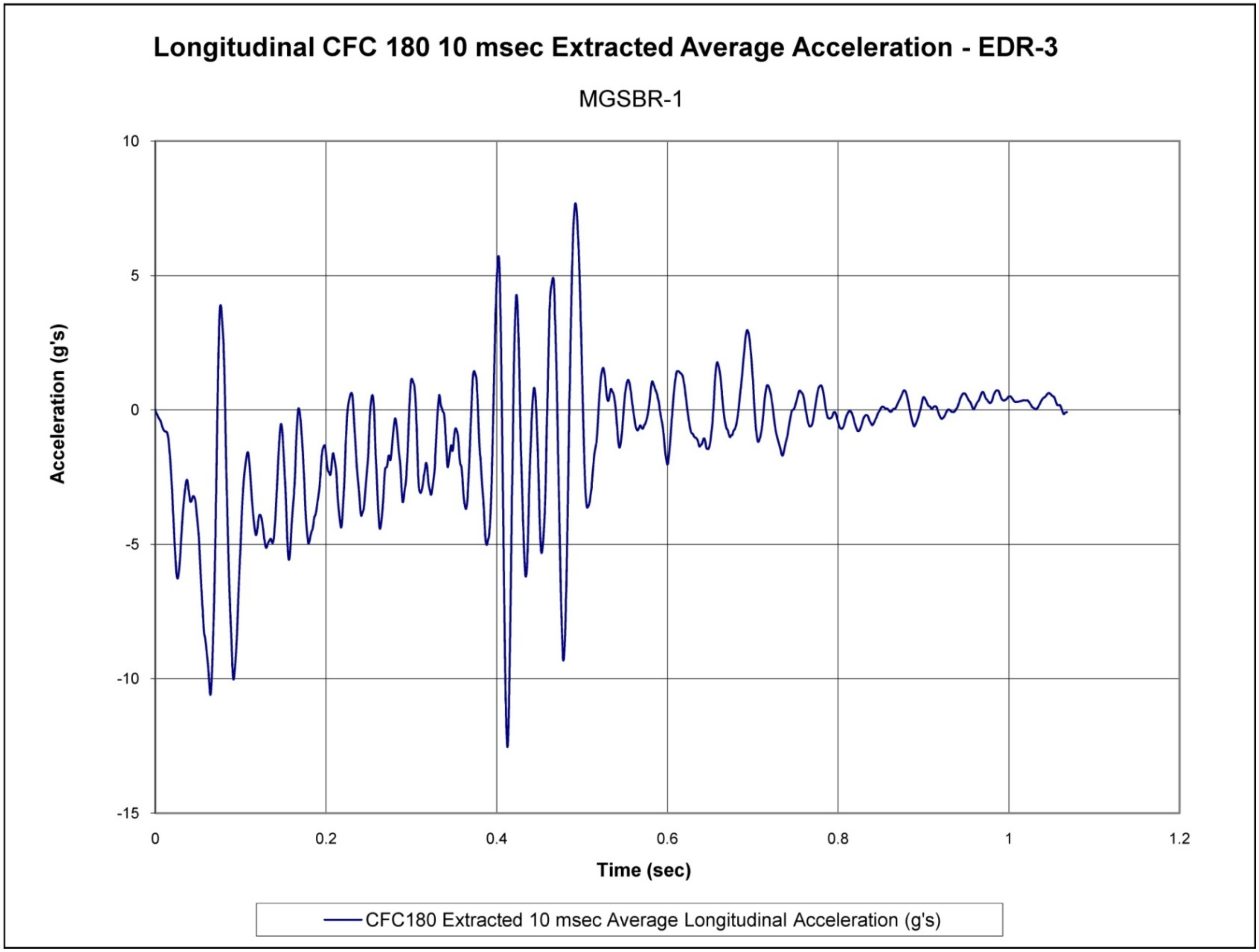

Figure E-15. 10-ms Average Longitudinal Deceleration (EDR-3), Test No. MGSBR-1

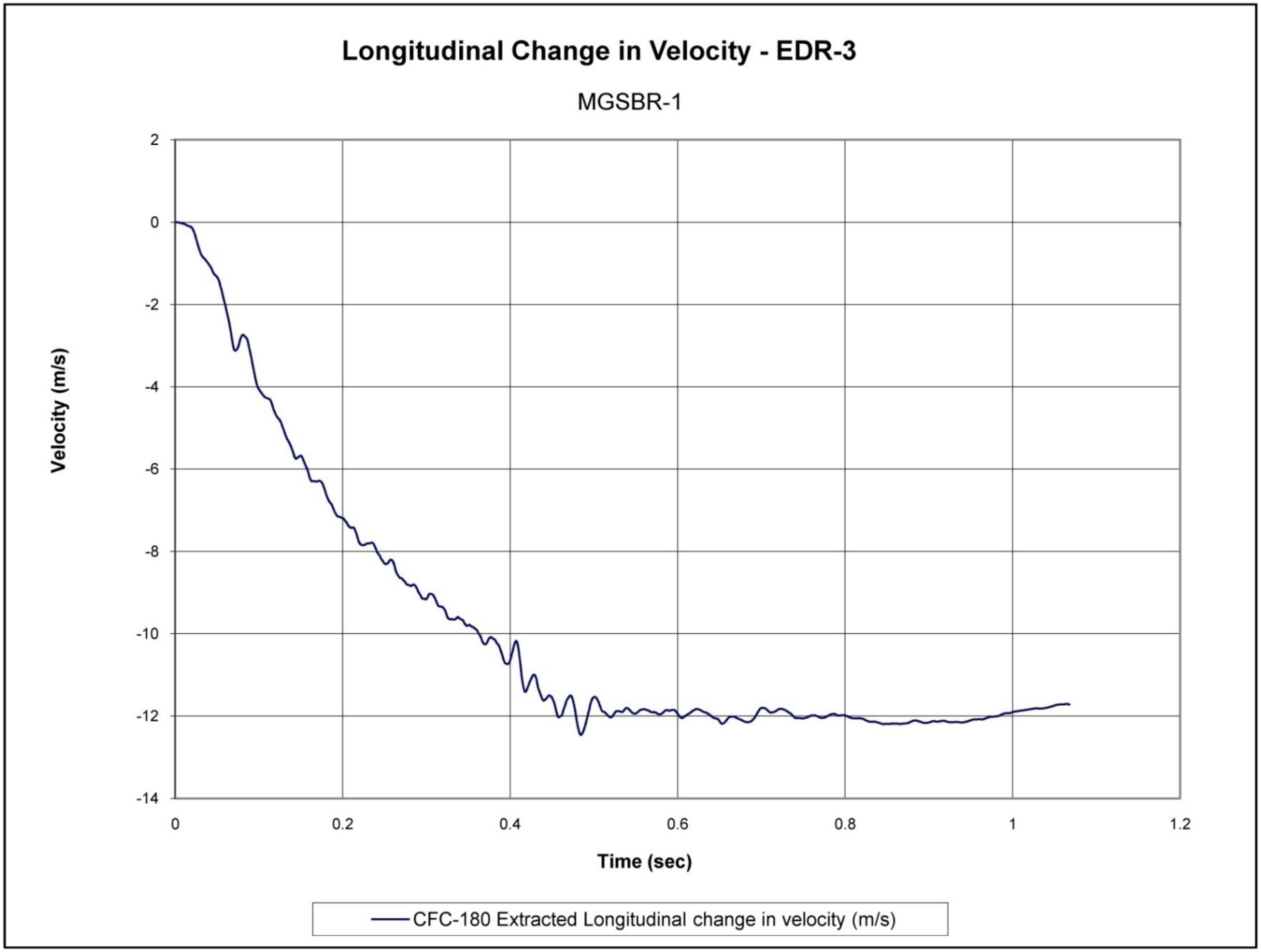

Figure E-16. Longitudinal Occupant Impact Velocity (EDR-3), Test No. MGSBR-1

Figure E-17. Longitudinal Occupant Displacement (EDR-3), Test No. MGSBR-1

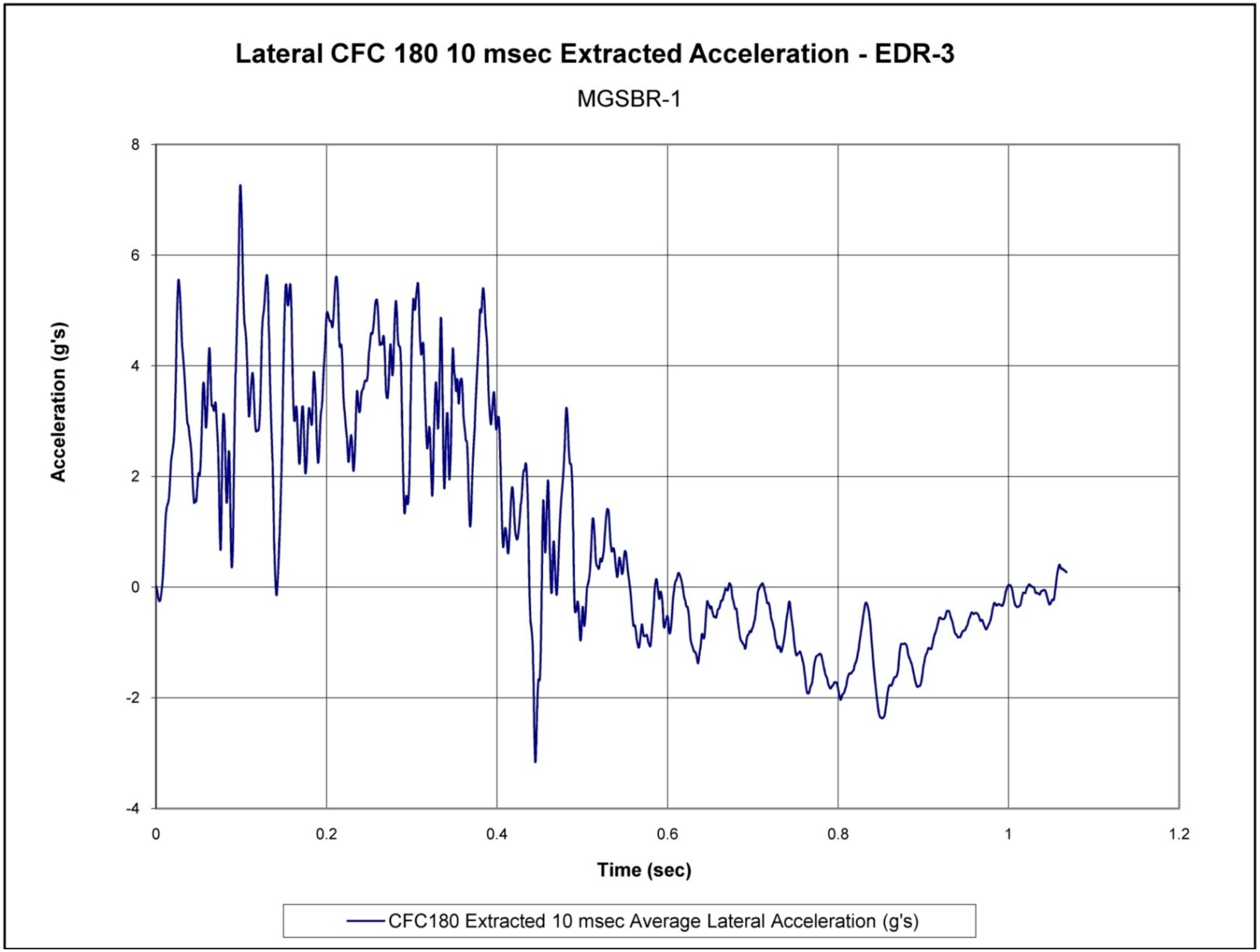

Figure E-18. 10-ms Average Lateral Deceleration (EDR-3), Test No. MGSBR-1

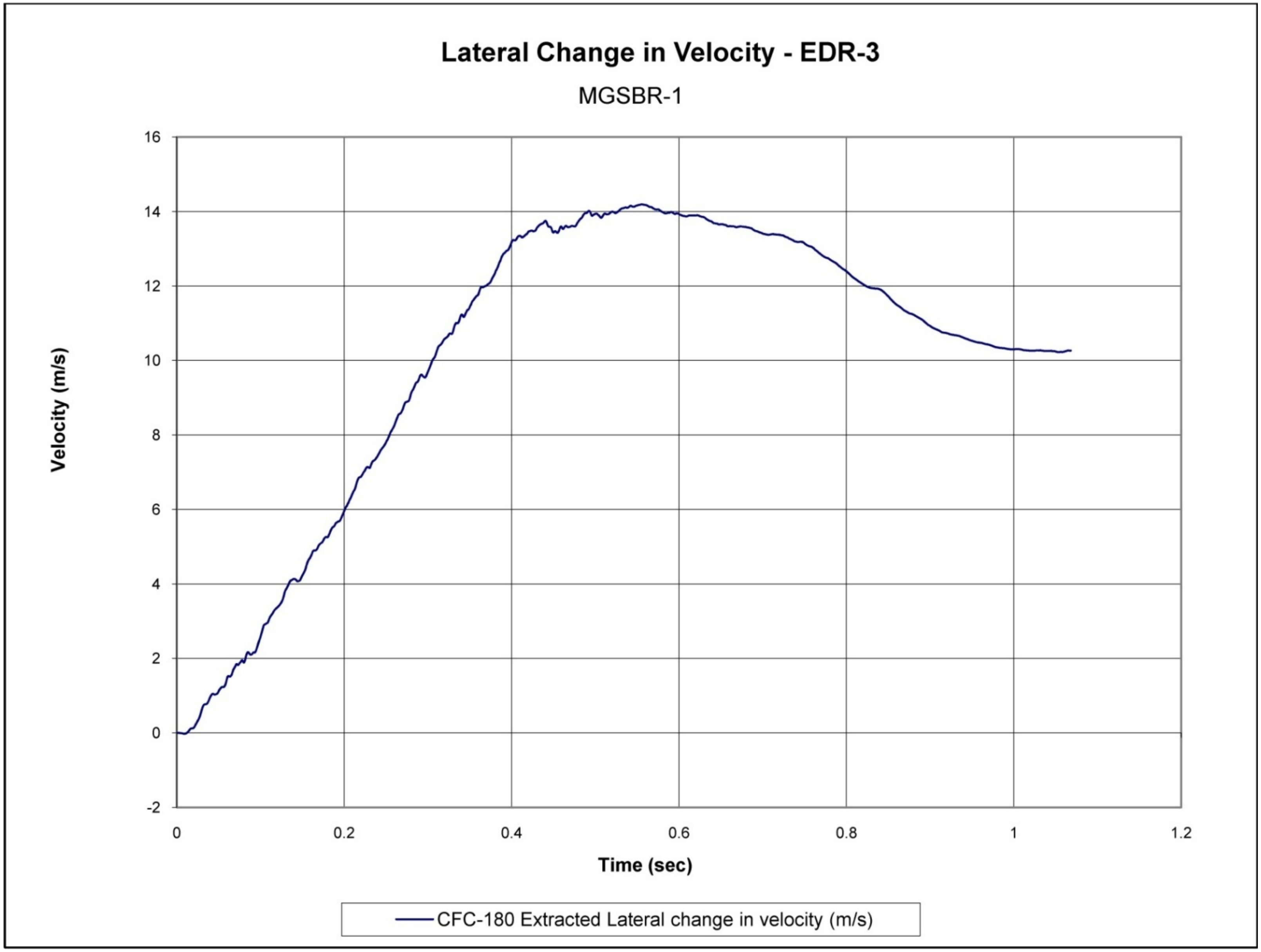

Figure E-19. Lateral Occupant Impact Velocity (EDR-3), Test No. MGSBR-1

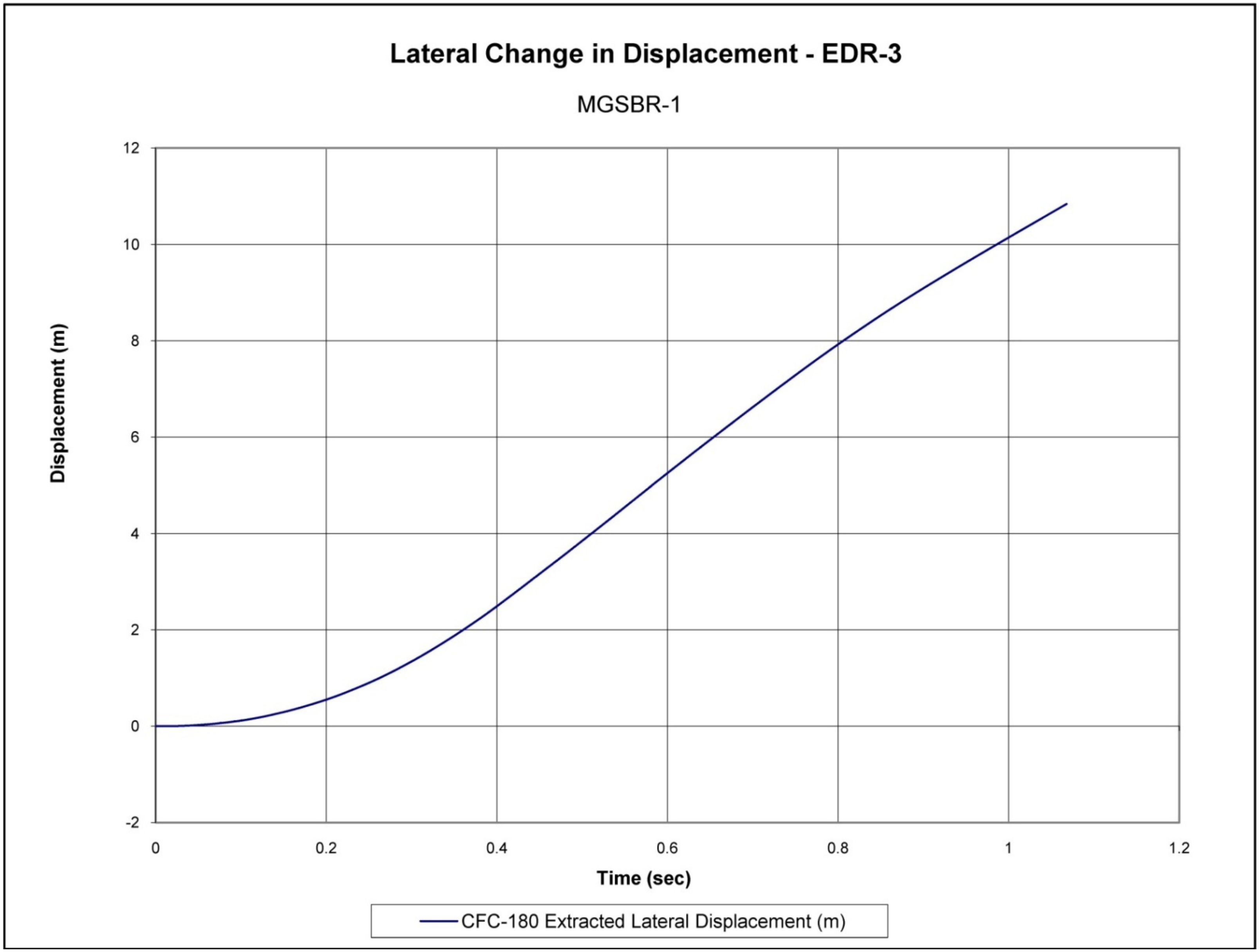

Figure E-20. Lateral Occupant Displacement (EDR-3), Test No. MGSBR-1

Appendix F. Accelerometer and Rate Transducer Plots, Test No. MGSBR-2

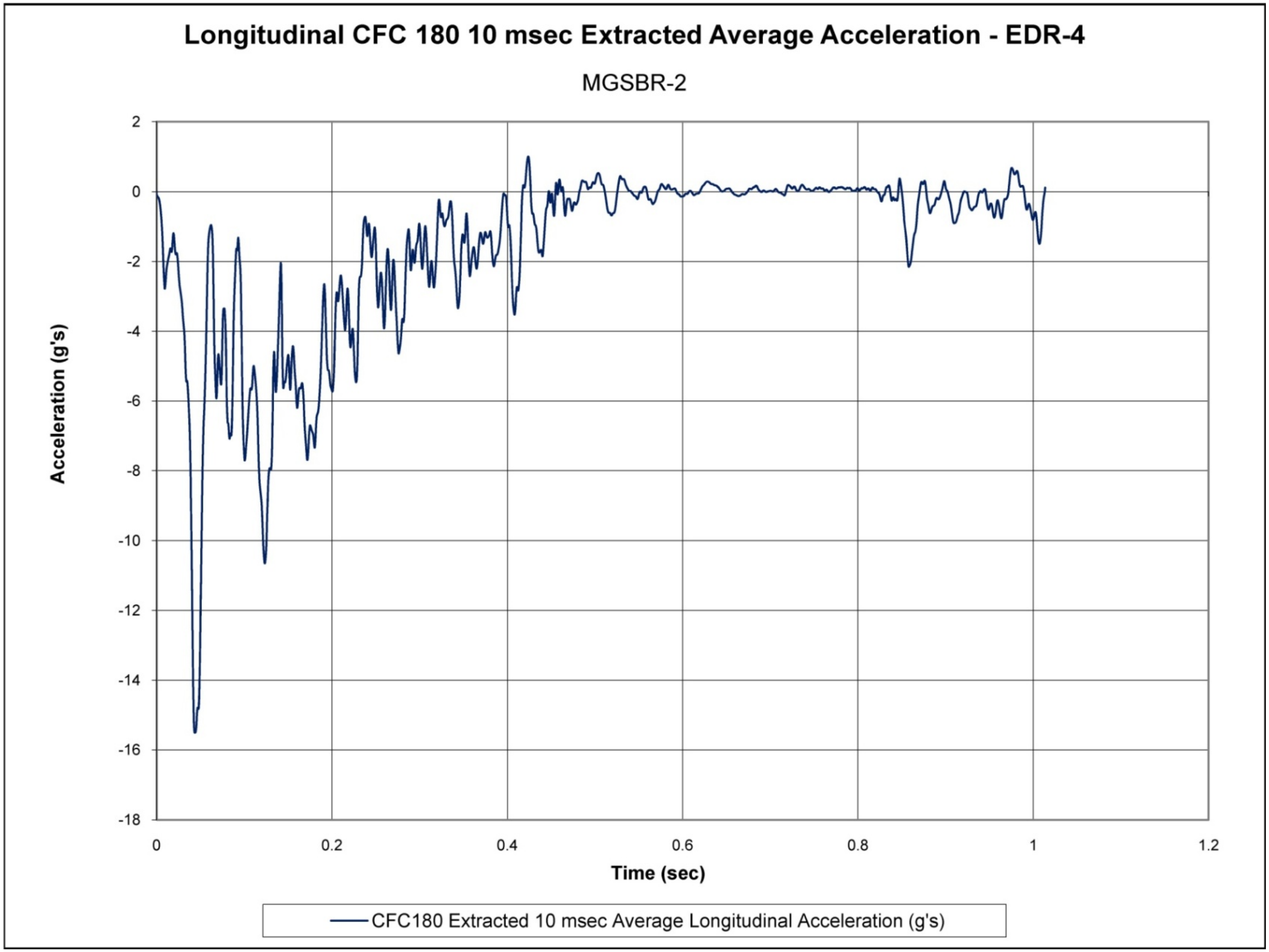

Figure F-1. 10-ms Average Longitudinal Deceleration (EDR-4), Test No. MGSBR-2

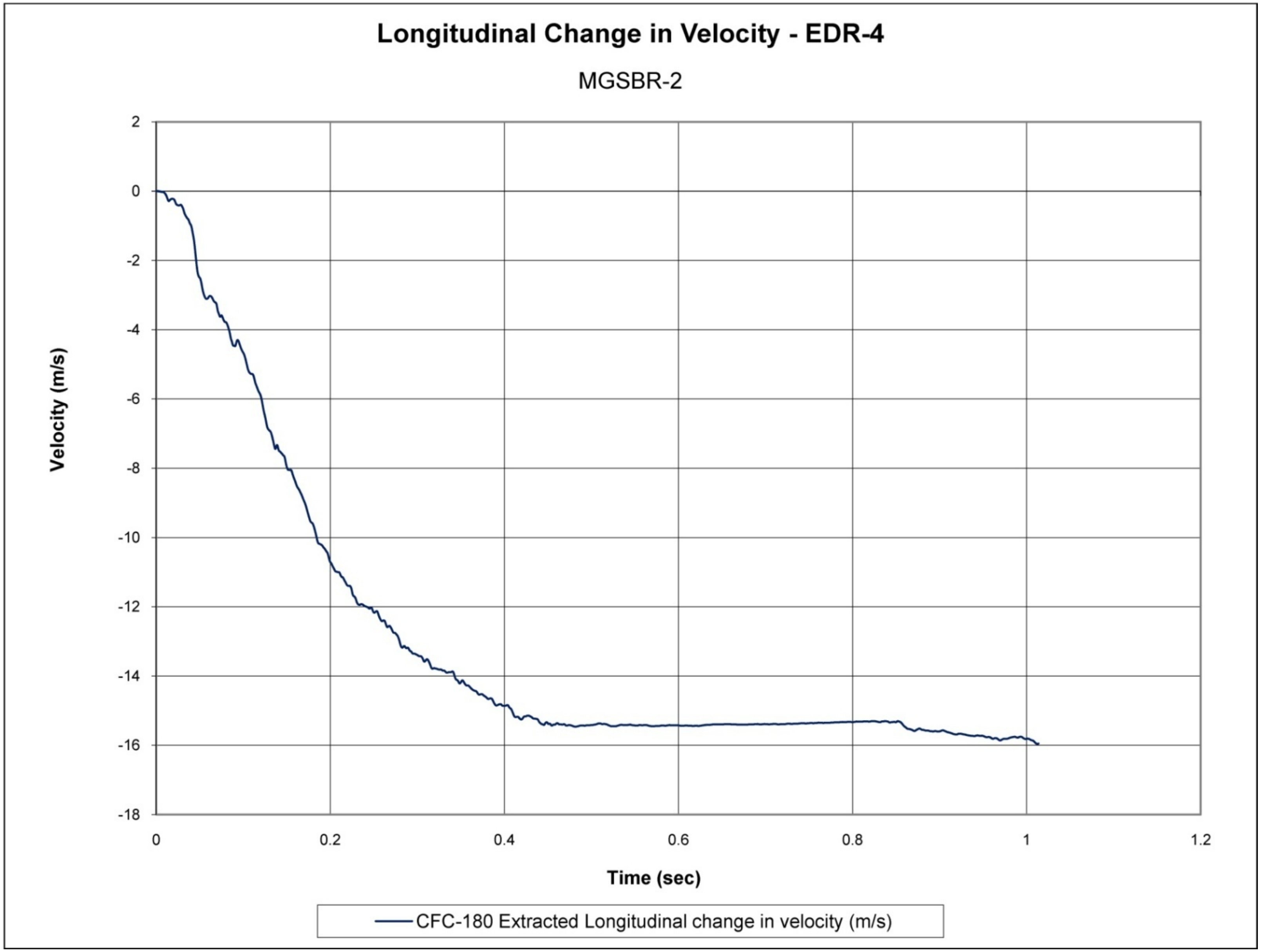

Figure F-2. Longitudinal Occupant Impact Velocity (EDR-4), Test No. MGSBR-2

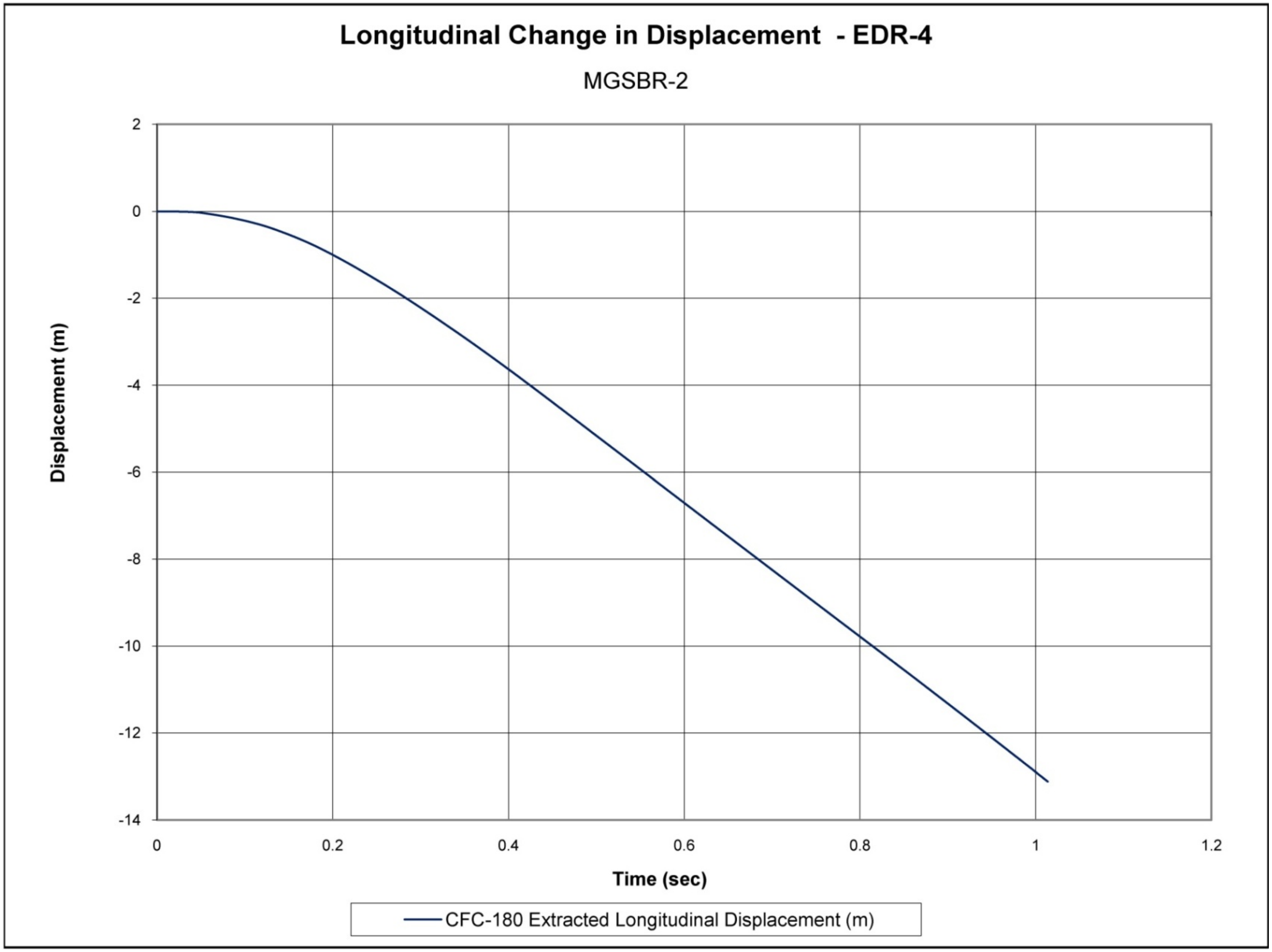

Figure F-3. Longitudinal Occupant Displacement (EDR-4), Test No. MGSBR-2

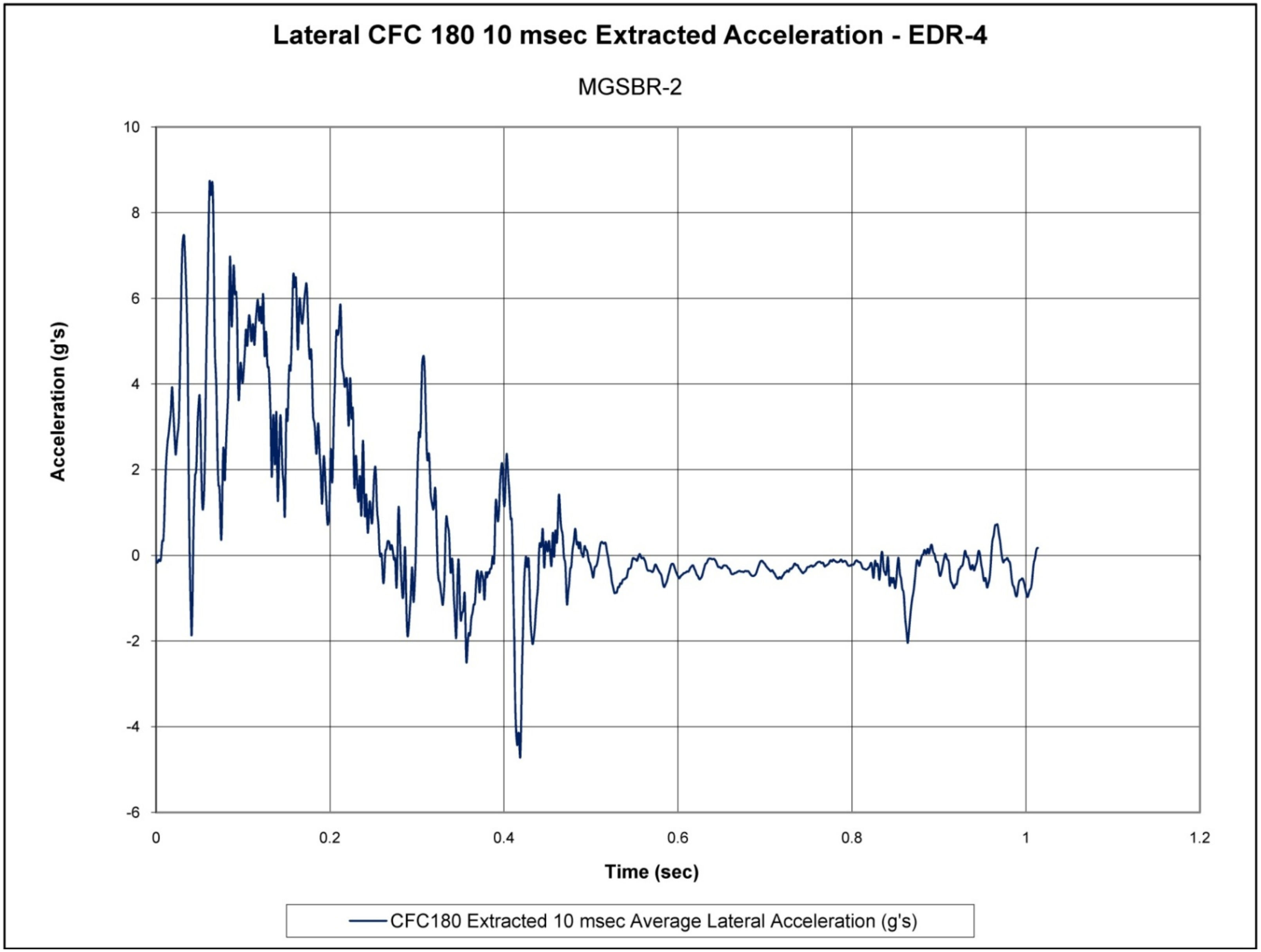

Figure F-4. 10-ms Average Lateral Deceleration (EDR-4), Test No. MGSBR-2

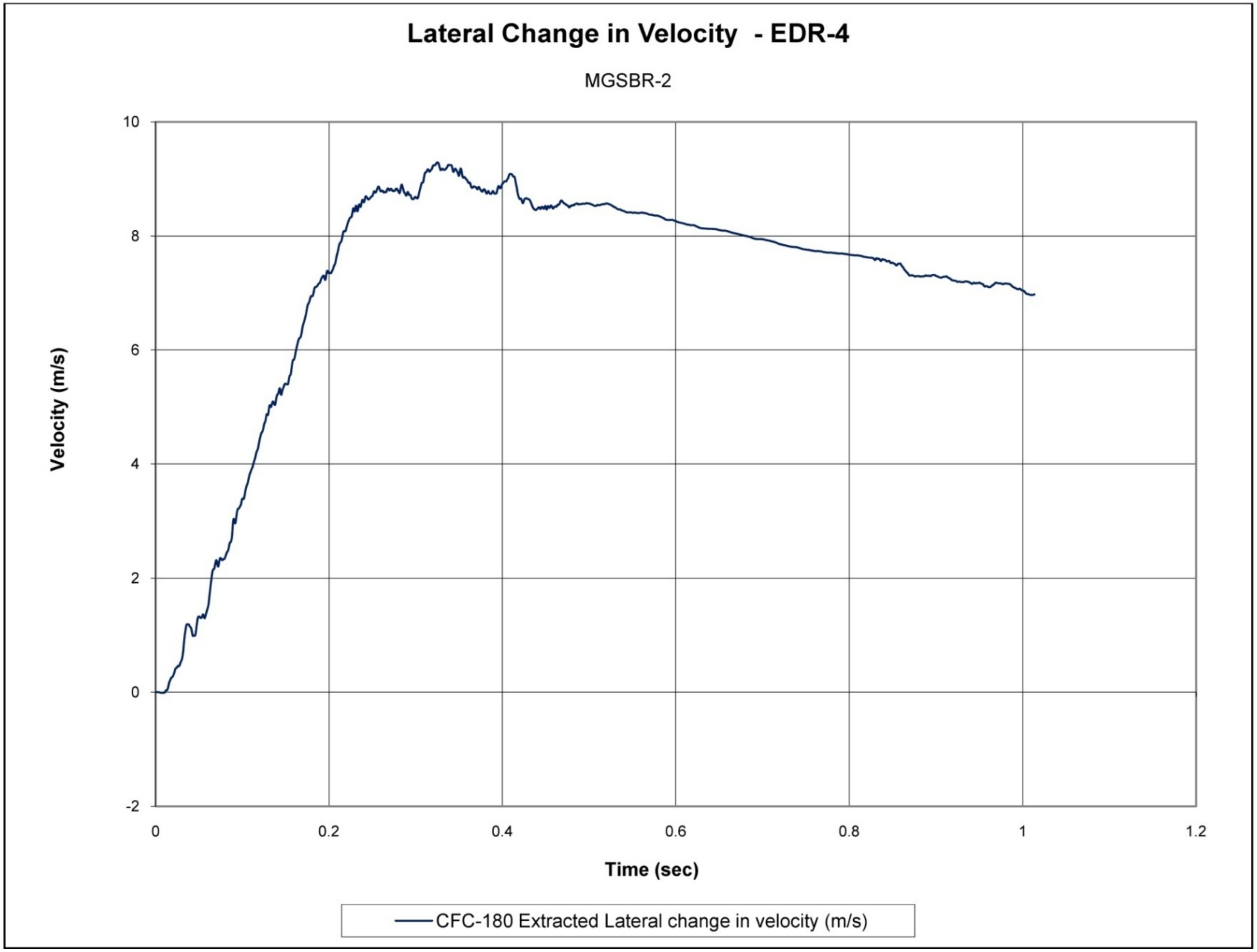

Figure F-5. Lateral Occupant Impact Velocity (EDR-4), Test No. MGSBR-2

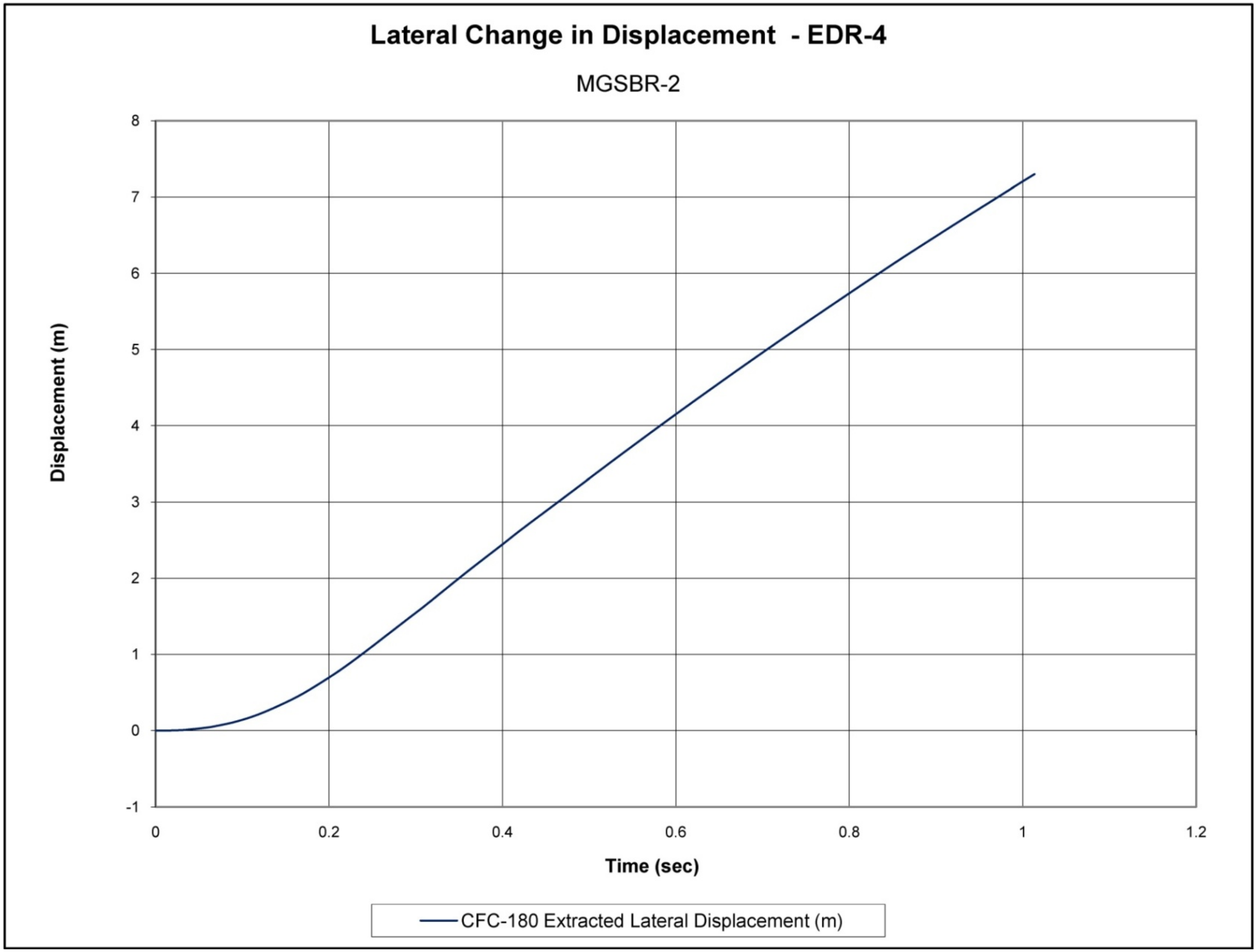

Figure F-6. Lateral Occupant Displacement (EDR-4), Test No. MGSBR-2

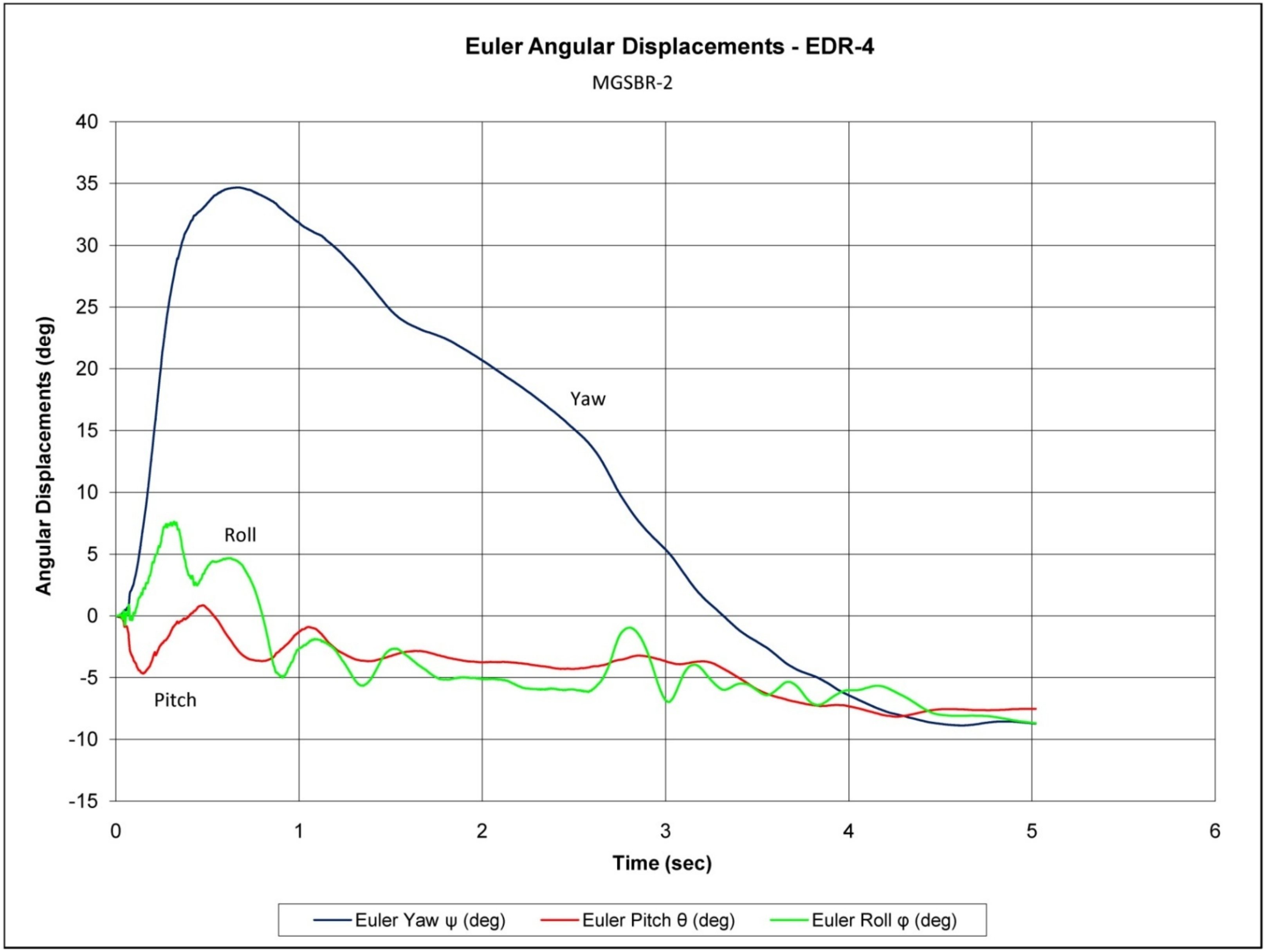

Figure F-7. Vehicle Angular Displacements (EDR-4), Test No. MGSBR-2

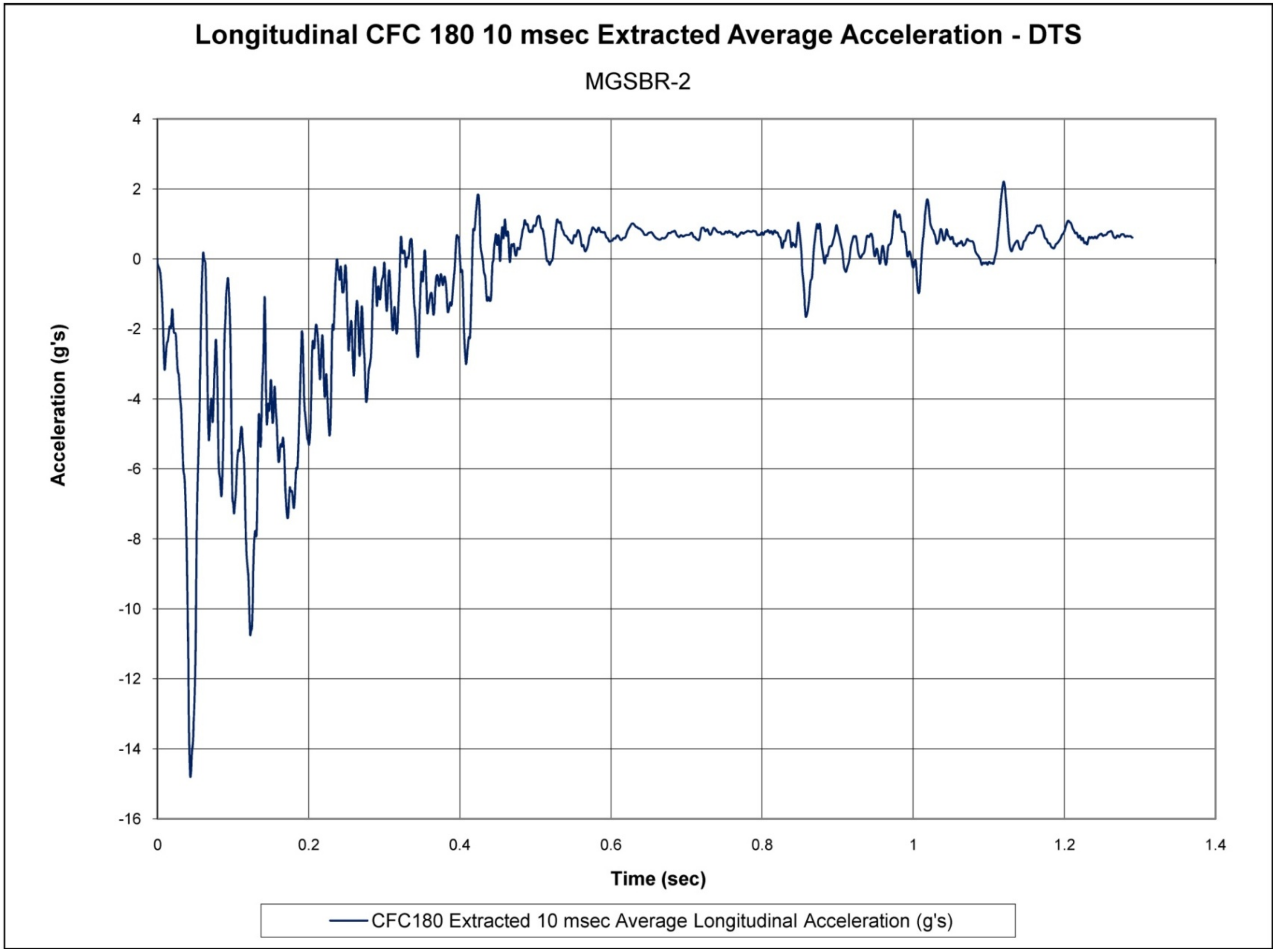

Figure F-8. 10-ms Average Longitudinal Deceleration (DTS), Test No. MGSBR-2

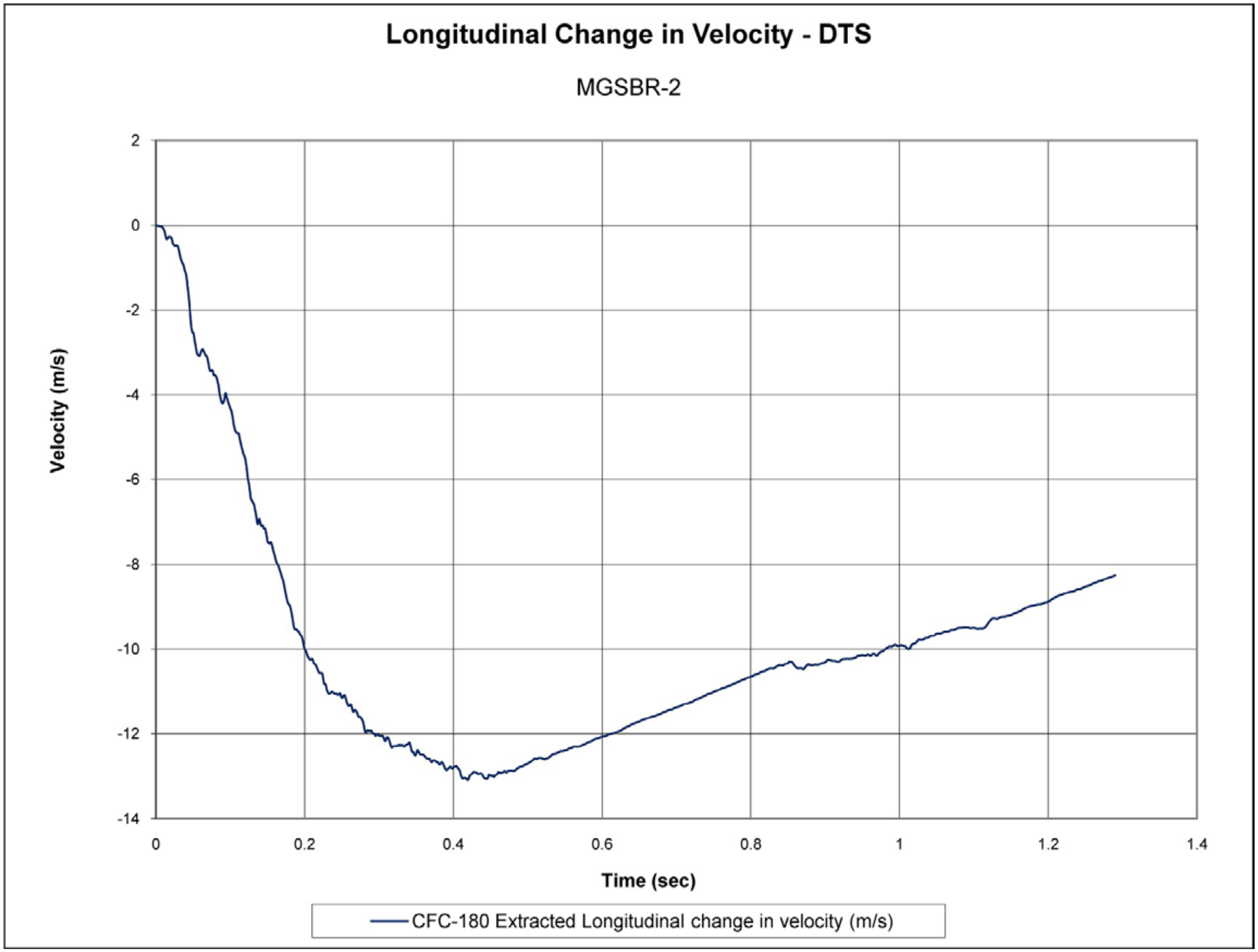

Figure F-9. Longitudinal Occupant Impact Velocity (DTS), Test No. MGSBR-2

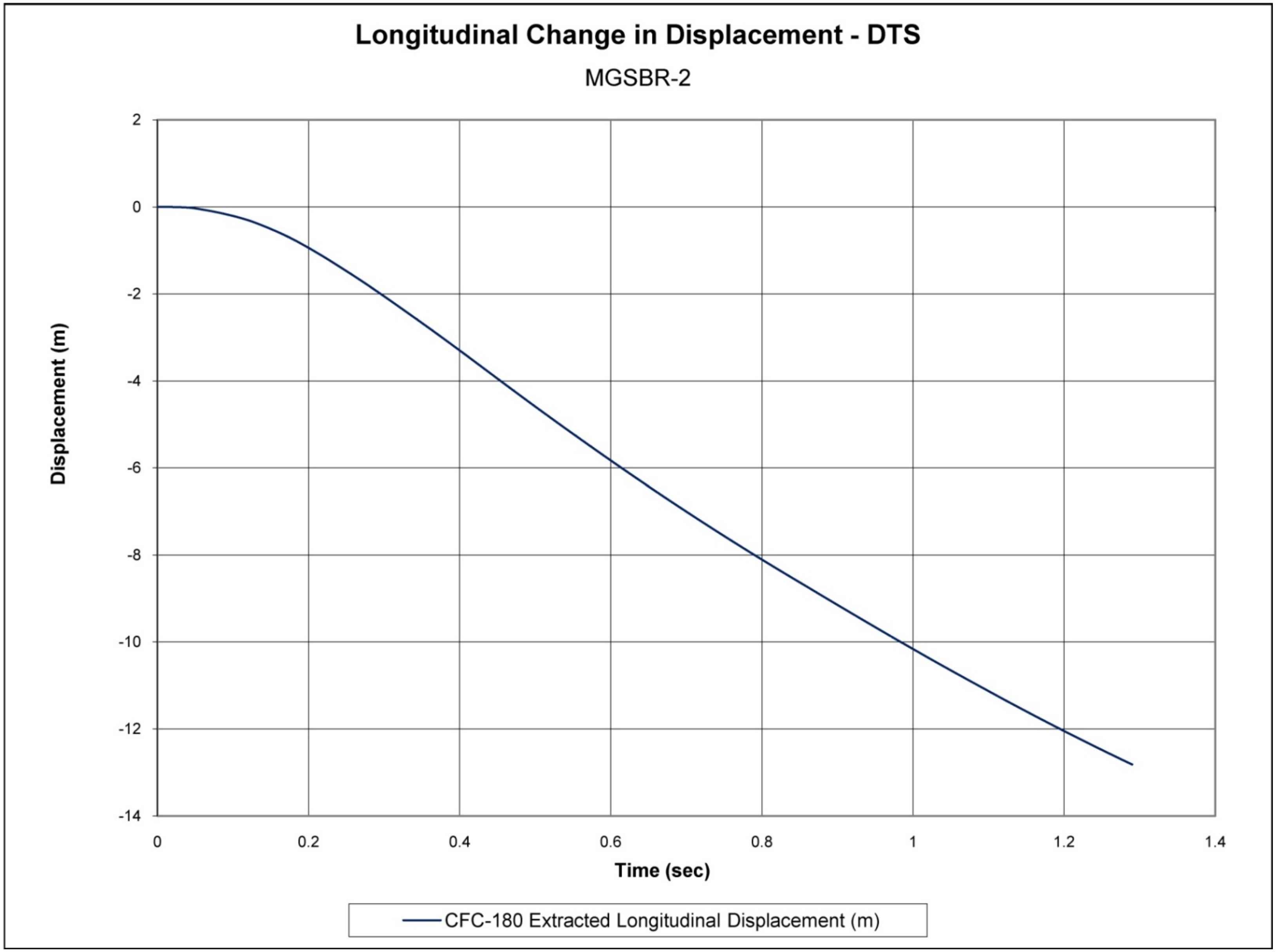

Figure F-10. Longitudinal Occupant Displacement (DTS), Test No. MGSBR-2

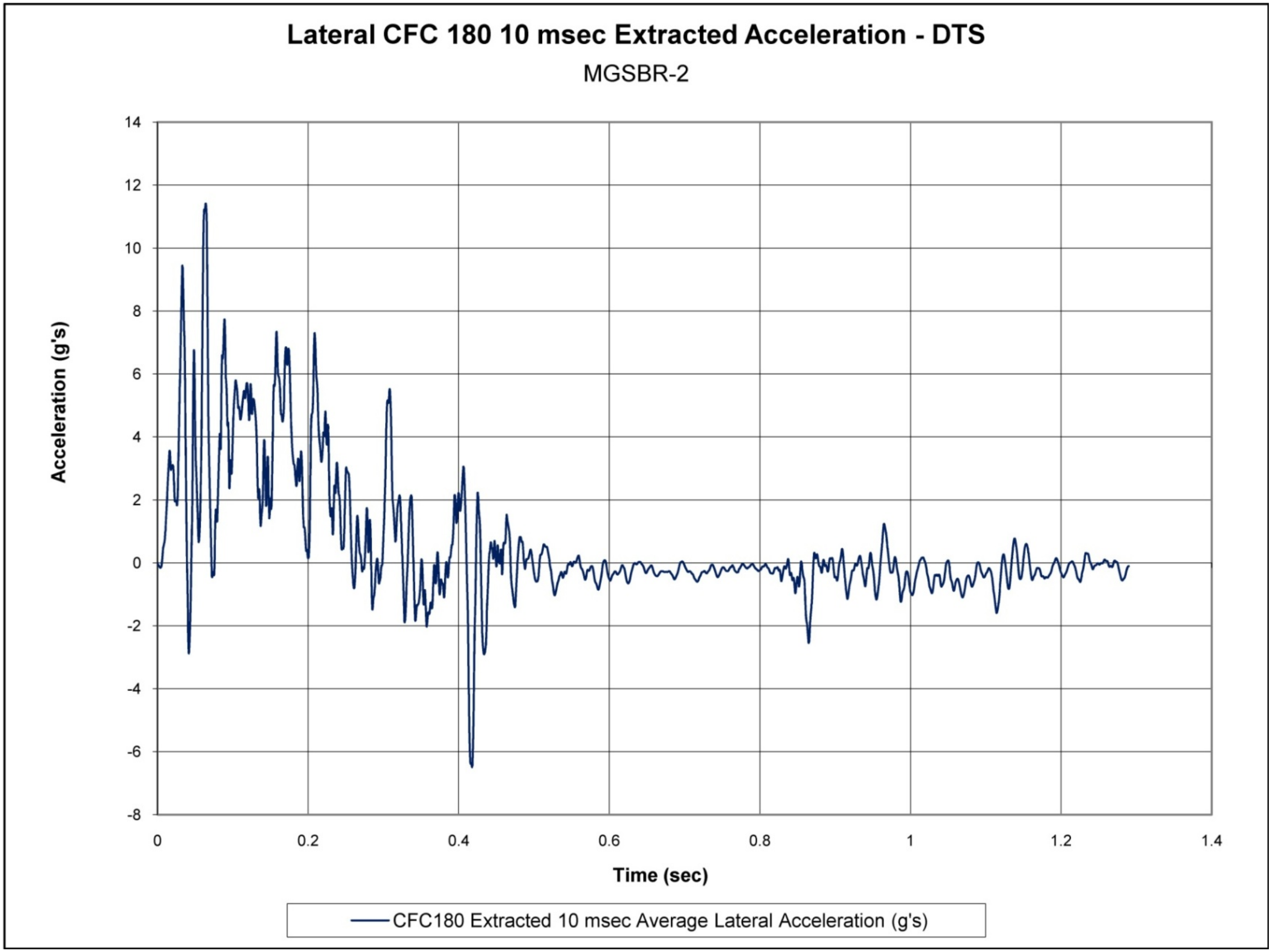

Figure F-11. 10-ms Average Lateral Deceleration (DTS), Test No. MGSBR-2

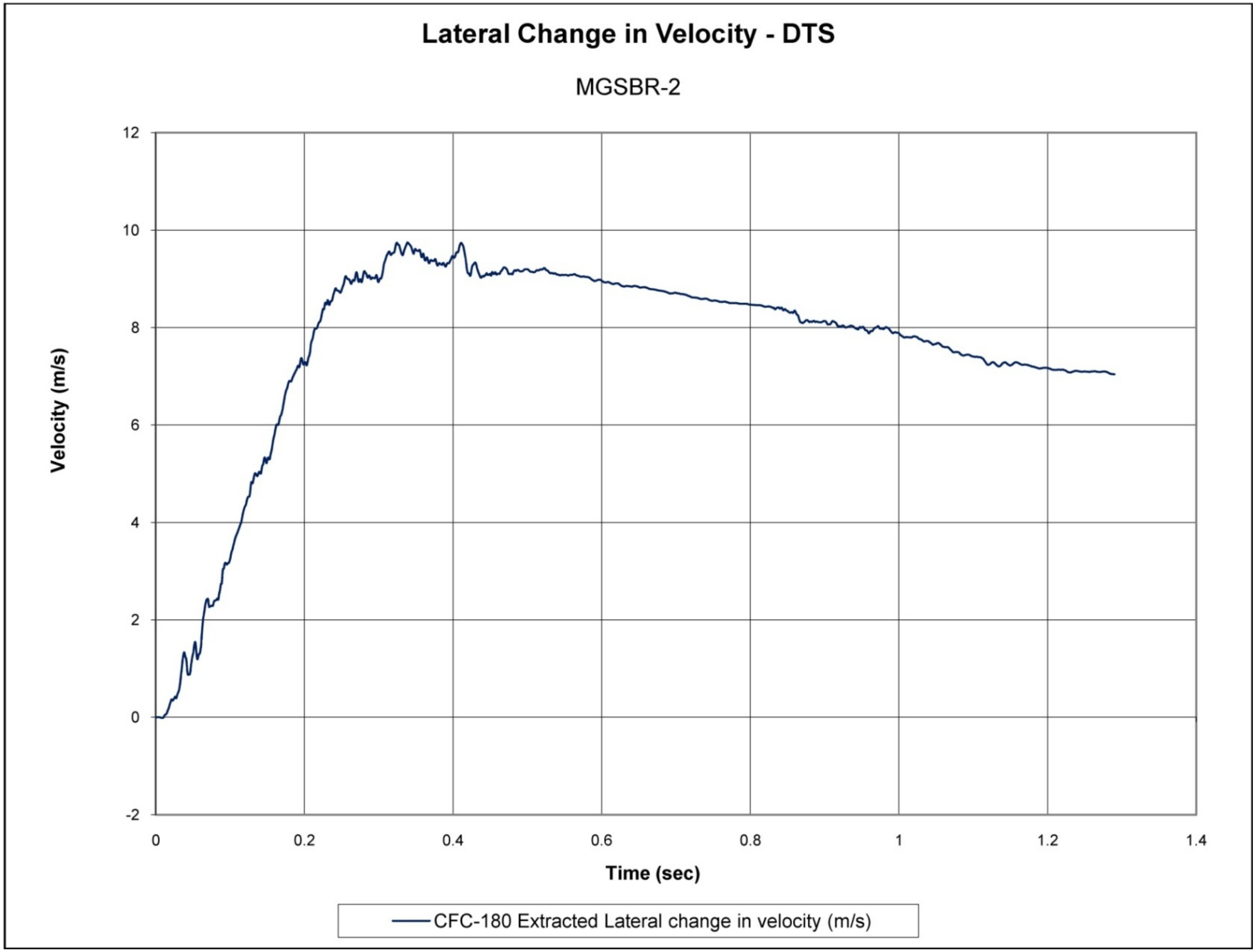

Figure F-12. Lateral Occupant Impact Velocity (DTS), Test No. MGSBR-2

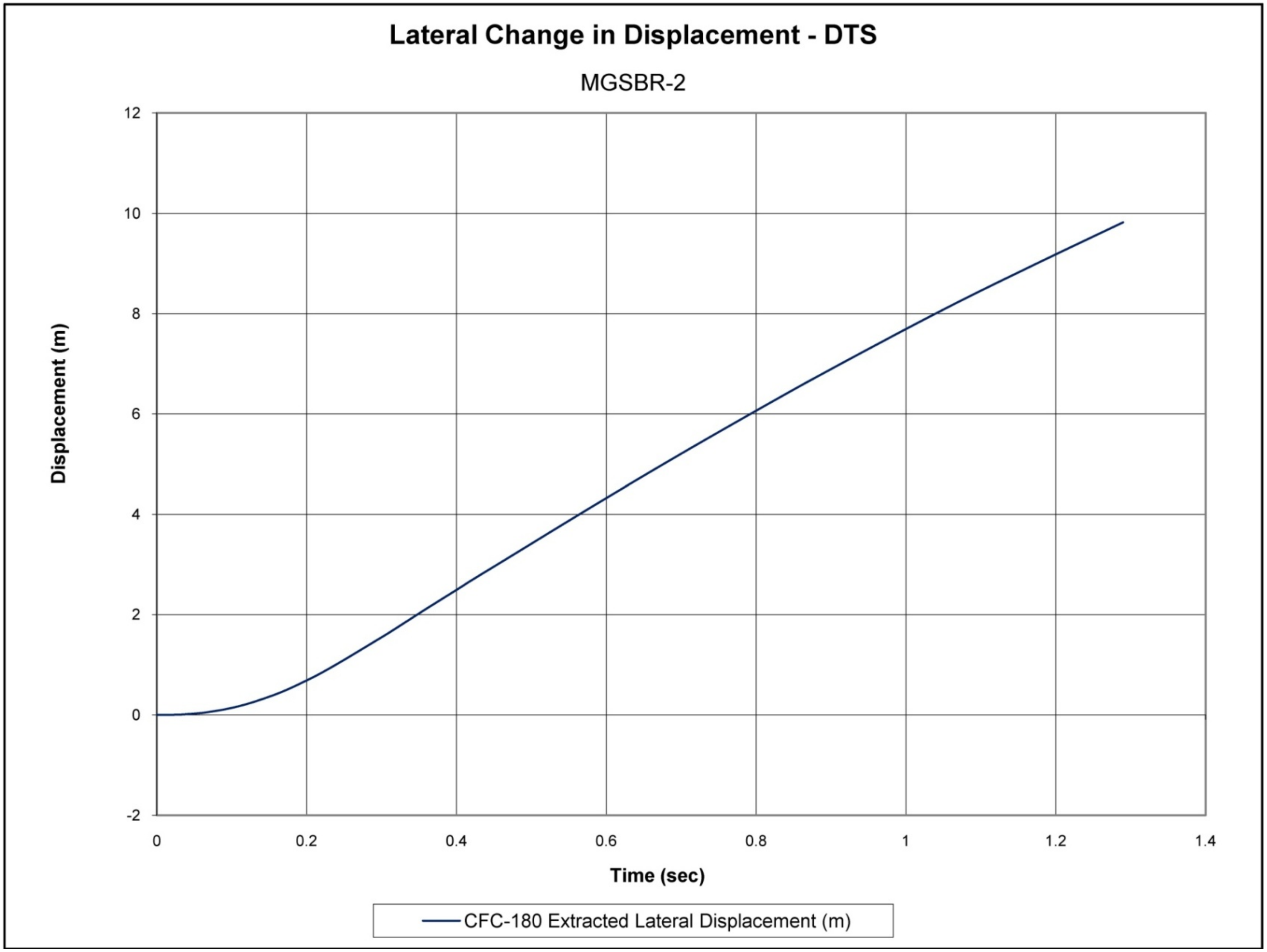

Figure F-13. Lateral Occupant Displacement (DTS), Test No. MGSBR-2

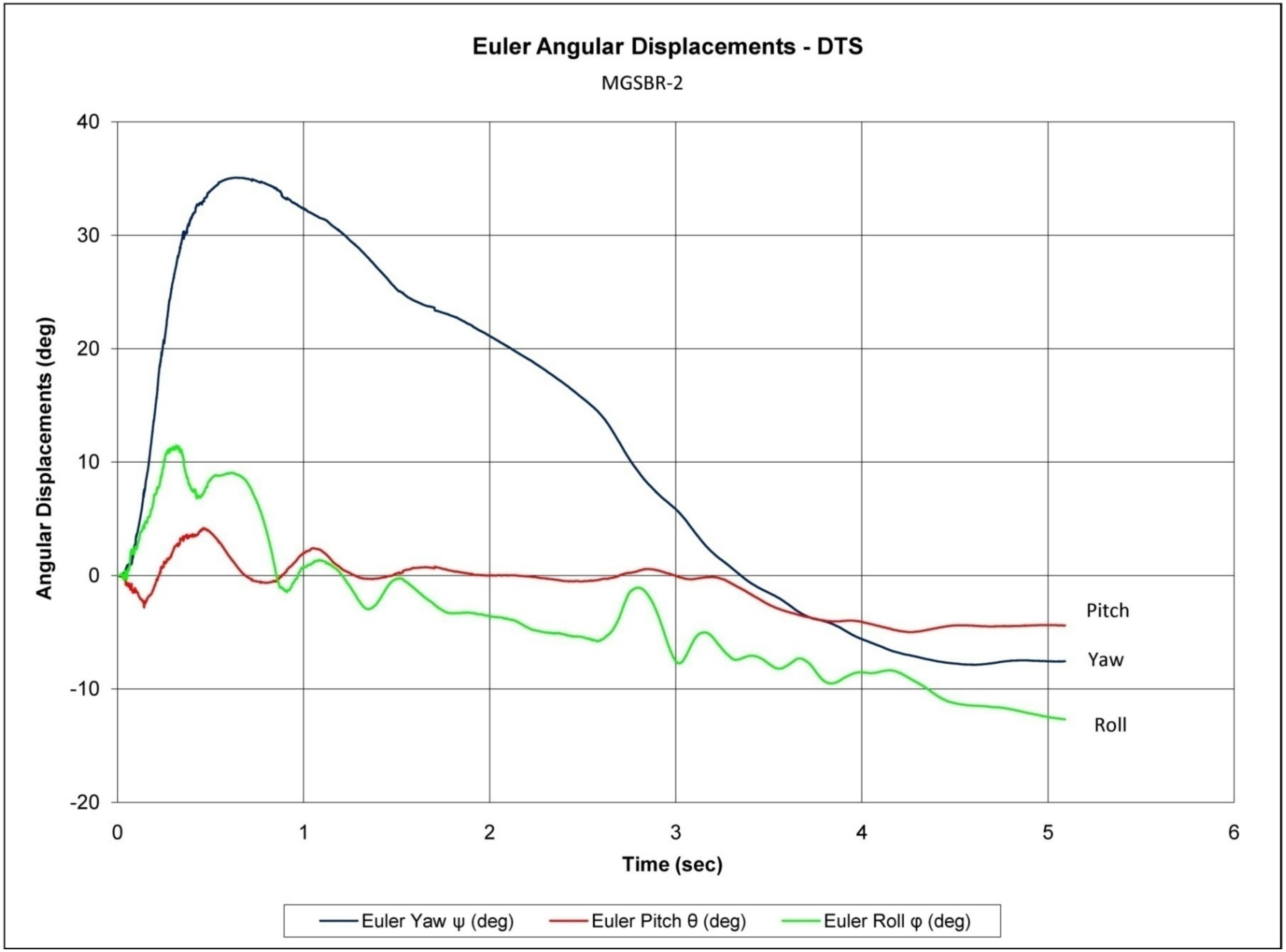

Figure F-14. Vehicle Angular Displacements (DTS), Test No. MGSBR-2

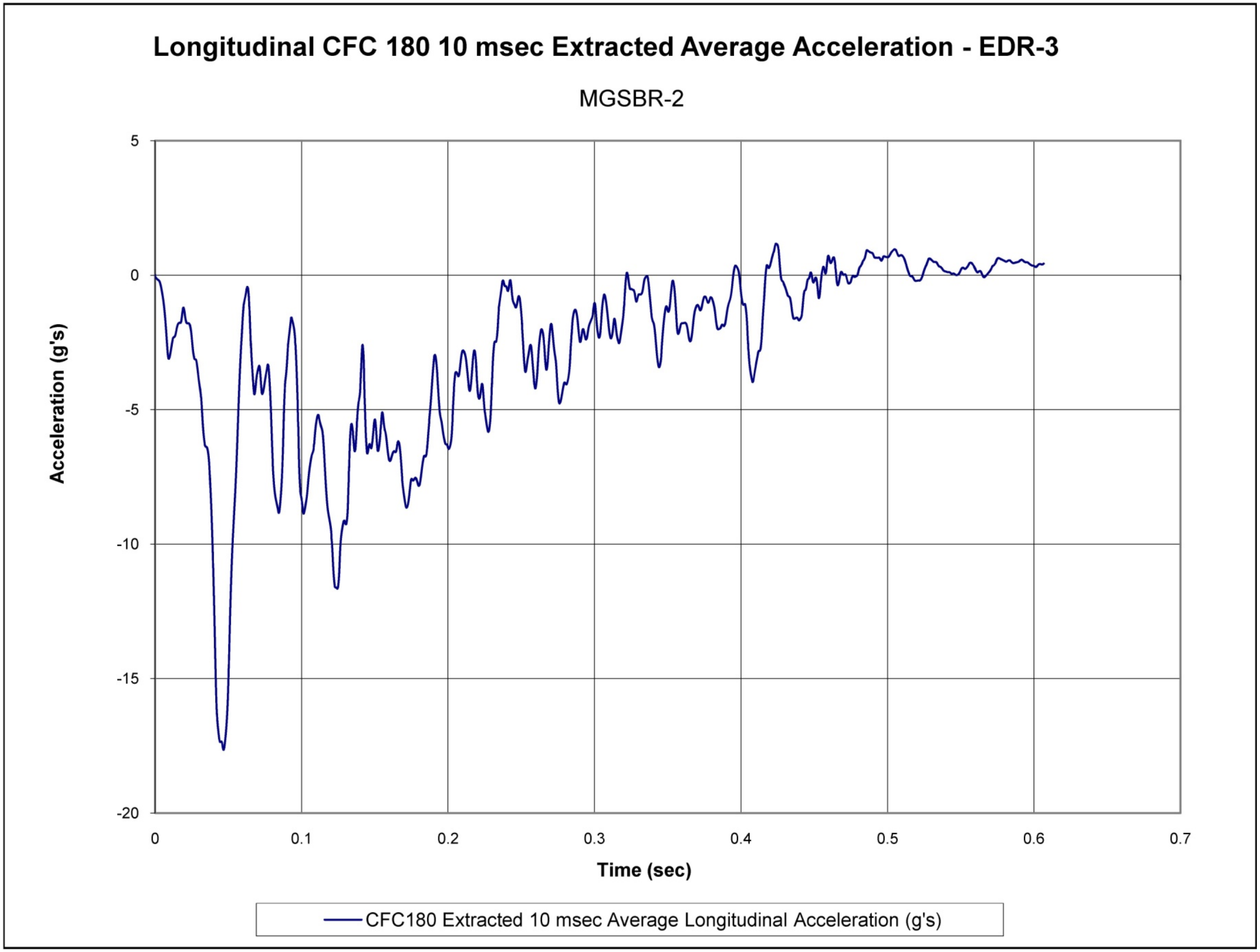

Figure F-15. 10-ms Average Longitudinal Deceleration (EDR-3), Test No. MGSBR-2

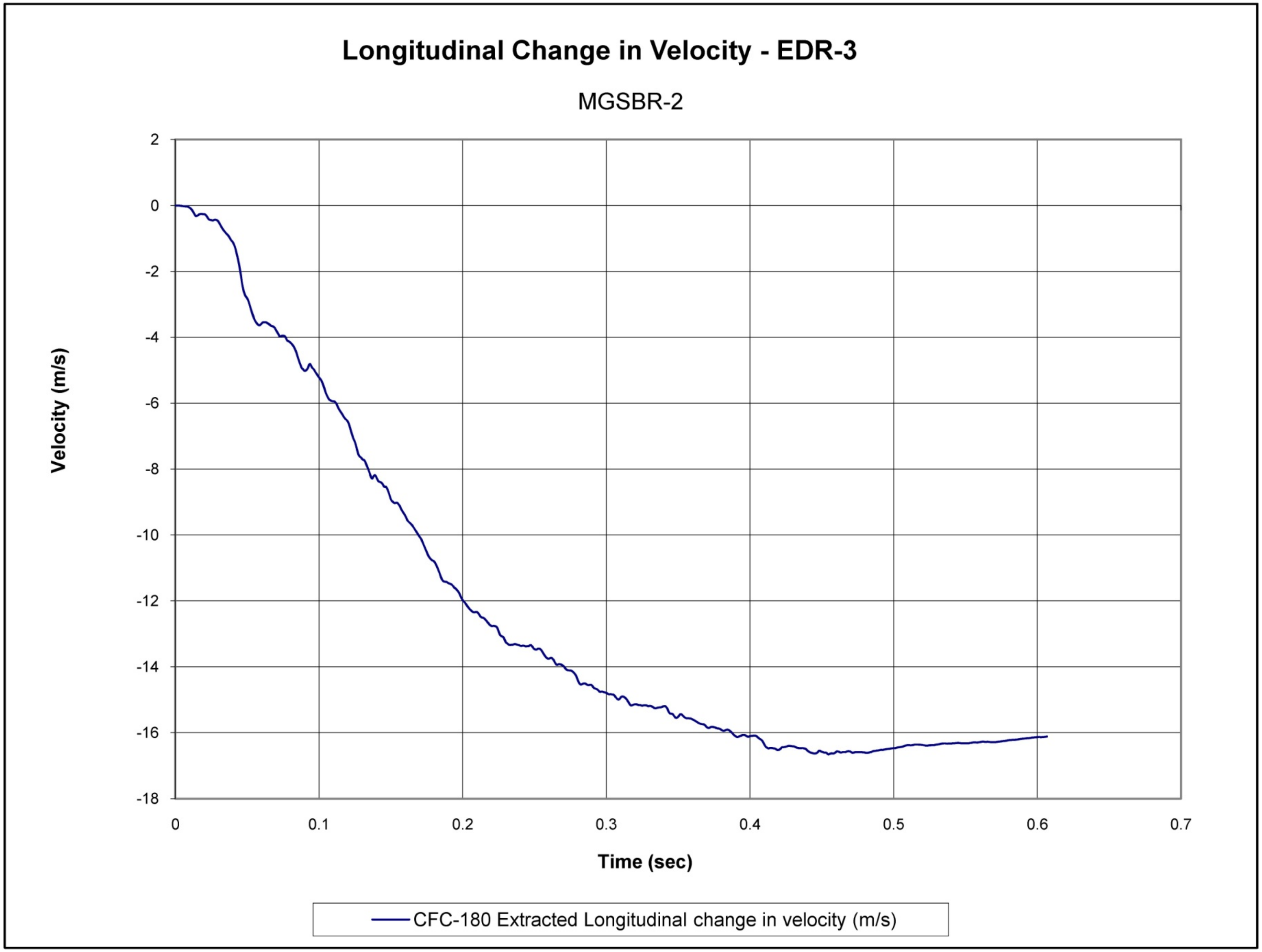

Figure F-16. Longitudinal Occupant Impact Velocity (EDR-3), Test No. MGSBR-2

Figure F-17. Longitudinal Occupant Displacement (EDR-3), Test No. MGSBR-2

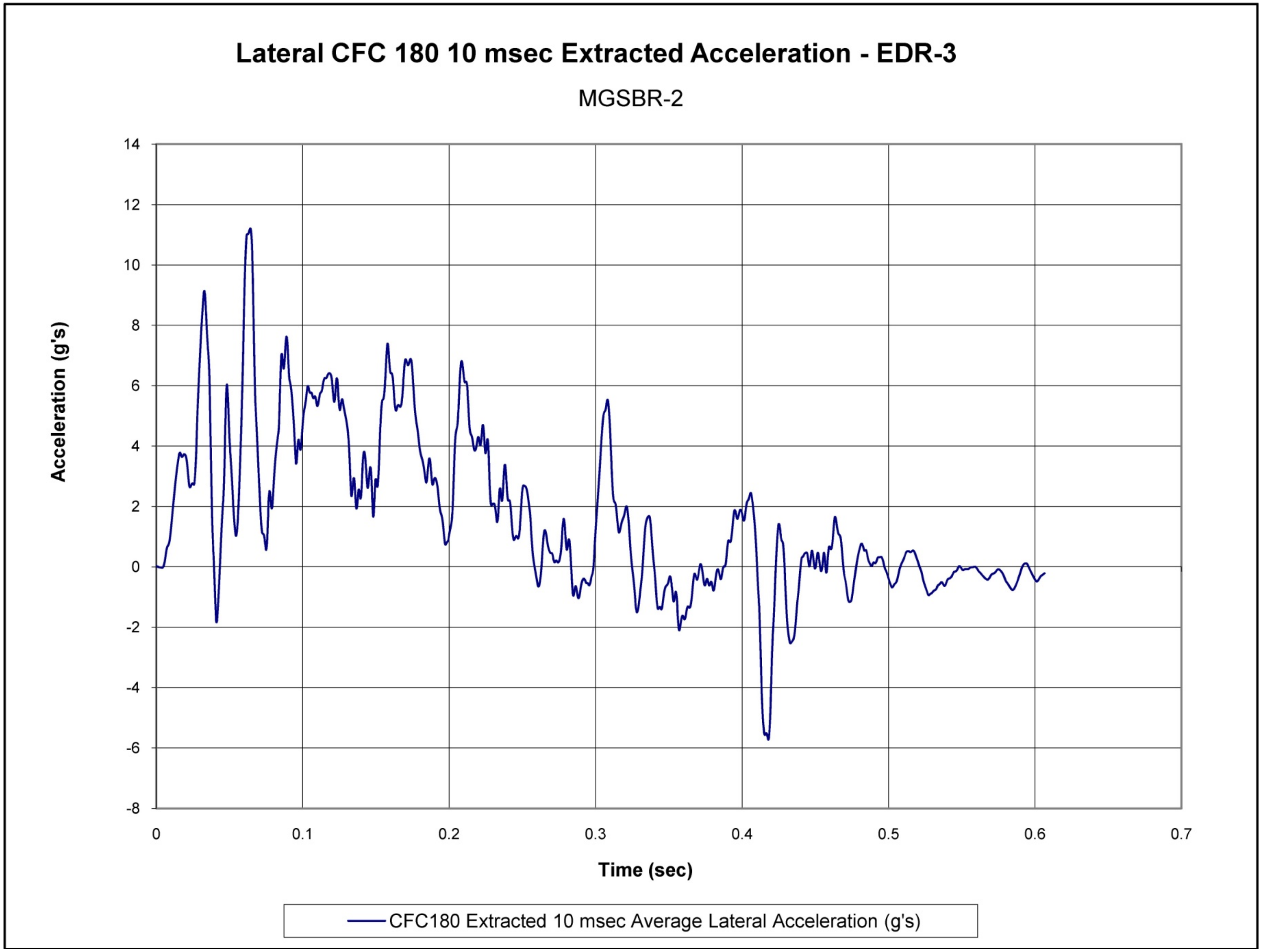

Figure F-18. 10-ms Average Lateral Deceleration (EDR-3), Test No. MGSBR-2

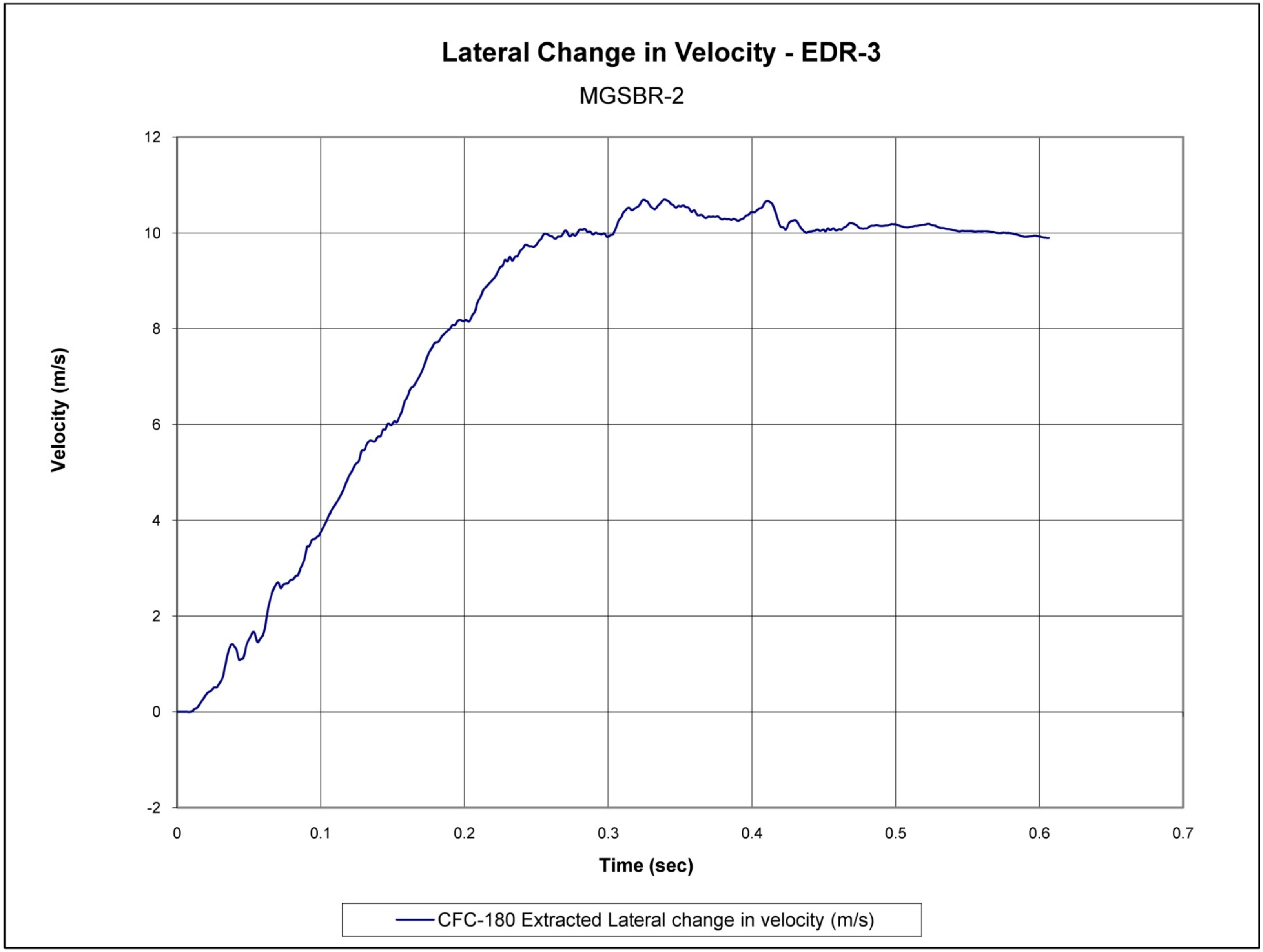

Figure F-19. Lateral Occupant Impact Velocity (EDR-3), Test No. MGSBR-2

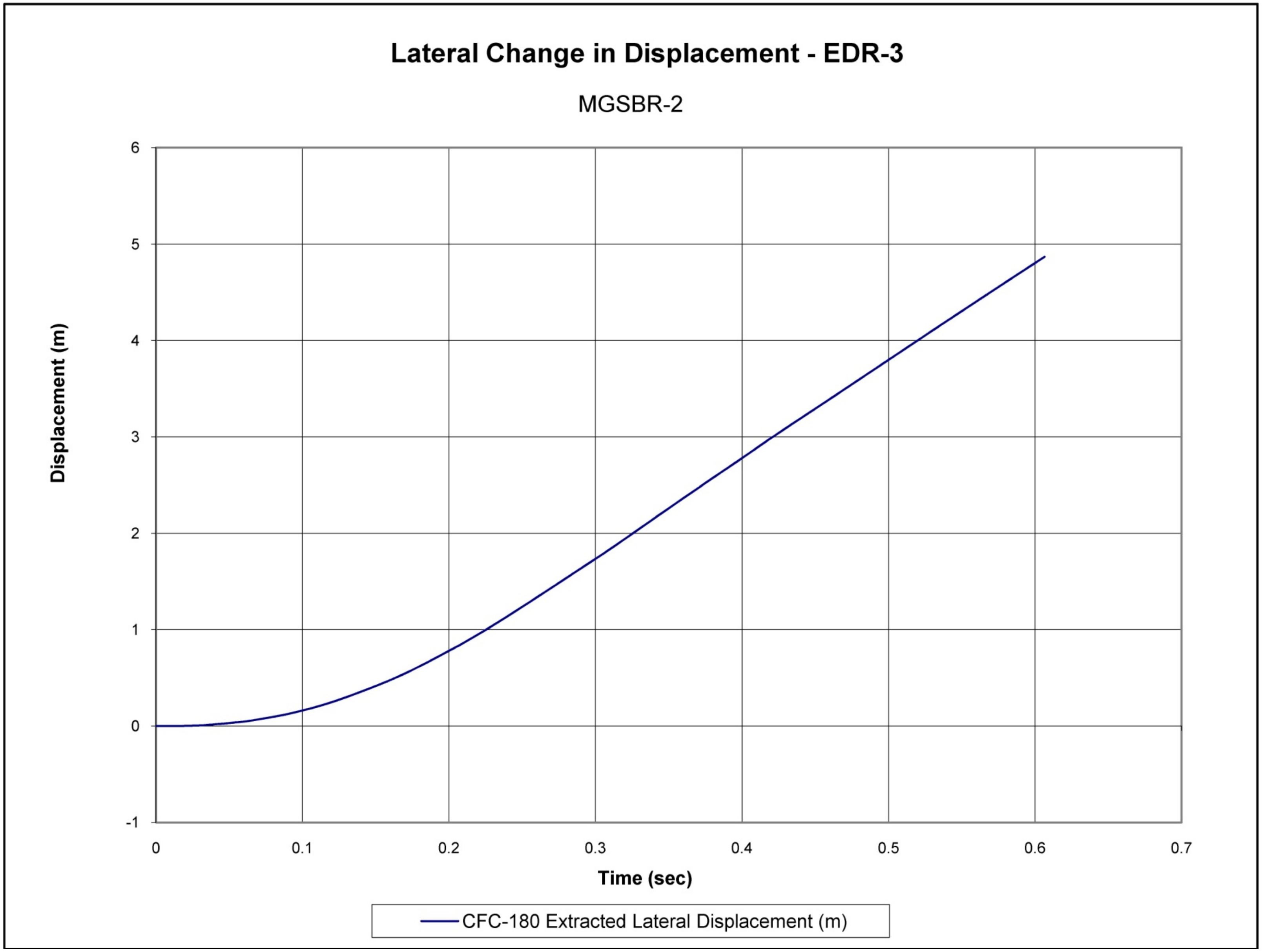

Figure F-20. Lateral Occupant Displacement (EDR-3), Test No. MGSBR-2

Appendix G. Calibrated BARRIER VII Input Files

```
Calibrated MGSBR-1 Model (Pickup), 30-Deg Post Data, 0.23 COF
  225    2    1    1  264    8    2    0
    0.0001    0.0001     2.000 2000    0       1.0    1
    1   10   10   10   10  500    1
    1       0.0       0.0
  225      2100       0.0
    1  225  223    1     9.375
    1  225      0.23
  225  224  223  222  221  220  219  218  217  216
  215  214  213  212  211  210  209  208  207  206
  205  204  203  202  201  200  199  198  197  196
  195  194  193  192  191  190  189  188  187  186
  185  184  183  182  181  180  179  178  177  176
  175  174  173  172  171  170  169  168  167  166
  165  164  163  162  161  160  159  158  157  156
  155  154  153  152  151  150  149  148  147  146
  145  144  143  142  141  140  139  138  137  136
  135  134  133  132  131  130  129  128  127  126
  125  124  123  122  121  120  119  118  117  116
  115  114  113  112  111  110  109  108  107  106
  105  104  103  102  101  100   99   98   97   96
   95   94   93   92   91   90   89   88   87   86
   85   84   83   82   81   80   79   78   77   76
   75   74   73   72   71   70   69   68   67   66
   65   64   63   62   61   60   59   58   57   56
   55   54   53   52   51   50   49   48   47   46
   45   44   43   42   41   40   39   38   37   36
   35   34   33   32   31   30   29   28   27   26
   25   24   23   22   21   20   19   18   17   16
   15   14   13   12   11   10    9    8    7    6
    5    4    3    2    1
  100    1
    1      2.29      1.99     9.375   30000.0      6.92      99.5      68.5 0.05 W-
Beam
  300    4
    1    24.875      0.00       6.0       6.0     100.0     675.0     675.0 0.05 BCT 1
     100.0     100.0      15.0      15.0
    2    24.875      0.00       3.0       3.0     100.0     150.0    225.00 0.05 BCT 2
      50.0      50.0      15.0      15.0
    3    24.875       0.0      4.00      6.03      54.0     92.88    143.65 0.05 W6x9
       6.0      15.0      15.0      15.0
    4    24.875       0.0     2.527     2.041      15.2    25.738    81.755 0.05
S3x5.7
       6.0      15.0      15.0      15.0
    1    1    2  224    1  101       0.0       0.0       0.0
  225    1                 301       0.0       0.0       0.0       0.0       0.0
  226    9                 302       0.0       0.0       0.0       0.0       0.0
  227   17       232    8  303       0.0       0.0       0.0       0.0       0.0
  233   65       255    4  304       0.0       0.0       0.0       0.0       0.0
  256  161       262    8  303       0.0       0.0       0.0       0.0       0.0
  263  217                 302       0.0       0.0       0.0       0.0       0.0
  264  225                 301       0.0       0.0       0.0       0.0       0.0
    5174.0   58310.0   20    6    4    0    1
    1     0.055      0.12      6.00      17.0
    2     0.057      0.15      7.00      18.0
    3     0.062      0.18     10.00      12.0
    4     0.110      0.35     12.00       6.0
    5      0.35      0.45      6.00       5.0
    6      1.45      1.50     15.00       1.0
    1    102.50    15.875    1      12.0    1    1    0    0
    2    102.50    27.875    1      12.0    1    1    0    0
    3    102.50    39.000    2      12.0    1    1    0    0
    4     88.75    39.000    2      12.0    1    1    0    0
    5     76.75    39.000    2      12.0    1    1    0    0
```

```
  6     64.75    39.000    2      12.0    1    1    0    0
  7     52.75    39.000    2      12.0    1    1    0    0
  8     40.75    39.000    2      12.0    1    1    0    0
  9     28.75    39.000    2      12.0    1    1    0    0
 10     16.75    39.000    2      12.0    1    1    0    0
 11    -13.25    39.000    3      12.0    1    1    0    0
 12    -33.25    39.000    3      12.0    1    1    0    0
 13    -53.25    39.000    3      12.0    1    1    0    0
 14    -73.25    39.000    3      12.0    1    1    0    0
 15    -93.25    39.000    3      12.0    1    1    0    0
 16   -125.35    39.000    4      12.0    1    1    0    0
 17   -125.35   -39.000    4      12.0    0    0    0    0
 18    102.50   -39.000    1      12.0    0    0    0    0
 19     62.40     33.90    5       1.0    1    1    0    0
 20    -77.85     33.90    6       1.0    1    1    0    0
  1     62.40     33.90       0.0      608.
  2     62.40    -33.90       0.0      608.
  3    -77.85     33.90       0.0      492.
  4    -77.85    -33.90       0.0      492.
  1       0.0       0.0
  3    823.00       0.0     24.91     61.89       0.0       0.0       1.0
```

```
Calibrated MGSBR-2 Model (Small Car), 30-Deg Post Data, 0.525 COF
  225    2    1    1  264    8    2    0
    0.0001    0.0001     2.000 2000    0       1.0    1
    1   10   10   10   10  500    1
    1       0.0       0.0
  225      2100       0.0
    1  225  223    1     9.375
    1  225     0.525
  225  224  223  222  221  220  219  218  217  216
  215  214  213  212  211  210  209  208  207  206
  205  204  203  202  201  200  199  198  197  196
  195  194  193  192  191  190  189  188  187  186
  185  184  183  182  181  180  179  178  177  176
  175  174  173  172  171  170  169  168  167  166
  165  164  163  162  161  160  159  158  157  156
  155  154  153  152  151  150  149  148  147  146
  145  144  143  142  141  140  139  138  137  136
  135  134  133  132  131  130  129  128  127  126
  125  124  123  122  121  120  119  118  117  116
  115  114  113  112  111  110  109  108  107  106
  105  104  103  102  101  100   99   98   97   96
   95   94   93   92   91   90   89   88   87   86
   85   84   83   82   81   80   79   78   77   76
   75   74   73   72   71   70   69   68   67   66
   65   64   63   62   61   60   59   58   57   56
   55   54   53   52   51   50   49   48   47   46
   45   44   43   42   41   40   39   38   37   36
   35   34   33   32   31   30   29   28   27   26
   25   24   23   22   21   20   19   18   17   16
   15   14   13   12   11   10    9    8    7    6
    5    4    3    2    1
  100    1
    1      2.29      1.99     9.375   30000.0      6.92      99.5      68.5 0.05 W-
Beam
  300    4
    1    24.875      0.00       6.0       6.0     100.0     675.0     675.0 0.05 BCT 1
     100.0     100.0      15.0      15.0
    2    24.875      0.00       3.0       3.0     100.0     150.0    225.00 0.05 BCT 2
      50.0      50.0      15.0      15.0
    3    24.875       0.0      4.00      6.03      54.0     92.88    143.65 0.05 W6x9
       6.0      15.0      15.0      15.0
    4    24.875       0.0     2.527     2.041      15.2    25.738    81.755 0.05
S3x5.7
       6.0      15.0      15.0      15.0
    1    1    2  224    1  101       0.0       0.0       0.0
  225    1               301       0.0       0.0       0.0       0.0       0.0
  226    9               302       0.0       0.0       0.0       0.0       0.0
  227   17       232    8  303       0.0       0.0       0.0       0.0       0.0
  233   65       255    4  304       0.0       0.0       0.0       0.0       0.0
  256  161       262    8  303       0.0       0.0       0.0       0.0       0.0
  263  217               302       0.0       0.0       0.0       0.0       0.0
  264  225               301       0.0       0.0       0.0       0.0       0.0
    2585.0   16264.9   20    1    4    0    1
    1     0.033     0.150       4.5      13.0
    1    75.750   -32.188    1    43.240    1    1    0    0
    2    75.750   -21.458    1    10.729    1    1    0    0
    3    75.750   -10.729    1    10.729    1    1    0    0
    4    75.750     0.000    1    10.729    1    1    0    0
    5    75.750    10.729    1    10.729    1    1    0    0
    6    75.750    21.458    1    10.729    1    1    0    0
    7    75.750    32.188    1    12.940    1    1    0    0
    8    60.600    32.188    1    15.150    1    1    0    0
    9    45.450    32.188    1    15.150    1    1    0    0
   10    30.300    32.188    1    15.150    1    1    0    0
```

11	15.150	32.188	1	15.150	1	1	0	0		
12	0.000	32.188	1	18.888	1	1	0	0		
13	-22.625	32.188	1	22.625	1	1	0	0		
14	-45.250	32.188	1	22.625	1	1	0	0		
15	-67.875	32.188	1	22.625	1	1	0	0		
16	-90.5	32.188	1	22.625	1	1	0	0		
17	-90.500	-32.188	1	45.250	1	1	0	0		
18	0.000	-32.188	1	45.250	1	1	0	0		
19	38.5	27.813	1	1.000	1	1	0	0		
20	38.5	-27.813	1	1.000	1	1	0	0		
1	38.5	27.813	0.00	380.250						
2	38.5	-27.813	0.00	380.250						
3	-57.0	27.813	0.00	264.500						
4	-57.0	-27.813	0.00	264.500						
1	0.00	0.00								
7	913.5	0.0	24.88	62.27	0.0	0.0	1.0			

END OF DOCUMENT